Impedance-Based Real-Time Monitoring of Mammalian Cells upon Introduction of Xenobiotics into the Cytoplasm by In Situ Electroporation

DISSERTATION

Zur Erlangung des

DOKTORGRADES DER NATURWISSENSCHAFTEN

(Dr. rer. nat.)

der Fakultät für Chemie und Pharmazie

der Universität Regensburg

vorgelegt von

Sonja Lukic

aus Sombor, Serbien

Im Jahr 2017

Die vorliegende Doktorarbeit entstand in der Zeit von Februar 2012 bis September 2015 am Institut für Analytische Chemie, Chemo- und Biosensorik an der Universität Regensburg.

Die Arbeit wurde von Prof. Dr. Joachim Wegener angeleitet.

Promotionsgesuch eingereicht am:	27. Juli 2017	
Tag der mündlichen Prüfung:	15. September 2017	
Prüfungsausschuss:	Apl. Prof. Dr. Rainer Müller	Vorsitzender
	Prof. Dr. Joachim Wegener	Erstgutachter
	PD Dr. Miriam Breunig	Zweitgutachter
	Prof. Dr. Antje J. Bäumner	Drittprüfer

Meiner Familie

Mojoj porodici

Table of Contents

1 Introduction

1.1 Cell-Based Biosensors

Biosensors incorporate biological components (biomolecules, organelles, membrane fragments, whole cells, tissues, organs, or even whole organism) as the sensing element closely connected to a transducer which converts the response of the biological/biochemical system into a corresponding electronic signal. (Turner, 1987, 2000; Luong et al., 1988; Gronow, 1984; Powner and Yalcinkaya, 1997).

Whole-cell biosensors have living cell(s) as the biological recognition element and any change in cellular behavior upon their exposure to different kinds of stimuli (biological, physical, chemical), will be converted (by a transducer) into a measurable signal (Keusgen, 2002; Bousse, 1996; Ziegler, 2000; Wang et al., 2005).

Cell-based biosensors and assays are broadly applied within bioanalysis, biotechnology, cell biology, pharmacology, toxicology, medicine, or environmental sciences. After initial studies are often performed on a molecular level, in a next stage results need to be verified within the living cells as the building blocks of life. Therefore, *in situ* analysis of cells is often applied as a readout. This approach allows the cells to spread and grow on the surface of a transducer, which will subsequently be used for analysis of the cellular behavior upon certain stimuli and in some cases, the transducer delivers specific stimuli itself. This enables a closer look into cellular mechanisms while the cells are in their natural environment, surrounded by other cells. This approach represents a basic concept for development of various lab-on-a-chip technologies and analytical devices which often involve microfluidics.

Widely spread transducer techniques which are extensively used for cell sensing are: surface plasmon resonance (SPR, Hide et al., 2002; Homola, 2008) and resonant waveguide grating (RWG; Fang, 2006; Fang, 2007, 2014; Fang et al., 2006). Both methods detect and analyze changes in the refractive index near the sensor surface which can be assigned to rearrangement of the proteins within cytoskeleton and to other cellular components, a phenomenon commonly known as dynamic mass redistribution (DMR; Yanase et al., 2007; Fang, 2014; Fang et al., 2006; Fang et al., 2009). Furthermore, quartz crystal microbalance (QCM) is a technique sensitive for changes in mass and viscoelacity (Gryte et al., 1993; Marx et al., 2001; Saitakis and Gizeli, 2012) which is mostly applied for studies of cell adhesion and changes in the viscoelastic properties of the cellular cytoskeleton (Heitmann and Wegener, 2007; Wegener et al., 1999a; Wegener et al., 2000b; Redepenning et al., 1993; Michaelis, 2010; Oberleitner, 2016). Moreover, there are field effect transistor sensors (FET; Sakata and Miyahara, 2008; Toshiya and Haruyo, 2011) and cell-based

electrochemical biosensors (Ziegler, 2000; Baumann et al., 1999). Finally, impedance-based sensing (ECIS; Giaever and Keese, 1984; Lo et al., 1995; Wegener et al., 2000a) is extensively applied to run various types of cell-based assays (Lukic and Wegener, 2015). The importance and relevance of cell-based biosensors is mirrored in the continuous development of new technologies and approaches for cell monitoring, such as latest example based on biolayer interferometry (Verzijl et al., 2017).

1.1.1 Biosensors for Cell Morphology

Changes in cell morphology are conventionally followed by microscopy. However, very sophisticated and sensitive technologies have been developed over time for sensing of very small and fast alterations in cell morphology (shape), cell-cell, or cell-substrate contacts. Certainly, one of the widest spread technologies to analyze changes in cell morphology is impedance sensing, which is based on observing the cells as dielectric insulating bodies. Great efforts have been made to develop various solutions for impedance sensing on a single-cell level, mostly using microfluidics and lab-on-a-chip systems (Sun and Morgan, 2010; Chen et al., 2015; Holmes and Morgan, 2010; Lan and Jang, 2011; Wang et al., 2011; Chen et al., 2014; Cho and Thielecke, 2007; Han et al., 2007). However, impedance sensing of cellular monolayer (Wolf et al., 2008) or even three dimensional spheroids (Kloss et al., 2008; Thielecke et al., 2001a, b) gains an equal attention.

Since monitoring of anchorage-dependent cells is relevant for this work, different setups for impedance monitoring of adherent cells will be discussed briefly. Analysis of cells grown on a porous filter membrane which separates two fluid compartments (Gitter et al., 1997; Hein et al., 1992; Wegener et al., 2004) is mostly applied for investigations of how endothelial and epithelial barrier function is being regulated (e.g. brain barrier, colon barrier), but also for drug delivery across the epithelial barrier (Cohen-Kashi Malina et al., 2009; Parmentier et al., 2010; Rehder et al., 2006). Some approaches are based on growing the cells on biocompatible solid substrates (made out of gold, ITO, etc.), which serve at the same time as a growth substrate and signal transducer to convert cellular behavior into electrical impedance signal. Cells can be grown within regular cell culture vessels and various geometric solutions for the layout of working and counter electrodes have been developed and implemented in such wells, for example: coplanar setup (Giaever and Keese, 1984; Wegener et al., 1996; Panke et al., 2011; Rahman et al., 2006; Wolf et al., 2008), and interdigitated electrodes layout with equally large working and counter electrode (Ehret et al., 1997).

Electric cell-substrate impedance sensing (ECIS) is a technology which uses two coplanar

electrodes to monitor behavior of the cells grown on electrodes surface (Giaever and Keese, 1984) and it has been applied as a main analytical tool within this work.

1.1.2 Introduction to Electric Cell-Substrate Impedance Sensing

Electric cell substrate impedance sensing (ECIS) is a versatile label-free analytical technique which allows non-invasive monitoring of adherent cells in a very sensitive and time-resolved manner. This method was born in the early 1980s with first published reports by Ivar Giaever and Charles R. Keese (Giaever and Keese, 1984, 1986) and has been commercialized and further developed within the company Applied BioPhysics Inc. (Troy, New York, USA). Over time, it has become one of the widest spread technologies for (impedimetric) analysis of adherent cells. Detection of changes in cellular morphology and motility is based on the similarity of anchorage-dependent cells with dielectric insulating bodies. Cells are grown on small planar electrodes made out of gold, which allow for non-invasive monitoring of the cells, but can also be used to deliver well-defined invasive electric pulses (Stolwijk et al., 2012). Once cells form a confluent monolayer, current is forced to flow mostly around the cell bodies and between the neighboring cells, which means this method is sensitive to record changes in cellular shape, morphology, or cellular movements (Giaever and Keese, 1991, 1993; Lo et al., 1995; Wegener et al., 2000a).

Measuring the complex impedance provides a wealth of information on the cellular population under study. Over years, the ECIS technique has become a well-established and popular technology which can be found within many laboratories in both the academic and the industrial world. It has been applied as readout in various types of cell-based assays covering different fields of application. To mention a few, ECIS has been applied for monitoring of: attachment and spreading of cells (Wegener et al., 2000a), cytotoxicity effects (Male et al., 2013; Arndt et al., 2004; Xiao et al., 2002; Xiao and Luong, 2003, 2005), cytotoxicity of nanoparticles (Male et al., 2008; Tarantola et al., 2009), cell proliferation (Stolwijk et al., 2012; Szulcek et al., 2014), signal transduction (Reddy et al., 1998; Wegener et al., 1999b; Qiao et al., 2006; Tiruppathi et al., 2000), cell motility - micromotion (Giaever and Keese, 1991; Lo et al., 1993), barrier function (Szulcek et al., 2015; Weidenfeller et al., 2005). Furthermore, the ECIS technique can be combined with the application of long invasive electric pulse(s), inducing irreversible cell damage and cell death (electric wounding) or short invasive pulses causing reversible permeabilization of the cell membrane (*in situ* electroporation). In the first case, automated wound healing and migration assay can be performed (Keese et al., 2004), whereas in the second case cellular behavior upon *in situ* electroporation is being monitored impedimetrically (Ghosh et al., 1993; Stolwijk et al., 2011;

Wegener et al., 2002). In addition, it has been demonstrated recently that the ECIS technique can be combined with other label-free analytical readouts, like SPR, for non-invasive combinatorial analysis of the cells (Michaelis et al., 2013).

1.2 Delivery of Xenomolecules into Cells - Challenges and Limitations

The cell cytoplasm with its inner cellular compartments (organelles) is separated and protected from the extracellular environment by the plasma membrane. As a consequence of this segregation as a natural protection mechanism, passive uptake of some exogenous molecules is rather poor, whereas certain molecules are entirely membrane-impermeable (due to their charge, size, etc.). Molecules which need assistance to cross the plasma membrane and accumulate within the cell cytosol can be various types of xenomolecules such as: nucleic acids, proteins, peptides, enzymes, drugs, etc. Many of those hold great potential as therapeutic agents or diagnostic tool, but the greatest obstacle in their wide application is usually their inability to reach their target or binding site within the cell interior and thus perform their function. The best example comes from DNA and RNA molecules that have a great potential in gene therapy. In therapies based on nucleic acids preferably, “naked” DNA and RNA molecules should be imported rapidly into the cell interior to assure their integrity and functionality, but on their way to the target (which is mostly in cell nucleus; Meister, 2008; Schraivogel and Meister, 2014; Chin et al., 1990; Dean and Gokay, 2005; Vacik et al., 1999) these molecules have to struggle with crossing the plasma membrane, denaturation by nucleases and uptake by acidic organelles (Juliano et al., 2008; Pereyra and Hereñu, 2013). For this reason, various strategies and technologies are being developed for simple, quick and efficient delivery of nucleic acids and other types of xenomolecules into the cell cytosol.

Initial activities to solve the delivery problem were directed towards viral vectors, as they are naturally predetermined for gene transfer, but due to safety reasons (immunogenicity) and their potentially oncogenic activity, efforts on molecule’s delivery are nowadays greatly concentrated on development of non-viral carriers.

Many approaches for delivering molecules are based on endocytosis, i.e. the cell’s natural mechanism for internalization of exogenous molecules. This method starts with binding of the external molecule to the cell membrane, thereafter it is being taken up by the acidic organelles (vesicles, endosomes, lysosomes) where its exposure to low pH values can often lead to degradation. This will prevent the molecule from being finally delivered to the cell cytoplasm. Therefore, efficient delivery of exogeneous molecule aims for what is called

"endosome escape", as well as rapid access to the cell cytosol (Conner and Schmid, 2003; Doherty and McMahon, 2009; Dominska and Dykxhoorn, 2010; Hoekstra et al., 2007). A majority of chemical reagents for cell transfection rely on complex formation with the molecule of interest (e.g. siRNA, DNA), subsequent binding to the cell surface and non-specific receptor-mediated endocytosis. Cationic lipid-based transfection reagents are in fact mostly exploited transfection agents which are being applied for a wide variety of cell types and various molecules (DNA, siRNA, proteins, drugs) (Almofti et al., 2003; Faneca et al., 2013; Wasungu and Hoekstra, 2006; Felgner et al., 1987; Sharma and Sharma, 1997). However, their performance in clinical trials raised issues with potential toxicity and insufficient efficiency for transfection of some cell types. As an alternative, cationic polymers (e.g. polyethylenimine - PEI, polylysine - PLL, polydiethylaminoethyl methacrylate - pDEAEMA) gain increasing attention and are being extensively developed as a tool for delivery (Boussif et al., 1995; Breunig et al., 2008; Breunig et al., 2007). Furthermore, transfection tools can include different kinds of nanoparticles (Elbakry et al., 2009) or cell penetrating peptides (CPPs; Temsamani and Vidal, 2004). In case of all the above mentioned transfection agents, it is still not fully clear if the endocytotic pathway is being completely mitigated and if potential cytotoxic effects can be excluded.

Direct transfer of "naked" (non-modified) molecules into cells has been achieved by various mechanical methods. One of them is microinjection, which can be applied for delivery of various molecules into cells with very high efficiency, but due to its very time- and labor-consuming experimental procedure, microinjection can be applied only for the treatment of a very low number of cells (Graessmann and Graessmann, 1983; Vaughan and Dean, 2006; Gruber et al., 2005). Other physical methods apply different types of stressors to permeabilize cell membrane: short pulses of laser light for optoporation (Kurata et al., 1986), ultrasonic cavitation for sonoporation (Miller et al., 2002), or mechanical deformation to "squeeze" the cells (Sharei et al., 2013).

Finally, electric pulses applied for transient permeabilization of the cells (electroporation) is the farthest developed and widest applied approach to shortly "open" the cell membrane (Neumann et al., 1982; Rols and Teissié, 1992). Although many studies are based on electroporation of suspended cells, electroporation *in situ* and *in vivo* has many advantages, since cells are present in their natural state.

1.3 *In Situ* Electoporation Monitored by Impedance Sensing

Electroporation is a transient reversible permeabilization of the cell membrane, induced by application of external electric field pulses and it is performed to allow diffusion of membrane-

impermeable compounds into the cell cytosol. Under well-defined and optimized conditions, electroporation allows a fast opening and resealing of the cell membrane and this allows exogenous molecules to enter and stay captured within the cell cytosol (schematic illustration given in **Figure 1.1**). More details on the physical background of electroporation are given in the chapter Theoretical Background (subchapter 3.2.2).

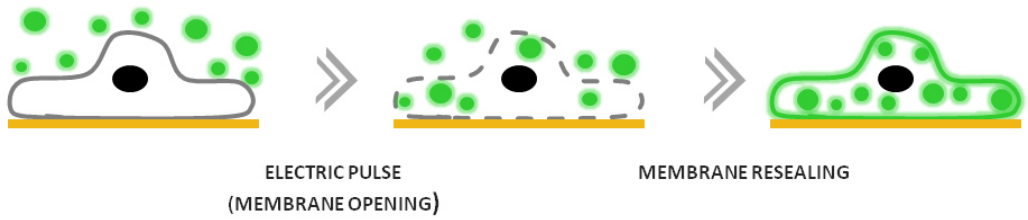

Figure 1.1 Schematic presentation of *in situ* electroporation of cells grown on the surface of thin gold film electrodes. Upon application of an electric pulse, small pores will be formed in the membrane (membrane opening) for a short period of time. Membrane-impermeable molecules surrounding the cells can thus freely diffuse into the cell cytosol, where they will remain entrapped after subsequent membrane resealing.

Electroporation allows for direct transfer of molecules into the cell interior (Golzio et al., 2002; Paganin-Gioanni et al., 2011; Pucihar et al., 2008). This is the greatest benefit of electroporation (and all other physical methods) over the conventional chemical reagents. Once xenomolecules have entered the cell interior, they are directly being located within the cytoplasm and can reach any location inside the cell by diffusion. Applied electric pulses have to be optimized and they need to be well-defined for application on a certain cell line and for the particular application. A well-optimized and adjusted electroporation procedure will provide a high efficiency of the method (by loading a major fraction of the cells under study with a high amount of material) and at the same time, minimize invasiveness of the operation. Namely, an unwanted side effect of electroporation, which may appear if pulse parameters and procedure are not carefully optimized, is cell damage, which may even lead to cell death. Therefore, optimization of electric parameters is essential for every electroporation protocol, regardless of the fact if cells are being treated in suspended, adherent or some other state.

Numerous publications have demonstrated that electroporation is well suited to allow for transfer of various types of xenomolecules into living cells (Rols et al., 2000; Rols, 2006; Rols and Teissié, 1998; Santra et al., 2013), most notably nucleic acids (Chabot et al., 2012; Chabot et al., 2013; Escoffre et al., 2009; Faurie et al., 2005; Rols, 2008). These studies

have shown internalization of DNA and RNA molecules into the cytoplasm and subsequently into the cell nuclei already within the first seconds or minutes after electric pulse application.

As already mentioned above, these fundamental studies have been mostly conducted on cells in suspension, but the great interest in the delivery of xenomolecules, especially for electrotransfer of nucleic acids and drugs (due to their great potential for therapeutic applications), has motivated scientists to investigate delivery of these molecules to the cells also under *in situ* and *in vitro* conditions. Thus, different groups have been working intensively on applying *in situ* electroporation for delivery of nucleic acids (DNA, siRNA) into adherent cells (Jain and Muthuswamy, 2007, Fujimoto et al., 2008, 2009, 2010; Koda et al., 2008; Yamauchi et al., 2004; Garcia-Sanchez and Marques-Garcia, 2016). In addition, the Raptis group has intensively worked on electrotransfer of peptides (Raptis et al., 1995a; Raptis et al., 1995b).

In situ electroporation combined with impedance sensing, allows for delivery of exogenous material into living cells and monitoring of the cell behavior in real time. This means that cellular behavior can be directly observed and compared before and after the electric manipulation, which is most interesting when particular (biologically active) compounds are transferred into the cell. Namely, cells are allowed to grow over small gold film electrodes, which serve for both, delivering of invasive electric pulses and for non-invasive monitoring of the cellular behavior. Online monitoring is sometimes crucial during the evaluation of electroporation experiment, since time point of cellular response to internalized xenomolecules may variate, be delayed or cannot be predicted at all.

In this work, *in situ* electroporation and concomitant impedance monitoring were performed (in most cases) using the ECIS instrumentation. A typical time course of *in situ* electroporation of a confluent cell layer that is monitored by the ECIS technology is given in **Figure 1.2**. Impedance-based monitoring of the cells using ECIS allows not only for an evaluation of cell type-specific cellular responses to electoporation and invasiveness of the pulse, but also reveals any potential effect of biologically active xenomolecules introduced into the cells by electric pulse application. This unique benefit of the combined ECIS-ISE technique was used in this thesis to study at the same time the electroporation-mediated transfer of bioactive molecules, like second messengers and nucleic acids, into the cells and to monitor the impact of these compounds on treated cells. In addition, impedance monitoring has been used to monitor cells during treatment using conventional chemical transfection methods in order to analyze and compare this approach with other means of cytoplasmic delivery.

Previously conducted studies of *in situ* electroporation combined with impedance sensing

using the ECIS technique (Ghosh et al., 1993; Ghosh et al., 1994; Wegener et al., 2002; Stolwijk et al., 2011) have provided an excellent basis to build on a further understanding of events and mechanisms associated with *in situ* electroporation and to demonstrate the versatility and applicability of this method even for very demanding applications.

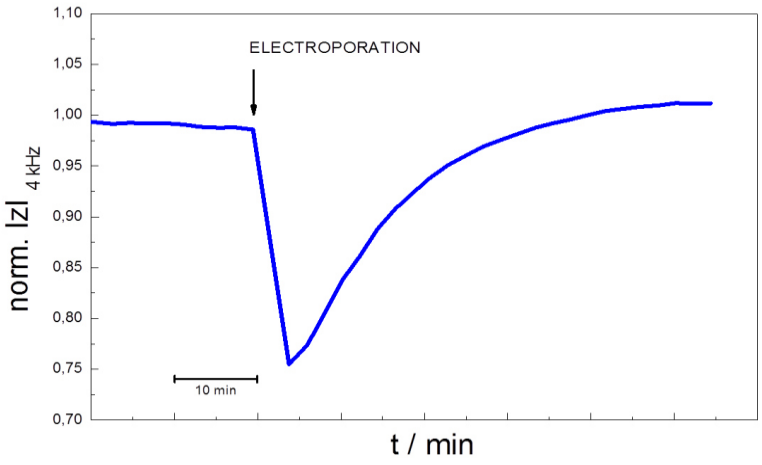

Figure 1.2 Typical time course of the normalized impedance magnitude measured before, during and after application of a short electroporating pulse (with pulse parameters: 40 kHz, 4 V, 200 ms) to the monolayer of NRK cells. The immediate decrease in impedance after application of the electric pulse (marked with an arrow) indicates morphological response of the cells to the transient disruption of the cell membrane (permeabilization) as *in situ* electroporation of the cells occurs. Impedance monitoring reveals a cell type-specific response of the cells to applied electric pulses and the progress of cell recovery in real time. Confluent monolayer of NRK cells was probed at 37 °C.

1.4 References

Arndt, S., Seebach, J., Psathaki, K., Galla, H.-J., and Wegener, J. (2004) Bioelectrical impedance assay to monitor changes in cell shape during apoptosis. *Biosensors and Bioelectronics* 19, 583–594.

Baumann, W.H., Lehmann, M., Schwinde, A., Ehret, R., Brischwein, M., and Wolf, B. (1999) Microelectronic sensor system for microphysiological application on living cells. *Sensors and Actuators B: Chemical* 55, 77-89.

Bousse, L. (1996) Whole cell biosensors. *Sensors and Actuators B: Chemical* 34, 270-275.

Boussif, O., Lezoualc'h, F., Zanta, M.A., Mergny, M.D., Scherman, D., Demeneix, B., and Behr, J.P. (1995) A versatile vector for gene and oligonucleotide transfer into cells in culture and in vivo: polyethylenimine. *Proceedings of the National Academy of Sciences of the United States of America* 92, 7297–7301.

Breunig, M., Hozsa, C., Lungwitz, U., Watanabe, K., Umeda, I., Kato, H., and Goepferich, A. (2008) Mechanistic investigation of poly(ethylene imine)-based siRNA delivery: Disulfide bonds boost intracellular release of the cargo. *Journal of Controlled Release* 130, 57–63.

Breunig, M., Lungwitz, U., Liebl, R., Klar, J., Obermayer, B., Blunk, T., and Goepferich, A. (2007) Mechanistic insights into linear polyethylenimine-mediated gene transfer. *Biochimica et Biophysica Acta* 1770, 196–205.

Chabot, S., Orio, J., Castanier, R., Bellard, E., Nielsen, S.J., Golzio, M., and Teissie, J. (2012) LNA-based oligonucleotide electrotransfer for miRNA inhibition. *Molecular Therapy* 20, 1590-1598.

Chabot, S., Pelofy, S., Teissie, J., and Golzio, M. (2013) Delivery of RNAi-based oligonucleotides by electropermeabilization. *Pharmaceuticals* 6, 510-521.

Chen, J., Xue, C., Zhao, Y., Chen, D., Wu, M.-H., and Wang, J. (2015) Microfluidic impedance flow cytometry enabling high-throughput single-cell electrical property characterization. *International Journal of Molecular Sciences* 16, 9804-9830.

Chen, N.-C., Chen, C.-H., Chen, M.-K., Jang, L.-S., and Wang, M.-H. (2014) Single-cell trapping and impedance measurement utilizing dielectrophoresis in a parallel-plate microfluidic device. *Sensors and Actuators B: Chemical* 190, 570-577.

Chin, D.J., Green, G.A., Zon, G., Szoka, F.C., Jr., and Straubinger, R.M. (1990) Rapid nuclear accumulation of injected oligodeoxyribonucleotides. *Nature: New Biology* 2, 1091-1100.

Cho, S., and Thielecke, H. (2007) Micro hole-based cell chip with impedance spectroscopy. *Biosensors and Bioelectronics* 22, 1764-1768.

Cohen-Kashi Malina, K., Cooper, I., and Teichberg, V.I. (2009) Closing the gap between the in-vivo and in-vitro blood-brain barrier tightness. *Brain Research* 11, 12-21.

Conner, S.D., and Schmid, S.L. (2003) Regulated portals of entry into the cell. *Nature* 422, 37-44.

Dean, D.A., and Gokay, K.E. (2005) Nuclear Import and Export in Plants and Animals. In Nuclear Import of DNA (Plenum Publishers, Springer US), pp. 187-205.

Doherty, G.J., and McMahon, H.T. (2009) Mechanisms of endocytosis. *Annual Review of Biochemistry* 78, 857-902.

Dominska, M., and Dykxhoorn, D.M. (2010) Breaking down the barriers: siRNA delivery and endosome escape. *Journal of Cell Science* 123, 1183-1189.

Ehret, R., Baumann, W., Brischwein, M., Schwinde, A., Stegbauer, K., and Wolf, B. (1997) Monitoring of cellular behaviour by impedance measurements on interdigitated electrode structures. *Biosensors and Bioelectronics* 12, 29-41.

Elbakry, A., Zaky, A., Liebl, R., Rachel, R., Goepferich, A., and Breunig, M. (2009) Layer-by-layer assembled gold nanoparticles for siRNA delivery. *Nano Letters* 9, 2059-2064.

Escoffre, J.-M., Portet, T., Wasungu, L., Teissie, J., Dean, D., and Rols, M.-P. (2009) What is (still not) known of the mechanism by which electroporation mediates gene transfer and expression in cells and tissues. *Molecular Biotechnology* 41, 286–295.

Fang, Y. (2006) Label-free cell-based assays with optical biosensors in drug discovery. *Assay and Drug Development Technologies* 4, 583-595.

Fang, Y. (2007) Non-invasive optical biosensor for probing cell signaling. *Sensors* 7, 2316–2329.

Fang, Y. (2014) Label-free drug discovery. *Frontiers in Pharmacology* 5, 52.

Fang, Y., Ferrie, A.M., Fontaine, N.H., Mauro, J., and Balakrishnan, J. (2006) Resonant waveguide grating biosensor for living cell sensing. *Biophysical Journal* 91, 1925-1940.

Fang, Y., Ferrie, A.M., and Tran, E. (2009) Resonant waveguide grating biosensor for whole-cell GPCR assays. *Methods in Molecular Biology* 552, 239-252.

Faurie, C., Golzio, M., Phez, E., Teissié, J., and Rols, M.P. (2005) Electric field-induced cell membrane permeabilization and gene transfer: theory and experiments. *Engineering in Life Sciences* 5, 179-186.

Felgner, P., Gadek, T., Holm, M., Roman, R., Chan, H., Wenz, M., Northrop, J., Ringold, G., and Danielsen, M. (1987) Lipofection: a highly efficient, lipid-mediated DNA transfection procedure. *Proceedings of the National Academy of Sciences of the United States of America* 84, 7413–7417.

Fujimoto, H., Kato, K., and Iwata, H. (2008) Electroporation microarray for parallel transfer of small interfering RNA into mammalian cells. *Analytical and Bioanalytical Chemistry* 392, 1309-1316.

Fujimoto, H., Kato, K., and Iwata, H. (2009) Prolonged durability of electroporation microarrays as a result of addition of saccharides to nucleic acids. *Analytical and Bioanalytical Chemistry* 393, 607-614.

Fujimoto, H., Kato, K., and Iwata, H. (2010) Layer-by-layer assembly of small interfering RNA and poly(ethyleneimine) for substrate-mediated electroporation with high efficiency. *Analytical and Bioanalytical Chemistry* 397, 571-578.

Garcia-Sanchez, A., and Marques-Garcia, F. (2016) Gene silencing delivery methods: lipid-mediated and electroporation transfection protocols. *Methods in Molecular Biology* 1434, 139-151.

Ghosh, P.M., Keese, C.R., and Giaever, I. (1993) Monitoring electropermeabilization in the plasma membrane of adherent mammalian cells. *Biophysical Journal* 64, 1602-1609.

Ghosh, P.M., Keese, C.R., and Giaever, I. (1994) Morphological response of mammalian cells to pulsed ac fields. *Bioelectrochemistry and Bioenergetics* 33, 121-133.

Giaever, I., and Keese, C.R. (1984) Monitoring fibroblast behavior in tissue culture with an applied electric field. *Proceedings of the National Academy of Sciences of the United States of America* 81, 3761-3764.

Giaever, I., and Keese, C.R. (1986) Use of electric fields to monitor the dynamical aspect of cell behavior in tissue culture. *IEEE Transactions on Biomedical Engineering* 33, 242-247.

Giaever, I., and Keese, C.R. (1991) Micromotion of mammalian cells measured electrically. *Proceedings of the National Academy of Sciences of the United States of America* 88, 7896-7900.

Giaever, I., and Keese, C.R. (1993) A morphological biosensor for mammalian cells. *Nature* 366, 591-592.

Gitter, A.H., Schulzke, J.D., Sorgenfrei, D., and Fromm, M. (1997) Ussing chamber for high-frequency transmural impedance analysis of epithelial tissues. *Journal of biochemical and biophysical methods* 35, 81-88.

Golzio, M., Teissie, J., and Rols, M.P. (2002) Direct visualization at the single-cell level of electrically mediated gene delivery. *Proceedings of the National Academy of Sciences of the United States of America* 99, 1292-1297.

Graessmann, M., and Graessmann, A. (1983) Microinjection of tissue culture cells. *Methods in Enzymology* 101, 482-492.

Gronow, M. (1984) Biosensors. *Trends in Biochemical Sciences* 9, 336-340.

Gruber, J., Manninga, H., Tuschl, T., Osborn, M., and Weber, K. (2005) Specific RNAi mediated gene knockdown in zebrafish cell lines. *RNA Biology* 2, 101-105.

Gryte, D.M., Ward, M.D., and Hu, W.S. (1993) Real-time measurement of anchorage-dependent cell adhesion using a quartz crystal microbalance. *Biotechnology Progress* 9, 105-108.

Han, A., Yang, L., and Frazier, A.B. (2007) Quantification of the heterogeneity in breast cancer cell lines using whole-cell impedance spectroscopy. *Clinical Cancer Research* 13, 139-143.

Hein, M., Madefessel, C., Haag, B., Teichmann, K., Post, A., and Galla, H.J. (1992) Implications of a non-lamellar lipid phase for the tight junction stability. Part II: Reversible modulation of transepithelial resistance in high and low resistance MDCK-cells by basic amino acids, Ca2+, protamine and protons. *Chemistry and Physics of Lipids* 63, 223-233.

Heitmann, V., and Wegener, J. (2007) Monitoring cell adhesion by piezoresonators: impact of increasing oscillation amplitudes. *Analytical Chemistry* 79, 3392-3400.

Hide, M., Tsutsui, T., Sato, H., Nishimura, T., Morimoto, K., Yamamoto, S., and Yoshizato, K. (2002) Real-time analysis of ligand-induced cell surface and intracellular reactions of living mast cells using a surface plasmon resonance-based biosensor. *Analytical Biochemistry* 302, 28-37.

Hoekstra, D., Rejman, J., Wasungu, L., Shi, F., and Zuhorn, I. (2007) Gene delivery by cationic lipids: in and out of an endosome. *Biochemical Society Transactions* 35, 68-71.

Holmes, D., and Morgan, H. (2010) Single cell impedance cytometry for identification and counting of CD4 T-cells in human blood using impedance labels. *Analytical Chemistry* 82, 1455-1461.

Homola, J. (2008) Surface plasmon resonance sensors for detection of chemical and biological species. *Chemical Reviews* 108, 462-493.

Jain, T., and Muthuswamy, J. (2007) Microsystem for transfection of exogenous molecules with spatio-temporal control into adherent cells. *Biosensors and Bioelectronics* 22, 863–870.

Juliano, R., Alam, M.R., Dixit, V., and Kang, H. (2008) Mechanisms and strategies for effective delivery of antisense and siRNA oligonucleotides. *Nucleic Acids Research* 36, 4158-4171.

Keese, C.R., Wegener, J., Walker, S.R., and Giaever, I. (2004) Electrical wound-healing assay for cells in vitro. *Proceedings of the National Academy of Sciences of the United States of America* 101, 1554-1559.

Keusgen, M. (2002) Biosensors: new approaches in drug discovery. *Naturwissenschaften* 89, 433-444.

Kloss, D., Fischer, M., Rothermel, A., Simon, J.C., and Robitzki, A.A. (2008) Drug testing on 3D in vitro tissues trapped on a microcavity chip. *Lab Chip* 8, 879-884.

Koda, S., Inoue, Y., and Iwata, H. (2008) Gene transfection into adherent cells using electroporation on a dendrimer-modified gold electrode. *Langmuir* 24, 13525-13531.

Kurata, S., Tsukakoshi, M., Kasuya, T., and Ikawa, Y. (1986) The laser method for efficient introduction of foreign DNA into cultured cells. *Experimental Cell Research* 162, 372-378.

Lan, K.C., and Jang, L.S. (2011) Integration of single-cell trapping and impedance measurement utilizing microwell electrodes. *Biosensors and Bioelectronics* 26, 2025-2031.

Lo, C.-M., Keese, C.R., and Giaever, I. (1995) Impedance analysis of MDCK cells measured by electric cell-substrate impedance sensing. *Biophysical Journal* 69, 2800-2807.

Lo, C.M., Keese, C.R., and Giaever, I. (1993) Monitoring motion of confluent cells in tissue culture. *Experimental Cell Research* 204, 102-109.

Lukic, S., and Wegener, J. (2015) Impedimetric monitoring of cell-based assays. In Encyclopedia of Life Sciences (John Wiley & Sons, Ltd.), pp. 1–8.

Luong, J.H.T., Mulchandani, A., and Guilbault, G.G. (1988) Developments and applications of biosensors. *Trends in Biotechnology* 6, 310-316.

Male, K.B., Hamzeh, M., Montes, J., Leung, A.C.W., and Luong, J.H.T. (2013) Monitoring of potential cytotoxic and inhibitory effects of titanium dioxide using on-line and non-invasive cell-based impedance spectroscopy. *Analytica Chimica Acta* 777, 78– 85.

Male, K.B., Lachance, B., Hrapovic, S., Sunahara, G., and Luong, J.H. (2008) Assessment of cytotoxicity of quantum dots and gold nanoparticles using cell-based impedance spectroscopy. *Analytical Chemistry* 80, 5487-5493.

Marx, K.A., Zhou, T., Montrone, A., Schulze, H., and Braunhut, S.J. (2001) A quartz crystal microbalance cell biosensor: detection of microtubule alterations in living cells at nM nocodazole concentrations. *Biosensors and Bioelectronics* 16, 773-782.

Meister, G. (2008) Molecular biology. RNA interference in the nucleus. *Science* 321, 496-497.

Michaelis, S. (2010) Non-invasive biosensors to characterize the cell-material interface. PhD thesis,Westfälische Wilhelms-Universität, Münster.

Michaelis, S., Wegener, J., and Robelek, R. (2013) Label-free monitoring of cell-based assays: Combining impedance analysis with SPR for multiparametric cell profiling. *Biosensors and Bioelectronics* 49, 63-70.

Miller, D.L., Pislaru, S.V., and Greenleaf, J.E. (2002) Sonoporation: mechanical DNA delivery by ultrasonic cavitation. *Somatic Cell and Molecular Genetics* 27, 115-134.

Neumann, E., Schaefer-Ridder, M., Wang, Y., and Hofschneider, P.H. (1982) Gene transfer into mouse lyoma cells by electroporation in high electric fields. *The EMBO Journal* 1, 841-845.

Oberleitner, M. (2016) Label-free and multi-parametric monitoring of cell-based assays with substrate-embedded sensors. PhD thesis, Universität Regensburg.

Paganin-Gioanni, A., Bellard, E., Escoffre, J.M., Rols, M.P., Teissié, J., and Golzio, M. (2011) Direct visualization at the single-cell level of siRNA electrotransfer into cancer cells. *Proceedings of the National Academy of Sciences of the United States of America* 108, 10443–10447.

Panke, O., Weigel, W., Schmidt, S., Steude, A., and Robitzki, A.A. (2011) A cell-based impedance assay for monitoring transient receptor potential (TRP) ion channel activity. *Biosensors and Bioelectronics* 26, 2376-2382.

Parmentier, J., Hartmann, F.J., and Fricker, G. (2010) In vitro evaluation of liposomes containing bio-enhancers for the oral delivery of macromolecules. *European Journal of Pharmaceutics and Biopharmaceutics* 76, 394-403.

Pereyra, A., and Hereñu, C. (2013) Gene delivery systems. In Current Issues in Molecular Virology - Viral Genetics and Biotechnological Applications, P.V. Romanowski, ed. (InTech)

Powner, E.T., and Yalcinkaya, F. (1997) Intelligent biosensors. *Sensor Review* 17, 107-116.

Pucihar, G., Kotnik, T., Miklavcic, D., and Teissie, J. (2008) Kinetics of transmembrane transport of small molecules into electropermeabilized cells. *Biophysical Journal* 95, 2837–2848.

Qiao, J., Huang, F., Naikawadi, R.P., Kim, K.S., Said, T., and Lum, H. (2006) Lysophosphatidylcholine impairs endothelial barrier function through the G protein-coupled

receptor GPR4. *American Journal of Physiology: Lung Cellular and Molecular Physiology* 291, 91-101.

Rahman, A.R.A., Lo, C.-M., and Bhansali, S. (2006) A micro-electrode array biosensor for impedance spectroscopy of human umbilical vein endothelial cells. *Sensors and Actuators B: Chemical* 118, 115-120.

Raptis, L.H., Firth, K.L., Brownell, H.L., Todd, A., Simon, W.C., Bennett, B.M., MacKenzie, L.W., and Zannis-Hadjopoulos, M. (1995a) Electroporation of adherent cells in situ for the introduction of nonpermeant molecules. *Methods in Molecular Biology* 48, 93-113.

Raptis, L.H., Liu, S.K., Firth, K.L., Stiles, C.D., and Alberta, J.A. (1995b) Electroporation of peptides into adherent cells in situ. *Biotechniques* 18, 104-114.

Reddy, L., Wang, H.-S., Keese, C.R., Giaever, I., and Smith, T.J. (1998) Assessment of rapid morphological changes associated with elevated cAMP levels in human orbital fibroblasts. *Experimental Cell Research* 245, 360–367.

Redepenning, J., Schlesinger, T.K., Mechalke, E.J., Puleo, D.A., and Bizios, R. (1993) Osteoblast attachment monitored with a quartz crystal microbalance. *Analytical Chemistry* 65, 3378-3381.

Rehder, D., Iden, S., Nasdala, I., Wegener, J., Brickwedde, M.K., Vestweber, D., and Ebnet, K. (2006) Junctional adhesion molecule-a participates in the formation of apico-basal polarity through different domains. *Experimental Cell Research* 312, 3389-3403.

Rols, M.P. (2006) Electropermeabilization, a physical method for the delivery of therapeutic molecules into cells. *Biochimica et Biophysica Acta* 1758, 423–428.

Rols, M.P. (2008) Mechanism by which electroporation mediates DNA migration and entry into cells and targeted tissues. *Methods in Molecular Biology* 423, 19-33.

Rols, M.P., Golzio, M., Delteil, C., and Teissié, J. (2000) In vitro delivery of drugs and other molecules to cells. *Methods in Molecular Medicine* 37, 83-97.

Rols, M.P., and Teissié, J. (1992) Experimental evidence for the involvement of the cytoskeleton in mammalian cell electropermeabilization. *Biochimica et Biophysica Acta* 19, 45-50.

Rols, M.P., and Teissié, J. (1998) Electropermeabilization of mammalian cells to macromolecules: control by pulse duration. *Biophysical Journal* 75, 1415-1423.

Saitakis, M., and Gizeli, E. (2012) Acoustic sensors as a biophysical tool for probing cell attachment and cell/surface interactions. *Cellular and Molecular Life Sciences* 69, 357-371.

Sakata, T., and Miyahara, Y. (2008) Noninvasive monitoring of transporter-substrate interaction at cell membrane. *Analytical Chemistry* 80, 1493-1496.

Santra, T.S., Wang, P.-C., and Tseng, F.G. (2013) Electroporation based drug delivery and its applications. In Advances in micro/nano electromechanical systems and fabrication technologies (InTech)

Schraivogel, D., and Meister, G. (2014) Import routes and nuclear functions of Argonaute and other small RNA-silencing proteins. *Trends in Biochemical Sciences* 39, 420-431.

Sharei, A., Zoldan, J., Adamo, A., Sim, W.Y., Cho, N., Jackson, E., Mao, S., Schneider, S., Han, M.J., Lytton-Jean, A., et al. (2013) A vector-free microfluidic platform for intracellular delivery. *Proceedings of the National Academy of Sciences of the United States of America* 110, 2082-2087.

Sharma, A., and Sharma, U.S. (1997) Liposomes in drug delivery: Progress and limitations. *International Journal of Pharmaceutics* 154, 123-140.

Stolwijk, J.A., Hartmann, C., Balani, P., Albermann, S., Keese, C.R., Giaever, I., and Wegener, J. (2011) Impedance analysis of adherent cells after in situ electroporation: Non-invasive monitoring during intracellular manipulations. *Biosensors and Bioelectronics* 26, 4720–4727.

Stolwijk, J.A., Michaelis, S., and Wegener, J. (2012) Cell growth and cell death studied by electric cell-substrate impedance sensing. In Electric cell-substrate impedance sensing and cancer metastasis, W.G. Jiang, ed. (Dordrecht: Springer Netherlands), pp. 85-117.

Sun, T., and Morgan, H. (2010) Single-cell microfluidic impedance cytometry: a review. *Microfluidics and Nanofluidics* 8, 423-443.

Szulcek, R., Bogaard, H.J., and van Nieuw Amerongen, G.P. (2014) Electric cell-substrate impedance sensing for the quantification of endothelial proliferation, barrier function, and motility. *Journal of Visualized Experiments:JoVE* 28, 51300.

Szulcek, R., van Bezu, J., Boonstra, J., van Loon, J.J., and van Nieuw Amerongen, G.P. (2015) Transient intervals of hyper-gravity enhance endothelial barrier integrity: Impact of mechanical and gravitational forces measured electrically. *PLoS One* 10

Tarantola, M., Schneider, D., Sunnick, E., Adam, H., Pierrat, S., Rosman, C., Breus, V., Sonnichsen, C., Basche, T., Wegener, J., et al. (2009) Cytotoxicity of metal and semiconductor nanoparticles indicated by cellular micromotility. *ACS Nano* 3, 213-222.

Temsamani, J., and Vidal, P. (2004) The use of cell-penetrating peptides for drug delivery. *Drug Discovery Today* 9, 1012-1019.

Thielecke, H., Mack, A., and Robitzki, A. (2001a) Biohybrid microarrays--impedimetric biosensors with 3D in vitro tissues for toxicological and biomedical screening. *Fresenius Journal of Analytical Chemistry* 369, 23-29.

Thielecke, H., Mack, A., and Robitzki, A. (2001b) A multicellular spheroid-based sensor for anti-cancer therapeutics. *Biosensors and Bioelectronics* 16, 261-269.

Tiruppathi, C., Yan, W., Sandoval, R., Naqvi, T., Pronin, A.N., Benovic, J.L., and Malik, A.B. (2000) G protein-coupled receptor kinase-5 regulates thrombin-activated signaling in endothelial cells. *Proceedings of the National Academy of Sciences of the United States of America* 97, 7440-7445.

Toshiya, S., and Haruyo, S. (2011) Continuous monitoring of electrical activity of pancreatic β-cells using semiconductor-based biosensing devices. *Japanese Journal of Applied Physics* 50

Turner, A.P.F. (1987) Biosensors: Fundamentals and applications, Vol 1 (Oxford University Press).

Turner, A.P.F. (2000) Biosensors-sense and sensitivity. *Science* 290, 1315-1317.

Vacik, J., Dean, B.S., Zimmer, W.E., and Dean, D.A. (1999) Cell-specific nuclear import of plasmid DNA. *Gene Therapy* 6, 1006-1014.

Vaughan, E.E., and Dean, D.A. (2006) Intracellular trafficking of plasmids during transfection is mediated by microtubules. *Molecular Therapy* 13, 422-428.

Verzijl, D., Riedl, T., Parren, P.W.H.I., and Gerritsen, A.F. (2017) A novel label-free cell-based assay technology using biolayer interferometry. *Biosensors and Bioelectronics* 87, 388-395.

Wang, P., Xu, G., Qin, L., Xu, Y., Li, Y., and Li, R. (2005) Cell-based biosensors and its application in biomedicine. *Sensors and Actuators B: Chemical* 108, 576-584.

Wang, W., Foley, K., Shan, X., Wang, S., Eaton, S., Nagaraj, V.J., Wiktor, P., Patel, U., and Tao, N. (2011) Single cells and intracellular processes studied by a plasmonic-based electrochemical impedance microscopy. *Nature Chemistry* 3, 249-255.

Wegener, J., Abrams, D., Willenbrink, W., Galla, H.J., and Janshoff, A. (2004) Automated multi-well device to measure transepithelial electrical resistances under physiological conditions. *Biotechniques* 37, 592-594.

Wegener, J., Janshoff, A., and Galla, H.J. (1999a) Cell adhesion monitoring using a quartz crystal microbalance: comparative analysis of different mammalian cell lines. *European Biophysics Journal* 28, 26-37.

Wegener, J., Keese, C.R., and Giaever, I. (2000a) Electric cell-substrate impedance sensing (ECIS) as a noninvasive means to monitor the kinetics of cell spreading to artificial surfaces. *Experimental Cell Research* 259, 158-166.

Wegener, J., Keese, C.R., and Giaever, I. (2002) Recovery of adherent cells after in situ electroporation monitored electrically. *Biotechniques* 33, 348 - 352.

Wegener, J., Seebach, J., Janshoff, A., and Galla, H.J. (2000b) Analysis of the composite response of shear wave resonators to the attachment of mammalian cells. *Biophysical Journal* 78, 2821-2833.

Wegener, J., Sieber, M., and Galla, H.-J. (1996) Impedance analysis of epithelial and endothelial cell monolayers cultured on gold surfaces. *Journal of biochemical and biophysical methods* 32, 151-170.

Wegener, J., Zink, S., Rosen, P., and Galla, H. (1999b) Use of electrochemical impedance measurements to monitor beta-adrenergic stimulation of bovine aortic endothelial cells. *Pflügers Archiv – European Journal of Physiology* 437, 925-934.

Weidenfeller, C., Schrot, S., Zozulya, A., and Galla, H.J. (2005) Murine brain capillary endothelial cells exhibit improved barrier properties under the influence of hydrocortisone. *Brain Research* 16, 1-2.

Wolf, P., Rothermel, A., Beck-Sickinger, A.G., and Robitzki, A.A. (2008) Microelectrode chip based real time monitoring of vital MCF-7 mamma carcinoma cells by impedance spectroscopy. *Biosensors and Bioelectronics* 24, 253-259.

Xiao, C., Lachance, B., Sunahara, G., and Luong, J.H.T. (2002) Assessment of cytotoxicity using electric cell-substrate impedance sensing: concentration and time response function approach. *Analytical Chemistry* 74, 5748-5753.

Xiao, C., and Luong, J.H. (2003) On-line monitoring of cell growth and cytotoxicity using electric cell-substrate impedance sensing (ECIS). *Biotechnology Progress* 19, 1000-1005.

Xiao, C., and Luong, J.H. (2005) Assessment of cytotoxicity by emerging impedance spectroscopy. *Toxicology and Applied Pharmacology* 206, 102-112.

Yamauchi, F., Kato, K., and Iwata, H. (2004) Spatially and temporally controlled gene transfer by electroporation into adherent cells on plasmid DNA-loaded electrodes. *Nucleic Acids Research* 32, e187.

Yanase, Y., Suzuki, H., Tsutsui, T., Hiragun, T., Kameyoshi, Y., and Hide, M. (2007) The SPR signal in living cells reflects changes other than the area of adhesion and the formation of cell constructions. *Biosensors and Bioelectronics* 22, 1081-1086.

Ziegler, C. (2000) Cell-based biosensors. *Fresenius' Journal of Analytical Chemistry* 366, 552-559.

2 Objectives

In situ electroporation (ISE) in combination with impedance analysis of the cells on the electrode surface has proven to be an efficient technique for the delivery of extracellular material across the cell membrane, while the cellular response is monitored in a time-resolved manner (Wegener et al., 2002; Stolwijk et al., 2011). A monolayer of cells grown on the small gold film electrodes is reversibly (or irreversibly) permeabilized and at the same time monitored noninvasively using impedance-based technology called electric cell-substrate impedance sensing (ECIS).

This work aimed to establish proof-of-principle assays implementing ISE for successful electropermeabilization of various cell lines in presence of different bioactive molecules. Not only that ISE can be applied for delivery of various xenobiotics into the cell cytoplasm, but one of the goals was also to demonstrate the release of intracellular material during the electroporation pulse. It was important to demonstrate that the ECIS technology in combination with *in situ* electroporation (ISE) can provide a wealth of information on the cellular population under study and as an analytical technique holds a great potential to be expanded to new emerging fields of application.

The overall objectives of this thesis were to:

1. Closer examine the impedance signal profiles after applying electric pulses in order to provide better and deeper understanding of events taking place during (electro)permeabilization of the cellular membrane. For these studies it was essential to acquire data points rapidly and therefore, a special experimental setup allowing for high time resolution impedance measurements was applied (Ghosh et al., 1993; Stolwijk et al., 2011).

2. Investigate and establish proof-of-principle assays for the release of intracellular material from adherent cells by applying ISE. Knowing that extracellular material can freely diffuse into the cellular interior upon application of electric pulses, it has been hypothesized (based also on some recent literature reports) that ISE is a bidirectional process and as such can be successfully applied for intracellular material release as well. Feasibility of release studies was (mostly) evaluated using confocal fluorescence microscopy.

3. Investigate if ISE can be applied for the delivery of second messengers into the cell cytosol, while monitoring cell signal transduction impedimetrically by the ECIS technology. This project was based on previous well-established studies on cell signal transduction by using impedance monitoring (often by ECIS technology; Wegener et al., 1996; Wegener et

al., 1999).

4. Investigate applicability of ISE for the delivery of (synthetic) nucleic acids into the cell cytosol. Aptamers and siRNA were taken as model compounds to establish proof-of-principle assays. It was a challenging goal to verify if it is possible to follow impedimetrically the cellular response to the cytoplasmic delivery of aptamers and siRNA, compounds delivered into the cells not only by ISE, but also by conventional chemical transfection methods (lipid-based delivery). Efficiency and effects of various transfection methods on the confluent cellular population were evaluated by non-invasive impedance measurements and by microscopy, where possible.

2.1. References

Ghosh, P.M., Keese, C.R., and Giaever, I. (1993) Monitoring electropermeabilization in the plasma membrane of adherent mammalian cells. *Biophysical Journal* 64, 1602-1609.

Stolwijk, J.A., Hartmann, C., Balani, P., Albermann, S., Keese, C.R., Giaever, I., and Wegener, J. (2011) Impedance analysis of adherent cells after in situ electroporation: Non-invasive monitoring during intracellular manipulations. *Biosensors and Bioelectronics* 26, 4720–4727.

Wegener, J., Keese, C.R., and Giaever, I. (2002) Recovery of adherent cells after in situ electroporation monitored electrically. *Biotechniques* 33, 348 - 352.

Wegener, J., Sieber, M., and Galla, H.-J. (1996) Impedance analysis of epithelial and endothelial cell monolayers cultured on gold surfaces. *Journal of biochemical and biophysical methods* 32, 151-170.

Wegener, J., Zink, S., Rosen, P., and Galla, H. (1999) Use of electrochemical impedance measurements to monitor beta-adrenergic stimulation of bovine aortic endothelial cells. *Pflügers Archiv – European Journal of Physiology* 437, 925-934.

3 Theoretical Background

3.1 Impedance Spectroscopy of Adherent Cells

Electrochemical impedance spectroscopy (EIS) or simply impedance spectroscopy (IS) is a widely applied characterization method for analysis of dielectric and conducting properties of different materials and interfacial layers in a variety of electrochemistry fields. (Ende and Mangold, 1993; Lisdat and Schafer, 2008; Wegener, 2010). This method is based on measuring complex impedance magnitude (*Z*), when the system under study is being excited by a low amplitude alternating current (AC) or voltage at different frequencies (Wegener, 2010). By recording changes in complex impedance over a certain range of frequencies, the impedance spectrum can be obtained. In fact, two modes of impedance measurements can be distinguished: (i) sequential data acquisition at pre-defined individual frequencies (continuous wave) and (ii) data acquisition for multiple frequencies at the same time, when the system is exposed to several superimposed sinusoidal waves in parallel.

Due to the small amplitudes of sinusoidal current or voltage applied for excitation of the system under study, impedance spectroscopy allows for non-invasive analysis, which makes impedance measurements especially convenient for time-resolved monitoring of living cells, tissues and some other biological systems.

Electrochemical impedance (*Z*) is a measure of resistance of the system under study exposed to alternating current flow. Ohm's Law describes impedance *Z* as a ratio between applied sinusoidal voltage *U(t)* and its resulting steady-state current *I(t)*:

$$Z = \frac{U(t)}{I(t)} \tag{3.1}$$

Taking into account the angular frequency $\omega=2\pi f$ with frequency *f* expressed in Hertz (Hz) and the fact that a phase shift φ between voltage *U(t)* and current *I(t)* might occur, U_0 and I_0 have to be introduced, representing amplitudes of voltage and current, respectively. Besides, to express the electrochemical impedance as a complex quantity, complex notation $i = \sqrt{-1}$ is necessary.

$$Z = \frac{Uo}{Io} exp(i \cdot \varphi) = |Z| exp\,(i \cdot \varphi) \tag{3.2}$$

Complex impedance is described by: the magnitude $|Z|$ (ratio of the amplitudes U_0 and I_0) and the phase angle φ between voltage and current (Wegener, 2010). The complex

impedance values can be illustrated in a diagram presented in a **Figure 3.1**. Complex impedance is represented by a vector in a complex plane and its length corresponds to the impedance magnitude |*Z*|. The angle *φ* corresponds to the phase shift.

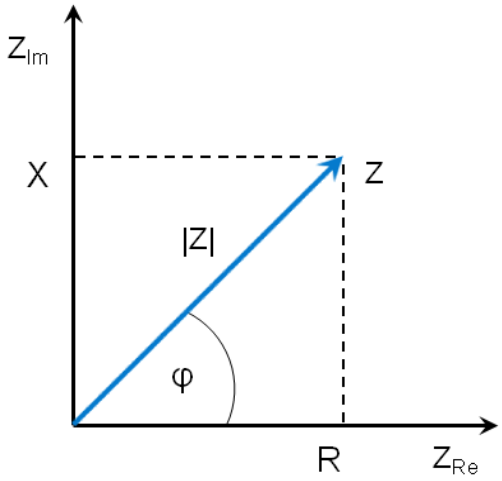

Figure 3.1 Complex impedance *Z* can be presented as a vector within the x-y plane with real (Re) and imaginary (Im) axis. The length of the vector *Z* corresponds to the impedance magnitude |*Z*|, whereas angle φ corresponds to the phase shift between voltage and current. Complex impedance *Z* can also be expressed in Cartesian coordinates, with *R* and *X* corresponding to real and imaginary part, respectively.

The complex impedance *Z* can also be expressed by the Cartesian coordinates, whereby *R* and *X* correspond to the real and imaginary part, respectively:

$$Z = R + i \cdot X \tag{3.3}$$

$$\text{With} \quad R = Re(Z) = |Z| \cdot \cos(\varphi) \tag{3.4}$$

$$\text{And} \quad X = Im(Z) = |Z| \cdot \sin(\varphi) \tag{3.5}$$

All components generating a phase shift contribute to the imaginary part which is termed reactance *X*, whereas components not producing any phase shift contribute to the real part which is called resistance *R*. Importantly, imaginary components include impedances of both capacitive Z_C and inductive Z_L elements.

When interpreting impedance data measured on mammalian cells and tissues, there is a general rule that resistance comes from their geometric dimensions and from intracellular and extracellular fluids, whilst measured capacitive reactance arises from the cell membranes.

There are different options to graphically present complex impedance data and some of the most common ways are (Chang and Park, 2010):
(i) The "Nyquist plot", where the imaginary part of impedance is plotted over the real part and
(ii) Bode diagram, where impedance magnitude $|Z|$ and the phase shift φ are plotted against the frequency f of the excitation signal on a logarithmic or semi-logarithmic scale.
It is important to understand that data acquired by impedance measurements represent the overall response of the system under study. In order to estimate contributions of individual components of the system, one may perform fitting of the experimental data with the help of a transfer function that expresses a physical model. However, appropriate model systems should not contain more parameters than necessary to fully describe all features of the impedance spectrum, in order to avoid redundancies, and inaccurate final results (Wegener, 2010; Macdonald, 2006).

3.1.1 Electric Cell-Substrate Impedance Sensing

There are different approaches available nowadays for label-free monitoring of whole cells and tissues (Scott and Peters, 2010) and among them, impedance-based biosensors are developed the farthest with broadest applicability and information content (Lukic and Wegener, 2015). At the same time, impedance-based methods offer certain advantages over other methods for detection of changes in cellular behavior, such as noninvasiveness, accuracy, sensitivity and speed (Ghenim et al., 2012; Sperber et al., 2016). Impedimetric monitoring of adherent cells has been first reported and described around 30 years ago by Ivar Giaever (Nobel laureate in physics) and Charles R. Keese, who named this technique Electric Cell-Substrate Impedance Sensing (ECIS; Giaever and Keese, 1984, 1986, 1991). The measurement principle of ECIS is to monitor the behavior of the cells grown to confluence on the surface of thin gold film electrodes in a non-invasive and time-resolved manner. Gold film electrodes are deposited on the bottom of a conventional cell culture vessel such as a multiwell plate. Small electrodes are made out of gold because this material provides an ideal growth surface for animal cells due to its hydrophilic surface (in presence of culture medium or buffer), chemical inertness and great overall biocompatibility.
Within the multiwell plate, pairs of planar electrodes are located on the bottom of each measurement unit (well). The two electrodes are connected via the overlaying physiological buffer or cell culture medium (as schematically presented in **Figure 3.2**). One of the electrodes (working electrode) is made with rather small surface size, with diameter of 250 µm, whereas the second electrode (counter electrode) within the electrode pair is made with much bigger surface area, approximately 500-1000 times bigger than the surface area of the

working electrode. The measured electrical impedance describes in principle behavior of the cells grown on both, working and counter electrode, but due to its very small size (impedance is inversely proportional to the electrode area), the working electrode represents a bottleneck of the overall measured signal and therefore, the electrical impedance will be dominated by the signal coming from the cell population present on the top of the small working electrode (Lo et al., 1995; Stolwijk et al., 2012). Contributions of the big counter electrode, wiring and the bulk electrolyte to the signal can be thus neglected. Such a two-electrode arrangement represents the original measurement layout which has been often modified over time depending on the specific needs and requirements of different assays and their applications.

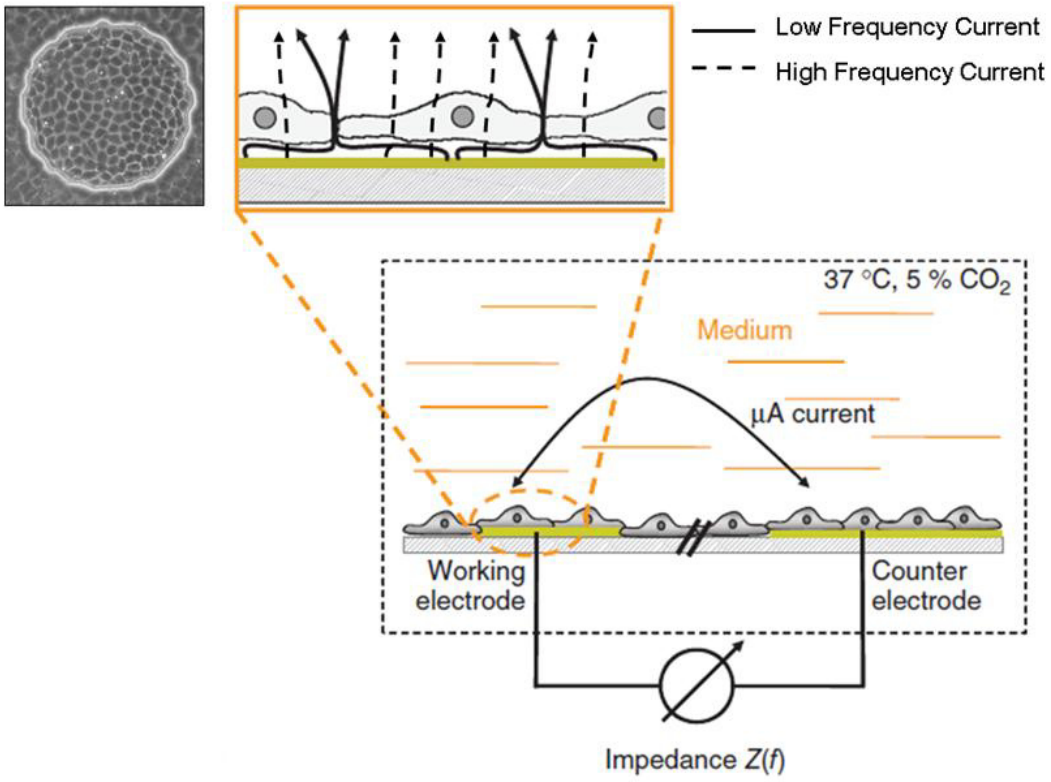

Figure 3.2 Schematic illustration of the basic ECIS measurement principle. Cells are grown to the confluence on planar gold film electrodes on the bottom of a cell culture dish. The cell-covered working electrode is depicted on the phase-contrast microscopic image in the upper left corner. Electric connection between the small (working) and significantly larger (counter) electrode is established by the overlaying physiological buffer or cell culture medium. Adherent cells on the electrodes represent dielectric bodies which increase the electrochemical impedance as the current is forced to flow around or through the cells. Portion of the current which flows around (low frequency current) and through (high frequency current) the cell bodies is illustrated in the upper left graph.

The small thickness of the electrodes (around 100 nm) allows for microscopic inspection of the cells by routine light microscopy (Wegener et al., 2000). Cells act like dielectric bodies (insulating particles) and with their attachment and spreading on the electrode surface, the impedance gradually increases (Wegener et al., 1996; Liu et al., 2009). In fact, as cell bodies cover the electrode surface, they impede current flow and once a confluent cellular monolayer is formed, the current is forced to flow underneath and between the neighboring cells. Such events take place in the lower range of frequencies (f < 1 kHz), whereas only at higher frequencies (f > 10 kHz), the current can flow even through the cell membrane and through the cells. Frequency-dependent current flow is illustrated in **Figure 3.2**. Taking this into consideration, one should conduct impedance readings at the appropriate frequencies, to get an insight into a certain cellular structure (cell-cell contacts, membrane topography) and thus obtain specific information about certain cellular behaviors. Typically, impedance readings are recorded from 1 Hz to 1 MHz to obtain full spectral information, but this frequency range can be adjusted depending on the cell type and assay requirements.

Obviously, the ECIS technique is sensitive to electrode coverage and the three-dimensional properties (morphology, shape) of the cells covering the electrodes. This leads to a conclusion that ECIS readings are a very powerful and convenient tool to monitor assays addressing (increasing or decreasing) number of cells on the electrode, changes in cell-cell and cell-substrate contacts, as well as the changes in cellular morphology. Electrode coverage and changes in cell morphology might be induced by different kinds of biological, chemical or physical stimuli (Giaever and Keese, 1984) and by using ECIS technique, cells are being probed in real time under conditions as similar as possible to their natural (*in vivo*) environment (37 °C, 5-10 % CO_2). Depending on the properties and morphology of each cell type, cells will form rather strong or weak cell-cell and cell-substrate contacts, which finally determine the characteristic impedance signal for a confluent monolayer of the cell type under study. Any changes in cell shape will be mirrored in the changes of the impedance signal. It has been shown that the ECIS technique is capable of detecting very small changes in cell shape (in the order of a few nanometers), which are practically non-detectable by an optical microscope (Giaever and Keese, 1991).

3.1.2 Cell-Based Assays Monitored by Impedance Readings

The sensitivity of the ECIS technique for changes in cell shape (morphology) and in electrode coverage qualifies this method as a versatile and multimodal approach applicable for analysis of different cell-based assays (Lukic and Wegener, 2015; Sperber et al., 2016). A variable number of individual compartments (wells) grouped to an electrode array (mostly 8-,

96- or 384-well format) allows for parallel monitoring and higher throughput, which might be of high importance for some assays. The basic ECIS measurement setup (described in the chapter 4.2.1.1) using 8-well format is applied for the majority of assays but it can be modified and tailored according to the special requirements of the experimental procedure (Szulcek et al., 2014).

To date, the ECIS technique has been applied for variety of different studies. Within this subchapter, various modes of impedance-based cellular assays will be briefly described.

Cell attachment and spreading is a fundamental and complex process relevant for many physiological and pathophysiological events. While suspended cells are allowed to attach and spread across the electrode surface, the associated increase in impedance is observed. For some studies, the substrate surface (electrodes) has been precoated with a protein of interest to observe how this could possibly influence attachment and spreading kinetics of the cells (Wegener et al., 2000).

Monitoring cell proliferation or cell growth is a very relevant assay in cancer biology and cancer research in general. Namely, uncontrolled cell growth is the most detrimental indicator of cancer. During proliferation studies conducted using ECIS, the growth of cells over a certain (often longer) period of time is being followed. Cells are seeded with lower densities upon the gold film electrodes and continuous cell growth is indicated by an impedance increase until constant values are reached. Usually, after several days cells will form a confluent monolayer. In fact, the time course of the impedance is being used as a measure for cell proliferation, so that the influence by different types of stimuli (biological, chemical, physical) can be studied in all detail. Hence, influence of different factors on the cells ability to grow and divide is available in an automated assay format (Stolwijk et al., 2012; Szulcek et al., 2014).

Monitoring cytotoxicity in real time using the ECIS platform is a great alternative to biochemical cytotoxicity assays present on the market, which are based on discontinuous (end-point) readings. Using ECIS, cell shrinking and membrane integrity can be probed as a relevant indicator of cytotoxicity for a given stimulus. When the cell membrane is being damaged, current is able to flow through the cells and this will cause a decrease in overall impedance. On the other hand, exposure of the cells to more moderate stress will not affect their membrane integrity but will most probably cause contraction and rounding up of the cell bodies. Such effects also reduce impedance values, as extracellular current pathways will be shorter and the cell body occupies less area on the electrode. There are many published reports on the successful application of the ECIS technology for cytotoxicity studies, and a concentration-dependent cellular response was observed upon exposure to various types of

different cytotoxic stimuli (Arndt et al., 2004; Xiao et al., 2002; Hofmann et al., 2012; Male et al., 2013; Kling et al., 2014; Widder et al., 2015).

Recording time-resolved response profiles and screening of GPCR activation can be performed using the ECIS instrumentation in a very sensitive manner. The crucial point is to know which part of the cell bodies needs to be monitored, as corresponding frequencies can be chosen for measurement of the impedance response profiles. G-protein-coupled receptors (GPCRs) belong to the pharmacologically most relevant cell-surface receptors. Upon (extracellular) receptor activation, (intracellular) signal cascades are being triggered and changes in cell shape are induced. These can be conveniently monitored in a very sensitive and time-resolved manner, which is the reason why the ECIS technique is routinely used for the screening of GPCR agonists and antagonists (Wegener et al., 1999; Scott and Peters, 2010; Stolwijk et al., 2014).

Cell motility – micromotion can be observed in a confluent monolayer of cells, which are dynamic even if they don't have much space to move around. In fact, numerous studies have shown that cells are in constant fluctuating motion due to their active metabolism and continuous movements of intracellular organelles within the cytoplasm. Since the ECIS technique allows for rapid data acquisition and very sensitive monitoring of the changes in cell morphology, it is very well suited for measurements of cellular micromotion with a time resolution in the milliseconds range (Giaever and Keese, 1991). Very often fluctuation patterns of different (or similar) cell lines are recorded and compared to find out more about their dynamics and metabolic activity (Lo et al., 1993), or their sensitivity for cytotoxic agents (Lovelady et al., 2009; Tarantola et al., 2009). In addition, micromotion of cancer cells might be a very valuable indicator for their invasiveness.

Endothelial and epithelial barrier function is based on the expression of functional tight junctions, which are highly specialized cell-cell contacts responsible for selective control of permeation and diffusion of solutes (various metabolites). Due to its high sensitivity for the paracellular current pathways at certain frequencies, the ECIS method has been extensively applied for studies of endothelial and epithelial barrier function (Wegener, 2010; Wegener and Seebach, 2014). Monitoring endothelial and epithelial barrier function is essential for drug development, as many drug candidates need to cross such biological barriers on their way to the final site of action/target.

In situ electroporation, as well as *cell migration and wound healing* are impedance-based cellular assays extensively studied within this work and as such they will be described in more details in chapters 3.2.3 and 3.2.4.

3.1.3 Presentation of the Impedance Data

The majority of reports within impedance-based studies describing cellular behavior contain data in which the impedance magnitude $|Z|$ is presented over a certain period of time at one particular frequency. The monitoring AC frequency used for the measurement will be chosen based on cell and assay type. However, it is highly recommended to record impedance data over a broad range of frequencies, whenever the assay setup allows it. This way, plenty of information about the cell population under study can be gathered within a single assay. An AC frequency of 4 kHz is often used for impedance monitoring as it allows for a sensitive observation of morphological changes and changes in cell motility (Giaever and Keese, 1993; Lo et al., 1993).

The complex impedance Z can be split into its real (resistance; R) and imaginary (capacitance; C) part. Depending on the assay and the focus of analysis, one may choose which of these two parameters is most relevant and appropriate to describe the cellular response. Whereas the real part of the impedance represents the overall resistance of the confluent cell monolayer and electrode, the imaginary part describes the capacitive behavior of the electrode and cell membrane. Giaever and Keese have developed a physical model which describes how individual impedance contributions of cellular structures make up the total impedance of the system for a confluent cell monolayer (Giaever and Keese, 1991). The impedance originating from the cells covering the electrode can be divided into three independent contributions: $\boldsymbol{R_b}$ which describes contributions originating from the intercellular current pathways and cell-cell contacts, $\boldsymbol{\alpha}$ which describes impedance contributions coming from the cell-substrate contacts and $\boldsymbol{C_m}$ quantifying capacitive contributions of the cell membranes. Changes in parameters R_b and α will have a big influence on resistance R and impedance $|Z|$. Paracellular pathway is mostly described by the impedance $|Z|$, but in some cases it can be also described by resistance R. On the other hand, analysis of capacitance at high frequencies (40 or 32 kHz) is often very useful to describe changes in membrane capacitance and changes of electrode coverage. When the applied frequency is high enough (above a cell type-dependent threshold), electrode capacitance will be linearly dependent on electrode coverage (Wegener et al., 2000). Hence, events like cell attachment, spreading and detachment can be appropriately monitored in a very sensitive manner by measuring the capacitance (or impedance) at higher frequencies (32 – 40 kHz). Therefore, for those assays within this work which involved cell detachment associated with cytotoxicity, apoptosis or changes in electrode coverage in general, the monitoring frequencies for impedance and capacitance values were predominantly set to values in the order of 32 – 40 kHz.

However, for the majority of studies within this work involving ISE (and cell signaling), the

recorded impedance data *IZI* are presented at 4 kHz, since at this frequency even slight changes within the confluent monolayer can be detected with high sensitivity. The exception was made with data for CHO cells, which were presented in most cases at 16 kHz as this was found to be the most appropriate frequency to look at. In order to decide which frequency is the most appropriate, spectral information of the different parameters (impedance, resistance, capacitance) is needed to find the most sensitive frequency for a given cell line. Normalized impedance spectra can be obtained after the complex impedance is measured for the electrodes covered with a confluent monolayer of the cells (cell-covered electrodes) and for the electrodes in absence of cells, covered only with the cell culture medium (cell-free electrodes). In **Figure 3.3 A** the impedance spectrum of electrodes covered with a confluent monolayer of NRK cells (cell-covered electrodes) is compared to cell-free electrodes. The complex impedance was measured over a range of frequencies (10^1-10^6 Hz) using 8W4Eμ electrode array (more details described in chapter 4.2.1.2). In **Figure 3.3 B** the ratio of impedance values for cell-covered and cell-free electrodes is presented as a function of frequency (frequency spectrum of the normalized impedance for $|Z|_{\text{cell-covered}}$ / $|Z|_{\text{cell-free}}$). In **Figure 3.4**, the impedance spectra for CHO-GFP cells are presented following to the same style. NRK and CHO-GFP/CHO-K1 are the cell lines which were applied for the majority of studies conducted within this thesis. For cell lines: BAEC, HaCaT and NIH 3T3, 4 kHz was chosen as the most appropriate monitoring frequency.

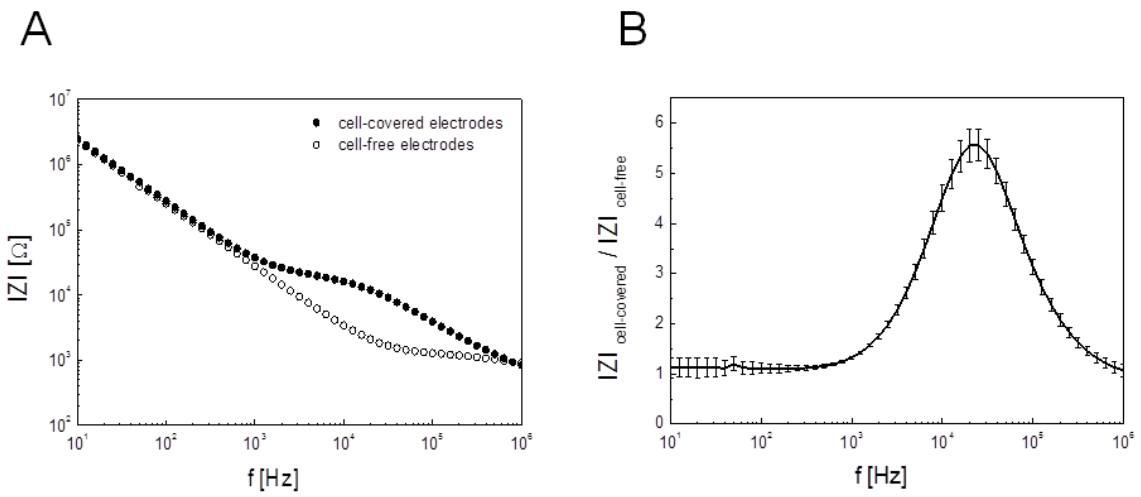

Figure 3.3 A Impedance spectra of cell-free electrodes and electrodes covered with confluent monolayers of NRK cells (measured at 37°C). Impedance spectra were recorded over a frequency range 10^1-10^6 Hz using 8W4Eμ electrode array. **B** Frequency spectra of the normalized impedance for $|Z|_{\text{cell-covered}}$ / $|Z|_{\text{cell-free}}$ recorded in a range 10^1-10^6 Hz and presented as mean value ± standard deviation; n=5 (impedance spectra recorded in 5 different wells).

For both cell lines observed here (NRK and CHO-GFP), as well as for the other cell lines, no major differences in impedance values for cell-covered and cell-free electrodes can be observed at low frequencies (< 10^3 Hz). The dielectric nature of the cell body becomes measurable starting with 10^3 Hz. The frequency value providing the highest sensitivity for impedance is determined by finding the maximum of the normalized impedance. For NRK cells, a frequency of 4 kHz was chosen as the most sensitive one, whereas for CHO-GFP cells, a frequency range between 10-20 kHz provides the best sensitivity of impedance measurements. Interestingly, every cell line will give slightly different, rather characteristic impedance spectra with an individual internal structure of the spectrum for cell-covered electrodes, as parameters *α*, *Rb* and *Cm* are defined by the cell line-specific morphological properties.

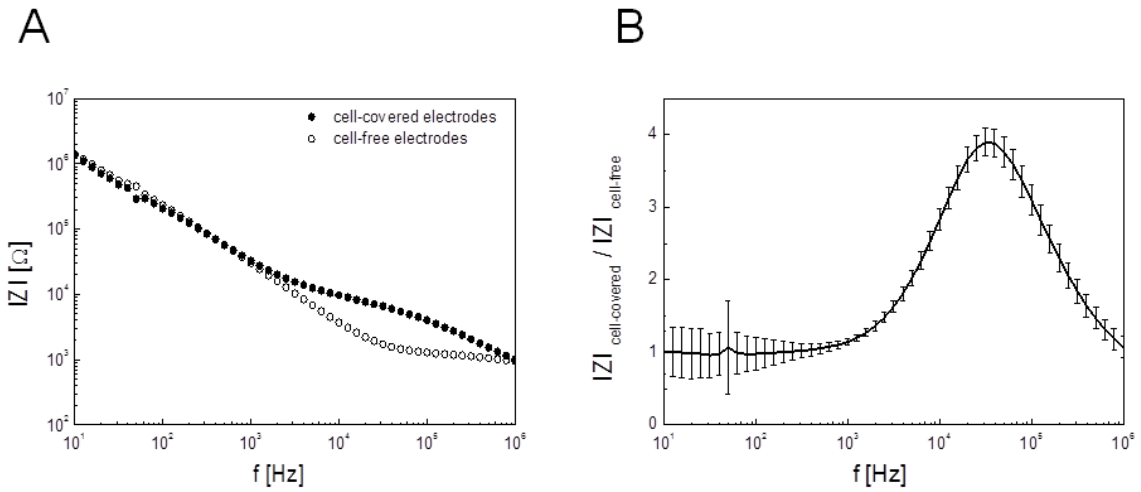

Figure 3.4 A Impedance spectra of cell-free electrodes and electrodes covered with confluent monolayers of CHO-GFP cells (measured at 37°C). Impedance spectra were recorded over a frequency range 10^1-10^6 Hz using an 8W4Eμ electrode array. **B** Frequency spectra of the normalized impedance for $|Z|_{cell\text{-}covered}$ / $|Z|_{cell\text{-}free}$ recorded in a range 10^1-10^6 Hz and presented as mean value ± standard deviation; n=5 (impedance spectra recorded in 5 different wells).

ECIS data are very rarely presented in a raw format. Instead, the time course of the impedance, resistance or capacitance values is often normalized to a certain reference point that is important for the given assay. The point of normalization may be the starting point of the assay (t = 0), but more often data will be normalized to the last point before certain stimuli are applied (e.g. compound addition, pulse application, etc.). Thus, effects of the applied stimuli can be better observed. Another important motivation or argument to apply normalization of the data is an improved comparability of the data acquired during various

experiments. Normalization of the absolute data was very often applied in this work and absolute values are mentioned only when they might be important for data evaluation.

3.2 Electroporation of Mammalian Cells

Reversible permeabilization of the cell membrane exposed very shortly to the external electric fields of high amplitudes is a phenomenon called electroporation (or electropermeabilization). As illustrated schematically in **Figure 3.5**, application of short but strong electric pulse(s) to the cell membrane will cause (b) a transient opening of the cell membrane which allows for diffusion of extracellular and membrane-impermeable material (xenomolecules) into the cell cytosol. Upon subsequent membrane resealing, xenomolecules will stay captured inside the cell cytosol (c). Application of stronger and/or longer electric pulse(s) may cause irreversible opening of the cell membrane, with the cell not recovering its membrane integrity (d) and hence, cell damage will be followed by cell death eventually.

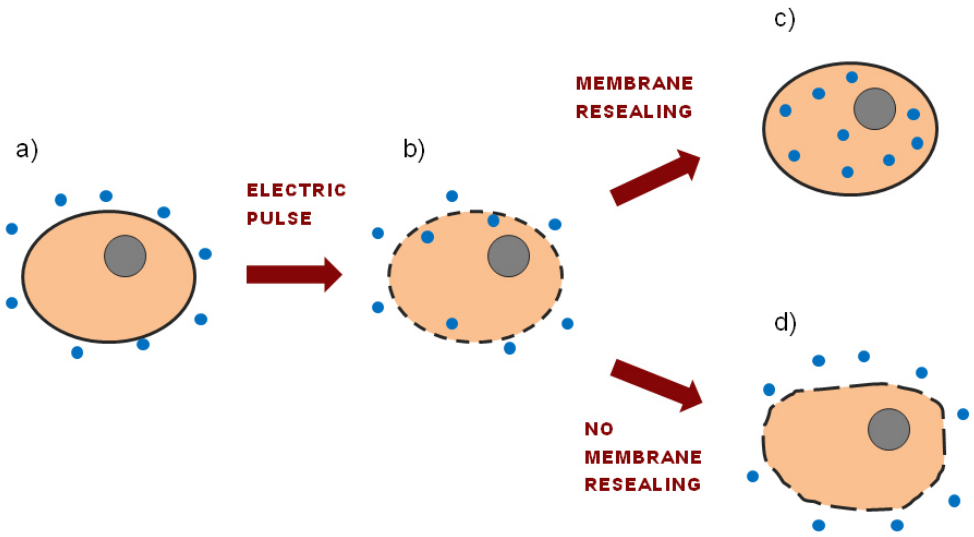

Figure 3.5 Simplified schematic illustration of events which occur as a consequence of exposure of the cell to an invasive electric field pulse. Firstly, **a)** an intact cell surrounded by the membrane-impermeable xenomolecules is exposed to a strong electric field pulse, which will cause disruption of the cell membrane. Thus, **b)** cell is electropermeabilized. Depending on the strength and invasiveness of the applied electric field, two following scenarios are possible. If the pulse causes only transient poration, the cell membrane will reseal shortly afterwards and **c)** the recovered cell will be loaded with xenomolecules. If the electric pulse causes a strong and persistent damage of the cell membrane, **d)** irreversibly damaged cell can hardly recover and cell death occurs.

The transient permeabilization of the cell membrane caused by applying a strong electric pulse allows for free diffusion of extracellular material into (and out of) the cell cytoplasm. These phenomena have been recognized as very advantageous for introduction of membrane-impermeable compounds into the cell interior, if they cannot cross the plasma membrane by simple diffusion or some other alternative transport mechanism. The term electroporation was introduced in the early 1980s with a first scientific report on cell loading with membrane-impermeable exogenous material by electric pulses (Neumann et al., 1982). Since then, electroporation and electropermeabilization have been extensively studied and developed. As a consequence, this method has been successively implemented into various fields of bioanalysis, diagnostics and therapeutics.

In the following subchapters, more details on the theoretical background associated with electroporation will be described.

3.2.1 Behavior of Cells in Electric Fields

Exposure of cells to external invasive electric field will disturb cell membrane integrity, either transiently or permanently, depending on the field strength. Transient and reversible permeabilization of the cell membrane (poration) allows membrane-impermeable compounds of different sizes to cross the cell membrane for a limited (short) period of time.

Cell membranes consist of lipids, proteins and carbohydrates which form a two-layer assembly – a diffusion barrier which separates the cell interior from the extracellular environment. More precisely, the bilayered cell membrane is predominantly constituted out of lipids (phospholipids) and upon application of strong external electric field, rearrangement of membrane components will occur, enabling formation of small aqueous hydrophilic pores within the membrane structure (Abidor et al., 1979; Benz et al., 1979; Weaver and Chizmadzhev, 1996; Weaver, 2003; Weaver and Powell, 1989). This allows for direct diffusion of ions and membrane-impermeable molecules into the cell interior (Pucihar et al., 2008). Basically, the two-layered lipid membrane acts as a dielectric (or insulating shell) which separates cell cytoplasm from the extracellular environment with electrolytic properties (Ramos and Teissié, 2000; Teissié, 2007). Under regular physiological conditions, a certain voltage (from –90 mV to –40 mV) is present across the cell membrane (resting transmembrane potential; Cole, 1972; Kotnik et al., 1997; Kotnik et al., 2010). Once the cell is exposed to an external electric field, the electric potential across the cell membrane will change and an induced transmembrane potential will be superimposed to the natural resting potential (Gabriel and Teissie, 1997; Rols, 2006). In other words, the induced transmembrane potential provides free energy which is necessary for the structural

rearrangement of the membrane phospholipids and as a consequence, small aqueous pores are formed. More details on how the transmembrane potential is being changed when a spherical cell is exposed to electric pulses is presented by the Schwan's equation (Neumann, 1989; Marszalek et al., 1990; Tsong, 1991; D.C. Chang et al., 1991; Kotnik et al., 1997). Various studies have shown that the membrane potential is asymmetrical and position-dependent, causing local diffusion of material across the cell membrane (Tekle et al., 1994; Gross et al., 1986; Hibino et al., 1993; Hibino et al., 1991).

Importantly, the majority of the above mentioned studies are based on changed cell suspensions and in principle, they model the cell as a spherical insulating shell (containing electrolyte). Such model systems are much simpler than the corresponding models of tissue or a cellular monolayer. In addition, most of the studies do not take into account a distribution of different cell shapes and morphology characteristics, but describe the cell as a simple uniform sphere or ellipsoid, which might be generally applicable for some cell types but is absolutely inappropriate for all of cell types. However, all these studies contributed to our current understanding of cellular behavior and events occurring in the cell membrane during exposure of the cells to strong external electric fields (Abidor et al., 1979; Chernomordik and Chizmadzhev, 1989).

Electric field pulses can be applied using direct (DC) or alternating current (AC) and most studies described in the literature are based on DC pulses applied for electropermeabilization. Pulse parameters such as amplitude and pulse duration are easier to describe and more intensely studied when DC pulses are applied. On the other hand, application of AC pulses will provide a different induced transmembrane potential than DC pulses, such that one has to be cautious when comparing the parameters for DC and AC pulses (Neumann, 1989; Tsong, 1991).

3.2.2 Electroporation

Electroporation can be defined as the transient permeabilization of the cell membrane caused by external short and well-defined electric pulses (Zimmermann et al., 1974; Neumann et al., 1982). It enables the transfer of hydrophilic molecules from the extracellular environment across the cell membrane into the cell cytoplasm where they will remain captured after membrane resealing (Gehl, 2003; Rols, 2006; Teissié et al., 2005; Faurie et al., 2005). A commonly accepted model explains electroporation by formation of aqueous hydrophilic pores in the lipid bilayer of the cell membrane which occurs upon cells being exposed to strong electric fields.

Depending on the strength and invasiveness of the applied electric pulse, electroporation can

be reversible or irreversible. Therefore, parameters of electric pulse have to be well defined, optimized and chosen carefully for each cell line, depending on application. The right combination of pulse parameters is needed which will create electric fields strong enough to trigger transient pore formation in the cell membrane, but which will not be too invasive to cause permanent cell damage. In other words, there is a certain threshold or critical value of induced transmembrane voltage, individual for every cell line, which has to be reached for reversible membrane poration by exposure of the cells to the corresponding external electric field (Kinosita and Tsong, 1979; Abidor et al., 1979; Neumann and Rosenheck, 1972; Neumann, 1989). Reversible electroporation is required for loading of the cells with different xenomolecules, or release of the intracellular material from the cells. When one aims for irreversible electroporation, the critical value/threshold has to be exceeded in order to achieve a permanent loss of cell membrane integrity, irreversible cell damage and finally loss of cell viability (Hamilton and Sale, 1967; Danfelter et al., 1998; Meaking et al., 1995).

There are numerous reports in the literature suggesting that selection of optimal electric pulse parameters which should be applied for reversible electroporation will strongly depend on the type of xenomolecules that need to be delivered into the cell (Golberg and Rubinsky, 2013; Kandušer and Miklavčič, 2008). For instance, trains of short electric pulses are recommended for introduction of small molecules (e.g. drugs, fluorescent dyes, etc.), whereas longer pulses are preferable for successful introduction of larger molecules (such as DNA plasmids), often in combination with a lower pulse voltage (Klenchin et al., 1991; Wolf et al., 1994;Teruel and Meyer, 1997; Santra et al., 2013; Dolinsek et al., 2016). The presence of macromolecules in the extracellular environment during pulse application is crucial to allow their diffusion into the cytosol (Rols and Teissié, 1998). On the other hand, small molecules can be transferred into the cells via electroporation even if they are added shortly after application of an electric pulse (Golzio et al., 2004; Pucihar et al., 2008; Rols et al., 2000). Several studies have demonstrated an efficient gene transfer achieved by using millisecond pulses for electroporation (Golzio et al., 2002; Rols, 2008; Escoffre et al., 2009; Phez et al., 2005; Smith et al., 2004; Favard et al., 2007; Orio et al., 2012).

Variable pulse parameters which should be optimized with respect to the specific cell line and type of application are: duration, amplitude, frequency, as well as the number of pulses and the repetition frequency (Rols and Teissié, 1990; Gabriel and Teissie, 1995; Wolf et al., 1994; Vernhes et al., 1999). Depending on pulse duration, electroporation (of suspended cells) can be divided to (i) classical electroporation (applying low intensity electric pulses with duration in μs to ms range; Rols and Teissié, 1998) and (ii) nanosecond electroporation (applying high intensity electric pulses with duration in the ns range; Sozer et al., 2016;

Pakhomov et al., 2015; Batista Napotnik et al., 2016).

Numerous studies have been conducted with the aim to unravel how different pulse parameters influence the outcome of the applied electroporation. Number of pores and their density within the cell membrane increases with an increasing voltage (Chernomordik and Chizmadzhev, 1989; Teissié et al., 2005), whereas pulse duration influences size of the pores established during the pulse application (Kinosita and Tsong, 1979; Rols and Teissié, 1990; Saulis and Saule, 2012).

Dye loading studies (conducted by Rols and Teissié, 1998 and Neumann et al., 1999) demonstrated that membrane permeabilization depends on pulse duration. Namely, dye loading efficiency increases linearly with longer pulses, until the point where saturation is reached. Every increase in pulse duration length above this point will lead to irreversible damage of the cell. Similar observations have been made when dye loading efficiency was monitored as a function of increasing number of sequentially applied electric pulses (multiple electroporation; Rols and Teissié, 1998). Nevertheless, cell vulnerability shortly after pulse application has to be taken into account when multiple electroporation trains are performed. Cells are in a very sensitive state for approximately 15 min after pulse application (Gehl et al., 1998) and additional invasive pulses could dramatically affect their viability (Golzio et al., 1998). Size of the pores formed within the cell membrane upon exposure of cells to invasive electric pulses was investigated by several groups and these studies concluded that size of the pores depends on the balance between the line tension of the pores and the membrane surface tension (Naumowicz and Figaszewski, 2013; Kaner et al., 2014; Rols et al., 2000; Tarek, 2005). Besides molecular simulations visualizing the process of electropermeabilization, electron microscopic images of pores in cell membranes upon electroporation have been reported (Chang and Reese, 1990) to support the pore formation theory.

According to Teissié et al., 2005, the process of electroporation of suspended cells can be divided into five different phases:

1) “Induction or triggering step” is the initial step during which the applied electric pulse induces an increase in transmembrane potential by which the critical permeabilization threshold is reached. Critical threshold field strength may be significantly influenced by the cell radius. Thus, larger cells can be readily permeabilized at lower electric field values (~ 200 V/cm) than the small bacteria (~ 1 – 2 kV/cm; Teissié and Rols, 1993). This step usually takes a few milliseconds.

2) “Expansion step” is time-dependent and lasts as long as the external electric field is maintained above the critical threshold value (usually in a range from hundreds of μs to ms).

During this phase, the size of the hydrophilic pores within the cell membrane expands (Naumowicz and Figaszewski, 2013; Kaner et al., 2014).

3) The “stabilization step” starts as soon as the applied external electric field decreases below the critical value. As a consequence, a membrane rearrangement takes place. This step usually takes a few milliseconds (ms).

4) The “resealing step” describes resealing of the lipid bilayer. This first order process might last from several seconds to several minutes, and it is strongly affected by the temperature (Kinosita and Tsong, 1979) and state of the cytoskeleton (Teissié and Rols, 1994; Rols and Teissié, 1992).

5) The “memory effect” is the last phase within the sequence of elementary electroporation steps and it means recovery of the cell metabolism back to the normal pre-pulse state. Yet, some previous electroporation-associated changes in cell membrane properties will still remain memorized (stored) during the following hours.

The majority of electroporation studies reported in the literature are performed using suspension of cells. This implies total absence of any cell-cell or cell-surface contacts, cells are rounded and more sensitive, most likely due to the enzymatic detachment from their growth surface (usually by trypsination). For suspension electroporation, cells in suspension are placed (in a cuvette) between two parallel electrodes (cathode and anode). Since in such setup a significant part of the applied electric current flows through the bulk electrolyte, high voltage amplitudes are required for successful electroporation of the cells. As a consequence, Joule heating has to be taken into account (Davalos et al., 2003) and cells have to be cooled down on ice. Besides, only special buffers with low ionic strength can be applied as assay buffer during electroporation. Subsequent analysis of electroporation efficiency can be performed either directly in suspension or with certain time delay after growing the cells on a culture substrate (Rols and Teissié, 1998; Golberg and Rubinsky, 2013; Wegener et al., 2002).

Most studies associated with electroporation and electropermeabilization are dedicated to an analysis of delivery of various xenomolecules into the cell cytosol. However, some researchers have attempted to show that diffusion of molecules through small hydrophilic pores during electroporation is bidirectional and electroporation as a method could be applied for targeted release of the intracellular material. Ghosh et al., 2013 reported on the development of an electrochemical microelectrode applied to electropermeabilize adjacent chromaffin cells and to measure the subsequent quantal catecholamine release using amperometry. Electroporation was also applied for release of proteins from adherent CHO cells (Zhan et al., 2012), release of molecules on a single-cell level (Agarwal et al., 2009;

Bao et al., 2008), or release of potassium ions from mouse hepatoma cells (Saulis et al., 2007). Lu et al., 2005 reported on a micro-electroporation device for cell lysis prior to subcellular analysis. In addition, reports on electroinduced release of ß-galactosidase from bacteria cells (Ganeva et al., 2015) and electroporation-mediated release of intracellularly stored secondary products from cultivated plant cells (Brodelius et al., 1988) can testify on relevance and necessity of electrically-induced release procedures.

Electroporation is a versatile method applicable for a variety of different cell types and biological systems (ranging from bacterial cells, over mammalian cell monolayer, three-dimensional spheroids to tissues and even skin). Over the past years, electroporation has been rapidly developed and it has been successfully implemented for many different types of application. Reversible electroporation is mostly applied for delivery of small molecules (e.g. drugs, synthetic nucleic acids) and macromolecules (proteins, DNA plasmids, etc.) into the intracellular environment, with preserved cell viability (Kandušer and Miklavčič, 2008; Wasungu et al., 2009). There is an increasing number of reports how electroporation can be efficiently applied for electrochemotherapy and genetherapy in medicine. Within various fields of biotechnology, irreversible electroporation is often applied for optimized and efficient cell killing, as an alternative method for liquid food sterilization, water purification (Kandušer and Miklavčič, 2008), or anti-cancer therapy (Harris et al., 2016).

3.2.3 *In Situ* Electroporation

Electroporation of cells in suspension is a very useful platform to study fundamental processes occurring during and after application of external electric field pulses to the cells and it provides great insight into events associated with membrane permeabilization. However, practical application of electroporation requires in many cases exposure of confluent cells, tissue, or even organs (e.g. skin) to the elevated electric fields and therefore, studies involving electroporation of more complex biological structures have to be performed. Requirements of modern bioanalytical and biomedical research led to the development of new approaches and instrumentation which will enable performing electroporation under *in situ* or *in vivo* conditions.

In situ electroporation and analysis of cellular behavior offers numerous advantages over classical electroporation of the cells in suspension. Anchorage-dependent cells are grown to confluence and are not detached from their growth substrate before their *in situ* exposure to electric pulse(s) is performed. This implies that membrane proteins, cytoskeleton, cell-cell and cell-substrate contacts are fully established, which significantly helps membrane recovery, by means of resealing and regeneration, after invasive pulse application (Raptis

and Firth, 1990; Stolwijk, 2012). Besides, in the moment of pulse application, cells are present in their natural "relaxed" state, different to the cells in suspension, which have been already exposed to stressful conditions during cell suspension preparation prior to electroporation. Therefore, it is not surprising that the cell viability after the *in situ* procedure is much higher than the viability of cells electroporated in suspension (Müller et al., 2003; Zheng and Chang, 1991). *In situ* studies provide a very solid basis for further *in vivo* investigations of the electroporation effects and efficiency of the method. Analysis of the experimental data can be assessed directly, without any time delay, and in some cases (e.g. using ECIS technology), it can be conducted in a time-resolved manner.

To date, different experimental setups for conducting *in situ* electroporation have been reported and described in the literature. Culturing and electroporation of the cells can be conducted on different types of substrate: conductive ITO (indiumtinoxide) electrodes (Raptis and Firth, 1990; Raptis et al., 1995a; Raptis et al., 1995b), glass (Teruel et al., 1999; Teruel and Meyer, 1997), porous membranes (Müller et al., 2003; Yang et al., 1995), gold electrodes coated with DNA (Yamauchi et al., 2004), ITO electrodes coated with siRNA (Jain et al., 2012), or silicon (Jain and Muthuswamy, 2007). The electrode(s) which are used to deliver electroporating pulses can be differently designed and arranged, for instance, in form of scanning electrodes (Olofsson et al., 2005, 2007) or spiral microelectrodes (Garcia-Sanchez et al., 2014; Garcia-Sanchez et al., 2012). However, there are several approaches for *in situ* electroporation, in which the cells are cultured on coplanar electrodes made from gold (Ghosh et al., 1993; Wegener et al., 2002) or ITO (Raptis and Firth, 1990; Raptis et al., 1995a; Raptis et al., 1995b; Raptis et al., 2003; Anagnostopoulou et al., 2007), which deliver invasive electric pulses and are used for online cell monitoring. In addition, cells can be grown on interdigitated electrodes (IDES) made out of gold, titanium (Chun-Ping et al., 2004), special polymers (Olbrich et al., 2008) or copper coated with nickel (Ni)/gold (Au) (Garcia-Sanchez et al., 2012). More approaches for *in situ* electroporation are discussed in some recent reviews (Towhidi et al., 2016; Luft and Ketteler, 2015; Geng and Lu, 2013).

All above mentioned methods and different approaches for *in situ* electroporation were developed with a common goal – to enable delivery of very different types of membrane-impermeable molecules into cells. Besides proof-of-principle studies which mostly include loading of the cells with fluorescent reporter dyes, some groups have managed to demonstrate applicability of their methods for loading of the cells with potential therapeutic and diagnostic candidates by using *in situ* electroporation. Delivery of siRNA into adherent cells has been demonstrated by several groups (Fujimoto et al., 2008, 2010; Jain et al., 2009; Jain et al., 2012; Jain and Muthuswamy, 2007; Teruel et al., 1999). Some approaches

apply the strategy to immobilize nucleic acids (DNA or siRNA) on the substrate surface prior to cell seeding (Fujimoto et al., 2008; Jain et al., 2012; Koda et al., 2008).

The Raptis lab developed an experimental setup to transfer proteins and peptides into the cytoplasm of anchorage-dependent cells (Raptis et al., 2003; Raptis and Firth, 1990; Raptis et al., 1995a; Raptis et al., 1995b; Anagnostopoulou et al., 2007), besides Schonenberger et al., 2011 loaded adherent chondrocytes with mechano-growth factor (MGF). *In situ* electroporation was also applied for delivery of radioactive compounds into cells (Tomai et al., 2003). All these studies show that *in situ* electroporation can be applied for cell loading with various bioactive molecules (ions, small molecules, macromolecules).

Whereas the majority of the above mentioned approaches are concentrated mostly on electroporation and its efficiency, some approaches are developed to study both, pulse application and monitoring of the cellular behavior. The ECIS technology allows at the same time application of elevated electric fields and non-invasive impedance-based monitoring of the cells under study. It has been demonstrated so far that such an approach enables loading of the cells with various molecules, from reporter molecules such as: Horseradish peroxidase (Ghosh et al., 1993), Lucifer yellow (Wegener et al., 2002), TRITC-phalloidin and FITC-dextran (Albermann, 2004; Stolwijk et al., 2011), up to different bioactive molecules such as: cytotoxic drugs (bleomycin), DNA, enzymes, proteins and antibodies (Stolwijk, 2012), pH sensitive nanocompounds (Peng et al., 2010; Wang et al., 2012) and nanoparticles (Sperber, 2016; Sperber et al., 2016). The cellular response to the introduction of all these molecules was monitored impedimetrically in real time.

Direct contact of cells with an electrode or substrate delivering electric pulses renders very small voltages to be sufficient for reversible electropermeabilization. Since there is no unwanted thermal effect present during the procedure, *in situ* electroporation can be conducted in any buffer with physiological ion content, under regular physiological conditions (37 °C, 5-10 % CO_2).

3.2.4 Electric Wounding

As already described in the previous subchapters, strong external electric pulses can be applied for irreversible damage of the cell population under study. Hence, an invasive assay mode of the ECIS technology uses well-defined long electric pulses of high voltage, which will kill the entire cell population grown on the surface of the electrode. It is the aim of this application to provide a well-defined lesion in the cell layer for subsequent analysis of the wound healing process. Great advantage of this system is its ability to combine the invasive mode for cell damage and the non-invasive mode for monitoring the repopulation of the

electrode after pulse application, thus offering a highly automated alternative to the standard wound healing or migration assays. *In vitro* wound healing assay starts with growing the cells of interest on the electrode surface until they reach full confluence and cover the entire bottom of the culture dish/well (including working and counter electrode). Upon application of highly invasive voltage or current pulses to the electrodes, cells attached to the small working electrode will be killed, whereas all surrounding cells will remain unaffected by the pulse. The elevated voltage will thus be applied only to the well-defined area of the small working electrode and irreversible cell damage will be mirrored by the dramatic decrease in impedance (down to the values of cell-free electrode). Shortly afterwards, unaffected cells surrounding the working electrode will start to migrate and fill up the free space. Cell migration from periphery to the center of the working electrode will be mirrored by an increase in impedance with time until the monolayer becomes completely confluent again. Wound healing studies are often conducted in presence of different (concentrations of) chemotherapeutic drugs, as the ability of the cells to migrate under these conditions is conveniently assayed and quantified, by monitoring the time course of the impedance recovery (Keese et al., 2004; Itokazu et al., 2014). Including electric wound healing in time-resolved impedance recordings offers a well-defined, automated and time-resolved assay as an alternative to the standard scratch assay (in which the wound needs to be created mechanically).

Obviously, assay setup for electric wounding and *in situ* electroporation conducted with the help of the ECIS instrumentation does not differ much. In both cases, non-invasive measuring mode is being combined with invasive electric pulses. Thus, cellular behavior before and after pulse application can be monitored in a non-invasive, sensitive and time-resolved manner. The only major difference between these two assay modes is the design of the electric pulse. Whereas it is crucial for ISE to apply optimized and a cell type-dependent combination of electric pulse parameters which will induce a reversible permeabilization of the cell membrane, to provide efficient loading of the cells with the xenomolecules of interest, the electric pulse used for cell wounding is adjusted to cause quick and irreparable cell damage.

3.3 References

Abidor, I.G., Arakelyan, V.B., Chernomordik, L.V., Chizmadzhev, Y.A., Pastushenko, V.F., and Tarasevich, M.P. (1979) Electric breakdown of bilayer lipid membranes. *Journal of Electroanalytical Chemistry and Interfacial Electrochemistry* 104, 37-52.

Agarwal, A., Wang, M., Olofsson, J., Orwar, O., and Weber, S.G. (2009) Control of the release of freely diffusing molecules in single-cell electroporation. *Analytical Chemistry* 81, 8001-8008.

Albermann, S. (2004) In situ Elektroporation adhärenter Säugerzellen. PhD Thesis, Westfälische Wilhelms-Universität Münster.

Anagnostopoulou, A., Cao, J., Vultur, A., Firth, K., and Raptis, L. (2007) Examination of gap junctional, intercellular communication by in situ electroporation on two co-planar indium-tin oxide electrodes. *Molecular Oncology* 1, 226 – 231.

Arndt, S., Seebach, J., Psathaki, K., Galla, H.-J., and Wegener, J. (2004) Bioelectrical impedance assay to monitor changes in cell shape during apoptosis. *Biosensors and Bioelectronics* 19, 583–594.

Bao, N., Wang, J., and Lu, C. (2008) Microfluidic electroporation for selective release of intracellular molecules at the single-cell level. *Electrophoresis* 29, 2939-2944.

Batista Napotnik, T., Rebersek, M., Vernier, P.T., Mali, B., and Miklavcic, D. (2016) Effects of high voltage nanosecond electric pulses on eukaryotic cells (in vitro): A systematic review. *Bioelectrochemistry* 110, 1-12.

Benz, R., Beckers, F., and Zimmermann, U. (1979) Reversible electrical breakdown of lipid bilayer membranes: A charge-pulse relaxation study. *The Journal of Membrane Biology* 48, 181-204.

Brodelius, P.E., Funk, C., and Shillito, R.D. (1988) Permeabilization of cultivated plant cells by electroporation for release of intracellularly stored secondary products. *Plant Cell Reports* 7, 186-188.

Chang, B.-Y., and Park, S.-M. (2010) Electrochemical impedance spectroscopy. *Annual Review of Analytical Chemistry* 3, 207-229.

Chang, D.C., and Reese, T.S. (1990) Changes in membrane structure induced by electroporation as revealed by rapid-freezing electron microscopy. *Biophysical Journal* 58, 1-12.

Chernomordik, L.V., and Chizmadzhev, Y.A. (1989) Electrical breakdown of lipid bilayer membranes: Phenomenology and mechanism. In Electroporation and Electrofusion in Cell Biology, E. Neumann, A. E. Sowers, and C.A. Jordan, eds., pp. 83-95.

Chun-Ping, J., Wei-Ming, W., Min, L., and Yu-Cheng, L. (2004) Site-specific enhancement of gene transfection utilizing an attracting electric field for DNA plasmids on the electroporation microchip. *Journal of Microelectromechanical Systems* 13, 947-955.

Cole, K.S. (1972) Membranes, ions and impulses: a chapter of classical biophysics (University of California Press).

D.C. Chang, B.M. Chassy, J.A. Saunders, and A.E. Sowers (1991) Guide to electroporation and electrofusion (Academic Press).

Danfelter, M., Engström, P., Persson, B.R.R., and Salford, L.G. (1998) Effect of high voltage pulses on survival of Chinese hamster V79 lung fibroblast cells. *Bioelectrochemistry and Bioenergetics* 47, 97-101.

Davalos, R.V., Rubinsky, B., and Mir, L.M. (2003) Theoretical analysis of the thermal effects during in vivo tissue electroporation. *Bioelectrochemistry* 61, 99-107.

Dolinsek, T., Prosen, L., Cemazar, M., Potocnik, T., and Sersa, G. (2016) Electrochemotherapy with bleomycin is effective in BRAF mutated melanoma cells and interacts with BRAF inhibitors. *Radiology and Oncology* 50, 274-279.

Ende, D., and Mangold, K.-M. (1993) Impedanzspektroskopie. In Chemie in unserer Zeit (WILEY-VCH Verlag GmbH), pp. 134-140.

Escoffre, J.-M., Portet, T., Wasungu, L., Teissie, J., Dean, D., and Rols, M.-P. (2009) What is (still not) known of the mechanism by which electroporation mediates gene transfer and expression in cells and tissues. *Molecular Biotechnology* 41, 286–295.

Faurie, C., Golzio, M., Phez, E., Teissié, J., and Rols, M.P. (2005) Electric field-induced cell membrane permeabilization and gene transfer: theory and experiments. *Engineering in Life Sciences* 5, 179-186.

Favard, C., Dean, D.S., and Rols, M.-P. (2007) Electrotransfer as a non viral method of gene delivery. *Current Gene Therapy* 7, 67-77.

Fujimoto, H., Kato, K., and Iwata, H. (2008) Electroporation microarray for parallel transfer of small interfering RNA into mammalian cells. *Analytical and Bioanalytical Chemistry* 392, 1309-1316.

Fujimoto, H., Kato, K., and Iwata, H. (2010) Layer-by-layer assembly of small interfering RNA and poly(ethyleneimine) for substrate-mediated electroporation with high efficiency. *Analytical and Bioanalytical Chemistry* 397, 571-578.

Gabriel, B., and Teissie, J. (1995) Control by electrical parameters of short- and long-term cell death resulting from electropermeabilization of Chinese hamster ovary cells. *Biochimica et Biophysica Acta* 28, 171-178.

Gabriel, B., and Teissie, J. (1997) Direct observation in the millisecond time range of fluorescent molecule asymmetrical interaction with the electropermeabilized cell membrane. *Biophysical Journal* 73, 2630-2637.

Ganeva, V., Stefanova, D., Angelova, B., Galutzov, B., Velasco, I., and Arevalo-Rodriguez, M. (2015) Electroinduced release of recombinant beta-galactosidase from Saccharomyces cerevisiae. *Journal of Biotechnology* 211, 12-19.

Garcia-Sanchez, T., Guitart, M., Rosell-Ferrer, J., Gomez-Foix, A.M., and Bragos, R. (2014) A new spiral microelectrode assembly for electroporation and impedance measurements of adherent cell monolayers. *Biomedical Microdevices* 16, 575-590.

Garcia-Sanchez, T., Sanchez-Ortiz, B., Vila, I., Guitart, M., Rosell, J., Gomez-Foix, A.M., and Bragos, R. (2012) Design and implementation of a microelectrode assembly for use on noncontact in situ electroporation of adherent cells. *The Journal of Membrane Biology* 245, 617-624.

Gehl, J. (2003) Electroporation: theory and methods, perspectives for drug delivery, gene therapy and research. *Acta Physiologica Scandinavica*, 437-447.

Gehl, J., Skovsgaard, T., and Mir, L.M. (1998) Enhancement of cytotoxicity by electropermeabilization: an improved method for screening drugs. *Anticancer Drugs* 9, 319-325.

Geng, T., and Lu, C. (2013) Microfluidic electroporation for cellular analysis and delivery. *Lab Chip* 13, 3803-3821.

Ghenim, L., Kaji, H., Nishizawa, M., and Gidrol, X. (2012) Impedance Sensing of Biological Processes in Mammalian Cells. In Integrated Biomaterials for Biomédical Technology (John Wiley & Sons, Inc.), pp. 293-308.

Ghosh, J., Liu, X., and Gillis, K.D. (2013) Electroporation followed by electrochemical measurement of quantal transmitter release from single cells using a patterned microelectrode. *Lab Chip* 13, 2083-2090.

Ghosh, P.M., Keese, C.R., and Giaever, I. (1993) Monitoring electropermeabilization in the plasma membrane of adherent mammalian cells. *Biophysical Journal* 64, 1602-1609.

Giaever, I., and Keese, C.R. (1984) Monitoring fibroblast behavior in tissue culture with an applied electric field. *Proceedings of the National Academy of Sciences of the United States of America* 81, 3761-3764.

Giaever, I., and Keese, C.R. (1986) Use of electric fields to monitor the dynamical aspect of cell behavior in tissue culture. *IEEE Transactions on Biomedical Engineering* 33, 242-247.

Giaever, I., and Keese, C.R. (1991) Micromotion of mammalian cells measured electrically. *Proceedings of the National Academy of Sciences of the United States of America* 88, 7896-7900.

Giaever, I., and Keese, C.R. (1993) A morphological biosensor for mammalian cells. *Nature* 366, 591-592.

Golberg, A., and Rubinsky, B. (2013) Mass transfer phenomena in electroporation. In Transport in biological media, S. Becker, and Kuznetsov, eds., pp. 455-492.

Golzio, M., Mora, M.P., Raynaud, C., Delteil, C., Teissie, J., and Rols, M.P. (1998) Control by osmotic pressure of voltage-induced permeabilization and gene transfer in mammalian cells. *Biophysical Journal* 74, 3015-3022.

Golzio, M., Rols, M.P., and Teissie, J. (2004) In vitro and in vivo electric field-mediated permeabilization, gene transfer, and expression. *Methods* 33, 126-135.

Golzio, M., Teissie, J., and Rols, M.P. (2002) Direct visualization at the single-cell level of electrically mediated gene delivery. *Proceedings of the National Academy of Sciences of the United States of America* 99, 1292-1297.

Gross, D., Loew, L.M., and Webb, W.W. (1986) Optical imaging of cell membrane potential changes induced by applied electric fields. *Biophysical Journal* 50, 339-348.

Hamilton, W.A., and Sale, A.J.H. (1967) Effects of high electric fields on microorganisms. *Biochimica et Biophysica Acta (BBA) - General Subjects* 148, 789-800.

Harris, J.C., Chen, A., Macias, V., Mahon, B., Chiu, B., and Pillai, S. (2016) Irreversible electroporation as an effective technique for ablating human metastatic osteosarcoma. *Journal of Pediatric Hematology/Oncology* 38, 182-186.

Hibino, M., Itoh, H., and Kinosita, K. (1993) Time courses of cell electroporation as revealed by submicrosecond imaging of transmembrane potential. *Biophysical Journal* 64, 1789-1800.

Hibino, M., Shigemori, M., Itoh, H., Nagayama, K., and Kinosita, K. (1991) Membrane conductance of an electroporated cell analyzed by submicrosecond imaging of transmembrane potential. *Biophysical Journal* 59, 209-220.

Hofmann, U., Michaelis, S., Winckler, T., Wegener, J., and Feller, K.-H. (2012) A whole-cell biosensor as in vitro alternative to skin irritation tests. *Biosensors and Bioelectronics*, 156-162.

Itokazu, Y., Pagano, R.E., Schroeder, A.S., O'Grady, S.M., Limper, A.H., and Marks, D.L. (2014) Reduced GM1 ganglioside in CFTR-deficient human airway cells results in decreased beta1-integrin signaling and delayed wound repair. *American Journal of Physiology: Cell Physiology* 306, C819-C830.

Jain, T., McBride, R., Head, S., and Saez, E. (2009) Highly parallel introduction of nucleic acids into mammalian cells grown in microwell arrays. *Lab Chip* 9, 3557-3566.

Jain, T., and Muthuswamy, J. (2007) Microsystem for transfection of exogenous molecules with spatio-temporal control into adherent cells. *Biosensors and Bioelectronics* 22, 863–870.

Jain, T., Papas, A., Jadhav, A., McBride, R., and Saez, E. (2012) In situ electroporation of surface-bound siRNAs in microwell arrays. *Lab Chip* 12, 939-947.

Kandušer, M., and Miklavčič, D. (2008) Electroporation in biological cell and tissue: an overview. In Electrotechnologies for extraction from food plants and biomaterials (Springer New York), pp. 1-37.

Kaner, A., Braslavsky, I., and Rubinsky, B. (2014) Model of pore formation in a single cell in a flow-through channel with micro-electrodes. *Biomedical Microdevices* 16, 181-189.

Keese, C.R., Wegener, J., Walker, S.R., and Giaever, I. (2004) Electrical wound-healing assay for cells in vitro. *Proceedings of the National Academy of Sciences of the United States of America* 101, 1554-1559.

Kinosita, K., and Tsong, T.Y. (1979) Voltage-induced conductance in human erythrocyte membranes. *Biochimica et Biophysica Acta (BBA) - Biomembranes* 554, 479-497.

Klenchin, V.A., Sukharev, S.I., Serov, S.M., Chernomordik, L.V., and Chizmadzhev Yu, A. (1991) Electrically induced DNA uptake by cells is a fast process involving DNA electrophoresis. *Biophysical Journal* 60, 804-811.

Kling, B., Bucherl, D., Palatzky, P., Matysik, F.M., Decker, M., Wegener, J., and Heilmann, J. (2014) Flavonoids, flavonoid metabolites, and phenolic acids inhibit oxidative stress in the neuronal cell line HT-22 monitored by ECIS and MTT assay: a comparative study. *Journal of Natural Products* 77, 446-454.

Koda, S., Inoue, Y., and Iwata, H. (2008) Gene transfection into adherent cells using electroporation on a dendrimer-modified gold electrode. *Langmuir* 24, 13525-13531.

Kotnik, T., Bobanovic, F., and Miklavcic, D. (1997) Sensitivity of transmembrane voltage induced by applied electric fields-a theoretical analysis. *Bioelectrochemistry and Bioenergetics* 43, 285-291.

Kotnik, T., Pucihar, G., and Miklavcic, D. (2010) Induced transmembrane voltage and its correlation with electroporation-mediated molecular transport. *The Journal of Membrane Biology* 236, 3-13.

Lisdat, F., and Schafer, D. (2008) The use of electrochemical impedance spectroscopy for biosensing. *Analytical and Bioanalytical Chemistry* 391, 1555-1567.

Liu, Q., Yu, J., Xiao, L., Tang, J.C.O., Zhang, Y., Wang, P., and Yang, M. (2009) Impedance studies of bio-behavior and chemosensitivity of cancer cells by micro-electrode arrays. *Biosensors and Bioelectronics* 24, 1305-1310.

Lo, C.-M., Keese, C.R., and Giaever, I. (1995) Impedance analysis of MDCK cells measured by electric cell-substrate impedance sensing. *Biophysical Journal* 69, 2800-2807.

Lo, C.M., Keese, C.R., and Giaever, I. (1993) Monitoring motion of confluent cells in tissue culture. *Experimental Cell Research* 204, 102-109.

Lovelady, D.C., Friedman, J., Patel, S., Rabson, D.A., and Lo, C.M. (2009) Detecting effects of low levels of cytochalasin B in 3T3 fibroblast cultures by analysis of electrical noise obtained from cellular micromotion. *Biosensors and Bioelectronics* 24, 2250-2254.

Lu, H., Schmidt, M.A., and Jensen, K.F. (2005) A microfluidic electroporation device for cell lysis. *Lab Chip* 5, 23-29.

Luft, C., and Ketteler, R. (2015) Electroporation knows no boundaries: the use of electrostimulation for siRNA delivery in cells and tissues. *Journal of Biomolecular Screening* 8, 932-942.

Lukic, S., and Wegener, J. (2015) Impedimetric monitoring of cell-based assays. In Encyclopedia of Life Sciences (John Wiley & Sons, Ltd.), pp. 1–8.

Macdonald, D.D. (2006) Reflections on the history of electrochemical impedance spectroscopy. *Electrochimica Acta* 51, 1376-1388.

Male, K.B., Hamzeh, M., Montes, J., Leung, A.C.W., and Luong, J.H.T. (2013) Monitoring of potential cytotoxic and inhibitory effects of titanium dioxide using on-line and non-invasive cell-based impedance spectroscopy. *Analytica Chimica Acta* 777, 78– 85.

Marszalek, P., Liu, D.S., and Tsong, T.Y. (1990) Schwan equation and transmembrane potential induced by alternating electric field. *Biophysical Journal* 58, 1053-1058.

Meaking, W.S., Edgerton, J., Wharton, C.W., and Meldrum, R.A. (1995) Electroporation-induced damage in mammalian cell DNA. *Biochimica et Biophysica Acta* 27, 357-362.

Müller, K.J., Horbaschek, M., Lucas, K., Zimmermann, U., and Sukhorukov, V.L. (2003) Electrotransfection of anchorage-dependent mammalian cells. *Experimental Cell Research* 288, 344-353.

Naumowicz, M., and Figaszewski, Z.A. (2013) Pore formation in lipid bilayer membranes made of phosphatidylcholine and cholesterol followed by means of constant current. In Cell Biochemistry and Biophysics (New York: Springer-Verlag), pp. 109-119.

Neumann, E. (1989) The relaxation hysteresis of membrane electroporation. (Plenum Press, New York, London).

Neumann, E., Kakorin, S., and Toensing, K. (1999) Fundamentals of electroporative delivery of drugs and genes. *Bioelectrochemistry and Bioenergetics* 48, 3-16.

Neumann, E., and Rosenheck, K. (1972) Permeability changes induced by electric impulses in vesicular membranes. *The Journal of Membrane Biology* 10, 279-290.

Neumann, E., Schaefer-Ridder, M., Wang, Y., and Hofschneider, P.H. (1982) Gene transfer into mouse lyoma cells by electroporation in high electric fields. *The EMBO Journal* 1, 841-845.

Olbrich, M., Rebollar, E., Heitz, J., Frischauf, I., and Romanin, C. (2008) Electroporation chip for adherent cells on photochemically modified polymer surfaces. *Applied Physics Letters* 92

Olofsson, J., Levin, M., Stromberg, A., Weber, S.G., Ryttsen, F., and Orwar, O. (2005) Generation of focused electric field patterns at dielectric surfaces. *Analytical Chemistry* 77, 4667-4672.

Olofsson, J., Levin, M., Stromberg, A., Weber, S.G., Ryttsen, F., and Orwar, O. (2007) Scanning electroporation of selected areas of adherent cell cultures. *Analytical Chemistry* 79, 4410-4418.

Orio, J., Coustets, M., Mauroy, C., and Teissie, J. (2012) Electric Field Orientation for Gene Delivery Using High-Voltage and Low-Voltage Pulses. *The Journal of Membrane Biology* 245, 661-666.

Pakhomov, A.G., Gianulis, E., Vernier, P.T., Semenov, I., Xiao, S., and Pakhomova, O.N. (2015) Multiple nanosecond electric pulses increase the number but not the size of long-lived nanopores in the cell membrane. *Biochimica et Biophysica Acta* 4, 958-966.

Peng, H.S., Stolwijk, J.A., Sun, L.N., Wegener, J., and Wolfbeis, O.S. (2010) A nanogel for ratiometric fluorescent sensing of intracellular pH values. *Angewandte Chemie International Edition* 49, 4246-4249.

Phez, E., Faurie, C., Golzio, M., Teissie, J., and Rols, M.-P. (2005) New insights in the visualization of membrane permeabilization and DNA/membrane interaction of cells submitted to electric pulses. *Biochimica et Biophysica Acta* 1724, 248 – 254.

Pucihar, G., Kotnik, T., Miklavcic, D., and Teissie, J. (2008) Kinetics of transmembrane transport of small molecules into electropermeabilized cells. *Biophysical Journal* 95, 2837–2848.

Ramos, C., and Teissié, J. (2000) Tension-voltage relationship in membrane fusion and its implication in exocytosis. *FEBS Letters* 465, 141-144.

Raptis, L., Balboa, V., Hsu, T., Vultur, A., Turkson, J., Jove, R., and Firth, K.L. (2003) In situ electroporation of large numbers of cells using minimal volumes of material. *Analytical Biochemistry* 317, 124–128.

Raptis, L., and Firth, K.L. (1990) Electroporation of adherent cells in situ. *DNA and Cell Biology* 9, 615-621.

Raptis, L.H., Firth, K.L., Brownell, H.L., Todd, A., Simon, W.C., Bennett, B.M., MacKenzie, L.W., and Zannis-Hadjopoulos, M. (1995a) Electroporation of adherent cells in situ for the introduction of nonpermeant molecules. *Methods in Molecular Biology* 48, 93-113.

Raptis, L.H., Liu, S.K., Firth, K.L., Stiles, C.D., and Alberta, J.A. (1995b) Electroporation of peptides into adherent cells in situ. *Biotechniques* 18, 104-114.

Rols, M.P. (2006) Electropermeabilization, a physical method for the delivery of therapeutic molecules into cells. *Biochimica et Biophysica Acta* 1758, 423–428.

Rols, M.P. (2008) Mechanism by which electroporation mediates DNA migration and entry into cells and targeted tissues. *Methods in Molecular Biology* 423, 19-33.

Rols, M.P., Golzio, M., Delteil, C., and Teissié, J. (2000) In vitro delivery of drugs and other molecules to cells. *Methods in Molecular Medicine* 37, 83-97.

Rols, M.P., and Teissié, J. (1990) Electropermeabilization of mammalian cells. Quantitative analysis of the phenomenon. *Biophysical Journal* 58, 1089-1098.

Rols, M.P., and Teissié, J. (1992) Experimental evidence for the involvement of the cytoskeleton in mammalian cell electropermeabilization. *Biochimica et Biophysica Acta* 19, 45-50.

Rols, M.P., and Teissié, J. (1998) Electropermeabilization of mammalian cells to macromolecules: control by pulse duration. *Biophysical Journal* 75, 1415-1423.

Santra, T.S., Wang, P.-C., and Tseng, F.G. (2013) Electroporation based drug delivery and its applications. In Advances in micro/nano electromechanical systems and fabrication technologies (InTech)

Saulis, G., Satkauskas, S., and Praneviciute, R. (2007) Determination of cell electroporation from the release of intracellular potassium ions. *Analytical Biochemistry* 360, 273–281.

Saulis, G., and Saule, R. (2012) Size of the pores created by an electric pulse: microsecond vs millisecond pulses. *Biochimica et Biophysica Acta* 12, 2.

Schonenberger, C., Schutz, A., Franco-Obregon, A., and Zenobi-Wong, M. (2011) Efficient electroporation of peptides into adherent cells: investigation of the role of mechano-growth factor in chondrocyte culture. *Biotechnology Letters* 33, 883-888.

Scott, C.W., and Peters, M.F. (2010) Label-free whole-cell assays: expanding the scope of GPCR screening. *Drug Discovery Today* 15, 704-716.

Smith, K.C., Neu, J.C., and Krassowska, W. (2004) Model of creation and evolution of stable electropores for DNA delivery. *Biophysical Journal* 86, 2813-2826.

Sozer, E.B., Wu, Y.H., Romeo, S., and Vernier, P.T. (2016) Nanometer-scale permeabilization and osmotic swelling induced by 5-ns pulsed electric fields. *The Journal of Membrane Biology* 19, 19.

Sperber, M. (2016) Impedance-based analysis of the cellular response to microparticles: Theory, assay development and model study. PhD Thesis, Universität Regensburg

Sperber, M., Hupf, C., Lemberger, M.-M., Goricnik, B., Hinterreiter, N., Lukic, S., Oberleitner, M., Stolwijk, J.A., and Wegener, J. (2016) Monitoring the impact of nanomaterials on animal cells by impedance analysis: a noninvasive, label-free, and multimodal approach. In Measuring Biological Impacts of Nanomaterials, J. Wegener, ed. (Springer International Publishing), pp. 45-108.

Stolwijk, J.A. (2012) Electric manipulation and impedance analysis of adherent cells on gold-film electrodes. PhD thesis, Universität Regensburg

Stolwijk, J.A., Hartmann, C., Balani, P., Albermann, S., Keese, C.R., Giaever, I., and Wegener, J. (2011) Impedance analysis of adherent cells after in situ electroporation: Non-invasive monitoring during intracellular manipulations. *Biosensors and Bioelectronics* 26, 4720–4727.

Stolwijk, J.A., Matrougui, K., Renken, C.W., and Trebak, M. (2014) Impedance analysis of GPCR-mediated changes in endothelial barrier function: overview and fundamental considerations for stable and reproducible measurements. *Pflügers Archiv* 10, 2193-2218.

Stolwijk, J.A., Michaelis, S., and Wegener, J. (2012) Cell growth and cell death studied by electric cell-substrate impedance sensing. In Electric cell-substrate impedance sensing and cancer metastasis, W.G. Jiang, ed. (Dordrecht: Springer Netherlands), pp. 85-117.

Szulcek, R., Bogaard, H.J., and van Nieuw Amerongen, G.P. (2014) Electric cell-substrate impedance sensing for the quantification of endothelial proliferation, barrier function, and motility. *Journal of Visualized Experiments:JoVE* 28, 51300.

Tarantola, M., Schneider, D., Sunnick, E., Adam, H., Pierrat, S., Rosman, C., Breus, V., Sonnichsen, C., Basche, T., Wegener, J., et al. (2009) Cytotoxicity of metal and semiconductor nanoparticles indicated by cellular micromotility. *ACS Nano* 3, 213-222.

Tarek, M. (2005) Membrane electroporation: a molecular dynamics simulation. *Biophysical Journal* 88, 4045-4053.

Teissié, J. (2007) Biophysical effects of electric fields on membrane water interfaces: a mini review. *European Biophysics Journal* 36, 967-972.

Teissié, J., Golzio, M., and Rols, M.P. (2005) Mechanisms of cell membrane electropermeabilization: A minireview of our present (lack of ?) knowledge. *Biochimica et Biophysica Acta* 1724, 270–280.

Teissié, J., and Rols, M.P. (1993) An experimental evaluation of the critical potential difference inducing cell membrane electropermeabilization. *Biophysical Journal* 65, 409-413.

Teissié, J., and Rols, M.P. (1994) Manipulation of cell cytoskeleton affects the lifetime of cell membrane electropermeabilization. *Annals of the New York Academy of Sciences* 720, 98-110.

Tekle, E., Astumian, R.D., and Chock, P.B. (1994) Selective and asymmetric molecular transport across electroporated cell membranes. *Proceedings of the National Academy of Sciences of the United States of America* 91, 11512-11516.

Teruel, M.N., Blanpied, T.A., Shen, K., Augustine, G.J., and Meyer, T. (1999) A versatile microporation technique for the transfection of cultured CNS neurons. *Journal of Neuroscience Methods* 93, 37-48.

Teruel, M.N., and Meyer, T. (1997) Electroporation-induced formation of individual calcium entry sites in the cell body and processes of adherent cells. *Biophysical Journal* 73, 1785-1796.

Tomai, E., Vultur, A., Balboa, V., Hsu, T., Brownell, H.L., Firth, K.L., and Raptis, L. (2003) In situ electroporation of radioactive compounds into adherent cells. *DNA and Cell Biology* 22, 339-346.

Towhidi, L., Khodadadi, D., Maimari, N., Pedrigi, R.M., Ip, H., Kis, Z., Kwak, B.R., Petrova, T.W., Delorenzi, M., and Krams, R. (2016) Comparison between direct and reverse electroporation of cells in situ: a simulation study. *Physiological Reports* 4

Tsong, T.Y. (1991) Electroporation of cell membranes. *Biophysical Journal* 60, 297-306.

Vernhes, M.C., Cabanes, P.A., and Teissié, J. (1999) Chinese hamster ovary cells sensitivity to localized electrical stresses. *Bioelectrochemistry and Bioenergetics* 48, 17-25.

Wang, X.D., Stolwijk, J.A., Lang, T., Sperber, M., Meier, R.J., Wegener, J., and Wolfbeis, O.S. (2012) Ultra-small, highly stable, and sensitive dual nanosensors for imaging intracellular oxygen and pH in cytosol. *Journal of the American Chemical Society* 134, 17011-17014.

Wasungu, L., Escoffre, J.-M., Valette, A., Teissié, J., and Rols, M.-P. (2009) A 3D in vitro spheroid model as a way to study the mechanisms of electroporation. *International Journal of Pharmaceutics* 379, 278–284.

Weaver, J.C. (2003) Electroporation of biological membranes from multicellular to nano scales. *IEEE Transactions on Dielectrics and Electrical Insulation* 10, 754-768.

Weaver, J.C., and Chizmadzhev, Y.A. (1996) Theory of electroporation: A review. *Bioelectrochemistry and Bioenergetics* 41, 135-160.

Weaver, J.C., and Powell, K.T. (1989) Theory of electroporation. In Electroporation and Electrofusion in Cell Biology, E. Neumann, A.E. Sowers, and C.A. Jordan, eds. (Plenum Press), pp. 111-126.

Wegener, J. (2010) Impedance analysis of cell junctions. *Nanotechnology* 6, 325-357.

Wegener, J., Keese, C.R., and Giaever, I. (2000) Electric cell-substrate impedance sensing (ECIS) as a noninvasive means to monitor the kinetics of cell spreading to artificial surfaces. *Experimental Cell Research* 259, 158-166.

Wegener, J., Keese, C.R., and Giaever, I. (2002) Recovery of adherent cells after in situ electroporation monitored electrically. *Biotechniques* 33, 348 - 352.

Wegener, J., and Seebach, J. (2014) Experimental tools to monitor the dynamics of endothelial barrier function: a survey of in vitro approaches. *Cell Tissue Research* 355, 485–514.

Wegener, J., Sieber, M., and Galla, H.-J. (1996) Impedance analysis of epithelial and endothelial cell monolayers cultured on gold surfaces. *Journal of biochemical and biophysical methods* 32, 151-170.

Wegener, J., Zink, S., Rosen, P., and Galla, H. (1999) Use of electrochemical impedance measurements to monitor beta-adrenergic stimulation of bovine aortic endothelial cells. *Pflügers Archiv – European Journal of Physiology* 437, 925-934.

Widder, M.W., Brennan, L.M., Hanft, E.A., Schrock, M.E., James, R.R., and van der Schalie, W.H. (2015) Evaluation and refinement of a field-portable drinking water toxicity sensor utilizing electric cell-substrate impedance sensing and a fluidic biochip. *Journal of Applied Toxicology* 35, 701-708.

Wolf, H., Rols, M.P., Boldt, E., Neumann, E., and Teissié, J. (1994) Control by pulse parameters of electric field-mediated gene transfer in mammalian cells. *Biophysical Journal* 66, 524-531.

Xiao, C., Lachance, B., Sunahara, G., and Luong, J.H.T. (2002) Assessment of cytotoxicity using electric cell-substrate impedance sensing: concentration and time response function approach. *Analytical Chemistry* 74, 5748-5753.

Yamauchi, F., Kato, K., and Iwata, H. (2004) Spatially and temporally controlled gene transfer by electroporation into adherent cells on plasmid DNA-loaded electrodes. *Nucleic Acids Research* 32, e187.

Yang, T.A., Heiser, W.C., and Sedivy, J.M. (1995) Efficient in situ electroporation of mammalian cells grown on microporous membranes. *Nucleic Acids Research* 23, 2803-2810.

Zhan, Y., Sun, C., Cao, Z., Bao, N., Xing, J., and Lu, C. (2012) Release of intracellular proteins by electroporation with preserved cell viability. *Analytical Chemistry* 84, 8102−8105.

Zheng, Q.A., and Chang, D.C. (1991) High-efficiency gene transfection by in situ electroporation of cultured cells. *Biochimica et Biophysica Acta* 17, 104-110.

Zimmermann, U., Pilwat, G., and Riemann, F. (1974) Dielectric breakdown of cell membranes. *Biophysical Journal* 14, 881-899.

4 Materials and Methods

4.1 Cell Culture Techniques

All work with mammalian cells was conducted according to the standard procedures and requirements of a cell culture laboratory. An overview of the cell lines used in this thesis, protocols for cell cultivation and preparation of the cells for experimental procedures are provided in the following subchapters.

4.1.1 Cell Lines

Experiments within this work were conducted with several different mammalian cell lines, grown as anchorage dependent (adherent) cultures: BAEC (bovine aortic endothelial cells), CHO-K1 (Chinese hamster ovary), CHO-GFP (Chinese hamster ovary cells genetically modified to express EGFP), HaCaT (human immortalized keratinocytes), NRK-52E (normal rat kidney cells, strain E52) and the fibroblastoid cell line NIH-3T3 (albino mouse embryo). Cell lines NRK-E52 and NIH-3T3 were obtained from the Leibniz-Institute DSMZ-German Collection of Microorganisms and Cell Cultures (Braunschweig, Germany). HaCaT cells were purchased from Cell Lines Service (CLS, Eppelheim, Germany), as a distributer of the German Cancer Research Center (DKFZ, Heidelberg, Germany). Bovine aortic endothelial cells (BAEC) were kindly provided by the Institute of Biochemistry of the University of Muenster. All cell lines and the most relevant details related to them are listed in a **Table 4.1**.

Table 4.1 List of the cell lines used in this work, along with their origin and relevant literature sources

Cell Line	Species	Cell Type	Purchase Source (No.)	Literature
BAEC	Bovine	Endothelial	/	Schwartz, 1978; Zink et al., 1993
CHO-K1	Chinese hamster	Ovary	/	Tjio and Puck, 1958; Kao and Puck, 1968
HaCaT	Human	Keratinocyte (skin)	CLS (300493)	Boukamp et al., 1988
NIH-3T3	Murine (Swiss mouse)	Fibroblast	DSMZ (ACC 59)	Jainchill et al., 1969
NRK-52E	Rat	Epithelial-like (clone 52E)	DSMZ (ACC 199)	de Larco and Todaro, 1978

For many gene silencing studies within this work, CHO-K1 cells chemically transfected to stably express enhanced green fluorescence protein (EGFP) were used. This cell line is for

convenience called CHO-GFP, although it is genetically modified to stably possess genes responsible for EGFP expression (CHO-K1/EGFP). Both cell lines, unmodified wild cell type CHO-K1 and genetically modified CHO-GFP were kindly provided by PD Dr. Miriam Breunig and Prof. Dr. Achim Göpferich from the Department of Pharmaceutical Technology (Faculty of Chemistry and Pharmacy) of the University of Regensburg. Their group conducted complete generation of CHO-GFP cells stably transfected with plasmid pEGFP-N1 (Breunig et al. 2008).

4.1.2 General Culture Conditions and Monolayer Subculturing

To ensure viability and reproducible growth of mammalian cells, they have to be maintained at 37 °C. Therefore, the cells were kept inside the humidified cell culture incubator where parameters are set to provide temperature of 37 °C and atmosphere with 5 % CO_2 and 95 % air. The entire cell culture work was conducted under sterile conditions in a laminar cell culture flow hood, according to standard cell culture procedures and requirements (Freshney, 2006, Freshney, 2005; Mericko et al., 2002). For subculturing and cell handling, sterile ready-to-use plastic disposables were mostly used, whereas non-sterile plasticware (e.g. pipette tips, tubes, etc.) and laboratory glassware was sterilized (in an autoclave) prior to use. Also, the majority of solutions used for routine cell culture and experiments (e.g. culture media, buffers, etc.) were purchased as already sterile, whereas all unsterile solutions (e.g. Milli-Q water) were autoclaved before use. All items (e.g. pipette controller, pipettes, tube racks, bottles, etc.) were cleaned with 70 % (v/v) ethanol before placing them inside the flow hood.

In order to assure cellular viability, stability and their normal living functions, regular subcultivation of the cells is necessary to maintain them in exponential growth. During this process, cells are split and seeded to new culture flasks (passage), according to standard subculturing protocol (Freshney, 2005). For some cell lines it is necessary to passage them before they reach full confluence (NIH-3T3: 70 - 80 % confluence; CHO-K1, CHO-GFP and HaCaT: ~ 80 % confluence; BAEC: ~ 90 % confluence), whereas NRK cells should be passaged shortly after they establish fully confluent cell monolayer. This implies that some cell lines were subcultured only once and some cell lines twice a week.

Adherent cell lines were maintained in culture by growing them on the bottom of sterile plastic culture flasks with the growth areas of either 25 cm^2 (T 25) or 75 cm^2 (T 75), in 4 or 10 mL of culture medium, respectively. Each cell line was cultured in a corresponding growth medium, with formulation adjusted for each cell type and supplemented with certain amounts of serum, antibiotics and L-glutamine. Ham's F-12 and Dulbecco's Modified Eagle's Medium (DMEM) with 3.7 g/L $NaHCO_3$ and either 1.0 g/L or 4.5 g/L D-glucose were used as basic cell

culture medium. They were supplemented with fetal bovine serum (FBS) to assure normal cell growth. Furthermore, the amino acid L-glutamine has to be added to the media, as an important factor for cell growth and function. The antibiotics penicillin and streptomycin were added to the medium to prevent cell culture contamination. **Table 4.2** summarizes applied culture media and corresponding amounts of supplements required for each cell line.

Table 4.2 Cell lines, basic culture medium and individual medium supplements.

Cell Line	Basal Medium	Supplementation
BAEC	DMEM with 3.7 g/L $NaHCO_3$ and 1.0 g/L D-glucose	10 % (v/v) FBS 100 µg/mL penicillin 100 µg/mL streptomycin 4 mM L-glutamine
CHO-K1	Ham's F-12	10 % (v/v) FBS 100 µg/mL penicillin 100 µg/mL streptomycin 2 mM L-glutamine
CHO-GFP	Ham's F-12	10 % (v/v) FBS 100 µg/mL penicillin 100 µg/L streptomycin 2 mM L-glutamine 400 µg/mL G418
HaCaT	DMEM with 3.7 g/L $NaHCO_3$ and 4.5 g/L D-glucose	10 % (v/v) FBS 100 µg/mL penicillin 100 µg/mL streptomycin 2 mM L-glutamine
NIH-3T3	DMEM with 3.7 g/L $NaHCO_3$ and 4.5 g/L D-glucose	10 % (v/v) FBS 100 µg/mL penicillin 100 µg/mL streptomycin 4 mM L-glutamine
NRK-52E	DMEM with 3.7 g/L $NaHCO_3$ and 4.5 g/L D-glucose	5 % (v/v) FBS 100 µg/mL penicillin 100 µg/mL streptomycin 2 mM L-glutamine

For the subcultivation of anchorage-dependent cells within this work, established general procedures (Freshney, 2005) have been used that are briefly described below. Considering that every cell line is specific, incubation times, number of washes or centrifugation parameters may vary from cell line to cell line.

Firstly, cell culture medium was removed out of the flask and the cell monolayer was washed twice with pre-warmed (37 °C) phosphate-buffered saline without Ca^{2+} or Mg^{2+} (PBS^{--}).

Provided in a sterile and ready-to-use form by a producer, PBS^{--} contains: 140 mM NaCl, 2.7 mM KCl, 8.1 mM Na_2HPO_4 and 1.5 mM KH_2PO_4 in deionized ultrapure water. As some cell lines form rather strong cell-surface contacts (HaCaT, NIH-3T3 and NRK), those cells have to be incubated with pre-warmed (37 °C) 1mM EDTA solution in PBS^{--} for a certain period of time (**Table 4.3**), whereas other cell lines (BAEC, CHO-K1 and CHO-GFP) adhere loosely to the surface. These cell lines were only briefly washed with EDTA solution. In a next step, a small amount of 0.05 % (w/v) trypsin-EDTA solution in PBS^{--} (thawed to 4 °C or to RT) was added to the cell layer. Only for NIH-3T3 cells 0.25 % (w/v) trypsin-EDTA solution in PBS^{--} was used. Incubation at 37 °C followed and, depending on a cell line, it took from 1 to 10 min. To support detaching of NRK cells from the substrate after trypsination, culture flasks were tapped gently to a solid surface. The trypsination step was followed by the addition of an extensive amount of cell culture medium in order to inactivate trypsin and prepare the cells for centrifugation.

Table 4.3 Subculturing protocol is similar for all cell lines. The main differences are the incubation times with EDTA/ PBS^{--} and trypsin-EDTA. Also, time span between consecutive subculturing differs from cell line to cell line.

Cell Line	Incubation Time with EDTA [min]	Incubation Time with Trypsin [min]	Time Span between Consecutive Subculturing [d]
BAEC	Only washing	2	4 – 7
CHO-K1	Only washing	2	3 – 4
CHO-GFP	Only washing	2	3 – 4
HaCaT	10 – 15	1 – 2	3 – 4
NIH-3T3	2	2 – 3	3 – 4
NRK-E52	8 – 10	8 – 10	7

Cells were gently resuspended two or three times in a medium and transferred into a centrifuge tube. Centrifugation of BAEC, CHO K1, CHO-GFP, NIH 3T3 and NRK-E52 cells was performed at 21 °C with 110 g for 10 min. Centrifugation of HaCaT cells was performed with 200 g for 5 min. After centrifugation, the cell pellet was gently resuspended several times in the corresponding cell culture medium (3-5 mL for T 25 flasks and 10 mL for T 75 flasks) and the cell suspension was subsequently filled into previously prepared culture flasks. The dilution ratio with which the cells were split and seeded into new flasks was dependent on cell line and cell age. Thereafter, flasks with the cells were placed into the

incubator. Their attachment and growth in the following days was controlled regularly using an inverted microscope. Culture medium of cells being passaged once a week (NRK and BAEC) was exchanged 3 or 4 days after seeding, sometimes also one day before the next passaging.

In order to keep selection pressure on the genetically-modified cell line CHO-GFP, the presence of the antibiotic G418 in culture medium is required. This aminoglycoside antibiotic was added to cells with a concentration of 400 µg/mL.

4.1.3 Cryopreservation

The long-term storage of the cells is possible by keeping them at temperatures below −130 °C, typically at −196 °C in a freezer loaded with liquid nitrogen. Cryopreservation is a standard procedure including first freezing of the cells slowly to the temperature below −80°C and then placing them into a liquid nitrogen tank at −196 °C. Before the cells are being frozen, they have to be suspended in a special cryoprotective solution, which contains 90 % (v/v) FCS and 10 % (v/v) dimethylsulfoxide (DMSO). DMSO acts as a cryoprotective agent during the freezing process because it prevents the formation of small ice crystals within the cells, by penetrating the cell membrane and reducing the water content in the cytoplasm, thus dehydrating the cells.

Before cryopreservation, cells were usually grown to confluence in the plastic flasks with the bigger growth area T 75 (75 cm^2), in order to obtain larger amounts of cells for freezing. Thereby, the standard subculturing protocol (Freshney, 2005) was applied, as described in a previous chapter 4.1.2. After collecting the cells by centrifugation, the cell pellet was resuspended in the cryoprotective solution, containing FCS and DMSO and split into small cryovials (as 1.8 mL aliquots), which were placed into a freezing container (chamber), where cells were frozen slowly with a cooling rate of −1 °C/minute down to −80 °C. Two days afterwards, cryovials containing frozen cells were finally stored at −196 °C in a liquid nitrogen tank. Thawing of the cryopreserved cells was done according to the following protocol. After taking the cryovial with cells out of the liquid nitrogen tank, it was immediately placed into a freezer at −20 °C, where the cells inside the cryovial could unfreeze slowly during 1 – 1.5 h. Complete thawing of the cells was initiated by keeping the cryovial in a water bath (at 37 °C) for 2-3 minutes, just enough to be able to release the cell suspension out of the cryovial. Thereafter, the cell suspension was transferred quickly into a centrifugation tube and it was diluted very slowly by addition of app. 18 mL of pre-warmed culture medium. The first 3 mL of cell culture medium were added dropwise. The remaining steps within this procedure were identical as for regular cell subculturing. Cells were centrifuged and the collected cell pellet

was slowly and carefully resuspended in fresh pre-warmed culture medium. The suspension of freshly thawed cells was divided into small culture flasks (T 25) containing pre-warmed culture medium. Dilution ratios were 1:2, 1:4 and 1:8 with respect to the former growth area. Cell attachment and growth was controlled in the following days, by observing the cells using the inverted microscope. Cell culture medium was exchanged 24 h after thawing and further subculturing was performed according to the standard protocol described in chapter 4.1.2, as soon as the cells reached the confluent state.

4.1.4 Preparation of Cellular Monolayers for Experiments

After applying the standard subculturing protocol described in chapter 4.1.2, cells were seeded into the cultureware for an experiment (ECIS electrode array or a Petri dish) at an appropriate cell density and in a corresponding volume. Cell counting took place after cells were being centrifuged and resuspended in the fresh cell culture medium. A small amount of cell suspension (30 µL) was taken out of the centrifuge tube and was pipetted between a thick glass slide and a small cell counting chamber, called Buerker hemocytometer in order to count the cells in the several fields (quadrants) of the hemocytometer (by observing them with the 10-fold magnification objective of the inverted microscope). After an average number of cells in the cell suspension was determined, dilution(s) of the cell suspension were prepared, if necessary. Thus prepared cell suspension(s) with the specific number of cells per milliliter (cells/mL) were seeded into the corresponding cultureware(s) for the experiment.
Cells were always counted before seeding them into cultureware prior to the experiment in order to maintain, as much as possible, the same cell density in all experiments with the same cell line. The appropriate cell number for experiments was optimized and standardized for each cell line separately. Different cell lines and their corresponding cell densities as applied in the experiments are summarized in **Table 4.4**. Cell densities are recalculated from cells/mL and expressed as cells/cm^2. Depending on the experiment (e.g. electroporation, wounding, chemical transfection, etc.) and the characteristics of each cell line, cells were seeded one (24 h) or two days (48 h) before the experiment. **Table 4.4** summarizes seeding densities for each cell line with respect to the time span between cell seeding and the experiment. Thus, for example, cells were seeded 48 h before electroporation or wounding and 24 h prior to chemical transfection or stimulation of the cells by second messengers.
To prepare wells of the cultureware (ECIS electrode array and Petri dish) and thus enable better adherence of the cells to the substrate, fresh cell culture medium (complete or serum-free) was added in an appropriate volume to each well 1 – 24 hours prior to cell seeding. Such pre-treatment is especially recommended for ECIS electrode arrays, as it assists better

attachment and spreading of the cells on the substrate. After the cell suspension was seeded upon the substrate, the electrode array or Petri dish with cells were left inside the flow hood (at RT) for additional 10 – 20 min, before they were finally placed into the incubator. This allows the cells to settle down on the substrate and start formation of cell-substrate contacts. Otherwise, sudden change of a temperature may disturb cells from adhering to the substrates, as they are transported convectively to the edges of the wells, thus leaving the center of the well (where electrodes are) less populated.

Table 4.4 Cell lines and their corresponding seeding densities dependent on the time prior to experiment.

Cell Line	Cell Density Seeded 48 h before Experiment [cells / cm^2]	Cell Density Seeded 24 h before Experiment [cells / cm^2]
BAEC	80 000	90 000
CHO-K1	/	80 000
CHO-GFP	/	80 000
HaCaT	220 000	240 000
NIH-3T3	100 000	200 000
NRK-E52	270 000	370 000 – 450 000

The attachment and spreading of the cells after seeding was monitored impedimetrically using ECIS, or it was occasionally controlled under the inverted microscope. Cell culture medium of the cells seeded 48 h before experiment was exchanged one day (app. 24 h) before experiment. All details on the electrode arrays and well size applied for different experiments, as well as on the working volumes, are given in chapters 4.2.1.2 and 4.2.1.3.

4.1.5 Coating of Culture Substrates with Adhesive Proteins

Cell lines BAEC, CHO-K1 and CHO-GFP form rather weak cell-substrate contacts and it is relatively easy for them to detach and dislodge from the substrate surface. This is particularly problematic when cells are electroporated, chemically transfected or exposed to consecutive washing steps prior to microscopy. Therefore, the growth substrates had to be coated with an adhesive protein prior to cell seeding and (cross-linked) gelatin was used for this purpose. Precoating protocol was applied both on ECIS electrode arrays and within the wells prepared inside Petri dish.

Firstly, 0.5 % (w/v) gelatin in Milli-Q was added to every well and was allowed to adsorb for 1.5 – 2 h at RT. After that, excess gelatin solution was removed, leaving the thin gelatin layer on the bottom of each well. Immediately afterwards, 2.5 % (v/v) glutaraldehyde (GDA) in Milli-Q was added to each well for 10 min at RT. GDA solution was removed and layer of a cross-linked gelatin was extensively washed (at least 10 times) with Milli-Q, in order to remove any excess of the cytotoxic GDA. The cross-linking with GDA improves the mechanical stability of the protein layer on the substrate surface (Reddy et al., 2008). These precoated substrates were kept under Milli-Q water at RT until cells were seeded onto them according to the standard protocol, usually on a next day. The volumes of gelatin solution, GDA solution and Milli-Q used for precoating protocol were adjusted to the size of wells. Different well types are presented and discussed in details in chapters 4.2.1.2 and 4.2.1.3. Briefly, besides regular 8-well chamber, small silicone tubes with the diameter of 3 and 5 mm served as the culture wells. The volumes of solutions applied for precoating protocol are listed in **Table 4.5**, with respect to the each well type.

Table 4.5 Depending on well type on the ECIS array (or inside the Petri dish) volumes of gelatin and GDA solutions, as well as of Milli-Q water (applied for extensive washing) were varied.

Type of the Well	Volume of Gelatin Solution / Well [µL]	Volume of Glutaraldehyde Solution / Well [µL]	Volume of Milli-Q / Well [µL]
8-Well Chamber	300	200	420
Ø 3 mm Silicone Tubes Inside the 8-Well Chamber	300	50	400
Ø 5 mm Silicone Tubes	60	40	80

4.1.6 Regeneration of Culture Substrates

The ECIS electrode arrays applied for experiments which did not involve cytotoxic molecules or any substances that might interfere with the substrate, have been reused. In that case, the electrode arrays were being regenerated immediately after the experiment and dried and stored until the next use. If the regeneration protocol was performed properly and the electrode array remained undamaged during experiments, it was reused several times. The regeneration protocol included steps very similar to those included in the standard

culturing protocol. After cells were rinsed twice with PBS^{--}, EDTA/PBS^{--} was added and incubation for 5 – 20 min at 37 °C followed. Thereafter, 0.05 % (w/v) trypsin-EDTA solution in PBS^{--} was added and the cells were incubated for 3 – 15 min at 37 °C. Detachment of the cells from the substrate surface was controlled under the inverted microscope. When all cells appeared round and completely dislodged from the substrate, they were removed and every well was extensively rinsed with Milli-Q or distilled water until all remnants were washed away. The electrode array was dried at RT and stored afterwards. Prior to next use, the electrode array was sterilized in Argon plasma for 20 – 27 s.

4.2 Electric Cell-Substrate Impedance Sensing Combined with *In Situ* Electroporation

Electric monitoring of adherent mammalian cells and manipulation of the cells by applying electric fields is based on the Electric Cell-Substrate Impedance Sensing (ECIS™) device. This highly automated impedance-based experimental technique has been first described around 30 years ago by Giaever and Keese (Giaever and Keese, 1984, 1986, 1991) and represents a versatile (multimodal) tool to monitor adherent cells on planar gold film electrodes electrically, in a non-invasive and label-free manner. The complex impedance provides information on the cellular monolayer under study in real time.

The key principle of this system and its non-invasive approach to the cells is based on a low amplitude sinusoidal AC voltage signal of varying frequency, being applied to the gold film electrodes deposited on the bottom of a conventional cultureware (cell culture vessel). Switching from the non-invasive to invasive mode for cell manipulation within the same system is possible by applying AC pulses with well-defined frequency, amplitude and duration to the cells on the electrodes. Using the invasive mode of ECIS device, either reversible transient cell membrane permeabilization (*in situ* electroporation) or irreversible cell membrane permeabilization, leading to cell damage (electric wounding), can be induced and combined with non-invasive cell monitoring. The non-invasive electrical monitoring of the events before, during and after application of electric pulses to the cells is carried out by recording the complex impedance in real time.

Therefore, the ECIS technique represents a powerful tool for an electrical observation of cell monolayers, which may be exposed to different kinds of stimuli. It is the main focus of the studies within this work to monitor cell response to different bioactive molecules delivered into confluent cells by *in situ* electroporation, with respect to the changes in cell morphology and viability.

4.2.1 Experimental Setup

The regular experimental setup applied to conduct assays using ECIS technique and all modifications which have been introduced due to cope with specific requirements of some studies are going to be described in the following sections.

4.2.1.1 Basic Measurement Setup

The basic measurement setup for impedance-based electric monitoring of adherent cells is schematically presented in **Figure 4.1** and it was applied for both, non-invasive impedimetric monitoring of cell monolayers, as well as for application of invasive electric pulses to the cells. The schematic illustration (adapted from Stolwijk, 2012) depicts the basic setup for the measurement. An electrode array was placed inside the regular cell culture incubator (with humidified 5 % CO_2 atmosphere at 37 °C), whereas all other parts of the electronic equipment remained outside the incubator. During the measurement, one or two electrode arrays, each containing 8 independent wells, were connected via a relay to an impedance analyzer (IA) and a frequency generator (FG). The role of the relay is to switch between different wells, making every well individually addressable for IA and FG. The micro-controller controls the relay and allows shifting between non-invasive mode (when IA is active) and invasive mode (when FG is active). A micro-controller, the relay, the impedance analyzer and the frequency generator were controlled by a personal computer (PC).

Two types of instrumentation can be distinguished here, although both are based on the measurement setup described above. A majority of experiments in this work was performed using a commercial ECIS 1600R device (Applied BioPhysics) which possesses all hardware (electronic) components (relay, impedance analyzer, frequency generator and micro-controller) integrated within one machine and applies an AC signal with frequency-dependent amplitudes. The user may select a single frequency measurement (SFT) or a multi frequency measurement (MFT) mode of data acquisition. When MFT mode was chosen, data acquisition included eleven different frequencies ranging from 62.5 to 64000 Hz (62.5, 125, 250, 500, 1000, 2000, 4000, 8000, 16000, 32000 and 64000 Hz). For electric manipulation (electroporation and electric wounding) of the cell monolayer, single invasive AC pulses were applied to the gold film electrodes with a frequency of 40 kHz (Wegener et al., 2002), whereas voltage amplitudes were varied in a range between 1 to 5 V and pulse durations in a range between 50 ms to 30 s. Evaluation of the measurements with the ECIS 1600R device was done with the commercial ECIS™ software (Applied BioPhysics).

For some experiments, particularly those engaging data acquisition with high time resolution, a special ECIS-based instrumentation with custom-made setup was used. This experimental

setup includes all essential electronic parts as individual components interfaced as depicted in **Figure 4.1**: relay, impedance analyzer (IA), frequency generator (FG), micro-controller and a personal computer (PC). This instrumental setup is capable of recording data at 51 individual frequencies, equally spaced on a logarithmic scale within a frequency range of 10^1 – 10^6 Hz (Stolwijk, 2012).

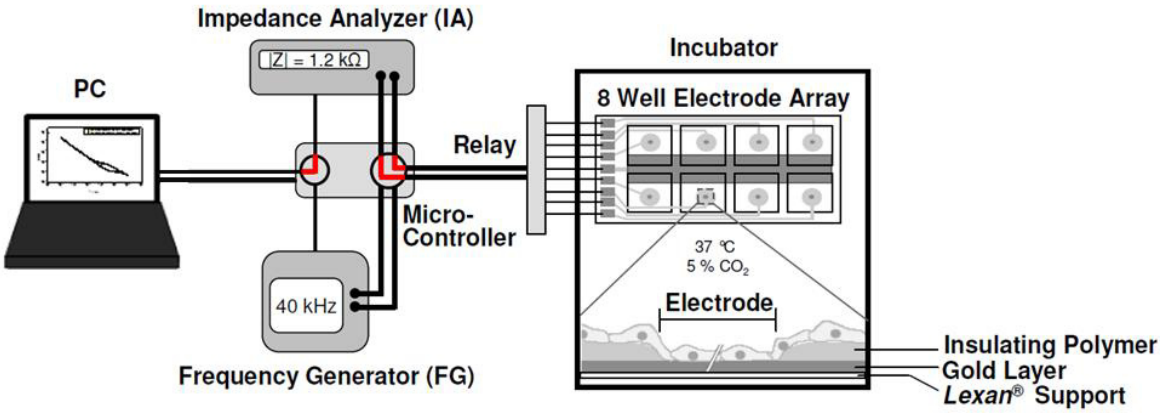

Figure 4.1 Basic experimental setup for impedance-based non-invasive monitoring of adherent cells and application of invasive electric pulses is presented by a schematic illustration. Switching between non-invasive and invasive mode is done by switching between the impedance analyzer (IA) and frequency generator (FG), with the help of a micro-controller connected to a personal computer (PC).

Sequential acquisition of impedance spectra in 8 wells was performed continuously with a time resolution of ~ 5.5 min. This was accomplished by applying an AC voltage at a preset frequency and amplitude of 50 mV to the electrodes. Experiments were controlled and evaluated with a LabView-based software (written by Prof. Dr. Joachim Wegener, University of Regensburg).

4.2.1.2 Electrode Arrays

There are different models of ECIS electrode arrays available, but for experiments in this work arrays containing 8 individual compartments (wells) were used. The thin gold film electrodes are deposited on the bottom of each individual well. The cultureware consisting of 8 wells has been created with a commercial chamber made of polystyrene, fixed and glued on the top of the electrode array and provided with the cover lid from the same material. Each individual well provides a cell growth area of 0.75 cm^2 and the liquid volume was typically kept in a range of 200 – 400 µL per well, with the possibility for further minimization (chapter 4.2.1.3). To protect them from a mechanical damage and to additionally assure

sterile conditions inside the wells, ECIS electrode arrays were always kept inside the sterile standard Petri dishes (100 x 20 mm), except during impedance measurements, when they were mounted in an array holder to provide their connection to the relay.

The ECIS culturewares were usually provided with a substrate made of polycarbonate (Lexan®), or polyethylene terephthalate (PET). The thin gold film electrode layout is deposited upon the substrate by sputter coating and subsequent photolithography. An insulating film made from photopolymer delineates the circular form of the electrode(s) with the diameter of 250 µm (www.biophysics.com). Thanks to the optical transparency of the gold film electrodes and their thickness of only ~ 100 nm, it is possible to observe the cells on the electrode surface even by routine light microscopy. **Figure 4.2** shows the monolayer of CHO-GFP cells grown on the top of the electrodes - insulating film substrate assembly.

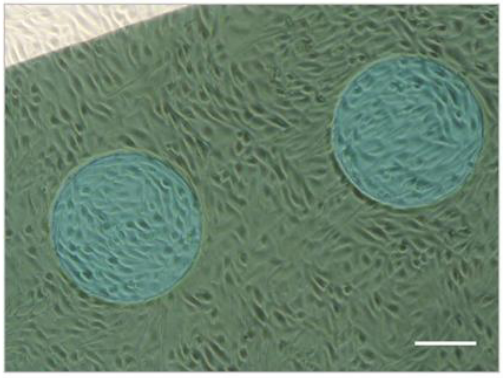

Figure 4.2 Exemplary phase-contrast micrograph shows the monolayer of CHO-GFP cells grown on the top of the electrode - insulating film substrate assembly (scale bar corresponds to 100 µm).

On the periphery of the array, outside of the measuring wells, there are contacts imprinted on the top of the substrate, providing the contact between electrodes (inside the measuring wells) and the rest of electronic equipment. For the array containing 8 culture wells, there are 8 corresponding contacts for each well, regardless of number of interconnected electrodes within one well. An additional contact (in the middle) is used for the common counter electrode. Electrode arrays containing 8 wells and either 1 or 4 gold-film electrodes within each well were used for the experiments in this work and their corresponding commercial designations are 8W1E and 8W4Eµ, respectively.

Electrode Array Type 8W1E

An acronym of the well-established array type 8W1E indicates the presence of 8 individual culture wells within the 8-well chamber and only one electrode within the each well (**Figure**

4.3 A, B). In fact, the layout within each well (**Figure 4.3 B, C**) consists of two coplanar electrodes: a small circular working electrode (with the diameter of 250 µm and area of ~ 0.049 mm^2) and a 1000-fold bigger counter electrode (Lukic and Wegener, 2015). Even though both electrodes are cell-covered, the contributions of the counter electrode, as well as those coming from wiring and the bulk medium can be neglected and the total impedance of the system is dominated mainly by the impedance of the small working electrode (Wegener et al., 2000).

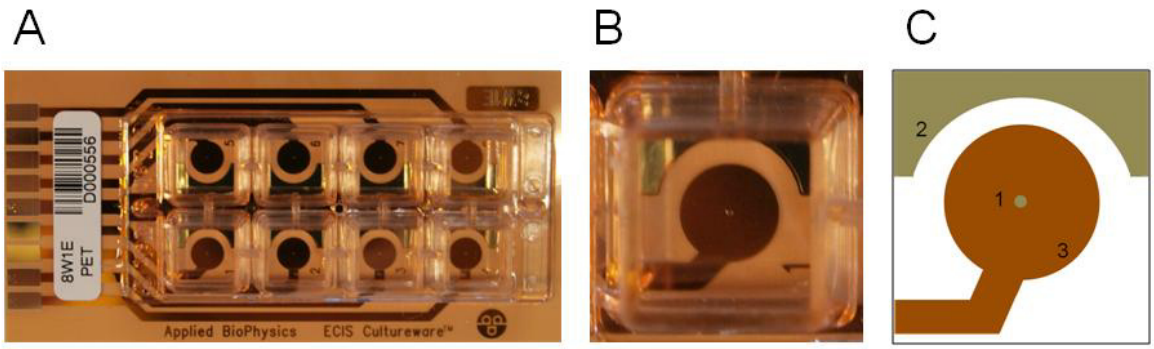

Figure 4.3 A The image shows an ECIS electrode array of type 8W1E with 8 individual culture wells, each containing 1 electrode deposited on the bottom. The 8-well chamber is fixed on the top of the array layout and provides the assembly of 8 independent culture wells. **B** A magnified photo of the culture well containing 1 electrode. **C** Schematic illustration of the two electrodes arrangement within the well of an 8W1E electrode array: **1.** Small working electrode and **2.** Significantly larger counter electrode. **3.** The layer of photopolymer delineates the circular working electrode area.

Electrode Array Type 8W4Eµ

The original 8W1E array type can be modified with respect to the electrode layout to be compliant with specific application requirements. Thus, array type 8W4Eµ contains 4 gold-film electrodes (instead of 1) in each of the 8 culture wells (**Figure 4.4**). The size of the electrodes stays the same as within 8W1E (diameter of 250 µm and growth area of ~ 0.049 mm^2). Since there are 4 small working electrodes within each well, their total area per well is ~ 0.196 mm^2 (4 * 0.049 mm^2). Two of four electrodes in each well act as counter electrodes, whereas other two electrodes act as working electrodes. The corresponding 8 contacts belonging to each of the culture wells are imprinted on the periphery of the electrode array (**Figure 4.4 A**). The 4 circular electrodes in each well are spatially divided into two electrode pairs (one pair giving working electrode and second pair providing counter electrode), separated by a narrow gap in the photopolymer layer (**Figure 4.4 B, C**). All four circular electrodes within one well produce a unique measuring signal and a mean value coming

from four electrodes is recorded. Despite of these modifications compared to array type 8W1E, 8W4Eμ allows unhindered impedimetric monitoring of the cells and application of electric pulses.

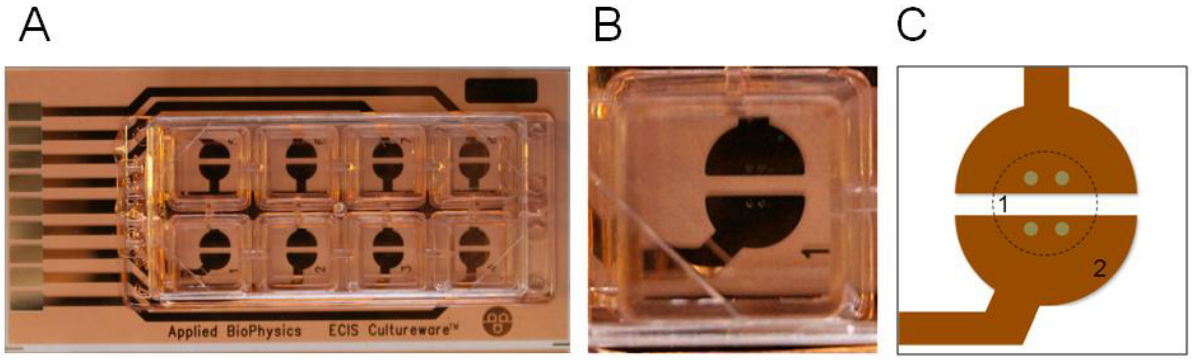

Figure 4.4 A The image shows an ECIS electrode array of type 8W4Eμ with 8 individual wells, each containing 4 electrodes deposited on the bottom. The 8-well chamber is fixed on the top of the array layout and provides the assembly of 8 independent culture wells. **B** A magnified photo of the culture well containing 4 electrodes. **C** Schematic illustration of the 4 electrodes within the well of 8W4Eμ electrode array: **1.** Four small circular electrodes divided spatially into two pairs (working electrodes and counter electrodes) are separated by a gap in the photopolymer layout. **2.** The layer of photopolymer delineates the areas of 4 circular electrodes.

The main advantages of an 8W4Eμ array type compared to 8W1E, relevant for various studies conducted within this work, are: (I) microscopic evaluation of the loading efficiency by *in situ* electroporation is possible at 4 independent electrodes (instead of 1), which allows one to obtain better statistics per experiment. (II) The electrode arrangement allows reducing the working volume when small silicone inserts are introduced within each well. (III) Increased number of electrodes and thus an increased number of cells directly engaged in the measurement and pulse application per well, accompanied by the reduction in working volume per well is an important precondition for some studies (e.g. release of the intracellular material by electroporation / wounding followed by LDH assay).

4.2.1.3 Array Modifications for Small Volume Applications

Work with rather costly chemicals and molecules (e.g. nucleic acids and proteins) requires a reduction of the working volume per well. Therefore, the 8W4Eμ electrode arrays combined with small silicon chambers, inserted into the culture wells to significantly reduce the working volume, appeared as a very good solution (Stolwijk, 2012). For studies of delivery of nucleic

acids into the cells by *in situ* electroporation, this strategy was extensively applied, taking the advantages of 8W4Eμ electrode array, described in a previous subchapter.

Electrode arrangement of 8W4Eμ array type allows insertion of the small chambers (tubes) around the electrodes, thus reducing the working volume necessary to perform experiments with costly molecules. Conducting cell culture medium and buffer provide the electric connection between the electrodes. Small round chambers used as inserts were out of silicone and their inner diameter was in the range 3 – 5 mm. Silicone rings were cut manually using a scalpel from commercial transparent silicone meter hoses. The small silicone rings with various inner diameters and various wall thicknesses can create chambers which provide a reduction of both, cell growth area and working volume compared to the standard 8-well chambers.

After being cut, silicone rings were cleaned according to the following protocol:

Around 30 mL of 5 % Elma clean was added into a 50 mL centrifuge tube containing silicone tubes and this was mixed at the ultrasonic water bath for 10 min at 20 °C. Thereafter, silicone tubes were rinsed three times with distilled water, kept in ethanol for 15 – 20 min and subsequently left to dry on a clean paper at RT. Silicone tubes were carefully glued and fixed onto the electrode array or inside standard tissue culture Petri dishes using a thin layer of the transparent and water-resistant silicone glue for aquaria.

One can differentiate between two types of chamber formed by round silicone inserts. They got acronyms according to electrode array type and the chamber size.

Chamber Type 8W4Eμ - Ø3

The first type was already described by Stolwijk (2012) and includes silicone rings with inner diameters of 3 – 3.5 mm and a wall thickness of 2 mm, cut with the scalpel to the height of app. 4 – 5 mm. Every silicone tube provides a cell growth area of 0.070 – 0.096 cm^2 and a reduction of the working volume from 200 – 400 µL (for 8-well chambers) to 30 – 40 µL per well. In fact, one still cultivates the cells in 400 µL volume (of the cell culture medium) per well, as the small silicone tubes are fixed and glued within the wells of 8-well chamber (**Figure 4.5 A**). Thereby, the cells are provided with sufficient fluid volume and long-term measurements are possible, if necessary. On the other hand, the experimental protocol for electroporation or wounding can be conducted with reduced volume inside the small chambers (30 µL) over several hours (**Figure 4.5 B**). Cells were cultivated in entire wells of the 8-well chamber but for electroporation and wounding, only the small silicone rings were filled with the working solutions (30 – 40 µL). To reduce the fluid loss due to evaporation, 100 µL of $EBSS^{++}$ buffer was added to the wells of 8-well chamber, around the silicone rings.

After electroporation and recovery of the cells, the regular volume of the fluid (400 µL) was added to each well again to monitor the cellular response over longer periods of time (several days) (Stolwijk, 2012).

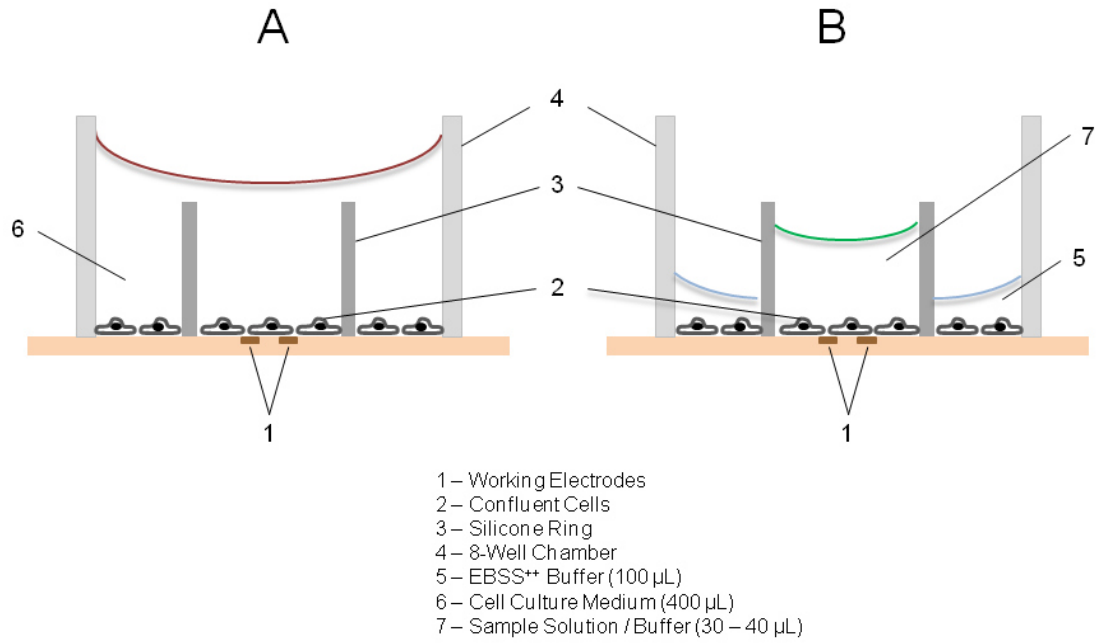

Figure 4.5 A Chamber type 8W4Eµ-Ø3 allows cultivation of the cells in 400 µL of cell culture medium within the wells of 8-well chamber. **B** Reduction of the working volume is possible from 150 – 200 µL to 30 – 40 µL within the small silicone rings. Drawings not to scale.

Chamber type 8W4Eµ-Ø3, with silicone tubes of 3 mm diameter fixed within a regular 8W4Eµ electrode array is shown in **Figure 4.6**.

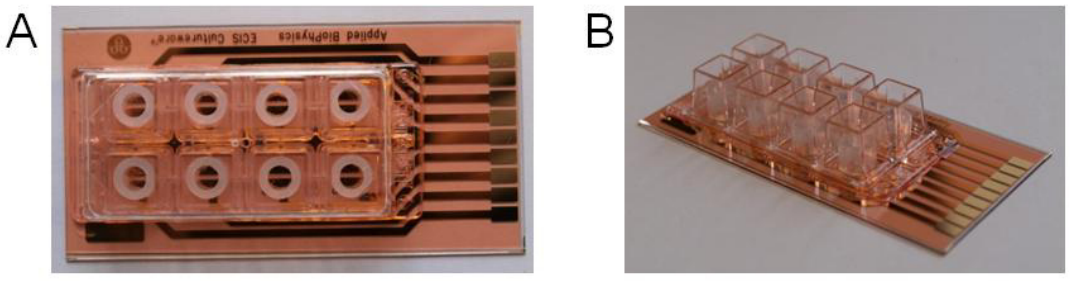

Figure 4.6 A Top view of the electrode array type 8W4Eµ-Ø3 with small silicone rings of 3 mm diameter are inserted in 8-well chambers of regular ECIS electrode array 8W4Eµ. **B** Side view of the chamber type 8W4Eµ-Ø3 (without the cover lid).

Chamber Type 8W4Eμ - Ø5

Due to the experimental requirements of *in situ* electroporation of the cells in presence of nucleic acids, which includes subsequent microscopic evaluation of the electroporation efficiency, another chamber type taking advantage of small silicone inserts was developed. A transparent silicone meter hose with slightly larger inner diameter (5 mm) and a wall thickness of 3 mm and 7 – 8 mm height was applied. Such silicone chambers enable a reduction of the working volume down to 40 µL per well, whereas a volume of 80 µL was used prior to the experiment to prevent fluid evaporation and drying of the cells (**Figure 4.7**).

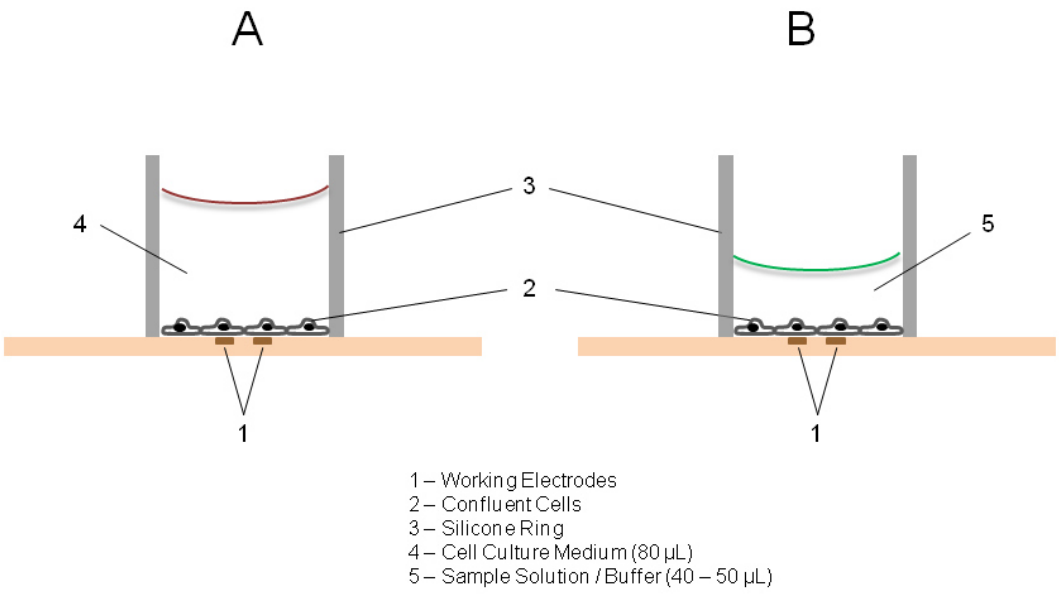

Figure 4.7 A Chamber type 8W4Eμ-Ø5 allows cultivation of the cells in 80 µL. **B** Working volume can be reduced to 40 – 50 µL within the small silicone rings. Drawings not to scale.

The cell growth area within each chamber was 0.196 cm^2. Nevertheless, the standard polystyrene lid for 8-well chambers was used as a cover, in order to prevent fluid evaporation and to maintain sterile conditions within the chambers. When cutting the silicone rings from the meter hose with the scalpel, a special effort has been made to create the chambers with the very same height in order to maximize closure of the chambers interior by the cover lid and thus assure sterile conditions and prevent over-evaporation of the fluid (**Figure 4.8**). The silicone tubes were cleaned and dried according to the same protocol as for Ø3 mm silicone tubes, before they were glued and fixed onto the electrode array layout in order to get 8W4Eμ-Ø5 (**Figure 4.8**) or inside the tissue culture Petri dish, using thin layer of the silicone glue. Both chamber types, 8W4Eμ-Ø3 and 8W4Eμ-Ø5 were sterilized in Argon plasma for app. 20 – 27 s prior to use.

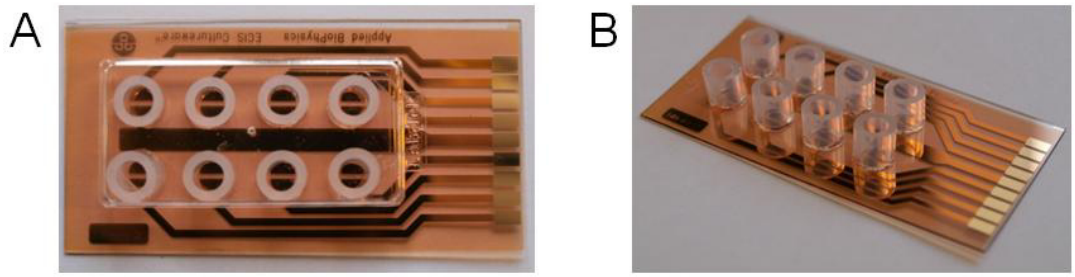

Figure 4.8 A Top view of the electrode array type 8W4Eμ-Ø5, where small silicone rings with a diameter of 5 mm are glued upon ECIS electrode array 8W4Eμ without the 8-well chamber. **B** Side view of the chamber type 8W4Eμ-Ø5 (without the cover lid).

4.2.1.4 Electrode Array Modifications for Combined Electroporation and Microscopy

For an optical *in situ* analysis of cells during electrical pulses, microscopic images were generated before and after pulse application. An appropriate time resolution (in seconds or in minutes) was chosen depending on the experiment and processes which were analyzed. For that, the standard experimental setup was modified and it included the following components: frequency generator (FG), water bath with a temperature control, electrical contacts for counter and working electrodes and a special holder for ECIS arrays (developed by Prof. Dr. Joachim Wegener), which was placed on the table of the confocal laser scanning microscope (schematic illustration shown in **Figure 4.9**).

The ECIS electrode array was placed in the special array holder on the microscope stage, so that cells could be approached directly from the top with an upright confocal microscope. A custom-made water-jacketed array holder was warmed to a temperature of 37 °C by a temperature-controlled water bath to maintain the cells at their physiological temperature (37 °C) during microscopy. On the front panel of the frequency generator (FG) parameters for electric pulses were predefined and applied to the cells. The electrical connection between FG and array in the holder was established thanks to the spring-loaded pogo contacts which were, from their bottom side, gently pressed to the array contact areas. Connection wires were manually fixed to the pogos (**Figure 4.10**). The pair of wires provided electric connection, when one of them (wire marked with 1 in **Figure 4.10**) was fixed to the counter electrode and another one (wire marked with 2 in **Figure 4.10**) to the working electrode(s) in the pre-selected well. The frequency generator was connected to the connection wires via coaxial cable.

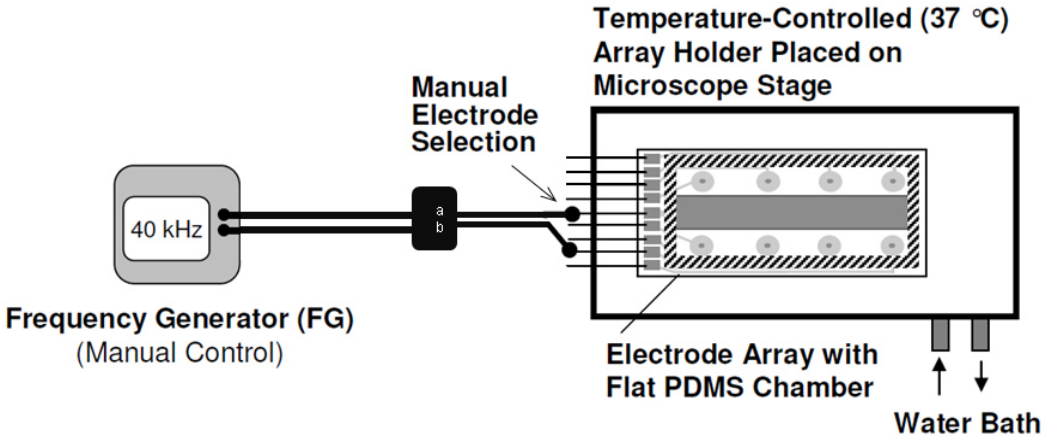

Figure 4.9 Schematic illustration of the experimental setup to conduct studies of *in situ* electroporation directly on the stage of a confocal laser scanning microscope, in order to obtain micrographs before and after pulse application. An ECIS electrode array was placed in an array holder warmed to a temperature of 37 °C (by a water bath) directly on the stage of the upright confocal microscope. The frequency generator (FG) provided electric pulses (with predefined parameters) to the cells via electric wires connected to the counter electrode and the working electrodes in a pre-selected well.

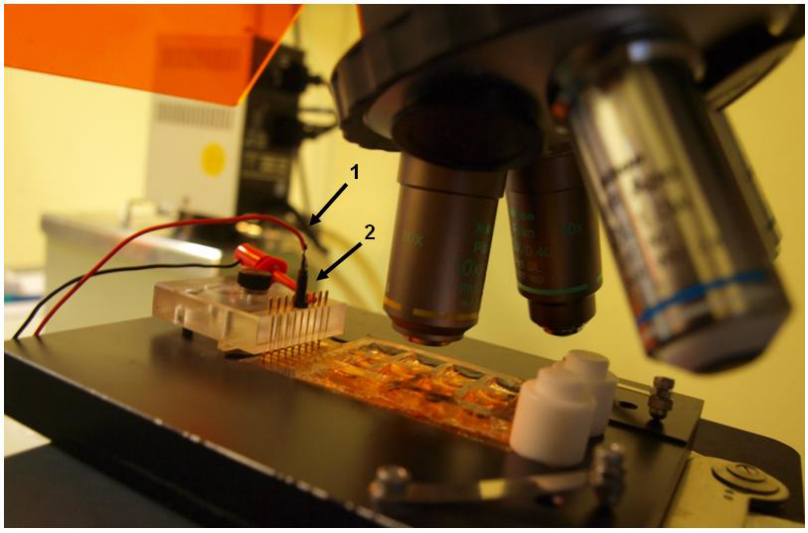

Figure 4.10 The photograph shows ECIS electrode array placed in the special (water-jacketed) array holder (warmed to 37 °C) on the microscope stage, in order to approach the cells from the top with an upright objective. Electric connection to the frequency generator (FG) was established by the connecting wires (marked with **1** and **2**).

For all studies involving *in situ* electroporation directly on the microscope stage, ECIS electrode array type 8W4Eμ was applied. Cellular monolayers were observed with the upright microscope from the top, either with 10- or 60-fold magnification objective. As

standard 8-well chambers could not be used because of their height, special chambers made from polydimethylsiloxane (PDMS) with low and flat walls were used instead. PDMS was prepared by mixing around 25 mL of PDMS base polymer with a curing agent in a ratio of 10:1, pouring it into a Petri dish to the height of roughly 5 – 6 mm and then incubating it for 12 – 24 h at 37 °C. After polymerization was complete, chambers were cut in a form of rectangle with outer dimensions of about 35 x 58 mm and wall thickness of app. 5 mm, thus providing one common chamber for all 8 wells. Finally, the chamber was glued onto commercial ECIS arrays (provided without the 8-well chamber) with the transparent and water-resistant silicone glue (**Figure 4.11 A**). In order to create 8 separate wells within the chamber, thin walls (~ 2 mm) were cut from a layer of PDMS and glued onto the electrode array substrate (**Figure 4.11 B**). This enabled better conditioning of cells during the experiment, as fast fluid evaporation and drying of the cells was avoided.

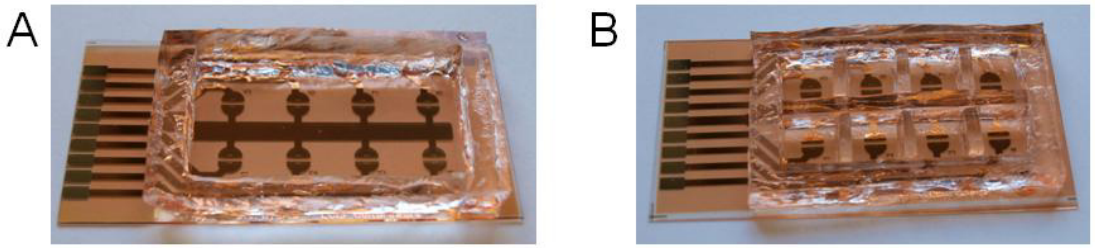

Figure 4.11 ECIS electrode array 8W4Eμ with PDMS chamber glued onto the array surface was used for combined *in situ* electroporation and microscopy using an upright microscope (CLSM). **A** Flat chamber without separate wells and **B** Flat chamber with 8 individual wells created from PDMS.

Whereas both PDMS chambers were convenient for microscopy with a 10-fold magnification objective (no immersion), as there must be a certain distance between the objective and the fluid, only the chamber without separate wells was applicable for microscopy with 60-fold magnification (water immersion) objective. PDMS chamber with one common well allowed placing of the water immersion objective into the fluid and thus unhindered approach of the objective to the cells. Electrode arrays with fixed and glued PDMS chambers were cleaned in the Argon plasma for 20 – 27 s before use and were kept inside a sterile Petri dish.

4.2.1.5 Cultureware and Chambers for Different Experimental Procedures

Besides the standard ECIS electrode arrays with 8-well chamber, other types of chambers and certain modifications were applied on ECIS electrode arrays, as well as inside the tissue

culture Petri dishes. All these are summarized and shortly described within this subchapter.

Table 4.6 Different chamber types in combination with ECIS electrode arrays or tissue culture Petri dishes.

Chamber Type and Substrate	Application	Cell Cultivation Volume / Well	Working Volume / Well
Standard 8W1E / 8W4Eμ	Electroporation, wounding, stimulation, ch. transfection	400 µL	150 – 400 µL
8W4Eμ - Ø3	Electroporation (long-term measurements), Wounding + LDH assay	400 µL	30 - 40 µL (100 µL of the buffer around the Ø3 chamber)
8W4Eμ - Ø5	Electroporation (short-term measurements), Wounding + LDH assay	80 µL	40 – 50 µL
8W4Eμ + PDMS chamber (one common well)	Electroporation with *in situ* microscopy	3 mL	1.5 mL
8W4Eμ + PDMS chamber (8 wells)	Electroporation with *in situ* microscopy	400 µL	200 µL
8-well chamber inside the Petri dish	Ch. transfection, permeabilization	400 µL	150 – 400 µL
Ø5 inside the Petri dish	Ch. transfection, permeabilization	80 µL	40 – 50 µL

ECIS electrode arrays with 8-well chamber (8W1E / 8W4Eμ) were used for electroporation studies (e.g. including fluorescent dyes and second messengers), cell wounding and for impedimetric monitoring of chemical transfections.

8W4Eμ - Ø3 were used for electroporation studies including costly molecules (nucleic acids). The cellular response after electroporation of the cells in presence of Cell Death siRNA or siRNA targeting EGFP was monitored up to ~ 96 hours after pulse application. This chamber type was also used to study a release of intracellular material by electric pulse application, combined with a subsequent LDH assay. A drawback of such small chambers was proximity of the electrodes to the chamber walls and therefore, it was difficult in some cases to conduct the experimental protocols including several successive washing steps prior to microscopy.

8W4Eμ - Ø5 was applied as well for studies of electroporation including nucleic acids (e.g. aptamers, siGLO Red). Long-term measurements were not conducted using this chamber type, as fluid evaporation was observed in contrast to 8W4Eμ-Ø3. However, such chamber type was very convenient for experimental protocols including extensive pipetting and washing steps prior to microscopy.

ECIS electrode arrays with PDMS chambers (with and without individual wells) were used only for time-resolved imaging of the cells before and after electroporation.

The 8-well chamber inside the Petri dish was applied for studies including chemical transfection and cell membrane permeabilization.

Small silicone chambers (Ø5) inside the Petri dish were used for studies of cell membrane permeabilization in presence of costly molecules.

4.2.1.6 Impedance Measurements with High Time Resolution

The experimental setup described in chapter 4.2.1.1 was usually applied for electrical monitoring of *in situ* electroporation, as it provides a direct insight into events occurring before and after application of the electric pulses. Nevertheless, such an experimental setup has to be operated entirely by the software. Software-controlled switching between invasive and non-invasive operational modes leaves a short time gap immediately after pulse application. A typical time resolution of ~ 1.5 min (Stolwijk, 2012) is insufficient to address events immediately after electric pulsation, especially since membrane resealing after electroporation is a very quick process. To be able to follow events before and (immediately) after electroporation with higher time resolution, the experimental setup was modified (**Figure 4.12**; Stolwijk, 2012) and a fast manual switch was introduced, replacing software-controlled switching. Therefore, the custom-made ECIS setup with all key electronic components as independent devices (chapter 4.2.1.1) was modified accordingly. Impedance analyzer (IA) and frequency generator (FG) were connected to the relay via a special manual switch, as it enables faster operation than the micro-controller with respect to the pulse application.

Since the custom-made software was only used for impedimetric monitoring of the cellular response during these experiments, the electric pulses were applied manually by controlling the frequency generator via its front panel. Rapid data acquisition by the IA was shortly interrupted by the manual switch, electric pulses were triggered via the front panel of the FG before the electric connection to the IA was reestablished manually. To facilitate faster data acquisition than usual and thus higher time resolution (~ 900 ms), complex impedance was

recorded at a single frequency (4 000 Hz) using 2000 cycles for integration. For electric pulse application, frequency was kept constant over all measurements (40 kHz), whereas voltage amplitude and pulse duration were varied.

For impedance measurements with high time resolution (HTR), ECIS electrode arrays of type 8W1E and 8W4Eμ were used. During all measurements, cells were maintained in 400 µL of $EBSS^{++}$ buffer per well.

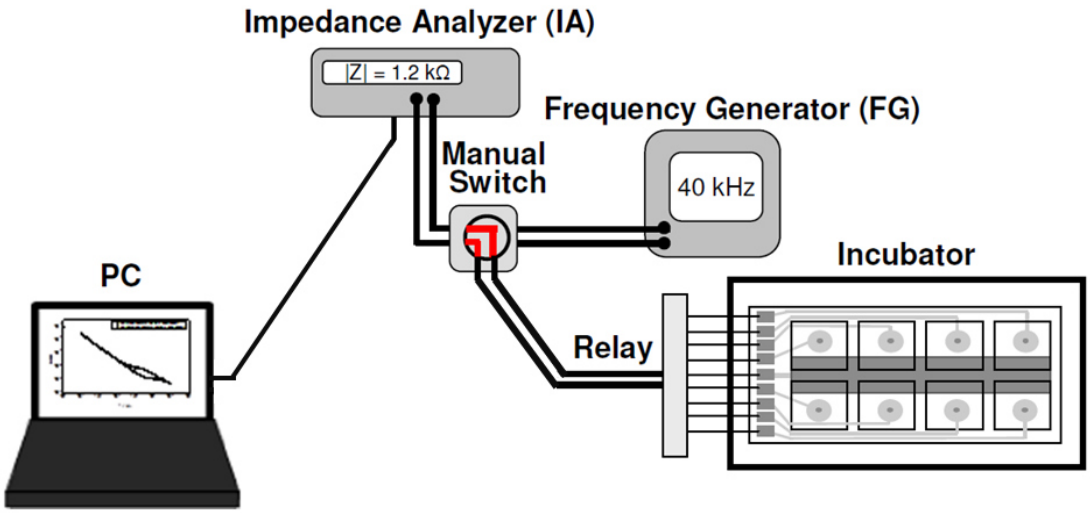

Figure 4.12 Experimental setup for impedimetric monitoring of *in situ* electroporation with high time resolution includes frequency generator (FG), impedance analyzer (IA) and a relay as separate devices, interfaced with PC and ECIS electrode array. Instead of controlling the electric pulses by the software, they were set and applied directly via the front panel of the frequency generator. Switching between the non-invasive impedimetric monitoring by the impedance analyzer and invasive electric pulses applied by the frequency generator was done manually with the special switch. This advanced setup allowed rapid data acquisition with high time resolution of ~ 900 ms.

4.2.2 Experimental Procedures for *In Situ* Electroporation

A standard experimental procedure for monitoring the morphological response of a cellular monolayer upon electroporation in real time includes the following steps: (i) array preparation, (ii) impedimetric monitoring with integrated pulse application and (iii) microscopic evaluation, if required. This experimental procedure was adjusted and optimized according to the special demands of different studies in the scope of the delivery / release of various probe types. For every cell line, the optimal combination of pulse parameters for efficient *in situ* electroporation was initially determined, with respect to maximal loading

efficiency of the material and minimal invasiveness of the method. For this purpose, confluent cells were electroporated using various combinations of pulse parameters, in presence of fluorescent dyes and results were evaluated subsequently by confocal microscopy.

One of the essential requirements for a successful application of *in situ* electroporation is a completely confluent cellular monolayer, as incomplete confluency of the cells can significantly affect the efficiency of the method. Therefore, every cell line, with an exception of CHO-K1 and CHO-GFP cells (only 24 hours before), was seeded in the electrode arrays app. 48 hours before the experiments including *in situ* electroporation were started. In order to assure homogeneous and healthy cellular monolayers on the day of the experiment, an additional medium exchange was performed 24 hours before starting the experiment.

4.2.2.1 Delivery of Fluorescent Probes by Electroporation

Delivery of fluorescent membrane-impermeable probes into confluent cell monolayer by *in situ* electroporation employing the ECIS instrumentation was conducted according to the standard protocol, which includes three main phases: (i) array preparation, (ii) impedimetric monitoring before and after application of electroporating pulses and (iii) subsequent evaluation of the loading efficiency by confocal microscopy. Fluorescent probes were used in most cases to initially optimize the electroporation procedure, before bioactive samples were applied. Optimization studies had to be performed for 8W4Eμ electrode arrays, as the optimization of experimental parameters for 8W1E arrays were already extensively examined by Stolwijk (2011).

Array preparation is described in chapter 4.2.1 and the preparation of cellular monolayers for experiments is given in chapters 4.1.4 and 4.1.5. Shortly before impedimetric monitoring was started, cell culture medium (400 μL) was exchanged with 100 – 200 μL of the buffer ($EBSS^{++}$ or L-15) in each culture well under sterile conditions.

Impedimetric monitoring started after the electrode array was mounted in the array holder and connection to other components of experimental setup was established (chapter 4.2.1.1). An initial pre-pulse data acquisition phase took usually 30 – 90 min, during which cells are allowed to equilibrate. A fluorescent probe (e.g. FITC-dextran, fluorescein, Lucifer yellow, propidium iodide) was always freshly prepared from a powder or a stock solution in a corresponding volume of the buffer ($EBSS^{++}$) necessary for the experiment. Addition of the fluorescent probe was done carefully under nonsterile conditions, without pausing the impedance measurement. When the electroporation pulses were applied, the non-invasive ECIS measuring mode was switched automatically, by the computer-controlled relay, to

application of invasive electric pulses (by the FG). The electrodes in selected wells received sinusoidal AC voltages of defined amplitude, duration and frequency. Whereas pulse amplitude and duration were varied during the process of optimization, frequency remained unchanged and set to 40 kHz, as it has been identified as the most suitable frequency for the cell monolayers (Wegener et al., 2002). Immediately after electric pulse application, the non-invasive measuring mode was automatically continued and the post-pulse cellular behavior was monitored (impedimetrically) in real time. During post-pulse phase, cells were allowed to recover after electric manipulation and to return to their normal (pre-pulse) state. Depending on the electric field strength applied for electroporation, as well as on the cell type, the time frame for cell recovery was usually from 15 min (for HaCaT cells) up to 60 min (for BAEC cells). The post-pulse incubation with the fluorescent probe should not be too long, as unspecific adsorption of the fluorescent dye to the cell surface or vesicle mediated uptake might take place and thus interfere with an evaluation of loading efficiency by confocal microscopy.

The FITC-labeled dextrans of different sizes (4 kDa – 250 kDa), fluorescein, Lucifer yellow and propidium iodide were used as fluorescent probes in order to imitate bioactive probes of nearly the same size. In **Table 4.7**, all fluorescent probes are summarized along with their molecular weight and the concentrations used in the analysis. The applied concentration of FITC-labeled dextrans and Lucifer yellow was 2 mg/mL according to the literature (Wegener et al., 2002). Fluorescent probes were used also to optimize the number of electric pulses, intracellular material release out of the cells and to obtain the additional controls within the studies of nucleic acid delivery into cells.

Table 4.7 Different fluorescent probes used to study *in situ* electroporation are listed with respect to their molecular weight and concentrations applied for the experiments.

Type of the Fluorescent Probe	Concentration [µmol / L]	Molecular Weight [g / mol]
FITC-dextran	8 – 500 (2 mg / mL)	4.000 – 250.000
Fluorescein	20 – 200	332.32
Lucifer yellow	3834.6 (2 mg / mL)	521.57
Propidium Iodide	100	668.39

The combination of pulse parameters has to be optimized for every cell line (**Table 4.8**) in order to achieve satisfactory loading efficiency of cells and high level of cell viability. The sinusoidal AC voltage pulses were applied at a frequency of 40 kHz, whereas the pulse

amplitude was varied in a range of 2 – 5 V and pulse duration was varied between 50 ms and 500 ms. After cells fully recovered, the impedance measurement was finished and the buffer containing the fluorescent probe was removed. The cells were carefully rinsed two or three times in each well. Washing steps were necessary to remove any unspecific or extracellularly bound fluorescent probe which may interfere with the optical determination of loading efficiency.

Table 4.8 Cell lines with their respective optimized combination of electric pulse parameters for *in situ* electroporation are listed, with respect to the pulse amplitude and pulse duration for 8W1E (Stolwijk, 2012) and 8W4Eμ electrode arrays. The frequency was set to 40 kHz in all cases.

Cell Line	8W1E	8W4Eμ
BAEC	/	4 V, 200 ms
CHO-K1	3 V, 500 ms	4 V, 500 ms
CHO-GFP	/	4 V, 500 ms
HaCaT	/	5 V, 500 ms
NIH-3T3	4 V, 200 ms	5 V, 200 ms
NRK-E52	4 V, 200 ms	4 V, 200 ms

Microscopic evaluation was performed using a confocal laser scanning microscope (CLSM) in order to determine the amount and localization of fluorescent material within the cell interior after delivery by *in situ* electroporation. More details on microscopy are given in chapter 4.3.

4.2.2.2 Multiple Electroporation

In order to increase the loading efficiency of *in situ* electroporation, the strategy of applying pulse trains was used. This means, electroporation pulses were repeated two or three times subsequently using the same pulse parameters with recovery times of 10 – 30 min between each pulse application. The pulse parameters were the same as for single pulse application. Application of multiple electroporation pulses was studied using propidium iodide as a membrane-impermeable fluorescent probe, which can enter the cells only if the cell membrane is damaged or reversibly permeabilized. The experimental procedure was completely the same as for other fluorescent probes, with the number of applied electroporating pulses as the only difference. Between every pulse application, it was waited for cells to recover to pre-pulse state. After the last pulse application and complete recovery

of the cells, the impedimetric measurement was finished and the microscopic inspection followed. Concentration of propidium iodide was 100 µM, as suggested for electroporation experiments in many literature sources (Tekle et al., 1994; Rols and Teissié, 1998; Pucihar et al., 2008). Studies addressing repeated electroporation pulses were conducted on 8W4Eµ electrode arrays.

4.2.2.3 Delivery of Second Messengers by Electroporation

The experimental procedure for delivery of bioactive compounds inducing signaling cascade in the cells, so called second messengers, included *in situ* electroporation and impedimetric monitoring of the cellular behavior before and after application of electric pulse.

Cells were seeded on the electrode array ~ 24 hours prior to experiment. After initial equilibration of the confluent cell monolayer in 200 µL of the buffer ($EBSS^{++}$, $EBSS^{+-}$, serum-free or complete medium), which took usually 60 – 90 min, a fresh solution of the second messenger (8-OH-cAMP, cAMP, cGMP) was prepared as a double concentrated solution in 200 µL volume and was added to the cells carefully, under non-sterile conditions, so that the total volume in every well was 400 µL.

When stimulating agents for certain signaling pathways (forskolin and calcimycin) or membrane-permeable analogues of second messengers (CPT-cAMP, CPT-cGMP) were studied, cellular response was monitored impedimetrically over several hours using non-invasive mode of ECIS instrumentation. On the other hand, when membrane-impermeable compounds were applied (cAMP, 8-OH-cAMP, cGMP), impedimetric measurement included equilibration phase, addition of the bioactive compound without pausing the measurement, reestablishment of the stable signal baseline and electric pulse application. Whereas 8-OH-cAMP, cAMP and cGMP were used as the membrane-impermeable second messengers, CPT-cAMP and CPT-cGMP were applied as the membrane-permeable analogues of the corresponding second messenger (concentrations are given in a **Table 4.9**). Forskolin triggers the cAMP signaling cascade by activating adenylate cyclase and served as a positive control for cAMP study.

Calcimycin acts as a calcium ionophore and allows a diffusion of extracellular Ca^{2+} ions present in the buffer solution through the cell-membrane into the cellular interior. Thus, the cellular response to influx of calcium was followed, in order to mimic the effect taking place after membrane permeabilization by electroporation when extracellular calcium ions from the buffer can enter the cell interior through the transient pores within the cell membrane.

Dilutions of 8-OH-cAMP and cAMP were freshly prepared from original aqueous solutions stored at – 20 °C, whereas cGMP, CPT-cAMP and CPT-cGMP were in a solid form stored at

– 20 °C. Small portions of the powder were dissolved in the corresponding buffer, usually as 1 – 2 mM stock solutions, which were used for further working dilutions and were stored at – 20 °C. The calcimycin and forskolin stock solutions were prepared by dissolving their powder in DMSO and they were stored at 4 °C and – 20 °C, respectively. When any of these two compounds was applied, a control was being run with the buffer containing DMSO at the same concentration.

Table 4.9 Cell membrane-impermeable second messengers and their corresponding membrane-permeable analogues are summarized, along with the concentration range applied for experiments and optimal concentration.

Type of the Probe	Bioactive Compound	Concentration Range [µM]	Optimal Concentration [µM]
Membrane-Impermeable Probes	8-OH-cAMP	100 – 800	100
	cAMP	100 – 1000	100
	cGMP	100 – 300	100
Membrane-Permeable Probes	CPT-cAMP	100 – 1000	100
	CPT-cGMP	/	100
	Forskolin	/	2.5
Calcium-Ionophore	Calcimycin	0.5 – 7.5	5

4.2.2.4 Delivery of Aptamers by Electroporation

The fluorescently-labeled DNA aptamers were delivered into confluent cell monolayer of different cell lines (CHO K1, HaCaT, NIH 3T3 and NRK) by *in situ* electroporation, following the experimental procedure similar to the standard protocol used for *in situ* electroporation of the cells in presence of fluorescent probes. Again, three main phases were included: (i) preparation of the electrode array with cells, (ii) impedimetric monitoring of the cells with integrated electric pulses application and (iii) microscopic evaluation of the loading efficiency. Nevertheless, considering DNA aptamers as expensive synthetic oligonucleotides, sensitive to denaturation and degradation by nucleases, higher temperature and pH change, work with them required very careful handling in a DNase-free environment during all experimental handling, as well as a reduction of the experimental volume to reduce costs.

Array preparation included initial preparation of electrode arrays prior to cell seeding, as for

this type of experiments arrays 8W4Eμ with small silicone chambers (8W4Eμ-Ø5) were used. Due to the aptamers' sensitivity to nucleases, the usual pre-equilibration of the cells in buffer ($EBSS^{++}$) before adding the probe was omitted. Instead, appropriate aptamer dilutions were prepared by mixing the 100 μM aptamer stock solution aliquots with the $EBSS^{++}$ buffer at RT and immediately afterwards, aptamer solutions were added to cells in a volume of 40 μL per well and at a final concentration of 15 μM.

Impedimetric monitoring was started after sample and control solutions were added to the cells on the array, which was then mounted onto an ECIS array holder. Typically, the first electroporating pulse was applied 8 – 12 min later, thus minimizing the possibility for oligonucleotide degradation, while still giving some time to the cells to equilibrate. Optimized electric pulses were applied three times successively, in order to increase the loading efficiency (chapter 4.2.2.2). After the third and final pulse application, cells were allowed to recover, which usually took 30 – 45 min. An extended post-pulse phase was avoided and microscopic evaluation followed soon afterwards, as aptamers localization within the cells is a dynamic process. Prior to microscopy by CLSM, cells were rinsed once with PBS^{++} very carefully. Due to small growth area within the Ø5 wells, multiple pipetting and washing steps could be invasive for the cell monolayer causing its damage and washing away of the cells. Therefore, buffer solution with or without aptamers was completely aspirated out of each well, silicone rings were carefully but quickly removed from the array substrate with tweezers and immediately afterwards, 90 μL of PBS^{++} was added to the cells. This was done for each well separately, in order to avoid cell drying between each of the steps.

To get a better insight into the spatial distribution of aptamers within the cells, some electroporation studies were followed by staining of lysosomes with LysoTracker® (chapter 4.3.4.3). Possible co-localization of the aptamers with this very selective lysosome marker was studied by CLSM.

Microscopic evaluation was performed by CLSM in order to determine the fraction of loaded cells and localization of fluorescent aptamers within the cell interior. More details on microscopy are given in chapter 4.3.

Working concentration of fluorescently-labeled DNA aptamers applied for *in situ* electroporation was 15 μM. During optimization, the concentration range was 2 – 20 μM and 15 μM was found to be sufficient for optimal microscopic evaluation.

4.2.2.5 Delivery of Small Interfering RNA by Electroporation

For the studies of sequence-specific gene knockdown by small interfering RNA (siRNA) delivered into cells by *in situ* electroporation, different types of siRNA oligonucleotides were

used: red fluorescing transfection indicator (siGLO Red), siRNA targeting genes responsible for EGFP expression (siEGFP), Cell Death siRNA (siCD), as well as a conventional negative control for all siRNA experiments, so called scrambled siRNA (siSCR). More details on siRNA are given in chapter 4.4.1.2. Since the above mentioned siRNA types address different targets and cause different effects within the cell cytosol, experimental protocols for each type had to be adjusted individually, in order to gain relevant information on their knockdown efficiency or localization.

Red fluorescing siGLO Red is a commercial siRNA transfection indicator containing an unspecific (random) sequence and a red fluorescent label. It serves conventionally as a non-targeting siRNA model to optimize any kind of transfection experiments before target-specific siRNA probes are applied (chapter 4.4.1.2). Using siGLO Red, the studies of siRNA delivery into cells by *in situ* electroporation were optimized with respect to the cell line, siRNA concentration, electroporation protocol, number of electric pulses, etc. For this, 8W4E-Ø5 arrays were used (working volume of 40 µL per well). The experimental protocol was almost identical to the one for *in situ* electroporation in presence of the fluorescently-labeled aptamers (chapter 4.2.2.4). The concentrations of siGLO Red applied for electroporation were in the range from 0.5 to 6 µM, depending on the cell line.

siRNA targeting genes responsible for EGFP expression (siEGFP) is a sequence-specific siRNA addressing the expression of enhanced green fluorescent protein (EGFP) and its silencing effects is observed 48 – 72 hours after entering an intracellular environment. Since experiments including siEGFP required a reduced working volume and monitoring of the cells for a longer period of time, array type 8W4E-Ø3 was used in all experiments (more details in chapter 4.2.1.3). Before starting every impedimetric measurement, working solutions were added to the cells in a nuclease-free environment. Due to the very small diameter of the Ø3 wells, it was essential to be very careful when adding the solutions, in order to minimize stress for the cellular monolayer. Around the small silicone chambers, 100 µL of $EBSS^{++}$ was added to limit evaporation, whereas 30 µL of the sample or control (prepared in $EBSS^{++}$) was added directly into the silicone tube within each well. After impedance monitoring was started, the baseline was only shortly recorded (for 8 – 10 min) before a first electroporating pulse was applied. *In situ* electroporation was applied three times successively to enhance loading of the cells with siRNA material and recovery of the cells was monitored by impedance readings. Thereafter, the buffer $EBSS^{++}$ around the silicone tubes was carefully removed and 400 µL of complete cell culture medium was added to each well of the electrode array, which was then placed in the cell culture incubator. App. 48 – 72 hours after siEGFP entered the cells its knockdown effect was studied. Evaluation of

the knockdown efficiency was performed app. 48 and app. 72 hours after electroporation, by taking phase-contrast and fluorescence micrographs using CLSM. 24 hours prior to microscopy, cell culture medium in each well was exchanged (400 µL). Since siEGFP induces solely a knockdown of genes responsible for expression of EGFP and this effect can be evaluated only by microscopy, impedimetric monitoring of the cells was not performed in the meantime. The cells were rinsed with PBS^{++} (once or twice), before small silicone tubes were quickly but very carefully removed from the array substrate using tweezers. Microscopic evaluation was performed according to the usual protocol.

Cell Death siRNA (siCD) is a commercially available double-stranded ready-to-use siRNA, which may serve as a positive control for siRNA studies. Since siCD aims for a knockdown of some vital genes in mice and rats, its successful delivery into the cytoplasm should induce significant level of cell death (Cell Death siRNA™). Different cell lines were tested on the cytotoxic effect of this siRNA oligonucleotide and for that, 8W4Eµ electrode arrays were used. For *in situ* electroporation of the cells in presence of siCD, an array with small chambers 8W4Eµ-Ø3 was applied and the experimental procedure was very similar to the procedure applied for delivery of siEGFP. The only significant difference compared to the protocol with siEGFP was that impedimetric measurement was performed continuously after electroporation and subsequent exchange of the $EBSS^{++}$ buffer with the cell culture medium. Impedance-based monitoring of the cells took 40 – 96 hours and allowed direct insight into the potential cytotoxic effect caused by the siCD. Impedance measurement was occasionally paused in order to take phase-contrast micrographs and evaluate cell viability. After completing impedance monitoring, microscopy by CLSM was conducted according to the usual protocol.

4.2.2.6 Impedance Monitoring of Electroporation with High Time Resolution

The experimental procedure for rapid data acquisition before and after *in situ* electroporation was rather simple. At least one hour (1 – 1.5 h) before the electrode array with cells (prepared according to the usual protocol) was used for impedance measurements with high time resolution, cell culture medium in each well was exchanged with 400 µL of pre-warmed $EBSS^{++}$. The array was returned to the incubator and NRK cells were allowed to equilibrate, while in the meantime the special hardware of this experimental setup (as described in chapter 4.2.1.6) was prepared. Impedance monitoring of *in situ* electroporation of the cells was conducted well by well in order to achieve high time resolution (HTR). For these experiments, 8W1E and 8W4Eµ electrode arrays were used. Electric pulses were applied

using different combinations of parameters, while voltage amplitude and/or pulse duration were varied systematically, frequency was kept constant at 40 kHz. The voltage amplitude was varied in a range of 2 – 5 V, whereas pulse duration was applied in a range of 50 ms – 1.25 s. The combinations of high voltage amplitude (5 V) and longer pulse durations (1 - 1.25 s) led to irreversible cell damage (electric wounding) and served as the controls for electroporation. Single and multiple electroporation pulse application were compared in one experiment. During all measurements cells were maintained in 400 µL of $EBSS^{++}$ buffer per well.

4.2.2.7 Release of Intracellular Material by Electroporation

For the studies of material release out of the cells induced by *in situ* electroporation, the fluorescent probes FITC-dextran (4 kDa) and calcein (~ 622 Da) were applied. The experimental procedures for these experiments were very similar to the previously described procedure for delivery of fluorescent probes into cells. However, several modifications were introduced and depending on the fluorescent probe, two approaches were applied as follows:

Loading of (NRK) cells with FITC-dextran (4 kDa) and subsequent release

Following the same protocol as for studies of delivery by *in situ* electroporation, confluent cells were allowed to equilibrate in $EBSS^{++}$ buffer and during this pre-pulse phase, FITC-dextran (4 kDa) was added (2 mg/mL) to the incubation buffer. Subsequently, electroporating pulses were applied and the post-pulse phase took 30 – 45 min until the cells fully recovered. Impedance measurement was paused and cells were rinsed two or three times in order to remove buffer containing fluorescent dye. Thereafter, 400 µL of fresh $EBSS^{++}$ buffer was added to each well and impedance measurement was continued. After the cells reached a stable equilibrium state again, electric pulses were applied (using optimized parameters) in order to release the FITC-dextran out of the cells. Electroporating pulses were applied in the corresponding wells once, twice or three times and in case of controls, there was no electric pulse application. **Figure 4.13 I** illustrates the experimental protocol and gives an overview of the procedure.

Loading of cells with calcein-AM and subsequent release studies

Initially, cells were loaded with calcein-AM (Ca-AM), which is often applied as a cell viability marker. After regular staining protocol was performed using 2 µM calcein-AM, cells were rinsed to remove PBS^{++} containing unbound calcein-AM. Thereafter, 400 µL of $EBSS^{++}$ buffer was added to each well, impedance measurement was started and the standard protocol for electroporation was performed including equilibration, electric pulse application and post-pulse recovery of the cells. In the corresponding wells, the electric pulses were applied once,

twice or three times, whereas in case of controls, there was no pulse application. After impedimetric measurement was finished, EBSS^{++} buffer was exchanged to PBS^{++} and the electrode array was prepared for microscopic evaluation by CLSM (**Figure 4.13 II**).

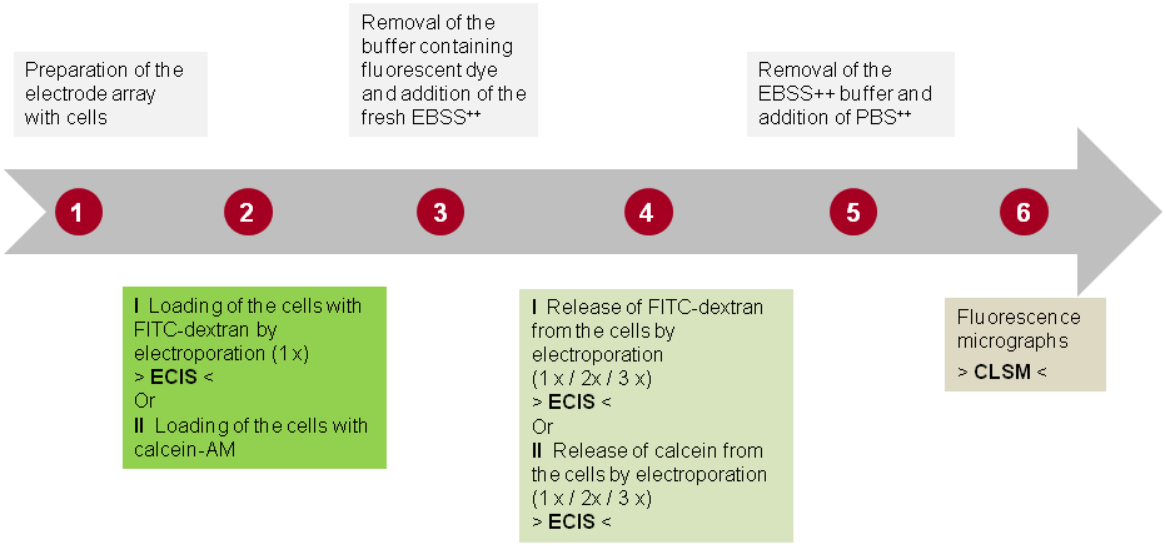

Figure 4.13 Schematic overview of the experimental procedure for studies of material release from the cytoplasm by *in situ* electroporation. **I** When FITC-dextran was applied as a fluorescent probe and **II** When calcein was applied as the fluorescent probe.

In addition, 2-aminoethoxydiphenyl borate (2-APB) was applied as an inhibitor of cell communication through gap junction (GJ) channels (Bai et al., 2006). The compound 2-APB was added to the buffer EBSS^{++} before impedimetric measurement was started (step 3 in the procedure flow shown in the **Figure 4.13**) and to PBS^{++} for sample preparation prior to microscopy in a final concentration of 50 µM (step 5 in **Figure 4.13**).

4.2.3 Experimental Procedure for Wounding

Electric wounding of the cells employing the ECIS technology was applied within several different projects: (i) impedimetric monitoring of the cells with high time resolution, (ii) as a positive control within the studies of intracellular material release by *in situ* electroporation and (iii) as a control for the studies of cytotoxicity effects by Cell Death siRNA. The experimental procedure for wound/healing experiments does not very much differ from the standard procedure for electroporation of adherent cells, including an identical electrode array preparation, non-invasive impedimetric monitoring of the cells with integrated invasive electric pulses and if needed, subsequent microscopic evaluation. This standard protocol

was adjusted according to the individual requirements of each study. When performing the experiment on commercial ECIS machines (with integrated frequency generator), standard pulse parameters for electric wounding were applied: 40 kHz, 5 V and 30 s, which are sufficient for effective and well-defined wounding (killing) of the cell population present on the working electrode(s). However, due to a technical limitation of the noncommercial but custom-made experimental setup, the maximum pulse duration was 1.25 s so that the respective parameters for electric wounding were: 40 kHz, 5 V and 1.25 s. Nevertheless, this combination of parameters was sufficient to irreversibly damage the cells residing on the working electrode(s). For wounding assays, both 8W1E and 8W4Eμ electrode arrays were used. Depending on the individual study, cells were wounded in $EBSS^{++}$ buffer (for HTR and intracellular material release evaluated by LDH assay), in Leibovitz's L-15 medium (for intracellular material release monitored directly on the microscope stage), or in complete cell culture medium (CM) for control experiments within the study involving Cell Death siRNA.
For comparison of the cell behavior after electric wounding and effects caused by Cell Death siRNA, cell recovery after wounding was followed for app. 20 – 24 hours and included occasional pausing of data acquisition in order to take phase-contrast images and thus document the level of cell viability. For all other studies mentioned above, cellular response after electric wounding was followed only for 10 – 60 min.

4.3 Microscopy

An important part of almost every experiment within this work was to get a microscopic insight into cell appearance by performing microscopy. Phase-contrast microscopy was performed on a regular basis to check for cell proliferation and the formation of a confluent cellular monolayer as an essential precondition to perform functional experiments. During and after experiments, phase-contrast micrographs provide basic information on cell shape, viability and level of confluency. Fluorescence micrographs provide much more detailed information on cell appearance, especially thanks to the specific staining of individual cell structures. Fluorescence microscopy was performed in this work to evaluate electroporation efficiency, as well as the loading of material into cells by chemical transfection or fixation and permeabilization. Microscopic evaluation was usually performed after impedimetric measurements and electric manipulation. In addition, some electroporation studies were conducted directly on the stage of the microscope (chapter 4.2.1.4). Loading of the cells with fluorescent probes, expression of recombinant fluorescent proteins (EGFP) and selective staining of cell structures using cytochemical probes was evaluated by fluorescence

microscopy and the following chapters are dedicated to the corresponding protocols and details.

4.3.1 Applied Microscopes

Phase-contrast and fluorescence micrographs were taken either with an inverted microscope Nikon Diaphot (objectives with 4-, 10- and 20-fold magnification) or with an upright microscope Nikon Eclipse 90i (objectives with 10- and 60-fold magnification).

Micrographs in epi-mode (Webb and Brown, 2013) were mostly taken using Nikon Eclipse 90i, with a mercury vapor lamp as a light source and corresponding filter cubes. Digital cameras were used for documentation of the microscopic images.

For confocal laser scanning microscopy (CLSM) a Nikon Eclipse 90i was used, equipped with a dry objective with 10-fold magnification and a water immersion objective with 60-fold magnification, as these were the most appropriate for imaging of the confluent cells. The applied microscopes and their most important properties are listed in a **Table 4.10** for an overview.

Table 4.10 Overview of the applied microscopes and their most relevant properties.

Microscope	Setup	Objectives
Nikon Diaphot	inverted	Plan 10 × / 0.25 Plan 20 × / 0.4
Nikon Eclipse 90i	upright	Plan 10 × / 0.25 NIR Apo 60 × / 1.0 W

4.3.2 Sample Preparation for Microscopy

Whereas phase-contrast images can be taken at almost any time point during cell cultivation or in the course of an experiment, fluorescence imaging is more demanding and requires often certain steps of sample preparation before cells are even observed under the microscope. This is especially true for imaging using upright microscopes, as the objective approaches the cells of interest from the top in order to obtain high quality micrographs. With inverted microscope, the objective approaches the cells from the back or from underneath their growth substrate, but unless these substrates are completely transparent and relatively thin, one cannot obtain fluorescence micrographs with high quality. Since thin gold film electrodes of the ECIS arrays are only semi transparent, phase-contrast images using

inverted microscope can be taken without any problems, whereas for fluorescence images there are some clear limitations. Therefore, an upright microscope was used for taking fluorescence images of the cells on ECIS electrode arrays, as well as on the majority of other substrates and culture dishes.

Washing steps prior to microscopy were necessary when fluorescent probes were added to the extracellular buffer (usually during experiments including electroporation or chemical transfection), as thus the extracellular environment gives an overwhelming fluorescence signal which interferes with the intracellular fluorescence of interest. Therefore, it was necessary to rinse the cells, at least once or twice, in order to remove any excess of the fluorescent probes and enable cellular imaging in a non-fluorescent buffer. As within almost every experiment, there was at least one control where cells were not exposed to the fluorescent probe, but to the other parameters of the particular experimental conditions, those cells were also rinsed and treated in the same way as cells in other wells, in order to avoid any handling artifacts. For washing, as well as for latter microscopy, pre-warmed PBS^{++} was used in a volume according to the size of the wells.

- When the cells on the electrode array or in a Petri dish with regular 8-well chamber were observed, they were rinsed twice with 200 µL of PBS^{++}. Washing was done in each well separately in order to avoid cell drying between each step. Eventually, 80 – 90 µL of PBS^{++} were added per well. The same protocol was applied for 8W4Eµ-Ø3 arrays as well, after the small silicone tubes were removed carefully and quickly with the tweezers.
- When the cells on the electrode array or in the Petri dish with Ø5 silicone tubes were observed, they were washed once or twice with 80 µL PBS^{++}. Aspiration and addition steps were performed very carefully in order to minimize cell stress due to the very small growth area around the electrodes. Again, each well was treated separately and a final volume of 80 – 90 µL of PBS^{++} was added as the final step.

In upright microscopy the objective has to have a free access to the cells of interest from the top. Therefore, after cells were supplied with 80 – 90 µL of PBS^{++} to avoid their drying, 8-well chamber and small silicone tubes Ø5 had to be removed. The 8-well chamber was removed from the substrate by pulling it carefully from each side, while at the same time keeping the substrate fixed on the table with the fingers. Small silicone tubes were removed also carefully, but rather quickly using tweezers, again keeping the substrate fixed on the table. Small weights made out of Teflon were used to keep the array fixed within a Petri dish during microscopy. Thus prepared, cells were ready for imaging with dry objectives. During microscopy, it is essential that the cells are entirely bathed in fluid, as otherwise they would

dry out and start dying very quickly. If necessary, a few drops of pre-warmed PBS^{++} were added to each well. Prior to microscopy with water immersion objective (60 × magnification), the Petri dish (with ECIS electrode array) was carefully flooded with around 20 mL of pre-warmed PBS^{++} to allow the immersion of an objective into the fluid and provide access to the cells in their aqueous environment.

4.3.3 Confocal Laser Scanning Microscopy

Pioneered by Marvin Minsky in 1955 at the Harvard University, confocal laser scanning microscopy (CLSM) has become an essential imaging technique in cell biology, biomedicine and materials science, as it offers several advantages over conventional optical microscopy. The key of its confocal approach is based on excluding (unwanted) scattered light, which is out of focus and collecting only the light coming from the focal plane of interest. Thus, instead of blurred images, sharp (true-to-life) images with fine and structured details of a specimen are obtained. CLSM incorporates sequential point-by-point illumination of an object and rejection of out-of-focus light (Semwogerere and Weeks, 2005), whereas pinhole apertures can be varied (Minsky, 1988). Although illumination point-by-point takes a long time, it is necessary in order to collect enough light. By reduction of lateral scattered light, one obtains sharp and detailed images. In a modern confocal laser scanning microscope, a laser is integrated as the light source of a very high intensity, available in a wide range of wavelengths. When the light from the laser is scanned across the specimen, the dye is excited, fluorescent light passes through the dichroic mirror and further through the pinhole as a spatial filter with the size that can be adjusted. Finally, the light gets to a highly sensitive detector (photomultiplier tube) and is stored as light intensity at given position (pixel) of the sample. Collected data are stored, analyzed and further processed with the help of image analysis software.

XY Image Stacks – Time-Resolved Imaging

To get a direct insight into (i) loading of the cells with a given fluorescent probe and (ii) release of fluorescent material out of the cells, both induced by *in situ* electroporation (ISE), sequential images of predefined xy-sections in certain time intervals were gathered over a given period of time. For time-resolved imaging the experimental setup described in chapter 4.2.1.4 was applied in order to perform electroporation directly on the stage of the upright microscope (Nikon Eclipse 90i). Cells were grown on the 8W4Eμ electrode arrays with the special PDMS chambers allowing a close approach of the objective to the cells from the top. Instead of $EBSS^{++}$ buffer (used for studies conducted inside the cell culture incubator)

Leibovitz's L-15 medium was applied, as it is independent of CO_2. During the entire experimental procedure, cells were maintained at their regular physiological temperature (37 °C). The electric pulse application was controlled by a frequency generator. For electroporation of NRK cells, optimized pulse parameters (40 kHz, 4 V and 200 ms) were applied, whereas for electric wounding, as an additional control, the following pulse parameters were applied: 40 kHz, 5 V and 1.25 s. For each well, a series of images was taken, beginning with the micrographs of the cell population before first electric manipulation, immediately afterwards and several minutes after the first pulse application, then directly before and immediately after the second pulse application, etc. Taken together, micrographs were taken in different time intervals, before and after pulse application almost every minute, and between the pulses every 3 or 5 min. For negative controls time-resolved imaging was performed on samples treated identically but in absence of electric manipulation.

Although photo bleaching could not be avoided due to acquisition of numerous micrographs of the same cell population, it could be reduced to some extent by using neutral density (ND) filters during microscopy. ND filters reduce the amount of incident light, thus allowing for an extended exposure time, if necessary. As the laser power cannot be manually adjusted, ND filters with different densities can be placed in the path of a laser beam. For the time-resolved imaging described here, ND8 was used (with optical density: 0.9 and transmittance: 12.5 %).

Online observation of delivery of fluorescent probes into the cells by ISE:

As a fluorescent probe, 2 mg/mL 250 kDa FITC-dextran in L-15 was applied. With the water immersion objective (60-fold magnification) dipping into the medium containing the fluorescent probe, only one electrode could be observed at a time.

Online release of fluorescent material out of the cells by ISE:

After loading the cells with 2 µM calcein-AM according to the regular protocol (chapter 4.3.4.1), buffer containing Ca-AM was entirely aspirated and replaced with L-15 medium. In one of the experiments 5 µM vitamin C (ascorbic acid) was applied as a potential photo-protective agent. Time-resolved imaging during multiple electric pulsing of the cells (electroporation/wounding) was carried out using a dry objective with 10-fold magnification, which allowed imaging of one electrode pair.

4.3.4 Cytochemical Stainings

Different structures within the cellular cytoplasm were stained specifically using protocols presented and shortly described in the following subchapters.

4.3.4.1 Live/Dead Staining with Calcein-AM and Ethidium Homodimer

Calcein acetoxymethyl ester or Ca-AM (Mw = 994.86 g/mol; λ_{ex} 495 nm; λ_{em} 517 nm) is commonly used as a vital stain. It addresses viability and membrane integrity of cells by reading the activity of an intracellular esterase. Thanks to acetoxymethyl ester in its structure, Ca-AM is a membrane-permeable derivative of calcein. After nonfluorescent Ca-AM enters the eukaryotic cell, acetoxymethyl esters are being hydrolyzed by endogenous esterases, present only in the healthy viable cells, with calcein rest becoming a green fluorescent anion that binds usually intracellular calcium and remains inside the cell, not able to diffuse out of it. As a result, the cytoplasm and the nuclei of living cells with an intact membrane are stained homogeneously, appearing bright green.

Ethidium homodimer-1 or EthD-1 (Mw = 856.77 g/mol; λ_{ex} 528 nm; λ_{em} 617 nm) is an indicator for dead cells. It addresses membrane integrity of the cells by a mechanism opposite to the one of calcein-AM. As EthD-1 is membrane-impermeable and can pass only across a compromised cell membrane, its bright red signal indicates the cell is dead or damaged. After diffusion into the cytosol of the cell across the damaged membrane, EthD-1 intercalates into the DNA. As a result, cell nuclei of dead or damaged cells appear bright red.

Since the emissions of these two indicators can be clearly distinguished, their simultaneous application has been commercialized in the form of LIVE/DEAD® cell viability assay. In this work, Ca-AM and EthD-1 were used both combined and separately for different studies including microscopic evaluation. Although both indicators are dissolved in DMSO, a 1 mM stock solution of Ca-AM was divided into aliquots and stored at – 20 °C, whereas a 2 mM stock solution of EthD-1 was kept (in original package) under 4 °C. The same protocol for both fluorophores makes their combined application very convenient. Before Ca-AM and/or EthD-1 were applied, cells were washed carefully with PBS^{++} once. Subsequently, PBS^{++} containing 1 - 2 µM Ca-AM and/or 4 µM EthD-1 was added to the cells (total volume per well of the 8-well chamber ~ 150 µL). The subsequent incubation time was between 35 and 45 min, in the dark at 37 °C and 5 % CO_2, followed by a careful removal of the staining solution and addition of fresh pre-warmed PBS^{++} to the cells prior to microscopy. For the studies of calcein release out of the cells, $EBSS^{++}$ or L-15 medium was added instead of PBS^{++} solution to the cells before impedance measurement or microscopy.
Since ethidium homodimer is potentially mutagenic or carcinogenic, it has to be handled with care. All solutions were handled very carefully, by wearing impermeable nitrile gloves and all leftovers were disposed into special waste.

4.3.4.2 DAPI Staining of the Cellular DNA

For a specific staining of the cell nucleus, 4',6-diamidino-2-phenylindole dihydrochloride or DAPI staining was used (Mw = 350.25 g/mol; λ_{ex} 358 nm; λ_{em} 461 nm). This nuclear stain exhibits bright blue fluorescence upon binding to AT-rich regions of the cellular DNA. DAPI is membrane-impermeable but after longer incubation or at higher concentration, it can enter living cells eventually. Stock solutions with a concentration of 100 ng/mL, prepared in Milli-Q water and stored at – 20 °C were diluted 1:10 in PBS^{++}, in order to obtain a working concentration of 10 ng/mL. Prior to staining of the cells with DAPI, usually fixation and permeabilization of the cells has to be performed, in order to facilitate diffusion of this stain across the cell membrane.

DAPI dissolved in PBS^{++} with the final concentration of 10 ng/mL was carefully added to the cells in a corresponding volume (~ 150 µL per well for the 8-well chamber and ~ 80 µL for Ø5 silicone tubes). As DAPI was used in this work for co-localization studies after loading of the cells with nucleic acids, fixation and permeablilization of the cells would possibly lead to a release of previously delivered material out of the cells. Therefore, the strategy of longer incubation times was applied for DAPI labeling. To let DAPI permeate across the cell membrane, cells were incubated for 15 min in the dark (at 37 °C and 5 % CO_2), instead for 2 min, as recommended for staining after cell fixation and membrane permeabilization. When cells were loaded with nucleic acids by cell fixation and permeabilization, subsequent DAPI staining was accomplished after only 2 min of incubation. Regardless of the incubation time, cell monolayers were rinsed once or twice with PBS^{++} in order to remove an excess of DAPI which did not enter the cell interior.

Since DAPI most probably intercalates with the cellular DNA, solutions were handled very carefully, by wearing impermeable nitrile gloves and all leftovers were disposed into special waste.

4.3.4.3 Staining of Cell Lysosomes with LysoTracker®

For selective staining of the cell lysosomes, the commercial probe LysoTracker® Blue DND-22 emitting blue fluorescence was applied (Mw = 524.403 g/mol; λ_{ex} 373 nm; λ_{em} 422 nm). This membrane-permeable probe is composed of a fluorophore coupled to a weak base and it accumulates within the acidic compartments (lysosomes) of living cells, thus labeling them. LysoTracker® was used in this work for co-localization studies with the DNA aptamers, after their delivery into the cell cytoplasm either by electroporation or chemical transfection.

LysoTracker® was stored at – 20 °C as a 1 mM stock solution and working solutions with a concentration of 1 µM in the corresponding cell culture medium were prepared shortly before

their application. LysoTracker® solutions were added to the cells in total volume of ~ 150 µL per well for the 8-well chamber and ~ 80 µL for Ø5 silicone tubes. The cells were subsequently incubated for 50 – 60 min in the dark at 37 °C and 5 % CO_2. Before microscopy, cells were rinsed with PBS^{++} to remove excess of extracellular LysoTracker®.

4.3.5 Microscopic Image Analysis by ImageJ

Phase-contrast and especially fluorescence microscopic images obtained in a digital format during microscopy had to be further processed using image processing software. For this purpose, the open source software ImageJ was used as a platform to process micrographs for statistical evaluation of microscopic features.

Within this work, molecule delivery into and release out of the cells by *in situ* electroporation has been studied. Some of the molecules used for these studies were either fluorescently-labeled (FITC-dextranes, calcein, fluorescent aptamers, etc.), cytotoxic (Cell Death siRNA) or they should interfere with the expression of fluorescent proteins (siRNA targeting EGFP genes). In any of those cases, an increase or a decrease in the fluorescence intensity was observed and quantified, in order to evaluate electroporation efficiency. As the pulse application took place only on the working electrodes, whereas cell population around the working electrodes (background) was not electrically manipulated, it was essential to compare the fluorescence intensity of the cells on the working electrodes with the remaining cell population within each well. For studies including microscopic imaging, electrode arrays 8W4Eµ were used, as they allow better statistics per well (4 circular electrodes instead of 1). With an objective providing 10-fold magnification, four electrodes within each well were observed and documented in pairs of two by two (**Figure 4.14 A**). Latter image analysis was carried out by selecting the electrodes area on each micrograph and subtracting it from the whole image area, in order to obtain intensity values for a background area (**Figure 4.14 B**). Values of integrated pixel brightness were measured and calculated for selected areas (ROI = region of interest) using ImageJ software. Fluorescence intensity of a given ROI was divided by the number of contributing pixels, in order to normalize and compare the brightness of cells on the electrodes with a background area that is used as an untreated control. The samples were compared with controls and corresponding statistic evaluation was conducted (including calculation of mean value and standard deviation). Electrodes/background calculations were performed for each well and for each condition (**Figure 4.15**). The value for a pair of electrodes was divided by the background value within each image in order to get normalized values and thus better comparison with respect to the possible image-to-image variations.

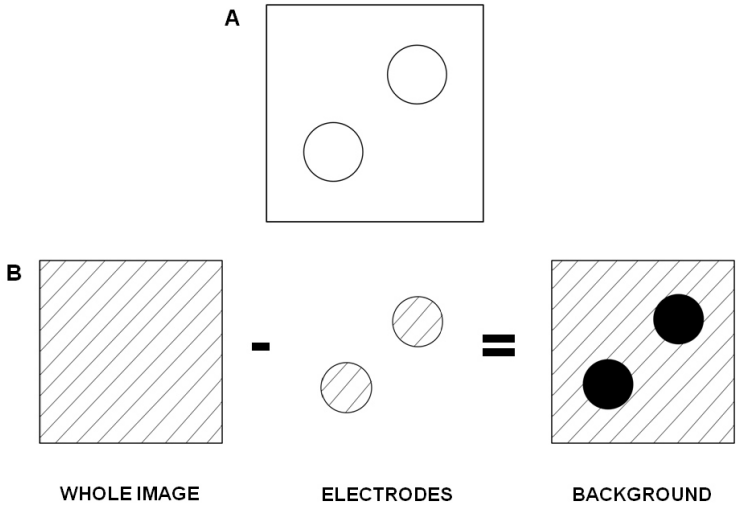

Figure 4.14 Schematically illustrated principle used for the evaluation of microscopic images of the cells on 8W4Eμ arrays. **A** A typical microscopic image shows two small electrodes (out of four in each well). **B** Areas of the sample covered by electrodes were subtracted from the integrated image intensity in order to obtain values for the brightness of the background area. Values for electrodes and background were used for further analysis.

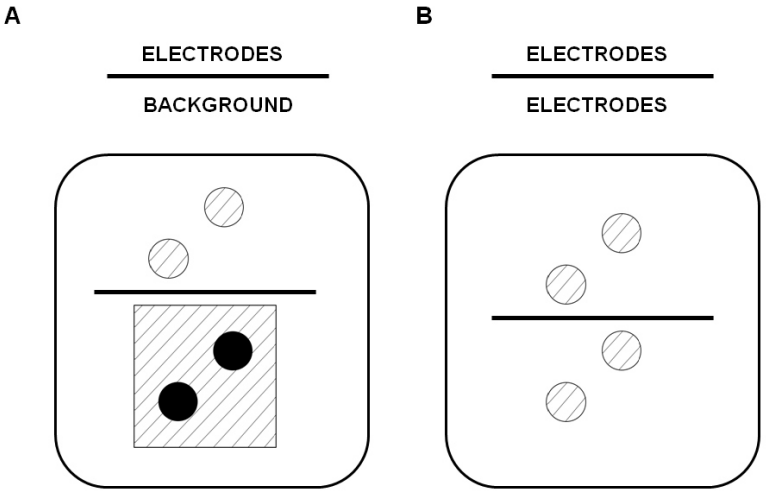

Figure 4.15 Schematically illustrated principle used for the evaluation of microscopic images on 8W4Eμ arrays. **A** Intensity values for a pair of electrodes were normalized to the average intensity of the background values within each image. **B** Intensity values for a pair of electrodes were compared to another electrode pair by only considering the average intensity on the electrode surface, without any background correction.

Different microscopic images were compared by taking the average brightness of pixels

representing the electrode, regardless from the background area. For evaluation of images obtained after chemical transfection (no electrodes involved), the whole image area was used for averaging of pixel brightness and subsequent comparison.

4.4 Nucleic Acids and Chemical Transfection

4.4.1 Nucleic Acids

In order to study delivery of nucleic acids into confluent cultures of mammalian cells by *in situ* electroporation and their fate once they enter the intracellular environment along with potential biological effect on cells, several models have been established and examined within this work, considering different types of oligonucleotides. These are the emerging types of oligonucleotides, which hold a very promising role in therapeutics and diagnostics nowadays, experiments were performed with (DNA) aptamers and small interfering RNA (siRNA). When working with oligonucleotides, especially with siRNA, it is necessary to maintain a nuclease-free environment (DNase- and RNase-free) to avoid their hydrolysis by the nucleases. Therefore, the flow hood was thoroughly cleaned before every experiment, in order to remove traces of DNases and RNases. Instead of standard pipette tips, special DNase/RNase-free filter tips were used, for up to 10 and 100 µL volume pipetting. Also, special DNase/RNase-free 0.5 mL plastic tubes were used to prepare small volume solutions. Whenever buffers for nucleic acids were being prepared, DNase/RNase-free Corning 50 mL centrifuge tubes were used. Instead of Milli-Q water, specially purified DNase/RNase-free water was used.

4.4.1.1 Aptamers

Delivery of aptamers into confluent cell monolayers was studied using DNA aptamers designed not to bind any extracellular nor intracellular target (containing random sequence), but to carry a green fluorescent label in order to be able to follow and localize aptamers once they enter the cells. Most of these studies were done using DNA aptamer 1 (APT 1). This single-stranded DNA oligonucleotide contains 50 nucleotides and a fluorescence modification (FAM-EX-5) coupled to the 5'- end (FAM-EX-5). DNA aptamer 1 (APT 1) was synthesized at 1.0 µmol scale (more details are listed in a **Table 4.11**). In addition, another non-targeting DNA aptamer 2 was applied (APT 2) to examine if there is any difference in binding pattern compared to APT 1 and basically to be sure, there is no specific binding of APT 1 inside the cells. The aptamer APT 2 was designed to have similar properties as APT 1 (number of nucleotides, the same fluorescent modification on 5'- end, molecular weight,

concentration, etc.), except the random sequence of APT 2 was different compared to APT 1 (the order of nucleobases was completely changed). The aptamer APT 2 was synthesized at 0.2 µmol scale and all relevant details for it can be found as well in **Table 4.11**).

Table 4.11 Overview of the most relevant properties for synthesis of DNA aptamers APT 1 and APT 2.

Oligonucleotide	Length (A,G,C,T)	E260 [cm^2/µmol]	Mw [g/mol]	Amount [nmol]	OD_{260nm}	Concentration [nmol/µL]
Aptamer 1 (APT 1)	50 (14,18,12,6)	507.24	16196.12	75.0	38.0	0.1
Aptamer 2 (APT 2)	50 (14,18,12,6)	507.24	16196.12	21.0	10.7	0.1

Both APT 1 and APT 2 contain random non-targeting sequence and these two sequences are given in **Table 4.12**.

Table 4.12 Sequences of the DNA aptamers APT 1 and APT 2.

Oligonucleotide	Sequence
Aptamer 1 (APT 1)	5'- AAG ATA CGC GTC TCC AGG GAT AAA TGA GGA CGA CCG CAG CGC GTG CGA GG - 3'
Aptamer 2 (APT 2)	5'- GTC GCG TGA CAT GAG GCG CGA CGT GCG AGC ACG ACA ACA GAG TGA ACA TG - 3'

Both oligonucleotides APT 1 and APT 2 have the same fluorescent modification with FAM-EX-5, covalently bound to the 5'- end of the oligonucleotides and its chemical structure with extended linker arm between oligonucleotide and dye is shown in **Figure 4.16**. The absorbance and emission for this dye are: 491 nm and 515 nm, respectively, with a molar absorbance coefficient of 86000 L/molcm.

Fluorescently-labeled DNA aptamers APT 1 and APT 2 were shipped as ready-to-use 100 µM stock solutions, both dissolved in TE-Buffer (10 mM Tris, 1 mM EDTA, brought to pH 8.0 with HCl) and were immediately stored at −20 °C upon receipt.

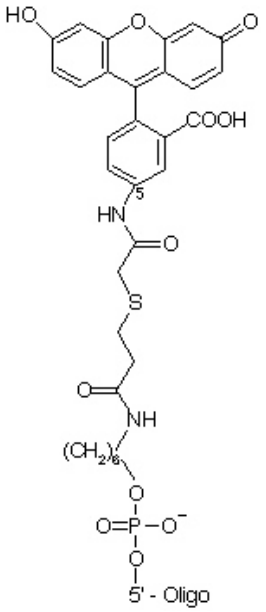

Figure 4.16 Chemical structure of the FAM-EX-5 modification coupled to the DNA aptamers APT 1 and APT 2.

4.4.1.2 Small Interfering RNA

In order to study the delivery of small interfering RNA (siRNA) into confluent cells by *in situ* electroporation, as well as to compare it with some other delivery methods (chemical transfection and permeabilization of fixed cells), different types of siRNA were applied.

Transfection Indicator (siGLO Red)

The commercially available transfection indicator siGLO™ Red was applied to optimize the experimental protocols for electroporation and chemical transfection and to visualize the localization of siRNA within the cells. This double-stranded, chemically synthesized RNA was chemically labeled with Thermo Scientific™ NuLight™ DY-547 fluorophore (absorption/emission max: 557 nm/ 570 nm). The manufacturer noted that the chemical modification of this oligonucleotide was done to prevent its uptake by RISC and to assure its optimal localization in the cell nucleus. This transfection indicator is not intended to provide information about siRNA function or duration of silencing, but to determine optimal siRNA transfection conditions and for monitoring relative efficiency of delivery when co-transfected with bioactive siRNA (information adapted from the producer's website http://dharmacon.gelifesciences.com). The siGLO Red was shipped as dried pellet in amber tubes and was stored at –20 °C upon receipt. In order to prepare ready-to-use 20 µM stock solution of readily anealed siGLO Red, 250 µL of 1 x siRNA buffer had to be added to 5 nmol

lyophilized siGLO Red in the tube. According to the producer's recommendations, first RNase-free 5 x siRNA buffer had to be prepared and subsequently it was diluted with RNase-free water, in order to obtain fresh 1 x siRNA buffer as a solvent for the siGLO Red pellet. 5 x siRNA buffer was prepared according to the recipe adapted from the producer's homepage (Dharmacon™ Protocol) and it contains: RNase-free water, 300 mM potassium chloride, 30 mM HEPES (free acid), 1.0 mM magnesium chloride hexahydrate and 2 M potassium hydroxide pellets. Buffer was adjusted to pH 7.5 and stored at 4 °C. By adding four volumes of RNase-free water to one volume of 5 x siRNA buffer, 250 µL of 1 x siRNA buffer was prepared and added to siGLO Red lyophlisate. The solution was mixed gently for 30 min at RT and ready-to-use 20 µM siGLO Red was aliquoted into smaller volumes subsequently stored at –20 °C.

Small Interfering RNA Targeting EGFP

Small interfering RNA (siRNA) causing sequence-specific knockdown of genes responsible for enhanced green fluorescent protein (EGFP) expression is called siEGFP. For studies including siEGFP, CHO-GFP cells served as a cell model. CHO-GFP are genetically modified CHO-K1 cells to stably express EGFP. This sequence-specific siRNA was purchased in a form of two unmodified single-stranded RNA oligonucleotides (sense and antisense strand), each containing 22 nucleobases and synthesized at 0.5 µmol scale (**Table 4.13**). Both strands were shipped in a dried form and were immediately stored at –20 °C upon receipt. These two single strands, sense and antisense had to be annealed before use, in order to get a stable double-stranded siRNA targeting EGFP (siEGFP).

Table 4.13 Overview of the most relevant properties for synthesis of two unmodified single strands (sense and antisense) of RNA, which are later annealed to obtain double-stranded sequence-specific siRNA targeting EGFP (siEGFP).

Oligonucleotide	Sequence (5' → 3')	OD_{260nm}	Amount [nmol]	Volume for 100 pmol/µL	Mw [g/mol]
Sense EGFP	GAA CUU CAG GGU CAG CUU GCC G (22)	12.0	51.2	512	7033
Antisense EGFP	GCA AGC UGA CCC UGA AGU UCA U (22)	2.3	9.5	95	7001

Lyophilized oligonucleotides were dissolved in RNase-free water, according to the manufacturer's recommendation and for that, 512 µL and 95 µL of RNase-free water was added to sense and antisense strand, respectively. Thus, solutions of sense and antisense

EGFP were obtained, each of them with the concentration of 100 pmol/µL. In order get a stable double-stranded siRNA, complementary single strands (sense and antisense) of RNA had to be annealed according to the standard protocol (Elbashir et al., 2001). This was done with the kind help of the working group of Prof. Dr. Göpferich (Pharmaceutical Technology Department, University of Regensburg).

For annealing of two RNA strands the 10 x annealing buffer was prepared, containing 100 mM TRIS-hydrochloride, 1 M sodium chloride and 10 mM ethylenediaminetetraacetic acid. The pH value of 10 x annealing buffer was adjusted to pH 7.5 by freshly prepared 1 M sodium hydroxide and controlled by pH paper.

To obtain 100 µL solution with 15 pmol/µL (15 µM) of double-stranded siEGFP:

15 µL of 100 pmol/µL of sense EGFP,

15 µL of 100 pmol/µL of antisense EGFP,

10 µL of 10 x annealing buffer and

60 µL of RNase-free water

were added into a small plastic PCR tube (0.2 mL), mixed and placed in the Thermocycler. The annealing process was started by heating the solution to 70 °C for 10 min. Subsequently, the oligonucleotide solution was allowed to cool down slowly to 25 °C. Freshly annealed 15 µM solution of siEGFP was aliquoted into small RNase-free plastic tubes and stored at –20 °C.

Small Interfering RNA Inducing Cell Death

Cell Death siRNA causes knockdown of genes responsible for cell viability and thus induces cell death (siCD). This siRNA is commercially available under the name “AllStars Mm/Rn Cell Death Control siRNA” and is meant to serve as a positive control for assays including siRNA, as well as for siRNA transfection optimization. The sequence and actual target gene(s) of Cell Death siRNA are proprietary and were not disclosed. Cell Death siRNA (or siCD) was provided as already annealed double-stranded oligonucleotide, in a lyophilized state and it was stored under –20 °C upon receipt. Each tube contained 1 nmol lyophilized siRNA and according to the producer's recommendation, 100 µL of sterile RNase-free water (provided together with the siCD) was added to the tube, in order to obtain 10 µM of ready-to-use stock solution, which was mixed, divided into aliquots and immediately stored at –20 °C.

Small Interfering RNA With Random Sequence

For all studies involving siEGFP and siCD, a conventional siRNA negative control was applied. This double-stranded siRNA has a random non-targeting sequence and is usually

called scrambled siRNA (siSCR). Scrambled siRNA is synthesized to have all properties of siRNA but its random (scrambled) sequence does not cause any gene knockdown within the cells. It serves as a control for any off-target effects, which may occur during experiments involving siRNA. A commercially available “AllStars Negative Control siRNA” was purchased as already annealed, double-stranded unmodified siRNA, with proprietary sequence. Upon receipt in a lyophilized state, siSCR was stored at –20 °C. To obtain the 20 µM ready-to-use stock solution of siSCR, 250 µL of RNase-free water (provided together with siSCR) was added to the 5 nmol of lyophilized siRNA, the solution was mixed and 20 µM siSCR was aliquoted and stored at –20 °C.

4.4.2 Chemical Transfection

Within all non-viral strategies for delivery of oligonucleotides into the cells, the most common and most frequently used method is chemical transfection. Among the most employed reagents or chemical assistants for transfection are cationic lipids (Felgner et al., 1987). Cationic lipid-mediated transfection reagents facilitate siRNA and DNA delivery into the cells (Chesnoy and Huang, 2000; Hirko et al., 2003) due to their polycationic nature. Thanks to the positively charged groups in their structure, cationic lipids, such as DOTMA, DOTAP (monovalent lipids) or DOGS (multivalent lipid), interact with negatively charged nucleic acids and form complexes with them (cationic liposome with DNA or siRNA), also known as lipoplexes (Faneca et al., 2013). The positively charged headgroup leads to an interaction with the phosphate backbone of the nucleic acid and after condensation, the resulting complex has a net positively charged surface which promotes its successful binding to the negatively charged cell membrane due to electrostatic interactions (Hoekstra et al., 2007). The higher number of positive charges (multivalent lipids) is often linked to an enhanced efficiency in condensing DNA, in comparison to the single positively charged (monovalent) lipids. Multivalent cationic lipids may be also more active than monovalent lipids, however in some cases they form less stable and more toxic lipoplexes (Faneca et al., 2013).

The cells take up the lipoplex and internalize it in intracellular vesicle through a process called endocytosis. Once inside the cell interior, the lipoplex should escape the endocytotic pathway, as the nucleic acid material should be released into the cell cytoplasm and furthermore possibly enter the cell nucleus, in order to find its targets or provide efficient gene expression (Wasungu and Hoekstra, 2006). Steps of lipoplex internalization are critical as they determine the fate of nucleic acids inside the cells and their mechanism of action.

Cationic lipid-mediated transfection allows relatively simple and cheap delivery of oligonucleotides in a wide variety of eukaryotic cells. There are many commercial chemical

transfection reagents on the market and the appropriate one should be chosen with respect to the cell type and the oligonucleotide of interest (DNA, siRNA). For chemical transfection studies within this work, the commercial transfection reagent Lipofectamine® was used, as it showed an appropriate transfection efficiency for both DNA and RNA molecules in a variety of different cell lines (Breunig et al., 2007; Hunt et al., 2010;Thompson et al., 1999).

4.4.2.1 Experimental Protocol for Chemical Transfection

Chemical transfection with the commercial transfection reagent Lipofectamine® was performed according to the protocol provided by the manufacturer. An important precondition for this experimental procedure was that the cells should not reach full confluency, but the monolayer should be in a subconfluent state (70 – 90 % confluency) when chemical transfection was performed. For the chemical transfection protocol serum-free medium is required, as it is essential to provide an environment free of enzymes/proteins normally present in serum, which can easily degrade and denaturate nucleic acids before they even enter the cells. Therefore, special commercially available OPTI-MEM® medium was used, as an improved nuclease-free substitute for self-prepared serum-free medium. For the chemical transfection experiments, either ECIS electrode arrays with 8-well chambers were used (8W4Eμ) in order to conduct impedimetric monitoring, or plastic chambers with 8 wells glued and fixed into tissue culture Petri dishes, when only microscopic investigation was necessary. The protocols provided by the manufacturer were adjusted with respect to the cell growth area and volume for wells of 8-well chambers.

A schematic illustration of the protocol is presented in a **Figure 4.17**. In order to perform chemical transfection in one well, two solutions had to be prepared in separate tubes. Firstly, the transfection reagent Lipofectamine® (1.2 µL) had to be diluted in a small volume (20 µL) of SFM in a small tube (solution B). In another tube (solution A), the nucleic acid solution had to be diluted in a small portion of SFM (20 µL per well) as well, independent of on its type (siRNA or DNA). The volume of nucleic acid solution used per well was calculated and applied with respect to the desired final concentration. Thus prepared solutions A and B were mixed gently and left for incubation at RT for 5 – 10 min. Thereafter, solution B was entirely added to solution A with the pipette, resuspended and mixed carefully a few times. Usually, the volume of a mixture A+B for one well was 45 – 50 µL and it was left for incubation at RT for 10 – 15 min in order to allow formation of liposome and oligonucleotide complexes – lipoplexes. Since there are 8 wells available for one experiment, transfection with nucleic acids of one concentration was conducted at least in duplicates (two wells). Usually two different concentrations were tested (two times two wells). Corresponding controls including

transfection reagent in SFM without nucleic acid and SFM only containing nucleic acid were also included within these experiments.

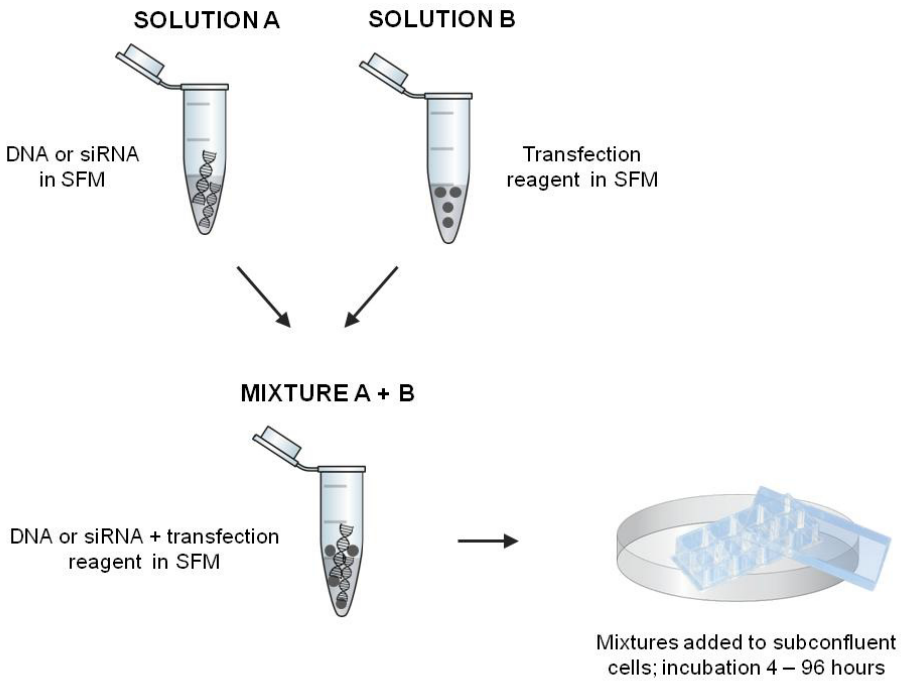

Figure 4.17 Schematic illustration of the experimental protocol for chemical transfection using the commercial transfection reagent Lipofectamine®. Drawings are not to scale.

Mixture A+B was added carefully to the cells after incubation, the whole array or Petri dish was "rocked" by moving it quickly but still gently for approximately 2 min. Thereafter, 200 µL of SFM was added to each well, independent of nucleic acid and transfection reagent content and cells were placed immediately into a cell culture incubator. An ECIS array with the cells was immediately connected to an ECIS machine and impedance monitoring of chemical transfection was started. According to the protocol provided by the manufacturer, evaluation of the chemical transfection efficiency (e.g. by microscopy) was performed at least four hours after transfection, as during this time period, lipoplex formation and internalization within the cells takes place.

4.4.2.2 Chemical Transfection with Aptamers

For delivery of DNA aptamers into cells by chemical transfection, Lipofectamine® 3000 Reagent was used, as it is recommended as "the most efficient versatile reagent" for cationic lipid-assisted delivery of DNA molecules into various cell types (www.thermofisher.com). The experimental protocol for chemical transfection was conducted as described in a previous

subchapter (4.4.2.1). In addition, a small amount of P3000™ Reagent (0.8 µL per well) was added to the DNA aptamer dissolved in SFM before the contents of the two tubes were mixed carefully and incubated at RT for 5 – 10 min. Reagent P3000™ was supplied by the manufacturer along with the Reagent Lipofectamine® 3000 in a separate tube, as its use is recommended only for transfection with DNA molecules (not for RNA). P3000™ is a nonionic detergent which acts as a dispersing agent for DNA oligonucleotides that may be relatively insoluble in aqueous solution and assists their internalization within the cells. According to the manufacturer, it has a low toxicity. After cells were transfected according to the standard protocol (chapter 4.4.2.1), 4 hours of incubation inside the cell culture incubator took place prior to microscopic investigation. In cases where co-staining of the lysosomes was necessary for the experiment (chapter 4.3.4.3), the incubation time after transfection was app. 3 hours. Thereafter, SFM (OPTI-MEM) was aspirated out of the wells and medium containing LysoTracker® was added to the cells for additional 60 min of incubation, followed by regular microscopic investigation using CLSM.

The DNA aptamer concentration applied for chemical transfection of the cells was 206 nM (205.8 nM). Chemical transfection of the cells in presence of aptamers was evaluated only by microscopy.

4.4.2.3 Chemical Transfection with Small Interfering RNA

For the delivery of small interfering RNA into cells by chemical transfection, Lipofectamine® RNAiMAX Reagent was used, as it is recommended by the literature (Breunig et al., 2008) for cationic lipid-assisted delivery of siRNA molecules into cells and gene knockdown studies. The protocol for chemical transfection was conducted as described in chapter 4.4.2.1. The incubation time was varied depending on the siRNA type in the range between 20 and 100 hours. As siGLO Red and siEGFP induced an increase or a decrease in the fluorescence of cell structures which was evaluated by fluorescence microscopy, cells were left inside the cell culture incubator for certain period of time prior to microscopy. For experiments including siCD, it was essential to obtain information on its cytotoxic effect. Therefore, chemical transfection was followed by impedance monitoring started immediately after addition of the transfection cocktail at the commercial ECIS machine (ECIS 1600R). In this case, microscopic evaluation was performed, if necessary, after finishing the impedance measurement, by taking fluorescence and phase-contrast images. 20 – 24 hours after performing chemical transfection, SFM was replaced by complete cell culture medium in each well under sterile conditions. For this, the impedimetric measurement was in most cases paused and the array was taken out of the array holder in order to perform medium

exchange in the flow hood under sterile conditions. After that, the array was remounted and the measurement was continued. Depending on the cell line, the concentration of siRNA used for chemical tansfection varied in the range from 25 to 200 nM (or from 6 to 48 pmol).
To facilitate more effective delivery of siRNA into cells by chemical transfection, manufacturer recommended seeding the cells in an antibiotic-free medium. Both antibiotics and siRNA oligonucleotides are negatively charged and during transfection, they could compete to form lipoplexes with cationic lipids, which can significantly affect transfection efficiency with siRNA molecules. Therefore, when NRK cells were chemically transfected with siCD, this strategy was applied and cells were seeded to the electrode array in absence of antibiotics in the cell culture medium.

4.5 Other Techniques and Procedures

4.5.1 Fixation and Permeabilization

Fixation of the cells and their subsequent membrane permeabilization is usually used as a method of preparation prior to staining of intracellular structures for microscopy. As this protocol allows membrane-impermeable compounds to enter the cells, it has been widely used in this work as an additional control for studies of electroporation and chemical transfection. The protocol is very simple and starts by washing of the cells with PBS^{++} buffer. Fixation of the cellular monolayer was performed using paraformaldehyde (PFA), which was added carefully as a 4 % (w/v) solution in PBS^{++} to the cells (~ 150 µL per well for the 8-well chamber and ~ 80 µL for Ø5 silicone tubes). Incubation followed for 10 min at RT. Thereafter, the PFA solution was aspirated and 0.2 % Triton-X-100 detergent in PBS^{++} was added to the cells in the corresponding volume (~ 150 µL per well for the 8-well chamber and ~ 80 µL for Ø5 silicone tubes) to permeabilize the cell membrane. The incubation took 10 min at RT and subsequently the detergent was carefully removed. Finally, the sample solution (aptamer, siRNA, Ca-AM, etc.) in PBS^{++} was added to the cells and the applied concentration was corresponding to the concentration used in electroporation studies. Incubation with the sample took usually 40 – 60 min at 37 °C and 5 % CO_2 in the dark. Afterwards, the cells were washed once and microscopic investigation was performed, following the usual protocol described in chapter 4.3.

4.5.2 LDH Assay

For the study of intracellular material release during *in situ* electroporation, the loss of a certain intracellular marker molecule induced by the short-term cell membrane

permeabilization was quantified by measuring its extracellular concentration. It is assumed that the opening of cell membrane and its resealing shortly afterwards will cause the release of cytosolic enzyme lactate dehydrogenase (LDH) out of the cells, which is expressed in a wide range of different cell lines. Upon damage (or permeabilization) of the cell membrane, LDH is released into the extracellular medium and quantification of extracellular LDH present in the media is performed by a commercial LDH assay (Pierce™ LDH Cytotoxicity Assay Kit). This colorimetric method is based on LDH catalyzed conversion of lactate to pyruvate by reduction of NAD+ to NADH (illustrated in a **Figure 4.18**).

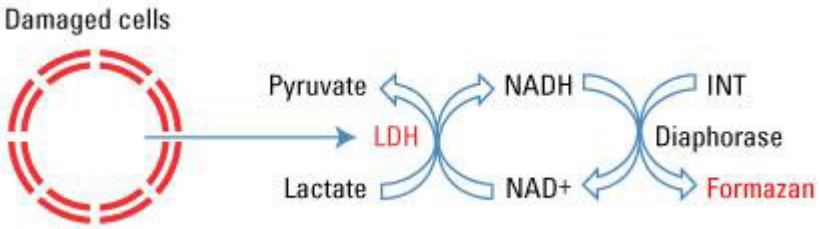

Figure 4.18 Schematic illustration of the mechanism of action for LDH assay, adapted from the producer's website (www.thermofisher.com).

In a coupled enzymatic reaction, NADH is used by a diaphorase for the reduction of a tetrazolium salt (INT) into its product formazan, which exhibits red color and can be quantified by photometry at 490 nm (www.thermofisher.com). As the amount of formazan is directly proportional to the amount of extracellular LDH, the LDH assay serves mostly as a cellular cytotoxicity assay.

Within the intracellular material release study, it was the initial idea to employ the LDH assay to evaluate and compare the levels of LDH released when cells are being electroporated once, twice and three times. In order to verify that the LDH assay is sensitive enough to be used in such release studies, the experimental procedure was first tested by performing the LDH assay after irreversible cell damage – electric wounding. In other words, the amount of released (extracellular) LDH present in the media was measured when the complete cell population present on the electrode(s) was irreversibly damaged. This way, wounding served as a positive control for LDH release by *in situ* electroporation.

The experimental procedure for electric wounding was conducted according to the standard protocol described in chapter 4.2.3, including application of the standard electric pulse parameters for wounding: 40 kHz, 5 V and 30 s. Array type 8W4Eμ was used in combination with either Ø5 silicone tubes (working volume was 50 μL per well), or Ø3 silicone tubes within the 8-well chambers (working volume of 40 μL per well and additional 100 μL of $EBSS^{++}$

around the small silicone tubes). Before the impedimetric measurement on commercial ECIS machine (ECIS 1600R) was started, complete cell culture medium was aspirated and 40 µL (for 8W4Eµ-Ø3) or 50 µL (for 8W4Eµ-Ø5) of $EBSS^{++}$ buffer was added into the silicone tubes in each well. Baseline data was recorded for 30 – 60 min prior to wounding pulses were applied and afterwards, post-pulse monitoring took 10 – 15 min in order to assure LDH molecules have enough time to diffuse into the extracellular buffer. Subsequently, impedimetric monitoring was finished and the buffer (without cells) from each well was transferred carefully to 8 independent wells of a 96-well plate (with flat bottom) in order to run the LDH assay according to its standard protocol. The next step included the addition of a corresponding volume of Reaction Mixture to each well (40 µL/well when 8W4Eµ-Ø3 was previously used and 50 µL/well when 8W4Eµ-Ø5 was previously used for electrical wounding). Afterwards, the 96-well plate was covered with aluminum foil to assure incubation of the samples in the dark at RT for 1 – 1.5 hour. Finally, a corresponding volume (40 µL/well for 8W4Eµ-Ø3 and 50 µL/well for 8W4Eµ-Ø5) of Stop Solution was added to each well, before the microplate was placed into a microplate reading spectrophotometer, where it was gently mixed for 10 seconds and absorbance values were measured at 492 nm.

As the membrane damage caused by wounding of the cells on the ECIS electrode arrays was induced only in the cells present directly on the working electrodes, whereas the rest of the cells in the well remain unaffected, it is clear that only a very small population of cells take part in the assay within each well. In contrast, standard LDH assay is set up for 96-well plate format with the entire cell population present in the well is under study. Therefore, an additional control was included within one of the experiments, in which the complete cell population in the Ø5 well was killed or damaged by addition of Lysis Buffer (to $EBSS^{++}$) at the beginning, before impedimetric measurement was started. Thus, the difference in LDH level between wells in which the entire cell population was damaged (by lysis) and wells in which only a small cell population was damaged (by wounding) were directly compared. All solutions for LDH cytotoxicity assay including: Reaction Mixture (prepared out of Substrate Mix and Assay Buffer), Stop Solution and Lysis Buffer were provided by the manufacturer and were ready-to-use.

Appropriate negative controls were included within each experiment, with all steps of the protocol, except the cells in the control wells were not exposed to the wounding.

4.6 References

Bai, D., del Corsso, C., Srinivas, M., and Spray, D.C. (2006) Block of specific gap junction channel subtypes by 2-aminoethoxydiphenyl borate (2-APB). *Journal of Pharmacology and Experimental Therapeutics* 319, 1452-1458.

Boukamp, P., Petrussevska, R.T., Breitkreutz, D., Hornung, J., Markham, A., and Fusenig, N.E. (1988) Normal keratinization in a spontaneously immortalized aneuploid human keratinocyte cell line. *The Journal of Cell Biology* 106, 761-771.

Breunig, M., Hozsa, C., Lungwitz, U., Watanabe, K., Umeda, I., Kato, H., and Goepferich, A. (2008) Mechanistic investigation of poly(ethylene imine)-based siRNA delivery: Disulfide bonds boost intracellular release of the cargo. *Journal of Controlled Release* 130, 57–63.

Breunig, M., Lungwitz, U., Liebl, R., and Goepferich, A. (2007) Breaking up the correlation between efficacy and toxicity for nonviral gene delivery. *Proceedings of the National Academy of Sciences of the United States of America* 104, 14454-14459.

Chesnoy, S., and Huang, L. (2000) Structure and function of lipid-DNA complexes for gene delivery. *Annual Review of Biophysics and Biomolecular Structure* 29, 27-47.

de Larco, J.E., and Todaro, G.J. (1978) Growth factors from murine sarcoma virus-transformed cells. *Proceedings of the National Academy of Sciences of the United States of America* 75, 4001-4005.

Elbashir, S.M., Lendeckel, W., and Tuschl, T. (2001) RNA interference is mediated by 21- and 22-nucleotide RNAs. *Genes and Development* 15, 188-200.

Faneca, H., Cardoso, A., Trabulo, S., Duarte, S., and de Lima Pedroso, M.C. (2013) Cationic liposome-based systems for nucleic acid delivery: From the formulation development to therapeutic applications. In Drug delivery systems: advanced technologies potentially applicable in personalised treatment, J. Coelho, ed. (Springer Netherlands), pp. 153-184.

Felgner, P., Gadek, T., Holm, M., Roman, R., Chan, H., Wenz, M., Northrop, J., Ringold, G., and Danielsen, M. (1987) Lipofection: a highly efficient, lipid-mediated DNA transfection procedure. *Proceedings of the National Academy of Sciences of the United States of America* 84, 7413–7417.

Freshney, R.I. (2005) Culture of specific cell types. In Culture of animal cells (John Wiley & Sons, Inc.)

Freshney, R.I. (2006) Basic principles of cell culture. In Culture of cells for tissue engineering (John Wiley & Sons, Inc.), pp. 1-22.

Giaever, I., and Keese, C.R. (1984) Monitoring fibroblast behavior in tissue culture with an applied electric field. *Proceedings of the National Academy of Sciences of the United States of America* 81, 3761-3764.

Giaever, I., and Keese, C.R. (1986) Use of electric fields to monitor the dynamical aspect of cell behavior in tissue culture. *IEEE Transactions on Biomedical Engineering* 33, 242-247.

Giaever, I., and Keese, C.R. (1991) Micromotion of mammalian cells measured electrically. *Proceedings of the National Academy of Sciences of the United States of America* 88, 7896-7900.

Hirko, A., Tang, F., and Hughes, J.A. (2003) Cationic lipid vectors for plasmid DNA delivery. *Current Medicinal Chemistry* 10, 1185-1193.

Hoekstra, D., Rejman, J., Wasungu, L., Shi, F., and Zuhorn, I. (2007) Gene delivery by cationic lipids: in and out of an endosome. *Biochemical Society Transactions* 35, 68-71.

Hunt, M.A., Currie, M.J., Robinson, B.A., and Dachs, G.U. (2010) Optimizing transfection of primary human umbilical vein endothelial cells using commercially available chemical transfection reagents. *Journal of Biomolecular Techniques: JBT* 21, 66-72.

Jainchill, J.L., Aaronson, S.A., and Todaro, G.J. (1969) Murine sarcoma and leukemia viruses: assay using clonal lines of contact-inhibited mouse cells. *Journal of Virology* 4, 549-553.

Kao, F.T., and Puck, T.T. (1968) Genetics of somatic mammalian cells, VII. Induction and isolation of nutritional mutants in Chinese hamster cells. *Proceedings of the National Academy of Sciences of the United States of America* 60, 1275-1281.

Lukic, S., and Wegener, J. (2015) Impedimetric monitoring of cell-based assays. In Encyclopedia of Life Sciences (John Wiley & Sons, Ltd.), pp. 1–8.

Mericko, P., Helmirch, A., Chen, L., Kusamoto, K., Toumadje, A., Chapline, C., Sato, D., and Barnes, D.W. (2002) Cell Culture: Basic Procedures. In Encyclopedia of Life Sciences (John Wiley & Sons, Ltd.)

Minsky, M. (1988) Memoir on inventing the confocal scanning microscope. *Scanning* 10, 128-138.

Pucihar, G., Kotnik, T., Miklavcic, D., and Teissie, J. (2008) Kinetics of transmembrane transport of small molecules into electropermeabilized cells. *Biophysical Journal* 95, 2837–2848.

Reddy, N., Tan, Y., Li, Y., and Yang, Y. (2008) Effect of Glutaraldehyde Crosslinking Conditions on the Strength and Water Stability of Wheat Gluten Fibers. *Macromolecular Materials and Engineering* 293, 614-620.

Rols, M.-P., and Teissié, J. (1998) Electropermeabilization of Mammalian Cells to Macromolecules: Control by Pulse Duration. *Biophysical Journal* 75, 1415–1423.

Schwartz, S.M. (1978) Selection and characterization of bovine aortic endothelial cells. *In Vitro Cellular and Developmental Biology* 14, 966-980.

Semwogerere, D., and Weeks, E.R. (2005) Confocal microscopy. In Encyclopedia of Biomaterials and Biomedical Engineering (CRC Press)

Stolwijk, J.A. (2012) Electric manipulation and impedance analysis of adherent cells on gold-film electrodes. PhD thesis, Universität Regensburg

Tekle, E., Astumian, R.D., and Chock, P.B. (1994) Selective and asymmetric molecular transport across electroporated cell membranes. *Proceedings of the National Academy of Sciences of the United States of America* 91, 11512-11516.

Thompson, C.D., Frazier-Jessen, M.R., Rawat, R., Nordan, R.P., and Brown, R.T. (1999) Evaluation of methods for transient transfection of a murine macrophage cell line, RAW264.7. *Biotechniques* 27, 824-832.

Tjio, J.H., and Puck, T.T. (1958) Genetics of somatic mammalian cells. II. Chromosomal constitution of cells in tissue culture. *The Journal of Experimental Medicine* 108, 259-268.

Wasungu, L., and Hoekstra, D. (2006) Cationic lipids, lipoplexes and intracellular delivery of genes. *Journal of Control Release* 116, 255-264.

Webb, D.J., and Brown, C.M. (2013) Epi-fluorescence microscopy. *Methods in Molecular Biology* 931, 29-59.

Wegener, J., Keese, C.R., and Giaever, I. (2000) Electric cell-substrate impedance sensing (ECIS) as a noninvasive means to monitor the kinetics of cell spreading to artificial surfaces. *Experimental Cell Research* 259, 158-166.

Wegener, J., Keese, C.R., and Giaever, I. (2002) Recovery of adherent cells after in situ electroporation monitored electrically. *Biotechniques* 33, 348 - 352.

Zink, S., Rösen, P., Sackmann, B., and Lemoine, H. (1993) Regulation of endothelial permeability by beta-adrenoceptor agonists: contribution of beta 1- and beta 2-adrenoceptors. *Biochimica et Biophysica Acta* 1178, 286-298.

5 *In Situ* Electroporation of Adherent Cells: Methodological Aspects

Since its introduction in the beginning of 1990s (Giaever and Keese, 1984; 1986; 1991), electric cell-substrate impedance sensing (ECIS) has been established over years as one of the most versatile and sensitive analytical methods for monitoring cell-based assays. In addition, ECIS is a label-free and non-invasive approach of cells sensing in real time, which attracts growing interest of researchers around the world, who would like to apply ECIS to monitor and assess diverse phenomena in living cell systems.

Among many various cell-based assays that can be investigated using ECIS technology is *in situ* electroporation (Lukic and Wegener, 2015). This well-established technique for delivery of membrane-impermeable molecules into confluent cells growing on the planar electrodes (Wegener et al., 2002; Stolwijk et al., 2011) has found application in biotechnology, biomedical research and cell biology (Stolwijk, 2012). Electroporating pulses are applied using planar gold film electrodes, which at the same time allow non-invasive monitoring of the cellular behavior. Electroporation is thus integrated into measurements of impedance magnitude. Impedance sensing by ECIS provides wealth of information on cell morphology, viability and motility. These parameters and their possible changes are monitored in real time, before and after application of electric pulses, in a non-invasive and sensitive manner.

The main focus of this work was to explore if *in situ* electroporation can be applied for introduction of certain bioactive molecules (i.e. nucleic acids, second messengers) into mammalian cells, while the cellular response is measured by ECIS. In addition, this work should contribute to further investigation and optimization of *in situ* electroporation. Therefore, in this section experiments are summarized which were done to: (i) optimize pulse parameters for every cell line applied in this work, (ii) verify and optimize application of multiple pulses as a strategy to increase electroporation efficiency, (iii) investigate membrane resealing after its permeabilization by *in situ* electroporation, monitored with high time resolution and finally (iv) to investigate the possibility to release intracellular material from the cells by *in situ* electroporation.

5.1 Optimization of Electric Pulses Used for *In Situ* Electroporation

Within this work various cell lines were applied for studies of *in situ* electroporation. Experimental procedures, like pulse parameters and number of pulses for efficient delivery of diverse xenomolecules into various cell lines were initially investigated and optimized using

fluorescently-labeled probes (250 kDa FITC-dextran and propidium iodide) as reporters for cell loading. Experiments were conducted on 8W4Eμ electrode arrays, and as a buffer during electroporation experiments, $EBSS^{++}$ was applied. Invasive electric pulses were applied by using alternating current (AC), whereby parameters for the applied electric field were varied with respect to frequency, pulse amplitude and pulse duration (Wegener et al., 2002). Whereas frequency of voltage pulses was kept constant during all electric manipulations (40 kHz; Wegener et al., 2002), pulse amplitude and duration of pulses were varied in order to find an appropriate combination, which provides effective loading of xenobiotics (here fluorescent probes) into the cells and at the same time minimize potential cytotoxic effect of the technique (Rols and Teissié, 1998a). The values of amplitude and duration applied for *in situ* electroporation by ECIS system (ISE) differ from the conventionally applied values for electroporation of the cells in suspension (more details are given in chapter 3.2.2. of Theoretical Background). Firstly, single pulses were optimized for different cell lines, with respect to amplitude and duration. After that, strategy of multiple pulse application was verified using NRK as a cell model.

5.1.1 Evaluation of Electroporation Efficiency

Optimal combination of parameters for single electroporation pulse was evaluated with respect to voltage (U [V]) and pulse duration (t [ms]). The frequency of AC sinusoidal voltage pulses was not varied and was always kept at 40 kHz. To assure that maximally efficient and minimally invasive electric pulses are going to be applied for *in situ* electroporation, for every cell line an ideal combination of frequency, amplitude and pulse duration had to be found. Amplitude values are varied in a range from 2 to 5 V. Pulse durations have been varied in a range from 50 to 700 ms and during optimization studies in this work, they were applied in the range 200 – 700 ms. *In situ* electroporation (ISE) with well-defined pulse parameters induces transient reversible permeabilization of the cell membrane, which allows diffusion of membrane-impermeable probes into cytosol. Fluorescently-labeled FITC-dextran (with size of 250 kDa) was applied here as a membrane-impermeable probe to study optimal pulsing conditions. As shown in **Figure 5.1 A**, events before and after *in situ* electroporation were monitored impedimetrically by ECIS in non-invasive and time-resolved fashion. Microscopic evaluation of fluorescent dye uptake to assess electroporation efficiency (**Figure 5.1 B**-**D**) was subsequently performed. In **Figure 5.1**, impedimetric monitoring of BAEC cells before and after ISE in presence of 250 kDa FITC-dextran illustrates a typical pulse optimization experiment. Initially, after culture medium in every well was replaced with the buffer ($EBSS^{++}$), measurement at ECIS was started and impedance magnitude was recorded for

several minutes, until the cells established a stable signal (baseline). Fluorescent probe 250 kDa FITC-dextran was added to cells (marked with a), to obtain final concentration of 2 mg/mL of fluorescent probe per well. After steady state was reestablished, electroporating pulses were applied with defined pulse parameters (marked with b). While other two parameters were kept constant (40 kHz, 4 V), pulse duration was varied (200 – 300 – 400 ms). ISE caused short membrane permeabilization and impedance signal dropped accordingly. The minimum in impedance after pulse application was directly proportional to the pulse duration. Thereafter, recovery of the cells after electroporation and return of impedance to pre-pulse values took place (in the example in graph **A**, not the entire recovery process was followed). Return of impedance magnitude takes usually 30 to 45 min.

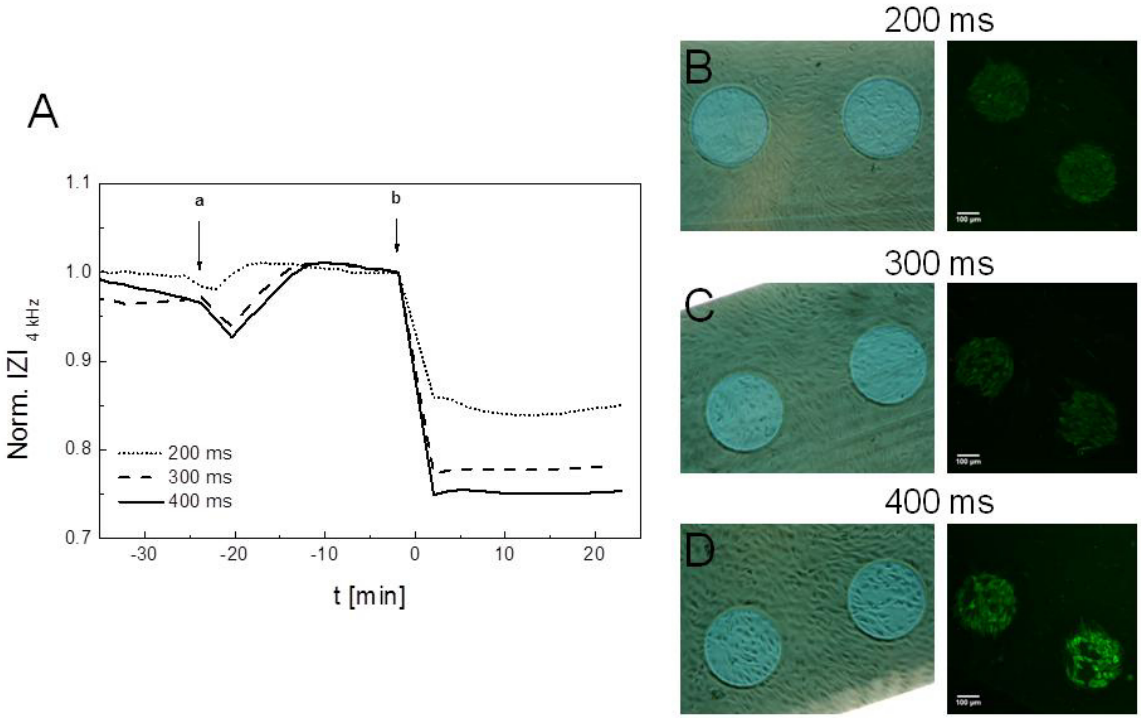

Figure 5.1 A Typical time course of the normalized impedance before, during and after *in situ* electroporation of BAEC cells in presence of 250 kDa FITC-dextran. The time point of FITC-dextran addition is marked with **a**. Pulses with constant frequency (40 kHz) and amplitude (4 V) were applied (at the time point marked with **b**), whereas pulse duration was varied. Impedance magnitudes were normalized to the last time point before electroporation. **B, C, D** Exemplary micrographs taken by CLSM with 10-fold objective to document electroporation efficiency (scale bar corresponds to 100 µm).

As already discussed in a theoretical part (chapter 3.2.2), resealing of membrane pores and recovery of the cells takes much shorter time (from several seconds to a few minutes), but reassembling of the confluent cell monolayer and return of the cells to steady state

morphology certainly takes a longer period of time, which is usually needed after ISE for signal to return to the pre-pulse values. In the example presented in **Figure 5.1 A**, the post-pulse time period was kept short in order to avoid unspecific adsorption of FITC-dextran to the cells, which is sometimes observed after long post-pulse incubation.

Fluorescence micrographs taken subsequently by CLSM with 10-fold magnification objective showed loading of BAEC cells with FITC-dextran. Fluorescent probe could enter the cells after ISE in all three cases, but longer duration of electric pulse led to damage of cell monolayer on the electrodes and loss of some cells from the electrodes. Shorter pulse duration facilitated transfer of FITC-dextran into entire cell population of BAEC cells on the electrodes and caused no visible damage in the cells. To better visualize the appearance of the cells on the electrodes, it is necessary to either take micrographs with (3 times) zoomed single electrodes, or to enlarge electrodes on existing micrographs, as it had been done for the micrographs presented in **Figure 5.1** (**B**, **C**, **D**). Images of single electrodes are summarized in **Figure 5.2**, to obtain a better overview of loading efficiency and invasiveness of applied pulses.

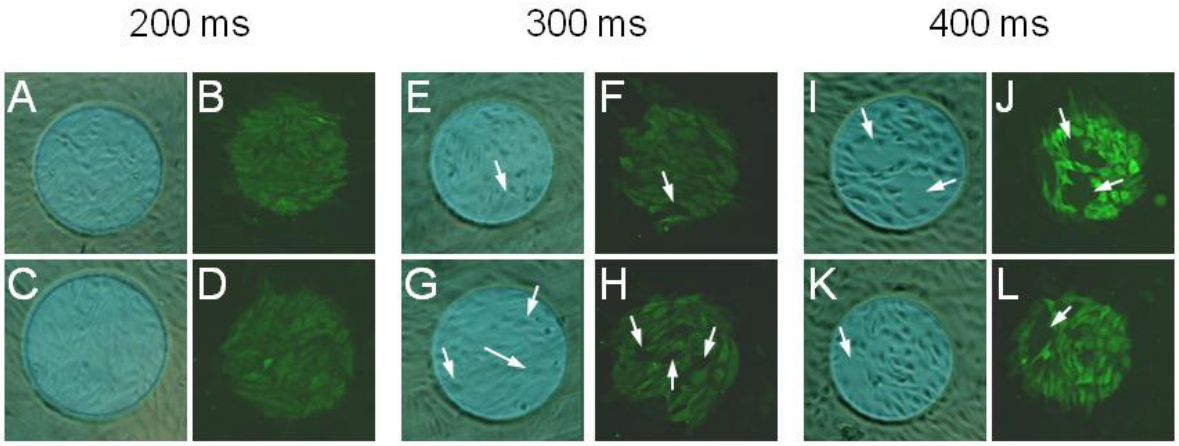

Figure 5.2 Exemplary microscopic images representing the respective enlarged micrographs given in **Figure 5.1**. Images **A-D** show electrodes with cells treated with 200 ms, images **E-H** electrodes with cells treated with 300 ms and images **I-L** show electrodes with BAEC cells treated with 400 ms long pulse duration, whereas frequency and amplitude were kept constant (40 kHz and 4 V, respectively). White arrows indicate damaged and missing cells on the electrodes.

Pulse duration of 200 ms (**A-D**) did not cause cell damage and detachment of the cells from the electrodes, while loading efficiency was very good and FITC-dextran was observed in the cytoplasm of every cell. Pulse duration of 300 ms (**E-H**) gave satisfactory loading with fluorescent probe but also caused loss of single cells from the electrodes (indicated by the

arrows). The BAEC cells exposed to pulse duration of 400 ms (**I-L**) exhibited high fluorescent signal (cytosol successfully loaded with FITC-dextran), but longer pulse duration obviously caused cell damage in some cells, which led to loss of the whole groups of cells, which detached from the electrodes and were probably washed away during rinsing steps before microscopy. After analysis of impedance recordings and micrographs taken after ISE, the conclusion was made on optimal combination of pulse parameters for given cell line. The ideal combination which gave the best results, with respect to the loading efficiency and cyotoxic effect is: f=40 kHz; U=4 V; t=200 ms.

5.1.2 *In Situ* Electroporation of Different Cell Lines

To investigate delivery of various xenobiotics into cytoplasm of cells by ISE, different cell lines were applied within this work. The appearance of applied cell monolayers grown to confluence on 8W4Eμ electrode array is given in **Figure 5.3**. Exemplary phase-contrast micrographs show monolayers of **A** BAEC, **B** CHO-GFP (CHO-K1), **C** HaCaT, **D** NIH-3T3 and **E** NRK cells (the scale bars correspond to 100 μm).

As previously mentioned, ISE was applied using different combinations of pulse parameters to find optimal combination appropriate for every cell line individually. Whereas pulse amplitude and duration of pulses were varied during optimization studies, frequency of voltage pulses was kept constant (40 kHz) during all electric manipulations. Studies of ISE conducted by Wegener et al., 2002 describe frequency-dependent voltage drop across the cell monolayer and their observations that only with the sufficiently high frequencies (> 10 kHz) applied for AC pulses, a significant voltage can be delivered to the cells (on the electrodes) to induce their membrane permeabilization. The optimal pulsing frequency for every cell line can be extracted from impedance spectra of the cell-covered and the cell-free electrodes. The optimal pulsing frequency for NRK cells was found to be 40 kHz (Wegener et al., 2002) and it is very well applicable for other cell lines studied in this work as well, since measured impedance spectra for every cell line (data not shown) did not show significantly different electrical properties (compared to NRK cells; chapter 3.1.3).

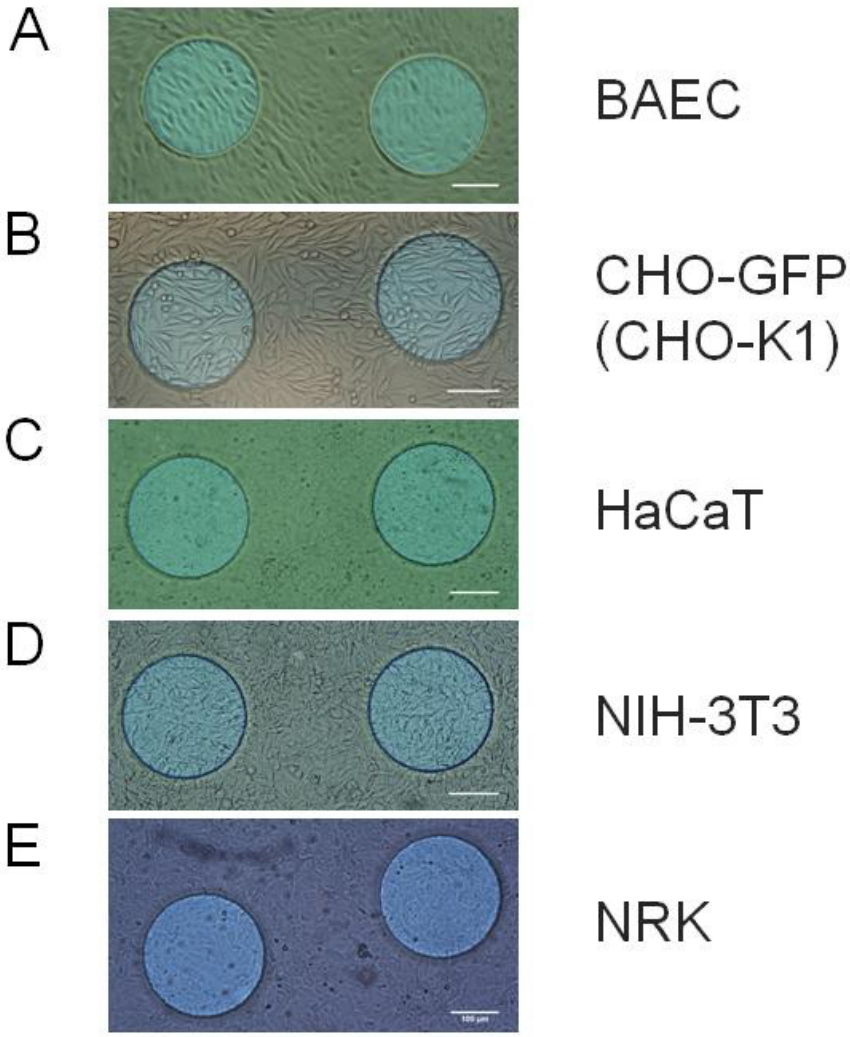

Figure 5.3 Exemplary phase-contrast micrographs of confluent cell monolayers: **A** BAEC; **B** CHO-GFP (CHO-K1); **C** HaCaT; **D** NIH-3T3 and **E** NRK cells grown on 8W4Eμ electrode array (scale bar corresponds to 100 μm). All cell lines were applied in this work as cell models within various studies of xenobiotics delivery into cytoplasm by *in situ* electroporation.

5.1.2.1 *In Situ* Electroporation of BAEC Cells

Confluent monolayers of BAEC cells grown on ECIS electrodes were exposed to electroporation in presence of 2 mg/mL FITC-dextran (250 kDa), dissolved in $EBSS^{++}$ buffer. According to the experimental protocol described in chapter 5.1.1, BAEC cells were pulsed with constant frequency (40 kHz) and pulse duration (200 ms), whereas pulse amplitude was varied (2 – 3 – 4 – 5 V). **Figure 5.4** shows time course of the normalized impedance at 4 kHz before, during and after ISE of BAEC cells. Fluorescent probe was added at the time point marked with a. After pulse application (b), impedance decrease was observed, when 3, 4

and 5 V were applied, whereas impedance signal slightly increased after the 2 V pulse. Profiles of normalized impedance gave insight into invasiveness of single pulses. After complete recovery of the cells, micrographs were taken by CLSM (with 10- and 60-fold magnification objective) to evaluate loading efficiency (exemplary micrographs are summarized in **Figure 5.5**).

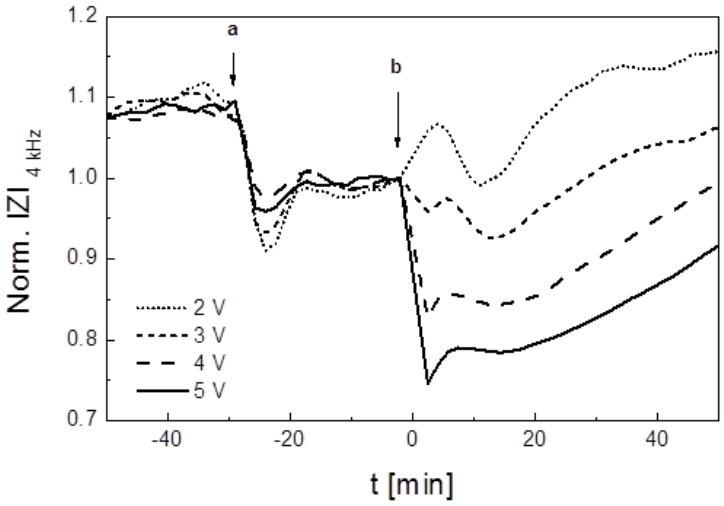

Figure 5.4 Typical time course of the normalized impedance at 4 kHz before and after *in situ* electroporation of BAEC cells in presence of 2 mg/mL FITC-dextran (250 kDa). After addition of fluorescent probe (**a**), cells were electroporated (**b**) using pulses of 40 kHz for 200 ms, whereas pulse amplitude was varied (2 – 3 – 4 – 5 V). Impedance magnitudes were normalized to the last time point before electroporation.

The cells pulsed with 2 V exhibited poor staining with FITC-dextran (**A**), as only several cells on the electrodes contained fluorescent probe in their cytoplasm. Dye uptake significantly improved after cells were pulsed with 3 V (**B**), 4 V (**C**) and 5 V (**D**) as the fluorescent dye entered most of the cells residing on the electrodes. It was concluded that the amplitude of 4 V gave the best results with respect to the loading efficiency and invasiveness of the pulse. In addition, unlike in other micrographs with BAEC cells, absence of nonspecific uptake of FITC-dextran by the cells was observed. Micrographs taken with higher magnification showed that the cells pulsed with 4 V gave the most satisfying results. It was observed that not all cells pulsed with 3 V were loaded with FITC-dextran and some cells on the electrodes were missing after pulsation with 5 V.

As already stated in chapter 5.1.1, the optimal combination of pulse parameters for *in situ* electroporation of BAEC cells on 8W4Eμ array is: f=40 kHz; U=4 V and t=200 ms.

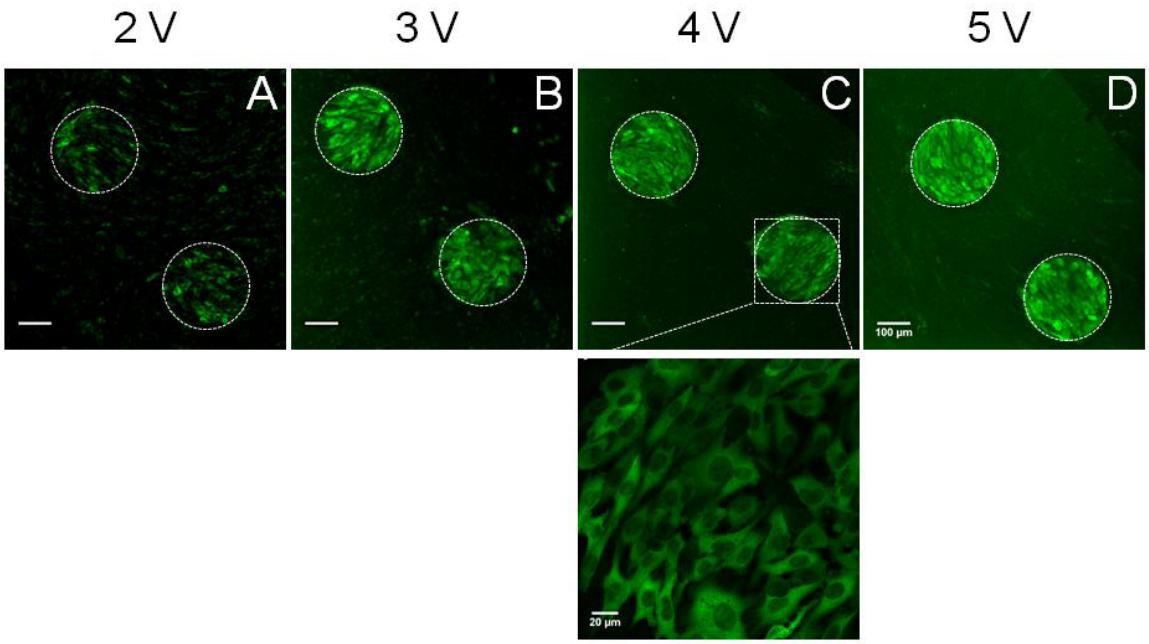

Figure 5.5 Exemplary confocal fluorescence micrographs taken with 10-fold magnification objective after *in situ* electroporation of BAEC cells in presence of 250 kDa FITC-dextran. Cells were pulsed at constant frequency (40 kHz) and pulse duration (200 ms), whereas amplitude was varied: **A** 2 V; **B** 3 V; **C** 4 V; **D** 5 V. In the top row, electrode areas are delineated by white circles and scale bar corresponds to 100 µm. Single micrograph in the lower panel represents a magnification of the cells on the electrode indicated by the dashed box in micrograph **C** (taken with 60-fold magnification; the scale bar corresponds to 20 µm).

5.1.2.2 *In Situ* Electroporation of CHO-K1 and CHO-GFP Cells

Pulse optimization for CHO cell lines was performed with CHO-K1 cells. This cell line grown on ECIS electrodes in a confluent state was exposed to electroporation in presence of 2 mg/mL FITC-dextran (250 kDa), dissolved in $EBSS^{++}$ buffer. According to the typical experimental protocol for ISE, CHO-K1 cells were pulsed with constant frequency (40 kHz), whereas amplitude and pulse duration were varied (3 V and 200 ms; 3 V and 500 ms; 4 V and 200 ms; 4 V and 500 ms). The experiment included controls where cells were not electroporated, but only incubated with the fluorescent probe. **Figure 5.6** shows typical time courses of the normalized impedance at 16 kHz before, during and after ISE of CHO-K1 cells. The FITC-dextran was added to the cells at the time point marked with a. After signal was stationary, electroporation pulses were applied (b). Normalized impedance signal of the cells pulsed with 3 V and 200 ms increased after pulse application and returned slowly over time to the baseline values. Impedance signal of the cells pulsed with 3 V and 500 ms and 4

V and 500 ms increased shortly after pulse application, then decreased and increased again until it reached certain higher values. A subsequent slow return to the lower impedance values took place over time. Finally, the normalized impedance signal of the cells pulsed with 4 V and 200 ms decreased after pulse application and then increase followed, after which impedance slowly decreased again. Obviously, time courses of the normalized impedance differ significantly after 3 V and 4 V pulse application. Whereas CHO-K1 cells pulsed with 3 V (either for 200 ms or 500 ms) exhibited lower signal increase, CHO-K1 cells pulsed with 4 V (both for 200 ms and 500 ms) showed higher increase of impedance signal after pulse application.

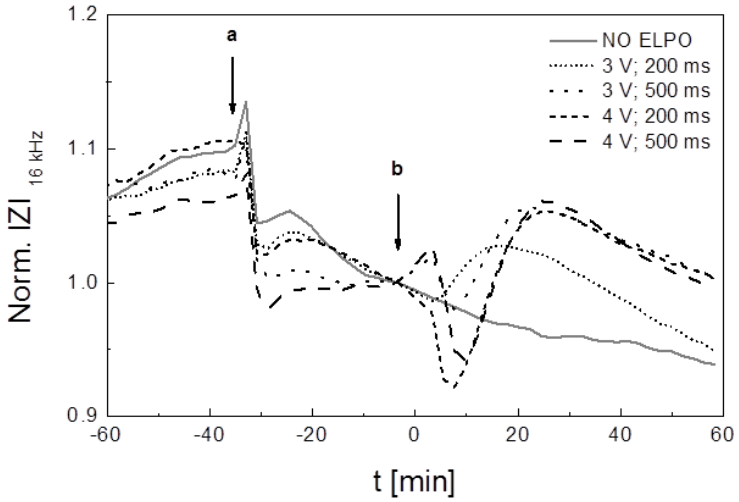

Figure 5.6 Typical time course of the normalized impedance at 16 kHz before and after *in situ* electroporation of CHO-K1 cells in presence of 2 mg/mL FITC-dextran (250 kDa). After addition of fluorescent probe (**a**), cells were electroporated (**b**) using pulses of 40 kHz, whereas pulse amplitudes and durations were varied: 3 V and 200 ms; 3 V and 500 ms; 4 V and 200 ms; 4 V and 500 ms. Impedance magnitudes were normalized to the last time point before electroporation.

After complete recovery of the cells after ISE, microscopy by CLSM (with 10-fold magnification objective) followed to evaluate loading efficiency. Exemplary fluorescence micrographs of CHO-K1 cells are summarized in **Figure 5.7**. In the control, when cells were not exposed to electroporation but only incubated in presence of fluorescence probe, no cell uptake was observed (**A**/**F**). Micrograph **A** shows that electrodes delineated with white circles exhibited a significant level of bright green fluorescence. This can be explained by the fact that very small diluted amount of fluorescent probe remained in the buffer during microscopy. Since the microscopic settings were set to higher gain in green channel in order to document even weak fluorescence signal and the gold electrodes' surface reflects the light, the circular

electrodes appear slightly brighter than the background. In the cells pulsed with 3 V and 200 ms, a very weak fluorescence signal was observed (**B**/**G**). Cells pulsed with 3 V and 500 ms (**C**/**H**) and with 4 V and 200 ms (**D**/**I**) were more efficiently loaded with FITC-dextran than in the previous sample (**B**/**G**), and the fluorescent probe entered only fraction of the cells on the electrodes. Dye uptake significantly improved after the cells were pulsed with 4 V and 500 ms (**E**/**J**), as fluorescent probe entered most of the cells residing on the electrodes. The optimal combination of pulse parameters for *in situ* electroporation of CHO-K1 and CHO-GFP cells on 8W4Eμ array was found to be: f=40 kHz; U=4 V and t=500 ms.

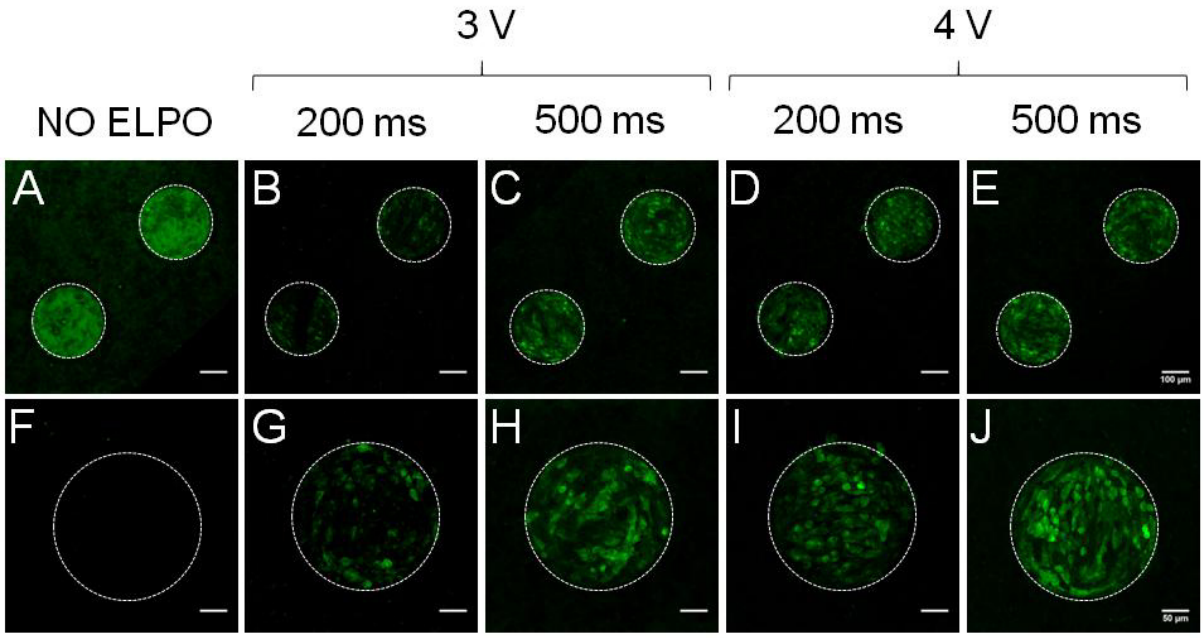

Figure 5.7 Exemplary confocal fluorescence micrographs taken with 10-fold magnification objective after *in situ* electroporation of CHO-K1 cells in presence of 250 kDa FITC-dextran. Cells were pulsed at constant frequency (40 kHz), whereas pulse amplitudes and durations were varied: **B**/**G** 3 V and 200 ms; **C**/**H** 3 V and 500 ms; **D**/**I** 4 V and 200 ms; **E**/**J** 4 V and 500 ms. The cells in control were not pulsed (**A**/**F**) The electrode areas are delineated by white circles, the scale bar in the top row corresponds to 100 μm and the scale bar in the lower panel corresponds to 50 μm.

5.1.2.3 *In Situ* Electroporation of HaCaT Cells

Confluent monolayers of HaCaT cells grown on ECIS electrodes were exposed to electroporation in presence of 2 mg/mL FITC-dextran (250 kDa), dissolved in $EBSS^{++}$ buffer. According to the standard experimental protocol for ISE, HaCaT cells were pulsed with constant frequency (40 kHz), whereas amplitudes and pulse durations were varied. Time

courses of the normalized impedance at 4 kHz are presented for two optimization experiments for HaCaT cells, one with rather weak electric fields and another with parameters causing more invasive pulses. This was done in order to demonstrate a need for stronger electric fields for ISE of this cell line.

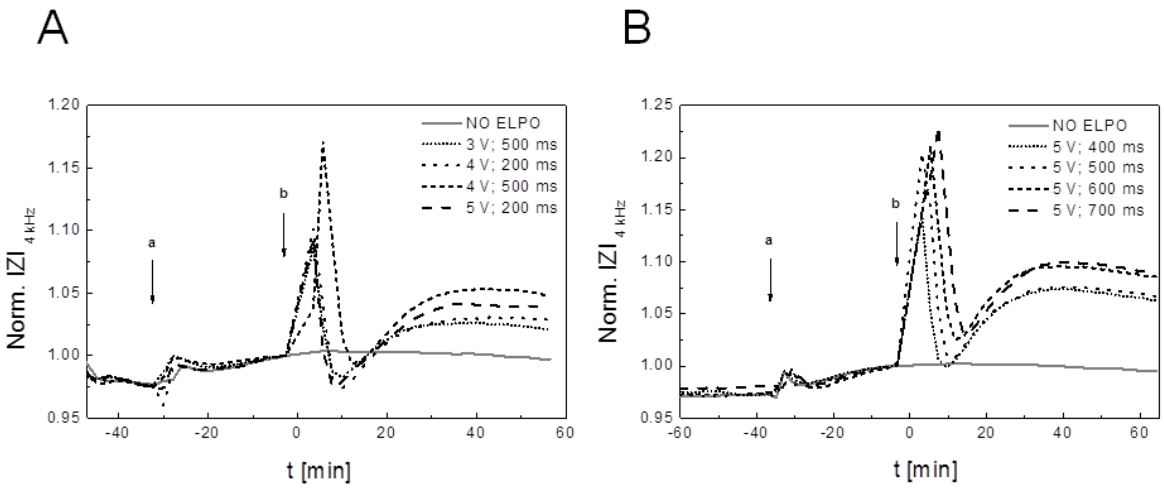

Figure 5.8 Typical time course of the normalized impedance at 4 kHz before and after *in situ* electroporation of HaCaT cells in presence of 2 mg/mL FITC-dextran (250 kDa) for two independent experiments. In both of them, after addition of the fluorescent probe (**a**), cells were electroporated (**b**) using pulse at 40 kHz, while **A** pulse amplitudes and durations were varied: 3 V and 500 ms; 4 V and 200 ms; 4 V and 500 ms; 5 V and 200 ms and in **B** pulse amplitude was constant (5 V) and durations were varied: 400 ms; 500 ms; 600 ms; 700 ms. Impedance magnitudes were normalized to the last time point before electroporation.

Fluorescent probe was added at the time point marked with a. After pulse application (b) in all samples, normalized impedance immediately jumped to the values in a range between 1.05 and 1.21, dependent on the invasiveness of the applied pulses. Immediately afterwards, signal dropped to either lower values and then increased again for less invasive pulses (**A**), or in the case of stronger pulses (**B**), returned to the baseline (pre-pulse values) and then increased once again slowly. After app. 40 min of post-electroporation recovery of the cells, micrographs were taken by CLSM (with 10-fold magnification objective) and loading efficiency was evaluated. The exemplary micrographs taken after experiment presented in graph **A** of the **Figure 5.8** are summarized in **Figure 5.9** and micrographs taken after electroporation presented in graph **B** are summarized in **Figure 5.10**.

In **Figure 5.9** micrographs show that loading of the cells with FITC-dextran increased with increasing invasiveness of electric pulses but it was still rather unsufficient. The best results

were obtained with 4 V and 200 ms, which was the most invasive combination of pulses applied within the experiment. In addition, impedimetric monitoring of events before and after *in situ* electroporation suggested that applied pulses were not very invasive for HaCat cells.

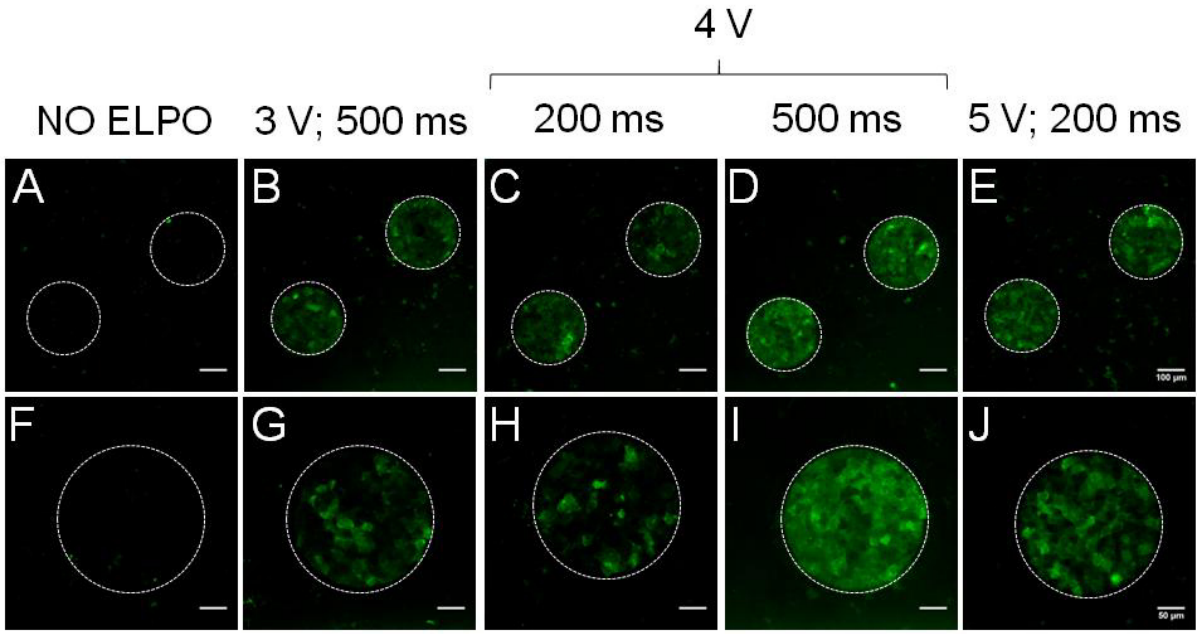

Figure 5.9 Exemplary confocal fluorescence micrographs taken with 10-fold magnification objective after *in situ* electroporation of HaCaT cells in presence of 250 kDa FITC-dextran. Cells were pulsed at constant frequency (40 kHz), while pulse amplitudes and durations were varied: **B**/**G** 3 V and 500 ms; **C**/**H** 4 V and 200 ms; **D**/**I** 4 V and 500 ms; **E**/**J** 5 V and 200 ms. The cells in control were not pulsed (**A**/**F**) The electrode areas are delineated by white circles. The scale bar in the top row corresponds to 100 µm, whereas the scale bar in the lower panel corresponds to 50 µm.

Therefore, another experiment was performed with more invasive electric pulses. The amplitude was kept at 5 V and pulse durations were varied along a relatively high range (400 – 700 ms). This resulted in a very good dye uptake in all four samples, whereas in control, no fluorescence signal was observed. Cells pulsed with 400 ms long pulses were still not entirely loaded with FITC-dextran, whereas cells pulsed with 700 ms exhibited several damaged cells on the electrodes. The cells pulsed with 500 and 600 ms long pulses showed the best results, with respect to the loading efficiency and almost no cell defects were seen. Since 600 ms is considered as rather long duration for *in situ* electroporation and may cause cell damage, pulse duration of 500 ms was chosen as the most appropriate to combine with 5 V, in order to successfully electroporate HaCaT cells. The optimal combination of pulse parameters for *in situ* electroporation of HaCaT cells on 8W4Eµ arrays, was found to be: f=40 kHz; U=5 V and t=500 ms.

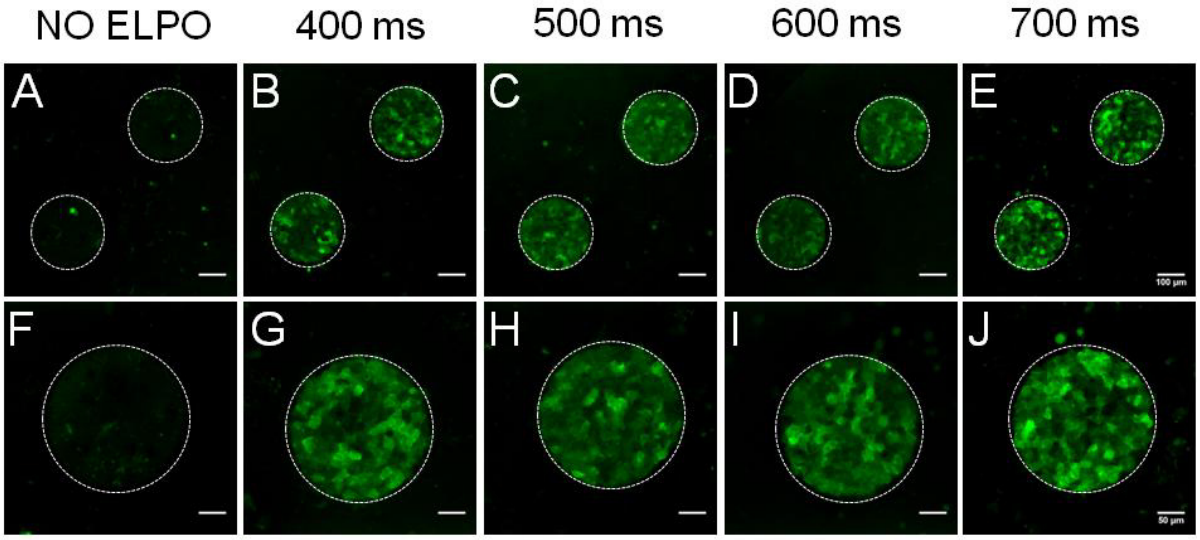

Figure 5.10 Exemplary confocal fluorescence micrographs taken with 10-fold magnification objective after *in situ* electroporation of HaCaT cells in presence of 250 kDa FITC-dextran. Cells were pulsed at constant frequency (40 kHz) and amplitude (5 V), whereas pulse durations were varied: **B**/**G** 400 ms; **C**/**H** 500 ms; **D**/**I** 600 ms; **E**/**J** 700 ms. The cells in control were not pulsed (**A**/**F**) The electrode areas are delineated by white circles. The scale bar in the top row corresponds to 100 µm, whereas the scale bar in the lower panel corresponds to 50 µm.

5.1.2.4 *In Situ* Electroporation of NIH-3T3 Cells

Confluent monolayers of NIH-3T3 cells grown on ECIS electrodes were exposed to electroporation in presence of 2 mg/mL FITC-dextran (250 kDa), dissolved in $EBSS^{++}$ buffer. According to the experimental protocol described in chapter 5.1.1, NIH-3T3 cells were pulsed with constant frequency (40 kHz), whereas pulse amplitude and pulse duration were varied (3 V and 500 ms; 4 V and 200 ms; 4 V and 500 ms; 5 V and 200 ms). **Figure 5.11** shows respective time courses of the normalized impedance at 4 kHz before, during and after ISE of NIH-3T3 cells. The fluorescent probe was added at the time point marked with a. After pulse application (b), impedance decrease was observed, dependent on invasiveness of the electrical pulse. The NIH-3T3 cells pulsed with 3 V and 500 ms exhibited only small and slightly delayed signal decrease, whereas NIH-3T3 cells exposed to pulses with 4 V and 200 ms, 4 V and 500 ms and 5 V and 200 ms exhibited immediate signal decrease and then increase, followed by slow signal recovery to pre-pulse levels. Magnitude of immediate normalized impedance decrease and increase after pulse application was dependant on pulse invasiveness, thus for NIH-3T3 cells pulsed with 4 V and 200 ms, signal decreased to 0.875, for cell pulsed with 4 V and 500 ms, signal decreased to 0.970, and for the cells

pulsed with 5 V and 200 ms, normalized impedance decreased to 0.945. The recovery of NIH-3T3 cells to pre-pulse levels took app. 20 - 25 min, whereby normalized impedance signal for cells exposed to 4 V and 500 ms and 5 V and 200 ms continued to increase after reaching the pre-pulse impedance levels. After recovery of the cells, micrographs were taken by CLSM with 10-fold magnification objective and loading efficiency was evaluated (exemplary micrographs are summarized in **Figure 5.12**).

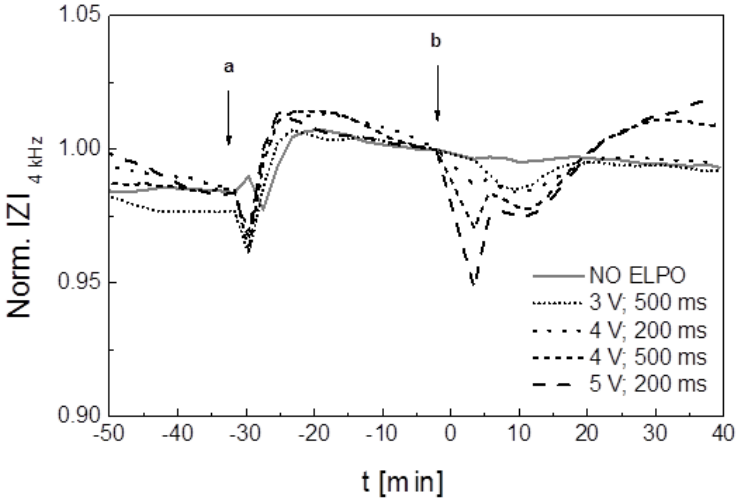

Figure 5.11 Typical time course of the normalized impedance at 4 kHz before and after *in situ* electroporation of NIH-3T3 cells in presence of 2 mg/mL FITC-dextran (250 kDa). After addition of fluorescent probe (**a**), cells were electroporated (**b**) using pulses with a constant frequency (40 kHz), whereas pulse amplitudes and durations were varied: 3 V and 500 ms; 4 V and 200 ms; 4 V and 500 ms; 5 V and 200 ms. Impedance data were normalized to the last time point before electroporation.

In the non-electroporated cells, several bright spots indicated weak non-specific uptake of FITC-dextran by NIH-3T3 cells. The cells pulsed with 3 V and 500 ms and 4 V and 200 ms were only partially loaded with FITC-dextran, whereas pulses of 4 V and 500 ms gave better results but still some partially blurred signals and unloaded cells were observed. Pulses of 5 V and 200 ms gave the best results, although some cells were missing on the electrodes.
In general, microscopy of NIH-3T3 cells was rather difficult, as they tend to detach from the substrate surface and the entire cell monolayer often rolled off as a carpet from the electrodes. Unfortunately, this hindered imaging of the cells on some electrodes with zoom and therefore, corresponding micrographs of single electrodes in **Figure 5.12** are missing. The optimal combination of pulse parameters for *in situ* electroporation of NIH-3T3 cells on 8W4Eμ array was found to be: f=40 kHz; U=5 V and t=200 ms.

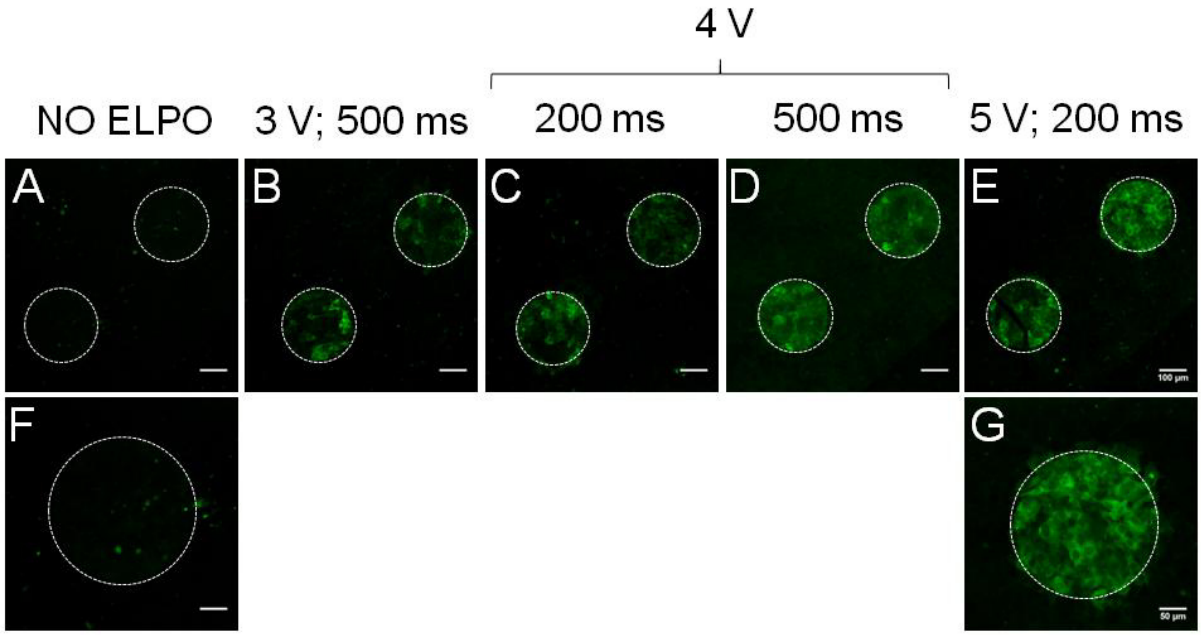

Figure 5.12 Exemplary confocal fluorescence micrographs taken with 10-fold magnification objective after *in situ* electroporation of NIH-3T3 cells in presence of 250 kDa FITC-dextran. Cells were pulsed at constant frequency (40 kHz), whereas amplitude and pulse duration were varied: **B** 3 V and 500 ms; **C** 4 V and 200 ms; **D** 4 V and 500 ms; **E**/**G** 5 V and 200 ms. The cells in control were not pulsed (**A**/**F**). The electrode areas are delineated by white circles. The scale bar in the top row corresponds to 100 µm, whereas the scale bar in the lower panel corresponds to 50 µm.

5.1.2.5 *In Situ* Electroporation of NRK Cells

NRK cells are well-established cell model for studies of ISE. Pulse parameters suitable for optimal *in situ* electroporation, with respect to the loading efficiency and invasiveness of the technique were found to be: f=40 kHz, U=4 V and t=200 ms, using fluorescent probe Lucifer yellow (Wegener et al., 2002). In addition, ISE in presence of 2 mg/mL FITC-dextran (250 kDa) was investigated on two different electrode layouts by Stolwijk, 2012 and the same results were obtained. Therefore, these optimized pulse parameters were applied in this work for ISE of NRK cells on 8W4Eµ and 8W1E electrode arrays. Nevertheless, experiments including ISE of NRK cells in presence of 2 mg/mL FITC-dextran (250 kDa) were performed to complete the optimization studies and to compare loading of NRK cells with FITC-dextran of relatively large size (250 kDa) with some bioactive molecules applied in this work. Confluent monolayers of NRK cells grown on ECIS electrodes were exposed to electroporation in $EBSS^{++}$ buffer. **Figure 5.13** shows time course of the normalized impedance at 4 kHz before, during and after ISE of NRK cells.

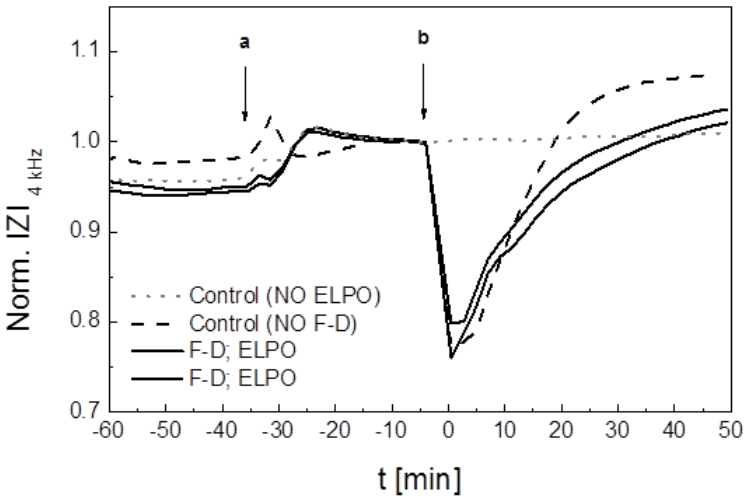

Figure 5.13 Typical time course of the normalized impedance at 4 kHz before and after *in situ* electroporation of NRK cells in presence of 2 mg/mL FITC-dextran (250 kDa). After addition of fluorescent probe (**a**), cells were electroporated (**b**) using optimized pulse parameters: 40 kHz, 4 V and 200 ms. Impedance magnitudes were normalized to the last time point before electroporation.

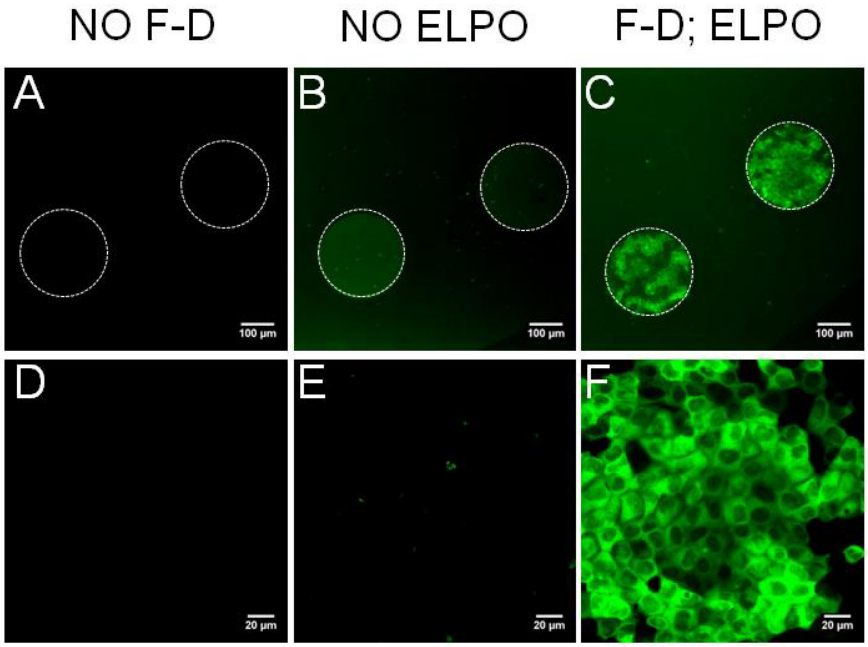

Figure 5.14 Exemplary confocal fluorescence micrographs taken with 10-fold (**A-C**) and 60-fold (**D-F**) magnification objective after *in situ* electroporation of NRK cells in presence of 250 kDa FITC-dextran. Cells were pulsed (**C**/**F**) using optimized pulse parameters: 40 kHz, 4 V and 200 ms. Two controls were made: ISE in absence of FITC-dextran (**A**/**D**) and cells were incubated with FITC-dextran, but not pulsed (**B**/**E**). The electrode areas are delineated by white circles. The scale bar in the top row corresponds to 100 µm, whereas the scale bar in the lower panel corresponds to 20 µm.

The fluorescent probe was added at the time point marked with a. After pulse application (b), significant impedance decrease was observed, followed by relatively fast recovery of the cells and return of impedance to pre-pulse values. Experiment included two controls: one with cells electroporated in absence of fluorescent probe and one with NRK cells being only incubated with FITC-dextran without pulse application. Subsequently, micrographs were taken by CLSM with 10- and 60-fold magnification objective. Exemplary micrographs are summarized in **Figure 5.14**. In the control where cells where pulsed only in buffer, no fluorescence signal was observed (**A**/**D**), control where cells were incubated with FITC-dextran in absence of pulse application (**B**/**E**) showed no fluorescence signal as well, with minor exceptions due to unspecific dye uptake. Cells on the electrodes, electroporated in presence of FITC-dextran were successfully loaded with the fluorescent dye. The FITC-dextran (250 kDa) was excluded from the nuclei due to its size, but filled entirely and homogeneously the cell cytoplasm (**C**/**F**). Most of the cells on the electrodes were successfully loaded with fluorescent dye, whereas only a few cells remained unloaded, or were damaged and washed away from the electrodes prior to microscopy. No cell damage was observed in NRK cells after optimized electroporation parameters were applied.

5.1.2.6 Survey of Optimized Parameters for *In Situ* Electroporation of Different Cell Lines

Optimized pulse parameters for different cell lines applied in this work are summarized in **Figure 5.15** with respect to the typical time course of the normalized impedance and exemplary micrograph taken by CLSM. The time necessary for impedance signal of each cell line to return to the pre-pulse values is indicated by the red part of the line.

This summary shows that individual cell lines require different periods of time for their complete recovery after ISE. Whereas normalized impedance of CHO-K1, CHO-GFP and HaCaT cells needs app. 10 – 20 min, NIH-3T3 cells app. 20 min and NRK cells 25 – 30 min to return to the pre-pulse values, recovery of impedance signal of BAEC cells takes app. 50 min. For most of the cell lines, normalized impedance values decrease after optimized pulse application. Only for HaCaT cells is characteristic that normalized impedance signal increases strongly and quickly returns to the pre-pulse values. Micrographs taken subsequently by CLSM show the cells residing on the electrodes after optimized ISE was applied in presence of 2 mg/mL FITC-dextran (250 kDa). Even when optimal combination of pulse parameter conditions is applied for ISE, certain differences in loading efficiency are observed between the different cell lines.

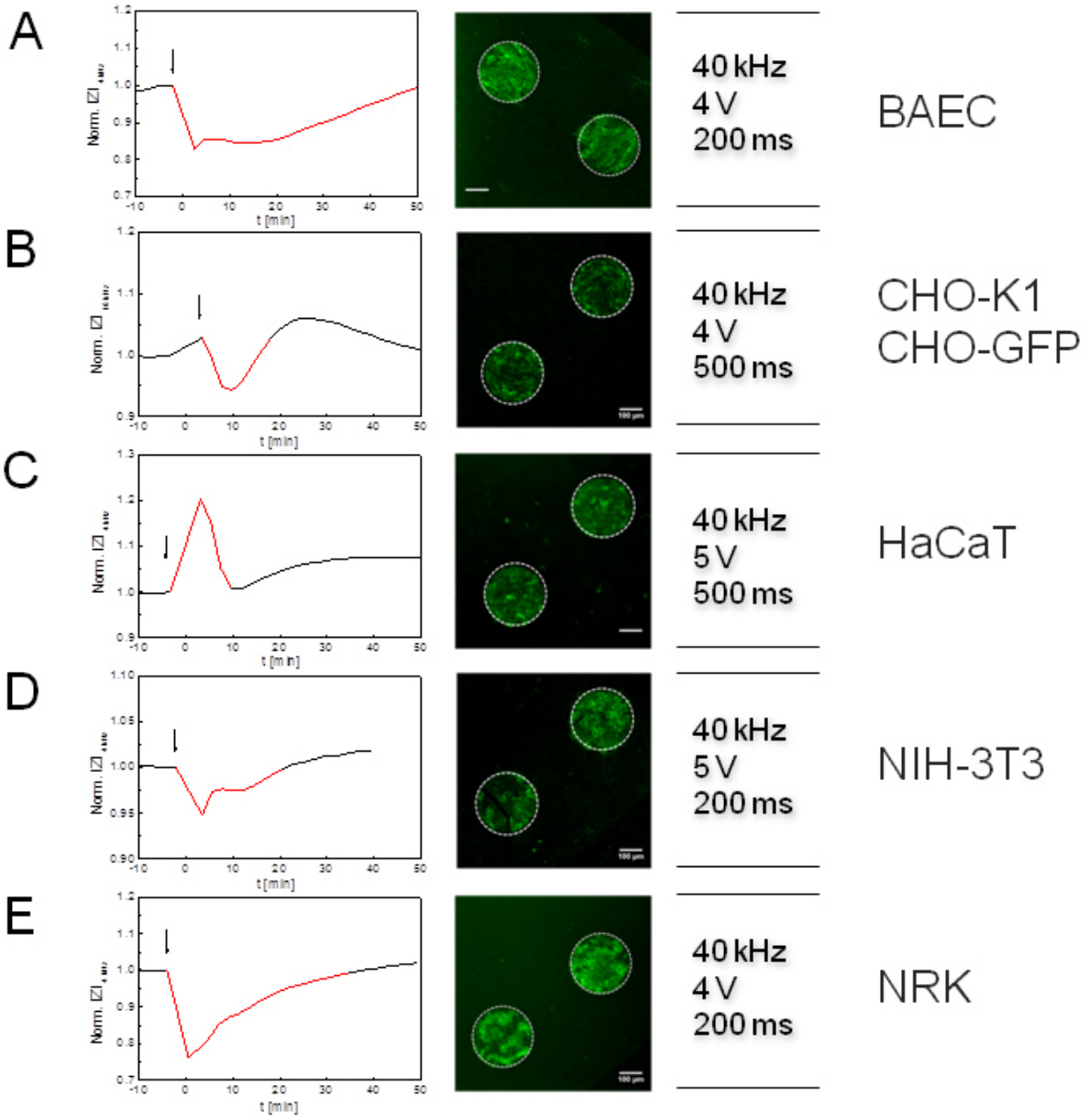

Figure 5.15 Survey presenting optimal combinations of pulse parameters for efficient *in situ* electroporation of various cell lines. For optimization experiments, 2 mg/mL (250 kDa) FITC-dextran was applied as a fluorescent probe. On the left side, time courses of the normalized impedance magnitude before and after application of ISE are presented. Arrow indicates the time point of pulse application. The red part of the lines indicates time period necessary for impedance signal to return to the pre-pulse values and corresponds to the recovery of the cell monolayers after their exposure to the electric pulse. Impedance data were normalized to the last time point before ISE. Exemplary fluorescence micrographs show the cells on the electrodes after optimal electric pulses were applied in presence of FITC-dextran. For all cells frequency was kept constant (40 kHz; Wegener et al., 2002) and pulse amplitude and duration were varied: **A** BAEC (4 V and 200 ms); **B** CHO-K1 / CHO-GFP (4 V and 500 ms); **C** HaCaT (5 V and 500 ms); **D** NIH-3T3 (5 V and 200 ms); **E** NRK (4 V and 200 ms).

5.1.3 *In Situ* Electroporation Using Multiple Voltage Pulses

Application of multiple electric pulses was applied as a strategy to enhance loading efficiency with the corresponding probe. Instead of single pulse applied to the confluent cell monolayer growing on planar ECIS electrodes, pulsation was applied two, three, or even four times (in some special cases). Pulse parameters for multiple pulsations were the same as for single pulses, previously optimized for every cell line.

To verify if two and three sequential pulses result in enhanced loading of the cells with xenobiotics, compared to the single pulses, NRK cells were used as a cell model. As a fluorescent probe 100 µM propidium iodide was applied. Propidium iodide (PI) is a membrane-impermeable red fluorescing dye which intercalates with DNA and is often applied as a reporter dye within the various electroporation studies (Rols and Teissié, 1998a; Pucihar et al., 2008). In this work, propidium iodide was a fluorescent probe of choice for studies of multiple ISE pulses, due to its ability to stain cell nuclei and to accumulate in the cells during repeatedly applied ISE. The aim of multiple electroporation studies was to investigate if and to which extent, subsequently repeated ISE pulses can lead to an increase of loading efficiency. Thus, PI seemed to be the best choice, as its presence and accumulation in the cell nuclei could be easily visualized, with regards to the number of applied pulses.

The cells grown to confluence on ECIS electrodes were exposed to single and multiple electroporation, and $EBSS^{++}$ was applied as an assay buffer. According to the typical experimental protocol for ISE, NRK cells were pulsed using optimal combination of pulse parameters: 40 kHz, 4 V and 200 ms. The experiment included control with cells not being electroporated, but only incubated with the fluorescent probe. **Figure 5.16** shows typical time course of the normalized impedance at 4 kHz before, during and after multiple ISE of NRK cells in presence of PI. The 100 µM propidium iodide was added to the cells at the time point marked with a. After signal became stationary, electroporation pulse was applied three time successively, as indicated by the arrows, b: 1^{st} pulse, **c**: 2^{nd} pulse and d: 3^{rd} pulse application. After every pulse, normalized impedance decreased immediately and returned within app. 20 - 30 min to the pre-pulse values. Between the pulses, cells were allowed to recover entirely to the state before pulse application, in order to avoid potential cytotoxic effect of ISE. After the third and last pulse, cells were allowed to completely recover and stabilize before impedimetric monitoring was finished.

Subsequently, micrographs were taken by CLSM (with 10-fold magnification objective) to evaluate loading efficiency and exemplary confocal fluorescence micrographs are summarized in **Figure 5.17**.

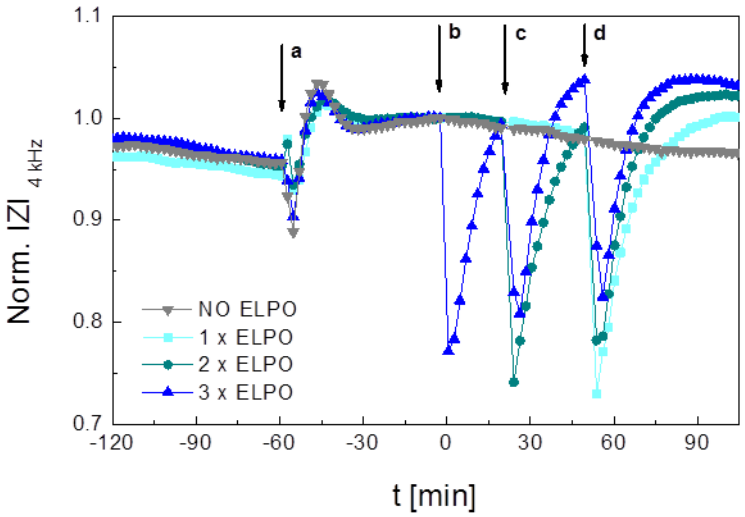

Figure 5.16 Typical time course of the normalized impedance at 4 kHz before and after multiple *in situ* electroporation of NRK cells in presence of 100 µM propidium iodide. After addition of the fluorescent probe (**a**), cells were electroporated three times successively - **b**: 1st pulse, **c**: 2nd pulse and **d**: 3rd pulse application. Impedance data were normalized to the last time point before electroporation.

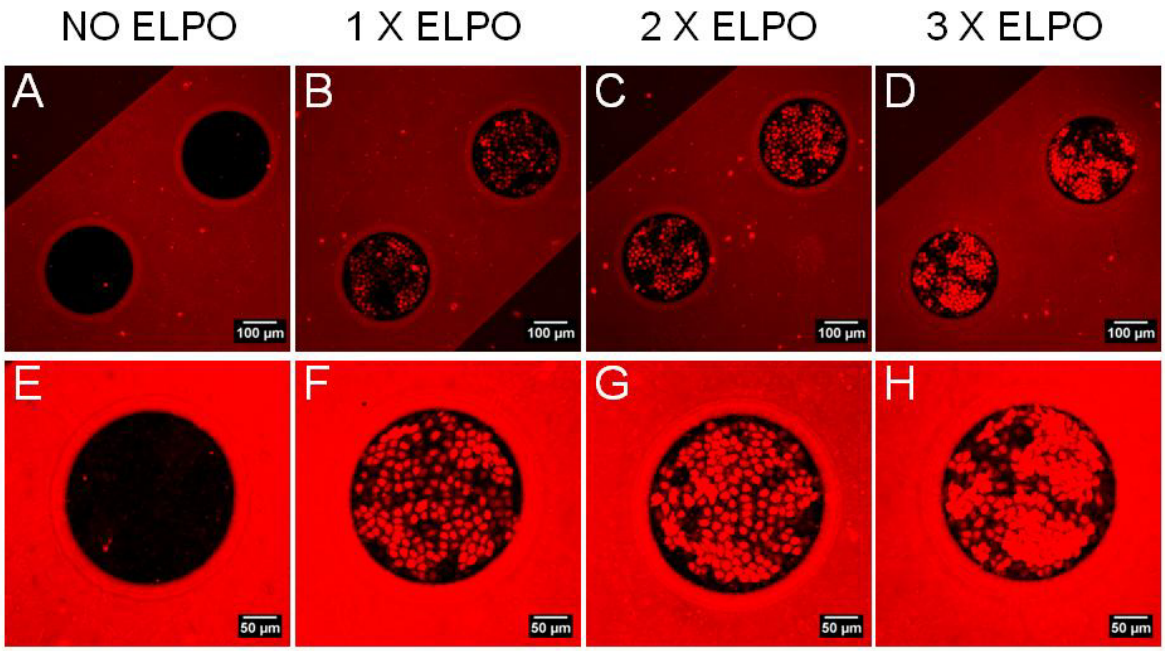

Figure 5.17 Exemplary confocal fluorescence micrographs taken with 10-fold magnification objective after *in situ* electroporation of NRK cells (40 kHz, 4 V and 200 ms) in presence of 100 µM propidium iodide, three times successively. NRK cells after: **A**/**E** No ISE; **B**/**F** Single pulse; **C**/**G** Two pulses and **D**/**H** Three pulses were applied. Micrographs in the top row were additionally zoomed 1.5 and in the lower panel 3 times, to better visualize cells on the electrodes. The scale bar in the top row corresponds to 100 µm, whereas the scale bar in the lower panel corresponds to 50 µm.

In the control (**A**/**E**), where cells were not exposed to electroporation but only incubated in presence of fluorescence probe, no cell uptake was observed. Cells electroporated once were successfully loaded with the probe and it is notable that increase of pulse number led to an increase of loading efficiency. Dye uptake in cells pulsed twice (**C**/**G**) is better than in the cells pulsed once and the cells pulsed three times exhibited the best loading efficiency, with respect to the number of loaded cells and amount of the fluorescent probe observed in the cell nuclei. In the micrographs taken after NRK cells were pulses twice or three times, accumulation of PI in nuclei and cytoplasm was observed. This led to conclusion that multiple application of optimized electric pulses does enhance the amount of probe, which enters the cells and efficiency of *in situ* electroporation can be thus increased.

5.1.4 Delivery of Fluorescent Probe into the Cells by Electroporation Monitored by Time-Resolved Imaging

The strategy to apply multiple subsequent electroporation pulses has been combined in this work with the time-resolved imaging of cells exposed to electric pulses directly on the microscope stage to study if release of material from the cells can be achieved by *in situ* electroporation. More details on release studies are described in chapter 5.3. However, before the release of fluorescent material from the cells by *in situ* electroporation (ISE) has been performed, simultaneous pulsing and microscopic observation was established and tested by loading of the cells with membrane-impermeable fluorescent probe. As a fluorescent probe 2 mg/mL (250 kDa) FITC-dextran was applied and its delivery into NRK cells by ISE was monitored in real time by taking micrographs in time intervals of ~ 60 or 120 seconds. This test was performed as a pre-experiment to investigate if loading/release of material in/out of the cells is possible with the applied experimental setup. Such control was necessary to provide an insight into the cell loading/release dynamics facilitated by ISE under the given conditions. Experimental setup and procedure are described in chapters 4.2.1.4 and 4.2.2.7.

For the experiment, NRK cells were grown on the 8W4Eμ electrode array and Leibovitz's medium (L-15) was applied as an assay buffer. The L-15 medium containing fluorescent probe 2 mg/mL (250 kDa) FITC-dextran was added to the NRK cells app. 30 min before pulse application took place. *In situ* electroporation was applied using the optimal pulse parameter combination for this cell line: 40 kHz, 4 V and 200 ms. Electric pulses were applied three times successively with 5 – 7 min break between the pulses. Shortly before and immediately after each pulse application, micrographs were taken. Between the pulses,

appearance of the cells on the electrodes was documented every one or two minutes. For the cell imaging, 60-fold magnification (water immersion) objective was applied and only cell population on the single electrode (out of four electrodes in each well) could be observed and evaluated. During time-resolved imaging of NRK cells upon delivery of FITC-dextran by ISE, impedimetric monitoring of the cells was not conducted.

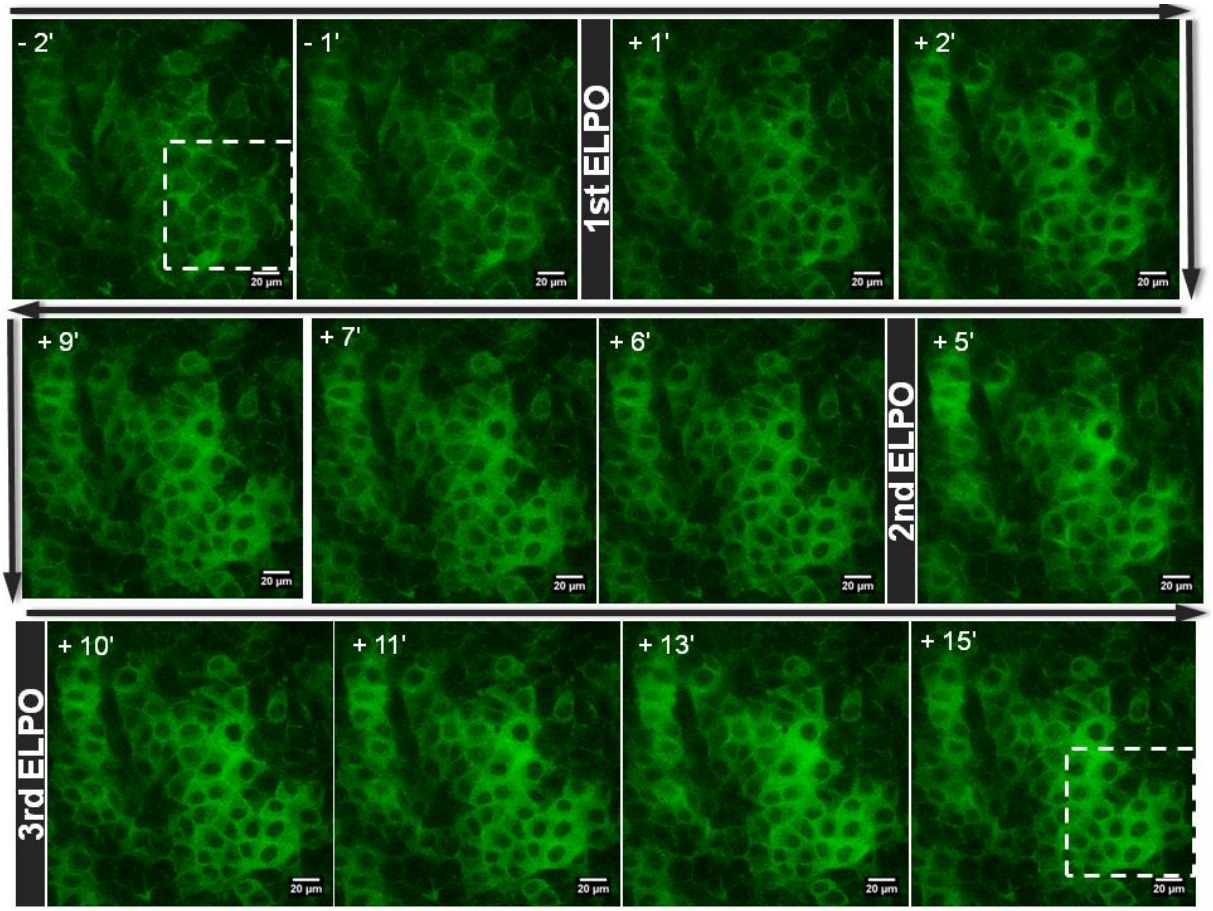

Figure 5.18 Exemplary microscopic images taken in real time by CLSM with 60-fold magnification objective before, during and after *in situ* electroporation of NRK cells, applied three times. Due to the presence of 2 mg/mL 250 kDa FITC-dextran (in the L-15 medium) during the entire experimental procedure, fluorescence signal was observed in the micrographs even before first pulse was applied. The appearance of the cells on the single electrode is shown and the scale bar corresponds to 20 µm in all images. Intracellular localization of 250 kDa FITC-dextran within the cytoplasm (excluding cell nuclei) increased with every electric pulse application.

The exemplary confocal fluorescence micrographs are summarized in **Figure 5.18** and the time scale of every micrograph (in minutes) is indicated in its upper left corner. First two images show the cells 2 and 1 minute before first pulse was applied. Further time points

indicate time periods after first pulse application. The dashed box marked in the first and the last image of the **Figure 5.18** indicate the cell population which was additionally zoomed in and presented in **Figure 5.19**, in order to visualize the appearance of the cells more closely, in the course of multiple pulse application.

In **Figure 5.18** and in **Figure 5.19**, (green) fluorescence signal of the probe was observed in the micrographs, as it surrounded the cells during the entire experimental procedure.

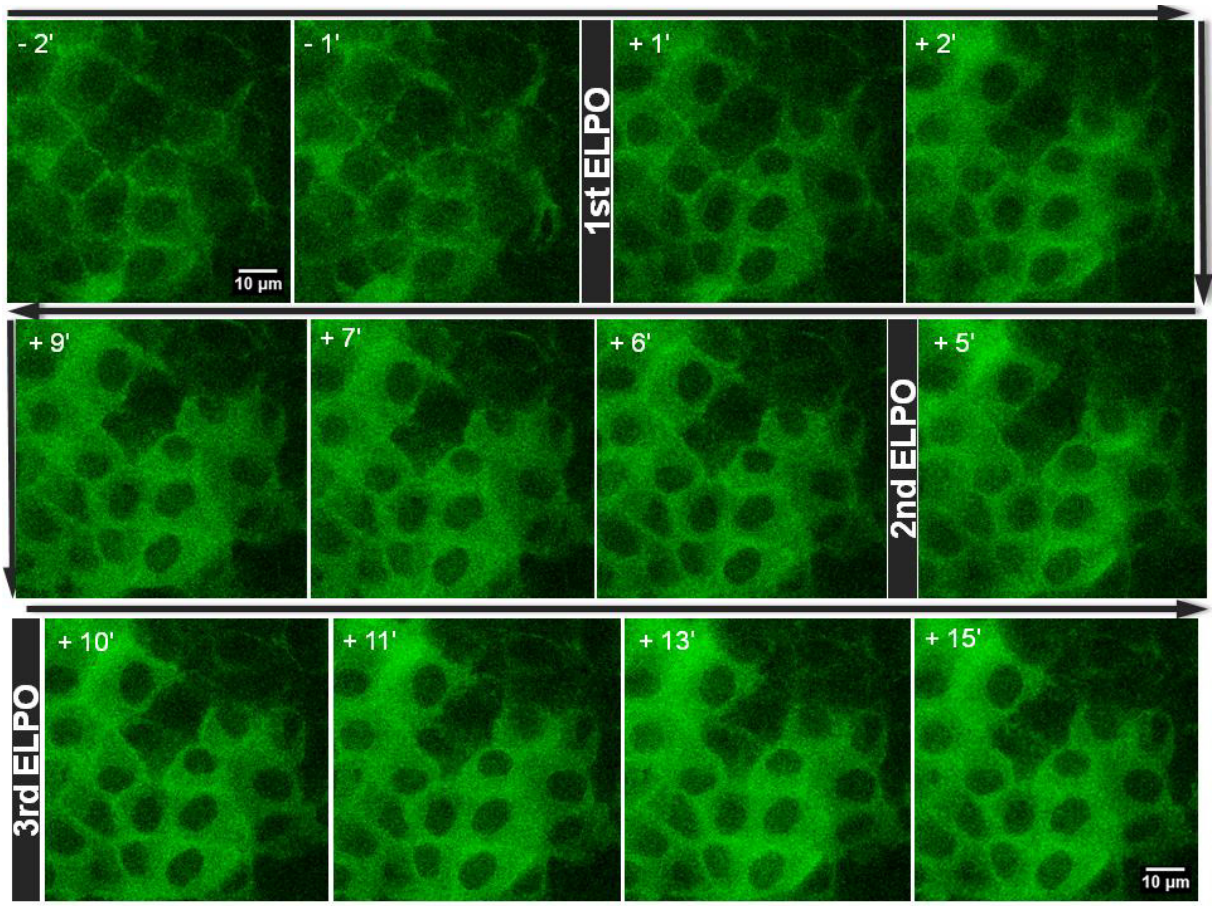

Figure 5.19 Exemplary microscopic images taken in real time by CLSM with 60-fold magnification objective before, during and after *in situ* electroporation of NRK cells, applied three times. Due to the presence of 2 mg/mL 250 kDa FITC-dextran (in the L-15 medium) during the entire experimental procedure, fluorescence signal was seen in the micrographs even before first pulse was applied. The scale bars represent 10 µm in all images. Intracellular localization of 250 kDa FITC-dextran within the cytoplasm (excluding cell nuclei) increased with every electric pulse application.

The focus of the objective was set towards the cell cytoplasm (and nuclei). However, by observing the first two micrographs, which show the cells before first pulse application, one can conclude that the small part of the dye may be taken up by the cells nonspecifically,

especially as the presence of the dye was seen within the cell membrane. After the first pulse application, the influx of the FITC-dextran into cell cytoplasm was clearly observed, as the fluorescent probe with the size of 250 kDa filled in the cell cytosol homogeneously and was excluded only from the cell nuclei due to its size. With every following pulse application, the fluorescence signal originating from the cytoplasm increased, as FITC-dextran accumulation within NRK cells interior got stronger. From the series of micrographs presented in **Figure 5.19**, it was observed that the cell population on the electrodes remained complete and undamaged in the course of the time-resolved imaging. This was confirmed by the phase-contrast micrograph of the cells taken after experimental procedure was finished (**Figure 11.1** of Appendix).

5.2 Impedance Monitoring of *In Situ* Electroporation with High Time Resolution

During studies including optimization of electric pulse parameters, it was seen that different cell lines respond differently after pulse application and time period necessary for their complete recovery also differs. It is well known from the theory of electroporation (Theoretical Background, chapter 3.2.2), that resealing of the cell membrane after electropermeabilization and its reassembling is a short time process, which takes from several seconds to several minutes (Rols and Teissié, 1998a; Neumann et al., 1998). Thanks to the time-resolved monitoring by ECIS, it is possible to follow recovery of the cell signal to the pre-pulse values after ISE. For some cell lines investigated in this work, post-pulse recovery takes 10 min (HaCaT), while for some even 50 min (BAEC). Considering the fact that post-pulse events on the cellular level are rather quick and time resolution of the typical ECIS measurement is relatively slow to record them, experiments were designed to monitor ISE with a high time resolution. The following hypothesis should be verified: post-pulse recovery of the cells is dependent on the invasiveness of the pulses but it takes relatively short time, slow signal return to the pre-pulse values corresponds to a monolayer reassembly, including cell-cell (and cell-substrate) contacts and to the return of the cells to their steady state. It was the aim of this section to follow events before and after single pulse application with the high time resolution, to document the kinetics of the impedance magnitude and thus behavior of the cells exposed to pulsation. A special experimental setup (described in chapter 4.2.1.6) was applied to conduct high time resolution monitoring of NRK cells grown on 8W1E and 8W4Eμ electrode arrays. Pulse parameters were varied, with respect to an amplitude and duration, whereas frequency was kept constant (40 kHz). All experiments were performed with NRK

cells grown to confluence on the ECIS electrodes. To avoid potential artifacts by cell age, previous treatment or some general differences in cell state, all experiments were performed with NRK cells seeded from the same cell suspension, which significantly contributed to the reproducibility of obtained results, since every pulse parameter combination was repeated at least twice.

5.2.1 Single Electroporation Pulses - Variation of Pulse Parameters

Graphs given in **Figure 5.20** show time course of the normalized impedance magnitude at 4 kHz, with impedance values normalized to the last value before pulse application (the time of the last data point before electric pulsing was set to zero). Impedance magnitude was recorded with the time resolution of app. 800 – 900 ms. In **Figure 5.20**, a typical dataset is presented, showing time course of the normalized impedance at 4kHz before and after NRK cells were pulsed by the optimal combination of pulse parameters (40 kHz, 4 V and 200 ms).

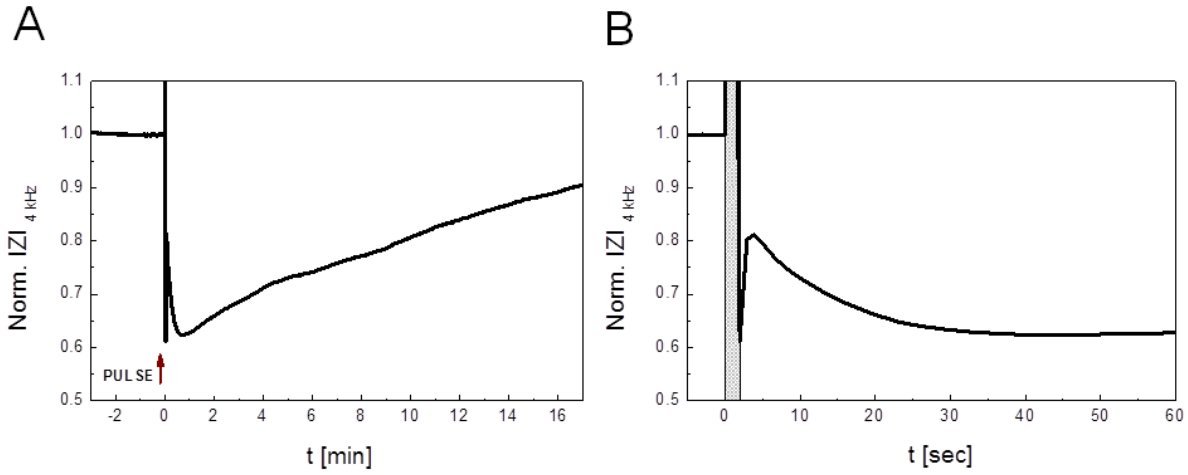

Figure 5.20 Typical time course of the normalized impedance magnitude at 4 Hz recorded with high time resolution. NRK cells were pulsed on 8W1E electrode array using the optimized pulse parameter combination for *in situ* electroporation: 40 kHz, 4 V, 200 ms. Results can be presented in different time frames: **A** After initial baseline, pulse was applied and monitoring of the cell response took app. 17 min afterwards **B** Cellular behavior several seconds before (4 sec) and 60 sec after pulse application is shown. Impedance magnitudes were normalized to the last time point before pulse application. Red arrow (in **A**) indicates moment of pulse application and grey shaded field (in **B**) indicates the short time interval of contact loss between electrodes with cells and IA, in order to apply electric pulse by FG.

In graph **A**, complete measurement is presented with the time scale in minutes. After

recording of the baseline data (app. 3 min), electric pulse was applied (by a manual switch) with well-defined parameters (indicated by the red arrow). During pulse application, electrodes contact had to be very shortly disconnected from IA and connected to the frequency generator (FG), which applied the pulse. Roughly 2 seconds were necessary to reestablish the contact of electrodes to the impedance analyzer and this time gap (including pulse application) can be seen in graph **B**, where it is marked by grey shaded field. The graph **B** is presented with the time scale in seconds, to better visualize events shortly before (4 sec) and after pulse application (60 sec). After the connection with IA was reestablished (app. 2 sec after pulse application), impedimetric monitoring of the cellular response was continued (with high time resolution). In both graphs, significant signal increase is observed, directly after pulse application, due to loss of the contact between electrodes and IA. After this contact was reestablished (after app. 2 sec; contact loss marked with grey shaded field), impedance data acquisition was continued. Switching between IA and FG without pulse application does not affect the measurement signal (data not shown).

The graph **A** shows that immediately after reestablishment of the contact (after pulse application) impedance value drop was recorded (to normalized value of 0.61). However, signal increases in the next moment to the normalized value of 0.8 and then decreases again (for a minute) and increases slowly back to the pre-pulse values. The drop of impedance signal and its increase shortly afterwards is better visualized in graph **B**, since it offers time scale in seconds and shows response of the cells app. 60 sec after pulse application. Impedance drop after pulse application and subsequent increase is followed by the relatively slow decrease of impedance signal to the normalized values of app. 0.63. From this value, the signal returns to the pre-pulse level over time. In the time course of impedimetric measurement with regular time resolution, such multistep process after pulse application cannot be observed, only the last part can be seen, including usually slow return of the signal to values before pulse application.

Based on such multiphasic cellular response, conclusion may be drawn that several processes take place upon pulse application. Electric pulse alternates affected cells immediately by permeabilizing them (immediate impedance drop). Subsequent and very fast increase in the signal suggests resealing of the cell membrane. Slow recovery of an impedance signal to the pre-pulse values, which takes several minutes, can be assigned to the rearrangement of the cells and reestablishment of the cell monolayer, due to morphological alterations such as loosen cell-cell and cell-surface contacts, or transient volume change. Above described experimental procedure and analysis was used to measure how NRK cells respond to electrical pulses of different invasiveness. Pulse parameters were

varied to deliver more and less invasive electric pulses. The response of the cells was analyzed to reveal what processes take place and dominate after application of less invasive and more invasive electric pulses.

For these studies, NRK cells were seeded to confluence on 8W1E and 8W4Eμ arrays. All pulse parameter combinations were repeated twice to evaluate their reproducibility. Since all measurements appeared to be very reproducible, a typical time course of the normalized impedance is given in the following figures, representing each of evaluated conditions. For all applied pulses, frequency was kept constant, whereas one of the other two parameters (pulse amplitude and pulse duration) was varied.

In **Figure 5.21**, typical time courses of the normalized impedance magnitude at 4 kHz are shown, for various pulse parameter combinations with constant pulse duration (200 ms) and variable pulse amplitude (2 – 5 V), measured on 8W1E and 8W4μ electrode arrays.

Curves measured with four different pulse parameter combinations are summarized and integrated in a single graph, which is presented either with the time scale in minutes (**A**/**B**), or with the time scale in seconds (**C**/**D**). In the graphs with the time scale in minutes (upper panel), infinite jump of impedance values (due to contact loss between electrodes and IA) is reduced during data evaluation to allow overlay of the multiple curves within one graph. Red arrows indicate time point of pulse application. In graphs of the lower panel (**C**/**D**), last data point before pulse application is connected by a dashed line to the first data point after reestablishment of the connection between electrodes and IA. Time frame of roughly 2 sec, during which connection between electrodes and IA was interrupted, is indicated with the grey shaded fields. Scale bars (corresponding to 0.2) in the graphs indicate normalized impedance values on y-axis.

Whereas graphs **A** and **B** (presenting events before and after pulse application on the time scale in minutes) show entire multistep process taking place after exposure of NRK cells to more or less invasive pulses, graphs **C** and **D** show only first 60 seconds after pulse application. Depending on the pulse amplitude, impedance drop after pulse increases In addition, subsequent fast return to the transient maximum varies depending on the voltage applied for the pulse. Thus, the cells pulsed with lower amplitude exhibited only small impedance decrease and subsequent return went to almost pre-pulse values (2 V and 3 V). Multistep process was continued by signal decrease and then slow increase over time, until they reached similar values as before pulse application. The cells pulsed with higher amplitude values (4 V and 5 V) exhibited significant impedance drop and only partial return of the signal immediately afterwards. Again, signal decrease within a minute and then slow increase was observed, as the phases of multistep process, seen also with the cells pulsed

with lower pulse amplitudes.

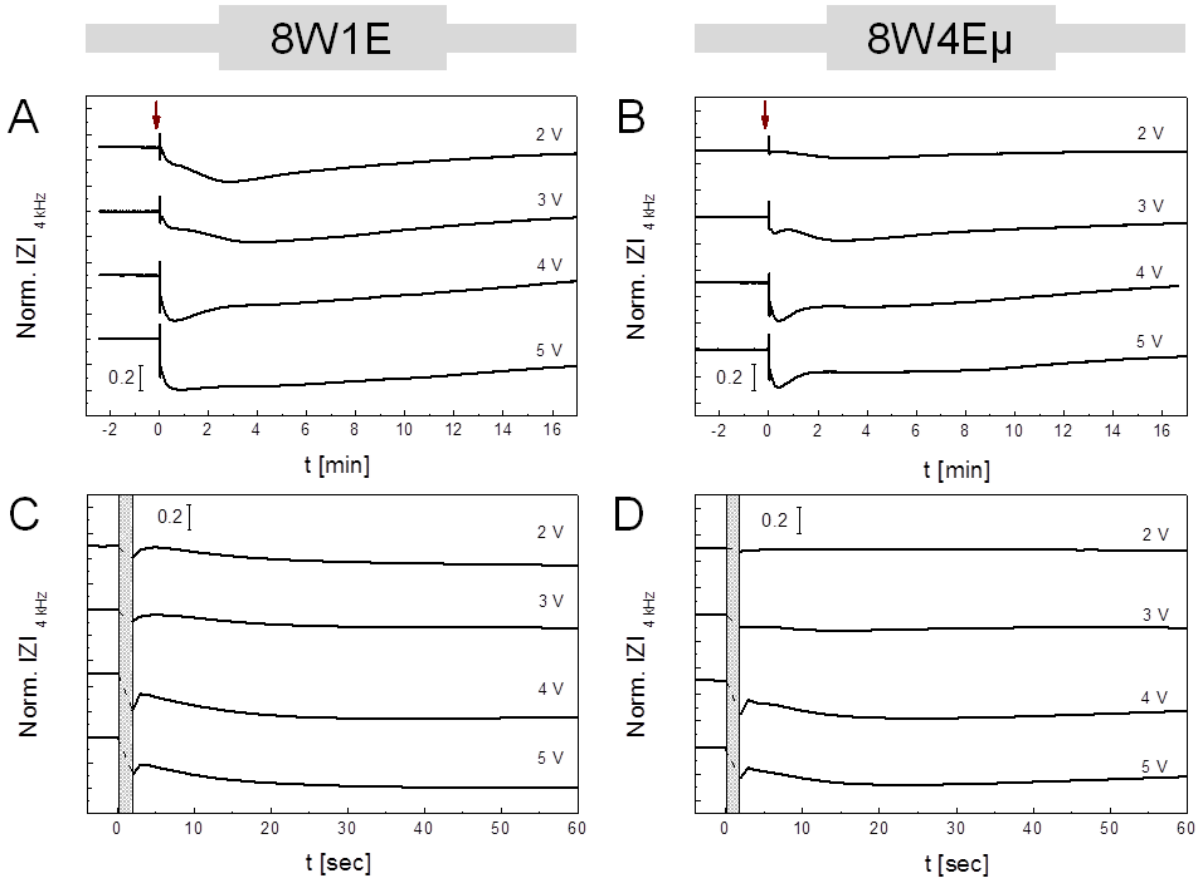

Figure 5.21 Typical time courses of the normalized impedance magnitude at 4 Hz recorded with high time resolution. NRK cells were pulsed on 8W1E (**A**/**C**) and 8W4Eμ (**B**/**D**) electrode arrays using pulses with constant frequency (40 kHz) and pulse duration (200 ms), whereas amplitude was varied (2 V – 3 V – 4 V – 5 V). Results are presented in different time frames: **A**/**B** In minutes time scale and **C**/**D** In seconds time scale. Impedance magnitudes were normalized to the last value before pulse application. Red arrows (in **A**/**B**) indicate moment of pulse application, while grey shaded fields (in **C**/**D**) indicate short time interval of contact loss between electrodes with cells and IA, in order to apply electric pulse by FG.

Very similar observations were made also for graphs presented in **Figure 5.22**. Here, typical time courses of the normalized impedance magnitude at 4 kHz are shown, for various pulse parameter combinations, whereby pulse amplitude was kept constant (4 V) and only pulse duration was varied (50 ms – 1 s). By measuring on 8W1E electrode arrays, results were obtained for five different pulse parameter combinations, whereas four different conditions were analyzed on 8W4Eμ electrode array. Similarly as in **Figure 5.21**, results are summarized in graphs with the time scale in minutes (**A**/**B**), and in seconds (**C**/**D**). Red

arrows in A/B indicate time point of pulse application and infinite jump of impedance values (due to contact loss between electrodes and IA) is reduced during data evaluation to allow overlay of the multiple curves within one graph. In graphs of the lower panel (**C**/**D**), last data point before pulse application is connected by a dashed line to the first data point after reestablishment of the connection between electrodes and IA. This short time interval of disconnection between electrodes and IA is indicated with the grey shaded fields. Scale bars (corresponding to 0.2) in graphs indicate normalized impedance values on y-axis.

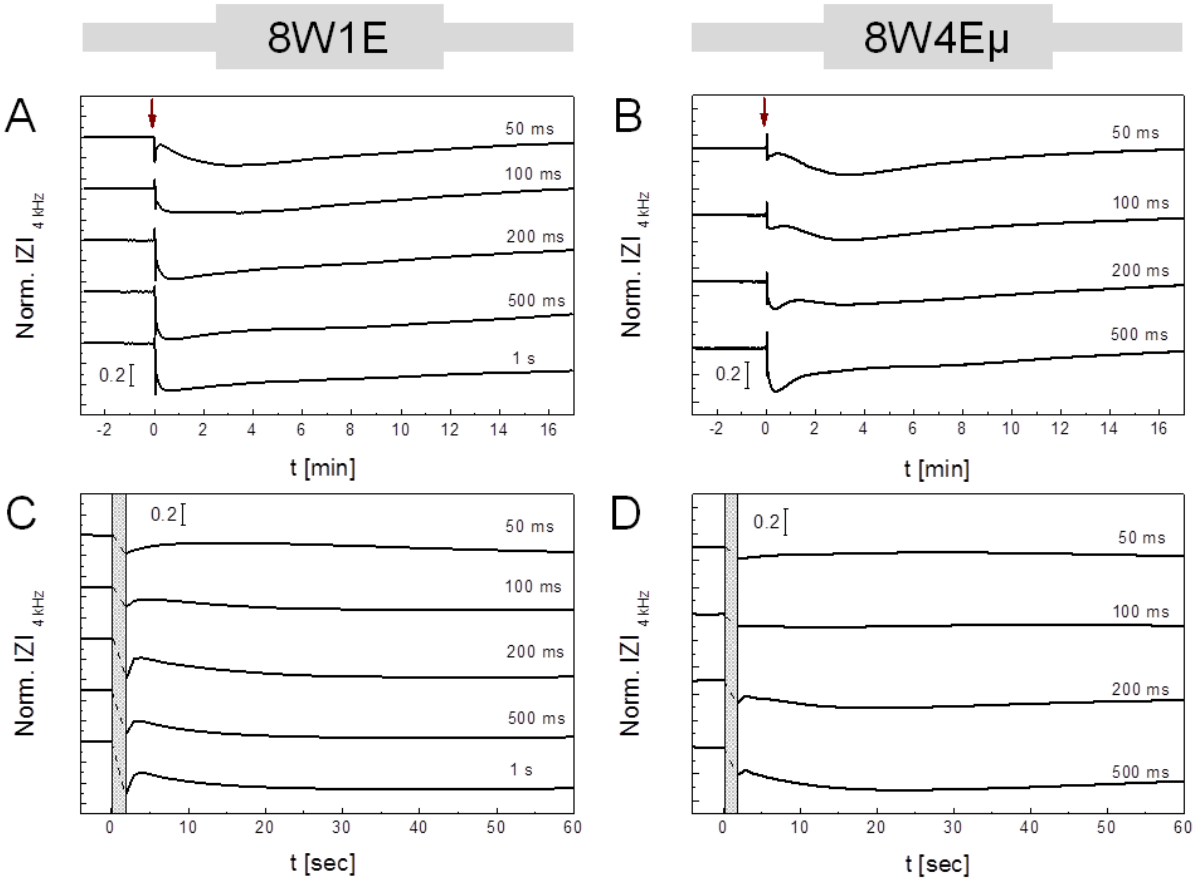

Figure 5.22 Typical time courses of the normalized impedance magnitude at 4 Hz recorded with high time resolution. NRK cells were pulsed on 8W1E (**A**/**C**) and 8W4Eµ (**B**/**D**) electrode arrays using pulses with constant frequency (40 kHz) and pulse amplitude (4 V), whereas pulse duration was varied (50 ms – 100 ms – 200 ms – 500 ms – 1 s). Results are presented in different time frames: **A**/**B** In the minutes time scale and **C**/**D** In the seconds time scale. Impedance magnitudes were normalized to the last value before pulse application. Red arrows (in **A**/**B**) indicate time point of pulse application, while grey shaded fields (in **C**/**D**) indicate short time interval of connection loss between electrodes with cells and IA, in order to apply electric pulse by FG.

With increasing pulse duration, impedance drop after pulse is larger. In addition, subsequent

fast return to the transient maximum of normalized impedance varies directly on pulse duration. Thus, the cells exposed to shorter pulses (50 ms and 100 ms) exhibited only small impedance decrease and subsequent return went to almost pre-pulse values. Afterwards, signals decreased and then slowly increased over time, until they reached values before pulse application. The cells exposed to longer pulses (200 ms and 500 ms) exhibited significant impedance drop and only partial return of the signal, immediately afterwards. Again, signal decrease within a minute and then slow increase was observed, as the phases of multistep process. Impedance signal of NRK cells exposed to 1 s long pulse, dropped significantly after pulse application and subsequent return to transient maximum of normalized impedance was very small. Nevertheless, multistep process was seen again with the difference that cells exposed to such a long pulse were mostly irreversibly permeabilized and required much longer time to recover to the pre-pulse level, compared to the cells exposed to shorter pulse durations.

In **Figure 5.23**, time courses of the normalized impedance magnitude at 4 kHz are shown for various pulse parameter combinations, whereby pulse amplitude was kept constant (5 V) and only pulse duration was varied (200 ms – 1.25 s). Results obtained for three different pulse parameter combinations are measured only on 8W1E electrode arrays, as during previous measurements no significant or systematic difference has been observed between these two electrode arrays. Results are summarized in a graph with the time scale in minutes (**A**) and in graph with the time scale in seconds (**B**). Scale bars (corresponding to 0.2) in these graphs indicate normalized impedance values on y-axis.

Similarly to the graphs in **Figure 5.22**, impedance drop after pulse application was larger, directly depending on pulse duration. Here, a pulse amplitude of 5 V was combined with various pulse durations. Thus, cells exposed to 5 V and either 200 ms, or 500 ms showed undoubtedly significant signal drop and subsequent fast return to the transient maximum of normalized impedance values was small. The cells exposed to 5 V and 1.25 s showed impedance drop to very low values and subsequent return of impedance signal was minimal. Multistep process including decrease and slow increase of the signal, due to return of impedance signal to the pre-pulse values was observed in the traces belonging to pulse parameter conditions: 40 kHz, 5 V; 200 ms and 40 kHz, 5 V, 500 ms. However, the cells exposed to 40 kHz, 5 V and 1.25 s long pulse showed minor recovery of the signal and increase to pre-pulse values surely takes a longer period of time. It is obvious that NRK cells were damaged in this case and membrane permeabilization was irreversible. The effect of such pulse parameters corresponds to electric wounding.

After exposing the NRK cells to various electric pulses, which invasiveness was varied by

varying pulse parameters (amplitude and duration), the comparison of cellular responses after pulse application was drawn. The observations made for cells monitored on 8W1E electrode arrays were very similar to those made for experiments conducted using 8W4Eμ electrode arrays.

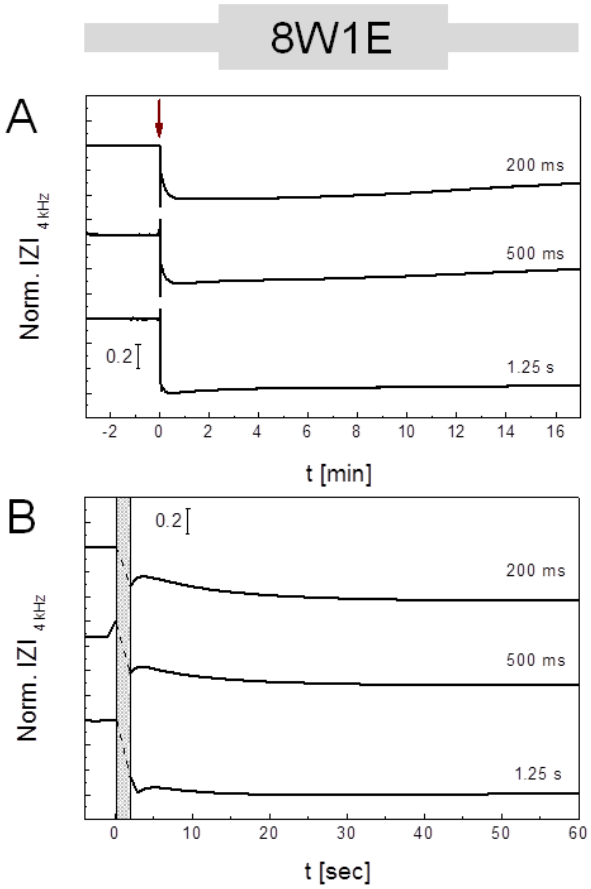

Figure 5.23 Typical time courses of the normalized impedance magnitude at 4 Hz recorded with high time resolution. NRK cells were pulsed on 8W1E electrode array using pulses with constant frequency (40 kHz) and pulse amplitude (5 V), whereas pulse duration was varied (200 ms – 500 ms – 1.25 s). Results are presented in different time frames: **A** In minutes time scale and **B** In seconds time scale. Impedance magnitudes were normalized to the last value before pulse application. Red arrow (in **A**) indicates moment of pulse application, while grey shaded field (in **B**) indicates short time interval of connection loss between electrodes with cells and IA, in order to apply electric pulse by FG.

Multistep process including: impedance drop, subsequent increase, repeated decrease and finally, slow increase until pre-pulse values are reached, was observed in measurements conducted on both array types. With increasing voltage, impedance drop after pulse was larger. What certainly was different in cellular responses measured on 8W4Eμ array,

compared to results obtained on 8W1E array, are minima of impedance signal reached after pulse application. Namely, by comparing normalized impedance traces for NRK cells on 8W1E and 8W4Eμ arrays, which are presented in **Figure 5.21** and **Figure 5.22**, it is observed that the cells exposed to the same pulse parameter conditions on different arrays, gave curves very similar in shape. However, minimal impedance values reached immediately after pulse application and subsequent return to transient maximum values were overall smaller (or less expressed) when measured on 8W4Eμ array, in comparison to the 8W1E array. To illustrate more precisely and quantify such trend, values of normalized impedance at the minimum (immediate drop upon pulse application) and at the transient maximum (subsequent increase in impedance signal after initial drop) are summarized in **Table 5.1**.

Table 5.1 Summary and comparison of response of NRK cells to various pulse parameter conditions measured on 8W1E and 8W4Eμ electrode arrays. Normalized impedance values for immediate signal drop (after pulse application) and for subsequent increase to the transient maximum are presented as mean value ± standard deviation for two repetitions (n=2).

		8W1E		8W4Eμ	
Pulse Parameters		**Normalized Impedance Decrease After Pulse (MV ± SD; n=2)**	**Subsequent Normalized Impedance Increase (MV ± SD; n=2)**	**Normalized Impedance Decrease After Pulse (MV ± SD; n=2)**	**Subsequent Normalized Impedance Increase (MV ± SD; n=2)**
40 kHz 200 ms	**2 V**	0.9076 ± 0.0011	0.9920 ± 0.0024	0.9815 ± 0.0091	0.9876 ± 0.0029
	3 V	0.8835 ± 0.0357	0.9197 ± 0.0521	0.8978 ± 0.0055	0.9071 ± 0.0013
	4 V	0.7259 ± 0.0264	0.8311 ± 0.0113	0.7949 ± 0.0611	0.8556 ± 0.0015
	5 V	0.6083 ± 0.1342	0.7729 ± 0.0153	0.8009 ± 0.0389	0.8403 ± 0.0080
40 kHz 4 V	**50 ms**	0.7410 ± 0.0345	0.9238 ± 0.0025	0.9296 ± 0.1138	0.9565 ± 0.0202
	100 ms	0.7357 ± 0.1006	0.8411 ± 0.0481	0.9074 ± 0.0038	0.9223 ± 0.0155
	200 ms	0.6764 ± 0.0927	0.8046 ± 0.0104	0.8382 ± 0.0011	0.8735 ± 0.0163
	500 ms	0.5704 ± 0.0119	0.7609 ± 0.0844	0.8283 ± 0.0452	0.8511 ± 0.0301
	1.0 s	0.5984 ± 0.1392	0.7309 ± 0.0395	n.d.	n.d.
40 kHz 5 V	**200 ms**	0.6081 ± 0.1345	0.7729 ± 0.0153	n.d.	n.d.
	500 ms	0.5117 ± 0.1809	0.6648 ± 0.0469	n.d.	n.d.
	1.25 s	0.4129 ± 0.0043	0.5536 ± 0.1374	n.d.	n.d.

Since the cellular response to electric pulses created by varying pulse parameter

combinations was measured in duplicates, comparison of 8W1E and 8W4Eμ array data is presented as the mean value of two repetitions, with the corresponding values of standard deviation (mean value ± standard deviation; n=2).

5.2.2 Multiple Electroporation Pulses

Besides single pulses, impedance monitoring of multiple electroporation pulses with high time resolution was performed with NRK cells grown to confluence on 8W1E array. Analysis of multiple electroporation pulses with high time resolution was performed three times and typical time course of the normalized impedance magnitude at 4 kHz is shown in **Figure 5.24**. *In situ* electroporation was applied three times successively (in $EBSS^{++}$), as indicated in **Figure 5.24** - **a**: 1st pulse, **b**: 2nd pulse and **c**: 3rd pulse application, using optimal pulse parameters for every pulsation: 40 kHz, 4 V and 200 ms.

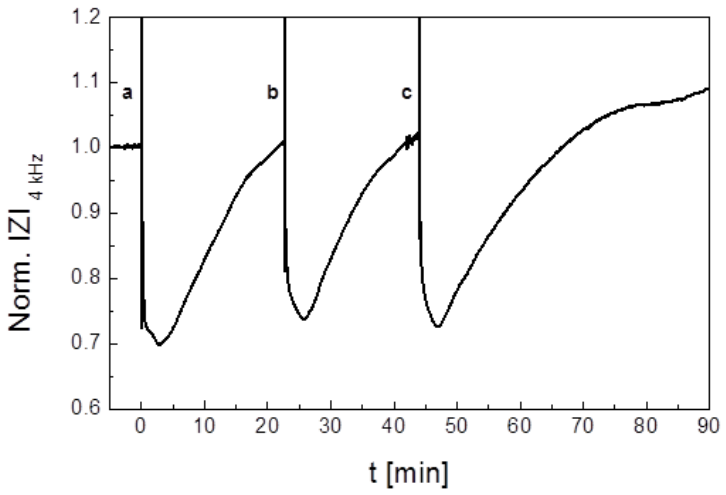

Figure 5.24 Typical time course of the normalized impedance magnitude at 4 kHz recorded with high time resolution. NRK cells were pulsed three times successively - **a**: 1st pulse, **b**: 2nd pulse and **c**: 3rd pulse application, using optimized pulse parameter conditions: 40 kHz, 4 V and 200 ms, on 8W1E electrode array. Impedance magnitudes were normalized to the last value before electroporation.

After every pulse application, cells gave impedance signal identical to the signal observed during single pulse application, using the same pulse parameters combination (presented in previous chapter 5.2.1, **Figure 5.21** and **Figure 5.22**). To get a better insight into events between every pulse application, the time course of every pulse is presented separately on the seconds scale in **Figure 5.25**. For every pulse individually, impedance magnitudes were normalized to the last value before pulse application. Thus, multiple step process after every

pulse application was observed more closely.

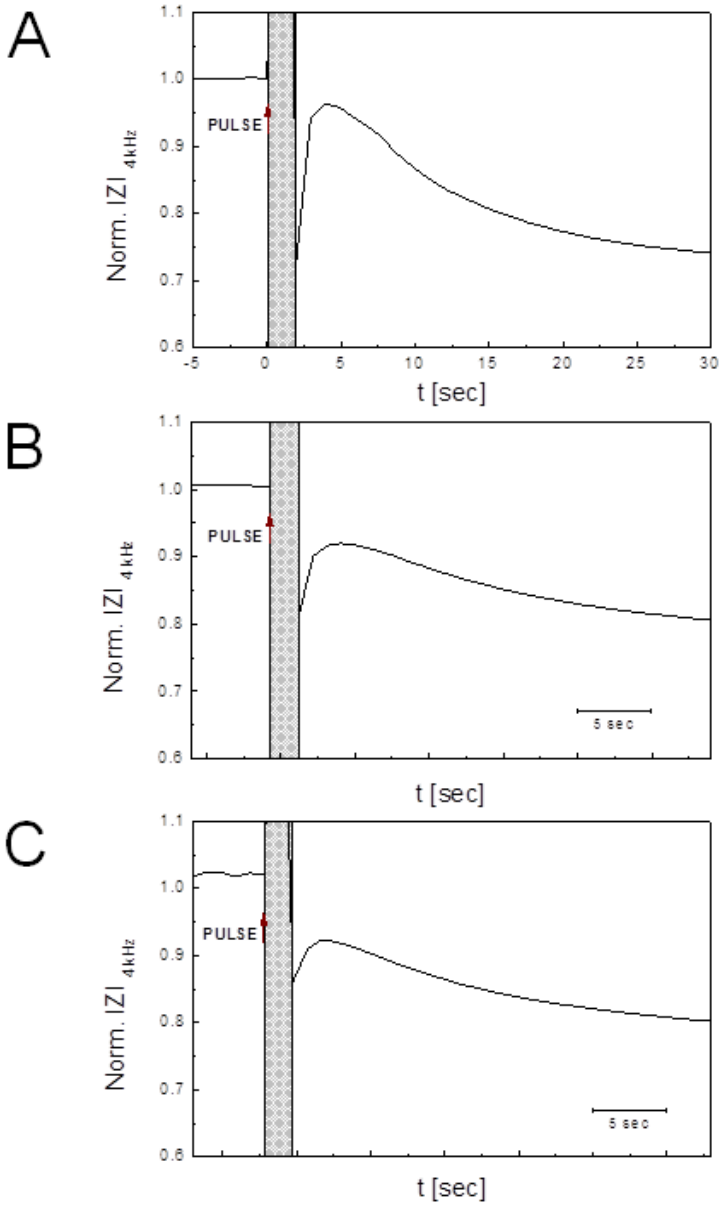

Figure 5.25 Typical time courses of the normalized impedance magnitude at 4 kHz recorded with high time resolution. NRK cells were pulsed on 8W1E electrode array three times successively, as presented in **Figure 5.24**. For each pulse, optimized pulse parameter conditions: 40 kHz, 4 V and 200 ms were applied. Here, time course of every pulse is presented separately: **A** First pulse; **B** Second pulse; **C** Third pulse; on the seconds time scale. For every pulse individually, impedance magnitudes were normalized to the last value before pulse application. Red arrows indicate moment of pulse application, while grey shaded fields indicate short time interval of disconnection between electrodes with cells and IA, in order to apply electric pulse by FG. Scale bars (corresponding to 5 sec) in graphs **B** and **C** indicate time values on x-axis.

Red arrows indicate the time point of pulse application, while grey shaded fields indicate the short time interval of disconnection between electrodes with cells and IA, in order to apply electric pulse by FG. Scale bars (corresponding to 5 sec) in graphs **B** and **C** indicate time values on x-axis.

Whereas after first pulse (presented in graph **A**), signal dropped significantly to the value of normalized impedance of app. 0.74, fast return of the signal took place subsequently and normalized impedance reached value of 0.95, before it decreased again and finally recovered to the pre-pulse values. After the second pulse (presented in graph **B**), signal dropped to the value of normalized impedance of app. 0.82 and quickly returned to the normalized impedance value of 0.9, before it decreased and increased again. After the third pulse was applied (presented in graph **C**), normalized impedance dropped to the value of only 0.85 and increased subsequently to the normalized value of 0.92, before short decrease and final increase took place, as slower phases of multistep post-pulse process.

5.3 Release of Intracellular Material by *In Situ* Electroporation

In situ electroporation combined with ECIS is a well-established technique for delivery of various xenomolecules into cytoplasm of the cells. After cell membrane permeabilization caused by well-defined electric pulse application, the molecules from extracellular space can freely diffuse into the cell cytosol and stay captured inside the cell after membrane pores reseal. The question arose if, instead of material introduction into the cells, intracellular material could be released from the cells by *in situ* electroporation. This hypothesis was verified by investigation of potential fluorescent material release from NRK cells by *in situ* electroporation. In addition, lactate dehydrogenase, as an intracellular enzyme was released from the cells by application of electric wounding, in order to investigate if LDH assay can be applied for evaluation of LDH release studies. As the fluorescent probes, FITC-dextran (4 kDa) and calcein (~ 660 kDa) were applied. Eventually, it turned out that the FITC-dextran is an inappropriate fluorescent probe for release studies, mostly because of its size. Release studies including initial loading of the cells with 4 kDa FITC-dextran and its subsequent release from the cells, by applying ISE, once, twice or three times, showed no visible nor reproducible results. Therefore, studies of material release from the cells were continued only with calcein as the florescent probe.

5.3.1 Release of Calcein from the Cells

Calcein-AM is a very small molecule (994 g/mol) giving a bright green fluorescent signal, upon binding to the intracellular Ca^{2+} within the cells. Prior to any release study conducted with calcein in this work, cells were routinely loaded with 2 µM calcein-AM (Ca-AM) in PBS^{++}, according to the common protocol described in chapter 4.3.4.1. Thereafter, PBS^{++} containing Ca-AM was removed and exchanged by the appropriate buffer. Subsequently, calcein release from the cells induced either by *in situ* electroporation or fixation and permeabilization of the cells was studied.

5.3.1.1 Release of Calcein from Fixed and Permeabilized Cells

Before release of calcein from NRK cells was attempted by applying *in situ* electroporation, the possibility to release calcein from the cells by fixation and permeabilization was investigated. This method was applied to provide disruption and irreversible permeabilization of the cell membrane, which could be thus easily crossed by intracellular calcein molecules and allow them to freely diffuse out from the cells. After initial loading of NRK cells with 2 µM Ca-AM, cells were fixed with 4 % (w/v) PFA and subsequently permeabilized with different percentages of Triton-X-100 (0.1 % / 0.3 % / 0.5 % (v/v)). The control population of the cells was neither fixed, nor permeabilized after initial Ca-AM staining. Micrographs were taken by CLSM with 10-fold magnification objective and exemplary micrographs are summarized in **Figure 5.26**. Images in the top row were zoomed 1.5 times and in the lower panel 3 times. Micrographs show that cells in all three samples, independently on applied Triton-X-100 percentage, allowed leakage of calcein from their cytosol. The cells treated with PFA and Triton-X-100 (micrographs **B**/**C**/**D** and **F**/**G**/**H** in **Figure 5.26**) appear significantly darker then the cells in controls, which were not exposed to the fixation and permeabilization (micrographs **A**/**E**). These fluorescence micrographs, along with the corresponding phase-contrast images (data not shown), indicate that significantly reduced fluorescence signals in micrographs of the samples (**B**/**C**/**D** and **F**/**G**/**H**) are not the consequence of the missing NRK cells, but the result of calcein release.

The cell fixation agent PFA permeabilizes the cell membrane as well, and calcein could thus diffuse from the cells even before permeabilization agent Triton-X-100 (of different percentages) was applied. The combination of PFA and Triton-X-100 applied to NRK cells clearly enhanced the effect of membrane permeabilization and allowed free diffusion of entire amount of previously loaded calcein from the cells. Such conclusion is drawn based on comparison between the micrographs which show control cells (no PFA and Triton-X-100

applied, bright green appearance) and cells in the sample (treated with PFA and Triton-X-100, appear almost completely dark).

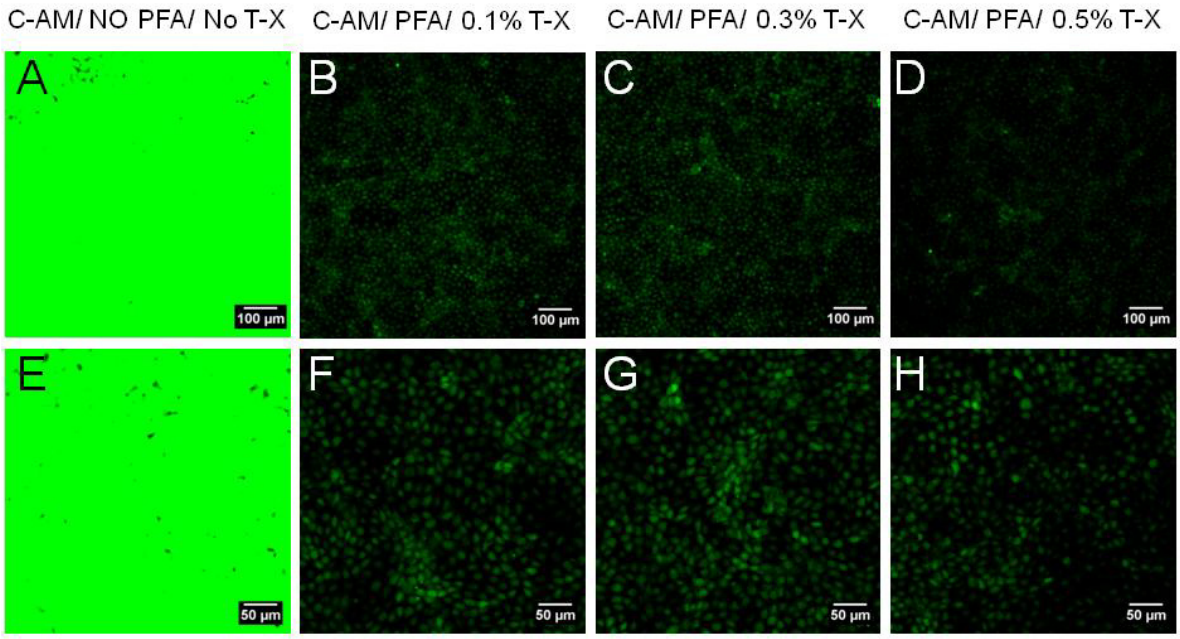

Figure 5.26 Exemplary confocal fluorescence micrographs taken with 10-fold magnification objective after fixation and permabilization of NRK cells in presence of 2 µM calcein-AM. Whereas in control **A**/**E** Neither fixation, nor permeabilization was applied, in samples fixation was performed with 4 % (w/v) PFA and permeabilization with various percentages of Triton-X-100 (v/v): **B**/**F** 0.1 %; **C**/**G** 0.3 %**; D**/**H** 0.5 %. Scale bar in the micrographs presented in the top row represents 100 µm, while the scale bar in the lower panel represents 50 µm.

5.3.1.2 Release of Calcein from the Cells by Electroporation Using Standard Experimental Setup

After successful release of calcein from NRK cells by fixation and permeabilization, release of calcein from NRK cells by electroporation was investigated. *In situ* electroporation was applied once, twice or three times to the cell monolayers grown on the electrodes of 8W4Eµ electrode array, using optimal pulse parameter conditions for NRK cells: 40 kHz, 4 V and 200 ms. In the controls, cells were not exposed to any electric pulses.

NRK cells loaded with 2 µM Ca-AM and dissolved in $EBSS^{++}$ buffer were exposed to electroporation pulses (applied at the time points indicated by the arrows - a: 1^{st} pulse, b: 2^{nd} pulse and c: 3^{rd} pulse application, in **Figure 5.27**). The experimental procedure for this assay is described more precisely in chapter 4.2.2.7. In graph **A** (**Figure 5.27**) time course of the

normalized impedance magnitude at 4 kHz is presented for the release of calcein from NRK cells by ISE. Between every pulse application, cells were allowed to completely recover and app. 35 min after final electric pulse, impedance monitoring was finished and release efficiency was evaluated by CLSM (exemplary micrographs are summarized in **Figure 5.28**).

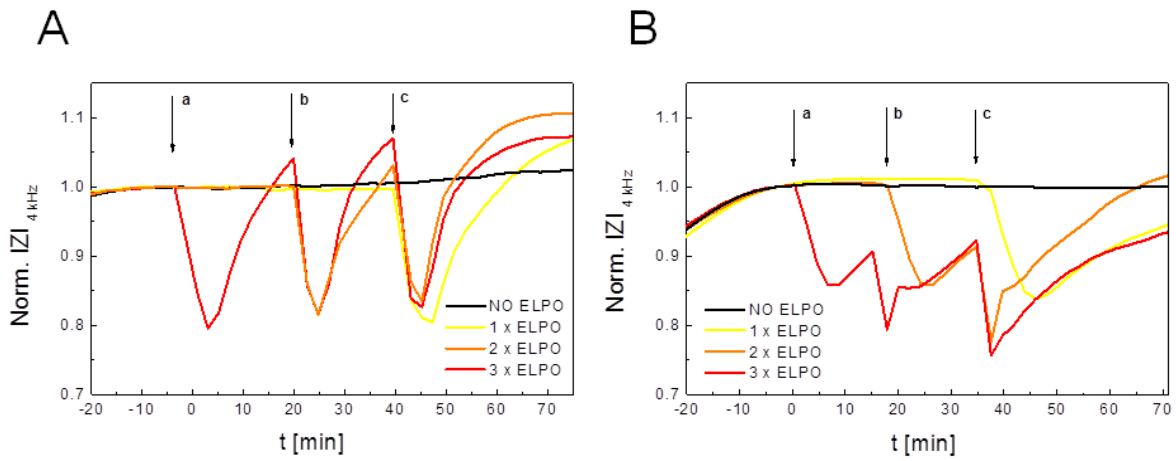

Figure 5.27 Time courses of the normalized impedance at 4 kHz before and after *in situ* electroporation of NRK cells to release calcein from the cell cytosol. Electric pulse was applied once, two or three times successively at the time points indicated by the arrows - **a**: 1st pulse, **b**: 2nd pulse and **c**: 3rd pulse application. Impedance magnitudes were normalized to the last time point before first electroporation. The release test shown in graph **A** was performed in presence of $EBSS^{++}$ as an assay buffer, while the release test given in graph **B** was conducted in presence of $EBSS^{++}$ containing 50 µM 2-APB. For both experiments, procedure was the same and it included impedimetric monitoring of ISE, followed by microscopy using CLSM, to evaluate release efficiency.

Furthermore, additional release test was performed, according to the same experimental procedure as for the experiment shown in graph **A**, except that the incubation buffer was composed of $EBSS^{++}$ and 50 µM 2-APB. Compound 2-APB was added to $EBSS^{++}$ buffer to circumvent potential exchange of calcein (between the cells) via gap junctions during electroporation. Impedimetric monitoring of this experiment is presented in graph **B** (**Figure 5.27**) and it shows that NRK cells recovered considerably slower after each pulse in presence of 50 µM 2-APB. Although recovery of the cells was slow, the time intervals between pulses were kept within 20 – 25 min range and app. 35 min after last pulse application, impedance measurement was finished. Microscopy by CLSM followed and corresponding exemplary micrographs are summarized in **Figure 5.29**.

Electrodes areas are delineated with the white circles. In the controls, (non-pulsed) cells on the electrodes and the cells around the electrodes (background) could not be clearly

distinguished. Moreover, cells on the electrodes appeared slightly brighter due to reflecting properties of the gold surface.

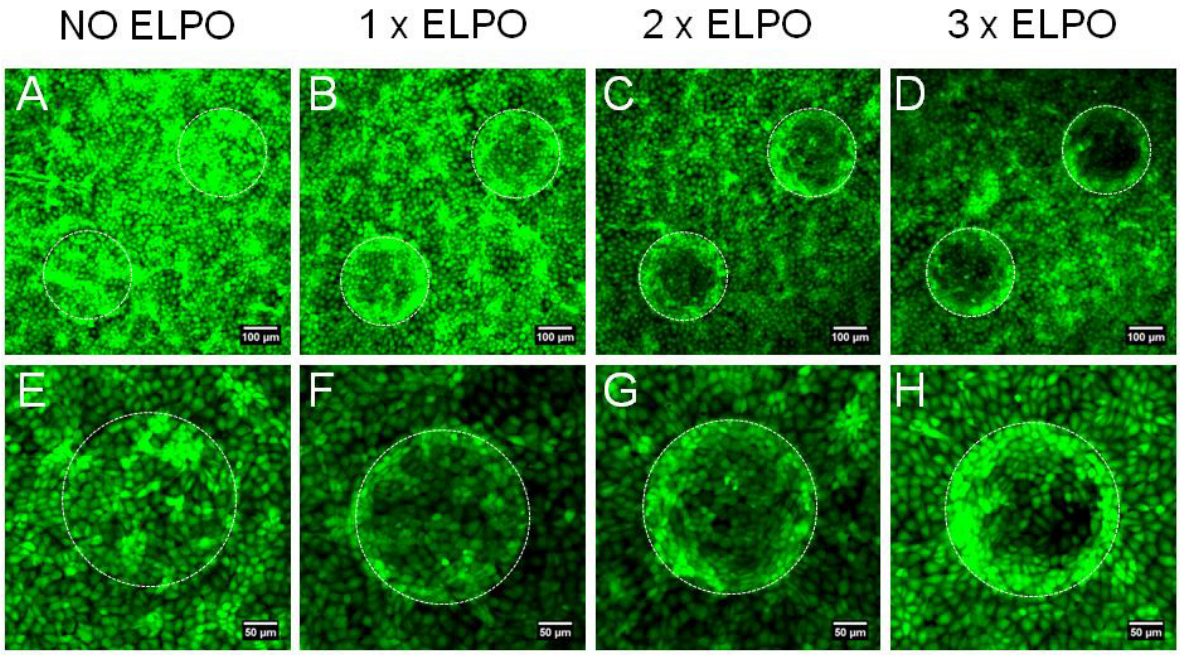

Figure 5.28 Exemplary confocal fluorescence micrographs taken with 10-fold magnification objective after no *in situ* electroporation of NRK cells was applied (**A**/**E**), or ISE was applied once (**B**/**F**), twice (**C**/**G**) or three (**D**/**H**) times. During ISE, NRK cells were dissolved in $EBSS^{++}$ buffer. White circles delineate electrodes area. Micrographs in the top row were zoomed 1.5 times and scale bars represent 100 µm, while micrographs in the lower panel were zoomed 3 times and scale bars correspond to 50 µm. The enhancement of calcein release from the cells is directly proportional to an increasing number of electric pulses.

Cell populations residing on the electrodes which were exposed to electric pulse(s) appear darker in the middle of the electrodes than the cells of the background (and the non-pulsed cells on the electrodes in control). Whereas cells pulsed once appear only slightly darker compared to the control, more significant reduction of the fluorescence signal was observed when the cells were pulsed twice or three times. More precisely, NRK cells exposed to electroporation (in $EBSS^{++}$ buffer) appeared darker in the middle of the electrode, while cells on the periphery of the electrode appeared brighter and built characteristic bright fluorescence ring around the cell population residing in the electrode center (**Figure 5.28**). Appearance of bright fluorescence rings can be explained by the fact that electric field is stronger in the middle of the electrode, but also by the fact that small compound as calcein can be exchanged between the NRK cells via gap junctions (Sperber, 2016). Therefore, in

the following experiment cells were pulsed in assay buffer ($EBSS^{++}$) containing 50 µM 2-APB (to prevent calcein exchange between the neighboring cells). Micrographs given in **Figure 5.29** show that electroporated cells exhibited reduction of the fluorescence signal within every electrode inhomogenously and in addition, bright fluorescent rings on the inner edges of the electrodes were not observed.

In the control, non-pulsed cells residing on the electrodes appeared slightly brighter than the cells of the background, due to reflecting properties of the gold surface.

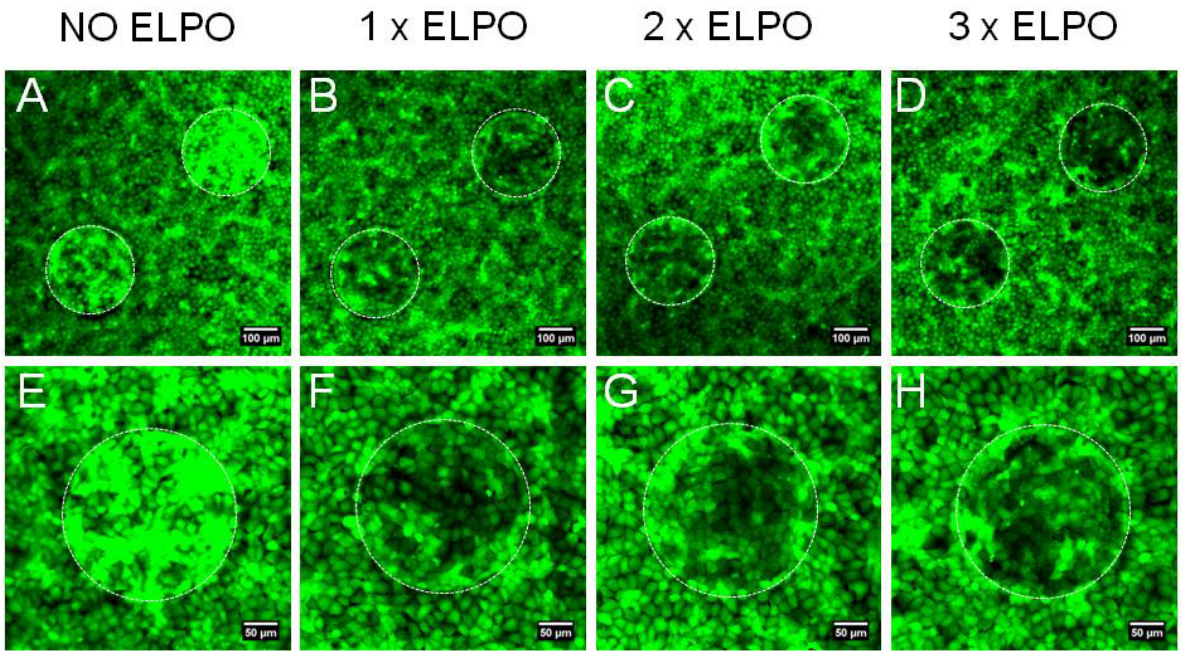

Figure 5.29 Exemplary confocal fluorescence micrographs taken with 10-fold magnification objective after no *in situ* electroporation of NRK cells was applied (**A**/**E**), or ISE was applied once (**B**/**F**), twice (**C**/**G**) or three (**D**/**H**) times. During ISE, NRK cells were dissolved in $EBSS^{++}$ buffer with 50 µM 2-APB. White circles delineate electrodes area. Micrographs in the top row were zoomed 1.5 times and scale bars represent 100 µm, while micrographs in the lower panel were zoomed 3 times and scale bars correspond to 50 µm.

Fluorescence micrographs documented after both experimental procedures were quantified using ImageJ program and evaluated statistically, according to the scheme described in **Figure 4.15 A** within chapter 4.3.5. The fluorescence intensity value for a pair of electrodes was normalized to the average intensity of the background at the micrographs taken for every measured experimental condition. The experimental procedure for calcein release from NRK cells by ISE (in $EBSS^{++}$ buffer) was conducted within two independent experiments and altogether 6 different micrographs were analyzed for each condition (n=6). The results are

evaluated in the form of bar plot presented in **Figure 5.30 A** (mean value ± standard deviation; n= 6). In **Figure 5.30 B**, bar plot shows results for the calcein release by ISE from NRK cells (in $EBSS^{++}$ containing 50 µM 2-APB). This experimental procedure was conducted only once and 2 different micrographs were taken and analyzed for every experimental condition (mean value ± standard deviation; n=2).

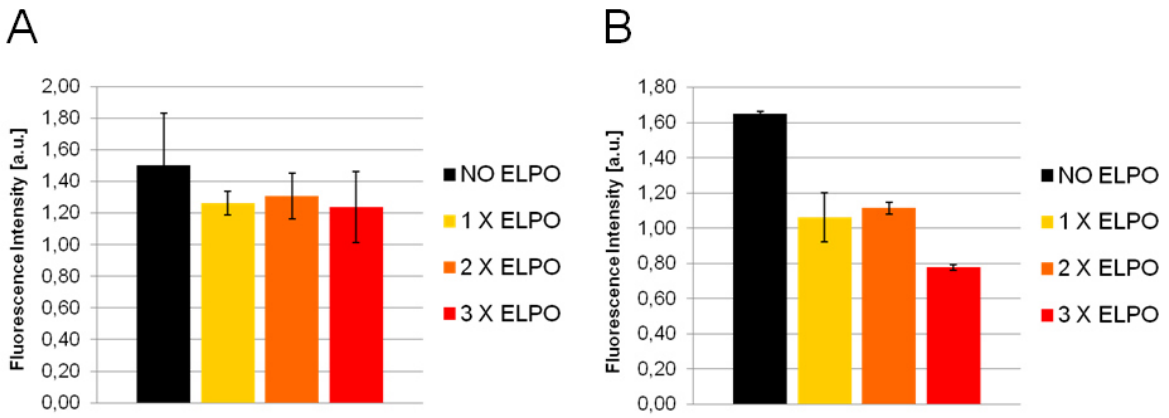

Figure 5.30 Bar plots presenting fluorescence intensity of calcein on the micrographs taken after *in situ* electroporation of NRK cells to facilitate release of calcein from the cell cytosol. Release of calcein by ISE was performed in: **A** $EBSS^{++}$ buffer (6 micrographs taken within two independent experiments were quantified using ImageJ; mean value ± standard deviation; n= 6) and **B** $EBSS^{++}$ buffer containing 50 µM 2-APB (2 different micrographs taken for every experimental condition within one experiment were quantified using ImageJ; mean value ± standard deviation; n= 2).

The calcein release experiment performed in $EBSS^{++}$ resulted in the fluorescence intensity of 1.50 ± 0.32 for the control and relatively small differences between mean values of three samples (1 x ELPO: 1.26 ± 0.07; 2 x ELPO: 1.31 ± 0.14; 3 x ELPO: 1.24 ± 0.22). Release of calcein by ISE from NRK cells in $EBSS^{++}$ containing 50 µM 2-APB resulted in the following values of fluorescence intensity: 1.06 ± 0.14 for 1 x ELPO; 1.11 ± 0.03 for 2 x ELPO and 0.78 ± 0.02 for 3 x ELPO. The fluorescence intensity of control was 1.65 ± 0.01. Based on the single experiment showed in graph **B**, it can be concluded that there was no significant difference in calcein release between the cells pulsed once and twice, whereas cells pulsed three times released slightly more calcein. Taken altogether, there was a clear difference in calcein release observed between these three conditions and a control. As expected, the cells pulsed three times exhibited lower fluorescence intensity than the cells pulsed one and two times.

5.3.1.3 Release of Calcein from the Cells by Electroporation Monitored by Time-Resolved Imaging

The results described in previous chapter demonstrated release of calcein from the cells by *in situ* electroporation. In order to explore release of calcein from NRK cells more closely, *in situ* electroporation of the cells was conducted directly under the objective of the CLSM microscope and was monitored by time-resolved imaging. It has been assumed that the direct insight into the cell appearance, shortly before and shortly after pulse application, will allow one to better visualize and evaluate loss of intracellular calcein from the cells. A special experimental setup (described in details in chapter 4.2.1.4) was applied to conduct pulse application on the microscopic stage. For this experimental procedure, NRK cells were grown on 8W4Eμ electrode arrays. After staining of NRK cells with 2 μM Ca-AM, L-15 medium was added to the cells and experimental setup (described in chapter 4.2.1.4) was mounted directly on the stage of the CLSM microscope.

The series of micrographs were taken with 10-fold magnification objective, thus documenting two electrodes out of four in every well. NRK cells in each well were pulsed four times successively (using optimal pulse parameters: 40 kHz, 4 V and 200 ms) with the time gap of app. 4 – 10 min between the pulses. Microscopic images were taken in short time intervals (every 1 – 2 min) between the pulses and shortly before and shortly after every pulse application.

Exemplary micrographs are summarized in **Figure 5.31**, with white circles delineating electrodes area. Images were taken either shortly before (**A**, **C**, **E**, **G**) or shortly after (**B**, **D**, **F**, **H**) every pulse application. Whereas release of calcein from the cytosol was not that obvious after first pulse application (**B**, **C**), after the second electric pulse was applied, diffusion of calcein from the cells was observed, as the cells on the electrodes appeared darker (**D**, **E**). With every following pulse application (third and fourth time), release of calcein from the cells was enhanced. This was concluded since the NRK cells directly on the electrodes appeared darker (**F**, **G**, **H**) than in the previous micrographs. The cells growing around the electrodes (on the surrounding photopolymer) did not exhibit change in the fluorescence signal. Nevertheless, a trend of an overall fluorescence decrease in the entire image was observed during the acquisition of micrographs series, due to the weak photobleaching effect. The loss of fluorescence signal observed in the cells on the electrodes was a result of both photobleaching and calcein release from the cells by ISE. However, it was not a result of cell damaging or cell detachment from the electrodes, and this was confirmed by the phase-contrast micrographs taken after imaging was finished. The

complete cell monolayer on the electrodes (after calcein release by ISE) is shown in **Figure 11.2** of Appendix and it shows that there were no missing cells on the electrodes.

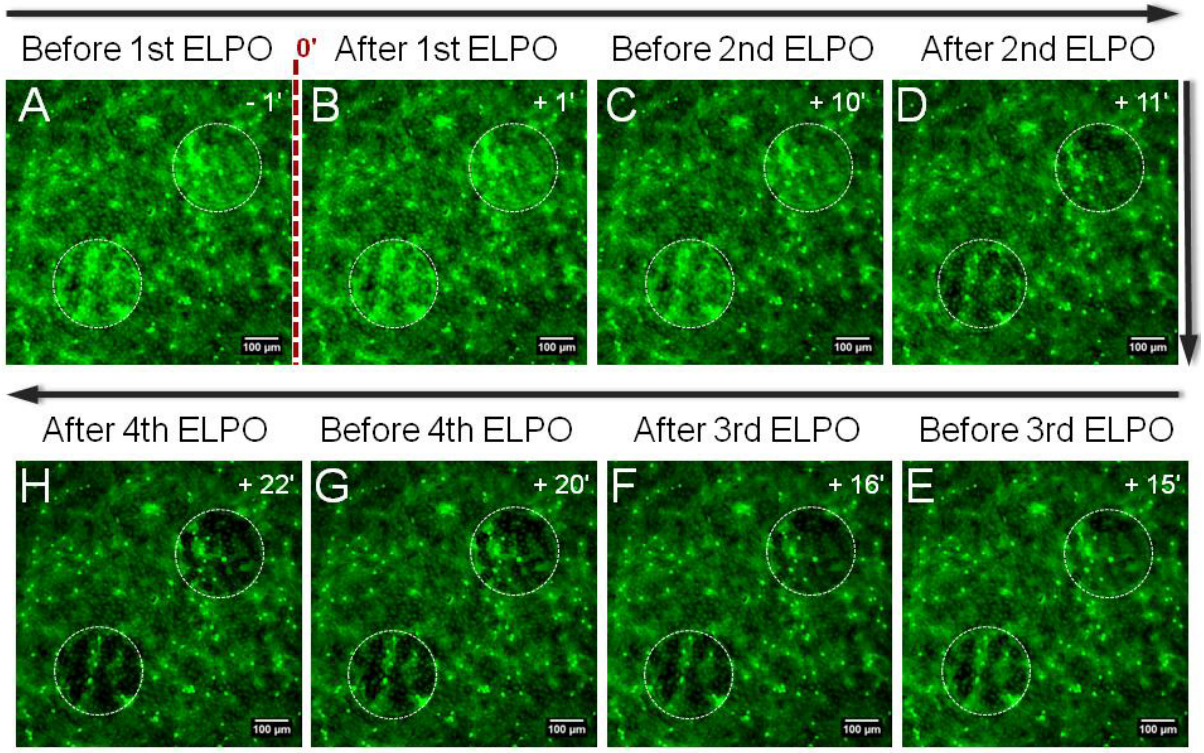

Figure 5.31 Exemplary microscopic images taken in real time by CLSM with 10-fold magnification objective before, during and after release of calcein from confluent NRK cells by *in situ* electroporation applied four times. The scale bars represent 100 µm. White circles in the images delineate electrodes area. The release of calcein from the cytoplasm increased with every electric pulse application.

Micrographs were quantified using ImageJ software, according to the scheme described in **Figure 4.15 A** in chapter 4.3.5. The experimental procedure for time-resolved imaging of cells exposed to ISE was performed once and at that occasion, three series of micrographs were analyzed (n=3) for the sample (w/ ISE). The results are presented in the form of bar plot (**Figure 5.32**; mean value ± standard deviation; n= 3).

These results indicate the loss of fluorescence signal from the cells on the electrodes after every pulse application. Before the cells were pulsed for the first time, the fluorescence intensity was at the value of 1.59 ± 0.16 and after first pulse application, fluorescence intensity decreased to 1.32 ± 0.12. It remained at 1.31 ± 0.11 before the second pulse application took place and thereafter, fluorescence intensity decreased to the value of 1.01 ± 0.06. In order to compensate a small effect of focus drift during microscopy, the focus was adjusted before the cells were pulsed for the third time and thus fluorescence intensity

slightly increased (1.06 ± 0.09). After the third pulse application, it dropped to 0.87 ± 0.10. Again, before the cells were pulsed for the fourth time, focus was adjusted and the fluorescence intensity was 0.95 ± 0.11, but after the fourth pulse application, it decreased to 0.80 ± 0.14.

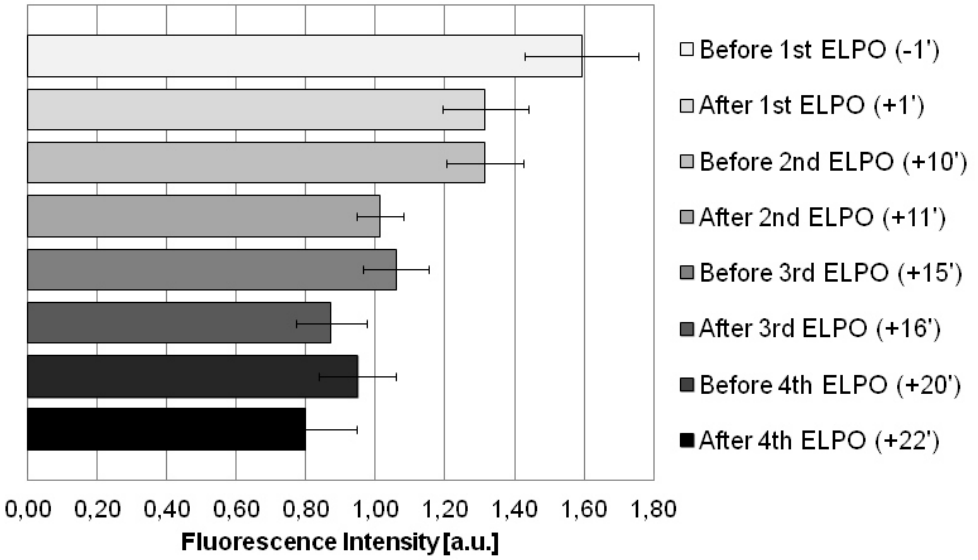

Figure 5.32 Bar plot presenting fluorescence intensity of calcein on the micrographs taken upon release of calcein from NRK cells by *in situ* electroporation applied four times successively. Three series of micrographs (taken within one experiment) were quantified using ImageJ; mean value ± standard deviation, n= 3. The fluorescence intensity value for a pair of electrodes was normalized to the fluorescence intensity of the background. With every pulse application, loss of fluorescence signal from the cells on the electrodes was observed due to release of calcein from the pulsed cells.

Within the same experiment, three series of micrographs (n=3) were taken in absence of electric pulses (w/o ISE) to obtain the corresponding controls. Micrographs were taken in app. the same time intervals as if multiple electroporation would be performed. The exemplary series of images showing NRK cells which were not exposed to electric pulses but only to imaging is presented in **Figure 5.33**. There was no release of calcein from the cells, neither on the electrodes, nor around them (background). However, a slight effect of focus drifting was seen in the course of image acquisition and this was compensated by adjusting the focus. Previous observations were confirmed after quantification of fluorescence intensity, as micrographs were evaluated using ImageJ (according to the scheme described in **Figure 4.15 A** in chapter 4.3.5) and the results were presented in the form of bar plot (**Figure 5.34**; mean value ± standard deviation; n= 3).

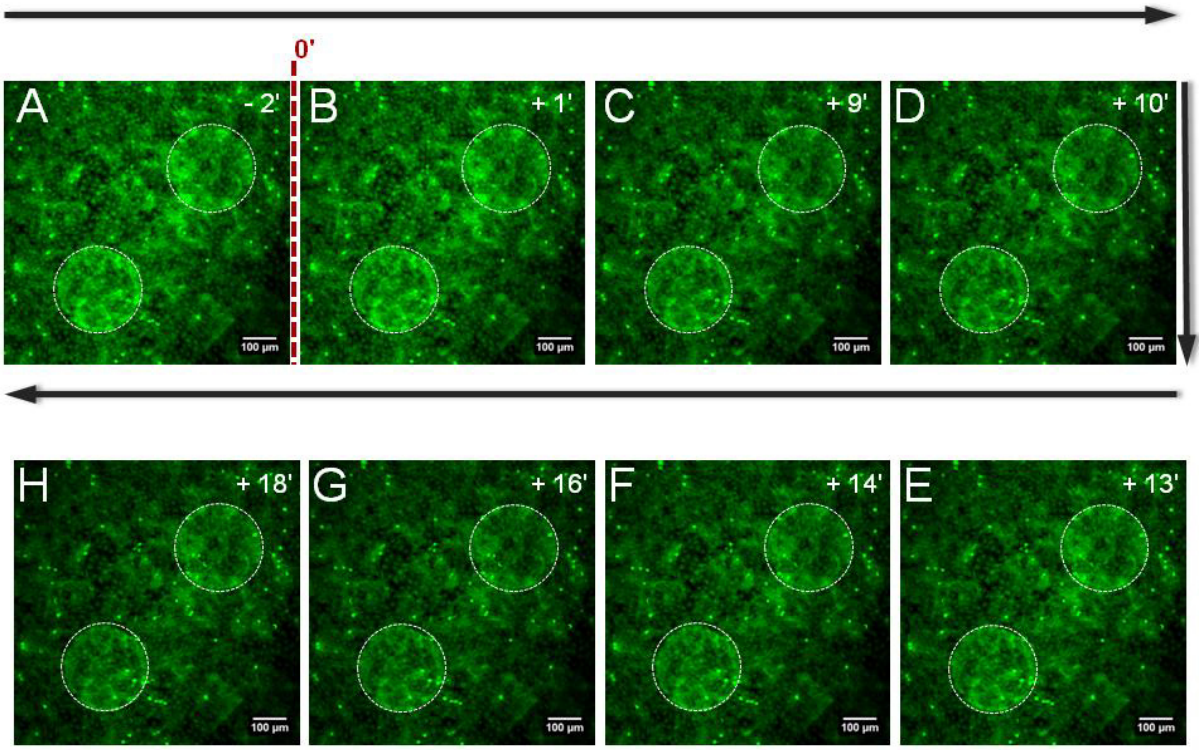

Figure 5.33 Exemplary microscopic images taken in real time by CLSM with 10-fold magnification objective in absence of electric pulse application. The scale bars represent 100 µm. White circles in the images delineate electrodes area. No release of calcein from the cytoplasm of NRK cells was observed.

Results indicated no loss of fluorescence signal from the cells in absence of electric pulses, but only slight increase of the overall fluorescence signal due to focus adjustment during the micrographs acquisition. The mean fluorescence intensity values obtained in the course of time-resolved imaging were as follows: 1.56 ± 0.10; 1.54 ± 0.11; 1.57 ± 0.15; 1.58 ± 0.16; 1.62 ± 0.12; 1.62 ± 0.13; 1.63 ± 0.12; 1.63 ± 0.10. After the series of fluorescence micrographs was taken in absence of ISE, the appearance of NRK cells was documented by the phase-contrast image given in **Figure 11.3** of Appendix.

In addition, in Appendix is given a series of micrographs taken in real time upon application of electric wounding to the NRK cells (using pulse parameters: 40 kHz, 5 V and 1.25 s), four times successively (**Figure 11.4**). The appearance of NRK cells, after they were irreversibly damaged in presence of calcein, was compared to the appearance of the cells during release of calcein by ISE. The series of micrographs showed that the cells were heavily damaged already after first wounding pulse application and after fourth application of strong electric pulses, there were only small populations of damaged cells present on the electrodes. The confluent cell monolayer on the electrodes was completely decomposed.

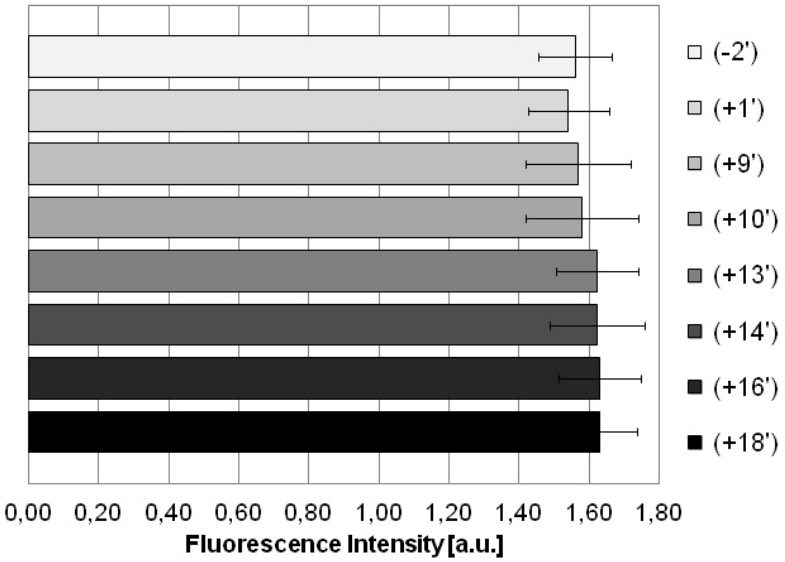

Figure 5.34 Bar plot presenting fluorescence intensity of calcein on the micrographs taken within the indicated short time intervals, in absence of pulse application. Three series of micrographs (taken within one experiment) were quantified using ImageJ; mean value ± standard deviation, n= 3. The fluorescence intensity value for a pair of electrodes was normalized to the fluorescence intensity of the background.

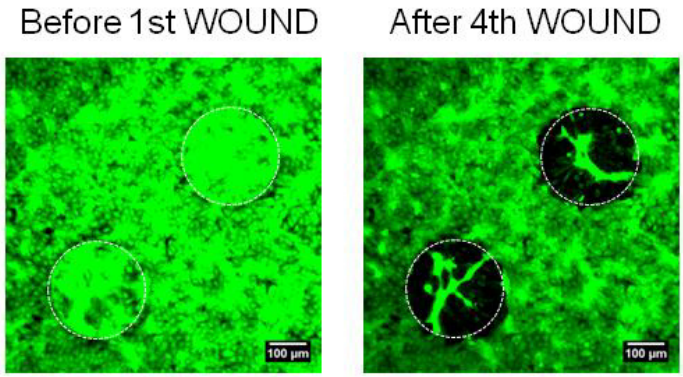

Figure 5.35 Exemplary micrographs taken by CLSM with 10-fold magnification objective, before first (left) and after fourth (right) application of electric wounding to the confluent NRK cells. The entire series of micrographs is given in Appendix (**Figure 11.4**). The scale bars represent 100 µm. White circles in the images delineate electrodes area. The loss of fluorescence signal (from calcein) was observed after electric wounding, due to cell damage and cell death.

To illustrate significant difference in appearance of the cells before and after wounding application, first (**A**, before 1st wounding) and the last image (**H**, after 4th wounding) within the

micrographs series shown in **Figure 11.4** are compared in **Figure 5.35**. Moreover, a comparison can be drawn between the appearance of the cells after electroporation (e.g. **Figure 5.31 H**) and after the electric wounding. In the case of ISE, fluorescence intensity within the electrodes area was mainly reduced due to calcein release by ISE and cell monolayer remained intact. In the latter case (wounding), electrodes area became darker with every wounding pulsation, as the cells detached from the electrodes, were killed and formed a group of dead and damaged cells on the top of the electrodes. Thus, the loss of fluorescence signal in these two cases comes as a consequence of completely different events. Moreover, appearance of the cells upon wounding is considered as an absolute "positive control" for studies of release by ISE, as it shows fluorescence change upon cell damaging and death, conditions upon which calcein can freely diffuse from the cell interior.
Since 5 mM Vitamin C was applied in this experiment as an anti-photobleaching agent, a corresponding control series of micrographs was taken under the same conditions, but in absence of pulse application (**Figure 11.5** of Appendix). These fluorescence micrographs corresponded to the controls obtained during time-resolved imaging of NRK cells in absence of pulse application shown in **Figure 5.33**.

5.3.2 Release of Lactate Dehydrogenase from the Cells and LDH Assay

The release of intracellular material from the cells was not only investigated by probing calcein, but also by releasing the intracellularly present enzyme lactate dehydrogenase (LDH). The initial idea was to release LDH from the cells by *in situ* electroporation and to evaluate the amount of released LDH from the cells by using standard, commercially available, LDH assay (more details described in chapter 4.5.2). Before ISE was applied for the release of LDH, a feasibility of this assay was verified by applying electric wounding to release LDH to the maximum extent from NRK cells, and to evaluate the amount of extracellular LDH by a commercial LDH assay. The experimental procedure was performed using 8W4Eμ electrode arrays, either with chamber type Ø3, or Ø5. In both cases, cell population in certain wells was exposed to irreversible damage by electric wounding (using pulse parameters: 40 kHz, 5 V and 30 s) and cells in other wells were not pulsed at all, in order to obtain the corresponding control. In addition, the entire cell populations in two wells of 8W4Eμ-Ø5 were exposed to lysis in order to estimate the maximal response, when all cells in one well release LDH (positive control). The results are listed in a **Table 5.2**, mean value ± standard deviation was calculated for each condition, either with number of

repetitions n=3 (w/ and w/o wounding), or with n=2 (cell lysis).

Table 5.2 Results after release of LDH from NRK cells by applying electric wounding to the cells grown on either 8W4Eμ-Ø3, or 8W4Eμ-Ø5. The mean values with corresponding standard deviation (n=3) are given for the case when cells were pulsed and when no pulse application took place. In addition, control was made on 8W4Eμ-Ø5, whereby all cells within the well were lysed (n=2).

	8W4Eμ-Ø3		**8W4E-Ø5**		
	W/ Wounding	**W/O Wounding**	**W/ Wounding**	**W/O Wounding**	**Lysis**
Mean Value (MV)	0.4180	0.2543	0.5033	0.3313	3.1375
Standard Deviation (SD)	0.1087	0.0636	0.0087	0.0657	0.0544
Number of Repetitions (n)	3	3	3	3	2

The cells exposed to electric wounding on 8W4Eμ-Ø3 released almost twice the amount of LDH, compared to non-pulsed cells. When the entire cell population in the well was lysed, it was released app. 6.2 times more LDH compared to the case when the cell population on the electrodes was exposed to wounding and app. 9.5 times more LDH compared to non-pulsed cells. It has been concluded that the sensitivity of an assay is insufficient and error bars are too high, so that it has been not preceded with LDH assay by ISE.

5.4 Discussion

In situ electroporation of adherent mammalian cell cultures grown on the planar electrodes, integrated within the electric cell-substrate impedance sensing (ECIS) technology, is a well-established method to introduce various non-permeable compounds into the cell cytosol (Wegener et al., 2002; Stolwijk et al., 2011). This section of the work is dedicated to: (i) optimization of pulse parameter conditions for every cell line applied in this work, with respect to the application of 8W4Eμ electrode arrays, (ii) evaluation of multiple pulse application as a strategy to enhance ISE loading efficiency, (iii) investigation of the post-electroporation events by impedimetric monitoring with the high time resolution and (iv) establishment of a proof-of-principle assay to demonstrate release of an intracellular material from the cells by

ISE. The cell morphology changes upon delivery and release by ISE were monitored noninvasively by the ECIS technology and by microscopy using CLSM (in cases when fluorescently-labeled probes were applied for electroporation studies).

5.4.1 Optimization of *In Situ* Electroporation for Different Cell Lines

Combination of very sensitive impedimetric monitoring of the confluent cells and conventional microscopy allowed for detailed investigation of events taking place before and after *in situ* electroporation. Before certain cell line was applied as a cell model to study delivery of the specific bioactive molecule into cell cytoplasm by ISE, optimal combination of parameters for pulse application had to be found. Valid for both single and multiple pulse application, the efficiency of ISE is ruled by successful loading of the cells with the probe and least possible damage of the cellular monolayer. Whereas frequency of 40 kHz was suitable for all cells and as such was kept constant (Wegener et al., 2002), pulse amplitude and pulse duration were varied in order to obtain optimal results, with respect to the maximal loading efficiency of the cells with the probe and minimal invasiveness of the method.

The ideal combination of pulse parameters is individual for every cell line and it depends mostly on the morphological characteristics of the given cell line. Therefore, systematic dye loading experiments (Neumann et al., 1999; Rols and Teissié, 1990; Raptis et al., 1995) were performed for every cell line, using 250 kDa FITC-dextran as a fluorescent probe to determine optimal pulse parameter conditions. In the literature can be found numerous reports on the application of FITC-dextrans with various molecular weights for dye loading studies, including electroporation (Prausnitz et al., 1993; Rols and Teissié, 1998a). For the studies of ISE of the cells grown on ECIS electrodes, in most cases fluorescent probes Lucifer yellow and FITC-dextrans were applied so far (Wegener et al., 2002; Albermann, 2004). Although within this work ISE was applied for delivery of bioactive molecules with much smaller molecular weight than 250 kDa (e.g. second messengers and nucleic acids), optimal pulse parameters were determined using FITC-dextran of that size to assure universal applicability of ISE, regardless of the probe size. Besides, it is well known from the literature that the FITC-dextran with the size of 2 MDa was successfully delivered into NRK cell by ISE, using optimal pulse parameter conditions for this cell line (Albermann, 2004). The distribution of the probe within the cells is ruled by the size exclusion of the nuclear membrane and thus molecules bigger than 40 - 50 kDa cannot cross the nuclear envelope by the passive diffusion (Fried and Kutay, 2003) and thus remain excluded from the nucleus.

Studies of dye loading efficiency after ISE on 8W4Eμ ECIS electrode arrays were conducted for cell lines: BAEC, CHO-K1 (CHO-GFP), HaCaT and NIH-3T3, whereas optimal combination of pulse parameters for NRK cells was already extensively studied and determined (Wegener et al., 2002; Stolwijk, 2012).

All cell lines applied in this work could be efficiently loaded with the fluorescent probe 250 kDa FITC-dextran by *in situ* electroporation. Impedimetric readings before and after electric pulse application demonstrated that each of the five cell lines showed characteristic time course of the (normalized) impedance after electroporating pulse application. Time course of the normalized impedance before and after ISE for all cell lines, except for CHO-K1 cells was evaluated and presented at 4 kHz, as at this frequency changes in cell-cell and cell-substrate contacts can be monitored in a very sensitive manner (Giaever and Keese, 1993). For CHO-K1 and CHO-GFP cells, frequency of 16 kHz was found to be the most sensitive to follow the alterations of the cell-cell and cell-substrate contacts.

A typical experimental procedure for ISE including the dye loading study was presented using an example of BAEC cells. In this case, impedimetric monitoring of the cells before and after ISE on ECIS electrodes allowed for evaluation of recovery kinetics after electric pulses of constant frequency (40 kHz) and constant amplitude (4 V), but different pulse durations were applied (200 ms, 300 ms and 400 ms). It was noticed that the impedance decrease after pulse application was bigger when the cells were exposed to electric pulse for the longer period of time. In correlation to that, cells needed more time to recover after they were exposed to longer pulse durations than to shorter. Subsequent microscopy by CLSM provided an insight into the loading efficiency and invasiveness of the method. The cells pulsed for shorter time (200 ms) were efficiently loaded with FITC-dextran and thereby no cell damage was observed. In contrast to that, the cells exposed to longer pulse durations (300 and 400 ms) were loaded very well with the fluorescent probe, but considerable number of the cells on the electrodes was damaged or even missing, due to the invasiveness of the electric pulses. Based on all these information gathered during dye loading studies, optimal combination of pulse parameters was determined for BAEC cells.

Similar dye loading studies were performed to determine the optimal pulse parameter conditions for other cell lines as well. Whereas for NIH-3T3 cells higher voltage (5V) is needed in combination with 200 ms, for CHO-K1 cells longer pulses (500 ms) in combination with 4 V needs to be applied to accomplish successful loading. On the other hand, HaCaT cells behave slightly different than the other cell lines studied in this work and this might be explained by their size, as the cell bodies of HaCaT are bigger compared to the other studied cell lines. For successful loading of HaCaT cells, voltage of 5 V and pulse duration not

shorter than 500 ms should be applied. Whereas cells exposed to 600 ms still appeared to be in a good condition after pulse application, several damaged or missing cells on the electrodes were observed when cells were exposed to 700 ms.

Previous observations regarding cell lines analyzed in this work correlate quite well with the published studies of Wegener et al., 2002 conducted on NRK cells. The group conducted detailed dye loading studies, with either voltage variations (while keeping frequency and pulse duration constant), or by varying pulse duration (while frequency and voltage were kept constant). It was observed (with 40 kHz and 200 ms) that the number of loaded NRK cells increased with an increasing voltage (up to 4 V), but the threshold was crossed with 5 V, when a considerable number of cells was irreversibly damaged. With the constant voltage (of either 3 V, or 4 V) and frequency (40 kHz) pulse durations were varied from 50 to 500 ms. Whereas loading efficiency increased gradually when NRK cells were exposed to pulses of duration from 50 to 200 ms, after their exposure to 500 ms long pulses, missing cells on the electrodes were observed, indicating that part of the cell population was irreversibly damaged.

In addition, the group conducted impedimetric monitoring of the cell recovery after pulse application, which showed that the NRK cells exposed to 40 kHz frequency, 4 V amplitude and different pulse durations from 50 to 200 ms needed approximately the same time (~ 20 min) to return to the pre-pulse levels. However, the cells exposed to longer pulse (500 ms), needed longer time for recovery. Time for complete post-electroporation recovery of different cell lines in this work varied from 10 min for HaCaT, over 15 – 20 min for CHO-K1 (CHO-GFP), 20 min for NIH-3T3 and 25 – 30 min for NRK cells, up to 50 min for BAEC cells. Such cell type-specific behavior upon *in situ* electroporation (Stolwijk, 2012) can be subscribed to individual morphological properties of every cell line. During all dye loading studies, it has been observed that the loading efficiency, invasiveness of the method and thus the time for recovery after pulse application depends on varied parameters (pulse amplitude and pulse duration). Whereas some cell lines (BAEC, NIH-3T3 and NRK) exhibited various levels of impedance decrease immediately after application of electric pulse, cell lines like CHO-K1 and HaCaT exhibited either impedance increase or signal alternating between decrease and increase successively after the pulse application.

Optimal pulse parameter conditions determined for every cell line were: f=40 kHz; U=4 V and t=200 ms for BAEC cells, f=40 kHz; U=4 V and t=500 ms for CHO-K1 and CHO-GFP cells, f=40 kHz; U=5 V and t=500 ms for HaCaT cells and f=40 kHz; U=5 V and t=200 ms for NIH-3T3 cells. Optimal pulse parameters for ISE of NRK cells are: f=40 kHz, U=4 V and t=200 ms. These results suggest that the pulse amplitude of 4 V is preferred for most cell lines

(BAEC, CHO-K1, CHO-GFP and NRK), whereas for two cell lines (HaCaT and NIH-3T3), amplitude of 5 V is necessary. BAEC and NRK cells need the same pulse parameter conditions for optimal ISE (40 kHz, 4 V and 200 ms). As previously mentioned, the HaCaT cells require pulses of higher amplitude (5 V) and longer duration (500 ms) for the efficient loading.

In the study conducted by Ghosh et al., 1993 optimal pulse parameters for electroporation of WI-38/VA13 (fibroblasts) cells on small gold film electrodes were found to be 4 kHz, 5 V and 200 ms. Loading efficiency was determined by the entry of a horseradish peroxidase (HRP). This study showed that only cells exposed to the voltage of 4V and 5V were largely loaded with HRP, whereas only a few cells exposed to 3 V showed HRP signal. On contrary, WI-38/VA13 cells exposed to lower voltages (1 and 2 V) were not loaded with HRP. Furthermore, previously described studies by Wegener et al., 2002 reported dye loading studies with Lucifer yellow conducted not only for NRK, but also for BSC-1, MDCK-I and MDCK-II cells. Whereas for the cell lines NRK and BSC-1 pulse parameter combination: 40 kHz, 4 V, 200 ms was found to be optimal, with regards to Lucifer yellow loading efficiency and recovery of the cells after pulse application, for the cell lines MDCK-I and MDCK-II, pulses of 40 kHz, 3 V and 200 ms were found to be most efficient, while not damaging.

Typically, with increasing pulse amplitude, loading efficiency gradually increases as well until the critical voltage is reached. Beyond critical voltage value, electric pulse causes irreversible permeabilization and damage of the cell membrane. On the other hand, too low pulse voltage (usually 1 or 2 V) in presence of 200 ms pulse duration cannot facilitate satisfying delivery of the probe into cell cytosol and thus the loading is inefficient (observed with BAEC cells). Therefore, amplitude of 3V was usually applied as the starting voltage value tested for ISE, which was further increased, along with the values of pulse duration, until the optimal combination of pulse parameters was achieved. According to the well-established theory of electroporation, number of pores and their density within the cell membrane, increases with the increasing voltage (Chernomordik and Chizmadzhev, 1989; Teissié et al., 2005), whereas pulse duration influences size of the pores established during the pulse application. Namely, application of longer pulses during electroporation causes a formation of the pores with bigger diameter than the pulses with shorter duration. Thus, the established pores within the cell membrane practically grow with an enhanced pulse duration, but only as long as the applied electric field is present (Weaver and Powell, 1989; Weaver and Chizmadzhev, 1996; Rols and Teissié, 1998a). The influence of an increasing pulse duration could be observed in the dye loading study conducted on BAEC cells, whereby it has been noticed that the fraction of stained cells did not change significantly with an elongation of the pulse, but the

fluorescence intensity increased, as well as the number of damaged cells, when critical pulse duration was exceeded. Although the cells seeded on the ECIS electrode array form confluent monolayer covering the entire area of the wells, only the cells present directly on the planar gold film electrodes are exposed to the electric pulses. Thus, during the electric pulse, an electric field is applied perpendicularly only to the cell population residing on the electrodes and to the cells adhering partially on the active electrode area. In the latter case, xenomolecules can diffuse into the cells through the permeabilized membrane on the one side and expand to the entire cytosol.

As already mentioned, significant differences in cell behavior upon ISE were observed for different cell lines and these can be subscribed to the individual morphological properties of every cell line. Since obvious differences in the shape and size of the various cell lines applied within this work were recognized, the cellular response to electric pulse application thus differentiated as well. Furthermore, many authors reported previously on influence of membrane composition (Benz and Zimmermann, 1981), content of membrane proteins (Tsong, 1991) and membrane conductivity (Kotnik et al., 1997) on efficiency of membrane permeabilization.

The experimental procedure for ISE on 8W4Eμ arrays was very well applicable for all cell lines used in this work, with only exception of NIH-3T3 cells, as certain difficulties had been experienced during the microscopy. Namely, the confluent monolayer of NIH-3T3 cells in most cases easily detached from the substrate surface, due to a buffer change and shear stress caused by pipetting. Nevertheless, dye loading studies following *in situ* electroporation of different cell lines within this work indicated that ISE can be applied as a highly efficient method to introduce membrane-impermeable compounds into cells. Furthermore, it has been demonstrated that ISE combined with impedimetric monitoring by ECIS allows for a direct evaluation of invasiveness of the technique and its impact on the cell morphology. Investigation of loading efficiency was completed by subsequent microscopy using CLSM to assess the appearance of the confluent cells, previously exposed to *in situ* electroporation.

5.4.2 Multiple *In Situ* Electroporation

Besides the optimization of experimental procedure for single electric pulses, application of multiple electroporation pulses was evaluated as a strategy, which can be further applied for delivery or release of the material in or out from the cells. The strategy behind the application of multiple electric pulses aims for enhanced loading efficiency, which can be achieved when electroporation is applied several times successively, whereby optimal combination of pulse parameters for the given cell line is applied. In this context, multiple electroporation was

already reported before by the different groups of scientist (Brown et al., 1992; Son et al., 2015, Pakhomov et al., 2015). Brown et al., 1992 measured an uptake of FITC-dextran in individual yeast cells (Saccharomyces cerevisiae) by the flow cytometry after their exposure to successive square 50 μs electric field pulses. Propidium iodide was added 25 min after pulsing to evaluate number of viable cells after the electric pulse application. When the optimal electric field strength (5 kV/cm) (for single pulse) was applied successively, fluorescence intensity inside the cells did not increase, while on the other hand percentage of cells with PI signal did increase. The group observed enhancement of the loading efficiency with increasing number of electric pulses applied only in combination with lower field strength (3 kV/cm). It would be the objective of future studies to investigate correlation between the number of electric pulses and pulse parameter conditions in order to assess if the application of pulse parameter conditions optimal for single pulse indeed is the best strategy for multiple pulse application as well. Multiple pulses of slightly lower voltage or pulse duration might result in the successful loading efficiency with the lower potential for cell damaging.

In the work performed by Sperber, 2016, sequential *in situ* electroporation was applied and monitored by the ECIS technology. As a fluorescent probe, 250 kDa FITC-dextran was applied. Studies within this work showed the enhanced fluorescence intensity of FITC-dextran in the cells electroporated two or three times, in comparison to the cells pulsed only once. In addition, time interval between the pulses was varied from 5 to 60 min and recovery of the cells was found to be similar with regards to different time intervals between the sequential pulses.

Within this work, propidium iodide (Tekle et al., 1994; Rols and Teissié, 1998a; Pucihar et al., 2008) was applied as the fluorescent probe to study application of multiple electric pulses successively to increase the loading efficiency. Due to its membrane impermeability, propidium iodide (PI) can enter only the cells with disrupted or porated membrane and thus accumulate in their nuclei where it intercalates with cell DNA. For the multiple electroporation protocol, 100 μM of propidium iodide was applied, since this concentration of PI was recommended by various literature sources (Tekle et al., 1994; Rols and Teissié, 1998a; Pucihar et al., 2008).

NRK cells were pulsed one, two or three times during the impedimetric monitoring at ECIS, by using optimal pulse parameters for this cell line: 40 kHz, 4 V and 200 ms. As a control served the population of non-pulsed cells on the electrodes exposed to PI. After every pulse application, normalized impedance signal decreased and recovery of the cells was followed by the signal increase to the pre-pulse state within 20 – 30 min. The cells were allowed to recover before the next pulse is applied, as thus possible cytotoxic effect of the experimental

procedure can be avoided. It has been noticed during multiple electroporation experiments that insufficient and uncompleted recovery of the cells between two successive pulse applications in some cases (data not shown) might lead to damage of the cells and eventually their detachment from the electrode surface. However, if the cells are given more time to recover between the pulses, no damaging effect of the method was observed. Similar observations were made by Sperber, 2016, where NRK cells were pulsed two times with 5, 30, 45 or 60 min of a time gap between the pulses. These studies showed that the cell recovery was independent of the inter-pulse delay time, and that all cells recovered eventually to the pre-pulse impedance values (within ~ 1 hour).

Even though cell membrane resealing takes place very quickly (within the several seconds or minutes; Kinosita and Tsong, 1979; Teissié and Rols, 1994), cell monolayer reassembly and return of the cells to the normal state after exposure to electric pulse takes more time. During post-pulse phase, cells are more sensitive and vulnerable and their exposure to the electric pulse during this phase could cause some irreversible damage. The studies of the effect of nanosecond-duration electric pulses applied in trains (1 to 100 pulses) conducted by Pakhomov et al., 2015 with cells in suspension showed that the increasing number of electric pulses leads to an increase of pore number, but not of the pore diameter.

After microscopic evaluation of the loading efficiency achieved by multiple ISE, it was concluded that the amount of material (propidium iodide) inside the cells increases with every additional pulse application. Namely, enhanced accumulation of propidium iodide inside the cells was observed after the NRK cells were pulsed twice and three times, compared to the cells pulsed only once. In addition, it was noticed that the number of loaded cells increases with every further pulse application. The cells which were not pulsed, but only incubated in the presence of propidium iodide appeared dark, indicating that this fluorescent probe did not cross the cell membrane in absence of electric pulse.

The group of Ghartey-Tagoe et al., 2004 did studies of electroporation on Caco-2 and T84 cells to investigate loading efficiency of the delivery as a function of voltage, pulse length, and pulse number. They did not observe a significant difference in the loading efficiency when the cells were exposed to the long single and to the short multiple pulses. However, such results are not in agreement with studies of Canatella et al., 2001 and Kim et al., 2007, who reported better loading efficiency and preserved viability when cells in suspension were exposed to short multiple pulses, compared to the application of long single pulses.

The results of multiple pulse application study conducted in this work suggested that application of multiple successive pulses can provide enhanced loading of the cells with the membrane-impermeable material and thus can be applied as a strategy to achieve

successful delivery or release of the material in or from the cells. Therefore, multiple *in situ* electroporation was applied to increase the efficiency of the delivery of various bioactive molecules into the different cell types and to demonstrate the ability of *in situ* electroporation as a method to release the intracellular material from the cells.

5.4.3 Impedance Monitoring of *In Situ* Electroporation with High Time Resolution

ECIS technology allows for non-invasive and time-resolved monitoring of the cellular behavior before and after *in situ* electroporation, thus enabling one to obtain a wealth of information, both on the effect of different bioactive molecules delivered into cells and on the cellular response to applied electric pulses. With the special experimental setup, data acquisition can be performed in a very fast manner and impedance can be monitored with the high time resolution (HTR).

Thus, events taking place shortly before and after pulse application can be monitored and recorded within the very short time intervals, with an aim to answer the question: what happens with the cells directly after electric pulse application. It is well known that the cell membrane resealing takes place within the very short time period (up to several seconds or minutes; Rols and Teissié, 1998a; Neumann et al., 1998), but the impedance magnitude signal observed upon pulse application returns to the pre-pulse values for most of the cells after some longer period of time (20 – 40 min). Such longer recovery of the signal should not be misinterpreted as the long time period necessary for the membrane resealing, but rather as the cell recovery phase, during which morphological changes within the cell monolayer take place, as the result of the pulse application (Stolwijk, 2012; Stolwijk et al., 2011). The study including impedance monitoring of ISE with high time resolution was performed to challenge an existing assumption that the post-electroporation recovery of the cells is a multistep process and to investigate how different pulse parameters affect the post-pulse recovery of the cells. NRK cells were chosen as a cell model for studies of ISE monitored with HTR, as this cell line was already extensively applied for various ISE studies and its optimal electric pulse parameters are well-known and established (Wegener et al., 2002; Stolwijk, 2012; Sperber, 2016). Usually, it takes 20 – 45 min for NRK cells to completely recover after their exposure to the electroporating pulse. *In situ* electroporation followed with the high time resolution was performed with NRK cells grown on the 8W1E and 8W4Eμ electrode arrays. Variation of single electric pulse parameters applied to NRK cells, using both electrode array types, is discussed in the following chapter.

5.4.3.1 Single Electroporation Pulses - Variation of Pulse Parameters

Having in mind optimal pulse parameter conditions for NRK cells: 40 kHz, 4 V and 200 ms, single electric pulses were applied and pulse parameters: amplitude and duration were varied (with the frequency always kept constant) in order to investigate parameter-dependent change in impedance signal with the high time resolution. Pulse parameter combinations were chosen and varied with an aim to create electric pulses of different invasiveness. Thus, applied pulses were ranging from almost noninvasive to strongly invasive and damaging (corresponding to the electric wounding), by varying just one of the parameters, either pulse duration, or pulse amplitude. All measurements were conducted at the single frequency (4 kHz) to achieve a rapid data acquisition. Frequency of 4 kHz was chosen as with this frequency the cell-cell contacts of NRK cells are monitored in a most sensitive manner. The measurement time was set to 20 min and only in cases when strongly invasive pulses were applied, measurement time was 25 min.

NRK cells grown on either 8W1E or 8W4Eμ arrays were exposed to well-defined pulse parameters applied to the cells manually and not via software to achieve rapid data acquisition. Regardless of electric pulse parameters applied and the electrode array used to grow the cells on, impedance signal showed an initial drop directly after pulse application, subsequent increase of the signal took place and the signal decreased again, but this time in a slightly slower manner. Thereafter, impedance was increasing back to the pre-pulse values in a very slow manner over certain period of time, depending on the pulse parameters. Such multistep process of cell recovery after pulse application can be explained by the stress caused by invasive pulse and some considerable morphological changes in the cell monolayer. Immediate impedance drop and subsequent increase, taking place already in less than a second, can be assigned to the effect on cell membrane (in this case transient) and its permeabilization (Hibino et al., 1991). Opening of the membrane pores allows current to flow directly through the cells. The resealing of the membrane pores takes place very quickly afterwards (Chang and Reese, 1990), which stops the current flow from going through the cells, and as a consequence, current is forced again to flow around the cells (at 4 kHz). This explains subsequent fast increase in the signal observed directly after initial drop. In fact, Saulis et al., 1991 proposed that there are three phases during the resealing process of membrane pores. After the pulse application stops, pore size decreases rapidly. During the subsequent second phase, pore size decreases (slightly) slower. The third phase corresponds to the complete pore resealing which takes place over longer period of time (in

minutes). Data presented within this study are in agreement with such timeline, since the cell recovery after ISE was observed as a multiphasic process. Certainly, invasive electric pulses cause alterations in morphology of the affected cells, their cell-cell and cell-substrate contacts need some time to reestablish entirely. It causes temporary changes in the cellular monolayer as well and certain period of time is necessary for the cells to return to the pre-pulse state. Thus, the impedance signal after pulse application exhibits the multiphase process, consisting of initial fast changes within the first 10 sec and slow changes in impedance signal taking place until the signal eventually returns to the pre-pulse values (20 – 45 min). Such observations of multiphase post-pulse recovery are also in line with the studies performed by Stolwijk et al., 2011 and Stolwijk, 2012, which reported on impedance drop directly after pulse application and the subsequent slow recovery of the normalized impedance signal to the pre-pulse values.

The current study showed that pulses of different invasiveness, created by varying pulse amplitude and/or pulse duration, highly influenced the impedance signal changes caused by cellular behavior after pulse application, as well as the time necessary for the complete recovery of the cells to the previous “normal” state. The increasing pulse amplitude or increasing pulse duration caused bigger impedance drop directly after application of electric pulse and also increased the time required for cells recovery to pre-pulse state afterwards. Such observations are in agreement with the previously reported results for different cell lines performed by: Ghosh et al., 1993 (VA13); Wegener et al., 2002 (NRK) and Stolwijk, 2012 (NRK, Hep G2 and HEK-293). In addition, study performed by Ghosh et al., 1994 described the multiphase signal change of impedance magnitude, indicating similar behavior of pulsed cells. In the study conducted by Ghosh et al., 1993, pore formation and resealing upon electric pulses applied to fibroblasts was monitored impedimetrically with the high time resolution. Data were acquired every 10 milliseconds and voltage was varied from 1 – 5 V, while the pulse duration and frequency were kept constant (200 ms and 4 kHz, respectively). Similarly to the observations made in this work with NRK cells, Ghosh and collaborators reported that the drop after pulse application was larger with the higher voltage applied. After the pulse was applied with 1 V, signal almost immediately returned to its original value and with higher voltages, recovery time was longer. The group explained large drop in (impedance) signal upon pulse application by drastic changes in cell morphology – pore formation. The resealing of the pores in cell membrane starts as soon as the electric pulse is turned off. Thereafter, multiphasic and slow recovery of the signal to the pre-pulse values was observed, which entirely corresponds to the observations made in this work. Interestingly, the group reported as well that the VA13 cells recovered in all cases to 96 % of

the initial signal, independently on the voltage applied and corresponding initial signal drop upon pulse application. It may be added that the results of their HTR studies were consistent and very small variations were observed between the experiments, which correlates well with the reproducibility of HTR study conducted in this work, observed both on 8W1E and 8W4Eμ electrode arrays (**Table 5.1**).

In addition, observations made during this study are in good agreement with the study performed by Ryttsén et al., 2000, who performed electroporation of single NG108-15 cells with carbon-fiber microelectrodes. Electroporation was characterized by patch-clamp recordings and fluorescence microscopy. Interestingly, the group applied patch-clamp recordings to describe transmembrane current responses of the cells pulsed with an increasing voltage (2.7 - 3.2 – 3.8 – 4.3 kV/cm). Current responses were measured with the high time resolution and their values increased with an increasing voltage, indicating that higher values of electric field induce increased number of pores which were formed, or a higher degree of pore expansion. Upon pulse application, signal drop was recorded and the drop was larger with an increasing voltage. Same as in the current study, the initial signal drop corresponded to the short membrane permeabilization. They observed recovery of the membrane within 0.5 – 1 seconds after pulse application and the recovery process was longer when higher voltages were applied. The group observed biphasic (membrane) recovery, which is in agreement with the observations made within the current study. Fast recovery process was happening in milliseconds and the current values almost returned to the pre-pulse levels during this phase, however, subsequent slow process followed. This second phase took seconds or even longer. The signal returned to the pre-pulse values indicating closing of the pores. Such observations are very much in agreement with the results of electroporation study with HTR conducted in this work, even though the system under study was completely different (current work was conducted on a confluent monolayer of the cells and the work described by Ryttsén et al., 2000 was performed on a single cell level).

The importance of investigation of ISE with the high time resolution is to understand what happens with the cells directly after pulse application. In all experiments performed with NRK cells using standard ECIS experimental setup, significant decrease of impedance signal was observed directly after pulse application, whereas subsequent recovery of the signal to the pre-pulse values takes app. 20 – 45 min and should not be false interpreted as a time necessary for the cell permeabilization and subsequent resealing. Namely, the impedance signal increase after pulse application can be subscribed to the overall alterations in cell morphology and recovery of the cells to the initial “normal” pre-pulse state, following up the

very short membrane permeabilization and resealing directly after pulse application. According to the literature reports (Escande-Geraud et al., 1988; Gabriel and Teissie, 1995; Rols and Teissié, 1998b), time necessary for the pores closure and the complete resealing of the cell membrane after electric pulse application is estimated to be in the range from several seconds to several minutes, in some rare cases even a few hours (Saulis et al., 1991). The reports of Escande-Geraud et al., 1988 showed that the CHO cells electroporated *in situ* at 37 °C exhibited resealing of their membrane within 10 min after pulse application. Similar observations were deduced after electroporation of the cells in muscle tissue (performed by Bier et al., 1999 and Gehl et al., 2002).

Chang and Reese, 1990 proposed that the application of invasive electric pulses leads to the following events: (a) dielectric breakdown due to the induced membrane potential (Zimmermann et al., 1980) and structural changes induced by mechanical stress; (b) secondary effects, such as movements of ions, water and mobile molecules, which can further cause local heating and membrane stress; (c) cell swelling or shrinking and disruption of cytoskeleton, as the effects of membrane permeabilization and changes in the local ionic environment.

Hence, the results of ISE study by HTR conducted in this work seem to be in a good agreement with the previous similar studies conducted by Ghosh et al., 1993 and Stolwijk, 2012, as well as with the above discussed reports indicating multiphasic events taking place after application of invasive electric pulses. The initial impedance drop and immediate subsequent increase of impedance signal within the first few seconds after pulse application can be ascribed to the poration (permeabilization) and subsequent resealing of the cell membrane (Teissié et al., 2005). Further decrease and subsequent slow increase of the impedance signal can be interpreted as the recovery of affected cells to the pre-pulse state, after considerable morphological changes were induced by external electric field application. In this work, variation of pulse parameters with HTR was studied using 8W1E and 8W4Eμ electrode array and depending on the parameters applied, it was observed that the NRK cells exhibit different initial response after pulse application, with regards to the impedance drop and subsequent impedance increase, as well with the secondary cell response and slow impedance increase to the pre-pulse values. A comparison of the impedance profiles obtained for electroporated NRK cells on 8W1E and 8W4Eμ electrode arrays led to a conclusion that the signals appear very similar, especially when pulse amplitude was varied. When pulse amplitude (and frequency) was kept constant and pulse durations were varied, differences in impedance signal were slightly more pronounced and an initial signal drop after pulse application, with the corresponding subsequent increase, was overall smaller on

8W4Eμ arrays, compared to the 8W1E electrode array.

5.4.3.2 Multiple Electroporation Pulses

After application of single electric pulses to NRK cells *in situ* was evaluated using special experimental setup, the impedimetric monitoring with high time resolution was employed to evaluate multiple electric pulse application. The NRK cells were grown on the electrodes of 8W1E array and only optimal electric pulse parameter conditions for this cell line were applied (40 kHz, 4 V and 200 ms). The aim of this study was to monitor cell response with the high time resolution and to investigate if multiple applications of electric pulses affect somehow the response of the cells directly after electroporation. The measurements were repeated three times in order to evaluate their reproducibility and one exemplary set of the data is presented in this work. The NRK cells were pulsed three times successively and the frequency of 4 kHz was chosen as a single measurement frequency at which impedimetric monitoring with HTR was conducted.

Neither the time course of the normalized impedance expressed in minutes, nor the time course expressed in seconds revealed the significant difference in the cell response between each of the three electric pulse applications. However, some slight differences in impedance signal, and thus in the cell response, were observed on a seconds scale by means of the impedance drop (after pulse application) and subsequent increase of the impedance signal. The impedance drop after first pulse was larger than the impedance drops after second and the third pulse application. Nevertheless, these differences are quite small and can be assigned to the statistical variations and the time interval between every pulse application. The possible explanation for such variations in the signal might be the fact that with every pulse application, and thus induced permeabilization of the cell membrane, a certain amount of an extracellular material diffuses into the cell interior and changes the ionic and metabolites composition within the cells. At the same time, intracellular material can be released from the cells during the membrane permeabilization and this influences metabolites composition and ionic changes within the cells as well. In addition, membrane might not be completely regenerated and recovered after the previous pulse(s). Even though the impedance signal returns to the pre-pulse values, it is known form the literature that the resealing of small pores and complete closure of the cell membrane might take several minutes (Chang and Reese, 1990). All these processes might influence the “size” of an impedance decrease directly after application of an external electric field.

In fact, during various studies including multiple electroporation of the cells which were conducted in this work in presence of the bioactive or fluorescent molecules (e.g. aptamers,

siRNA, FITC-dextran), certain upward stepwise trend of the impedance signal was observed quite often with every following pulse application. This might be assigned to the diffusion of the material from an extracellular environment into the cells.

5.4.4 Release of Intracellular Material by *In Situ* Electroporation

Besides extensive investigation of delivery of the membrane-impermeable material into the cells by *in situ* electroporation, one part of this work was dedicated to the studies which should provide an answer if application of ISE by ECIS technology can be employed for the controlled release of the intracellular material from the cells. Various assays were performed to investigate the release of either fluorescent material (calcein and FITC-dextran), or an intracellular compound (lactate dehydrogenase) from the adherently grown mammalian cells. The NRK cells were applied as a cell model for release studies, as this cell line is previously optimized for ISE and represents a well-established reference for various types of assays involving ISE by ECIS technology. All studies of the release by ISE using ECIS technology were conducted on 8W4Eμ electrode arrays.

There are quite a few examples known from the literature which reported on intracellular material release from the cells by electropermeabilization. The electroporation was applied as a tool for a single cell lysis to release calcein (600 Da) and protein kinase Syk-EGFP (72 kDa) from chicken B cells (Bao et al., 2008). A microfluidic chip was mounted on an inverted fluorescence microscope in order to detect fluorescence of the cells directly before and after the pulse application. The group varied electric field intensity in a range 0 – 1200 V/cm and field duration in a range 50 – 150 ms with an aim to study if and how change of these parameters affects calcein and Syk-EGFP release from the cells. They found out that calcein was released at lower field intensities and shorter field durations, in comparison to the Syk-EGFP. No significant decrease in the fluorescence intensity was observed when applied electric field intensity was below 400 V/cm. When the field intensity was between 600 and 1200 V/cm, calcein release was dependent on the field duration (in the range of 50 – 150 ms) and more calcein was released with longer field duration. In addition, the group was able to demonstrate the selective release of intracellular molecules (calcein and SykEGFP) at the single-cell level, by tuning the electroporation parameters.

Another microfluidic approach was developed and applied for the release of material on the single cell level. Poration of the cells based not on application of external electric field but on mechanical deformation, was applied to deliver and subsequently to release 3 kDa and 70 kDa fluorescently-labeled dextran (Sharei et al., 2013). Saulis et al., 2007 investigated cell membrane permeability for ions during and after application of electric pulses. They

measured release of intracellular potassium ions and experiments were carried out on mouse hepatoma MH-A22 cells. After generating the calibration graph by measuring known amounts of KCl (0.2–100 mM), they plotted the obtained corresponding potential readings against the concentrations. The single square-wave pulses were applied with duration of 1 or 2 ms, while the amplitude was ranging from 0.25 to1.2 kV/cm. An increase of the applied electric field strength resulted in an increase of the fraction of electroporated cells.

Since the controlled and reproducible release of intracellular material from the cells without killing them (e.g. chemical lysis) is very challenging, electroporation holds a great potential to become an alternative method of choice for release studies. It is of great importance to fine-tune the experimental parameters in order to achieve an efficient material release, while preserving the high level of cell viability after electroporation. A group of researchers (Zhan et al., 2012) investigated correlation between the cell viability and release of intracellular protein (GFP-tagged NF-κB) from the adherent CHO cells by electroporation. They applied laser-induced fluorescence (LIF) detection to evaluate efficiency of electroporation and to quantify the release of the protein. It was observed that the release of cytosolic protein NF-κB (~ 115 kDa) was more successful with single pulses of longer duration and with higher field intensity. Whereas pulse duration was varied in a range 10 – 50 ms, applied electric field intensity was in a range 400 – 1100 V/cm. During release studies with pulse duration of 10 ms, the group observed that the significant release of NF-κB took place only when the field intensity exceeded 900 V/cm (most probably due to the relatively large size of this protein), even though the electroporation threshold for CHO cells was 300−400 V/cm. With longer pulse duration (and higher strength of electric field), release of NF-κB increased. On the other hand, cell viability decreased significantly with the higher field intensity and longer pulse duration. Interestingly, the group reported there was no direct correlation between an increased protein release and the probability for cell death, when the release study was conducted on a single cell level. It was counterintuitive that the cell death probability was found to be lower when more of the protein was released, although this might suggest the activation of special recovery mechanisms within the cell when large amount of protein is released.

5.4.4.1 Release of Calcein from Adherent Cells

Whereas the release of 4 kDa FITC-dextran from NRK cells by ISE gave rather irreproducible and inconsistent results (data were not shown), calcein served as a much more appropriate probe to investigate release of fluorescent material from the cells by ISE, and to establish proof-of-principle assay. The reason why release study with 4 kDa FITC-

dextran was difficult to establish is most probably the size of the fluorescent probe. Bao et al., 2008 monitored release of calcein (600 Da) and Syk-EGFP protein (72 kDa) from cytosol on a single cell level and concluded that the release of Syk-EGFP was quite different from the calcein release. This protein could not be significantly released (with any of applied pulse durations) when electric field intensity was below 800 V/cm, whereas calcein was successfully released already at 600 V/cm, with any pulse duration. They explained such observations with much bigger molecular size of SykEGFP, compared to calcein, but did not exclude influence of some other physical properties as well, such as diffusivity and electrophoretic mobility. Having on mind theory of electroporation and the fact that pulse duration influences the size of the pores, electric pulse parameters might be re-optimized in order to increase the size of the pores formed in the cell membrane upon ISE and thus to enable release of bigger molecules.

A majority of release studies performed in this work are conducted with calcein (662 Da) as a fluorescent probe and NRK cells were loaded with 2 μM calcein-AM at the beginning of the experimental procedure. The ability of NRK cells to release calcein from the cytoplasm was firstly investigated by fixing and permeabilizing their cell membrane with PFA and different percentages of detergent Triton-X-100. It appeared that all cells exposed to fixation and permeabilization, regardless of Triton-X-100 percentage, were able to release calcein, which freely diffuse out of the cell cytosol. This experiment was very encouraging and studies of calcein release from NRK cells by application of *in situ* electroporation followed.

The calcein release was initially conducted using standard experimental setup for ISE on the ECIS device and the cells were electroporated once, twice or three times successively. Thereafter, the release efficiency was evaluated by CLSM and the pulsed cells did appear darker than the non-pulsed cells. The fluorescence intensity within the electrode area was substantially lower with an increasing number of the applied pulses, indicating that calcein can be successfully released from NRK cells by ISE. However, the appearance of darker middle area of the electrodes (indicating higher extent of release) and the bright fluorescence rings on the electrode edge can be explained by the fact that the electric field is stronger in the middle of the electrode, but also by the fact that small compound as calcein can be transferred between the neighboring cells through their gap junction channels (Bai et al., 2006, Anagnostopoulou et al., 2007, Sperber, 2016).

Quantification of fluorescence intensity on the micrographs taken after electroporation showed minor difference in fluorescence intensity between the three samples (ISE applied once, twice and three times) and the control (no ISE applied), indicating that the release of calcein was rather inefficient. However, such results should not be discouraging having on

mind that the analysis of fluorescence intensity included also the bright fluorescence rings appearing within the electrode area.

To exclude (or at least minimize) the exchange of calcein through the gap junction channels during the release study, compound 2-aminoethoxydiphenyl borate (2-APB) was applied, as it reversibly blocks and inhibits the communication between the gap junction channels in normal rat kidney cells (Bai et al., 2006; Harks et al., 2003). As previously mentioned, the release of calcein by ISE and its transfer between the neighboring cells most probably overlap and it was essential to distinguish between these two events. In the following experiment, ISE of NRK cells was conducted once, two or three times in presence of 50 µM 2-APB (Goto et al., 2010; Sperber, 2016). Subsequently taken microscopic images revealed the presence of fluorescence signal on the edge of the electrode area, but the fluorescence intensity was much weaker compared to the bright fluorescence rings observed when cells were pulsed in absence of 2-APB. The cells residing on the electrodes appeared overall darker than the cells of the background. Such observations suggested that the calcein exchange between the neighboring cells (through the gap junction channels) was inhibited. The effect of calcein release from NRK cells induced by *in situ* electroporation was evaluated by the quantification of fluorescence intensity in the micrographs taken after experimental procedure. A clear difference in fluorescent signal was observed between the pulsed and non-pulsed cells. The NRK cells electroporated twice showed higher fluorescence signal than the cells electroporated once, and this can be assigned to variation, concluding that there is no significant difference in calcein release between the cells pulsed once or twice. However, cells pulsed three times obviously released significant amount of calcein compared to the control, indicating that multiple pulse application is a good strategy to enhance release of the material from the cells.

Similarly to some previously reported release studies from the literature (Bao et al., 2008; Zhan et al., 2012), further investigation of the calcein release by ISE was conducted directly on the microscopic stage. The time-resolved imaging of NRK cells upon consecutively applied electric pulses showed no significant release of calcein after the application of one electric pulse. However, after every following pulse application, fraction of the cells on the electrodes, which appeared darker than before the pulse, was increasing. Thus, by observing the appearance of the cells on the electrodes after the third pulse application (**Figure 5.31 F**) and by comparing it with the appearance of the same cells before the first electric pulse was applied (**Figure 5.31 A**), it is obvious that release of intracellular calcein took place, due to the application of ISE. The fourth elecroporation (**Figure 5.31 G** and **H**) was applied to investigate how the cells respond to another pulse application, to check whether they would

collapse and how this can influence the fluorescence signal coming from the affected cells on the electrodes. Nevertheless, the fourth pulse application did not cause visible cell death, but only further reduced the fluorescence signal due to the additional release of calcein. The viability of the cells on the electrodes was confirmed by the phase-contrast micrographs taken after experiment was finished (Appendix, **Figure 11.2**). Quantification of these micrographs indicated that with every pulse application, there was a reproducible gradual decrease of the fluorescence signal due to the release of calcein from NRK cells (**Figure 5.32**). In contrast to that, the cells in control, which were not exposed to any electric pulses, exhibited the same fluorescence intensity over time (**Figure 5.34**). The reduction of fluorescence signal due to the calcein release by ISE can be clearly distinguished from the reduction of fluorescence signal due to the cell death, which was observed during the time-resolved imaging of electric wounding of the cells (Appendix; **Figure 11.4**). The wounded cells exhibited clear loss of the fluorescence signal already after first pulse application and this trend was continued with every following electric wounding applied. When the applied electric pulses are too invasive, cells were damaged, killed and they detached from the electrode surface, which was confirmed by the subsequently taken phase-contrast image (data not shown).

Above discussed observations made during calcein release studies are in agreement with the previously reported release studies. Similarly to the report of Bao et al., 2008, calcein could be successfully released from the cells using electric pulse parameters which do not affect the cell viability. The group suggested that the release of a certain bigger molecule by electroporation requires a set of threshold conditions, however in this work, pulse duration and voltage were not increased beyond the optimal values, but the strategy of multiple pulse application was applied to enhance release efficiency. The release studies presented in this work suggested that multiple pulse application is necessary to achieve successful release of the material from adherent cells and this is agreement with the study conducted by Saulis et al., 2007, which showed that the successful release of material from the cells (in suspension) was achieved by treating the cells with three consecutive electric pulses (using an amplitude of 1.2 kV/cm and the pulse duration of 2 ms).

In the release study performed by Zhan et al., 2012 optimized electroporation parameters were applied as well, with an aim to preserve the cell viability and potentially carry out the pulsation multiple times to enhance the release efficiency. Both previously mentioned release studies employed the experimental setup which allowed for direct evaluation of release efficiency shortly after the pulse application. Similarly as the calcein release study conducted in this work, where NRK cells were exposed to the electric pulses directly on the microscope

stage, the experimental setup of Bao et al., 2008 also included a direct evaluation of the fluorescence intensity of the pulsed cells (within the microfluidic chip) on the microscope stage. The release of the material from the cells is obviously more demanding to measure than the material loading into the cell cytosol. Whereas within dye loading studies fluorescence signal needs to be detected when the entire or most of the cell population appears dark, within dye release studies, reduction of an overall bright signal needs to be detected and evaluation of such signal changes in many cases is very difficult or not very precise. Therefore, direct evaluation of the fluorescent material release immediately after pulse application appears to be the best and most accurate option for the evaluation of release efficiency, which is obviously recognized and extensively applied by different research groups for release studies. Another electroporation study which confirmed that the real-time monitoring of the material release is worthy, in terms of assessing efficiency of the method, and which correlates very well with the release study presented in this work was performed by Park et al., 2014. This group monitored the release of RFP molecules from the RFP-expressing HUVEC cells exposed to electroporation. They used an inverted epi-fluorescent microscope with a 10-fold magnification objective to achieve a time-lapse image capturing (with an interval of 2 sec) for 40 min. The transparent indium tin oxide (ITO) electrodes were enabling visualization of the cell transfection (in real time). In their studies, the release of RFP molecules from the cells was an indicator for the cell membrane disruption by irreversible electroporation and the electroporation parameters applied for release were compared to the electrporation parameters used for delivery of propidium iodide into the cells. The results suggested that electroporation induces the release of the RFP molecules across the membrane and with the 10 V pulse amplitude and pulse durations of either 0.5 ms, or 1 ms, which are considered to be in the range of reversible electroporation, the fluorescent intensity decreased slightly compared to the lower pulse amplitude or to the control cells (0 V). Thereby, the cells viability was preserved within the following 24 h. Even though this study was conducted with the cells in suspension, the approach to the release investigation and the evaluation of the release efficiency was quite comparable to the time-resolved imaging of calcein release conducted in this work.

An important aspect which needs to be mentioned here is that the difficulty and complexity of a release study depends on the number of the cells under study. Namely, the fact that the most release studies found in the literature are conducted on the suspended cells or on a single cell level should not be underestimated. In contrary, it must be taken into account that the release of the material from the cell monolayer, or the release from large population of cells exhibiting bright fluorescence does influence the sensitivity of the release method.

Measuring decrease of fluorescence intensity for only one or several cells is in principle more straightforward than measuring of the fluorescence intensity decrease for entire cell population. Besides difficulty to extract the release-correlated signal decrease from the high background, one of the experimental obstacles (which was observed during release studies in this work as well) is that the living cells are able to communicate and exchange the material between the neighboring cells, which makes the evaluation of release studies more complicated. In addition, expectations for release studies need to be set properly. Whereas loading studies by electroporation often demonstrate high increase of the signal upon pulse application, none of the above discussed release studies (including study conducted and presented within this work) showed complete signal reduction, as the result of material release. In fact, the complete signal reduction can be mostly linked with the loss of cell viability and the cell death.

The proof-of-principle experiments which were established within this work should pave the way for further investigation of controlled, efficient and reproducible material release by *in situ* electroporation, while maintaining the high level of cell viability.

5.4.4.2 Release of Lactate Dehydrogenase from Adherent Cells

Besides calcein, lactate dehydrogenase (LDH) was released from NRK cells after their exposure to electric pulses and amount of released material was evaluated using standard and commercially available LDH assay. The aim was to establish another assay for cytosolic material release using ECIS technology. It was assumed that *in situ* electroporation applied once, twice and three times will cause different levels of LDH release from the cells, which would proportionally increase with an increasing number of electric pulses applied to the cells. Before such hypothesis was verified, the amount of LDH released from the cells was firstly evaluated after application of electric wounding, as it should serve as a positive control for proposed release assay including *in situ* electroporation.

The commercially available LDH assays are developed and adjusted for the use in 96-well plate format, with an entire area of the flat bottomed wells taken into account. The question arose if such assay would be sensitive enough to detect LDH released from very small cell population residing on the gold film electrodes of the ECIS array, which is affected by electroporation or electric wounding. Even with four electrodes in each well of the 8W4Eμ electrode arrays, active surface area is significantly smaller (4 x 0.049 mm^2 ~ 0.196 mm^2) than the area of the 96-well plate well (~ 32 mm^2). This is summarized in **Table 5.2**. Obviously, in case when ECIS electrode arrays are applied, the rest of a cell population (background cells), surrounding the affected cells on the electrodes, play a significant role in

the release evaluation. This undesired side-effect comes from a high dilution of the released LDH from the cells, since relatively high working volume needs to be applied for every well. Therefore, the assays on ECIS electrode arrays were performed using 8W4Eμ-Ø3 and 8W4Eμ-Ø5 chamber setups, where working volumes per well were kept 40 and 50 μL, respectively. The working volume per well for LDH assay performed in the 96-well plate was 100 μL. The NRK cells were electrically wounded on either 8W4Eμ-Ø3, or 8W4Eμ-Ø5 electrode arrays and the samples with pulsed cells were compared to the controls where cells were not exposed to any electric pulses. In addition, the entire cell populations in the wells of 8W4Eμ-Ø5 were lysed in order to compare the values for complete ("maximal") LDH release with the values obtained when the cells on the electrodes were wounded. The results are summarized in **Table 5.2** and indicate that there was an obvious difference in the LDH release between the wounded and non-wounded cells. The wounded NRK cells released less than twice the amount of LDH, compared to the untreated cells, and results indicated high values of a standard deviation. In addition, the lysis of entire cell population present in Ø5 wells resulted in almost ten times higher values for LDH release, compared to the values obtained after LDH release from the cells by electric wounding.

The lack of sensitivity observed in this assay comes from the high background and under such circumstances it is difficult to measure precisely the release of LDH from the treated cells. This is in agreement with the release study performed by Saulis et al., 2007, where the authors also had difficulties to get a noticeable increase of the concentration of potassium ions after electroporation, which would be above the high background level (3–5 mM).

Table 5.2 The comparison of the well surface area for the electrode arrays 8W4Eμ-Ø3 and 8W4Eμ-Ø5 with the wells of 96-well plate. In addition, a surface area of four electrodes per well is given for an overview. The area of one well of the flat bottomed 96-well plate is app. 163 bigger than the total area of the four gold film electrodes in one well of the 8W4Eμ electrode array.

	8W4Eμ-Ø3	**8W4E-Ø5**	**96-Well Plate**
Area of the Well [mm^2]	7 – 9.6	~ 19.6	32
Area of the Electrodes [mm^2]	~ 0.196 (4 x 0.049)	~ 0.196 (4 x 0.049)	/

Since these results demonstrated that standard LDH assay cannot be applied for the evaluation of LDH release from NRK cells by electric wounding, due to the lack of

reproducibility and sensitivity, further experiments involving release of LDH from the electroporated cells were not performed.

5.5 References

Albermann, S. (2004) In situ Elektroporation adhärenter Säugerzellen. PhD Thesis, Westfälische Wilhelms-Universität Münster.

Anagnostopoulou, A., Cao, J., Vultur, A., Firth, K., and Raptis, L. (2007) Examination of gap junctional, intercellular communication by in situ electroporation on two co-planar indium-tin oxide electrodes. *Molecular Oncology* 1, 226 – 231.

Bai, D., del Corsso, C., Srinivas, M., and Spray, D.C. (2006) Block of Specific Gap Junction Channel Subtypes by 2-Aminoethoxydiphenyl Borate (2-APB). *Journal of Pharmacology and Experimental Therapeutics* 319, 1452-1458.

Bao, N., Wang, J., and Lu, C. (2008) Microfluidic electroporation for selective release of intracellular molecules at the single-cell level. *Electrophoresis* 29, 2939-2944.

Benz, R., and Zimmermann, U. (1981) The resealing process of lipid bilayers after reversible electrical breakdown. *Biochimica et Biophysica Acta* 640, 169-178.

Bier, M., Hammer, S.M., Canaday, D.J., and Lee, R.C. (1999) Kinetics of sealing for transient electropores in isolated mammalian skeletal muscle cells. *Bioelectromagnetics* 20, 194-201.

Brown, R.E., Bartoletti, D.C., Harrison, G.I., Gamble, T.R., Bliss, J.G., Powell, K.T., and Weaver, J.C. (1992) Multiple-pulse electroporation: Uptake of a macromolecule by individual cells of Saccharomyces cerevisiae. *Bioelectrochemistry and Bioenergetics* 28, 235-245.

Canatella, P.J., Karr, J.F., Petros, J.A., and Prausnitz, M.R. (2001) Quantitative study of electroporation-mediated molecular uptake and cell viability. *Biophysical Journal* 80, 755-764.

Chang, D.C., and Reese, T.S. (1990) Changes in membrane structure induced by electroporation as revealed by rapid-freezing electron microscopy. *Biophysical Journal* 58, 1-12.

Chernomordik, L.V., and Chizmadzhev, Y.A. (1989) Electrical breakdown of lipid bilayer membranes: Phenomenology and mechanism. In Electroporation and Electrofusion in Cell Biology, E. Neumann, A. E. Sowers, and C.A. Jordan, eds., pp. 83-95.

Escande-Geraud, M.L., Rols, M.P., Dupont, M.A., Gas, N., and Teissie, J. (1988) Reversible plasma membrane ultrastructural changes correlated with electropermeabilization in Chinese hamster ovary cells. *Biochimica et Biophysica Acta* 939, 247-259.

Fried, H., and Kutay, U. (2003) Nucleocytoplasmic transport: taking an inventory. *Cellular and Molecular Life Sciences* 60, 1659-1688.

Gabriel, B., and Teissie, J. (1995) Control by electrical parameters of short- and long-term cell death resulting from electropermeabilization of Chinese hamster ovary cells. *Biochimica et Biophysica Acta* 28, 171-178.

Gehl, J., Skovsgaard, T., and Mir, L.M. (2002) Vascular reactions to in vivo electroporation: characterization and consequences for drug and gene delivery. *Biochimica et Biophysica Acta* 15, 1-3.

Ghartey-Tagoe, E.B., Morgan, J.S., Ahmed, K., Neish, A.S., and Prausnitz, M.R. (2004) Electroporation-mediated delivery of molecules to model intestinal epithelia. *International Journal of Pharmaceutics* 270, 127-138.

Ghosh, P.M., Keese, C.R., and Giaever, I. (1993) Monitoring electropermeabilization in the plasma membrane of adherent mammalian cells. *Biophysical Journal* 64, 1602-1609.

Ghosh, P.M., Keese, C.R., and Giaever, I. (1994) Morphological response of mammalian cells to pulsed ac fields. *Bioelectrochemistry and Bioenergetics* 33, 121-133.

Giaever, I., and Keese, C.R. (1984) Monitoring fibroblast behavior in tissue culture with an applied electric field. *Proceedings of the National Academy of Sciences of the United States of America* 81, 3761-3764.

Giaever, I., and Keese, C.R. (1986) Use of electric fields to monitor the dynamical aspect of cell behavior in tissue culture. *IEEE Transactions on Biomedical Engineering* 33, 242-247.

Giaever, I., and Keese, C.R. (1991) Micromotion of mammalian cells measured electrically. *Proceedings of the National Academy of Sciences of the United States of America* 88, 7896-7900.

Giaever, I., and Keese, C.R. (1993) A morphological biosensor for mammalian cells. *Nature* 366, 591-592.

Goto, J., Suzuki, A.Z., Ozaki, S., Matsumoto, N., Nakamura, T., Ebisui, E., Fleig, A., Penner, R., and Mikoshiba, K. (2010) Two novel 2-aminoethyl diphenylborinate (2-APB) analogues differentially activate and inhibit store-operated Ca(2+) entry via STIM proteins. *Cell Calcium* 47, 1-10.

Harks, E.G., Camina, J.P., Peters, P.H., Ypey, D.L., Scheenen, W.J., van Zoelen, E.J., and Theuvenet, A.P. (2003) Besides affecting intracellular calcium signaling, 2-APB reversibly blocks gap junctional coupling in confluent monolayers, thereby allowing measurement of single-cell membrane currents in undissociated cells. *The FASEB Journal* 17, 941-943.

Hibino, M., Shigemori, M., Itoh, H., Nagayama, K., and Kinosita, K. (1991) Membrane conductance of an electroporated cell analyzed by submicrosecond imaging of transmembrane potential. *Biophysical Journal* 59, 209-220.

Kim, J.A., Cho, K., Shin, Y.S., Jung, N., Chung, C., and Chang, J.K. (2007) A multi-channel electroporation microchip for gene transfection in mammalian cells. *Biosensors and Bioelectronics* 22, 3273-3277.

Kinosita, K., and Tsong, T.Y. (1979) Voltage-induced conductance in human erythrocyte membranes. *Biochimica et Biophysica Acta (BBA) - Biomembranes* 554, 479-497.

Kotnik, T., Bobanovic, F., and Miklavcic, D. (1997) Sensitivity of transmembrane voltage induced by applied electric fields-a theoretical analysis. *Bioelectrochemistry and Bioenergetics* 43, 285-291.

Lukic, S., and Wegener, J. (2015) Impedimetric monitoring of cell-based assays. In Encyclopedia of Life Sciences (John Wiley & Sons, Ltd.), pp. 1–8.

Neumann, E., Kakorin, S., and Toensing, K. (1999) Fundamentals of electroporative delivery of drugs and genes. *Bioelectrochemistry and Bioenergetics* 48, 3-16.

Neumann, E., Toensing, K., Kakorin, S., Budde, P., and Frey, J. (1998) Mechanism of electroporative dye uptake by mouse B cells. *Biophysical Journal* 74, 98-108.

Pakhomov, A.G., Gianulis, E., Vernier, P.T., Semenov, I., Xiao, S., and Pakhomova, O.N. (2015) Multiple nanosecond electric pulses increase the number but not the size of long-lived nanopores in the cell membrane. *Biochimica et Biophysica Acta* 4, 958-966.

Park, S., Bassat, D.B., and Yossifon, G. (2014) Individually addressable multi-chamber electroporation platform with dielectrophoresis and alternating-current-electro-osmosis assisted cell positioning. *Biomicrofluidics* 8, 024117.

Prausnitz, M.R., Lau, B.S., Milano, C.D., Conner, S., Langer, R., and Weaver, J.C. (1993) A quantitative study of electroporation showing a plateau in net molecular transport. *Biophysical Journal* 65, 414-422.

Pucihar, G., Kotnik, T., Miklavcic, D., and Teissie, J. (2008) Kinetics of transmembrane transport of small molecules into electropermeabilized cells. *Biophysical Journal* 95, 2837–2848.

Raptis, L.H., Liu, S.K., Firth, K.L., Stiles, C.D., and Alberta, J.A. (1995) Electroporation of peptides into adherent cells in situ. *Biotechniques* 18, 104-114.

Rols, M.-P., and Teissié, J. (1998a) Electropermeabilization of Mammalian Cells to Macromolecules: Control by Pulse Duration. *Biophysical Journal* 75, 1415–1423.

Rols, M.P., and Teissié, J. (1990) Modulation of electrically induced permeabilization and fusion of Chinese hamster ovary cells by osmotic pressure. *Biochemistry* 29, 4561-4567.

Rols, M.P., and Teissié, J. (1998b) Electropermeabilization of mammalian cells to macromolecules: control by pulse duration. *Biophysical Journal* 75, 1415-1423.

Ryttsén, F., Farre, C., Brennan, C., Weber, S.G., Nolkrantz, K., Jardemark, K., Chiu, D.T., and Orwar, O. (2000) Characterization of single-cell electroporation by using patch-clamp and fluorescence microscopy. *Biophysical Journal* 79, 1993-2001.

Saulis, G., Satkauskas, S., and Praneviciute, R. (2007) Determination of cell electroporation from the release of intracellular potassium ions. *Analytical Biochemistry* 360, 273–281.

Saulis, G., Venslauskas, M.S., and Naktinis, J. (1991) Kinetics of pore resealing in cell membranes after electroporation. *Journal of Electroanalytical Chemistry and Interfacial Electrochemistry* 321, 1-13.

Sharei, A., Zoldan, J., Adamo, A., Sim, W.Y., Cho, N., Jackson, E., Mao, S., Schneider, S., Han, M.J., Lytton-Jean, A., et al. (2013) A vector-free microfluidic platform for intracellular delivery. *Proceedings of the National Academy of Sciences of the United States of America* 110, 2082-2087.

Son, R., Gowrishankar, T., Smith, K., and Weaver, J. (2015) Modeling a conventional electroporation pulse train:Decreased pore number, cumulative calcium transportand an example of electrosensitization. *IEEE Transactions on Biomedical Engineering* 20, 20.

Sperber, M. (2016) Impedance-based analysis of the cellular response to microparticles: Theory, assay development and model study. PhD Thesis, Universität Regensburg

Stolwijk, J.A. (2012) Electric manipulation and impedance analysis of adherent cells on gold-film electrodes. PhD thesis, Universität Regensburg

Stolwijk, J.A., Hartmann, C., Balani, P., Albermann, S., Keese, C.R., Giaever, I., and Wegener, J. (2011) Impedance analysis of adherent cells after in situ electroporation: Non-invasive monitoring during intracellular manipulations. *Biosensors and Bioelectronics* 26, 4720–4727.

Teissié, J., Golzio, M., and Rols, M.P. (2005) Mechanisms of cell membrane electropermeabilization: A minireview of our present (lack of ?) knowledge. *Biochimica et Biophysica Acta* 1724, 270–280.

Teissié, J., and Rols, M.P. (1994) Manipulation of cell cytoskeleton affects the lifetime of cell membrane electropermeabilization. *Annals of the New York Academy of Sciences* 720, 98-110.

Tekle, E., Astumian, R.D., and Chock, P.B. (1994) Selective and asymmetric molecular transport across electroporated cell membranes. *Proceedings of the National Academy of Sciences of the United States of America* 91, 11512-11516.

Tsong, T.Y. (1991) Electroporation of cell membranes. *Biophysical Journal* 60, 297-306.

Weaver, J.C., and Chizmadzhev, Y.A. (1996) Theory of electroporation: A review. *Bioelectrochemistry and Bioenergetics* 41, 135-160.

Weaver, J.C., and Powell, K.T. (1989) Theory of electroporation. In Electroporation and Electrofusion in Cell Biology, E. Neumann, A.E. Sowers, and C.A. Jordan, eds. (Plenum Press), pp. 111-126.

Wegener, J., Keese, C.R., and Giaever, I. (2002) Recovery of adherent cells after in situ electroporation monitored electrically. *Biotechniques* 33, 348 - 352.

Zhan, Y., Sun, C., Cao, Z., Bao, N., Xing, J., and Lu, C. (2012) Release of intracellular proteins by electroporation with preserved cell viability. *Analytical Chemistry* 84, 8102−8105.

Zimmermann, U., Vienken, J., and Pilwat, G. (1980) Development of drug carrier systems: Electrical field induced effects in cell membranes. *Bioelectrochemistry and Bioenergetics* 7, 553-574.

6 Delivery of Second Messengers into Cells

6.1 Introduction

The cells receive various signals from their environment and very often have to respond to the different chemical stimulators, such as hormones, growth factors, neurotransmitters, or components of an extracellular matrix. When the ligands bind to a receptor protein on the cell surface, cell receives a signal and series of biochemical reactions within the cytosol are initiated. A stimulation of the cell receptors by the extracellular molecules (chemical compounds), conventionally called “first messengers” is followed by the synthesis of “second messengers” inside the cell and these small molecules act to transmit received signals to the target molecules in the cytosol or nucleus. Such signal pathway is usually referred to as a signal transduction cascade. The second messengers relay the signal and even amplify it. Moreover, the second messengers are able to coordinate the signal pathways for several targets and thus a signal transmission can be expanded (Serezani et al., 2008; Hofer and Lefkimmiatis, 2007).

The most common second messengers can be classified into the three major groups:

(i) Cyclic nucleotides (e.g. cyclic adenosine monophosphate and cyclic guanosine monophosphate);

(ii) Chemical derivatives of phospholipid (produced by the enzyme phospholipase): Inositol 1,4,5-triphosphate (IP3) and diacylglycerol (DAG) and

(iii) Calcium ions (Ca^{2+}).

Cyclic adenosine monophosphate (cAMP)

Adenosine monophosphate (cAMP) is not only the most common, but also the first discovered second messenger. Dr. Earl Wilbur Sutherland discovered cAMP during his studies of hormone action (in 1957) and was awarded with the Nobel Prize in 1971 for his second messenger concept. The work of Dr. Sutherland on cAMP was recognized since he discovered that the hormones (first messengers) do not enter the cell, but bind to its surface and induce production of small cAMP molecules (second messenger), which regulate various metabolic processes in the cell (Sutherland, 1972). Thus, the cAMP is involved in various biological processes, among others: gene regulation, metabolism, immune function, memory, etc. (Montminy, 1997; Beavo and Brunton, 2002).

When hormones, like for example adrenaline, bind to a corresponding adrenergic receptor on the cell surface, G-protein coupled to the receptor undergoes a conformational change. As a result of its activation, the enzyme adenylyl cyclase (attached to the plasma membrane)

synthesizes cyclic AMP from ATP (adenosine triphosphate). The small cAMP molecules further activate the enzyme cAMP-dependent protein kinase A (PKA) and phosphorylation of the protein substrates follows (signal transduction cascade is shown in **Figure 6.1**). The signal is thus transmitted in the cell nucleus or cytosol. Eventually, cAMP is degraded to the AMP by the enzyme phosphodiesterase and stops signaling (Alberts et al., 2014; Kilpatrick and Major, 1970).

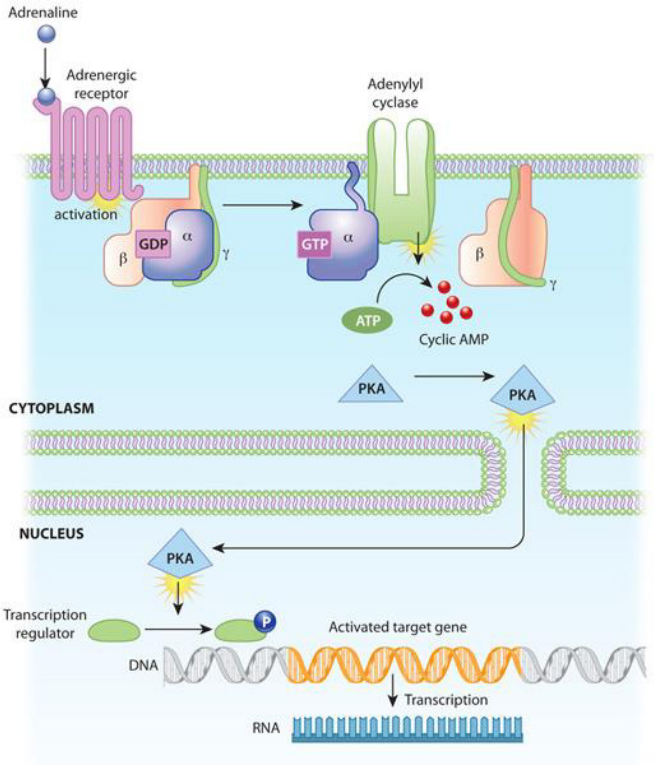

Figure 6.1 An example of a signal transduction cascade involving cyclic AMP. The binding of adrenaline to an adrenergic receptor initiates a cascade of reactions inside the cell. The signal transduction cascade begins when adenylyl cyclase, a membrane-bound enzyme, is activated by the G-protein molecules associated with the adrenergic receptor. The adenylyl cyclase creates multiple cyclic AMP molecules, which fan out and activate protein kinases (here PKA). Protein kinases can enter the nucleus and affect transcription. Adapted from Essentials of Cell Biology, © 2010 *Nature Education* (http://www.nature.com/scitable/ebooks/essentials-of-cell-biology-14749010/118241092).

Cyclic guanosine monophosphate (cGMP)

Similarly to the cAMP, cyclic guanosine monophosphate (cGMP) is produced from GTP (guanosine triphosphate) by removing two phosphate groups from its molecule and forming a cyclic phosphodiester bond. This is done by the enzyme guanylyl cyclase attached to the plasma membrane. Same as for cAMP, the synthesized cGMP molecules activate cGMP-

dependent protein kinase G (PKG) and the signal can be further amplified and transmitted to the targets within the cell cytoplasm or nucleus (Alberts et al., 2014; Murad et al., 1979).

Calcium ions (Ca^{2+})

The intracellular concentration of calcium ions is an important parameter for numerous cellular functions (Tran et al., 2000). On a regular basis, the level of calcium in the cell cytosol is rather low and main storage of the calcium ions is in the cell organelles: endoplasmic reticulum and mitochondria. Therefore, when a significant increase of the calcium concentration is elevated within the cell, it may trigger different types of effects (e.g. exocytosis, apoptosis, excitability, biochemical changes mediated by protein kinase C, etc.). An acceptance of the calcium ion as a second messenger was proposed by Lewis Victor Heilbrunn in the 1940s (Carafoli, 2002) and it increased over years, as the signaling role of calcium was becoming more clear. Inside the cell interior calcium ions can bind to the various types of proteins and thus induce changes in their localization, association, and function. In addition, the gap junction channels can be closed by Ca^{2+}, while the calcium ions can be exchanged between the adjacent cells by transmitter-gated Ca^{2+}-permeant ion channels (Clapham, 2007). Various signaling molecules can induce the activation of the cell surface receptors and thus trigger the signal transduction cascades within the cells, or even send the signals to the other neighboring cells. Signaling pathways may differ from very short to very long distance.

Over years, it became clear how important it is to monitor signaling pathways, from receptor stimulation by the chemical activator (first messenger), over activation of second messengers and further signaling routes and effects triggered within the cells. Accordingly, the knowledge on stimulation and signaling pathways increased, along with the number of proposed bioanalytical methods which should reveal the mechanisms and scenarios behind the cell action. As a logical consequence, the Nobel Prize in Physiology and Medicine was awarded to Alfred G. Gilman and Martin Rodbell in 1994 "for their discovery of G-proteins and the role of these proteins in signal transduction in the cells" and in 2012, Robert Lefkowitz and Brian Kobilka received the Nobel Prize in Chemistry for their groundbreaking discoveries helping to understand the inner workings of the family of receptors greatly involved in the cell signaling: G-protein-coupled receptors (GPCRs). The fact which illustrates the importance of GPCRs in the best way is that, nowadays, around a half of all medications are based on the effect through G-protein-coupled receptors. Therefore, it is essential to recognize if certain compounds (molecules) elicit the response of the cells and what kind of the effect do they have on the different kinds of cells. Agonists are considered as ligands that bind to the GPCreceptor, thus stabilizing its conformation and activating the G-protein. An antagonist is,

on the other hand, a molecule that prevents the conformational change which activates the G-protein, binds to and stabilizes the inactive form of the receptor. Agonists and antagonists have to compete for the binding site. Based on this, GPCRs are very important drug targets in the pharmaceutical research.

6.1.1 Monitoring Second Messengers-Based Signaling Pathways

Different stimulators (agonists) and inhibitors (antagonists) of the receptors on the cell surface can be used for studies of diverse signaling pathways. Over the past years, radioactively-labeled agonist ligands (radioligands) have been extensively applied for various studies involving cell surface receptors. Radioligands were developed to be specific for certain type of receptors and were often applied for quantification of the dissociation constant, as well as for the studies of the effects caused/triggered by different compounds. Also, studies of the thermodynamic coupling, as well as on binding affinity of molecular interactions between ligand and receptor gave important insights into the signaling mechanisms (Zhang and Xie, 2012; Lefkowitz et al., 1970; Brooker et al., 1979).

Most of the currently present assays for cAMP determination are usually end-point assays involving cell lysis. Radioimmunoassay (RIA) can be applied as a very sensitive method for determination of cAMP concentrations in *in vitro* conditions. The radiolabeled cAMP is mixed with the cAMP-specific antibody in order to couple them in a specific manner. After cAMP from the sample is added to them, it has to compete with the radiolabeled cAMP for the binding site on the antibody. Sample-originating cAMP replaces radiolabeled cAMP and reduces an antibody-coupled radioactivity. The radioactivity of the unbound cAMP (measured using a gamma counter) is thus inversely proportional to the concentration of cAMP in the sample. Although highly sensitive and specific, this method allows only discontinuous measurement with an end-point evaluation (Brooker et al., 1979; Manolopoulos and Lelkes, 1993; Zink et al., 1993). Besides that, radio labeling is rather undesirable method of analysis, which tends to be replaced, where possible. Alternatively, bioanalytical studies dedicated to the measurements of the intracellular levels of cAMP, can be conducted using non-radioactive ELISA immunoassay (Spindler et al., 2010). To determine the spatial and temporal dynamics of action for second messengers (cAMP and Ca^{2+}) in living cells, digital fluorescence ratio imaging using a FRET-based sensor FlCRhR was developed (DeBernardi and Brooker, 1996; Adams et al., 1991; Nikolaev and Lohse, 2006). Although *in vitro* studies based on the cell culture models can give the important information on dose-dependency, kinetics and toxicology of various compounds, they cannot always precisely predict how the living organisms (with all their complexity) will respond to those compounds (Frampton et al.,

2008). Besides above mentioned methods, a special technology for a real-time monitoring of the changes in cAMP levels within the living cells was developed. This method employs a modified cyclic nucleotide-gated channel (CNG) and changes in cAMP levels are translated into changes of free calcium ions, measured by fluorimetric imaging plate reader (FLIPR) in the 96-well format (fluorometric imaging technologies) (Reinscheid et al., 2003). There are also reporter gene assays developed based on the luciferase reporter system, which employs cAMP-mediated gene transcription. These end-point assays can be also problematic as integration of cAMP concentrations are being followed over longer period of time and the results can be influenced by different compounds over that time period as, for instance, hydrolysis by phoshphodiesterase (Stratowa et al., 1995).

The real-time monitoring of signaling molecules, e.g. cAMP in living cells upon stimulation with ß-adrenergic receptor agonist was demonstrated using low-cost FRET measurements system (Sprenger et al., 2012). Since label-free technologies such as: impedance spectroscopy and optical-based techniques (e.g. surface plasmon reference - SPR) bring many advantages, their potential has been recognized and different innovative label-free technology platforms emerged over past years. Overview of these whole-cell technologies is nicely presented by Scott and Peters, 2010. The group of Ye Fang developed a method for label-free real-time detection of integrated cellular responses in living cells based on the dynamic mass redistribution (DMR; Fang et al., 2005). This optical technology relies on the detection of refractive index alterations by resonance wave-guides close to the sensor surface. It was demonstrated that the cell reaction to activation of second messengers cAMP and Ca^{2+} can be thus detected (Schroder et al., 2010; Schroder et al., 2011).

The Robitzki group developed the sensor chip for non-invasive measurements of the cell alterations to detect hNPY-receptor activation in living cells, based on the impedance spectroscopy in a time-resolved and label-free manner. The experiments were conducted to demonstrate how pre-incubation of the cells with hNPY inhibits cellular response to forskolin (Wolf et al., 2008). Wegener and collaborators reported on a label-free and time-resolved monitoring of the beta-adrenergic receptors stimulation in BAEC cells performed by ECIS technology (Wegener et al., 1999). This study showed that the ECIS technology can be successfully employed to study stimulation and inhibition of the receptors when the cells are grown to confluence on the thin gold film electrodes. At the same time, Reddy et al., 1998 reported on the assessment of rapid morphological changes associated with the elevated cAMP levels in fibroblasts using ECIS technology. Over years, numerous reports followed demonstrating the successful implementation of ECIS technology for various investigations of signal transduction and signaling pathways (Pearse et al., 2003; Kim et al., 2004, etc).

Nowadays, there are plenty of methods employed to study cell signaling and the communication of the cells with the outer environment with the help of GPCRs. Chemical compounds acting as the analogues of second messengers or stimulators of the appropriate receptors, which after binding trigger the signaling cascades in the cells, are often applied. In most cases, the membrane-permeable analogues of second messengers are applied for these studies. To investigate signaling events the cAMP is engaged in, forskolin is often applied as a stimulator of the cAMP production in the cells (Manolopoulos and Lelkes, 1993; Novara et al., 2004). Also, very often employed compound within the studies of cAMP is 8-(4-chlorophenylthio) adenosine 3',5'-cyclic monophosphate (CPT-cAMP). This analogue of cAMP acts as an activator of the cAMP signaling cascade, which can easily cross the cell membrane thanks to 8-(4-chlorophenylthio) moiety. Used as a selective activator of cAMP dependent protein kinase (PKA), it inhibits cGMP-specific phosphodiesterase and, at higher concentrations, inhibits cAMP-specific phosphodiesterase. (Miller et al., 1973; Chavis et al., 1998; Carroll et al., 1990). For the studies of cGMP as a second messenger, its membrane-permeable analogue 8-(4-chlorophenylthio) guanosine 3′,5′-cyclic monophosphate (CPT-cGMP) was applied (Butt et al., 1995; Miller et al., 1973).

To study the role of calcium as a second messenger and potential influx of calcium ions into the cells from the extracellular medium, calcimycin was applied. Calcimycin (A-23187) is the ionophore highly selective for calcium ions (Boot and Van Hilten, 1996; Pressman, 1976) and is often applied within different studies involving calcium to increase its intracellular levels.

6.1.2 Methods for Introducing Second Messengers into Cells

The second messengers (e.g. cAMP) cannot enter the cytoplasm due to their insolubility in lipids (hydrophilic nature). To be able to study mechanisms of action elicited by stimulation compounds and the subsequent signaling pathways involving second messengers, it may be very useful to allow direct entry of the second messengers into the cells. The aim of this work was to demonstrate that with the ECIS technology, it is not only possible to monitor the signaling events in the living cells (Wegener et al., 1999), but also to deliver second messengers or their membrane-impermeable analogues into confluent cells by *in situ* electroporation (ISE).

To the best of my knowledge, only several studies have combined introduction of second messengers into the cells with monitoring of the cellular response to them. The activity of beta-adrenergic receptors was investigated in glioma cells after electropermeabilization. The plated cells were assayed for their affinity to isoproterenol and the density of beta-adrenergic receptors (Volker et al., 1989). The group of Schoen et al., 1989 investigated the subcellular

localization of the nascent cAMP and its release from Dictyostelium discoideum cells after electropoermeabilization (under controlled conditions). In another study, the effects of cyclic nucleotides cAMP and cGMP on calcium-induced release of vitamin B12 binding protein and B-glucuronidase from electoporated cells were investigated. The neutrophils were electropermeabilized in a cuvette. The cell surface receptor-ligand interactions could be thus bypassed and the neutrophils were directly exposed to the μM concentrations of cAMP or cGMP to investigate their stimulation ability more closely (Smolen et al., 1991).

Some unpublished works performed by J. Wegener indicated that *in situ* electroporation can be successfully employed to deliver membrane-impermeable analogue (8-OH-cAMP) into the NRK cells, while at the same time, cellular response before and after delivery can be noninvasively monitored using ECIS technology, in a time-resolved manner. These studies served as a basis and an initial point for the studies conducted in this work, which were dedicated to the investigation of second messenger's delivery by *in situ* electroporation. The second messengers were delivered by ISE into the cells grown to confluence on ECIS electrodes. The signaling cascades regulated through the cAMP- and cGMP-dependent pathways are responsible for the wide range of different physiological, metabolic and functional processes within the cells. For this reason, these cyclic nucleotides and the enzymes related to them are very important targets and there is a great interest in clarifying their role, especially for the various diseases (e.g. cancer, diabetes).

6.2 Non-Invasive Impedance Monitoring of the Cellular Response to the Membrane-Permeable Analogues of Second Messengers

Previously reported studies (Wegener et al., 1999; Reddy et al., 1998; Pearse et al., 2003) demonstrated that the ECIS technique is a valuable tool to monitor signaling events and response of the cells to various compounds in real time and in non-invasive manner. In these reports, confluent mammalian cells grown on the gold film electrodes within ECIS arrays were exhibited to various activators and inhibitors of particular receptors, and their response to such compounds was followed. Since the ECIS technology has been successfully applied to monitor effect of membrane-permeable compounds to the cells, the question arose if *in situ* electroporation by ECIS could facilitate entry of the potent membrane-impermeable compounds into the cytoplasm. At the same time, cellular response was studied in real time. Based on previous reports, studies within this work were performed starting with membrane-permeable compounds, to establish the references and after that, a delivery of membrane-impermeable second messengers into the cells by *in situ* electroporation (ISE) was

conducted. Stimulation of the cells with second messengers (cAMP, cGMP and Ca^{2+}) was performed to investigate how signaling pathways and signaling cascades can be optimally monitored noninvasively on the ECIS platform. The stimulation of corresponding receptors on the cell surface by the "first messengers" and (further) activity of "second messengers" through the cell signaling cascades was followed impedimetrically. For most of the experimental procedures conducted during second messenger studies, NRK and BAEC cells were used as cell models. These two cell lines possess corresponding receptors, which presence is necessary in order to conduct investigation of cAMP or cGMP signaling triggered by extracellular compounds, based on the literature (Wegener et al., 1999; Rodríguez et al., 1999; Feschenko et al., 2002) and on previously conducted tests.

Table 6.1 Besides BAEC and NRK cells applied as the cell models within the second messengers studies, different cells lines were tested to investigate whether they show the response to second messengers and their corresponding activators. Cell lines, compounds and concentrations of each compound applied are listed in this table. The cells were exposed to the membrane-permeable (forskolin, CPT-cAMP, CPT-cGMP, calcimycin) and membrane-impermeable (cAMP) compounds.

Cell Line	Membrane-Permeable Compounds				Impermeable Compound
	Forskolin	**CPT-cAMP**	**CPT-cGMP**	**Calcimycin**	**cAMP**
CHO-GFP	/	100 µM	100 µM	5 µM	/
HaCaT	2.5 µM	100 µM	100 µM	/	100 µM
MCF-7	/	100 µM	100 µM	5 µM	100 µM
MDCK II	/	100 µM	100 µM	5 µM	100 µM
U373	/	100 - 200 µM	100 µM	5 – 7.5 µM	/

Interestingly, not all cells are equally capable of giving a response to the certain second messengers, or in other words, second messengers cannot conduct their function in all cell types equally. Presence of receptors and potential response to the second messengers was tested in different cell lines, other than BAEC and NRK cells. It was investigated if CHO, HaCaT, MCF-7, MDCK II and U373 cells potentially give a significant response to the different membrane-permeable analogues of second messengers, as the stimulators of the corresponding signaling pathways. The analyzed cell lines are listed in **Table 6.1**, along with

the compounds tested (membrane-permeable and impermeable analogue of second messenger), and the corresponding concentrations which were applied. All tests were performed according to the experimental protocol described in chapter 4.2.2.3.

6.2.1 Membrane-Permeable Analogues of Second Messengers and NRK Cells

The studies on cAMP signaling using ECIS technology which were performed in the past indicated that the NRK cells may be successfully applied as a cell model for further investigation of second messengers and their introduction into the cells by ISE. In addition to that, there are several more examples from the literature which demonstrated that the NRK cells are appropriate cell model for the studies of elevated cAMP within the cells and the signaling pathways associated with the PKA (Feschenko et al., 2002; Rodríguez et al., 1999). Therefore, the NRK cells were chosen as the appropriate cell model for the studies involving second messengers conducted in this work.

Before delivery of membrane-impermeable second messengers (cAMP, cGMP or Ca^{2+}) by *in situ* electroporation (ISE) was attempted, cellular behavior before and after the addition of membrane-permeable second messenger analogues was studied using non-invasive mode of the ECIS technology. The NRK cells were firstly stimulated using forskolin, cell membrane-permeable compound which increases the levels of cAMP, by directly activating the enzyme adenylyl cyclase. Once the intracellular levels of cAMP increased, one may encounter the activation of corresponding signaling pathways and the cellular response. In **Figure 6.2**, time course of the normalized impedance is presented, where behavior of confluent NRK cells was monitored before, during and after addition of 2.5 µM forskolin. Cellular monolayer was grown to the confluence according to the standard procedure and the experimental protocol was conducted as described in chapter 4.2.2.3. The monolayer of NRK cells was exposed to 2.5 µM forskolin. This concentration of forskolin was chosen based on previously published studies performed on BAEC cells (Wegener et al., 1999) and the known activity range (Kottra and Fromter, 1993; Zink et al., 1993). A highly concentrated stock solution of forskolin was prepared in DMSO. All further dilutions were prepared in the corresponding assay buffer. When 2.5 µM of forskolin was applied for the experiment, a final DMSO concentration in the assay buffer was 0.05 % (v/v). The experiment was conducted on 8W1E electrode array and as an assay buffer $EBSS^{+-}$ ($EBSS^{--}$with Mg^{2+}, without Ca^{2+}) was applied. The measurement was started with 200 µL of the buffer in each well. The cells were allowed to equilibrate and in the moment of addition (marked with an arrow in **Figure 6.2**), 200 µL of a double concentrated forskolin (5 µM) was added to the sample wells (to obtain the final

concentration of 2.5 µM in 400 µL of a total/ end volume per well). The volume of 200 µL of the assay buffer, containing the same amount of DMSO as in the forskolin sample, was added to the control wells. After the addition, cellular monolayers were monitored noninvasively for app. 4 hours, to follow their response to forskolin. Both, sample and the (buffer) control were run in triplicates and these data are presented in **Figure 6.2** (mean value ± standard deviation; n=3). Impedance measurement is presented at 4 kHz and the normalization of the data was applied to the last time point before the addition of 200 µL of 5 µM forskolin/ $EBSS^{+-}$ (or $EBSS^{+-}$only).

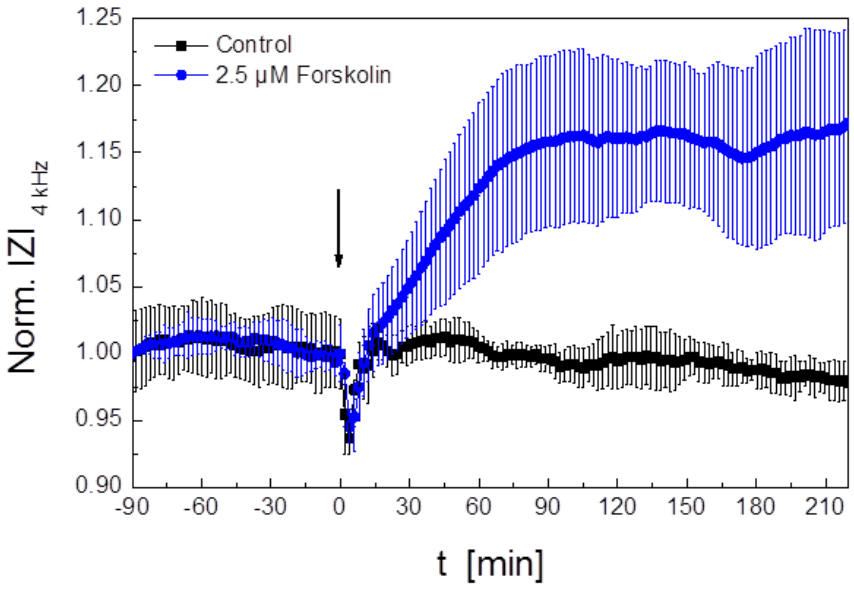

Figure 6.2 Time course of the normalized impedance magnitude at 4 kHz before, during and after stimulation of NRK cells with 2.5 µM forskolin, membrane-permeable compound which triggers the intracellular cAMP synthesis and cAMP-dependent signaling cascade within the cells. Data are normalized to the last time point before the addition of forskolin was conducted (marked with arrow). Immediately after addition of forskolin to NRK cells, impedance increased significantly, compared to the addition of buffer in the control. Error bars correspond to the values of standard deviation (mean value ± standard deviation; n=3).

A slight response of the NRK cells to addition of the fresh fluid is visible in **Figure 6.2**, as the decrease in the signal directly after the addition occured, both in sample and in the buffer control. After 10 – 15 min normalized impedance signal belonging to the control stabilized, whereas the signal belonging to the sample continued to increase for an hour after the addition, and then eventually, stabilized at the value of 1.17 ± 0.07. The raw non-normalized data indicated an increase in impedance signal after the addition forskolin from 14.5 kΩ to 17.3 kΩ at 4 kHz (data not shown). The measurement was run for additional 3 hours and the

signal remained at the higher values of normalized impedance during this time, although some small fluctuations in the signal were observed. The error bars indicate that three samples gave similar profiles of the signal, but the increase of the signal measured in three different wells varied. On the opposite, the NRK cells dissolved only in buffer (control) exhibited continuously stable signal throughout the measurement and no significant difference in impedance signals was observed between the three wells.

Furthermore, the cellular response to the membrane-permeable analogue of cyclic AMP (CPT-cAMP) was investigated. **Figure 6.3** shows time course of the normalized impedance where confluent monolayer of NRK cells was monitored noninvasively before, during and several hours after the addition of 200 µM CPT-cAMP (to obtain the final concentration of 100 µM CPT-cAMP). Prior to this experiment, series of experiments was performed (with BAEC cells) in order to find the optimal concentration of CPT-cAMP. The monolayer of NRK cells was monitored for app. 4.5 hours to follow the cellular response to CPT-cAMP.

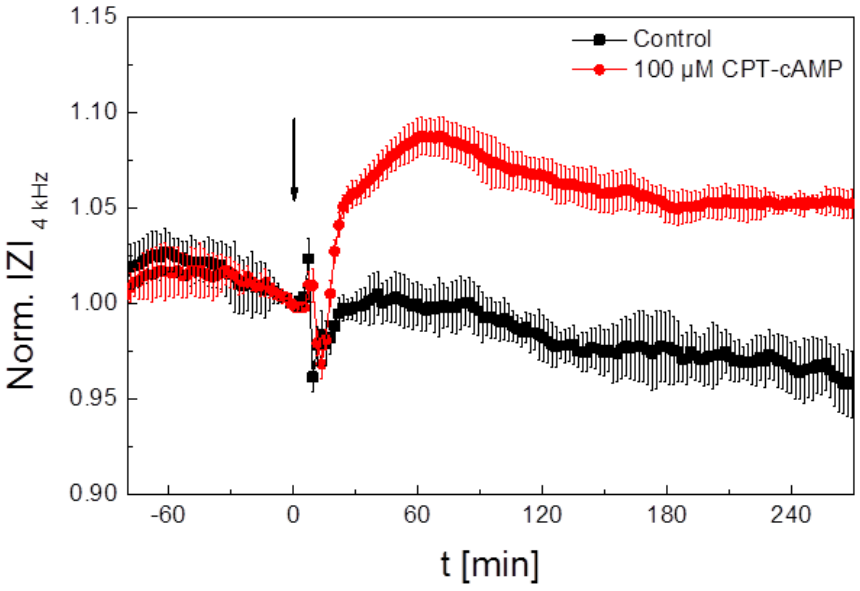

Figure 6.3 Time course of the normalized impedance magnitude at 4 kHz before, during and after stimulation of NRK cells (at passage number P10) with 100 µM CPT-cAMP. Data are normalized to the last data point before the addition of CPT-cAMP (marked with arrow). Immediately after the addition of CPT-cAMP, impedance of the NRK cells increases significantly, compared to the addition of buffer in the control. Error bars correspond to the values of standard deviation (mean value ± standard deviation; n=4).

Both sample and the (buffer) control were run in four wells in parallel to obtain four replicates for each condition. The impedance measurement is presented in **Figure 6.3** (mean value ± standard deviation; n=4). The impedance monitoring is presented at the frequency of 4 kHz

and the data were normalized to the last data point before the addition of 200 µL of 200 µM CPT-cAMP/ $EBSS^{+-}$ (or $EBSS^{+-}$ only) to the cells (marked with the arrow). **Figure 6.3** shows that the buffer control exhibited a trend of small signal decrease throughout the measurement. This can be explained by the fact that applied buffer $EBSS^{+-}$ does not contain Ca^{2+} and thus has caused interference (to some small extent) for the previously established cell-substrate contacts. The sample curves exhibited similar trend, although to much smaller extent. Nevertheless, it is obvious that directly after addition of the fresh fluid, both cells in the sample and in the control wells reacted in a same way, with the decrease in impedance signals, which returned to the pre-addition state within app. 20 min. At the same time, as soon as the addition effect passed, the cells that received CPT-cAMP exhibited significant increase in the normalized impedance signal. **Figure 6.3** shows that app. 70 min after the addition took place, normalized impedance signal reached its maximum at 1.09 ±.0.003. Looking at the raw non-normalized data (not shown here), an increase in the signal at 4 kHz was from 13.3 kΩ to 14.7 kΩ for all sample wells, whereas cells in the control wells (dissolved only in buffer) did not show any significant signal increase.

The signals belonging to the samples decreased slightly after reaching the maximal values, but still remained at the higher impedance values throughout the rest of the measurement.

The only significant difference in the cellular response to 100 µM CPT-cAMP was noticed when the NRK cells were applied for the measurements at the different age. Namely, it was noticed that the cells with lower passage number give higher and more pronounced response to the CPT-cAMP, than the cells with higher passage number. This observation can be deduced by analyzing **Figure 6.3** and **Figure 11.6** (presented in Appendix), which both show behavior of NRK cells before, during and after addition of 100 µM CPT-cAMP. However, the measurement shown in **Figure 6.3** was performed with the NRK cells with the passage number P10, whereas measurement presented in **Figure 11.6** was performed with NRK cells with the passage number P28. The cells with higher passage number showed much slower increase of impedance signal after the addition of 100 µM CPT-cAMP and the maximal values of normalized impedance reached app. 80 min after stimulation of the cells with membrane-permeable analogue of cAMP were 1.075 ± 0.035. Thereby, error bars indicate fairly high values of the standard deviation throughout the rest of the measurement, after CPT-cAMP was added to the cells. At the same time, cells dissolved only in buffer during the measurement did not exhibit high variations in the impedance signal, and thus high values of standard deviation. The raw data for the NRK cells with passage number P28 indicated an average increase in impedance signal at 4 kHz of app. 0.5 – 0.9 kΩ, app. 90 min after addition of CPT-cAMP to the cells.

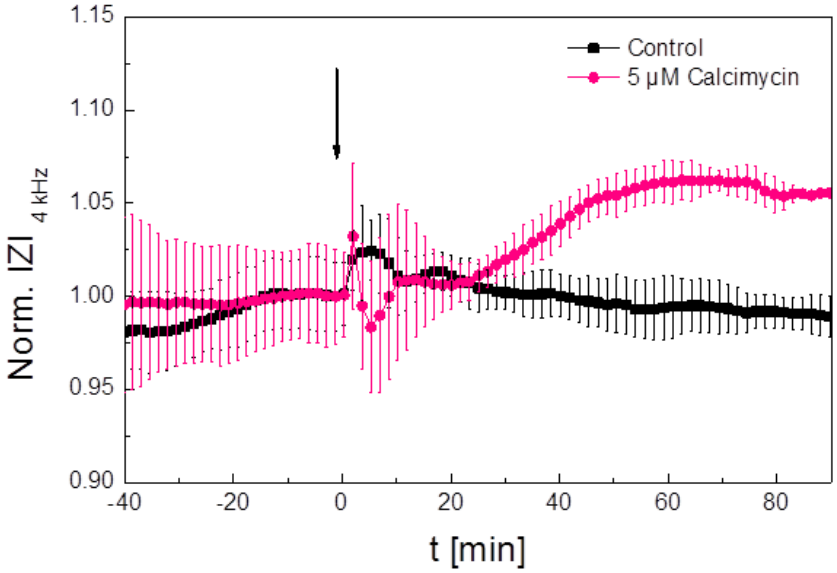

Figure 6.4 Time course of the normalized impedance magnitude at 4 kHz before, during and after addition of 5 µM calcimycin to the NRK cells. The data are normalized to the last time point before the addition of calcimycin (marked with arrow). Immediately after addition, NRK cells reacted to the fluid addition (by the signal decrease) and after app. 20 min, subsequent impedance increase indicated response of the cells to the influx of Ca^{2+} into their cytoplasm. Error bars correspond to the values of standard deviation (mean value ± standard deviation; n=2).

In **Figure 6.4**, time course of the normalized impedimetric measurement is presented, where NRK cells were exposed to the calcium-ionophore calcimycin, in order to investigate their response to influx of Ca^{2+} ions into the cytoplasm. During the experimental procedure conducted on 8W4Eµ array, NRK cells were dissolved in $EBSS^{++}$ containing Ca^{2+} ions. After 5 µM of calcimycin was added to the cells, cellular membrane became permeable for the extracellular calcium ions, which could diffuse from the buffer into the intracellular environment. Appropriate concentration of calcimycin for stimulation experiments was optimized on BAEC cell line (more details described in chapter 6.2.2). The concentration of 5 µM was chosen as the best one to apply, having on mind efficiency and a potential cytotoxic effect that calcimycin could induce. Since highly concentrated stock solution of calcimycin was prepared by dissolving it in DMSO, the addition of calcimycin was always followed by addition of the same amount of DMSO in the buffer to the cells of control.

Figure 6.4 shows that the cells initially react to the addition of fresh fluid (by a small signal decrease). Thereafter, signal returns quickly to the pre-addition values. App. 20 min after calcimycin addition, the effect of Ca^{2+} influx into the cells is observed, as the normalized impedance signal increased and such trend took place within the following 30 - 40 min until the normalized impedance signal reached its maximum value (of app. 1.06 ± 0.015 at 4 kHz).

Analysis of raw non-normalized data showed that the average impedance increase was app. 500 Ω. Such effect of calcium ions on NRK cells lasted at least 3 hours after the addition of calcimycin, as impedance signal remained constant at maximal values during that time and only some small fluctuations in the signal were observed.

The above described assays conducted on NRK cells confirmed that the response of NRK cells to membrane-permeable analogues of second messengers (forskolin, CPT-cAMP and calcimycin) are measured in a very sensitive and reproducible manner by the ECIS platform. These experiments provide solid basis for implementation of ISE for second messengers delivery into NRK cells, which is presented in one of the following chapters.

6.2.2 Membrane-Permeable Analogues of Second Messengers and BAEC Cells

Previous studies on stimulation of beta-adrenergic receptors in the living cells and their involvement in the various signaling pathways were successfully performed using ECIS technology as these reports demonstrated that the impedance measurements are an appropriate and very sensitive analytical method to monitor cell response (Wegener et al., 1999). The BAEC cells were applied as a cell model within these studies, since they possess beta-adrenergic receptors on the surface of a plasma membrane. The response of BAEC cells was successfully monitored before, during and after the addition of agonists and antagonists of beta-adrenergic receptors. In the current work, applicability of BAEC cells for electroporation studies and optimization of experimental procedure for *in situ* electroporation (ISE) of these cells was investigated and described in details in chapter 5.1.2.1. In parallel, assays involving stimulation of BAEC cells with the different membrane-permeable compounds were conducted, to initiate signaling pathways involving second messengers.

Experiments presented in this chapter were performed to confirm applicability of BAEC cells as a cell model for second messengers studies and to generate appropriate controls for the following experiments involving delivery of membrane-impermeable second messengers into BAEC cells by *in situ* electroporation.

Similarly as with NRK cells, the response of BAEC cells to forskolin was firstly investigated. Cellular behavior before, during and after the addition of 5 µM forskolin (to obtain a final concentration of 2.5 µM) to confluent layers of BAEC cells was monitored using the non-invasive mode of ECIS platform and a time course of this impedimetric measurement is presented in **Figure 6.5**. The experimental protocol was conducted as described in chapter 4.2.2.3. The concentration of 2.5 µM forskolin was applied based on the previously published studies conducted on BAEC cells (Wegener et al., 1999) and the known activity range (Kottra

and Fromter, 1993; Zink et al., 1993).

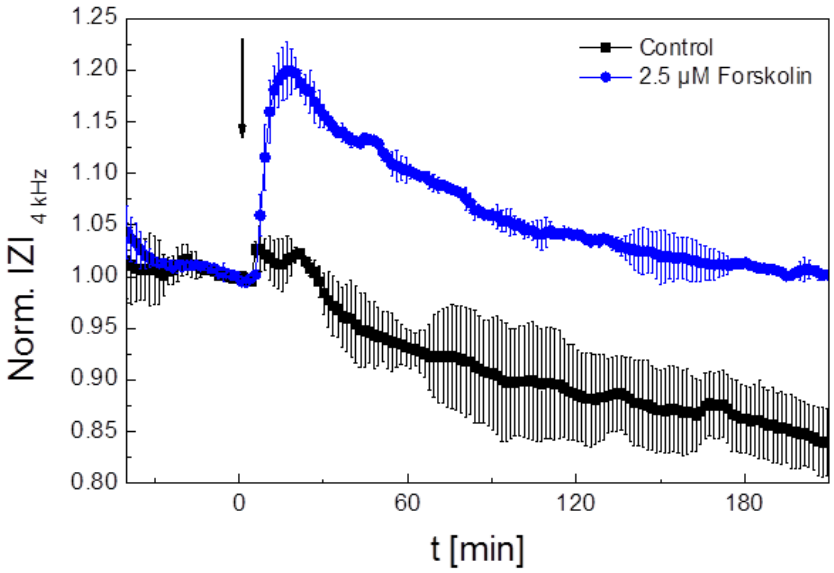

Figure 6.5 Time course of the normalized impedance magnitude at 4 kHz before, during and after stimulation of BAEC cells with 2.5 µM forskolin. Data are normalized to the last time point before the addition of forskolin (marked with arrow). Error bars correspond to the values of standard deviation (mean value ± standard deviation; n=2).

Experiment was conducted on 8W4Eµ electrode array and as an assay buffer, complete BAEC culture medium was applied. The assay was started with 200 µL of the buffer in each well, cells were allowed to equilibrate and afterwards, 200 µL of double concentrated forskolin (5 µM) was added to the sample wells (to obtain the final concentration of 2.5 µM in 400 µL of total/ end volume per well). To the control wells, 200 µL of the assay buffer containing the same amount of DMSO as in the forskolin sample was added. After the addition, cellular response was monitored noninvasively for app. 3.5 hours. Both sample and the (buffer) control were run in duplicates.

Figure 6.5 shows that the BAEC cells responded instantly to the addition of forskolin, as the normalized impedance signal jumped from 1.00 to 1.20 in only a few minutes. At the same time, cells in the controls exhibited only very small increase of the normalized impedance (due to the addition of fresh fluid). Applied forskolin obviously immediately triggered a cAMP-dependent signaling pathway within the BAEC cells and the maximal value of normalized impedance (average 1.20 ± 0.025) was reached already within 15 – 20 min. Analysis of raw (non-normalized) data indicated that the impedance value went from app. 10.25 kΩ (in the moment of addition) to 12.4 kΩ, when it reached maximum. After maximal values were reached, impedance signal started to decrease and it returned to the pre-addition values very

slowly. Throughout the whole experiment, blank controls exhibited constantly decreasing signal and relatively high error bars which appeared app. 1 hour after the addition. On the other hand, very small variations in signal were observed in traces belonging to the cells exposed to forskolin.

In **Figure 6.6**, the response of BAEC cells before, during and after their exposure to the membrane-permeable analogue of cyclic AMP (CPT-cAMP) is presented. This figure shows time course of the normalized impedance where confluent BAEC cells (grown on 8W4Eμ array) were stimulated with 100, 500 or 1000 μM of CPT-cAMP and their behavior was monitored noninvasively using ECIS. Experiment was conducted in presence of complete medium applied as the assay buffer. The compound CPT-cAMP was added to the BAEC cells at different concentrations, to investigate if concentration-dependent response of BAEC cells will be observed. An immediate cellular response was recorded after the addition of all three concentrations of CPT-cAMP. In all three cases, the impedance signals reached maximal values app. 15 – 20 min after the addition. For 100 μM CPT-cAMP, the maximum was app. 1.18, for 500 μM CPT-cAMP app. 1.22 and for 1000 μM CPT-cAMP, the maximum of normalized impedance was reached at app. 1.2. These values indicate very small differences in initial cellular response, by means of maximal normalized impedance signal, after which (in case of all 3 CPT-cAMP concentrations), signal started to decrease slowly.

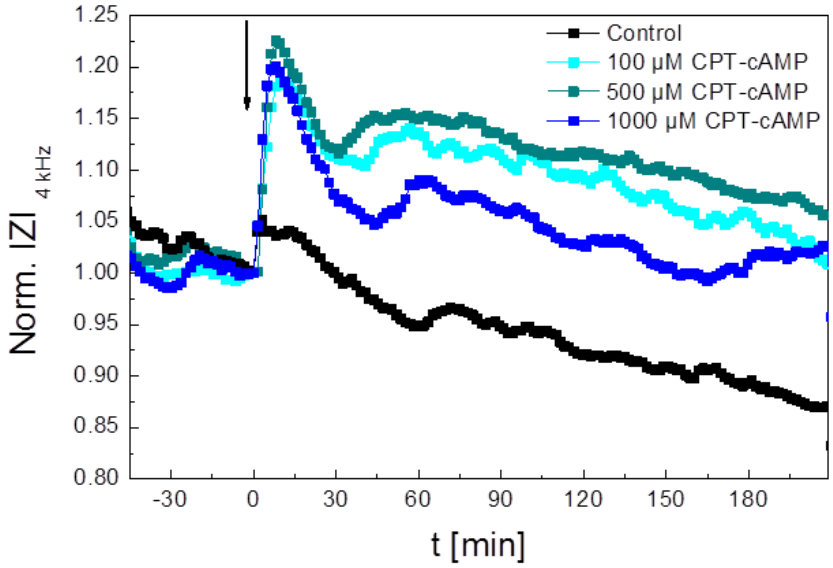

Figure 6.6 Time course of the normalized impedance magnitude at 4 kHz before, during and after stimulation of BAEC cells with 100, 500 and 1000 μM CPT-cAMP. Raw data are normalized to the last time point before the addition of CPT-cAMP (marked with arrow).

Again, the constantly decreasing signal in the trace belonging to the buffer control was

observed and such decreasing trend must be taken into account for control and sample traces. However, it is clear that the impedance signals belonging to samples did not return back to the baseline within the time frame of app. 4 hours after the addition, which was covered in this measurement. By analyzing the traces belonging to different concentrations of CPT-cAMP, no significant difference was seen in behavior of the cells stimulated with 100 and 500 µM of CPT-cAMP. The cells stimulated with the highest CPT-cAMP concentration (1000 µM) did not give the highest response, as it was expected. Such trend was observed also in some other experiments performed with BAEC, where the presence of concentration-dependent response of BAEC to CPT-cAMP was investigated (data not shown). Certain small differences between the traces of different CPT-cAMP concentrations were observed but overall reproducibility of the data was not very good. This might be explained by the fact that these CPT-cAMP concentrations are quite high and the saturation point was reached. It is recommended to apply lower concentrations of CPT-cAMP in order to follow concentration-dependent response of BAEC cells to this cAMP analogue.

In **Figure 6.7**, time course of the normalized impedance at 4 kHz before, during and after stimulation of BAEC cells with 100 µM CPT-cGMP is presented. This membrane-permeable analogue of cGMP was applied to investigate how BAEC cells respond to the stimulation of cGMP-dependent signaling pathway. For this measurement (conducted in complete medium), BAEC cells were grown on 8W4Eµ electrode array.

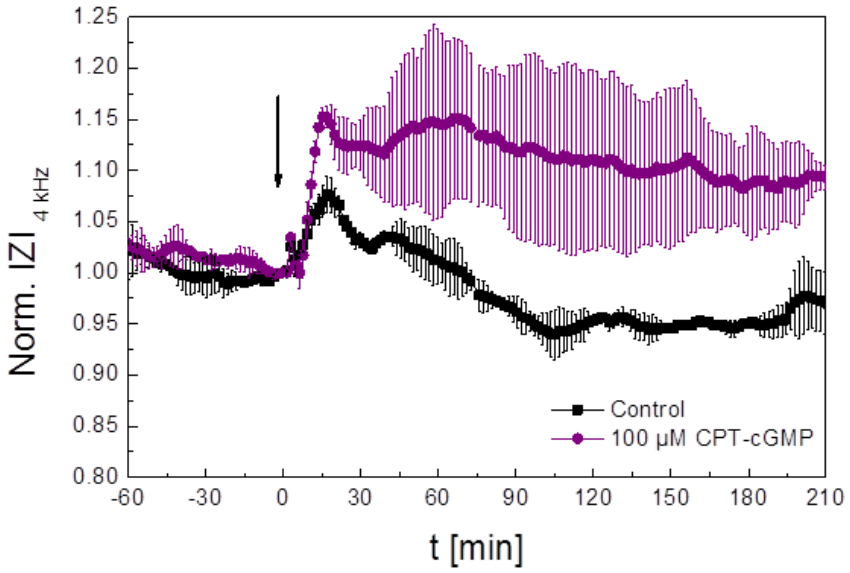

Figure 6.7 Time course of the normalized impedance magnitude at 4 kHz before, during and after stimulation of BAEC cells with 100 µM CPT-cGMP. Raw data are normalized to the last time point before the addition of CPT-cGMP (marked with arrow). The error bars correspond to the values of standard deviation (mean value ± standard deviation; n=2).

Both sample and the (buffer) control were studied in duplicates. After the addition of 100 µM CPT-cGMP to the cells, immediate increase of normalized impedance to app. 1.16 ± 0.001 was observed. This was the maximum recorded for the average normalized impedance, however, in the course of experiment, traces fluctuated quite differently and for one of them, even higher values of normalized impedance were recorded throughout the measurement. Therefore, high values of standard deviation (indicated by the error bars) are observed in traces belonging to the samples, after the addition of CPT-cGMP. The average values of normalized impedance showed many fluctuations and a trend of the slow signal decrease was observed in the traces belonging to both, sample and control.

Given the Ca^{2+} ions are known as second messengers, triggering intracellular signaling cascades, an influence of the extracellular calcium entry into the cytosol was investigated using calcium-ionophore calcimycin. This should be especially considered since the calcium ions are in most cases present in the buffer applied during *in situ* electroporation and thus can easily enter the cellular interior, along with the other membrane-impermeable compounds. In **Figure 6.7**, time course of the normalized impedance is shown at 4 kHz, where the BAEC cells were exposed to 5 µM calcimycin. For this measurement, the BAEC cells were grown on 8W4Eµ electrode array and during the experimental procedure, they were bathed in $EBSS^{++}$ (containing Ca^{2+} ions).

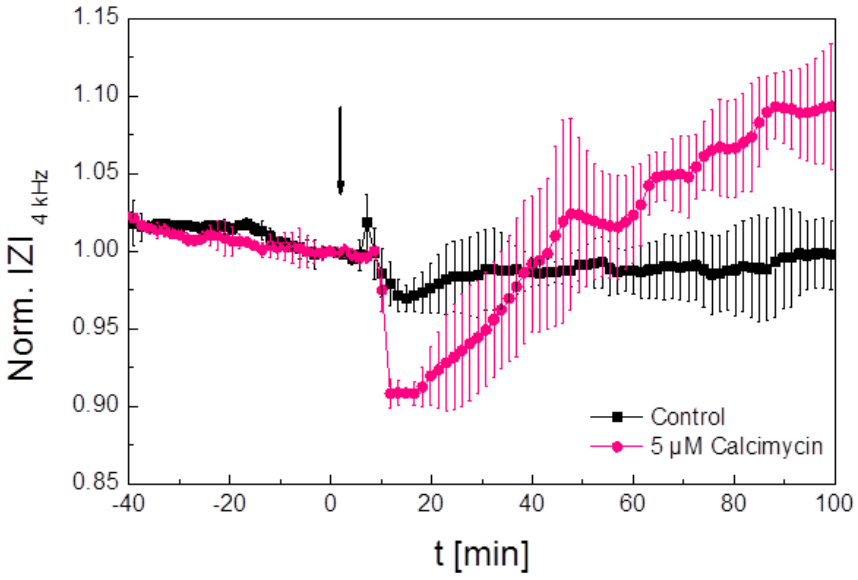

Figure 6.8 Time course of the normalized impedance magnitude at 4 kHz before, during and after the addition of 5 µM calcimycin to BAEC cells. Raw data are normalized to the last time point before the addition of calcimycin (marked with arrow). The error bars correspond to the values of standard deviation (mean value ± standard deviation; n=2).

In order to evaluate which concentration of the calcimycin would be optimal for experiments including stimulation of the cells with calcium ions same experimental procedure was conducted in presence of 5 and 7.5 µM calcimycin. Based on results obtained with BAEC cells (data not shown), it was concluded that 5 µM calcimycin is the most appropriate concentration to apply, with respect to the cellular response and to avoid a potential cytotoxic effect that calcimycin could cause. In addition, lower concentrations of calcimycin were tested (0.5, 1 and 2 µM; data not shown), however, they appeared to be too low, as no significant and reproducible response of BAEC was observed. The stock solution of calcimycin was prepared by dissolving it in DMSO, therefore, the addition of calcimycin was followed by the addition of the buffer containing the same amount of DMSO as in the sample, in order to obtain the corresponding blank controls.

After addition of calcimycin to the cells, cellular membrane became permeable for the extracellular calcium ions present in the assay buffer ($EBSS^{++}$), which could freely diffuse into the cytosol. **Figure 6.8** shows that the addition of calcimycin caused immediate decrease of the normalized impedance, which reached minimum at app. 0.91 ± 0.01 after only a few minutes. Thereafter, the signal slowly started to increase and such trend continued (with many fluctuations) until the signal eventually stabilized (app. 90 min after the addition of calcimycin). In contrast, traces belonging to the cells which were only exhibited to the assay buffer containing DMSO, remained relatively stable throughout the measurement, with some smaller fluctuations visible in the signal.

The assays described in this chapter confirmed that ECIS platform can be successfully implemented to monitor the response of BAEC cells to the membrane-permeable analogues of second messengers (forskolin, CPT-cAMP, CPT-cGMP and calcimycin), in a sensitive and reproducible manner.

6.2.3 Cell Response to Membrane-Permeable Analogues of Second Messengers: an Overview

The cell lines NRK and BAEC were exposed to different membrane-permeable analogues of second messengers and their response was successfully followed by ECIS in a time-resolved and non-invasive manner. These experiments were conducted with an aim to investigate how NRK and BAEC cells respond to second messengers, to optimize these assays and establish proof-of-principle for further studies which will include delivery of second messenger by *in situ* electroporation.

NRK cells give immediate response once they are exposed to 2.5 µM forskolin or 100 µM CPT-cAMP. The addition of these compounds causes an immediate increase in impedance

signal and the effect on the cells remains visible at least within the following 2-3 hours. During the exposure of NRK cells to 100 µM CPT-cGMP, no significant signal increase or specific cell response was observed (data not shown), suggesting that stimulation of NRK cells with cGMP does not significantly affect these cells and induces signaling cascades. Therefore, delivery of cGMP to NRK cells was not investigated in this work. The NRK cells certainly do show response to the influx of calcium ions into their cytosol (induced by 5 µM calcimycin), although signal change is rather small and, in comparison to the BAEC cells, it is slightly delayed. In **Table 6.2**, response of NRK and BAEC cells to various compounds acting as the membrane-permeable analogues of the second messenger is summarized.

Table 6.2 The response of BAEC and NRK cells to different membrane-permeable analogues of second messengers is summarized, with regards to the experiments conducted in this work. The cells were exposed to: forskolin, CPT-cAMP, CPT-cGMP and calcimycin.

	NRK		**BAEC**	
Compound	**Response**	**Comment**	**Response**	**Comment**
Forskolin	Yes	Positive control for cAMP experiments. Impedance increase significant and reproducible	Yes	Positive control for cAMP experiments. Impedance increase significant and highly reproducible
CPT-cAMP	Yes	Important control for delivery of cAMP by ISE. Impedance increase specific and reproducible	Yes	Important control for delivery of cAMP by ISE. Impedance increase specific and profile very similar to the signal profile of forskolin
CPT-cGMP	No	No specific cell response	Yes	Impedance increase shows high variations. Impedance profile very similar to the signal profile of CPT-cAMP (and forskolin)
Calcimycin	Yes	Response of the cells not immediate but delayed for app. 20 min	Yes	Response of the cells immediate, after initial decrease, impedance signal increases over time

BAEC cells exposed to 2.5 µM forskolin and concentrations ≥ 100 µM CPT-cAMP show immediate increase in impedance signal, followed by the slow decrease in the following hours. These results suggest that increased concentrations of cAMP induce signaling cascades within BAEC cells and therefore this cell line was applied for further studies of cAMP delivery by ISE. On the other hand, BAEC cell showed response to CPT-cGMP as well, the signal change/increase appeared to be very similar to the signal increase after CPT-

cAMP addition. Therefore, delivery of cGMP to BAEC was attempted. The BAEC cells respond instantly to the increasing concentrations of calcium in the cytoplasm (induced by 5 µM calcimycin), firstly by signal decrease and then by the slow and constant signal increase (over the following 1-2 hours). Such signal changes seem to partially overlap with the cell response after ISE and the delivery of calcium by ISE was not attempted within this work.

6.3 Delivery of Second Messengers into Cells by *In Situ* Electroporation

Studies which are described in the previous chapters were conducted with an aim to investigate how different cell lines respond to the increased levels of second messengers within the cytoplasm and thus initiated signaling pathways. The cell response was monitored noninvasively in real time using ECIS technology. The information and results obtained during these studies serve as the basis for establishment of proof-of-principle assays demonstrating that the ECIS technology can be conveniently applied for the delivery of membrane-impermeable second messengers into the cells and for the time-resolved and non-invasive monitoring of the cellular response to second messengers.

Impedance monitoring of the delivery of membrane-impermeable second messengers into the NRK and BAEC cells by *in situ* electroporation (ISE) is presented and evaluated within the following chapters. To establish the proof-of-principle assays, it was aimed for delivery of membrane-impermeable compounds cAMP and 8-OH-cAMP into the cell cytoplasm, whereas delivery of cGMP into the cytoplasm of BAEC cells was attempted without the success. The BAEC cells did not show significant response (i.e. no significant impedance increase) after they were exposed to ISE in presence of cGMP. Hence, these data are not presented in this work.

6.3.1 Nonpermeable Analogues of Second Messengers and NRK Cells

The first attempts to deliver second messenger cAMP into the NRK cells by ISE and record the cell response upon activation of cAMP-specific signaling pathways by ECIS were conducted using membrane-impermeable and unmodified cAMP. **Figure 6.9** shows an exemplary measurement performed on 8W4Eµ electrode array. The NRK cells were exposed to different concentrations of cAMP (100, 300, 400, 500, 800 and 1000 µM) and serum-free culture medium was applied as assay buffer. Different concentrations of the second messenger cAMP were added to the NRK cells at the time point marked with arrow a.

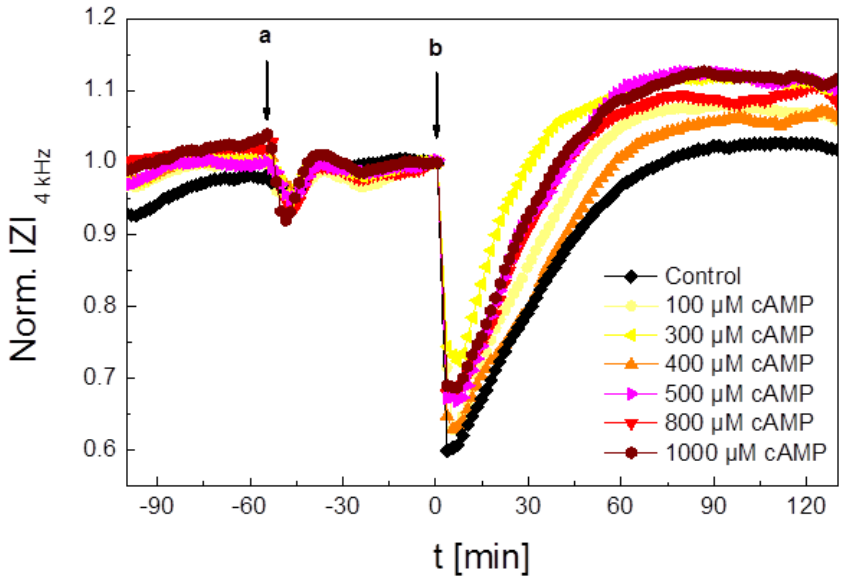

Figure 6.9 Exemplary time course of the normalized impedance magnitude at 4 kHz before, during and after *in situ* electroporation of NRK cells in presence of different concentrations of cAMP (added at the time point marked with arrow **a**). Impedance magnitudes were normalized to the last time point before electroporation was applied (marked with arrow **b**), using optimal combination of pulse parameters for NRK cells: 40 kHz, 4 V and 200 ms.

After re-equilibration of the cells, ISE was applied (marked with arrow b) using optimal combination of pulse parameters for NRK cells: 40 kHz, 4 V and 200 ms. **Figure 6.9** shows that there was no consistent difference in the cell response between the samples and the control (ISE in absence of cAMP). Furthermore, no concentration-dependent cellular behavior was observed. Even though the cells exposed to ISE in presence of cAMP show overall higher impedance signal (compared to the cells exposed to ISE in absence of cAMP) after the pulse application, it is difficult to draw any conclusion about the cell response to cAMP based on these data. In addition, a series of experiments was conducted where NRK cells were exposed to different concentrations of cAMP and the assay buffer was varied (serum-free medium, complete medium, or $EBSS^{++}$), however these experiments showed either inconsistent NRK response to cAMP, or there was no significant cell response to cAMP at all (data not shown). Therefore, it was concluded that the pure cAMP is inappropriate for studies of second messenger delivery and it was decided to move on with another (modified) cAMP probe. For the further assays, 8-OH-cAMP was applied as an active compound, which was aimed to be delivered into the cells by ISE. This second messenger cAMP is slightly modified (by introducing hydroxyl group: 8-OH into its structure) in order to improve its membrane impermeability and resistance against mammalian cyclic nucleotide-dependent phosphodiesterases.

The preliminary studies, conducted with various membrane-permeable compounds, were performed in different assay buffers. Most common buffer applied for studies with NRK cells was $EBSS^{+-}$ (w/ magnesium, w/o calcium), but the experiments were also conducted in $EBSS^{++}$ (w/ magnesium, w/ calcium). For studies with BAEC cells, additionally serum-free culture medium or even complete culture medium were applied. The first assays involving *in situ* electroporation of NRK cells (in presence of cAMP) were conducted in $EBSS^{++}$ buffer, serum-free and complete culture medium. However, there was a concern that some of the contents of serum-free or complete culture medium diffuse into the cytosol during electroporation and thus potentially interfere with the cell response to the second messenger cAMP. Therefore, serum-free and complete culture medium were excluded as the assay buffers for ISE of NRK cells. At that point, it was assumed the $EBSS^{++}$ buffer is an optimal assay buffer, as it provides appropriate content of salts, physiological pH and does not contain many other additional compounds (like it is the case with the culture medium), that could eventually enter the cytosol during the membrane permeabilization and cause some unwanted artifacts.

However, looking at the experiments conducted with calcimycin an during the optimization of assays, where membrane-permeable initiators of cAMP signaling pathways were applied (CPT-cAMP and forskolin), it was noticed that the $EBSS^{+-}$ buffer provided the best conditions to monitor cellular response. This EBSS buffer contains Mg^{2+}, but not Ca^{2+} ions and its application should exclude any artifacts coming from the calcium effect. Taking into the account that Ca^{2+} ions are able to act as second messengers as well, especially encountering the cell response upon their treatment with calcimycin, it was assumed that the buffer containing calcium might cause interference in signals coming from the specific signaling cascades. There was a certain concern that not only the second messenger cAMP (dissolved in assay buffer) might enter the cytosol upon the electroporation of the cell membrane, but also the calcium ions present in the buffer ($EBSS^{++}$). Therefore, the effect of the applied buffer itself on *in situ* electroporation had to be addressed first. A potential influence of calcium present in the EBSS buffer during *in situ* electroporation was investigated within a simple experiment. In **Figure 6.10**, time course of the normalized impedance is presented, where the behavior of confluent NRK cells was monitored impedimetrically before, during and after *in situ* electroporation (ISE) in presence of buffers: $EBSS^{++}$ (w/ Mg^{2+} and w/ Ca^{2+}) and $EBSS^{+-}$ (w/ Mg^{2+} and w/o Ca^{2+}). During the experimental procedure, no active compounds (including second messengers) were present in the buffers. The experiment was conducted on 8W1E electrode array. The assay was started with 400 µL of the corresponding buffer in each well and the NRK cells were allowed to equilibrate for

app. an hour, before ISE was applied (using optimal combination of parameters for this cell line: 40 kHz, 4 V and 200 ms). Thereafter, the cell recovery and the response were monitored noninvasively for app. 3 hours, in order to evaluate if any differences in cell behavior will be observed, regarding the cell exposure to calcium ions during the electroporation. For each of the two conditions (ISE in presence and absence of calcium), the assay was run in triplicates.

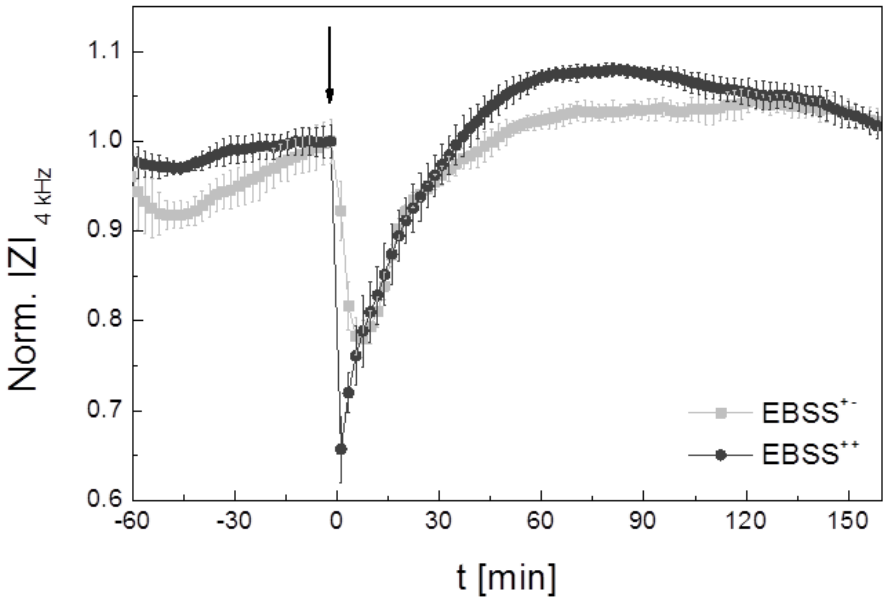

Figure 6.10 Time course of the normalized impedance magnitude at 4 kHz before, during and after *in situ* electroporation of NRK cells in absence of any active compound. The effect of calcium ions during ISE was evaluated using two different assay buffers: $EBSS^{+-}$ and $EBSS^{++}$. Impedance magnitudes were normalized to the last time point before electroporation was applied (marked with arrow), using optimal combination of parameters for NRK cells: 40 kHz, 4 V and 200 ms. The error bars correspond to the values of standard deviation (mean value ± standard deviation; n=3).

Data presented in **Figure 6.10** show mean value ± standard deviation (n=3) of the normalized impedance magnitude at 4 kHz and the data were normalized to the last time point before ISE was applied to the cells (indicated with the arrow). During this measurement, overall impedance values for the cells bathed in $EBSS^{+-}$ were lower than for the cells bathed in $EBSS^{++}$. Thus, after the equilibration and shortly before ISE was applied, raw non-normalized impedance values for the cells dissolved in $EBSS^{+-}$ were around 12 kΩ and for the cells dissolved in $EBSS^{++}$ around 14 kΩ. Cells surrounded by $EBSS^{+-}$ also need longer time to equilibrate. Upon *in situ* electroporation of NRK cells, immediate drop in impedance signal was observed, but minimum values for cells in $EBSS^{+-}$ and $EBSS^{++}$ were not the same. The minimum of normalized impedance after ISE reached by the cells bathed

in $EBSS^{+-}$ was 0.78 ± 0.01, whereas the cells bathed in $EBSS^{++}$ showed bigger drop and reached the minimum of normalized impedance at 0.65 ± 0.04. Thereafter, the changes of normalized impedance suggested that the cells in both buffers recover equally fast. However, after the signals returned to the pre-pulse values, the impedance signal of the cells electroporated in $EBSS^{+-}$ remained app. at the same levels (1.025 ± 0.001), whereas the impedance signals of the cells electroporated in $EBSS^{++}$ continued to increase for app. 30 - 40 min, reached values of 1.075 ± 0.001 of the normalized impedance and then returned slowly back to the pre-pulse values, indicating final stabilization of the cells.

It is reasonable to assume that such slight increase in impedance signal after ISE, observed after the cells where electroporated in $EBSS^{++}$, comes as an effect of calcium to the cells. In fact, similar cell response to the calcium ions was observed when the NRK cells were exposed to calcimycin in presence of the same $EBSS^{++}$ buffer. The NRK cells treated with 5 µM calcimycin showed an impedance increase from 1.00 ± 0.025 to 1.06 ± 0.015 (therefore, $\Delta_{calcymicin}$ = 1.06 – 1.00 = 0.06), and the cells electroporated in $EBSS^{++}$ buffer showed the impedance increase from 1.00 ± 0.02 to 1.075 ± 0.001 (therefore, $\Delta_{ISE/EBSS++}$ = 1.075 – 1.00 = 0.075). Furthermore, if the impedance increase after ISE in $EBSS^{++}$ buffer (1.075 ± 0.001) is compared to the impedance "increase" after ISE in $EBSS^{+-}$ buffer (1.025 ± 0.001), following difference is calculated: $\Delta_{ISE/EBSS}$ = 1.075 – 1.025 = 0.05. Obviously, both impedance increase $\Delta_{ISE/EBSS++}$ = 0.075 and $\Delta_{ISE/EBSS}$ = 0.05 measured upon ISE, are in a good agreement with the impedance increase $\Delta_{calcymicin}$ = 0.06, measured after treatment of the cells with calcymicin, suggesting that the calcium ions have rather small but distinct influence on the NRK behavior after ISE. This is supported by the fact that the effect of calcium ions was mostly pronounced during the time interval of 40 -70 min after calcium influx into the cytosol, which was observed in both measurements, including calcimycin and ISE in $EBSS^{++}$.

Based on these observations, it was concluded that the $EBSS^{+-}$ buffer is more appropriate than $EBSS^{++}$ to address cellular response to the increased intracellular levels of second messengers, elevated by the application of ISE.

Figure 6.11 shows time course of the normalized impedance before, during and after ISE of NRK cells in presence of 100 µM 8-OH-cAMP. This experiment was conducted with NRK cells (with the passage number P12), grown on 8W1E array and $EBSS^{+-}$ was applied as assay buffer. Both, sample (ISE in presence of 8-OH-cAMP) and the control (ISE in buffer only), were run in four replicates. **Figure 6.11** shows average values of normalized impedance and the error bars correspond to the values of standard deviation (n=4). The assay was started with 200 µL of assay buffer ($EBSS^{+-}$) in each well, the cells were allowed to equilibrate and in the moment of addition (marked with a), 200 µL of double concentrated

8-OH-cAMP (200 µM) was added to the sample wells (to obtain the final concentration of 100 µM 8-OH-cAMP in 400 µL of the total/end volume per well). Furthermore, 200 µL of the assay buffer was added to the control wells. After addition, cell monolayers were allowed to re-equilibrate and subsequently, electroporating pulses were applied (marked with b), using optimal combination of pulse parameters for NRK cells: 40 kHz, 4 V and 200 ms. Recovery of the NRK cells after ISE and their response to delivery of cAMP into the cytosol was monitored noninvasively for app. 2.5 hours.

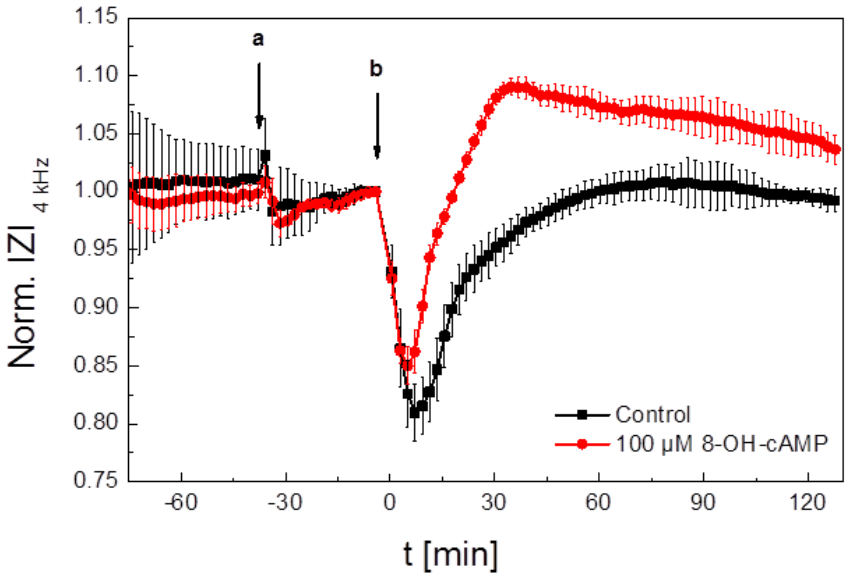

Figure 6.11 Time course of the normalized impedance magnitude at 4 kHz before, during and after *in situ* electroporation (marked with **b**) of NRK cells in presence of 100 µM 8-OH-cAMP (added at the time point marked with **a**). Impedance magnitudes were normalized to the last time point before electroporation was applied, using optimal combination of pulse parameters for NRK cells: 40 kHz, 4 V and 200 ms. The error bars correspond to the values of standard deviation (mean value ± standard deviation; n=4).

Immediately after pulse application, (normalized) impedance dropped to average values of 0.85 ± 0.010 and 0.81 ± 0.018, for cells electroporated in presence of 8-OH-cAMP and cells electroporated only in buffer, respectively. Whereas the cells exposed to electric pulses in buffer recovered slowly and returned to pre-pulse values after app. 45 min, impedance signal of the cells electroporated in presence of 8-OH-cAMP, started to increase more rapidly after the initial drop and reached maximum values at 1.09 ± 0.007 app. 35 min after pulse application. Shortly after plateau was observed, impedance signal started to decrease very slowly. Within the measured time frame, return of the signal to pre-pulse value was not observed, indicating that triggered signal cascade and the subsequent recovery of the cells

to the initial state before the pulse, takes longer than 2.5 hours.

Since during different second messenger studies both 8W1E and 8W4Eμ electrode arrays were applied, it was decided to monitor and compare the cellular response after delivery of second messengers (8-OH-cAMP) by ISE on both electrode arrays in parallel. Thus, it was evaluated if the choice of the array will have any impact on the results. For this purpose, previous experiment (presented in **Figure 6.11**) was repeated, with a difference that the same protocol was conducted in parallel on the array 8W4Eμ, in addition to 8W1E. Both measurements including delivery of 100 μM 8-OH-cAMP into NRK cells by ISE were performed in parallel, at the same ECIS device and at the same time. In addition, the NRK cells were seeded to both arrays from the same cell suspension prior to the experiment.

In graphs presented in **Figure 6.12**, time courses of the normalized impedance magnitude at 4 kHz are given for NRK cells electroporated in presence of 100 μM 8-OH-cAMP on 8W1E (**A**) and 8W4Eμ (**B**) electrode array. Cell behavior was monitored on ECIS before and after application of electroporating pulses, optimal for NRK cells: 40 kHz, 4 V and 200 ms. This experiment was conducted in the assay buffer EBSS^{+-}. Both, sample (ISE in presence of 8-OH-cAMP) and the control (ISE in buffer only), were run in triplicates (within each of the two arrays). After initial equilibration of the cells, 100 μM of 8-OH-cAMP was added (time point marked with a) and after several minutes of re-equilibration, electroporation was applied to the cells (at the time point marked with arrow b).

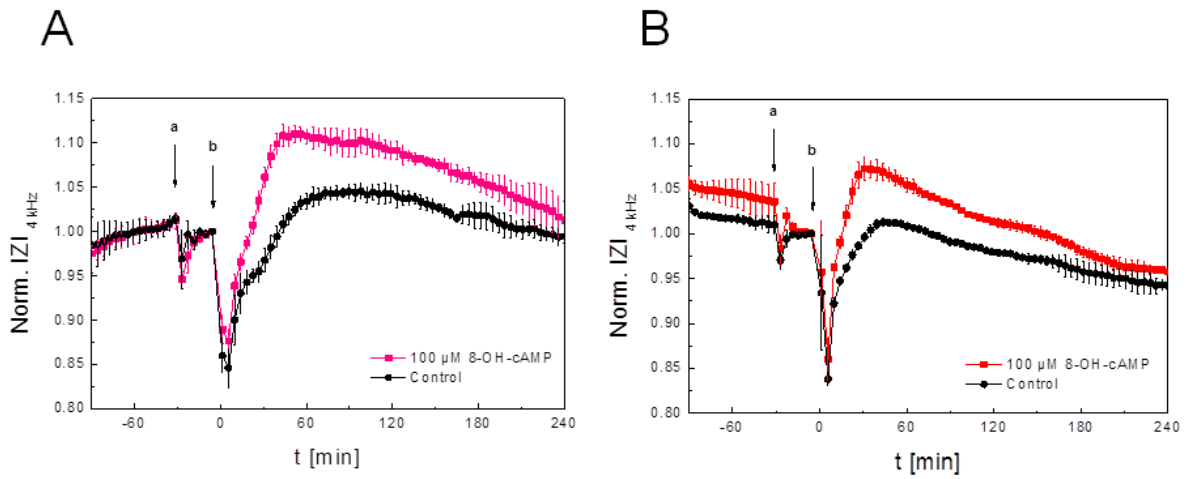

Figure 6.12 Time courses of the normalized impedance magnitude at 4 kHz before, during and after *in situ* electroporation of NRK cells in presence of 100 μM 8-OH-cAMP (added at the time marked with arrow **a**). Assay was performed on: **A** 8W1E and **B** 8W4Eμ electrode array in parallel. Impedance magnitudes were normalized to the last time points before electroporation was applied (marked with arrow **b**), using optimal combination of pulse parameters for NRK cells: 40 kHz, 4 V and 200 ms. The error bars correspond to the values of standard deviation (mean value ± standard deviation; n=3).

Impedance recordings were normalized to the last time points before ISE. Before ISE was applied, non-normalized impedance values for NRK cells on 8W1E electrode array were app. 11.5 kΩ, on average, whereas for NRK cells on 8W4Eμ array, impedance values were around 13.7 kΩ. Regardless of electrode array applied for the experiment, the cell response to *in situ* electroporation and delivery of 8-OH-cAMP into the cytosol was approximately the same. Impedance profiles recorded on both electrode arrays appear very similar in shape and with regards to the impedance magnitude. After initial impedance drop, due to transient membrane permeabilization, normalized impedance signal started to increase very fast and the cells in control and sample wells were recovering to pre-pulse values. However, traces belonging to the cells exposed to ISE in presence of 8-OH-cAMP showed faster recovery of the signal, compared to the cells in control, and their signal continued to increase until the maximal values were reached (app. 35 min after ISE). This significant impedance increase suggests fast and distinct response of NRK cells to the activation of cAMP-dependent signaling cascade on both arrays. Thereafter, impedance signal started to decrease slowly and it returned close to the pre-pulse values app. 4 hours after ISE. The impedance signal of the control cells recovered to the pre-pulse values within app. 35 – 45 min.

These experiments demonstrated successful delivery of membrane–impermeable second messenger 8-OH-cAMP into the NRK cells by *in situ* electroporation. Cell recovery after electric pulse and subsequent response of the cells to the increased concentrations of intracellular cAMP was reproducible and consistent, regardless of the electrode array applied for the analysis (8W1E or 8W4Eμ). The $EBSS^{+-}$ buffer was found as the optimal assay buffer.

6.3.2 Nonpermeable Analogues of Second Messengers and BAEC Cells

Based on previous studies performed on BAEC cells (chapter 6.2.2), where the cell response to the activation of second messengers-dependent signaling pathways was successfully monitored upon the addition of membrane-permeable compounds, delivery of second messengers by application of invasive electric pulses was evaluated. The proof-of-principle studies for delivery of second messengers into the BAEC cells by ISE were conducted in parallel to the studies conducted on NRK cells.

The first experiments where the stimulation of BAEC cells with membrane-permeable CPT-cAMP was investigated were performed in $EBSS^{++}$ buffer, serum-free or in the complete culture medium. Therefore, the first tests of the delivery of membrane-impermeable cAMP into the BAEC cells by ISE were also performed using these assay buffers. Before 8-OH-cAMP was applied for the studies of second messenger delivery by ISE, unmodified cAMP

was used for the experimental procedure. However, in some experiments was noticed that directly after the addition of cAMP, the characteristic increase in impedance signal is observed (as an indicator that cAMP-dependent pathway is activated), even before the electric pulse was applied. One of these experiments is presented in **Figure 6.13**, where the assay with BAEC cells was performed on 8W4Eμ electrode array, in serum-free medium applied as the assay buffer. The second messenger cAMP was added to BAEC cells at different concentrations (100, 300, 400, 500, 800, 1000 μM), during the experiment (marked with arrow a). After re-equilibration of the cells, ISE was applied (at the time point marked with arrow b) using optimal combination of pulse parameters for this cell line: 40 kHz, 4 V and 200 ms. The subsequent cell response was monitored impedimetrically for app. 3 hours after pulse application.

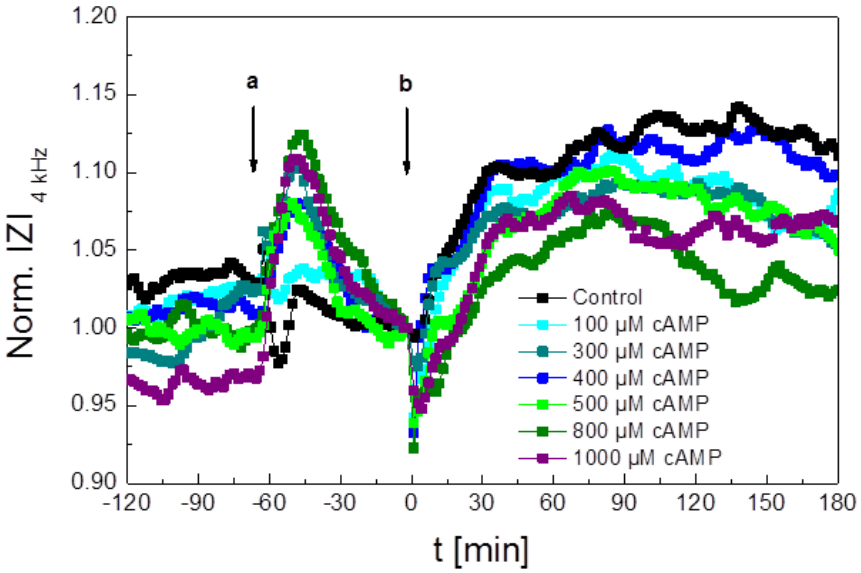

Figure 6.13 Exemplary time course of the normalized impedance magnitude at 4 kHz before, during and after *in situ* electroporation of BAEC cells in presence of different concentrations of cAMP (added at the time point marked with arrow **a**). Impedance magnitude was normalized to the last time point before electroporation was applied (marked with arrow **b**), using optimal combination of pulse parameters for BAEC cells: 40 kHz, 4 V and 200 ms.

During this measurement, it was observed that already after the addition of cAMP (at different concentrations), BAEC cells started to respond in a cAMP-characteristic manner, as an immediate impedance increase and then relatively fast return to the pre-addition values took place within 60 min. The cell response to the activation of cAMP-specific signaling pathway was not entirely concentration-dependent, however, it was observed that the cells exposed to the higher concentrations of cAMP (e.g. 500, 800 and 1000 μM), exhibited more

pronounced response after the addition, whilst their response after the pulse application was rather reduced. Obviously, the cells which showed more significant response to the cAMP addition, exhibited bigger drop in impedance signal after the pulse application. Moreover, **Figure 6.13** shows that, from the moment of addition (marked with arrow a), BAEC cells exposed to cAMP behaved completely different compared to the control cells, which were exposed only to the buffer. All this indicated that compound cAMP is not entirely membrane-impermeable, on the contrary, cAMP seemed to be able to diffuse into the cytosol of BAEC cells even in absence of the electric pulse. Interestingly, similar issue was not obvious when NRK cells were exposed to the unmodified cAMP (**Figure 6.9**). Nevertheless, unmodified cAMP was replaced with 8-OH-cAMP for further assays conducted with BAEC and NRK cells. In **Figure 6.14**, time course of the normalized impedance at 4 kHz before, during and after *in situ* electroporation of BAEC cells in presence of 100 µM 8-OH-cAMP is presented. This experiment was conducted on 8W1E electrode array and EBSS^{+-} was applied as the assay buffer to exclude any potential artifacts due to the influx of calcium ions during ISE. Both, sample (ISE in presence of 8-OH-cAMP) and the control (ISE only in buffer), were measured in duplicates (n=2).

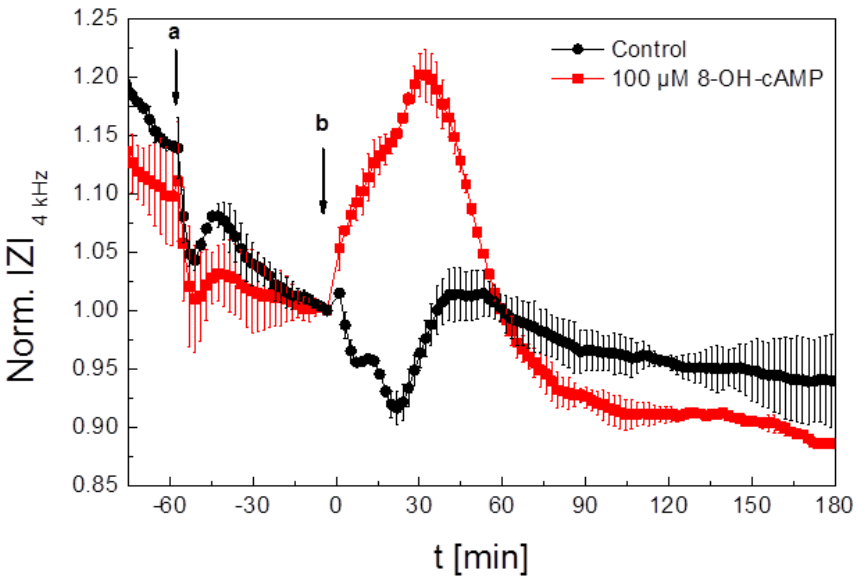

Figure 6.14 Time course of the normalized impedance magnitude at 4 kHz before, during and after *in situ* electroporation (marked with arrow **b**) of BAEC cells in presence of 100 µM 8-OH-cAMP (added at the time point marked with arrow **a**). Impedance magnitudes were normalized to the last time point before electroporation was applied using optimal combination of pulse parameters for BAEC cells: 40 kHz, 4 V and 200 ms. The error bars correspond to the values of standard deviation (mean value ± standard deviation; n=2).

The measurement was started with 200 µL of the assay buffer ($EBSS^{+-}$) in each well, the BAEC cells were allowed to equilibrate and subsequently, the addition was performed (at the time point marked with arrow a). 200 µL of the double concentrated 8-OH-cAMP (200 µM) was added to sample wells (to obtain a final concentration of 100 µM in 400 µL of the total/end volume per well). To the control wells, 200 µL of the assay buffer was added. After the cells re-equilibrated, electroporating pulses were applied (marked with arrow b), using optimal combination of pulse parameters for BAEC cells: 40 kHz, 4 V and 200 ms.

The behavior of BAEC cells after *in situ* electroporation and their response to the delivery of membrane-impermeable cAMP analogue into the cytosol was monitored noninvasively for app. 3 hours. Immediately after pulse application, increase in impedance signal was recorded for the cells exposed to 8-OH-cAMP. Such significant increase in impedance signal continued for around 30 min until the maximal values of normalized impedance were reached (1.20 ± 0.02). Thereafter, the impedance signals started to decrease and app. 60 min after pulse application, they were at the pre-pulse level. However, the impedance decreased continuously for the following 30 min, when the signal finally stabilized. On the other hand, the BAEC cells pulsed in absence of 8-OH-cAMP showed small biphasic signal decrease after electroporation and they recovered to the pre-pulse values in less than 45 min. Such cellular response to the electroporation and the effect of 8-OH-cAMP on BAEC cells was different from what was observed with NRK cells. However, the response of BAEC cells to 8-OH-cAMP and the impedance profiles after ISE were very similar and comparable to the cell response and impedance profiles observed upon stimulation of these cells with membrane-permeable cAMP analogue (CPT-cAMP) and activator of the cAMP-dependent signaling pathway (forskolin). Moreover, the response of the BAEC cells after delivery of 8-OH-cAMP by ISE appears very similar to the response of the cells observed after the addition of unmodified cAMP (**Figure 6.13**). During the measurement presented in **Figure 6.14**, a drifting of the signal, by means of constant signal decrease, was observed, most probably due to the loosening of cell-substrate contacts, caused by the absence of calcium ions in the assay buffer $EBSS^{+-}$.

These experiments demonstrated successful delivery of second messenger 8-OH-cAMP into BAEC cells by *in situ* electroporation. The compound 8-OH-cAMP was applied as the membrane-impermeable second messenger, since it was found that unmodified cAMP diffuses into the cytosol of BAEC cells even in absence of electric pulses. Cell response to the increased concentrations of intracellular cAMP (induced by 8-OH-cAMP) was reproducible and consistent with the previous measurements conducted with membrane-permeable analogues of the second messenger cAMP (CPT-cAMP and forskolin).

6.4 Discussion

The cell response to increased concentrations of second messengers within the cytosol was investigated using ECIS technology as the analytical method. In addition, invasive mode of ECIS was applied to deliver electric pulses over the cell monolayer and thus open transiently the cell membrane, allowing the second messengers to diffuse into the cytoplasm. Using non-invasive mode of ECIS, cell recovery after electroporation and the response to activation of second messengers-dependent signaling pathways was monitored over several hours. The impedance profiles acquired after stimulation of the cells with second messengers were analyzed and compared. The cell lines NRK and BAEC were applied as cell models, which were exposed to second messengers cAMP, calcium and cGMP. Whereas both cell line gave consistent and reproducible response to stimulation of cAMP- and calcium-specific signaling pathways (after application of membrane-permeable analogues), only BAEC cells showed certain specific response after addition of membrane-permeable analogue of cGMP. Therefore, studies conducted within this work were focused on following the cell response to second messengers cAMP and calcium. Membrane-permeable compounds forskolin and CPT-cAMP were applied to stimulate confluent NRK and BAEC cells in order to record their behavior and impedance profiles upon activation of cAMP-specific signaling pathways. These experiments served as basis to establish proof-of-principle assay for delivery of membrane-impermeable 8-OH-cAMP into cells by *in situ* electroporation, using optimal combination of pulse parameters (investigated and established within the dye loading studies described in chapter 5.1.2.

Besides NRK and BAEC cells, other cell lines were investigated for their response to different second messengers. CHO-GFP, HaCaT, MCF-7, MDCK II and U737 were exposed to membrane-permeable CPT-cAMP, CPT-cGMP, calcimycin and forskolin. However, these cell lines showed only certain specific response to the influx of calcium into the cytoplasm. Some of these cell lines were even exposed to ISE in presence of cAMP, but no significant cell response was found.

The studies involving second messengers conducted within this work were based on the previous reports which showed the applicability of impedance analysis for monitoring the response of adherent cells, grown on small gold film electrodes, to the biologically active compounds (Wegener et al., 1999; Reddy et al., 1998; Gagliardi et al., 2015).

6.4.1 Response of NRK Cells to Second Messengers

The behavior of NRK cells, upon their stimulation with second messengers was firstly monitored using forskolin, as a bioactive compound. Forskolin activates enzyme adenylyl

cyclase and thus directly increases the intracellular levels of cAMP. The applied concentration of forskolin (2.5 µM) was chosen based on previously reported studies performed on BAEC cells (Wegener et al., 1999; Zink et al., 1993; Kottra and Fromter, 1993). After forskolin addition, short-termed response of the cells to the fresh fluid was observed, however, immediately afterwards, impedance signal started to increase and it reached the maximal values within an hour. Such response of the NRK cells to forskolin is in agreement with the response of this cell line observed after their exposure to CPT-cAMP. The addition of this membrane-permeable cAMP analogue (at the concentration 100 µM) caused immediate increase in impedance signal (after the initial short signal change due to the fluid addition). The maximal values of normalized impedance were reached within an hour and similarly to the cell response observed after the treatment with forskolin, impedance signal remained relatively close to the maximal values for the following 2 -3 hours measurement time, with only very small signal decrease observed over time. The recorded cell response of NRK cells to the increased cAMP levels is in agreement with the studies performed on BAEC by Wegener et al., 1999, regarding the significant initial increase in impedance signal. However, the effects of forskolin and CPT-cAMP on BAEC cells seemed to be on a shorter term compared to the NRK cells, since this reference indicates that impedance signal started to rapidly decrease shortly after the maximal values were reached. In addition, treatment of NRK cells with CPT-cAMP resulted in overall lower impedance values (maximal values reached at 1.09 ±.0.003) compared to the treatment of this cell line with forskolin (maximal values reached at 1.17 ± 0.07), whereas during studies conducted by Wegener and collaborators on BAEC cells, the situation was vice versa.

Studies involving stimulation of cAMP-specific signaling pathway in NRK cells showed that age of the cells (passage number; P) is an important parameter, which has to be taken into account, in order to assure consistent and reproducible response of the cells. ECIS recordings have demonstrated that the cells with higher passage number (P28) show much slower initial increase in impedance signal after addition of 100 µM CPT-cAMP. Thus, the maximal values are reached app. 20 min later than in the experiments where NRK cells at lower passage number (P10) were applied for analysis. In addition, lower impedance magnitude was observed in the measurements where “older” NRK cells were exposed to CPT-cAMP. Such observations might be explained by the possible alterations in the cell morphology and increased stiffness of the cells with an increasing passage number (Fletcher and Mullins, 2010). The increased levels of cAMP within the cell cytoplasm cause the activation of protein kinase A (PKA), which regulates different processes and mechanisms within the cell, and plays an important role in the various signaling cascades. Furthermore,

PKA is linked to the numerous components of the cytoskeleton (e.g. actin) and thus plays an essential role in cytoskeletal organization and cell migration (Howe, 2004; Nadella et al., 2009). This implies that signaling cascades involving cAMP/ PKA cause changes in the cellular morphology, or cell migration.

Successful impedance monitoring of response of the NRK cells upon their treatment with forskolin and CPT-cAMP paved the way for investigation of cAMP delivery by ISE into cytosol of NRK cells. It is important to mention that concentration-dependent stimulation of NRK cells with CPT-cAMP and forskolin was not investigated within this work. It would be the aim of future studies involving second messengers to examine if and within which range concentration-dependent response of NRK cells to CPT-cAMP (and forskolin) can be observed, similarly as it was conducted by Lieb and collaborators (Lieb et al., 2016), who demonstrated successfully concentration-dependent response of U373 cells to histamine, and response of BAEC cells to isoprenaline, monitored by ECIS.

Capability of *in situ* electroporation as a method to deliver second messengers into NRK cells grown on small gold film electrodes was firstly investigated using unmodified cAMP. Even though these assays were repeated several times, in various buffers and with various concentrations of cAMP, the results showed that there was either no significant cell response, or the NRK response was rather inconsistent (not reproducible) after the electric pulse was applied to the cells in presence of cAMP. Considering the response of NRK to forskolin and CPT-cAMP, it is difficult to understand such outcome of the analysis. However, assays conducted in parallel on BAEC cells showed that unmodified cAMP can enter the cytosol of BAEC cells even without application of electric pulses. Although similar observations were not made during impedance measurements conducted on NRK cells in presence of cAMP, it remains unclear if unexpected (partial) membrane-permeability of cAMP affected in some way investigation of cAMP delivery by ISE.

Instead of cAMP, 8-OH-cAMP was applied as the membrane-impermeable probe. Delivery of 100 µM 8-OH-cAMP into confluent monolayers of NRK cells was accomplished by application of optimal pulse parameters for this cell line: 40 kHz, 4 V and 200 ms. Directly after pulse application, characteristic impedance drop indicated effect of transient membrane permeabilization. For the NRK cells exposed to ISE in presence of 8-OH-cAMP, impedance drop was smaller than for the cells in control (bathed only in buffer). The NRK cells exposed to 8-OH-cAMP showed significantly faster subsequent recovery of the signal, compared to the cells in controls. Moreover, their rapid rise of impedance signal reached the maximal values already within 30 – 35 min after pulse application, whereas impedance of the cells pulsed only in buffer recovered slowly to the pre-pulse values within app. 60 min. These data

are entirely in agreement with the previously conducted (but not published) studies performed by J. Wegener, where NRK cells were exposed to ISE in presence of 100 µM 8-OH-cAMP (data not shown).

To investigate if the choice of array for analysis (8W1E or 8W4Eµ) will influence the outcome of the experiment, delivery of 100 µM 8-OH-cAMP into NRK cells by ISE was conducted in parallel on both electrode arrays, under the same conditions and with the NRK cells seeded to both arrays from the same cell suspension. This experiment showed that the response of NRK cells to 8-OH-cAMP delivery by ISE is very similar on these two electrode array types. **Figure 6.15** shows time courses of the normalized impedance for stimulation of NRK cells with 100 µM CPT-cAMP (**A**) and delivery of 100 µM 8-OH-cAMP into NRK cells by *in situ* electroporation (**B**) for comparison of NRK response recorded based on these two protocols.

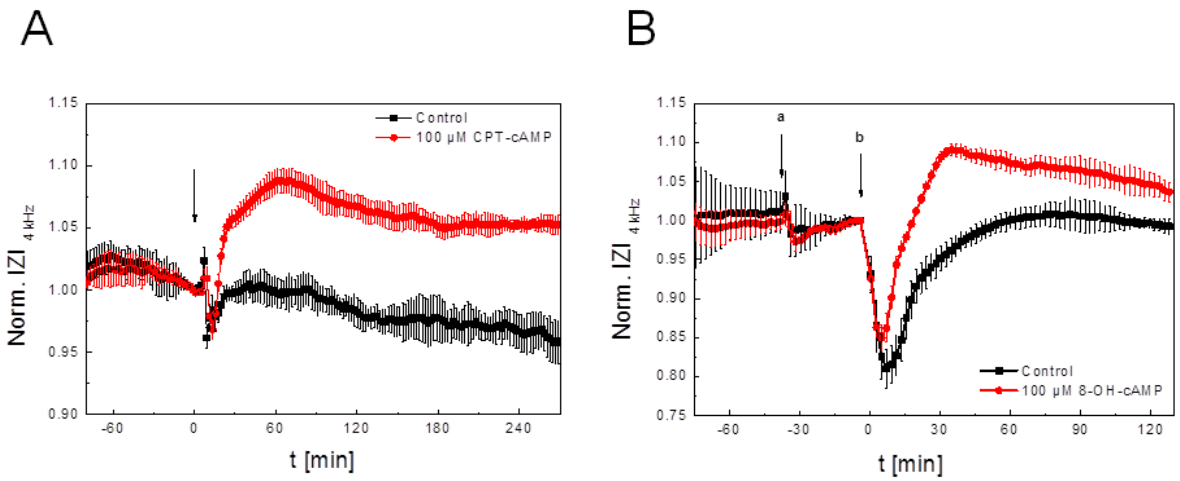

Figure 6.15 The comparison of time courses of the normalized impedance magnitude at 4 kHz before, during and after (**A**) addition of 100 µM CPT-cAMP and (**B**) *in situ* electroporation of NRK cells in presence of 100 µM 8-OH-cAMP. Impedance magnitudes were normalized to the last time points before addition (**A**) or electroporation (**B**). The error bars correspond to the values of standard deviation (mean value ± standard deviation; n=4).

By comparing the time courses of these two experiments, it is obvious that in both cases an initial rapid and steep increase of impedance signal takes place after cAMP influx into the cytosol, followed by slightly slower impedance rise to the maximal values. Such biphasic impedance increase is highly reproducible and it may be even concluded that the second impedance rise is faster when the NRK cells are pulsed in presence of 8-OH-cAMP. Time course of the NRK stimulation with forskolin did not show similar biphasic impedance increase. Nevertheless, the maximal values of normalized impedance are reached much faster after ISE of NRK cells in presence of the second messenger (within 30 - 35 min after

the pulse), in comparison to the treatment of NRK cells with CPT-cAMP, when the maximal values were reached app. 60 – 70 min after the addition. The time necessary for NRK cells to reach maximal values of impedance after forskolin addition was even longer (app. 70 – 80 min). This leads to the conclusion that NRK cells show much faster response to an activated cAMP-specific signaling pathway after the pulse, due to the fact that cAMP instantly reaches the cytoplasm (and thus its targets) when delivered by ISE. Based on these observations, the conclusion may be drawn that not only the *in situ* electroporation facilitates efficient delivery of the second messengers into the cells, but it also allows for their rapid and direct entry into the cytoplasm, thus accelerating their action, which can be critical in some cases.

One of the aims of potential future studies on second messengers would certainly be to investigate if concentration-dependent response of NRK cells to 8-OH-cAMP can be achieved after its delivery by ISE.

After several initial experiments were conducted in $EBSS^{++}$, serum-free and complete culture medium within the project involving second messengers, the choice of an appropriate assay buffer for these assays arose. The buffer $EBSS^{++}$ is usually applied as the assay buffer within studies of ISE, as it supplies the cells with essential salts and allows for optimal physiological conditions during the experimental procedure. However, for studies including second messengers, it was important to investigate if extracellular calcium, as a well-known second messenger itself, might cause interference and produce artifacts, when present in the assay buffer. The behavior of NRK cells before and after *in situ* electroporation in presence of $EBSS^{++}$ (w/ calcium) and $EBSS^{+-}$ (w/o calcium) buffer was analyzed and it was observed that the cells pulsed in absence of calcium showed smaller initial impedance drop after the pulse application than the cells pulsed in presence of calcium. Furthermore, cells pulsed in absence of calcium recovered to pre-pulse values, whereas the impedance signal belonging to the cells pulsed in presence of calcium, continued to increase beyond the pre-pulse pulse values for app. 30 – 40 min and finally reached values of normalized impedance that were for 0.05 higher ($\Delta_{ISE/EBSS} = 0.05$) than the values reached by the NRK cells pulsed in absence of calcium. This observation is in agreement with the results obtained after addition of 5 µM calcimycin to the NRK cells. The influx of extracellular calcium (from $EBSS^{++}$) into the cytoplasm resulted in increase of normalized impedance for 0.06 ($\Delta_{calcymicin} = 0.06$), compared to the signal of cells which were not treated with calcimycin. The time scale in these two experiments is also very comparable, since the calcium effect was mostly pronounced within 40 – 70 min after the entry of calcium ions into the cytoplasm in both cases.

It is well known from the literature that increased intracellular levels of calcium may trigger some calcium-dependent processes and thus affect cell morphology. For instance, higher

intracellular concentrations of calcium can induce regulatory volume decrease (RVD) within the kidney cells (Tinel et al., 2000). A sensitivity of rat kidney cell types to elevated intracellular calcium might well explain why distinct calcium effect upon calcimycin addition was observed with NRK cells, much more than in BAEC cells (where the effect of calcium influx was different). The fact that NRK cells might be prone to calcium-induced volume decreases could be an explanation why with NRK cells exposed to ISE in presence of calcium clearly more pronounced (bigger) impedance drop was observed, compared to the NRK cells pulsed in absence of calcium. The reason for such phenomenon might be that regulatory volume decrease leads to the short opening of the cell-cell contacts. This effect allows for current to flow between the cells (rather than around them) and results in transiently lower impedance values (as observed shortly after pulse application). Golzio et al., 1998 investigated the effects of buffer osmotic pressure during electroporation (and in the following 10 min) in CHO cells exposed to ms square wave pulses. They followed under the microscope how cell diameter changes after pulsing (10 pulses of 5 ms, 0.8 kV/cm and 1 Hz) in hypo-, iso- and hypertonic buffers. The cell size increases with a decrease in osmolarity and it decreases with the increase in osmolarity. Upon membrane permeabilization, osmotic balance is interrupted and this causes swelling of the cells (Kinosita and Tsong, 1977a; Kinosita and Tsong, 1977b). The cell size first increases and then a regulated volume decrease (RVD) takes place. CHO cells re-estabish their size within 10 min after the pulse. The group found that the effect of osmolarity exists only during the application of the pulses and increase in the cell size was observed regardless of osmolarity of the pulsing buffer. Furthermore, the group studied the effect of hypo-, iso- and hypertonic buffers on cells after the pulse. They pulsed the cells in isotonic buffer and exchange it 1 sec later. They observed that the cell size after pulse increased in hypotonic buffer and it was followed by RVD, whereas the size of the cells in hypertonic buffer decreased after the pulse and it was followed by RVI (regulated volume increase). The size of size cells in isotonic buffer did not significantly changed after the pulse.

There are also several reports in the literature indicating an importance of the assay buffer and ionic strength during electropermeabilization of the cell membrane. Hibino et al., 1991 reported that membrane conductance appears to be independent of ionic strength when the same electric field intensity is applied. The size of the pores formed within the cell membrane that remain open after application of electric pulse appeared to be (much) larger in buffer with low ionic strength (Kinosita and Tsong, 1977b; Kinosita and Tsong, 1977a). These reports suggest that the recovery of cell membrane after pulsation is highly dependent on the ionic strength. Furthermore, Rols and Teissié, 1989 investigated the effect of ionic strength

on the electroporation of CHO cells grown in Petri dishes and in suspension. They studied how pulses with different duration, number and electric field intensity influence the extent of permeabilization in presence of iso-osmolar buffers with lower and higher ionic content. They observed that the extent of permeabilization of the plated cells increased with increasing ionic strength of the buffer. Also, permeabilization of the cells was only dependent on the ionic strength during pulsation. With the higher ionic strength of the assay buffer, permeabilization was enhanced. Even though within this work the effect of the buffer was not considered regarding the peremabilization efficiency, but with the respect to its influence and possible interference of the second messenger studies, it is clear that the assay buffer and its content is an important aspect which has to be encountered during the protocol for *in situ* electroporation.

Based on all these considerations and observations made during experiments performed within this work, it was concluded that the extracellular calcium during electroporation will influence and it might possibly overlap with the response of NRK cells to other second messengers under study. Hence, it was decided to apply buffer without calcium ions - $EBSS^{+-}$ for the further monitoring of cell response after triggering the cAMP-specific signaling cascades.

The effect of calcium ions on the electroporation of the cells in presence and absence of second messengers was investigated also by Rickords and White, 1993. This group compared increase of calcium levels in murine secondary oocytes (loaded with fluo-3) after their exposure to electroporation in presence of IP3 (inositol 1,4,5-triphosphate) in the PBS buffer containing calcium and in the calcium-free PBS. They observed dramatic increase in calcium signal, as a result of calcium release from intracellular compartments, as well as periodic oscillations in calcium signal indicating periodic calcium release (within 20 min), when oocytes where pulsed in calcium-free PBS containing IP3. On the other hand, no changes in calcium signal were observed when oocytes were pulsed in calcium-free PBS in absence of IP3. Such results are in good agreement with the studies of delivery of 8-OH-cAMP by ISE conducted in this work. In addition, the group compared behavior of oocytes after their electroporation in presence with IP3 with the release of calcium ions from the intracellular compartments by 7% ethanol, in presence of PBS with and without calcium ions. The calcium signal in both buffers was very similar, with an immediate calcium increase after the exposure of the cells to ethanol, suggesting that initial increase in calcium signal comes from the release of calcium from intracellular stores (induced by ethanol), and not due to the influx of extracellular calcium into the secondary oocytes. Such results are different from the results obtained within this work, when electroporation in EBSS buffer with and without

calcium was compared and the clear effect of extracellular calcium was observed.

Another interesting study conducted by Decrock et al., 2015a, b describes electroporation as a method to load caged IP3 into the monolayer of C6 glioma cells and after the application of flash photolysis, intracellular IP3 levels are increased, inducing calcium changes and intracellular calcium waves (ICWs). The group also applied *in situ* electroporation to load the cells with different membrane-impermeable agents that interfere with IP3 and calcium signaling. They usually applied 15 pulse trains with 0.5 sec breaks to permeabilize adherent cells and emphasized that *in situ* electroporation allows for loading of the cells within a certain defined zone, as a part of entire cell population, with different calcium-interfering agents. That way, corresponding response of the loaded cells within the defined zone was directly compared to the response of unloaded cells, allowing for “paired” experimental approach.

Golzio et al., 2003 and Frandsen et al., 2015 described delivery of defined concentrations of calcium into the cells by applying high voltage electric pulses and demonstrated that the high concentrations of calcium can selectively induce cell death of tumor cells. Namely, the study of Frandsen and collaborators showed that normal fibroblast spheroids were not affected after electroporation in presence of calcium. In contrast, cell death was induced in tumor cells after pulsation with calcium, which makes this method very promising for anti-cancer treatment.

Besides cAMP-, the response of NRK cells to stimulation of cGMP-specific signaling pathway was investigated in this work. The cell were subjected to 100 µM CPT-cGMP, however, no significant response of NRK cells was recorded. For that reason, delivery of cGMP by ISE was not attempted within this work.

The response of NRK cells to second messengers cAMP and calcium was successfully monitored using ECIS technology and impedance recordings allowed for detailed analysis of the cell behavior either after treatment of NRK cells with membrane-permeable compounds, or after exposure of the cells to ISE do deliver second messengers directly into the cell cytosol. Cell response upon loading of the NRK cells with second messengers by ISE was absolutely comparable and in agreement with the cell response recorded after treatment of the cells with the corresponding membrane-permeable compounds. In addition, it was demonstrated that *in situ* electroporation allows for direct and rapid delivery of second messengers into the cytoplasm, allowing them direct approach to their targets and thus accelerating their action.

6.4.2 Response of BAEC Cells to Second Messengers

Due to the fact that the BAEC cells possess beta-adrenergic receptors on the cell surface, they are chosen as an appropriate system for studies of signal transduction studies. Morphological changes of BAEC cells before and after stimulation of the cAMP-specific signaling pathway with forskolin was monitored using ECIS. Concentration of this activator of adenylyl cyclase (2.5 µM) was chosen based on previously reported studies performed on BAEC cells (Wegener et al., 1999) and known activity range (Zink et al., 1993; Kottra and Fromter, 1993). Immediately after forskolin addition, a steep impedance increase was observed and the maximal values of (normalized) impedance were reached already within 15 - 20 min. Thereafter, signal was constantly decreasing. Such response of BAEC cells was in agreement with the response of BAEC cells reported by Wegener et al., 1999, where the cells were subjected to 2.5 µM forskolin in serum-free medium. The group conducted impedimetric measurements with the BAEC cells grown on arrays containing three individual, small working electrodes. Not only that time courses (shapes of the curves) observed in both studies appear very similar, but also the time scales are in a very good agreement, considering that maxima of the curves in both studies were reached within first 15 – 20 min after forskolin addition.

Furthermore, the response of BAEC cells was analyzed after their exposure to three different concentrations of membrane-permeable analogue of cAMP (CPT-cAMP; 100, 500 and 1000 µM). Regardless of the CPT-cAMP concentration, immediately after its addition to BAEC cells, (normalized) impedance signal increased and reached maximal values within 10 min after the addition. The concentration-dependent behavior of BAEC cells was not observed, as the highest CPT-cAMP concentration (1000 µM) did not induce the highest cell response. Most probably, the applied concentration range was leading to the saturation of the CPT-cAMP-dependent response. Nevertheless, cell response after the addition of CPT-cAMP was very similar to the cell response after the addition of forskolin. Compounds CPT-cAMP and forskolin have different chemical structure and are not related chemically, however, they both activate cAMP-dependent signal transduction (by different mechanism). Besides similar profile/shape of the response curves and comparable impedance magnitudes, time scales of the both assays (forskolin vs. CPT-cAMP) were in a very good agreement, indicating that described impedance recordings were picking up cAMP-specific response of the cells. Moreover, the response of BAEC cells to addition of CPT-cAMP was in a very good agreement with the response reported by Wegner and collaborators (Wegener et al., 1999), both regarding the impedance profiles (shape) and time scale of the cell response. Delivery of membrane-impermeable cAMP into BAEC by *in situ* electroporation was initially

conducted using unmodified cAMP and serum-free medium was applied as the assay buffer. However, it was observed that cAMP can diffuse into the cells even before electric pulse is applied, since already after its addition (at different concentrations), BAEC cells showed cAMP-characteristic cell response in an almost concentration-dependent manner. After pulse application, cell response was partially concentration-dependent, but in a reverse order: cells exposed to higher concentrations of cAMP (which showed higher signal increase after cAMP addition) exhibited lower signals than the cells exposed to lower cAMP concentrations (which showed lower impedance signals after cAMP addition). Such results indicated that cAMP can be taken up by the BAEC cells and therefore, it is inappropriate probe for studies of second messenger delivery into the cells by ISE.

Following studies of second messenger delivery by ISE were conducted with 8-OH-cAMP as a membrane-impermeable compound. $EBSS^{+-}$ was applied as assay buffer to avoid any possible artifacts coming from the extracellular calcium. BAEC cells were exposed to electric pulse with optimal combination of pulse parameters for this cell line (40 kHz, 4 V and 200 ms) in presence of 100 µM 8-OH-cAMP. An immediate steep increase in impedance signal was observed after pulse application, and maximal values were reached within app. 30 min. Thereafter, fast decrease of impedance signals took place and their return to the baseline values was observed within 70 – 80 min after pulse application. Interestingly, no characteristic impedance drop directly after pulse application was observed when BAEC cells were exposed to 8-OH-cAMP, but the impedance signal immediately increased. On the other hand, BAEC cells in controls, subjected to ISE only in buffer, did show typical impedance drop and biphasic signal change after ISE, as described in chapter 5.1.2.1 for ISE of BAEC cells using optimal pulse parameters.

Figure 6.16 shows time courses of the normalized impedance for stimulation of BAEC cells with 100/ 500/ 1000 µM CPT-cAMP (**A**) and delivery of 100 µM 8-OH-cAMP into BAEC cells by *in situ* electroporation (**B**). The impedance profiles after ISE in presence of 8-OH-cAMP were very much comparable with to the impedance profiles observed after treatment of BAEC cells with CPT-cAMP (and forskolin). However, comparison of the time scales for both assays reveals that the maximal values of impedance reached after ISE were slightly shifted/delayed, compared to the maximal impedance values reached after CPT-cAMP (or forskolin) addition. After ISE, maximal (normalized) impedance values were reached within app. 30 min. The reason for such effect was not further investigated, however, one of the possible explanations could be also overlapping of the cell response to the increased concentrations of cAMP and to the ISE itself. On the other hand, the comparison between experiments where cAMP and 8-OH-cAMP were applied as second messengers leads to

conclusion that cell response after delivery of 8-OH-cAMP by ISE appears very similar to the cell response after addition of cAMP to BAEC cells (before ISE was applied). This suggests that the same functional response of BAEC cells - to the increased levels of cAMP was triggered during both experiments.

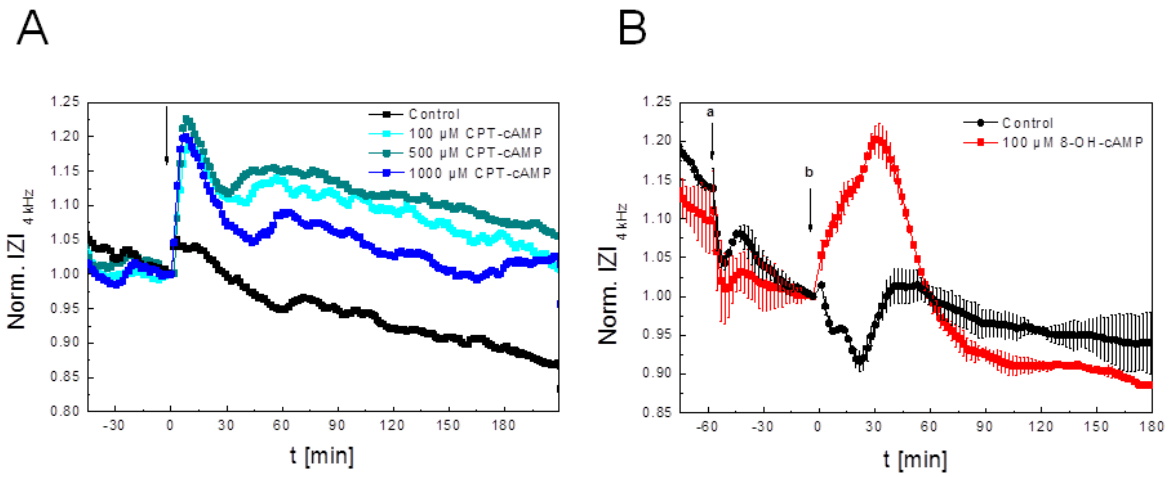

Figure 6.16 The comparison of time courses of the normalized impedance magnitude at 4 kHz before, during and after (**A**) addition of 100/ 500/1000 µM CPT-cAMP and (**B**) *in situ* electroporation of BAEC cells in presence of 100 µM 8-OH-cAMP. Impedance magnitudes were normalized to the last time points before addition (**A**) or electroporation (**B**). The error bars in the graph **B** correspond to the values of standard deviation (mean value ± standard deviation; n=2).

The buffer without calcium EBSS^{+-} was applied as an assay buffer for stimulation of BAEC cells with forskolin and for delivery of 8-OH-cAMP into cells by ISE. During these experiments, constant decrease in impedance signal (drifting) was observed throughout the measurement. This is due to the loosening of cell-cell and cell-substrate contacts which obviously took place over time in absence of calcium. Such trend was observed in both sample and control traces. Interestingly, such signal drifting was not observed when NRK cells were bathed in EBSS^{+-} buffer. This might be a good indicator that NRK cells form tighter cell-cell and cell-substrate contacts than BAEC cells. In addition, maintaining of BAEC cell culture and microscopic images of this cell line indicate that BAEC cells are prone to form rather weak cell-substrate and cell-cell contacts.

Furthermore, the response of BAEC cells to the membrane-permeable cGMP analogue (CPT-cGMP) was investigated. Immediately after addition of 100 µM CPT-cGMP, a rapid increase of impedance signal was observed. Even though response of BAEC cells subjected to CPT-cGMP (sample) and only to the medium (control) was clearly different, fluctuations and rather high variations between the time courses of normalized impedance were

observed when cells were treated with CPT-cGMP. Later on BAEC cells were subjected to ISE in presence of unmodified cGMP (data not shown), however, no significant difference in impedance signal was observed between the cells exposed to cGMP and only to the buffer.
Since calcium acts as a second messenger, increased levels of calcium ions were induced in the cytoplasm of BAEC cells using calcium ionophore calcymicin and cell response was followed impedimetrically. The BAEC cells were exposed to 5 µM calcimycin in $EBSS^{++}$ buffer and after the addition of calcimycin, a small impedance decrease (0.91 ± 0.01) was observed. Thereafter, slow but constant impedance increase was recorded, until the signal stabilized app. 90 min after addition of calcimycin. Such response of BAEC cells was different from the response observed upon treatment of NRK cells with calcimycin. These results showed that influx of calcium into the cytoplasm causes rather small signal change directly after the addition, but it induces slow and constant impedance increase over longer period of time (within almost 2 hours after calcimycin addition). This suggests that BAEC cells respond very slowly to the increased concentrations of calcium and the calcium-specific signaling pathways within BAEC cells require longer time to induce changes in cell morphology measurable by ECIS. Such response of BAEC cells to calcium overlaps with their response after ISE (impedance signal drop and subsequent slow recovery). However, compared to the cell response after stimulation of cAMP-specific signaling pathway (forskolin, CPT-cAMP, cAMP and 8-OH-cAMP), or after treatment of the cells with CPT-cGMP, response of BAEC cells to calcium, recorded by ECIS, appears completely different. Considering the fact that BAEC cells respond to forskolin and CPT-cAMP within first 10 – 20 min after the addition, by the significant impedance increase, and then slow decrease of the signal, reaction of BAEC to calcium is completely opposite (first impedance drop, then slow impedance increase), with much smaller impedance magnitudes. Such results suggest that the presence of calcium in the assay buffer interferes the analysis of BAEC response to membrane-permeable and -impermeable compounds inducing cAMP-specific effects only to a very small extent. This rather small effect of calcium should be taken into account only as a factor which slightly reduces initial impedance increase, when cAMP-or cGMP-specific pathway is activated (e.g. with forskolin, CPT-cAMP, cGMP, 8-OH-cAMP), or slightly enhances immediate impedance drop upon application of electric pulse to BAEC cells.
Nevertheless, studies conducted in this work showed that electroporation allows for successful and rapid loading of BAEC cells with the second messenger 8-OH-cAMP, as elevated cAMP induced activation of cAMP-specific signaling cascades. The concentration-dependent response of BAEC to 8-OH-cAMP was not investigated and it would be the aim of future projects to acquire response of BAEC cells to 8-OH-cAMP in a concentration-

dependent manner. It is reasonable to expect that higher concentrations of 8-OH-cAMP will induce higher levels of intracellular cAMP and thus enhance cAMP-specific response of the cells. Similar study was performed by Amano and collaborators (Amano et al., 2004), who investigated correlation between activation, development and rise in calcium ions (released from intracellular stores) and the level of IP3 delivered into porcine oocytes by (micro)injection. They found that rate of development and duration of the calcium signal rise increased with the increasing concentration of IP3.

On the other hand, Semenov et al., 2013 applied various high-intensity nanosecond pulses (nsEP) to open the cell membrane and release calcium ions from the intracellular compartments. A ratiometric calcium imaging with Fura-2 was applied as a quantifying method after pulsation of CHO-K1 cells in calcium-free medium. Interestingly, the group found that the release of intracellular calcium increases with shorter electric pulses and thus the release of calcium from intracellular stores can be tuned. In addition, 2 mM of external calcium was introduced in the cells by electric pulses and the group was able to measure actual concentration of calcium within the cells.

Dahlgren et al., 2005 employed electroporation from an electrolyte-filled capillary to deliver different energy metabolites into the mouse islets and thus investigate closer the important factors influencing the oscillations in insulin secretion of single islets. They measured fluorescence signal of the islets previously loaded with Fura-2 to calculate intracellular calcium concentrations and during their studies they investigated if and how influx of extracellular calcium (from the buffer) influences the measured calcium concentrations. Interestingly, they found that the increase in calcium concentrations after electroporation with ATP was due to calcium influx through the voltage-gated channels and not due to calcium release from intracellular stores or leakage through the pores. These conclusions correlate well with the conclusions deduced in this work after treatment of BAEC cells with calcimycin, where no significant influence of calcium influx was observed that might affect cAMP or cGMP studies. In fact, Dahlgren and collaborators expected to observe more significant effect of extracellular calcium on oscillations (due to calcium diffusion through the transient pores) however, they found eventually that membrane resealing is a very rapid process, taking place before any higher levels of calcium can enter the cells from the buffer.

An ultimate goal of this project was to investigate if ECIS technology can be applied as a system with dual role: (i) to facilitate delivery of membrane-impermeable biologically active second messengers into the cytoplasm by *in situ* electroporation (ISE) and (ii) to be employed as the analytical method for monitoring of the corresponding cell response. Studies conducted in this work demonstrated that membrane-impermeable second

messenger 8-OH-cAMP was successfully delivered into two cell lines: NRK and BAEC by applying *in situ* electroporation and the respective cell response monitored impedimetrically using ECIS was in agreement with the cell response when both cell lines were treated with the corresponding membrane-permeable compounds inducing increased levels of second messengers within cell cytoplasm. The proof-of-principle assay for delivery of second messengers into confluent cells by ISE was established and evaluated regarding experimental protocol, second messenger probe, assay buffer content and electrode array type. The scope of the future studies on second messengers should be addressing potential concentration dependency of the cell response, further investigation of the cell response regarding calcium influx and correlation between the cell response and level/concentration of applied calcium. The effect of cGMP on BAEC cells might be further investigated and the strategy for delivery of membrane-impermeable cGMP should be reconsidered. Finally, delivery of other second messengers (e.g. IP3) into the cytoplasm by ISE might be considered, based on proof-of-principle assays established in this work and previously discussed reports from the literature.

6.5 References

Adams, S.R., Harootunian, A.T., Buechler, Y.J., Taylor, S.S., and Tsien, R.Y. (1991) Fluorescence ratio imaging of cyclic AMP in single cells. *Nature* 349, 694-697.

Alberts, B., Johnson, A., Lewis, J., Morgan, D., Raff, M., Roberts, K., and Walter, P. (2014) Molecular Biology of the Cell. 6th edition (New York: Garland Science)

Amano, T., Mori, T., and Watanabe, T. (2004) Activation and development of porcine oocytes matured in vitro following injection of inositol 1,4,5-trisphosphate. *Animal Reproduction Science* 80, 101-112.

Beavo, J.A., and Brunton, L.L. (2002) Cyclic nucleotide research-still expanding after half a century. *Nature Reviews Molecular Cell Biology* 3, 710-718.

Boot, J.H., and Van Hilten, J.A. (1996) The use of the divalent calcium-ionophore A23187 as a biochemical tool in pharmacological and in vitro toxicological studies. *Cell Structure and Function* 21, 97-99.

Brooker, G., Harper, J.F., Terasaki, W.L., and Moylan, R.D. (1979) Radioimmunoassay of cyclic AMP and cyclic GMP. *Advances in Cyclic Nucleotide Research* 10, 1-33.

Butt, E., Pohler, D., Genieser, H.G., Huggins, J.P., and Bucher, B. (1995) Inhibition of cyclic GMP-dependent protein kinase-mediated effects by (Rp)-8-bromo-PET-cyclic GMPS. *British Journal of Pharmacology* 116, 3110-3116.

Carafoli, E. (2002) Calcium signaling: A tale for all seasons. *Proceedings of the National Academy of Sciences of the United States of America* 99, 1115–1122.

Carroll, R., Juhasz, A., and Severson, D.L. (1990) Treatment of cardiac myocytes with 8-(4-chlorophenylthio)-adenosine 3',5'-cyclic monophosphate, forskolin or cholera toxin does not stimulate cellular or heparin-releasable lipoprotein lipase activities. *Biophysical Journal* 270, 391-395.

Chavis, P., Mollard, P., Bockaert, J., and Manzoni, O. (1998) Visualization of cyclic AMP-regulated presynaptic activity at cerebellar granule cells. *Neuron* 20, 773-781.

Clapham, D.E. (2007) Calcium signaling. *Cell* 131, 1047-1058.

Dahlgren, G.M., Nolkrantz, K., and Kennedy, R.T. (2005) Effect of intracellular delivery of energy metabolites on intracellular Ca2+ in mouse islets of Langerhans. *Life Sciences* 77, 2986-2997.

DeBernardi, M.A., and Brooker, G. (1996) Single cell Ca2+/cAMP cross-talk monitored by simultaneous Ca2+/cAMP fluorescence ratio imaging. *Proceedings of the National Academy of Sciences of the United States of America* 93, 4577-4582.

Decrock, E., De Bock, M., Wang, N., Bol, M., Gadicherla, A.K., and Leybaert, L. (2015a) Electroporation loading and flash photolysis to investigate intra- and intercellular Ca2+ signaling. *Cold Spring Harbor Protocols* 2, 239-249.

Decrock, E., De Bock, M., Wang, N., Bol, M., Gadicherla, A.K., and Leybaert, L. (2015b) Electroporation loading of membrane-impermeable molecules to investigate intra- and intercellular Ca2+ signaling. *Cold Spring Harbor Protocols* 2, 284-288.

Fang, Y., Ferrie, A.M., Fontaine, N.H., and Yuen, P.K. (2005) Characteristics of dynamic mass redistribution of epidermal growth factor receptor signaling in living cells measured with label-free optical biosensors. *Analytical Chemistry* 77, 5720-5725.

Feschenko, M.S., Stevenson, E., Nairn, A.C., and Sweadner, K.J. (2002) A novel cAMP-stimulated pathway in protein phosphatase 2A activation. *Journal of Pharmacology and Experimental Therapeutics* 302, 111-118.

Fletcher, D.A., and Mullins, R.D. (2010) Cell mechanics and the cytoskeleton. *Nature* 463, 485-492.

Frampton, J.P., Shuler, M.L., Shain, W., and Hynd, M.R. (2008) Biomedical technologies for in vitro screening and controlled delivery of neuroactive compounds. *Central Nervous System Agents in Medicinal Chemistry* 8, 203-219.

Frandsen, S.K., Gibot, L., Madi, M., Gehl, J., and Rols, M.-P. (2015) Calcium electroporation: evidence for differential effects in normal and malignant cell lines, evaluated in a 3D spheroid model. *PLoS One* 10, e0144028.

Gagliardi, P.A., Puliafito, A., di Blasio, L., Chianale, F., Somale, D., Seano, G., Bussolino, F., and Primo, L. (2015) Real-time monitoring of cell protrusion dynamics by impedance responses. *Scientific Reports* 5

Golzio, M., Gabriel, B., Boissier, F., Deuwille, J., Rols, M.P., and Teissie, J. (2003) [Calcium and electropermeabilized cells]. *Journal De La Societe De Biologie* 197, 301-310.

Golzio, M., Mora, M.P., Raynaud, C., Delteil, C., Teissie, J., and Rols, M.P. (1998) Control by osmotic pressure of voltage-induced permeabilization and gene transfer in mammalian cells. *Biophysical Journal* 74, 3015-3022.

Hibino, M., Shigemori, M., Itoh, H., Nagayama, K., and Kinosita, K. (1991) Membrane conductance of an electroporated cell analyzed by submicrosecond imaging of transmembrane potential. *Biophysical Journal* 59, 209-220.

Hofer, A.M., and Lefkimmiatis, K. (2007) Extracellular calcium and cAMP: second messengers as "third messengers"? *Physiology* 22, 320-327.

Howe, A.K. (2004) Regulation of actin-based cell migration by cAMP/PKA. *Biochimica et Biophysica Acta* 5, 2-3.

Kilpatrick, R., and Major, P.W. (1970) The functions of adenosine 3':5'-cyclic monophosphate. *Biochemical Journal* 120, 1P-3P.

Kim, Y.V., Di Cello, F., Hillaire, C.S., and Kim, K.S. (2004) Differential Ca2+ signaling by thrombin and protease-activated receptor-1-activating peptide in human brain microvascular endothelial cells. *American Journal of Physiology - Cell Physiology* 286, C31-C42.

Kinosita, K., Jr., and Tsong, T.Y. (1977a) Voltage-induced pore formation and hemolysis of human erythrocytes. *Biochimica et Biophysica Acta* 471, 227-242.

Kinosita, K., and Tsong, T.Y. (1977b) Formation and resealing of pores of controlled sizes in human erythrocyte membrane. *Nature* 268, 438-441.

Kottra, G., and Fromter, E. (1993) Tight-junction tightness of Necturus gall bladder epithelium is not regulated by cAMP or intracellular Ca2+. II. Impedance measurements. *Pflügers Archiv* 425, 535-545.

Lefkowitz, R.J., Roth, J., and Pastan, I. (1970) Radioreceptor assay of adrenocorticotropic hormone: new approach to assay of polypeptide hormones in plasma. *Science* 170, 633-635.

Lieb, S., Michaelis, S., Plank, N., Bernhardt, G., Buschauer, A., and Wegener, J. (2016) Label-free analysis of GPCR-stimulation: The critical impact of cell adhesion. *Pharmacological Research* 108, 65-74.

Manolopoulos, V.G., and Lelkes, P.I. (1993) Cyclic strain and forskolin differentially induce cAMP production in phenotypically diverse endothelial cells. *Biochemical and Biophysical Research Communications* 191, 1379-1385.

Miller, J.P., Boswell, K.H., Muneyama, K., Simon, L.N., Robins, R.K., and Shuman, D.A. (1973) Synthesis and biochemical studies of various 8-substituted derivatives of guanosine cyclic-3',5' phosphate, inosine cyclic-3',5' phosphate, and xanthosine cyclic-3',5' phosphate. *Biochemistry* 12, 5310-5319.

Montminy, M. (1997) Transcriptional regulation by cyclic AMP. *Annual Review of Biochemistry*, 807–822.

Murad, F., Arnold, W.P., Mittal, C.K., and Braughler, J.M. (1979) Properties and regulation of guanylate cyclase and some proposed functions for cyclic GMP. *Advances in Cyclic Nucleotide Research* 11, 175-204.

Nadella, K.S., Saji, M., Jacob, N.K., Pavel, E., Ringel, M.D., and Kirschner, L.S. (2009) Regulation of actin function by protein kinase A-mediated phosphorylation of Limk1. *EMBO Reports* 10, 599-605.

Nikolaev, V.O., and Lohse, M.J. (2006) Monitoring of cAMP synthesis and degradation in living cells. *Physiology* 21, 86-92.

Novara, M., Baldelli, P., Cavallari, D., Carabelli, V., Giancippoli, A., and Carbone, E. (2004) Exposure to cAMP and β-adrenergic stimulation recruits Ca(V)3 T-type channels in rat chromaffin cells through Epac cAMP-receptor proteins. *The Journal of Physiology* 558, 433-449.

Pearse, D.B., Shimoda, L.A., Verin, A.D., Bogatcheva, N., Moon, C., Ronnett, G.V., Welsh, L.E., and Becker, P.M. (2003) Effect of cGMP on lung microvascular endothelial barrier dysfunction following hydrogen peroxide. *Endothelium* 10, 309-317.

Pressman, B.C. (1976) Biological applications of ionophores. *Annual Review of Biochemistry* 45, 501-530.

Reddy, L., Wang, H.-S., Keese, C.R., Giaever, I., and Smith, T.J. (1998) Assessment of rapid morphological changes associated with elevated cAMP levels in human orbital fibroblasts. *Experimental Cell Research* 245, 360–367.

Reinscheid, R.K., Kim, J., Zeng, J., and Civelli, O. (2003) High-throughput real-time monitoring of Gs-coupled receptor activation in intact cells using cyclic nucleotide-gated channels. *European Journal of Pharmacology* 478, 27-34.

Rickords, L.F., and White, K.L. (1993) Electroporation of inositol 1,4,5-triphosphate induces repetitive calcium oscillations in murine oocytes. *Journal of Experimental Zoology* 265, 178-184.

Rodríguez, A., Martinez, I., Chung, A., Berlot, C.H., and Andrews, N.W. (1999) cAMP regulates Ca2+-dependent exocytosis of lysosomes and lysosome-mediated cell invasion by trypanosomes. *Journal of Biological Chemistry* 274, 16754-16759.

Rols, M.P., and Teissié, J. (1989) Ionic-strength modulation of electrically induced permeabilization and associated fusion of mammalian cells. *European Journal of Biochemistry* 179, 109-115.

Schoen, C.D., Arents, J.C., Bruin, T., and Van Driel, R. (1989) Intracellular localization of secretable cAMP in relaying Dictyostelium discoideum cells. *Experimental Cell Research* 181, 51-62.

Schroder, R., Janssen, N., Schmidt, J., Kebig, A., Merten, N., Hennen, S., Muller, A., Blattermann, S., Mohr-Andra, M., Zahn, S., et al. (2010) Deconvolution of complex G protein-coupled receptor signaling in live cells using dynamic mass redistribution measurements. *Nature Biotechnology* 28, 943-949.

Schroder, R., Schmidt, J., Blattermann, S., Peters, L., Janssen, N., Grundmann, M., Seemann, W., Kaufel, D., Merten, N., Drewke, C., et al. (2011) Applying label-free dynamic mass redistribution technology to frame signaling of G protein-coupled receptors noninvasively in living cells. *Nature Protocols* 6, 1748-1760.

Scott, C.W., and Peters, M.F. (2010) Label-free whole-cell assays: expanding the scope of GPCR screening. *Drug Discovery Today* 15, 704-716.

Semenov, I., Xiao, S., Pakhomova, O.N., and Pakhomov, A.G. (2013) Recruitment of the intracellular Ca2+ by ultrashort electric stimuli: the impact of pulse duration. *Cell Calcium* 54, 145-150.

Serezani, C.H., Ballinger, M.N., Aronoff, D.M., and Peters-Golden, M. (2008) Cyclic AMP: master regulator of innate immune cell function. *American Journal of Respiratory Cell and Molecular Biology: AJRCMB* 39, 127-132.

Smolen, J.E., Stoehr, S.J., and Kuczynski, B. (1991) Cyclic AMP inhibits secretion from electroporated human neutrophils. *Journal of Leukocyte Biology* 49, 172-179.

Spindler, V., Vielmuth, F., Schmidt, E., Rubenstein, D.S., and Waschke, J. (2010) Protective endogenous cyclic adenosine 5'-monophosphate signaling triggered by pemphigus autoantibodies. *The Journal of Immunology* 185, 6831-6838.

Sprenger, J.U., Perera, R.K., Götz, K.R., and Nikolaev, V.O. (2012) FRET microscopy for real-time monitoring of signaling events in live cells using unimolecular biosensors. *Journal of Visualized Experiments: JoVE*, 4081.

Stratowa, C., Himmler, A., and Czernilofsky, A.P. (1995) Use of a luciferase reporter system for characterizing G-protein-linked receptors. *Current Opinion in Biotechnology* 6, 574-581.

Sutherland, E.W. (1972) Studies on the mechanism of hormone action. *Science* 177, 401-408.

Tinel, H., Kinne-Saffran, E., and Kinne, R.K. (2000) Calcium signalling during RVD of kidney cells. *Cellular Physiology and Biochemistry* 10, 297-302.

Tran, Q.-K., Ohashi, K., and Watanabe, H. (2000) Calcium signalling in endothelial cells. *Cardiovascular Research* 48, 13-22.

Volker, T.T., Pianet, I., Labouesse, J., and Teissie, J. (1989) Signal transduction by membrane receptors in viable electropermeabilized cells: isoproterenol-stimulated cyclic AMP synthesis in C6 glioma cells. *Biochimica et Biophysica Acta* 984, 243-251.

Wegener, J., Zink, S., Rosen, P., and Galla, H. (1999) Use of electrochemical impedance measurements to monitor beta-adrenergic stimulation of bovine aortic endothelial cells. *Pflügers Archiv – European Journal of Physiology* 437, 925-934.

Wolf, P., Rothermel, A., Beck-Sickinger, A.G., and Robitzki, A.A. (2008) Microelectrode chip based real time monitoring of vital MCF-7 mamma carcinoma cells by impedance spectroscopy. *Biosensors and Bioelectronics* 24, 253-259.

Zhang, R., and Xie, X. (2012) Tools for GPCR drug discovery. *Acta Pharmacologica Sinica* 33, 372-384.

Zink, S., Rösen, P., Sackmann, B., and Lemoine, H. (1993) Regulation of endothelial permeability by beta-adrenoceptor agonists: contribution of beta 1- and beta 2-adrenoceptors. *Biochimica et Biophysica Acta* 1178, 286-298.

7 Delivery of Aptamers into Cells

7.1 Introduction

Aptamers are usually short single- or double-stranded oligonucleotides (DNA, RNA) or peptide molecules designed to bind certain targets, differing in size from very small to big molecules, having simple or complex structures and they are even capable of binding the whole cells or viruses. Target recognition with high affinity and specificity is possible due to the fact that aptamer changes its three-dimensional conformation upon binding to its target. The name of aptamer comes from the Latin *aptus* – to fit and Greek *meros* – part. The credit for the discovery of aptamers belongs to two groups of researchers, who independently found and described the process of selection of aptamers in 1990. The lab of Larry Gold and Craig Turk called it SELEX process: **s**ystematic **e**volution of **l**igands by **ex**ponential enrichment, as they demonstrated the selection of RNA ligands against T4 DNA polymerase (Tuerk and Gold, 1990) and the lab of Andrew Ellington and Jack Szostak described an *in vitro* selection of RNA molecules binding to a variety of organic dyes (Ellington and Szostak, 1990, 1992).

The process of selection of specific aptamer (SELEX protocol), starting from a large pool of random sequences is depicted in **Figure 7.1** and it can be performed manually at the bench top or with the fully automated equipment, which has been developed over past years.

The initial screening library used to generate specific aptamers consists of vast numbers of potential ligands, usually 10^{13} – 10^{16} of random oligonucleotides, which can be screened rapidly (Sampson, 2003). The pool with random nucleic acids is incubated together with the target of interest and all bound molecules are separated from the unbound molecules which can be removed. Bound molecules are eluted and nucleic acids are amplified in the next step using PCR (polymerase chain reaction), so they can serve as an enriched nucleic acids library within the next cycle. It is necessary to perform 8 – 15 cycles (Luzi et al., 2003) in order to obtain specific aptamers with high affinity to the target, which can be further cloned, sequenced and optimized. After successful SELEX procedure, there are usually several aptamers identified and each can be further tested for its binding properties to the target. Additionally, some modifications can be added, for example: 2′-fluoro or 2′-O-methyl, to increase *in vivo* stability of an aptamer (Pendergrast et al., 2005), as well as some other modifications and labels like: fluorescence marker, thio, phosphorothioate and others.

Recently, the SELEX process has been modified and adapted to generate (DNA) aptamers binding specifically to a certain cell type (cell-SELEX). These aptamers hold a great therapeutic potential, as they are able to distinguish between different cell types of interest

or, for instance, cancer cells from normal cells (Sefah et al., 2010).

Aptamers are relatively short oligonucleotides, containing in most cases 12 – 80 nucleobases (Meyer et al., 2011). The binding affinity of aptamers highly depends on its target and it ranges from the picomolar (10^{-12} M) to the nanomolar scale (10^{-7} M) for different protein targets (Cho et al., 2009). Since their discovery in 1990, hundreds of aptamers against various types of targets have been generated, whereby targets range from very small molecules (e.g. organic dyes, antibiotics, amino acids, etc.), over proteins and peptides (e.g. enzymes, growth factors, immunoglobulins, HIV-related proteins, etc.) to viruses and cells (Pendergrast et al., 2005).

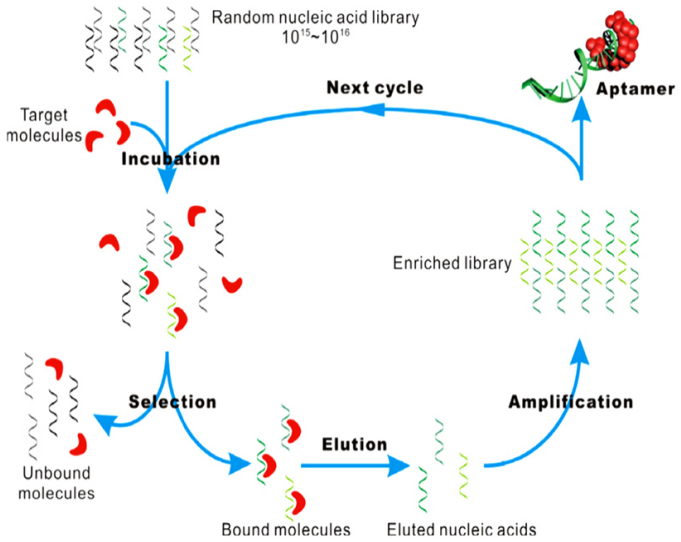

Figure 7.1 SELEX protocol starts with a nucleic acids library with the large number of random sequences, mixed with the target. Unbound molecules are removed and bound molecules are further eluted to obtain eluted nucleic acids which can be amplified by PCR in a next step and serve as enriched library of nucleic acids in a following cycle of SELEX. Procedure takes usually 8 – 12 cycles until several specific aptamers are obtained and can be further tested and optimized. Scheme adapted from Song et al., 2008; © 2008 Elsevier Ltd. doi:10.1016/j.trac.2007.12.004.

Aptamers, also referred to as chemical antibodies, have become important alternative to the antibodies and even tend to replace them in the scope of some application aspects (Jayasena, 1999). Some of the most important advantages of aptamers over antibodies are: chemical *in vitro* production of aptamers does not require any organisms, nor cellular biochemistry, which makes it free of contamination, much quicker, more scalable, simpler and thus more cost-effective, whereas batch-to-batch variations common for antibodies can be eliminated, as aptamers are purified to a high degree after production (Luzi et al., 2003). Whereas antibodies are larger in size, sensitive to irreversible denaturation and often

immunogenic, aptamers are small enough to enter many biological compartments (high bioavalibility and biodistribution) and to be released rapidly from the bloodstream. In most cases, aptamers can be reversibly denaturated and thanks to a variety of available modifications, their resistance to nucleases and thus stability can be significantly enhanced (Keefe et al., 2010). In addition, they are non-immunogenic. Both aptamers and antibodies, have binding affinities to their targets ranging from picomolar to higher nanomolar scale. But aptamers can be selected against virtually any target, and they can be selected to bind specific region of the target and keep the specific binding properties even under different binding conditions and storage in different buffers and solvents (Ireson and Kelland, 2006). Still, when choosing the appropriate aptamers, it is important to take into account that there are certain differences between DNA and RNA counterparts: although RNA molecules offer more (structural) versatility and diversity compared to DNA, selection procedure for DNA aptamers is simpler and the libraries including DNA molecules are usually available at lower price compared to those for RNA. Furthermore, DNA molecules are less susceptible to hydrolysis than RNA and thus the final DNA aptamers have higher level of stability than the RNA (Orava et al., 2010).

For all above mentioned highly appreciated properties, aptamers have become emerging candidates for various applications in therapy (White et al., 2000), diagnostics (Brody and Gold, 2000) and for various analytical applications (Scheller et al., 2001). For therapeutical applications, aptamers can be developed for wide range of targets present intracellularly, extracellularly or on the cell-surface. The choice of last two cases has an advantage of avoiding a cell membrane as a barrier for aptamers to reach their targets (Keefe et al., 2010). At the moment, there are several aptamers being evaluated for commercial applications and before they find their way to the market, various stages of pre-clinical trials have to be completed. So far, one aptamer managed to accomplish all necessary requirements and is now present on the market as a therapeutic agent under the name Macugen Pegaptanib (produced by Eyetech Pharmaceuticals and Pfizer). This RNA aptamer is selected against vascular endothelial growth factor (VEGF)-165 and is highly effective in treatment of choroidal neovascularization associated with age-related macular degeneration (Ng et al., 2006). Some of the aptamers currently being under study for commercial therapeutical applications are: aptamer AS1411 (targeting nucleolin) that induces mRNA instability, as well as the cytotoxicity in MCF-7 and MDA-MB-231 cells (Soundararajan et al., 2008); aptamer REG-1, or more precisely factor IXa-inhibiting aptamer RB-006, which is under development by Regado Biosciences and can serve as an anticoagulant system for potential treatment of arterial thrombosis (Becker and Chan, 2009). Many aptamers appropriate for systemic

administration have been developed recently. Most of their targets are in the bloodstream (e.g. thrombin) or on the cell-surface, such as epidermal growth factor receptor (EGFR). To obtain an effective anticancer drug, aptamer can be developed either as agonist or as antagonist for cancer-related receptors (Keefe et al., 2010; Ireson and Kelland, 2006). Great efforts to implement aptamers in different applications in therapy are based on their characteristics: high specificity and affinity, biological efficacy, predictable pharmacokinetics, relative nuclease resistance and stability, rapid clearance, non-toxicity, non-immunogenicity and chemical production process which is scalable and inexpensive (Pendergrast et al., 2005).

Furthermore, aptamers are very applicable for bioimaging as they are not cytotoxic. Conjugated to a fluorophore, quantum dots or some other kinds of material, aptamers can be easily applied for imaging of cells or single proteins (Song et al., 2012; Dirks and Tanke, 2006). Over time, a special type of oligonucleotides has been developed, so-called optical switches or molecular beacons, which are short nucleic acids very similar to aptamers. The specific advantage of optical switches is that they can turn on or modify their light emission upon binding to the specific target and thus hold a great potential as very promising optical nanosensors (Giannetti et al., 2013; Huang and Martí, 2012). Thus, there is a range of oligonucleotides developed to be a recognition element coupled with fluorescent labels in order to provide highly sensitive and selective assays (Juskowiak, 2011; Nutiu and Li, 2005).

For their numerous valuable features, great potential of aptamers for various analytical applications was quickly recognized. Since aptamers can be rapidly synthesized at low costs and then easily modified with various functional groups, linkers, fluorescent labels or reporter molecules (Luzi et al., 2003), many possibilities for their incorporation in sensors or biosensors were found. A (bio)sensor based on aptamer as a recognition element is called an aptasensor (Lim et al., 2009). They are an alternative to antibodies for the detection of proteins and small molecules, whereby different types of assays can be considered: switching, sandwich, competitive and dissociation (or displacement) (Han et al., 2010), also in the combination with antibodies. Thereby, aptamers can be immobilized on the different types of solid support and on the electrodes made of different materials. For example, a conventional antibody sandwich assay has been modified by using aptamers as a capturing moiety. The aptamer targeting cytochrome c is linked to multi-walled carbon nanotube screen printed electrode (via diazonium electrochemical grafting). A biotinylated antibody against cytochrome c is then applied in a sandwich type of assay to improve selectivity of the biosensor. Detection of the binding events is conducted by electrochemical impedance spectroscopy and using a streptavidin-gold nanoparticle conjugate (Ocaña et al., 2015). In

general, various methods can be employed in order to obtain highly specific aptamer-based competitors of traditional immunochemical assays (Radi, 2011). Within the bioanalytical techniques, aptamers represent a recognition element to target an analyte, whereas translation of the biorecognition event into the electrical signal can be conducted by SPR, BLI, or QCM techniques, as a physical transducer (Luzi et al., 2003; Zichel et al., 2012; Roh et al., 2011). Aptamer-based biochemical biosensors develop and expand rapidly (Velasco-Garcia and Missailidis, 2009) and thanks to their unique characteristics, aptamers can be employed within various analytical techniques: electrochemical, colorimetric, optical, or mass-sensitive methods (Song et al., 2012). Since aptamers are quite small and their molecular mass is usually around 10 kDa, there are claims that they can diffuse into cells and even serve as the carrier for other nucleic acids (Stanlis and McIntosh, 2003). Aptamers binding to internalized cell surface receptors are developed to deliver drugs, toxins, siRNA, or some other non-permeable cargos into the cells. An example is given with the prostate-specific membrane antigen (PSMA), as a valuable marker for prostate cancer and aptamer against this target has been extensively studied (Song et al., 2012). The aptamer-drug chimeras are based on the recognition and binding of aptamers to the (prostate cancer) cell and subsequent cell uptake of aptamers (together with the conjugated drug) by the mechanism of endocytosis. Thus, drug can be delivered into the target cell (Meyer et al., 2011). Drug delivery to tumor cells facilitated by aptamers as a vehicle has been widely described in a literature (Zhang et al., 2011).

7.1.1 Methods for Delivery of Aptamers into Living Cells

Aptamers are composed of negatively charged oligonucleotides or peptides. Due to their total negative charge and their size, aptamers cannot cross the cell membrane and their bioavailability is thus significantly restricted. Nevertheless, it is of crucial importance for aptamers directed against intracellular targets to enter the cell cytosol and be able to reach their targets. Especially because many targets important in therapy, diagnostics or analytics are inside the cell interior and require an agent/ligand to cross the cell envelope. The same is valid for imaging of specific cell structures and examination of a certain target.

The importance of intracellular targets is mirrored in the recent struggles to develop RNA aptamers which can be synthesized directly by transcription machinery of the cells and which would be used to target certain proteins in their natural environment. The aptamers aiming for targets within the cell cytosol are also referred to as intramers and can be excellent tools to specifically inhibit signal transduction, cell growth, transcription, translation, or some other intracellular processes (Famulok et al., 2000; Blind et al., 1999). In any case, for practical

therapeutic applications *in vivo* systems have to be considered, as the delivery of aptamers into living cells becomes even more difficult in that case. So far, most of the methods for aptamer delivery into cells rely on standard protocols applied for antisense and siRNA oligonucleotides (Meyer et al., 2011). Using lipid-based chemical transfection, an RNA aptamer against N-terminal part of cytohesin-2 was delivered into cells (Theis et al., 2004). Furthermore, liposomes as a carrier have been employed to construct Apt-PEG-LPs (aptamer-polyethylene glycol-liposome) system in order to target primary cultured mouse tumor endothelial cells (mTEC) *in vitro* and *in vivo* (Ara et al., 2014). For the delivery of optical switches (molecular beacons) into various cell types, either microinjection, or different compounds (Streptolysin O, Lipofectamine, polyethylenamine, etc.) have been used (Giannetti et al., 2013).

It has been reported that some aptamers like RNA aptamer with specificity for the human IL-6 receptor (IL-6R) can be taken up by the cells via macropinocytosis or receptor mediated endocytosis (Meyer et al., 2012). A distribution and metabolism of fluorescently-labeled oligonucleotides within the cells after microinjection was evaluated earlier using confocal fluorescence microscopy (Fisher et al., 1993). To compare different available methods, single- and double-stranded DNA molecules were introduced into living cells using electroporation, microinjection and lipid-based transfection. For comparison, same DNA molecules were also added to fixed cells with disrupted membrane (Bamford et al., 2014). The transfection efficiency and DNA integrity within the cells was evaluated by the fluorescence resonance energy transfer (FRET) technology, relying on the close proximity of two compatible fluorophores Cy3 and Cy5. Moreover, a possibility to apply aptamers as probes for protein localization in the cells was studied after diffusion of oligonucleotides (ssDNA) into aldehyde-permeabilized mammalian (PtK1) cells (Stanlis and McIntosh, 2003). Interestingly, a group of M. Berezovski selected DNA aptamers targeting cell organelles and nucleus of cancer cells in order to induce cell death. They selected aptamer NAS-24 binding to vimentin (intermediate filament protein) and delivered it into cells by natural polysaccharide arabinogalactan as a carrier reagent (Zamay et al., 2014). NAS-24 caused apoptosis of mouse ascites adenocarcinoma cells *in vitro* and *in vivo*, whereby the mixture of arabinogalactan and aptamer was injected intraperitoneally into mice.

Due to all above mentioned virtues of aptamers and the great potential they hold, there is an emerging interest to find an appropriate strategy to facilitate their fast entry into the cytosol and thus support targeting of numerous intracellular targets. *In situ* electroporation offers rapid delivery of unmodified “naked” aptamers into the cells. In order to demonstrate applicability of electroporation as an appropriate system for delivery of aptamers into cells,

proof-of-principle experiments were performed in this work. Fluorescently-labeled aptamers with random non-targeting sequence have been chosen as a model aptamer. Two DNA aptamers (APT 1 and APT 2) were tested within this study and both of them contained 50 nucleobases, had same molecular mass and only differed with respect to their sequence (details given in chapter 4.4.1.1). As a fluorescent label, fluorescein with absorption of the light at 488 nm was chosen and the label was linked to 5'- end. As illustrated in **Figure 7.2**, after successful delivery of aptamers into the cells (by transfection), bright green fluorescence should be observed within the cell interior, using confocal laser scanning microscopy (CLSM). No specific binding was expected.

Different cell lines were applied as a model system and delivery of aptamers by *in situ* electroporation was compared to their delivery by chemical lipid-based transfection, as a widespread conventional transfection method. Besides living cells, fixed and permeabilized cells were also loaded with aptamers.

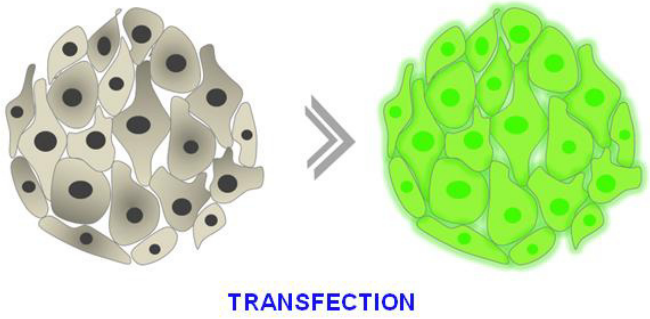

Figure 7.2 Schematic illustration showing adherent cells before (left) and after (right) their transfection in presence of fluorescently-labeled DNA aptamers. Successful delivery of aptamers into cells should induce bright green fluorescence signal coming from the cytosol.

7.2 Delivery of Aptamers into NRK Cells

7.2.1 Delivery of Aptamers by *In Situ* Electroporation

NRK cells were applied as a first cell model to study an introduction of fluorescently-labeled DNA aptamers into confluent mammalian cells using three different strategies. For this, two similar aptamers were used, which only differed in their sequences. Experimental procedure for *in situ* electroporation was performed for both aptamers in a completely same manner, according to the experimental protocol described in chapter 4.2.2.4).

Aptamer 1

The experimental procedure for *in situ* electroporation of NRK cells in presence of fluorescein-labeled DNA aptamer 1 (abbreviated APT 1) was optimized with respect to the different experimental parameters: array preparation, working volume, aptamer concentration, duration of impedimetric measurement and microscopy conditions.

Experiments were performed in EBSS^{++} buffer and working volume was 40 µL per well. During optimization process, a single electroporation pulse was applied to the cells in presence of lower aptamer concentrations: 2, 4 and 6 µM (data not shown). As such conditions produced only some unspecific fluorescence signals, strategy of multiple successive electroporation pulses (three times) was further employed and aptamer concentrations in the bathing fluid were increased. Concentration of APT 1 was varied in a range from 10 to 20 µM (data not shown) and since the samples with 15 µM of APT 1 showed quite satisfactory staining of the cells, it was decided to proceed with this concentration for all further electroporation studies involving aptamers.

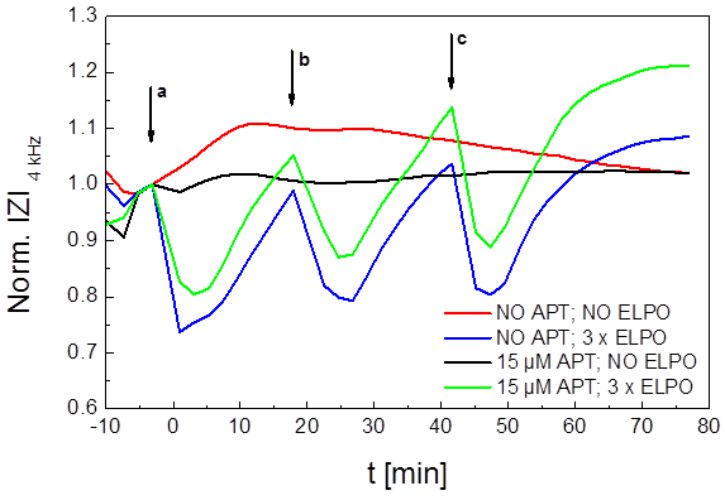

Figure 7.3 Typical time course of the normalized impedance at 4 kHz before, during and after *in situ* electroporation of NRK cells in presence of 15 µM APT 1. ISE was applied three times successively - **a**: 1st pulse, **b**: 2nd pulse and **c**: 3rd pulse application, using optimal combination of pulse parameters for this cell line: 40 kHz, 4 V and 200 ms. Impedance values are normalized to the last time point before first electroporation pulse was applied. After recovery of the cells, impedance measurement (at 37 °C) was finished and microscopy by CLSM followed to evaluate electroporation efficiency.

Strikingly, concentration of 10 µM APT 1 did not provide nice and clear staining of the cell structures but rather unspecific, whereas 20 µM of APT 1 gave clear and bright staining of NRK cells, with some additional unspecific background signal originating from the cells which

were not electroporated. Therefore, it was concluded that concentration of aptamer 15 µM is sufficient and aptamers were applied at this concentration for studies of delivery by ISE.

Figure 7.3 shows typical time course of the normalized impedance during *in situ* electroporation of NRK cells in presence of 15 µM APT 1. The experiment was conducted on 8W4Eµ electrode array and NRK cells were electroporated three times successively, as indicated by the arrows - a: 1st pulse, b: 2nd pulse and c: 3rd pulse application, using optimal combination of pulse parameters for this cell line: 40 kHz, 4 V and 200 ms. Impedance measurement is presented at 4 kHz and data are normalized to the last time point before first electroporation pulse was applied. After every pulse application, impedance decreased and it was waited until the impedance signals returned to the pre-pulse values before next pulse was applied. After the third pulse, cells were allowed to fully recover before impedance measurement was finished. Buffer containing fluorescent aptamers was removed and microscopy by CLSM followed in order to document micrographs and thus estimate electroporation efficiency. Corresponding controls where cells were exposed to aptamers without pulse application and where cells were electroporated in absence of aptamers were acquired during the experiment.

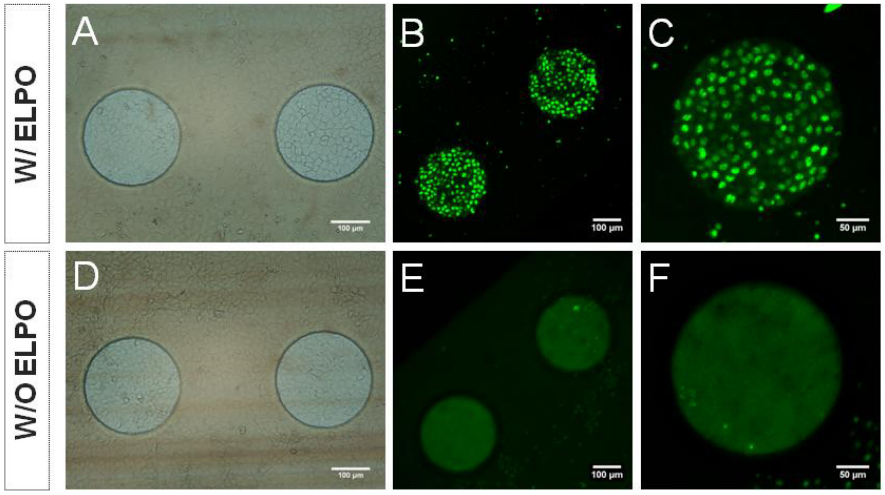

Figure 7.4 Exemplary phase-contrast (**A**, **D**) and confocal fluorescence micrographs (**B**, **C**, **E**, **F**) taken after *in situ* electroporation was applied for delivery of 15 µM APT 1 into NRK cells. Experiment was performed at 37 °C. All fluorescence micrographs were taken using the same imaging settings for comparison. The scale bar in micrographs **A**, **B**, **D** and **E** corresponds to 100 µm and in the micrographs **C** and **F** to 50 µm. All micrographs were taken using 10-fold magnification objective.

Micrographs presented in **Figure 7.4** were taken with 10-fold magnification objective and confocal fluorescence micrographs **B** and **E** were additionally zoomed 1.5 times, whereas

confocal fluorescence micrographs **C** and **F** were zoomed 3.5 times to obtain a better insight into localization of aptamers within the cells. Micrographs in the top row (**A**-**C**) show NRK cells exposed to 15 µM APT 1 and electroporation (applied three times) during impedance measurement, whereas the cells in the lower panel (**D**-**F**) were subjected to 15 µM APT 1 in absence of electric pulses. By observing the phase-contrast micrographs (**A** and **D**), no considerable difference between the cells in a sample and control are visible. However, fluorescence micrographs (**B**, **C**, **E** and **F**) reveal the difference in appearance of the cells on the gold film electrodes. NRK cells directly on the electrodes (**B**), exposed to electroporation in presence of aptamers appear bright green and aptamers were mostly localized within the cell nuclei (**C**), which appear brighter than the cytoplasm. Cells present on the photopolymer surrounding the electrodes appear dark as they did not receive electric pulses and aptamers could not enter their cytosol. The latter situation was observed in the control (**E** and **F**) as well, where aptamers could not enter the cells via electroporation and therefore cells appear dark. All fluorescence micrographs were taken using the same imaging settings.

In all micrographs, the area of circular electrodes appears slightly brighter than the background. This can be explained by the fact that cells were not extensively washed before microscopy and the small amount of fluorescent probe remained in the buffer during imaging, while at the same time gold electrode surface reflects the light. Similar effect was observed during some dye loading studies, where FITC-dextran was applied as a fluorescent probe. Micrographs corresponding to the controls where cells were exposed to electroporation in absence of aptamers are not presented here. As expected, fluorescence signal was neither detected in the cells on the electrodes, nor in the cells of the background.

After impedance measurement was finished, cells were stained with specific marker for acidic cell organelles lysosomes, so-called LysoTracker®. Micrographs were taken with 60-fold magnification objective in order to evaluate localization of aptamers within the cell interior and investigate if there is a co-localization of aptamers and LysoTracker®.

Figure 7.5 shows exemplary phase-contrast micrograph (**A**) and confocal fluorescence micrographs (**B**-**E**) taken during microscopy. Fluorescence micrograph **B** shows an accumulation of aptamers predominantly in the nuclei, whereas fluorescence signal in the cytoplasm is observed only to some lower extent. Image **C** shows the staining of lysosomes by LysoTracker® and overlay in **D** shows no co-localization of the lysosome marker with the fluorescent aptamer. Fluorescence micrograph **E** is taken with 2x zoom to better visualize previous observations. Although this is visible already at the images taken with 10-fold magnification, images taken with higher magnification objective (**B-E**) show even better that APT 1 accumulated in cell nucleus and stained nucleoli, which appear brighter than the rest

of nucleus. From the micrographs **B** in **Figure 7.4** and **Figure 7.5** is concluded that most of the cells present on the electrodes were successfully loaded with APT 1. Corresponding phase-contrast micrographs (**A**) reveal this cannot be attributed to the damaged or missing cells, as fully confluent cell monolayer was present on the electrodes.

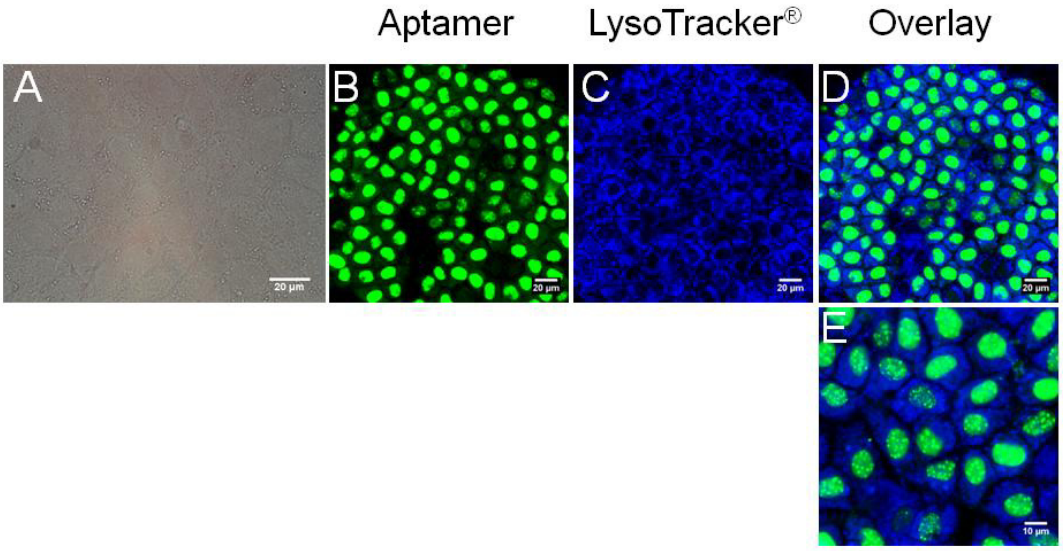

Figure 7.5 Typical phase-contrast (**A**) and confocal fluorescence micrographs (**B-E**) taken after *in situ* electroporation was applied for delivery of 15 µM APT 1 into NRK cells and the lysosome marker LysoTracker® was applied to stain lysosomes. Scale bar in micrographs **A**, **B**, **C** and **D** corresponds to 20 µm and in micrograph **E** to 10 µm. All micrographs were taken with 60-fold magnification objective.

Aptamer 2

To compare loading and localization pattern with APT 1, DNA aptamer 2 (abbreviated APT 2) with the concentration 15 µM was applied for *in situ* electroporation of NRK cells in $EBSS^{++}$ (**Figure 7.6**). Experimental procedure was conducted using electrode array 8W4Eµ and NRK cells were electroporated three times successively (using optimal combination of pulse parameters for this cell line: 40 kHz, 4 V and 200 ms), as indicated by the arrows - a: 1^{st} pulse, b: 2^{nd} pulse and c: 3^{rd} pulse application.

Typical time course of the normalized impedance at 4 kHz is presented in **Figure 7.6** and normalization of the data was applied to the last time point before first electroporation pulse. After every pulse application, impedance signal decreased and it was waited until impedance signals returned to the pre-pulse values before the next pulse was applied, which was not the case after the second pulse. It seems that cells recovered slower after second pulse than after the first one, but the reason for that is unknown. Nevertheless, the third pulse was

applied and cells were allowed to fully recover before impedance measurement was finished. Microscopy by CLSM followed in order to document corresponding electroporation efficiency.

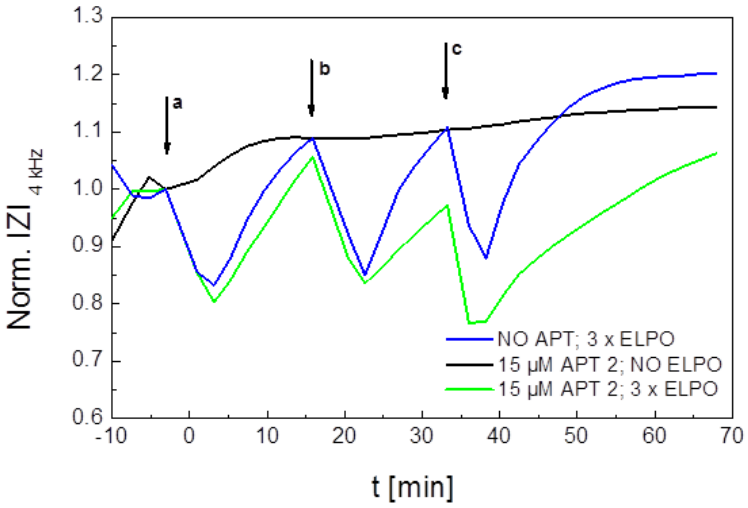

Figure 7.6 Typical time course of the normalized impedance at 4 kHz before, during and after *in situ* electroporation of NRK cells in presence of 15 µM APT 2. ISE was applied three times successively - **a**: 1st pulse, **b**: 2nd pulse and **c**: 3rd pulse application, using optimal combination of pulse parameters for this cell line: 40 kHz, 4 V and 200 ms. Impedance values are normalized to the last time point before first electroporation pulse was applied. After recovery of the cells, impedance measurement (at 37 °C) was finished and microscopy by CLSM followed to evaluate electroporation efficiency.

The cells exposed to APT 2 and ISE and the cells exposed to APT 2, but not subjected to ISE were imaged and typical micrographs are summarized in **Figure 7.7**. Micrographs were taken with 10-fold magnification objective for the sample (**A**-**C**) and control (**F**-**H**). Confocal fluorescence micrographs **B** and **G** were additionally zoomed 1.5 times and a clear difference between NRK cells incubated with APT 2 in presence (**B**) and absence (**G**) of electric pulses is visible. Confocal fluorescence micrograph **C** shows one of the electrodes zoomed 3 times and it reveals localization of APT 2 predominantly in the nuclei. This observation was supported with 60-fold magnification images (**D** and **E**).

The phase-contrast micrographs (**A** and **F**) show no difference between the cells in the sample and control. However, it is noticeable that loading of NRK cells with APT 2 was not as successful as with APT 1, since the number of loaded cells on the electrodes was smaller when APT 2 was applied as a probe, compared to APT 1. Apart from some minor unspecific signals observed for the cells surrounding the electrodes (background), overall, these cells appeared dark and the same was true for the whole cell population of the controls.

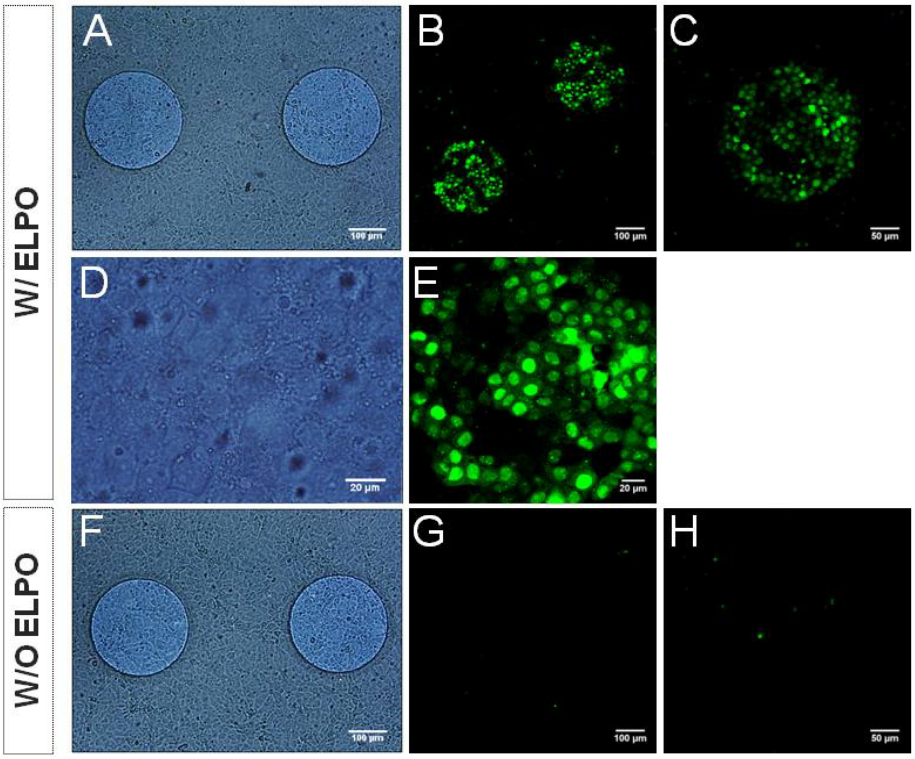

Figure 7.7 Exemplary phase-contrast (**A**, **D**, **F**) and confocal fluorescence micrographs (**B**, **C**, **E**, **G**, **H**) taken after *in situ* electroporation was applied for delivery of 15 µM APT 2 into NRK cells. Experiment was performed at 37 °C. The scale bar in micrographs **A**, **B**, **F** and **G** corresponds to 100 µm, in micrographs **C** and **H** to 50 µm and in micrographs **D** and **E** to 20 µm. Micrographs were taken with 10-fold (**A-C** and **F-H**) and with 60-fold (**D-E**) magnification objective.

Fluorescent Aptamer versus Conventional Fluorescent Probe

During work with fluorescently-labeled aptamers (APT 1 and APT 2), it was noticed that they mostly accumulate within the nuclei and to some lower extent in the cytoplasm. This was in contrast with the loading pattern of fluorescently-labeled dextrans (FITC-dextran) applied as common fluorescent probes for *in situ* electroporation so far.

From such observations arose several questions and therefore, an additional experiment was performed to directly compare electroporation efficiency and localization of aptamer and FITC-dextran within the cells. Aptamer APT 1 has a size of ~ 16 kDa and fluorescein label linked to the oligonucleotide. Fluorescently-labeled FITC-dextran was chosen in a similar size (10 kDa) in order to have two as much as possible comparable fluorescent probes. NRK cells were electroporated (using optimal combination of pulse parameters: 40 kHz, 4 V and 200 ms) in presence of these two fluorescent probes in parallel on 8W4Eµ electrode array. Confluent monolayers of NRK cells were exposed to *in situ* electroporation in presence of either 15 µM APT 1, or 2 mg/mL of 10 kDa FITC-dextran. Appropriate controls for both

probes (without pulse application) were included, as well as a common control for electroporation with NRK cells being electroporated in absence of any fluorescent probe. After three successive electroporation pulses, cells were allowed to recover. Thereafter, buffer containing fluorescent probes was removed and microscopy by CLSM was conducted. Exemplary micrographs are summarized in **Figure 7.8**.

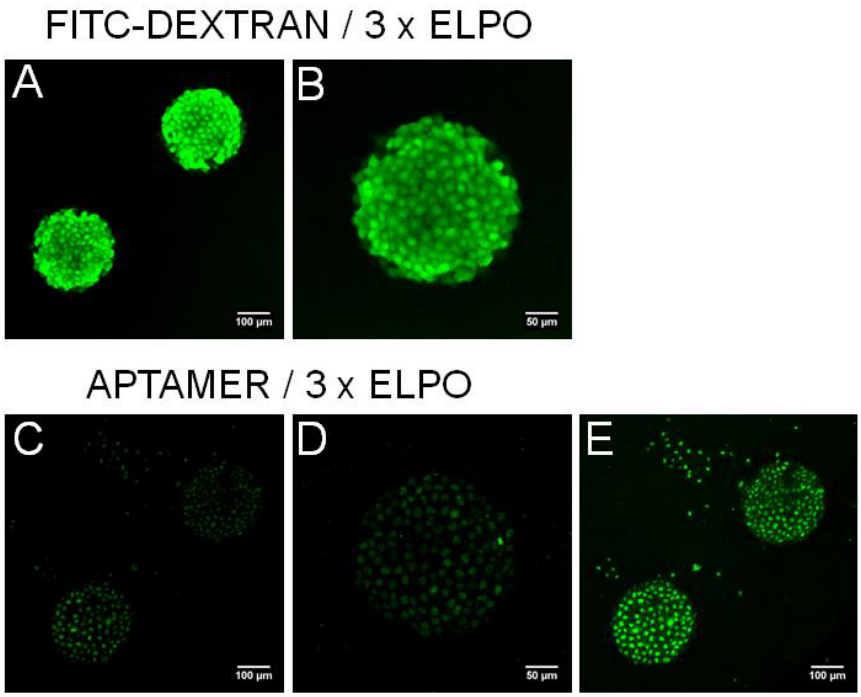

Figure 7.8 Exemplary confocal fluorescence micrographs taken after *in situ* electroporation of NRK cells in presence of either 2 mg/mL FITC-dextran (**A** and **B**), or in presence of 15 µM APT 1 (**C-E**). Experiment was performed at 37 °C. Fluorescence micrographs **C** and **E** show the same cell population, except the image **E** was taken with the higher detector gain. The scale bar in micrographs **A**, **C** and **E** corresponds to 100 µm, whereas in the micrographs **B** and **D** scale bar corresponds to 50 µm. All micrographs were taken with 10-fold magnification objective.

Since there was a certain difference in fluorescence intensity (FITC-dextran appeared much brighter than APT 1), imaging settings were adjusted with respect to both probes and were kept constant during microscopy in order to obtain comparable results. All images were taken with 10-fold magnification objective, whereby **A**, **C** and **E** were zoomed 1.5 times and **B** and **D** 3 times. Fluorescence micrographs **A** and **B** show bright and homogenous fluorescence signal coming from the cytoplasm and nuclei of NRK cells electroporated in presence of FITC-dextran. Fluorescence micrographs **C** and **E** show that NRK cells electroporated in presence of APT. NRK cells on electrodes in **C** showed rather weak fluorescence, although it was evident that fluorescence signal originates mostly from the cell nuclei. Micrograph **E**

shows the same population of NRK cells as in **C**, only with the gain set to a higher value to better visualize localization of aptamer within NRK cell bodies. In addition, micrographs showing cells exposed to APT 1 revealed some unspecific uptake of aptamer by the cells of the background (not exposed to electroporation). A loading pattern between these two fluorescent probes is obvious as 10 kDa FITC-dextran is homogeneously distributed in both cytoplasm and nuclei, whereas aptamer (~ 16 kDa) is localized mostly within the cell nuclei.

7.2.2 Delivery of Aptamers by Chemical Transfection

To make a comparison between aptamer delivery by *in situ* electroporation and aptamer delivery by widespread chemical lipid-based transfection (abbreviated CH TR), commercial chemical transfection reagent Lipofectamine® was applied. NRK cells were chemically transfected in presence of aptamers APT 1 and APT 2 and results are described within this chapter.

Aptamer 1

NRK cells were chemically transfected in presence of 206 nM APT 1 according to the common protocol (described in chapter 4.4.2.2) and as recommended by manufacturer, transfection efficiency was evaluated after app. 4 hours. Exemplary phase-contrast and confocal fluorescence micrographs taken by CLSM with 10-fold magnification objective are summarized in **Figure 7.9**. Micrographs **A**, **B** and **C** show NRK cells app. 4 hours after chemical transfection in presence of 206 nM APT 1, whereas **D**, **E** and **F** show corresponding control, where NRK cells were not chemically transfected, but only incubated with 206 nM APT 1 for 4 hours. Whereas in phase-contrast micrographs no difference between the sample and control cells was observed, fluorescence micrographs reveal the difference between them. Fluorescence micrographs **B** and **E** were additionally zoomed 1.5 times, however, staining pattern and localization of APT 1 within the cells can be better visualized in micrograph **C** (**C** and **F** were zoomed 3 times). Even though chemical transfection reagent allowed for introduction of APT 1 into NRK cells, fluorescence signal was clearly not found within cell nuclei. Based on punctuated fluorescence pattern seen on the micrographs **B** and **C,** it is concluded that aptamer accumulated predominantly in the cell vesicles. In addition, no cytoxicity after chemical transfection was observed. As indicated in **E** and **F**, in absence of chemical transfector, aptamer could not enter NRK cells and cells appeared completely dark. In addition, marker for acidic cellular compartments lysosomes LysoTracker® was added to the cells, in order to evaluate if there is any co-localization with the aptamer. Phase-contrast and confocal fluorescence micrographs were taken with 60-fold

magnification objective app. 5 hours after chemical transfection in presence of 206 nM APT 1. Exemplary micrographs are summarized in **Figure 7.10**.

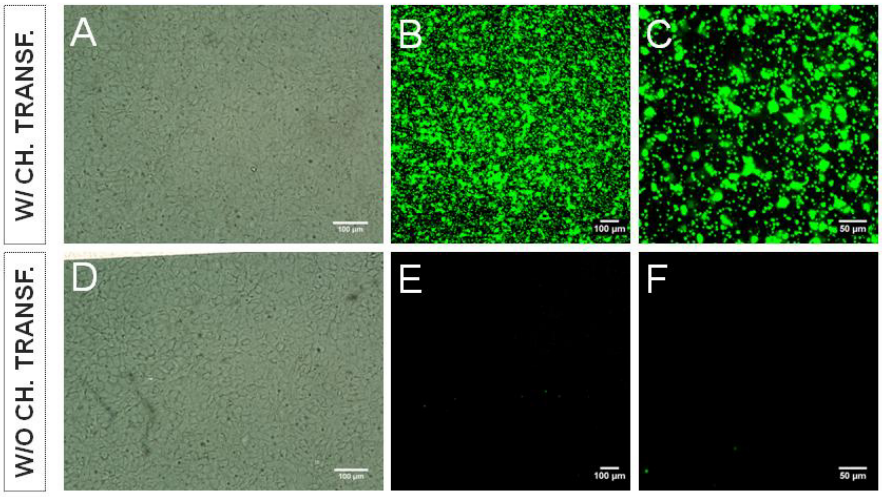

Figure 7.9 Exemplary phase-contrast (**A**, **D**) and confocal fluorescence micrographs (**B**, **C**, **E**, **F**) taken after chemical transfection of NRK cells in presence of 206 nM APT 1 (**A-C**) and incubation of NRK cells with 206 nM APT 1 in absence of the transfection mediator (**D-F**). Experiment was performed at 37 °C. The scale bar in **A**, **B**, **D** and **E** corresponds to 100 µm and in **C** and **F** to 50 µm. All micrographs were taken with 10-fold magnification objective.

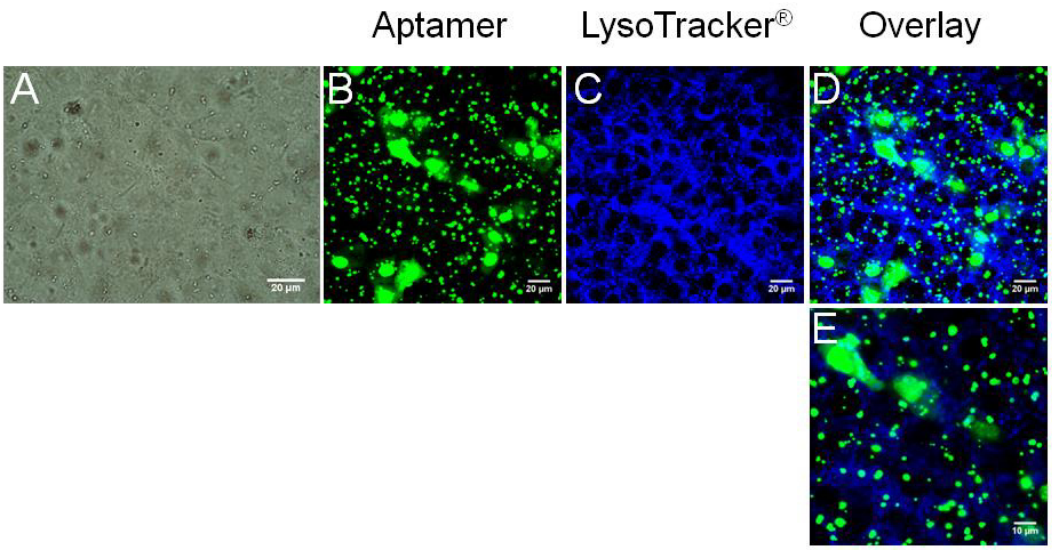

Figure 7.10 Exemplary phase-contrast (**A**) and confocal fluorescence micrographs (**B-E**) taken app. 5 hours after chemical transfection of NRK cells in presence of 206 nM APT 1. The lysosome marker LysoTracker® was applied after chemical transfection. Scale bar in **A**, **B**, **C** and **D** corresponds to 20 µm and in **E** to 10 µm. All micrographs were taken with 60-fold magnification objective.

High magnification images give an insight into localization of aptamer within NRK cells after transfection and micrograph **B** shows that APT 1 accumulated only in the vesicles, which is indicated by the characteristic punctuated pattern. Fluorescence signal was not found in the nuclei. Fluorescence micrograph **B** shows staining of the cells with LysoTracker® and overlay image **D**, along with its 2 times zoomed image presented in **E,** show that aptamers reached nucleus only in very rare cases. Fluorescence signal originates predominantly from vesicles and there is a certain co-localization of aptamer and lysosomes marker indicated by the bright blue dots.

Aptamer 2

To compare transfection efficiency, loading and localization pattern with APT 1, NRK cells were chemically transfected in presence of 206 nM DNA aptamer APT 2. Transfection efficiency was evaluated after app. 4 hours and exemplary micrographs, taken by CLSM with 10- and 60-fold magnification objective, are summarized in **Figure 7.11**.

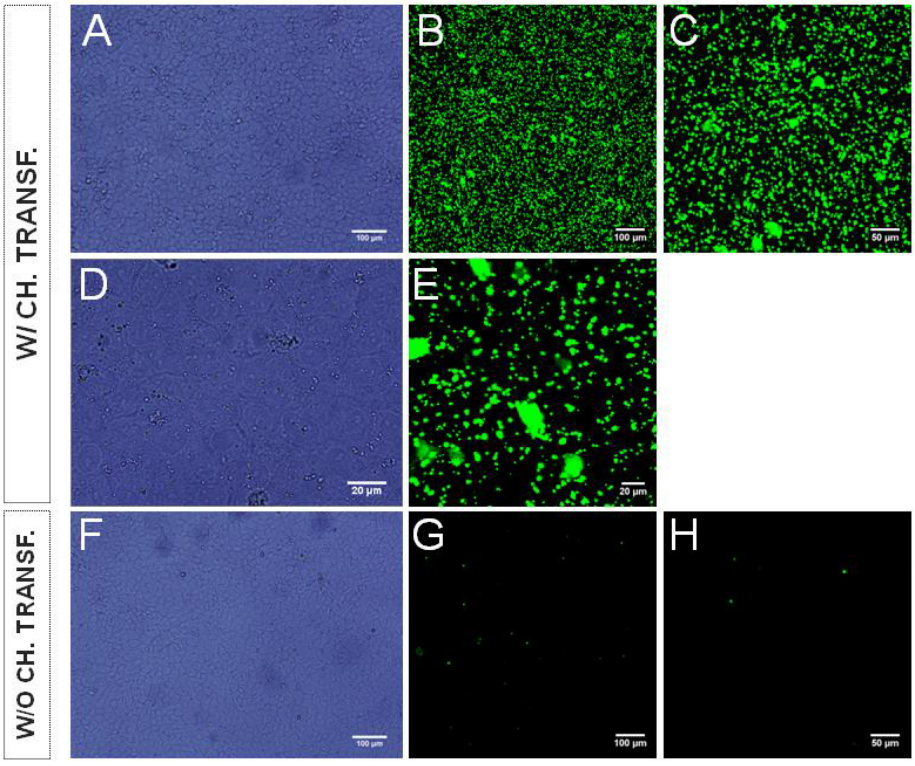

Figure 7.11 Exemplary phase-contrast (**A**, **D**, **F**) and confocal fluorescence micrographs (**B**, **C**, **E**, **G**, **H**) taken after chemical transfection of NRK cells in presence of 206 nM APT 1 (**A-E**) and incubation of NRK cells with 206 nM APT 2 in absence of chemical transfector (**F-H**). Experiment was performed at 37 °C. The scale bar in micrographs **A**, **B**, **F** and **G** corresponds to 100 µm, in micrographs **C** and **H** to 50 µm and in micrographs **D** and **E** to 20 µm. Micrographs were taken with 10-fold (**A-C** and **F-H**) and with 60-fold (**D-E**) objective.

NRK cells subjected to both APT 2 and chemical transfection reagent, are presented in the micrographs **A**-**C** and **D**-**E,** whereas NRK cells exposed to APT 2 in absence of chemical transfector are presented in micrographs **F**-**H**. Phase-contrast micrographs show no difference between the sample (**A**) and control (**F**), whereas confocal fluorescence micrographs reveal loading of NRK cells app. 4 hours after chemical transfection in presence of 206 nM APT 2 (**B**, **C** and **E**). Similarly to the results previously described with APT 1, APT 2 did not manage to reach cell nuclei, but it mostly accumulated in the cell vesicles. This is concluded based on the punctuated pattern which dominates the fluorescence micrographs belonging to sample (in the upper and middle panel), and which is especially visible in the fluorescence micrograph **E**. On the other side, NRK cells incubated with 206 nM APT 2 in absence of chemical transfector did not exhibit fluorescence signal. The exceptions were only a few unspecifically stained dots.

7.2.3 Delivery of Aptamers into Fixed and Permeabilized Cells

The fate of DNA aptamers APT 1 and APT 2 after their diffusion through disrupted membrane of fixed and permeabilized cells (abbreviated F + P) was studied to obtain an insight into what happens when aptamers have a free entrance into the cell cytosol. The localization of aptamers under such conditions was investigated with an aim to better understand why aptamers accumulate in cell nuclei after *in situ* electroporation. The spatial distribution of aptamers within fixed and permeabilized cells was documented by CLSM.

Aptamer 1

NRK cells served as a cell model and they were exposed to fixation and permeabilization agents, paraformaldehyde and Triton-X-100, respectively, before 15 µM APT 1 was added to them. Irreversibly permeabilized cell membrane allowed aptamer to diffuse freely into cell environment and it was the aim of this experiment to find out where its accumulation takes place. Exemplary phase-contrast and confocal fluorescence micrographs are summarized in **Figure 7.12**. Micrographs were taken with 10-fold (**A**-**C**) and 60-fold (**D**-**E**) magnification objective app. 1 hour after addition of APT 1 to fixed and permeabilized NRK cells. Aptamer APT 1 was able to diffuse into every cell and accumulated predominantly in the nuclei. In contrast to bright fluorescent signals originating from cell nuclei, fluorescent signal from cytoplasm was very weak. The boarders of cell membrane became slightly visible in the micrographs taken with higher magnification (**E**). Nuclei of the cells were not homogenously stained but numerous bright dots within almost every cell nucleus was observed (indicated by the small arrows in **E**).

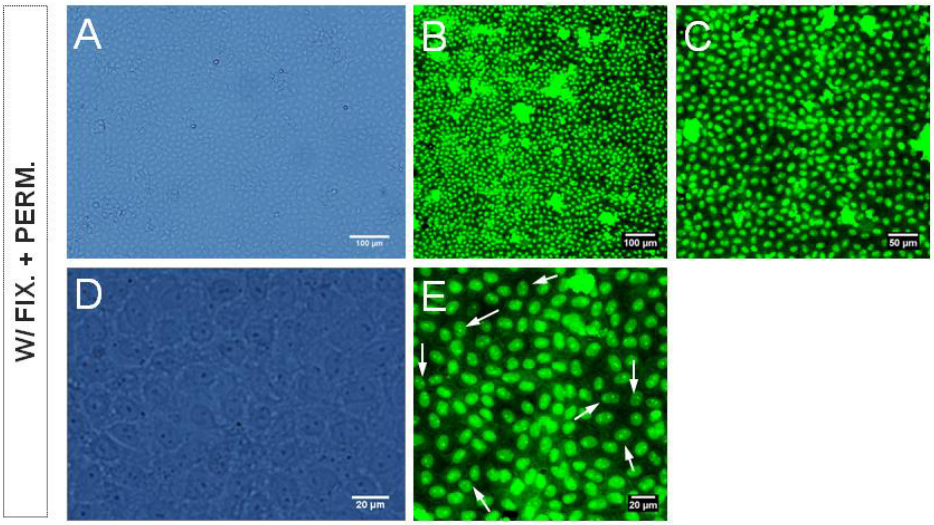

Figure 7.12 Exemplary phase-contrast (**A**, **D**) and confocal fluorescence micrographs (**B**, **C**, **E**) taken app. 1 hour after 15 µM APT 1 was added to fixed and permeabilized NRK cells. Incubation of NRK cells with APT 1 was performed at 37 °C. The scale bar in micrographs **A** and **B** corresponds to 100 µm, in **C** to 50 µm and in micrographs **D** and **E** to 20 µm. Micrographs were taken with 10-fold (**A-C** and **F-H**) and with 60-fold (**D-E**) magnification objective.

Aptamer APT 1 entered almost every cell after its addition to fixed and permeabilized NRK cells and it accumulated predominantly in the cell nuclei. Such observations are entirely in agreement with the outcome of APT 1 delivery by *in situ* electroporation,

Aptamer 2

Localization of APT 2 within fixed and permeabilized NRK cells was investigated with an aim to draw a comparison with spatial distribution of APT 1 within NRK cells under the same conditions and with the spatial distribution of APT 2 after electroporation. NRK cells were fixed and permeabilized and subsequently 15 µM of APT 2 was added to them. Exemplary phase-contrast and confocal fluorescence micrographs are summarized in **Figure 7.13**. Micrographs were taken with 10-fold (**A**-**C**) and 60-fold (**D** and **E**) magnification objective app. 1 hour after addition of APT 2 to fixed and permeabilized cells. APT 2 diffused into every cell and accumulated mainly within the cell nuclei, whereby fluorescence signal appeared rather homogeneous.

Fluorescence of APT 2 appeared brighter than the fluorescence of APT 1. It was concluded that APT 1 and APT 2 distribute within fixed and permeabilized cells in a very similar manner. In addition, these results show a good agreement with the localization of APT 2 within cell nuclei after *in situ* electoporation.

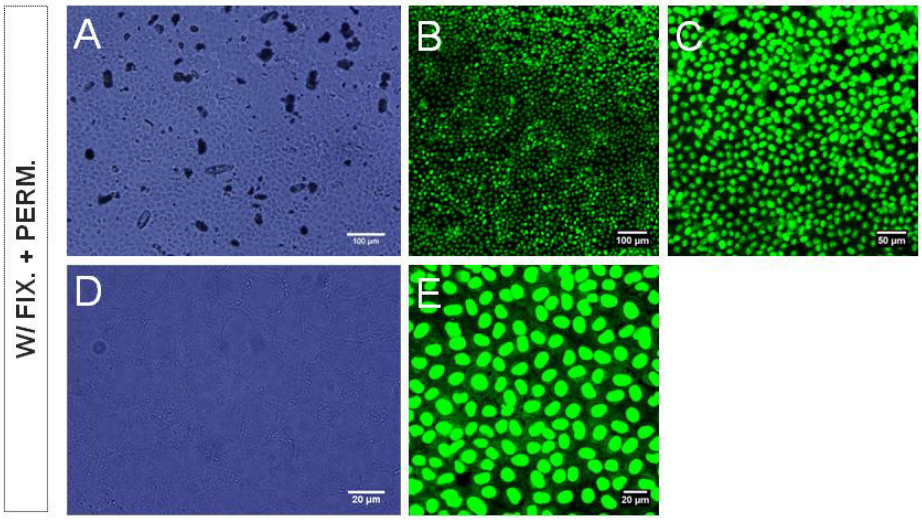

Figure 7.13 Exemplary phase-contrast (**A**, **D**) and confocal fluorescence micrographs (**B**, **C**, **E**) taken app. 1 hour after 15 µM APT 2 was added to fixed and permeabilized NRK cells. Incubation of NRK cells with APT 2 was performed at 37 °C. The scale bar in micrographs **A** and **B** corresponds to 100 µm, in **C** to 50 µm and in micrographs **D** and **E** to 20 µm. Micrographs were taken with 10-fold (**A-C** and **F-H**) and with 60-fold (**D-E**) magnification objective.

Fluorescein-Labeled Aptamer versus Fluorescein

To be sure the aptamers are not denatured on their way from extracellular environment through the cell membrane and to their final destination within the intracellular environment, spatial distribution of fluorescein-labeled aptamers APT 1 and APT 2 and pure fluorescein label (MW = 332 kDa) was studied after their diffusion into fixed and permeabilized cells. According to the common protocol (described in chapter 4.5.1), NRK cells were fixed and permeabilized and either 20 µM, or 200 µM fluorescein was added to them. These two concentrations were chosen since the lower (20 µM) corresponds nearly to the concentration of fluorescently-labeled aptamers (15 µM) and the higher was chosen as it corresponds closely to the concentrations applied for delivery of FITC-dextrans into cells. Exemplary confocal fluorescence micrographs are summarized in **Figure 7.14**. They were taken with 60-fold magnification objective app. 1 hour after fluorescein was added to fixed and permeabilized NRK cells. Exemplary fluorescence micrographs taken for 20 µM (**C**) and 200 µM (**D**) fluorescein are summarized along with the previously presented exemplary micrographs for APT 1 (**A**) and APT 2 (**B**), taken with the same magnification.

As already described, APT 1 (**A**) and APT 2 (**B**) accumulated in the cell nuclei. Thereby, bright dots were observed within nuclei loaded with APT 1 and more homogeneous signal was seen within cell nuclei loaded with APT 2. Micrographs showing NRK cells after diffusion of 20 µM and 200 µM fluorescein through their disrupted cell membrane reveal homogenous

staining of fluorescein within cytoplasm of every cell, whereas nuclei remained much darker, practically unstained and without any bright dots. The difference in fluorescence intensity between two applied concentrations of fluorescein 20 and 200 µM was noticeable, however, staining pattern was the same.

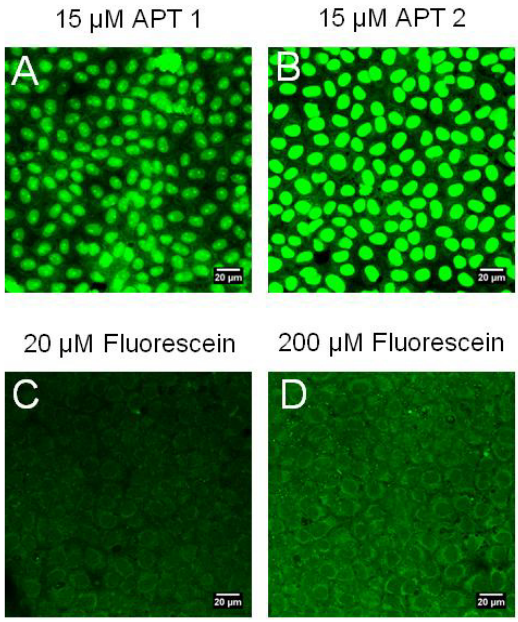

Figure 7.14 Exemplary confocal fluorescence micrographs taken app. 1 hour after 15 µM APT 1 (**A**), 15 µM APT 2 (**B**), 20 µM fluorescein (**C**), or 200 µM fluorescein (**D**) was added to fixed and permeabilized NRK cells. Incubation of NRK cells was performed at 37 °C. Scale bars correspond to 20 µm and all micrographs were taken with 60-fold magnification objective.

Whereas APT 1 and APT 2 predominantly accumulated in cell nuclei after their diffusion into fixed and permeabilized NRK cells, both 20 µM and 200 µM fluorescein stained only the cytoplasm in a homogenous manner.

7.3 Delivery of Aptamers into HaCaT Cells

7.3.1 Delivery of Aptamers by *In Situ* Electroporation

Besides NRK cells, another cell line was applied to investigate delivery of fluorescently-labeled DNA aptamers into adherent cells. HaCaT cells were applied as a cell model for delivery of aptamers into cell interior employing three different delivery strategies. Previously optimized with NRK cells, experimental procedure for *in situ* electroporation was applied here in the same manner. NRK is the only cell line investigated using both DNA aptamers (APT 1

and APT 2). For HaCaT cells, as well as for the studies including all further cell lines, only aptamer 1 (APT 1) was applied and therefore, in further text abbreviation APT corresponds to APT 1, unless specifically stated (APT 1 or APT 2).

Delivery of aptamers into HaCaT cells by *in situ* electroporation was conducted on electrode array 8W4Eμ and EBSS^{++} was applied as assay buffer. HaCaT cells were electroporated (using optimal combination of pulse parameters for this cell line: 40 kHz, 5 V and 500 ms) three times successively, as indicated by the arrows - a: 1st pulse, b: 2nd pulse and c: 3rd pulse application) in **Figure 7.15**.

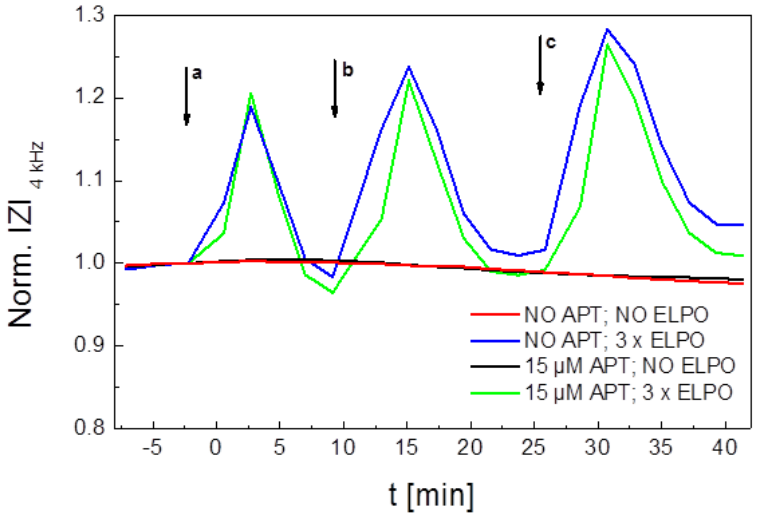

Figure 7.15 Typical time course of the normalized impedance at 4 kHz before, during and after *in situ* electroporation of HaCaT cells in presence of 15 μM APT 1. ISE was applied three times successively - **a**: 1st pulse, **b**: 2nd pulse and **c**: 3rd pulse application, using optimal combination of pulse parameters for this cell line: 40 kHz, 5 V and 500 ms. Impedance values are normalized to the last time point before first electroporation pulse was applied. After recovery of the cells, impedance measurement (at 37 °C) was finished and microscopy by CLSM followed to evaluate electroporation efficiency.

Figure 7.15 shows typical time course of the normalized impedance before, during and after *in situ* electroporation of HaCaT cells in presence of 15 μM APT. Exemplary impedance measurement is presented at 4 kHz and data are normalized to the last time point before first electroporation pulse was applied. HaCaT cells, in comparison to the other investigated cell lines, recover quite fast after the application of electric pulses and return to pre-pulse impedance values within app. 10 min. In addition, impedance signal does not decrease after electroporation, but increases rapidly and returns back to the baseline after a few minutes. Nevertheless, after every pulse application, it was waited until impedance of the cells returned to the pre-pulse values before next pulse was applied. After the third pulse,

impedance measurement was finished and microscopy by CLSM followed, in order to take fluorescence micrographs and thus estimate electroporation efficiency. Experiment included controls where cells were incubated in presence of aptamers but no electroporation was applied and where cells were electroporated in absence of aptamers.

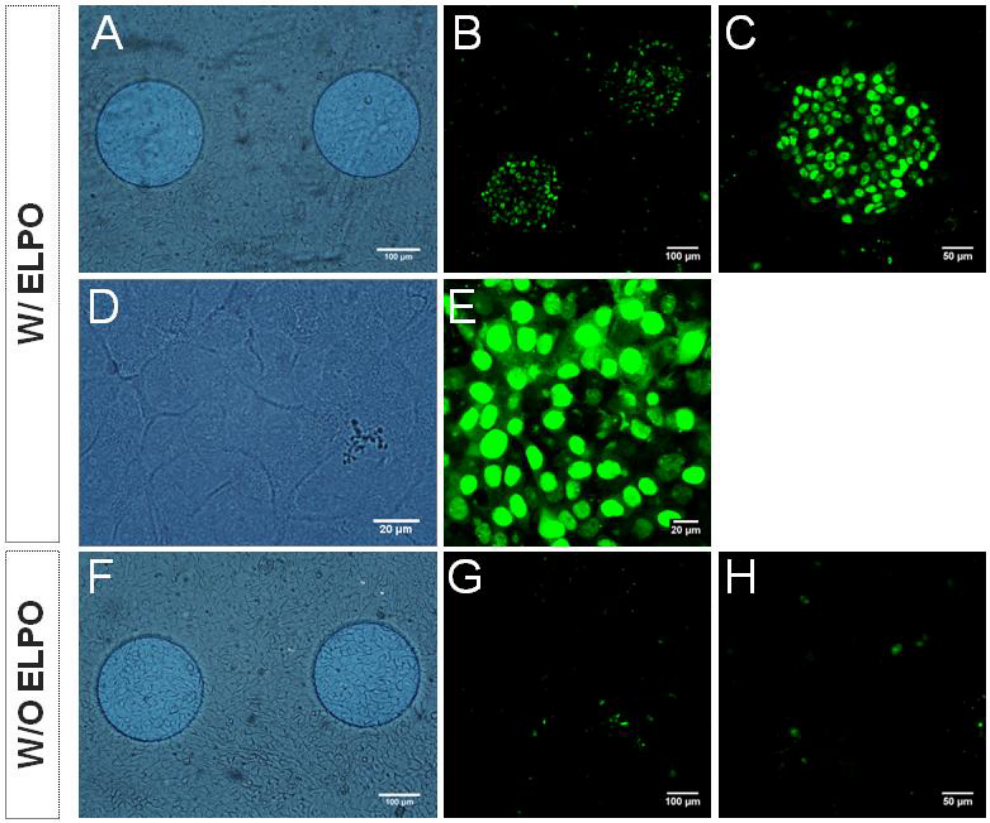

Figure 7.16 Exemplary phase-contrast (**A**, **D**, **F**) and confocal fluorescence micrographs (**B**, **C**, **E**, **G**, **H**) taken after *in situ* electroporation was applied for delivery of 15 µM APT into HaCaT cells. Scale bar in micrographs **A**, **B**, **F** and **G** corresponds to 100 µm, in **C** and **H** to 50 µm and in **D** and **E** to 20 µm. Micrographs were taken with 10-fold (**A-C** and **F-H**) and with 60-fold (**D-E**) magnification objective.

Exemplary phase-contrast and confocal fluorescence micrographs are presented in **Figure 7.16**. Micrographs were taken with 10-fold (**A-C** and **F-H**) and 60-fold (**D-E**) magnification objective. HaCaT cells subjected to ISE in presence of 15 µM APT are shown in the micrographs **A**-**E** and cells exposed to 15 µM APT in absence of electric pulse are shown in the micrographs **F**-**H**. Whereas phase-contrast micrographs do not show difference between the sample (**A**) and control (**F**), fluorescence images **B** and **G**, additionally zoomed 1.5 times, reveal loading of HaCaT cells on the electrodes with the fluorescing aptamer. Aptamers accumulated only within nuclei of the cells present on the electrodes. The cells surrounding the electrodes (background) appeared dark, as aptamers did not enter the cell envelope and

the same was true for the whole cell population of the controls. However, some minor unspecific uptake of aptamers by the HaCaT cells was observed.

Loading of HaCaT cells with aptamers was even better visualized by comparing the fluorescence micrographs **C** (sample) and **H** (control), which were zoomed 3 times. Most of the cells residing on the electrodes were loaded with aptamers. Additionally, micrographs of the sample were also taken using 60-fod magnification objective (**D** and **F**). Aptamers were localized predominantly in cell nuclei and within some nuclei characteristic small bright dots were recognized. Much smaller amount of fluorescence signal came from the cytoplasm and it was rather homogeneous.

7.3.2 Delivery of Aptamers by Chemical Transfection

To better understand loading efficiency and pattern observed after electroporation, HaCaT cells were chemically transfected in presence of 206 nM APT according to the common protocol (described in chapter 4.4.2.2). App. 4 hours after transfection, efficiency of aptamer delivery was evaluated by CLSM. Exemplary phase-contrast and confocal fluorescence micrographs are summarized in **Figure 7.17**. Micrographs were taken with 10-fold (**A**-**C**) and 60-fold (**D**-**E**) magnification objective and were additionally zoomed 1.5 (**B**) and 3 times (**C**).

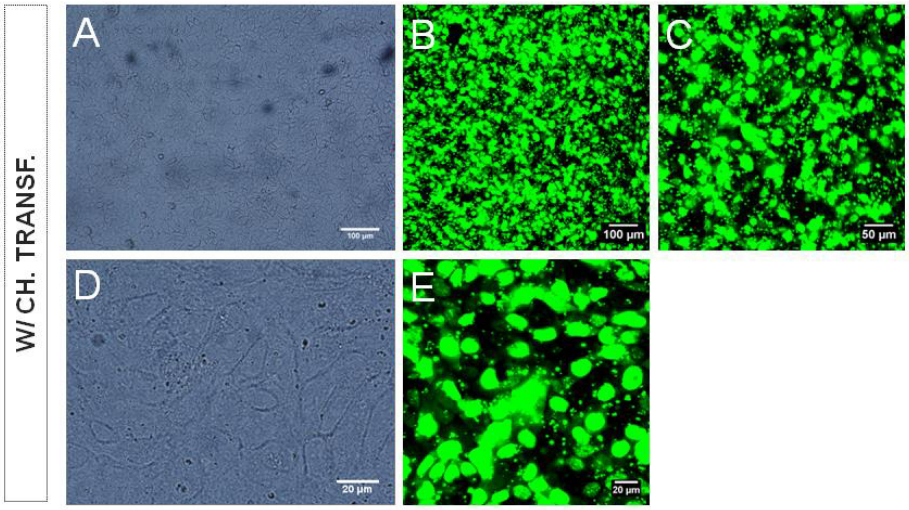

Figure 7.17 Exemplary phase-contrast (**A** and **D**) and confocal fluorescence micrographs (**B**, **C** and **E**) taken after chemical transfection of HaCaT cells in presence of 206 nM APT. Experiment was performed at 37 °C. The scale bar in micrographs **A** and **B** corresponds to 100 µm, in **C** to 50 µm and in micrographs **D** and **E** to 20 µm. Micrographs were taken with 10-fold (**A-C**) and 60-fold (**D-E**) magnification objective.

Chemical transfection reagent facilitated entry of aptamer into the HaCaT cells. The

fluorescence signal was predominantly localized in the cell vesicles, as punctuated pattern, typical for endocytotic mechanism of delivery, was recognized within most of the cells. Aptamers were found to some very small extent in the cell cytoplasm, however, it was surprising to see that fluorescence signal was localized also within several cell nuclei. This is visible in the micrograph taken with high magnification objective (**E**). Such results indicate that chemical transfection of HaCaT cells with aptamers was more successful than the chemical transfection of NRK cells.

7.3.3 Delivery of Aptamers into Fixed and Permeabilized Cells

After the *in situ* electoporation and chemical transfection were applied for delivery of aptamers into living HaCaT cells, localization of aptamers within fixed and permeabilized HaCaT cells was investigated. HaCaT cells were subjected to 15 µM APT, added after the common fixation and permeabiliization protocol was applied to disrupt the cell membrane. Irreversibly permeabilized cell membrane of HaCaT cells allowed for diffusion of aptamer into the cell cytosol. This is shown in the exemplary confocal fluorescence micrographs, summarized along with the respective phase-contrast micrographs, in **Figure 7.18**. Micrographs were taken using 10-fold (**A**-**C**) and 60-fold (**D**-**E**) magnification objective, app. 1 hour after addition of 15 µM APT to the cells.

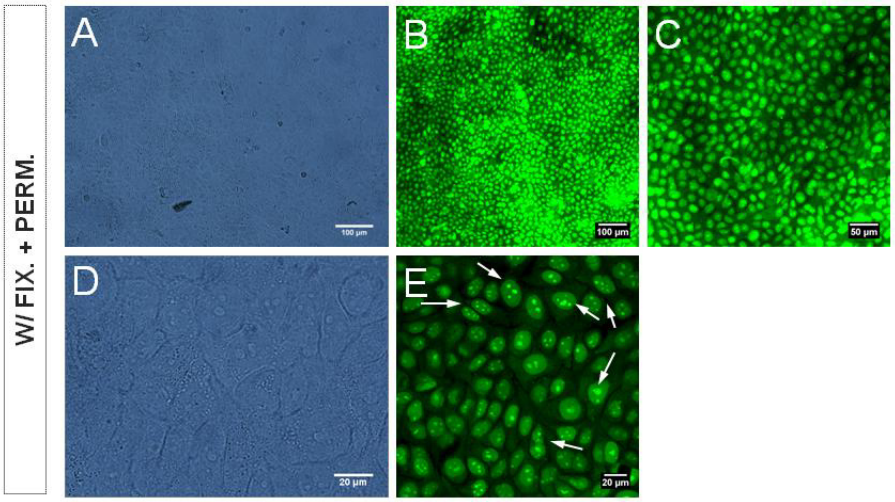

Figure 7.18 Exemplary phase-contrast (**A**, **D**) and confocal fluorescence micrographs (**B**, **C**, **E**) taken app. 1 hour after 15 µM APT was added to fixed and permeabilized HaCaT cells. Incubation of HaCaT cells with aptamer was performed at 37 °C. The scale bar in micrographs **A** and **B** corresponds to 100 µm, in **C** to 50 µm and in micrographs **D** and **E** to 20 µm. Micrographs were taken with 10-fold (**A-C** and **F-H**) and with 60-fold (**D-E**) magnification objective.

Fluorescence micrographs, taken with the lower magnification objective (**B** and **C**), show bright fluorescence signal of aptamers, originating from every cell. Cell nuclei appeared very bright as aptamers accumulated in them. The bright dots were observed within most of cell nuclei and it hypothesized that this structures are in fact nucleoli. Micrograph taken with the higher magnification objective (**E**) shows such staining pattern even more clearly, as bright dots (indicated by the small arrows) were recognized within almost every cell nucleus. Fluorescence signal observed within the cytoplasm was very low and homogeneously distributed.

7.4 Delivery of Aptamers into CHO-K1 Cells

7.4.1 Delivery of Aptamers by *In Situ* Electroporation

Cell line CHO-K1 was applied as an additional model system to investigate delivery of fluorescently-labeled DNA aptamers into cells. Experimental procedure for *in situ* electroporation was applied in a same manner as for all other cell lines. CHO-K1 cells were subjected only to DNA aptamer APT 1 and not to APT 2. Therefore, abbreviation APT will be used in the further text.

Experimental procedure including delivery of aptamers into CHO-K1 cells by *in situ* electroporation was conducted on electrode array 8W4Eμ and $EBSS^{++}$ was applied as assay buffer. Typical time course of the normalized impedance before, during and after *in situ* electroporation of CHO-K1 cells in presence of 15 μM APT is presented in **Figure 7.19**. Electroporation was applied three times successively, as indicated by the arrows - a: 1^{st} pulse, b: 2^{nd} pulse and c: 3^{rd} pulse application, using optimal combination of pulse parameters for this cell line: 40 kHz, 4 V and 500 ms. Impedance measurement is presented at 16 kHz and data are normalized to the last time point before first electroporation pulse was applied. After first pulse application, impedance signal decreased and cells needed app. 30 min to return to the pre-pulse impedance values. After second and the third pulse application, impedance shortly increased and then decreased subsequently, whereby recovery of the cells to the pre-pulse impedance values again took place within 30 min. After the third pulse, cells were allowed to fully recover and stabilize before impedance measurement was finished and the microscopy by CLSM followed.

Exemplary phase-contrast and confocal fluorescence micrographs are presented in **Figure 7.20** and all micrographs were taken with 10-fold magnification objective. CHO-K1 cells subjected to ISE in presence of 15 μM APT are shown in the top row (**A**-**C**), whereas cells exposed to 15 μM APT in absence of electric pulse are shown in the lower panel (**D**-**F**).

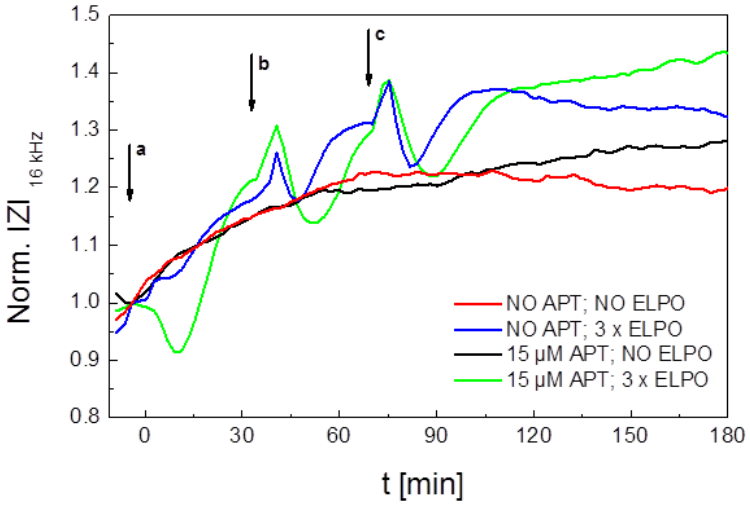

Figure 7.19 Typical time course of the normalized impedance at 16 kHz before, during and after *in situ* electroporation of CHO-K1 cells in presence of 15 µM APT. ISE was applied three times successively - **a**: 1st pulse, **b**: 2nd pulse and **c**: 3rd pulse application, using optimal combination of pulse parameters for this cell line: 40 kHz, 4 V and 500 ms. Impedance values are normalized to the last time point before first electroporation pulse was applied. After cellular recovery from the third and final pulse, impedance measurement (at 37 °C) was finished and microscopy by CLSM followed to evaluate electroporation efficiency.

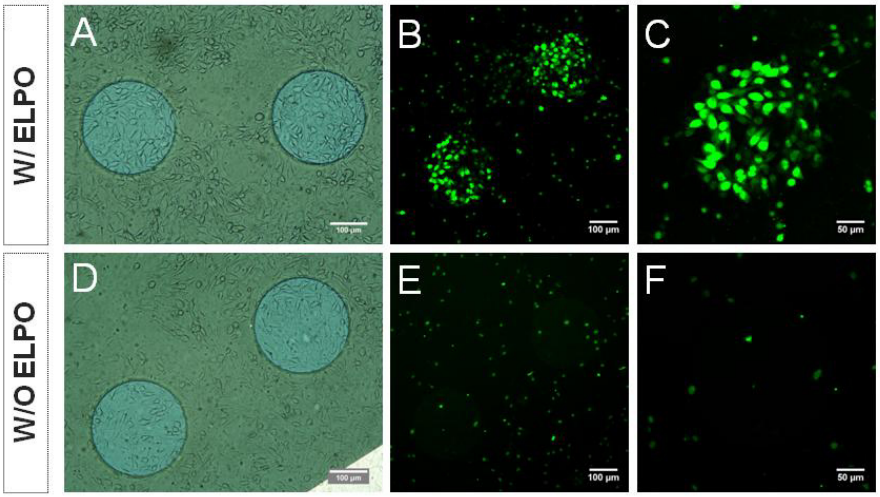

Figure 7.20 Exemplary phase-contrast (**A**, **D**) and confocal fluorescence micrographs (**B**, **C**, **E**, **F**) taken after *in situ* electroporation was applied for delivery of 15 µM APT into CHO-K1 cells. Experiment was performed at 37 °C. The scale bar in micrographs **A**, **B**, **D** and **E** corresponds to 100 µm and in **C** and **F** to 50 µm. All micrographs were taken using 10-fold magnification objective.

Exemplary phase-contrast micrographs (**A** and **D**) illustrate the biggest issue faced during

the experimental procedure conducted on CHO-K1 cells. During washing steps prior to microscopy, it was often happening that the CHO-K1 cells were washed away and confluent cell monolayer was damaged. The cells were missing on and around the electrodes. Microscopic examination of pulsed and non-pulsed CHO-K1 cells was conducted before and after impedance monitoring of the multiple *in situ* electroporation. It was observed that cell monolayers were complete and undamaged after impedance measurement, regardless of electric pulse application. However, after washing and before microscopy, monolayers were often damaged and this led to conclusion that the shear stress during pipetting causes detachment of some CHO-K1 cells from the substrate, during washing steps.

Nevertheless, fluorescence micrographs taken after ISE in presence of aptamers, showed that a number of the cells residing on the electrodes was still successfully loaded with aptamer, and the fluorescence signal was mostly accumulated within cell nuclei (**B** and **C**). Besides, in all fluorescence micrographs was visible that an unspecific uptake of the aptamer took place, most probably by the damaged cells.

7.4.2 Delivery of Aptamers by Chemical Transfection

To compare delivery of aptamers into CHO-K1 cells by *in situ* electroporation and with the lipid-based transfection agent, CHO-K1 cells were transfected in presence of 206 nM APT according to the common protocol (chapter 4.4.2.2), using commercial chemical transfector.

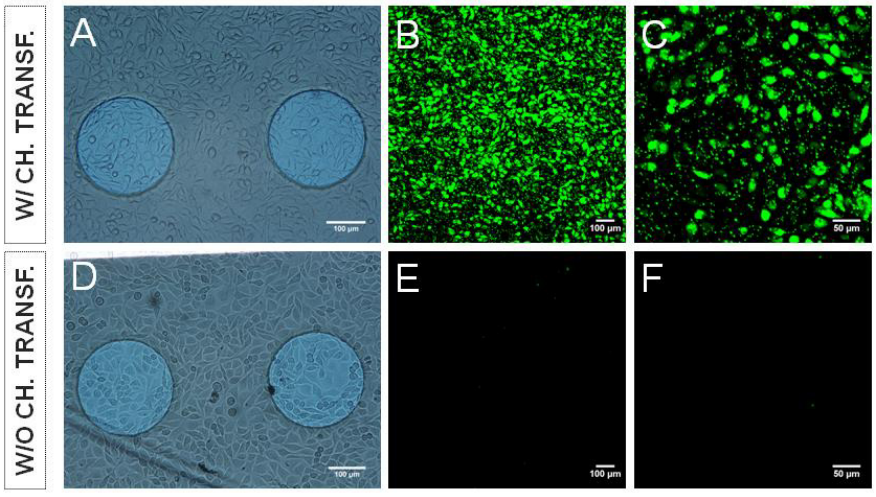

Figure 7.21 Exemplary phase-contrast (**A** and **D**) and confocal fluorescence micrographs (**B**-**C** and **E**-**F**) taken app. 4 hours after chemical transfection of CHO-K1 cells in presence of 206 nM APT (**A-C**) and incubation of CHO-K1 cells with 206 nM APT in absence of the transfection mediator (**D-F**). Experiment was performed at 37 °C. The scale bar in micrographs **A, B, D** and **E** corresponds to 100 µm and in **C** and **F** to 50 µm. All micrographs were taken with 10-fold magnification objective.

Exemplary phase-contrast and confocal fluorescence micrographs are summarized in **Figure 7.21**. All micrographs were taken with 10-fold magnification objective and were additionally zoomed 1.5 (**B** and **E**) and 3 times (**C** and **F**). As the phase-contrast micrographs are showing (**A** and **D**), experimental procedure was performed on 8W4Eμ array in order to investigate if any significant morphological changes of the cells, measurable by ECIS, can be captured during and after chemical transfection (data not shown). However, impedance measurement did not reveal significant signal changes which could be ascribed to the effects of chemical transfection. Nevertheless, fluorescence micrographs taken after chemical transfection showed that aptamer was mostly accumulated within cell vesicles, as indicated by the characteristic punctuated pattern. Small number of cells exhibited fluorescence signal within their nuclei. The cells incubated with aptamer in absence of chemical transfection reagent appeared dark, as aptamer did not enter the cells. No cytoxicity after chemical transfection was observed.

Chemical transfection allowed for entrance of the fluorescent aptamer into the CHO-K1 cells, however aptamer was mostly entrapped within vesicles and only in small number of cells it reached cell nuclei.

7.4.3 Delivery of Aptamers into Fixed and Permeabilized Cells

To investigate the fate of aptamer after its free diffusion into intracellular environment, fixation and permeabilization of CHO-K1 cells was performed to disrupt the cell membrane. Thereafter, 15 µM APT was added to the cells and incubation at 37 °C took place for app. 40 min. Subsequently, localization of aptamers within CHO-K1 cells was evaluated by CLSM.

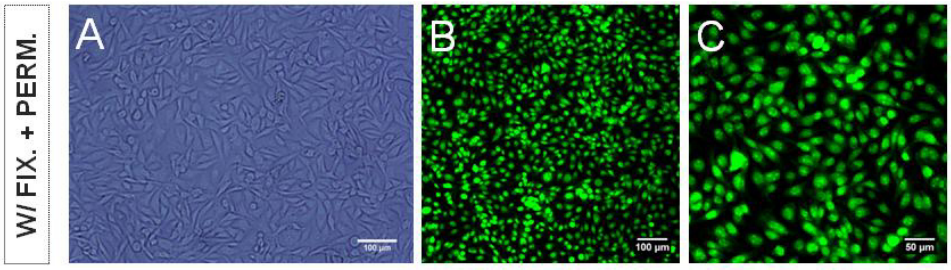

Figure 7.22 Exemplary phase-contrast (**A**) and confocal fluorescence micrographs (**B**, **C**) taken app. 1 hour after 15 µM APT was added to fixed and permeabilized CHO-K1 cells. Incubation of CHO-K1 cells with aptamer was performed at 37 °C. The scale bar in micrographs **A** and **B** corresponds to 100 µm and in micrograph **C** to 50 µm. All micrographs were taken with 10-fold magnification objective.

Exemplary phase-contrast and confocal fluorescence micrographs are summarized in **Figure**

7.22. Micrographs taken with 10-fold magnification objective were zoomed either 1.5 (**B**), or 3 times (**C**), to visualize better spatial distribution of fluorescent aptamer within the CHO-K1 cells. Bright fluorescence signal was observed in the nucleus of every cell, whereas cytoplasm staining was hardly seen. Loading of cell nuclei did not appear homogenous, as small bright dots (probably originating from nucleoli) were recognized within most of the cells. After its addition to fixed and permeabilized CHO-K1 cells, aptamer was found in the cytosol of every cell. It accumulated mostly in the cell nuclei, whereas very small amount of fluorescence signal was homogeneously distributed within cytoplasm.

7.5 Delivery of Aptamers into NIH-3T3 Cells

7.5.1 Delivery of Aptamers by *In Situ* Electroporation

The last cell line applied as a cell model for investigation of aptamer delivery was NIH-3T3. NIH-3T3 cells were exposed to the fluorescently-labeled DNA aptamer APT 1 (and not to APT 2). Therefore, abbreviation APT in further text corresponds to APT 1. Experimental procedure for *in situ* electroporation was applied on NIH-3T3 cells in the same manner as for all other cell lines (more details in chapter 4.2.2.4).

Typical time course of the normalized impedance before, during and after *in situ* electroporation of NIH-3T3 cells in presence of 15 µM APT is presented in **Figure 7.23**. Experimental procedure was conducted on electrode array 8W4Eµ and $EBSS^{++}$ was applied as assay buffer. Electroporation of NIH-3T3 cells (using optimal combination of pulse parameters for this cell line: 40 kHz, 5 V and 200 ms) was applied three times successively, as indicated by the arrows - a: 1^{st} pulse, b: 2^{nd} pulse and c: 3^{rd} pulse application. Impedance measurement is presented at 4 kHz and data are normalized to the last time point before first electroporation pulse was applied. After every pulse application, impedance signal decreased and cells needed app. 20 minutes to return to the pre-pulse impedance values. After the third and final pulse, cells were allowed to fully recover and stabilize to the pre-pulse impedance values, before impedance measurement was finished and microscopy by CLSM followed to evaluate electroporation efficiency.

Exemplary phase-contrast and confocal fluorescence micrographs are presented in **Figure 7.24**. All micrographs were taken with 10-fold magnification objective. NIH-3T3 cells subjected to ISE in presence of 15 µM APT cells are shown in the upper panel (**A**-**C**), whereas cells exposed to 15 µM APT in absence of electric pulse are shown in the lower panel (**D**-**F**). Whereas phase-contrast micrographs do not show difference between a sample (**A**) and a control (**D**), fluorescence micrographs **B** and **E** (additionally zoomed 1.5 times)

show that only fraction of NIH-3T3 cells residing on the electrodes was loaded with the aptamer. Localization of aptamers within cells was evaluated more closely by analyzing fluorescence micrographs **C** and **F** (zoomed 3 times). Obviously, aptamers accumulated within nuclei of the cells present on the electrodes and the characteristic small bright dots were recognized within some nuclei. In addition, rather weak fluorescence signal was originating from the cytoplasm of the cells on the electrodes.

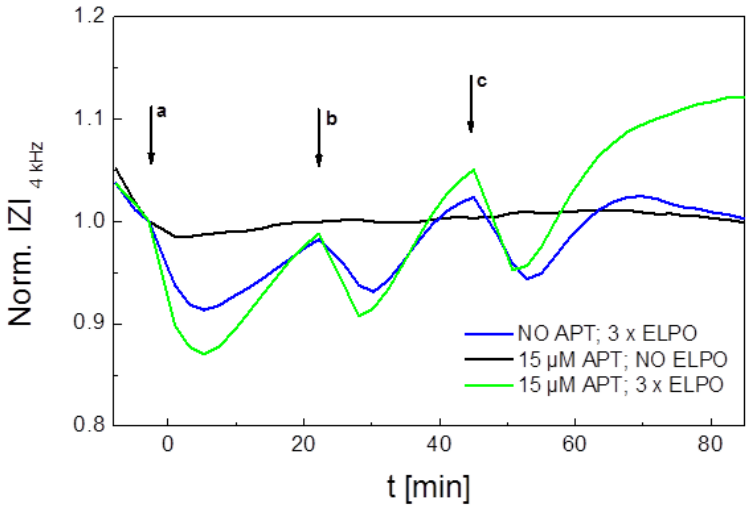

Figure 7.23 Typical time course of the normalized impedance at 4 kHz before, during and after *in situ* electroporation of NIH-3T3 cells in presence of 15 µM APT. ISE was applied three times successively - **a**: 1st pulse, **b**: 2nd pulse and **c**: 3rd pulse application, using optimal combination of pulse parameters for this cell line: 40 kHz, 5 V and 200 ms. Impedance values are normalized to the last time point before first electroporation pulse was applied. After cellular recovery from the third and final pulse, impedance measurement (at 37 °C) was finished and microscopy by CLSM followed to evaluate electroporation efficiency.

However, efficiency of *in situ* electroporation for delivery of aptamers was difficult to evaluate more precisely on NIH-3T3 cells, as a relatively high amount of aptamer was unspecifically taken up by the cells. Fluorescence stains and punctuated structures were observed on all micrographs, regardless of the pulse application. It is difficult to say if such unspecific fluorescence signals originate from the damaged cells, since cytotoxicity or missing cells were not an issue during the procedure. Possible explanation for unspecific uptake of aptamers could be also endocytosis, as punctuated pattern in this case appears to be similar to the pattern observed when aptamers were entrapped within the vesicles (mostly after chemical transfection). Unfortunately, micrographs could not be taken with the higher magnification objective, as the confluent monolayer of NIH-3T3 cells mostly detached from

the substrates after microscopy with 10-fold magnification objective and latest, when additional volume of the buffer was added to the cells, before microscopy with the higher magnification objective was attempted.

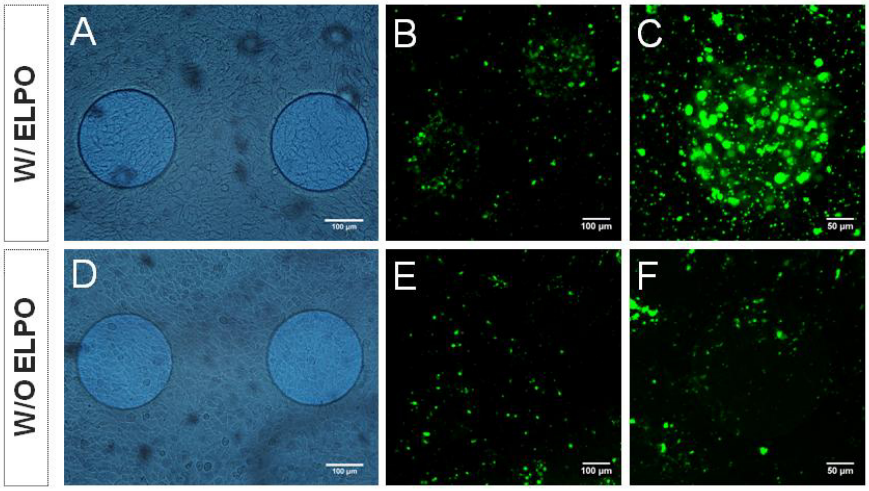

Figure 7.24 Exemplary phase-contrast (**A**, **D**) and confocal fluorescence micrographs (**B**, **C**, **E**, **F**) taken after *in situ* electroporation was applied for delivery of 15 µM APT into NIH-3T3 cells. Experiment was performed at 37 °C. The scale bar in micrographs **A**, **B**, **D** and **E** corresponds to 100 µm and in **C** and **F** to 50 µm. All micrographs were taken using 10-fold magnification objective.

In situ electroporation facilitated delivery of aptamers into NIH-3T3 cells and allowed their accumulation within cell nuclei. To a very small extent, signal was also observed in the cytoplasm. However, relatively high level of unspecific uptake was observed in all micrographs, suggesting possible endocytosis (or damage of the cells) during procedure.

7.5.2 Delivery of Aptamers by Chemical Transfection

NIH-3T3 cells were chemically transfected in presence of 206 nM APT, following usual experimental protocol (described in chapter 4.4.2.2), in order to compare transfection efficiency and loading pattern of lipid-based delivery with *in situ* electroporation. App. 4 hours after transfection of NIH-3T3 cells in presence of 206 nM APT, localization of aptamers was evaluated by CLSM. Exemplary phase-contrast and confocal fluorescence micrographs are summarized in **Figure 7.25**. Micrographs were taken with 10-fold (**A**-**C**) and 60-fold (**D**-**E**) magnification objective. Micrograph **B** was additionally zoomed 1.5 and micrograph **C** 3 times. Fluorescence micrographs show that chemical transaction reagent facilitated entry of aptamers into NIH-3T3 cells, although not entire cell population was loaded with the aptamer. Again, punctuated pattern, typical for endocytotic mechanism of uptake, was dominating the

micrographs and it indicated that aptamers mostly accumulated in the cell vesicles. Fluorescence signal was also localized within cell nuclei, partially in the cell cytoplasm as well, but both to much lower extent, compared to the fluorescence signal originating from the vesicles. Such localization of aptamers within the cells was confirmed by the fluorescence micrograph(s) taken with higher magnification (**E**).

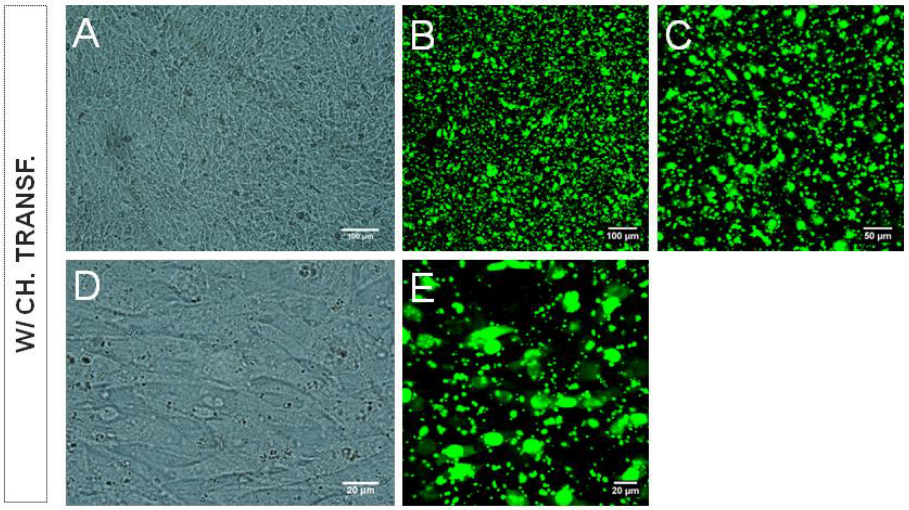

Figure 7.25 Exemplary phase-contrast (**A** and **D**) and confocal fluorescence micrographs (**B**, **C** and **E**) taken after chemical transfection of NIH-3T3 cells in presence of 206 nM APT. Experiment was performed at 37 °C. The scale bar in micrographs **A** and **B** corresponds to 100 µm, in micrograph **C** to 50 µm and in **D** and **E** to 20 µm. Micrographs were taken with 10-fold (**A-C**) and 60-fold (**D-E**) magnification objective.

Chemical transfection allowed entry of aptamers into the cytosol of NIH-3T3 cells, however, aptamers accumulated predominantly in cell vesicles, only partially in nuclei and cytoplasm.

7.5.3 Delivery of Aptamers into Fixed and Permeabilized Cells

Finally, after delivery of aptamers into the living NIH-3T3 cells, their diffusion into fixed and permeabilized cells was investigated. After fixation and permeabiliization of NIH-3T3 cells, they were subjected to 15 µM APT and incubated at 37 °C for app 40 min. Localization of aptamers was evaluated by CLSM and exemplary phase-contrast and confocal fluorescence micrographs are summarized in **Figure 7.26**. Micrographs were taken with 10-fold (**A**-**C**) and 60-fold (**D**- **E**) magnification objective. Micrograph **B** was additionally zoomed 1.5 times and micrograph **C** 3 times. Aptamers diffused across irreversibly permeabilized cell membrane into the cell cytosol and accumulated predominantly within nuclei, which appeared much brighter than the cytoplasm. In addition, bright dots (most probably corresponding to nucleoli)

were recognized within the structure of some nuclei. Such observations were confirmed by the micrograph taken with higher magnification objective (**E**). Fluorescence signal in cytoplasm of NIH-3T3 cells appeared considerably higher than in all previously analyzed cell lines, with certain grained pattern of staining recognized within the cytoplasmatic structure.

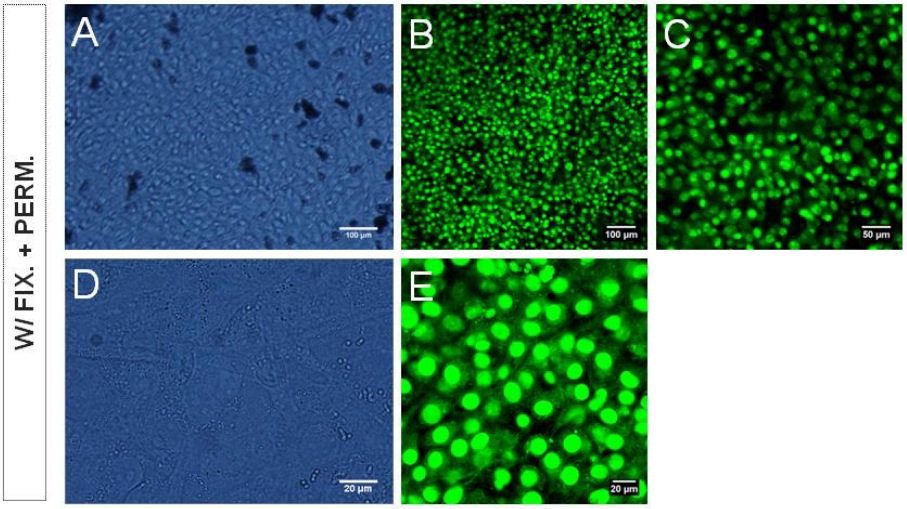

Figure 7.26 Exemplary phase-contrast (**A**, **D**) and confocal fluorescence micrographs (**B**, **C**, **E**) taken app. 1 hour after 15 µM APT was added to fixed and permeabilized NIH-3T3 cells. Incubation of NIH-3T3 cells with aptamer was performed at 37 °C. The scale bar in micrographs **A** and **B** corresponds to 100 µm, in **C** to 50 µm and in micrographs **D** and **E** to 20 µm. Micrographs were taken with 10-fold (**A-C** and **F-H**) and with 60-fold (**D-E**) magnification objective.

Aptamers freely diffused across the disrupted membrane of fixed and permeabilized NIH-3T3 cells and accumulated predominantly within the cell nuclei. Besides, fluorescence signal was found within cell cytoplasm.

7.6 Discussion

This section of the work was dedicated to the introduction of aptamers into various cell lines by *in situ* electroporation employing ECIS technology. Main goal was to explore a possibility to apply *in situ* electroporation for delivery of aptamers and to compare it with the most common method for oligonucleotides delivery in the cells – chemical lipid-based transfection. In addition, the fate of aptamers after their free diffusion into the cytosol of fixed and permeabilized cells was investigated.

Aptamers belong to an emerging class of novel synthetic nucleic acids and hold a great potential for different fields of application. However, the greatest obstacle for taking advantage of aptamers with intracellular target nowadays is the negative charge of their

molecules, which hinders their transit across the cell membrane. Therefore, it is crucial to find a versatile and an effective tool for transfer of aptamers into the intracellular environment, where they can target diverse types of molecules. *In situ* electroporation combined with ECIS technology is a well-established technique for delivery of various xenomolecules into mammalian cells (Wegener et al., 2002; Albermann, 2004; Stolwijk et al., 2011) and within this chapter, proof-of-principle experiments are described to demonstrate the capability of such experimental setup to be effectively employed, in order to overcome poor membrane permeability of aptamers. In addition, ECIS technology offers sensitive and precise monitoring of events before and after introduction of xenobiotics into cells, thus giving one an opportunity to analyze the impact of delivered molecules in real time, before spatial distribution of probes are evaluated by CLSM.

Delivery of membrane-impermeable compounds into cells brings certain demand and challenges which should be overcome in order to achieve their applicability in real systems. For instance, cell viability after transfection should be as much as possible preserved and especially in case of sensitive probes such as nucleic acids, denaturation or digestion within the cells should be avoided in order to preserve biological activity of the probe.

Whereas lipid-based delivery of aptamers was already described (Theis et al., 2004) and serves in general as a very common tool for the delivery of various nucleic acids into cells (Wasungu and Hoekstra, 2006; Faneca et al., 2013), examples for aptamers delivery by electroporation were hard to find in the literature. Hence, additional motivation has come out to put efforts to demonstrate that *in situ* electroporation is an appropriate method for delivery of aptamers. Behavior of cells before, during and after introduction of aptamers into cells by electroporation (ISE) and chemical transfection was monitored impedimetrically using ECIS technology. The fate of DNA aptamers within living cells after *in situ* electroporation and after chemical transfection with Lipofectamine® was investigated using microscopy (CLSM). Fixation and permeabilization of cells leads to irreversible membrane permeabilization and, since the probe can thus freely diffuse into the cytosol, it was interesting to observe, where the accumulation of fluorescent probes takes place within the cell. In addition, digestion of oligonucleotides by nucleases within the cells is hindered this way and therefore, this assay represents a valuable control for oligonucleotide delivery.

NRK cells were applied as a main cell model to verify the hypothesis that *in situ* electroporation employing ECIS facilitates effective delivery of aptamers into cells. This cell line was subjected to two very similar fluorescently-labeled aptamers (APT 1 and APT 2), as well as to the other fluorescently-labeled probes (FITC-dextran) and fluorescent label itself. Other cell lines (HaCaT, CHO-K1 and NIH-3T3) served as the additional cell models to

revise, control and confirm findings obtained with NRK cells. They were tested in order to estimate reproducibility and versatility of *in situ* electroporation as a delivery method, as well as to evaluate its applicability for wide range of different mammalian cell types. Since the results acquired for NRK cells were highly reproducible and generally applicable for all evaluated cell lines, delivery of aptamers into NRK cells will be discussed in details in the scope of different methodological aspects. Delivery of aptamers using *in situ* electroporation and chemical transfection will be discussed and compared, with fixation and permeabilization applied as a control. Thereafter, observed similarities and differences regarding delivery of aptamers into different cell lines in this work will be compared and discussed.

7.6.1 Delivery of Aptamers into NRK Cells – Methodological Aspects

Cell line NRK served as a main model system for the delivery of aptamers into adherent mammalian cells. Fluorescently-labeled DNA aptamer APT 1 was initially applied to conduct *in situ* electroporation and chemical transfection for aptamers delivery and to perform any optimization steps necessary for these experimental procedures. Another DNA aptamer APT 2 was applied additionally to establish a control for APT 1 and to explore if there is any sequence-specific or sequence-dependent binding of intracellular structures by APT 1. Since the localization of APT 1 was observed within cell nuclei in all four different cell lines tested in this work, a question arose if by chance, APT 1 has a particular ability to bind structures within cell nuclei. To investigate and eliminate this possibility, another non-specific DNA aptamer (APT 2) with random sequence was obtained, whereby all parameters including fluorescent label, molecular mass and number of nucleobases was kept constant and only the sequence (order of nucleobases) was completely different, compared to APT 1.

Initially, NRK cells were electroporated (according to the optimized protocol) three times consecutively in presence of 15 µM APT 1, using standard optimized combination of pulse parameters: 40 kHz, 4 V and 200 ms. Experimental procedure for *in situ* electroporation was repeated several times and the acquired results were very reproducible. After every pulse application impedance signal decreased immediately, since the cell membrane was transiently permeabilized (Stolwijk et al., 2011; Wegener et al., 2002) and NRK cells were allowed to recover to the pre-pulse impedance values. Electroporation efficiency was evaluated always app. 45 – 90 min after pulse application to document the results relatively soon after their introduction into cell cytosol, as the oligonucleotides distribution within the cells after electrotransfer may vary in the course of time (Orio et al., 2013). This group examined temporal and spatial distribution of locked nucleic acid (LNA)/DNA (composed of

LNA bases - ribonucleotide analogues with locked 3′-endo conformation; Kaur et al., 2007) in the electoporated cells. Orio and collaborators reported that 2 hours after electrotransfer, the locked nucleic acid (LNA)/DNA oligomer was observed mainly in the nucleus of electroporated cells and thereafter, signal started to disappear from nucleus and concentrated in the cytoplasm over time.

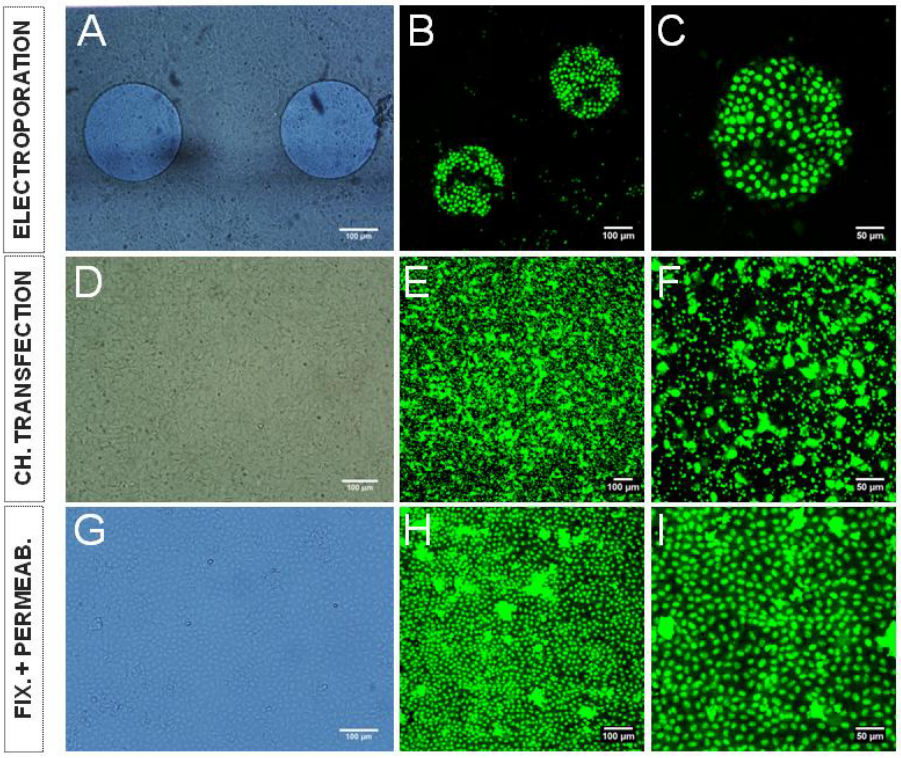

Figure 7.27 Exemplary phase-contrast (**A**, **D**, **G**) and confocal fluorescence micrographs (**B**-**C**, **E**-**F**, **H**-**I**) after *in situ* electroporation (**A-C**), chemical transfection (**D-F**) and fixation and permeabilization (**G-I**) of NRK cells in presence of fluorescent aptamer APT 1. Survey reveals the similarities and differences in delivery efficiency between these three strategies. The scale bar in micrographs **A**, **B**, **D**, **E**, **G** and **H** corresponds to 100 µm and in micrographs **C**, **F** and **I** to 50 µm. All micrographs were taken with 10-fold magnification objective.

In **Figure 7.27**, micrographs are summarized for all three delivery strategies and the fluorescence micrographs **B** and **C** reveal that most of the cells residing on the gold film electrodes of 8W4Eµ electrode array, which received electroporating pulses in presence of APT 1, were successfully loaded with the fluorescent aptamer. Although the fraction of the cells loaded with aptamers varied from electrode to electrode, it is concluded that in all cases most of the cells exhibited strong fluorescence signal coming from fluorescently-labeled aptamers. In all cases, aptamers accumulated predominantly in the cell nuclei. In addition, small bright dots within nucleus structure were observed. This was in agreement with earlier

reports that fluorescein-labeled (DNA) oligonucleotides accumulated rapidly in the nucleus after microinjection into epithelial cells and primary human fibroblasts. In addition, pattern including bright dots was observed app. 60 min after DNA oligonucleotide injection into the cell – nuclear incorporation of DNA (Chin et al., 1990). The mechanism of DNA entry into the cell nucleus and its accumulation there, especially in the form of small dots, is still unknown but it is suggested that transport of oligonucleotides across the nuclear envelope is NLS-assisted and size-dependent (Ludtke et al., 1999). Furthermore, it had been speculated that oligonucleotides might enter the nucleus either by active nuclear transport or by simple diffusion through the nuclepores, which may depend on the affinity of given oligonucleotide for protein binding partners. NLS-containing proteins bind to the DNA and forward it to the nucleus (Dean and Gokay, 2005). There were many efforts made to explore and learn mechanisms of nuclear import of single-stranded DNA (ssDNA). Although one would expect (synthetic) oligonucleotides will aim for cytoplasm as a site of action, it had been demonstrated that small single-stranded oligonucleotides can diffuse freely into the cell nucleus after microinjection or membrane permeabilization (Hagstrom et al., 1997; Leonetti et al., 1991). In the present system, incorporation of fluorescently-labeled aptamers within the nuclei was not extensively explored, but having in mind size of the APT 1 (and APT 2), a scenario including free diffusion into cell nuclei should also not be excluded.

In **Figure 7.28** fluorescence micrographs taken with higher magnification objective demonstrate even more clearly localization of DNA APT 1 (and APT 2) after its delivery using three various strategies. As indicated in the micrograph **A**, after *in situ* electroporation, accumulation of APT 1 takes place within the cell nuclei and the characteristic dotted pattern is observed. Homogenous staining of cytoplasm is obvious, although it is considerably weaker, compared to the fluorescence signal coming from cell nuclei. The number of NRK cells which were effectively loaded with aptamers after chemical transfection is significantly lower, compared to the results obtained after *in situ* electroporation. Although at the first glance, it seems that NRK cells are very well loaded with the fluorescent aptamer, by lipid-mediated transfection (**Figure 7.27 E**), in the micrograph **F** was recognized that, despite the fact fluorescence signal is rather high, a distribution of aptamers within the cells is not optimal in most cases. Besides high level of punctuated staining pattern, only cytoplasm and nucleus of a very small number of cells appeared to contain APT 1. Such observations and number of successfully transfected cells were estimated by looking into the micrograph taken with higher magnification objective (**Figure 7.28 C**).

In contrast to co-localization study of APT 1 with LysoTracker® after electroporation (**Figure 7.5 E**), which showed no overlap, since aptamers accumulated mostly in the nuclei, co-

localization study of aptamer APT 1 and LysoTracker® after chemical transfection showed certain level of overlapping, as aptamers accumulated in the vesicles and formed small bright dots around nucleus (perinucelarly) (**Figure 7.10 E**). Similar observations were published by (Chin et al., 1990), who noticed that after addition of DNA oligonucleotides to the cells (in culture medium), perinuclear and punctuate staining in the cytoplasm occurred, as an indicator of endocytosis and low membrane permeability (Loke et al., 1989).

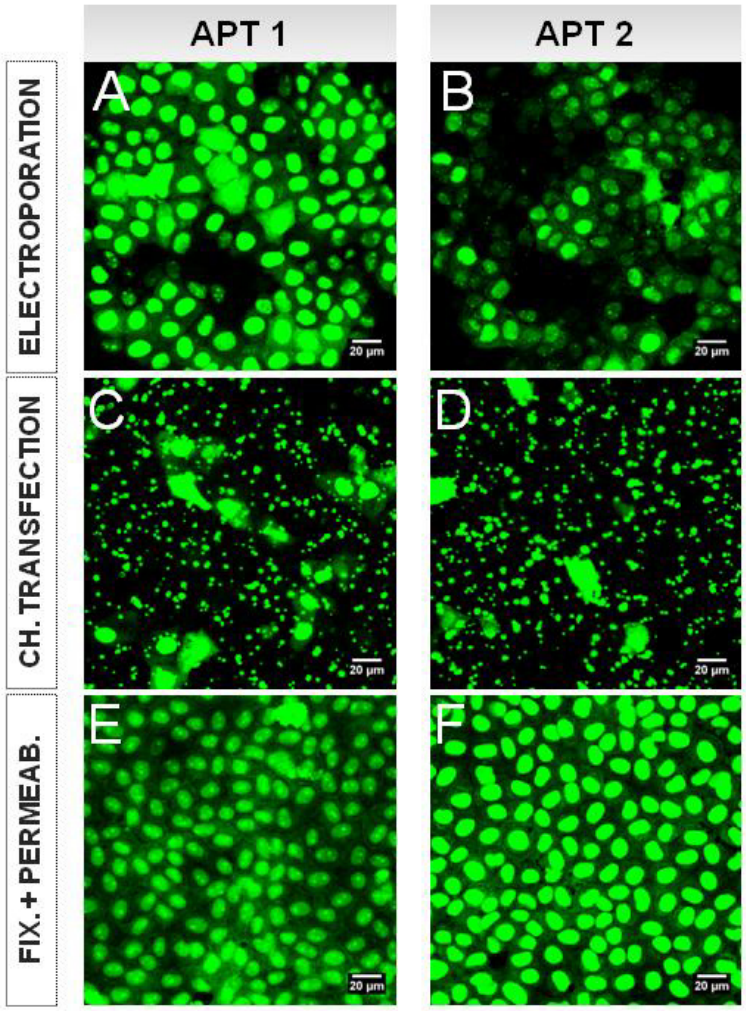

Figure 7.28 Exemplary confocal fluorescence micrographs taken after *in situ* electroporation (**A**, **B**), chemical transfection (**C**, **D**) and fixation and permeabilization (**E**, **F**) of NRK cells in presence of fluorescent aptamer APT 1 (micrographs in the left column) and aptamer APT 2 (micrographs in the right column). Survey reveals the similarities and differences in delivery of APT 1 and APT 2 using these three strategies. The scale bar corresponds to 20 µm. All micrographs were taken with 60-fold magnification objective.

The investigation of extent and localization of aptamer-modified liposomes after their entry into the intracellular environment has been often investigated using the lysosome staining

with LysoTracker®. Similarly to the results obtained in this work (chapters 7.2.1 and 7.2.2), Ara et al., 2014 observed that Apt-PEG-LPs (aptamer-polyethylene glycol-liposomes) co-localized with LysoTracker® and they concluded that less than a half of the staining originating from the aptamer-modified PEG-LPs did not overlap with the lysosomes, as some aptamers managed to escape from endosomes.

There are many reports on cationic liposomes applied as a delivery method for transfer of oligonucleotides into various cell types. However, great amount of oligonucleotides which cross the cell membrane this way remain associated in vesicles with the same protein to which they were initially binding on the cell surface. In contrast, only small percentage of oligonucleotides can be observed in cytosol, not associated to the proteins (Dean and Gokay, 2005). In the current work, delivery of aptamers into living cells by electroporation and cationic lipid-based transfection was additionally compared to the free diffusion of aptamers into cells after their fixation and permeabilization. Although in this case it cannot be discussed on the living cells system, this method has been already extensively applied for different studies of oligonucleotides entry to cells (Bamford et al., 2014). Nucleic acids can thus freely cross disrupted cell membrane and find their targets or the site of interest without any barriers or obstacles in a form of nucleases, for example. In a given cell system, investigation of oligonucleotides journey after their addition to fixed and permeabilized cells can be considered as a sort of a positive control.

The results obtained in this work after addition of APT 1 to fixed and permebilized NRK cells are compared with two delivery methods in **Figure 7.27** (**H** and **I**) and in **Figure 7.28 E**. These fluorescence micrographs reveal that the fluorescence signal originates from every cell, as APT 1 was able to diffuse into all cells through their irreversibly permeabilized membrane. Regarding of localization pattern after aptamer entry in fixed and permeabilized cells, the situation can be very much compared to the localization pattern after aptamer delivery by *in situ* electroporation. Nuclei of the cells appeared bright, since the fluorescent aptamers accumulated predominantly within this part of the cell and small bright dots were exhibited in most of the nuclei (**Figure 7.28 E**), similarly as after electroporation (**Figure 7.28 A**). Fluorescent signal was also found in cytoplasm (rather homogenously distributed), however, fluorescence intensity was significantly weaker than in the cell nuclei, the same is valid for cell borders, corresponding to the cell membrane, which was recognized in some cells. From these observations, it might be concluded that aptamers aim for nucleus of the cells and that in the case of electroporation, they can easily reach their target, whereas after chemical transfection, oligonucleotides only partially manage to reach their target. Such observations made after addition of APT 1 to fixed and permeabilized cells are in line with

the previously reported studies from the literature (Bamford et al., 2014). Thus, fluorescently-labeled DNA with different sequences, delivered into cells permeabiliized with digitonin, remained partially in cytoplasm, but with the great part entered nuclei (Hagstrom et al., 1997). Furthermore, an attempt by the group of researchers to select and develop single-stranded aptamer binding to the green fluorescent protein (GFP) was not quite successful, however, they also studied diffusion of such oligonucleotides into fixed and aldehyde-permeabilized PtK cells. As reported, entry of single-stranded DNA was very fast and it shuttled directly to the nuclei of cells (Stanlis and McIntosh, 2003).

The group of researchers from England applied FRET technology to track single- and double-stranded DNA molecules after their transfer into CHO cells by four different methods. FRET (fluorescence resonance energy transfer) is based on the close proximity of two compatible fluorophores (here Cy3 and Cy5) for energy transfer. Complementary DNA strands forming stable dsDNA, or both ends of ssDNA were tagged with the respective fluorophores and exhibited FRET outside of the cellular environment. The group investigated if FRET will be still observed after dsDNA and ssDNA enter the cells, indicating that integrity of ssDNA and dsDNA is not compromised after their introduction into the cytosol (Bamford et al., 2014). The results indicated successful delivery of DNA into cells by electroporation (in a cuvette) and by microinjection, whereby these two invasive methods gave very similar results. In both cases, ssDNA and dsDNA remained intact. On the other hand, chemical transfection (with Lipofecamine®) facilitated cell transfection with single- and double-stranded DNA but no FRET signal was observed, indicating decomposition of DNA by nucleases and the appeareance of bright fluorescing spots suggested that DNA remained captured within the endocytotic vesicles. After DNA readily permeated into the fixed and permeabilized cells (using methanol), intact DNA duplex, as well as the single-stranded DNA were evidenced by FRET (Bamford et al., 2014).

After *in situ* electroporation of APT 1 was investigated and compared to chemical transfection and diffusion of APT 1 into fixed and permeabilized cells, another fluorescently-labeled non-specific aptamer was tested using all three delivery strategies, in order to avoid any doubt that results acquired with APT 1 were, by chance, linked to the aptamer sequence. Aptamer APT 2 contained completely different sequence compared to APT 1. However, results with APT 2 were still very similar to the results acquired with APT 1, which showed that the results are consistent, regardless of aptamer sequence. Surprisingly, APT 2 exhibited overall slightly lower fluorescence intensity within the cells after electroporation and chemical transfection, whereas results for fixed and permeabilized cells were consistent with APT 1. Difference in intensity of fluorescence signal observed between APT 1 and APT 2 was rather small and

the reason for such difference is unknown, having on mind these two aptamers were labeled using the same fluorescein label.

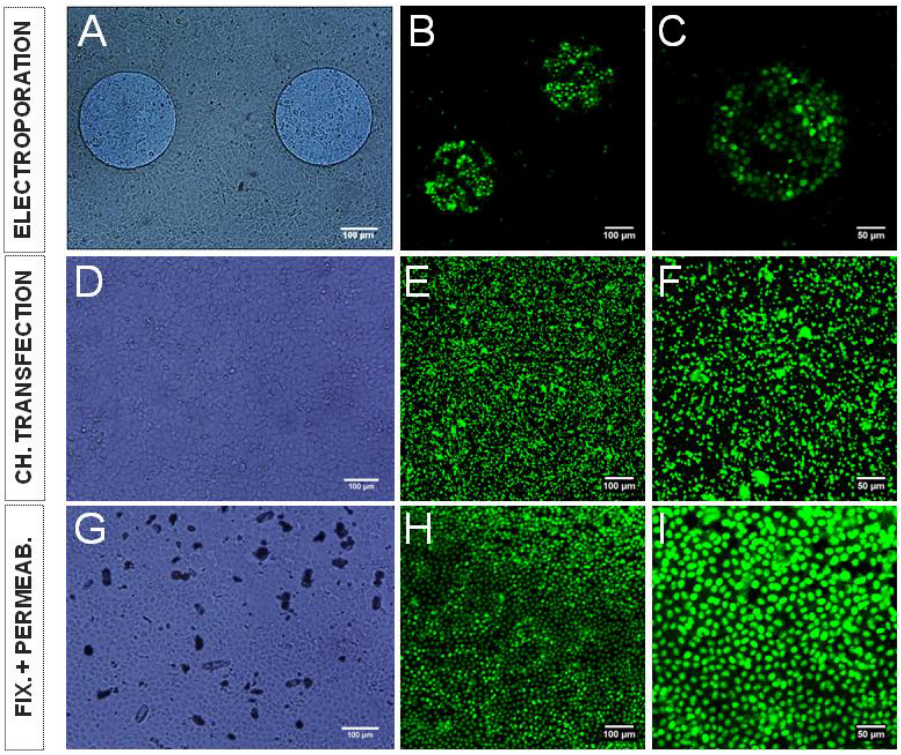

Figure 7.29 Exemplary phase-contrast (**A**, **D**, **G**) and confocal fluorescence micrographs (**B**-**C**, **E**-**F**, **H**-**I**) after *in situ* electroporation (**A-C**), chemical transfection (**D-F**) and fixation and permeabilization (**G-I**) of NRK cells in presence of fluorescent aptamer APT 2. Survey reveals the similarities and differences in delivery efficiency between these three strategies. The scale bar in micrographs **A**, **B**, **D**, **E**, **G** and **H** corresponds to 100 µm and in micrograhs **C**, **F** and **I** to 50 µm. All micrographs were taken with 10-fold magnification objective.

Figure 7.29 summarizes exemplary micrographs taken after *in situ* electroporation (**A**-**C**), chemical transfection (**D**-**F**) and fixation and permeabilization (**G-I**) of NRK cells. Analysis of these micrographs leads to the same conclusions which were already extracted with APT 1 (**Figure 7.27**). Comparing the micrographs taken for APT 1 and APT 2, loading of the cells with APT 2 can be described as slightly reduced, compared with the loading with APT 1, although no precise explanation is found for that, since all parameters for both aptamers and delivery strategies were the same, except that sequences of these two oligonucleotides were different. In addition, it has been noticed during impedance measurements including triple successive electroporation of NRK cells in presence of APT 2 that the cells recovered slower after second and especially after the third pulse application. Again, since the experimental procedure and applied buffer for *in situ* electroporation of NRK cells in presence of APT 1

and APT 2 were kept constant, it remained unclear, what led to such small differences in loading efficiency between those two probes. Micrographs taken with higher magnification objective after uptake of APT 2 into NRK cells using *in situ* electroporation (**B**), chemical transfection (**D**) and fixation and permeabilization (**F**) are summarized in **Figure 7.28** and clearly demonstrate staining/loading pattern of APT 2 within the cells described previously.

Fluorescent Aptamer versus Conventional Fluorescent Probes

Delivery of fluorescently-labeled DNA aptamers into cells and loading pattern seen primarily after *in situ* electroporation was compared with delivery of other fluorescent probes to the intracellular environment. Considering the susceptibility of oligonucleotides to nucleases-mediated degradation, there was a concern that strong fluorescence signal coming from cell nuclei may be a consequence of denaturation of fluorescently-labeled aptamer. Thereby, nucleic acid would be possibly digested by enzymes nucelases and fluorescent label (fluorescein) could diffuse, due its small size, through the nucleopores into the nuclei and accumulate within its structure. This possible scenario was investigated by the addition of pure fluorescein to fixed and permeabilized NRK cells. The action of nucleases in fixed cells, which could digest the nucleic acids, was thus rather unlikely. However, after pure fluorescein freely permeated into NRK cells, it did not accumulate in the cell nuclei, but only stained the cell cytoplasm to some extent. Cell nuclei appeared dark and unstained in that case, or with very less fluorescence signal, probably as an artifact since the gain during microcopy was set to higher levels to document the fluorescence signal precisely. In addition, no bright spots within nuclear structure were observed. The results were shown in **Figure 7.14** (in chapter 7.2.3) and the same observations were made for 20 µM and 200 µM fluorescein present in the cells. These results indicate that above described hypothesis on degradation of fluorescently-labeled aptamer is not correct and can be rejected. After addition of fluorescently-labeled APT 1 and APT 2 to fixed and permeabilized cells, they accumulated mostly in the nuclei and much less in the cytoplasm, in contrast to the fluorescein, which accumulated only in cytoplasm. In addition, aptamers exhibited characteristic bright dots within the nuclear structure. Interestingly, by comparing the micrographs of NRK cells showing staining with 15 µM APT 1 and 15 µM APT 2 on the one and 20 µM fluorescein on the other side, it may be even concluded that cytoplasmic staining of all three probes is almost the same. Concentration of fluorescein 20 µM was chosen to be nearly the same as of the label in applied aptamers, in order to correlate the better fluorescence intensity and staining pattern between aptamers and fluorescein. This leads to several conclusions: (i) since the staining pattern of both aptamers is completely different

from the fluorescein after their free entry into the cells (in absence of nucleases), these two probes act completely different although they carry the same fluorescent label (ii) this implies that the DNA aptamer aims for cell nucleus, not the fluorescent label, after it enters the cell by crossing the plasma membrane (iii) integrity of DNA aptamer during *in situ* electroporation is not an issue since the staining pattern is very much the same (or at least) very similar to the one obtained after free diffusion of aptamers into fixed and permeabilized cells and finally, (iv), since cytoplasmic staining by 15 µM aptamers and 20 µM fluorescein appears to be the same, it is possible that aptamer probe contains a certain amount of unbound fluorescent label (in a solution), which remains intracellularly mostly in the cytoplasm, as similar effect was observed with the pure fluorescein. Concentration of 200 µM fluorescein was chosen to assure that sufficient fluorescence signal can be documented during microscopy, since the fluorescent probes such as FITC-dextran of different sizes are usually applied using concentration of that order (Stolwijk et al., 2011; Albermann, 2004). Observations made during this experiment are in good agreement with the study performed by Ryttsén et al., 2000, who performed electroporation of single NG108-15 cells with carbon-fiber microelectrodes and applied 5 µM fluorescein as a fluorescent probe. Electroporation was characterized by patch-clamp recordings and fluorescence microscopy and they reported internalization of fluorescence signal from fluorescein in the cytosol of NG108-15 cells. However, loading pattern of fluorescein (332 kDa) observed within cytoplasm of NRK cells after their exposure to ISE in the present work is not in agreement with the studies of ISE conducted on NRK cells using Lucifer yellow (444 kDa), performed by Wegener et al., 2002 and Sperber et al., 2016. Even though fluorescent dye Lucifer yellow is only slightly bigger than fluorescein, previous studies showed its rather homogenous distribution within the NRK cell bodies and its presence in both cytoplasm and nucleus. Therefore, it remains unclear if the size of the molecules, in this case fluorescein, does predominantly determine its distribution and its staining pattern within the cells.

Furthermore, an additional experiment was conducted to investigate the difference in loading pattern between 2 mg/mL FITC-dextran (concentration 200 µM) and 15 µM fluorescently-labeled APT 1. Delivery of these two probes into NRK cells by *in situ* electroporation was conducted in parallel, within one experiment, in order to keep experimental conditions the same. **Figure 7.8** (chapter 7.2.1) shows drastic difference in fluorescence intensity between these two probes, as the fluorescence signal of FITC-dextran was much brighter and stronger than the fluorescence signal exhibited by fluorescein-labeled aptamers. Such difference is most probably caused by the difference in concentration of fluorescent material. Besides, staining pattern of FITC-dextran and APT 1 was very different, considering the fact

that their molecules have comparable molecular masses (FITC-dextran: 10 kDa; APT 1: 16 kDa). Aptamer stained predominantly cell nuclei and showed bright spots within nuclear structure, whereas FITC-dextran homogeneously stained cell cytoplasm and nuclei.

Previously discussed assays conducted on NRK cells demonstrated successful transfer of fluorescent aptamers APT 1 and APT 2 across the cell membrane into cytosol, using *in situ* electroporation. Aptamers accumulated predominantly in cell nuclei and the loading pattern was clearly different from the loading pattern of FITC-dextan or the fluorescein label solely.

In addition, loading efficiency and fluorescence pattern were completely different when aptamers were delivered into NRK cells by ISE and by chemical transfection. In the latter case, punctuated staining indicated localization of aptamers in vesicles and thus predominantly endocytotic uptake of oligomers. Based on these findings, proof-of-principle assay for delivery of aptamers into confluent cell monolayers was established and its applicability for different cell types was evaluated by testing it on three additional cell lines.

7.6.2 Delivery of Aptamers into Different Cell Lines – Comparative Analysis

Protocols for *in situ* electroporation, chemical transfection and fixation and permeabilization, previously applied and established on NRK cells, were implemented to investigate introduction of aptamers into other cell mammalian lines. Thus, applicability, reproducibility and versatility of investigated methods were addressed, especially regarding *in situ* electroporation. Since both fluorescent aptamers APT1 and APT 2 were tested only on NRK cells and all other cell lines were subjected only to APT 1, in the further text abbreviation APT is applied and it corresponds to APT 1, unless specified differently. Besides NRK, cell lines HaCaT, CHO-K1 and NIH-3T3 were applied as the cell models for aptamers study and the aim of this chapter is to compare, discuss and summarize similarities and differences in morphology and response of the different cell types, upon their exposure to the fluorescent DNA aptamer.

Figure 7.30 provides overview of (previously presented) exemplary confocal fluorescence micrographs taken after *in situ* electroporation, chemical transfection and fixation and permeabilization of every cell line. Such overview helps comparison of results acquired with different cell lines. This summary of exemplary micrographs taken with 10-fold magnification objective is completed by the respective summary of exemplary confocal fluorescence micrographs of different cell types taken with higher (60-fold) magnification (**Figure 7.31**).

HaCaT cells were successfully loaded with the fluorescent aptamer by *in situ* elecroporation and the loading efficiency was very comparable to the loading efficiency of NRK cells, if not

even better. Bright fluorescence signal was found in the nuclei of almost every HaCaT cell residing on the electrodes. Besides, cytoplasm of many cells was homogeneously loaded with aptamer. However, chemical transfection of HaCaT was also rather successful, taking into account that aptamer managed to reach nuclei of considerable number of cells. Transfection efficiency after Lipofectamine treatment was surely the best in HaCaT cells, compared to other three evaluated cell lines. Such conclusion is based on the fact that the fluorescence signal was not only observed within vesicles (or in lysosmes and endosomes), but the aptamer obviously managed to escape endocytic pathway in some cases and it reached cytoplasm and nuclei of the cells. Even though significant amount of aptamer was still within vesicles, as indicated by the characteristic punctuated pattern, vesicular localization of the fluorescent signal was not absolutely dominating, as it was the case with other three investigated cell lines.

Loading of CHO-K1 and NIH-3T3 cells with aptamers was quite similar to the loading of NRK and HaCaT cells after ISE, with the bright fluorescence signal mostly originating from cell nuclei. However, fraction of loaded cells on the electrodes was fairly smaller than it was the case with NRK and HaCaT cells, which is explained by detachment of CHO-K1 cells from the substrate before or during microscopy (due to shear stress during pipetting) and most probably increased endocytosis observed on NIH-3T3 cells. Cell lines CHO-K1 and NIH-3T3 exhibited more unspecific uptake of aptamer than NRK and HaCaT cells, and this was especially the case with NIH-3T3 cells, which made the assessment of loading efficiency more difficult for this cell line. Chemical transfection of CHO-K1 and NIH-3T3 cells gave similar results as with NRK cells, with high level of fluorescence signal coming from cell vesicles and only in some rare cases, aptamers were located within nuclei or cell cytoplasm. After crossing the membrane of these cells, aptamer mostly remained entrapped in vesicles. Observations made after fixation and permeabilization of the cells to allow free diffusion of aptamers into cells were very consistent for all four cells lines evaluated in this work.

Addition of aptamer to fixed and permeabilized cells resulted in its accumulation predominantly in cell nuclei, and much weaker signal was originating from homogeneously stained cell cytoplasm. Small bright dots within nuclei structure were observed in most of the cells. Such aptamer localization was very comparable with the localization of aptamers after their delivery by ISE. It is hypothesized that these bright dots are in fact nucleoli, however, literature resources do not provide applicable explanations or confirmation in this case, as the mechanisms of oligonucleotides accumulation within the cell nuclei are still poorly understood.

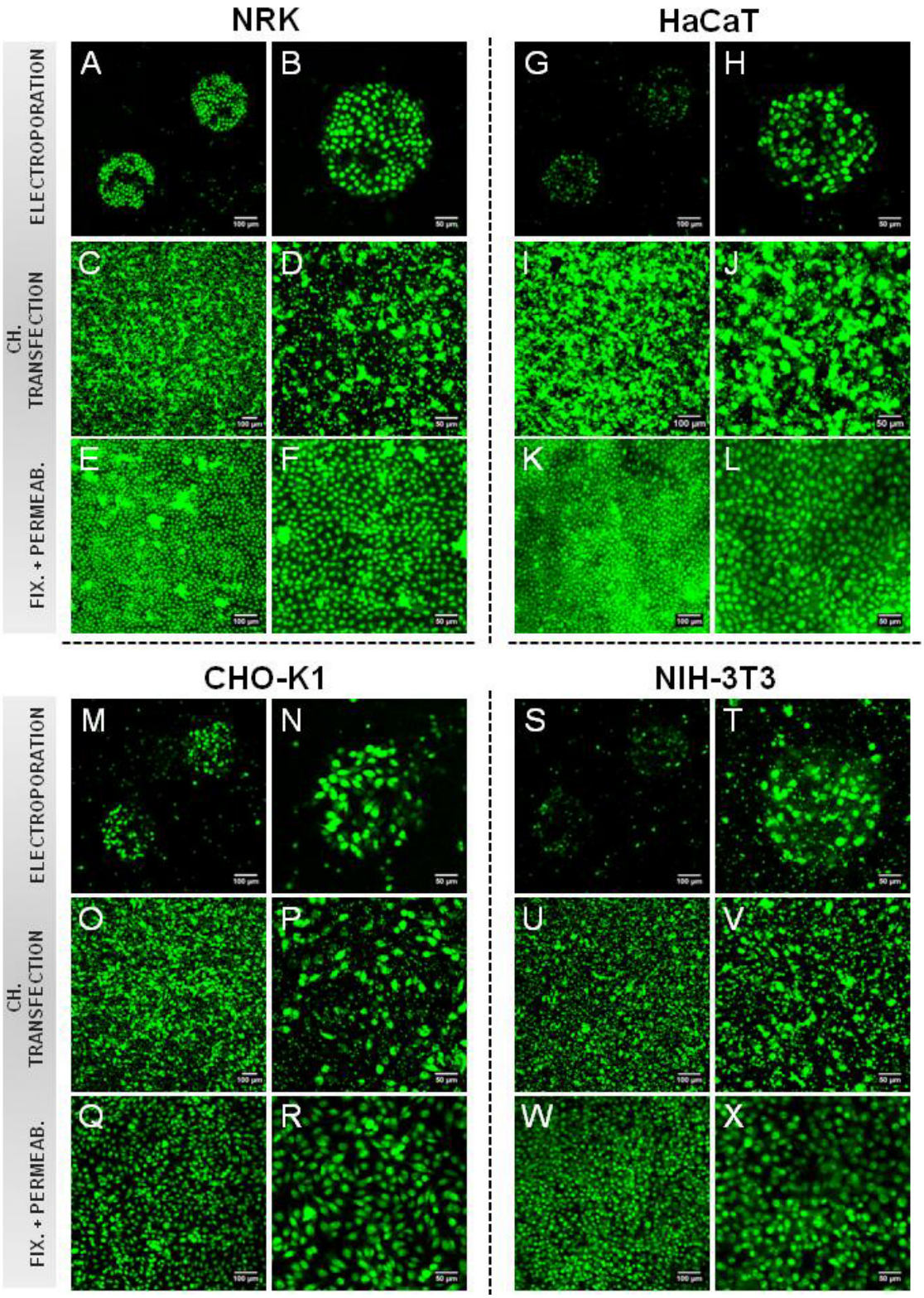

Figure 7.30 Overview and comparison of confocal fluorescence micrographs taken on different cell lines: NRK (**A-F**), HaCaT (**G-L**), CHO-K1 (**M-R**) and NIH-3T3 (**S-X**) after *in situ* electroporation, chemical transfection, and fixation and permeabilization in presence of fluorescent aptamer APT 1. Scale bar of the micrographs in the first and third column corresponds to 100 µm and in the second and fourth column to 50 µm. All micrographs were taken with 10-fold magnification objective.

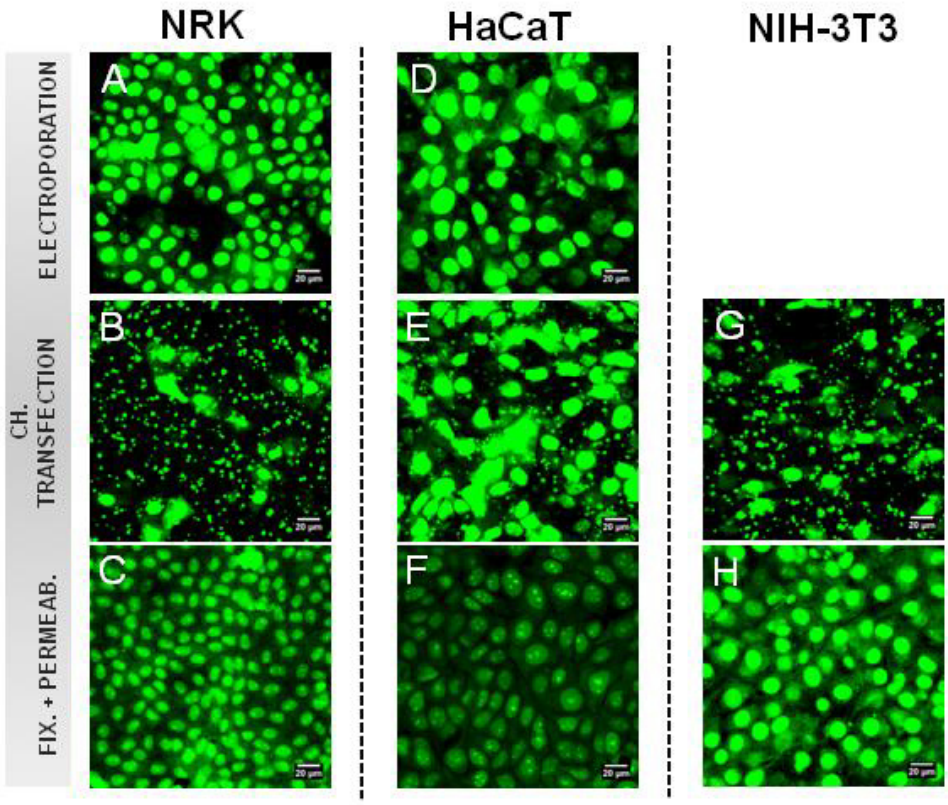

Figure 7.31 Overview and comparison of confocal fluorescence micrographs taken on different cell lines: NRK (**A-C**), HaCaT (**D-F**) and NIH-3T3 (**G-H**) after *in situ* electroporation, chemical transfection, and fixation and permeabilization in presence of fluorescent aptamer APT 1. Scale bar corresponds to 20 µm. All micrographs were taken with 60-fold magnification objective.

Chemical transfection facilitated entrance of aptamers in all cell lines, however, micrographs clearly showed their localization within vesicles, cell lysosomes (when co-localization study was conducted on NRK cells) and endocytic uptake (NIH-3T3 cells), as characteristic punctuated pattern was recognized. This is in agreement with the study performed by Nicol et al., 2013 and Cesur et al., 2015 who applied chemical transfection for delivery of aptamers into different cell lines. The aim of their study was to select RNA aptamer (named A2) binding to HPV16 E7 oncoprotein (Human papillomavirus 16) with the high affinity and to apply chemical transfection mediator Oligofectamine for its introduction into E7-positive cell lines (SiHa and CaSki) and cell lines HeLa, C33A and HaCaT, which do not express E7, to measure off-target effects. However, before they looked into specific effect of A2 aptamer, they studied uptake of Cy3-labeled RNA aptamer (not binding to E7) by the cells chemically transfected with Oligofectamine. They counted the cells containing aptamers after their incubation with Oligofectamine and determined the transfection efficiency of 87% (n = 90). However, they observed that 3 hours after transfection, aptamer was mostly localized in early

endosomes (63.3%), whereas 6 hours after transfection, amount of aptamer was reduced within the cells, and it was distributed both in early and late endosomes / lysosomes (45.5% and 33.2% respectively). In addition, they investigated spatial and temporal distribution of another aptamer within the SiHa cells, however, the results were very similar. Based on such results, the group concluded that RNA aptamers land in early or late endosomes and lysosomes upon their entry to the cells by chemical transfection. Such results correspond very well to the outcome of experiments conducted in this work with the fluorescent aptamer where Lipofectamine® was applied as chemical transfection reagent.

Hu et al., 2015 described isolation of single-stranded DNA (ssDNA) aptamer Ras-a1 targeting human Ras protein with high affinity and specificity. Electroporation was applied to deliver Cy3-labeled Ras-a1 into vascular smooth muscle cells (VSMCs) in suspension. Electric pulse of 200 V for 20 ms was applied and the group determined the transfection efficiency of 82.11 ± 6.03 %, calculated as the ratio of electroporated cells labeled with Cy3 red fluorescence in the dark field (fluorescence micrographs) to the cells in the bright field (phase-contrast micrographs). Interestingly, the survival rate of the cells was 83.04 ± 1.74 %. In addition, the group followed proliferation and migration of VSMCs after aptamer Ras-a1 was introduced in the cells by electroporation. Proliferation and migration of VSMC cells is mediated by Ras protein and these processes are crucial for restenosis after PCI (percutaneous coronary intervention) and CABG (coronary artery bypass graft). Therefore, they selected ssDNA aptamer against Ras protein and investigated if aptamer Ras-a1 can influence proliferation and migration of VSMC cells. They found that both proliferation and migration of VSMCs were significantly inhibited in cells transfected with Ras-a1 compared to controls (cells pulsed in absence of aptamer). Inhibition of proliferation (by targeting Ras protein) was measured after 12, 24, 36 and 48 h and the maximal inhibition rates were obtained at 24 h (40 %), whereas prolonged treatment did not improved the inhibition rate. The success of aptamer delivery by electroporation in the work of Hu and collaborators is in agreement with the results of aptamer delivery by ISE demonstrated in this work. It provides also a nice example for targeted application of (DNA) aptamers within the cells, which is enabled and even enhanced by the direct delivery of aptamers in the cell cytosol by electroporation. The group of Hu followed proliferation of VSMCs cells and thus progress of proliferation inhibition by using commercial CCK-8 kit (cell counting kit-8 assay), whereas migration was determined using a Transwell assay. However, having on mind versatility of an ECIS platform and its applicability for electric manipulation of the cells (Stolwijk et al., 2011; Wegener et al., 2002), as well as for the monitoring of cell proliferation (Szulcek et al., 2014; Sperber, 2016; Stolwijk et al., 2012) and cell migration (Keese et al., 2004), a study similar to

the one described by Hu and collaborators could be also performed entirely on the ECIS platform. The great advantage of such approach would be assessment of the cellular response within the confluent monolayer, in a time-resolved manner, whereby possible artifacts of end-point assays are eliminated.

Studies conducted in the current work demonstrated successful and highly efficient delivery of DNA aptamers into different cell lines by ISE and proved that *in situ* electroporation should be seriously considered as a delivery method during future attempts to develop aptamers against intracellular targets. Not only that cells are efficiently loaded with oligonucleotides in their natural state (close to their natural environment, in contrast to cells in suspension), but the delivery of oligonucleotides is also facilitated for the specific and well-defined cell population (residing on the electrodes).

7.7 References

Albermann, S. (2004) In situ Elektroporation adhärenter Säugerzellen. PhD Thesis, Westfälische Wilhelms-Universität Münster.

Ara, M.N., Matsuda, T., Hyodo, M., Sakurai, Y., Hatakeyama, H., Ohga, N., Hida, K., and Harashima, H. (2014) An aptamer ligand based liposomal nanocarrier system that targets tumor endothelial cells. *Biomaterials* 35, 7110-7120.

Bamford, R.A., Zhao, Z.Y., Hotchin, N.A., Styles, I.B., Nash, G.B., Tucker, J.H., and Bicknell, R. (2014) Electroporation and microinjection successfully deliver single-stranded and duplex DNA into live cells as detected by FRET measurements. *PLoS One* 9

Becker, R.C., and Chan, M.Y. (2009) REG-1, a regimen comprising RB-006, a Factor IXa antagonist, and its oligonucleotide active control agent RB-007 for the potential treatment of arterial thrombosis. *Current Opinion in Molecular Therapeutics* 11, 707-715.

Blind, M., Kolanus, W., and Famulok, M. (1999) Cytoplasmic RNA modulators of an inside-out signal-transduction cascade. *Proceedings of the National Academy of Sciences of the United States of America* 96, 3606-3610.

Brody, E.N., and Gold, L. (2000) Aptamers as therapeutic and diagnostic agents. *Journal of Biotechnology* 74, 5-13.

Cesur, Ö., Nicol, C., Groves, H., Mankouri, J., Blair, G.E., and Stonehouse, N.J. (2015) The subcellular localisation of the human papillomavirus (HPV) 16 E7 protein in cervical cancer cells and its perturbation by RNA aptamers. *Viruses* 7, 3443-3461.

Chin, D.J., Green, G.A., Zon, G., Szoka, F.C., Jr., and Straubinger, R.M. (1990) Rapid nuclear accumulation of injected oligodeoxyribonucleotides. *Nature: New Biology* 2, 1091-1100.

Cho, E.J., Lee, J.W., and Ellington, A.D. (2009) Applications of aptamers as sensors. *Annual Review of Analytical Chemistry* 2, 241-264.

Dean, D.A., and Gokay, K.E. (2005) Nuclear import and export in plants and animals. In Nuclear import of DNA (Plenum Publishers, Springer US), pp. 187-205.

Dirks, R.W., and Tanke, H.J. (2006) Advances in fluorescent tracking of nucleic acids in living cells. *Biotechniques* 40, 489-496.

Ellington, A.D., and Szostak, J.W. (1990) In vitro selection of RNA molecules that bind specific ligands. *Nature* 346, 818-822.

Ellington, A.D., and Szostak, J.W. (1992) Selection in vitro of single-stranded DNA molecules that fold into specific ligand-binding structures. *Nature* 355, 850-852.

Famulok, M., Mayer, G., and Blind, M. (2000) Nucleic acid aptamers from selection in vitro to applications in vivo. *Accounts of Chemical Research: ACR* 33, 591-599.

Faneca, H., Cardoso, A., Trabulo, S., Duarte, S., and de Lima Pedroso, M.C. (2013) Cationic liposome-based systems for nucleic acid delivery: From the formulation development to therapeutic applications. In Drug delivery systems: advanced technologies potentially applicable in personalised treatment, J. Coelho, ed. (Springer Netherlands), pp. 153-184.

Fisher, T.L., Terhorst, T., Cao, X., and Wagner, R.W. (1993) Intracellular disposition and metabolism of fluorescently-labeled unmodified and modified oligonucleotides microinjected into mammalian cells. *Nucleic Acids Research* 21, 3857-3865.

Giannetti, A., Tombelli, S., and Baldini, F. (2013) Oligonucleotide optical switches for intracellular sensing. *Analytical and Bioanalytical Chemistry* 405, 6181–6196.

Hagstrom, J.E., Ludtke, J.J., Bassik, M.C., Sebestyen, M.G., Adam, S.A., and Wolff, J.A. (1997) Nuclear import of DNA in digitonin-permeabilized cells. *Journal of Cell Science* 110, 2323-2331.

Han, K., Liang, Z., and Zhou, N. (2010) Design strategies for aptamer-based biosensors. *Sensors* 10, 4541-4557.

Hu, X., Wang, Z., Wu, H., Jiang, W., and Hu, R. (2015) Ras ssDNA aptamer inhibits vascular smooth muscle cell proliferation and migration through MAPK and PI3K pathways. *International Journal of Molecular Medicine* 35, 1355-1361.

Huang, K., and Martí, A.A. (2012) Recent trends in molecular beacon design and applications. *Analytical and Bioanalytical Chemistry* 402, 3091-3102.

Ireson, C.R., and Kelland, L.R. (2006) Discovery and development of anticancer aptamers. *Molecular Cancer Therapeutics* 5, 2957-2962.

Jayasena, S.D. (1999) Aptamers: an emerging class of molecules that rival antibodies in diagnostics. *Clinical Chemistry* 45, 1628–1650.

Juskowiak, B. (2011) Nucleic acid-based fluorescent probes and their analytical potential. *Analytical and Bioanalytical Chemistry* 399, 3157–3176.

Kaur, H., Babu, B.R., and Maiti, S. (2007) Perspectives on chemistry and therapeutic applications of Locked Nucleic Acid (LNA). *Chemical Reviews* 107, 4672-4697.

Keefe, A.D., Pai, S., and Ellington, A. (2010) Aptamers as therapeutics. *Nature Reviews Drug Discovery* 9, 537-550.

Keese, C.R., Wegener, J., Walker, S.R., and Giaever, I. (2004) Electrical wound-healing assay for cells in vitro. *Proceedings of the National Academy of Sciences of the United States of America* 101, 1554-1559.

Leonetti, J.P., Mechti, N., Degols, G., Gagnor, C., and Lebleu, B. (1991) Intracellular distribution of microinjected antisense oligonucleotides. *Proceedings of the National Academy of Sciences of the United States of America* 88, 2702-2706.

Lim, Y.C., Kouzani, A.Z., and Duan, W. (2009) Aptasensors design considerations. In Computational intelligence and intelligent systems, Z. Cai, Z. Li, Z. Kang, and Y. Liu, eds. (Springer Berlin Heidelberg), pp. 118-127.

Loke, S.L., Stein, C.A., Zhang, X.H., Mori, K., Nakanishi, M., Subasinghe, C., Cohen, J.S., and Neckers, L.M. (1989) Characterization of oligonucleotide transport into living cells.

Proceedings of the National Academy of Sciences of the United States of America 86, 3474-3478.

Ludtke, J.J., Zhang, G., Sebestyen, M.G., and Wolff, J.A. (1999) A nuclear localization signal can enhance both the nuclear transport and expression of 1 kb DNA. *Journal of Cell Science* 112, 2033-2041.

Luzi, E., Minunni, M., Tombelli, S., and Mascini, M. (2003) New trends in affinity sensing: aptamers for ligand binding. *TrAC: Trends in Analytical Chemistry* 22, 810-818.

Meyer, C., Eydeler, K., Magbanua, E., Zivkovic, T., Piganeau, N., Lorenzen, I., Grötzinger, J., Mayer, G., Rose-John, S., and Hahn, U. (2012) Interleukin-6 receptor specific RNA aptamers for cargo delivery into target cells. *RNA Biology* 9, 67-80.

Meyer, C., Hahn, U., and Rentmeister, A. (2011) Cell-specific aptamers as emerging therapeutics. *Journal of Nucleic Acids*, 1-19.

Ng, E.W.M., Shima, D.T., Calias, P., Cunningham, E.T., Guyer, D.R., and Adamis, A.P. (2006) Pegaptanib, a targeted anti-VEGF aptamer for ocular vascular disease. *Nature Reviews Drug Discovery* 5, 123-132.

Nicol, C., Cesur, Ö., Forrest, S., Belyaeva, T.A., Bunka, D.H.J., Blair, G.E., and Stonehouse, N.J. (2013) An RNA aptamer provides a novel approach for the induction of apoptosis by targeting the HPV16 E7 oncoprotein. *PLoS One* 8, e64781.

Nutiu, R., and Li, Y. (2005) Aptamers with fluorescence-signaling properties. *Methods* 37, 16–25.

Ocaña, C., Lukic, S., and del Valle, M. (2015) Aptamer-antibody sandwich assay for cytochrome c employing an MWCNT platform and electrochemical impedance. *Microchimica Acta* 182, 2045–2053.

Orava, E.W., Cicmil, N., and Gariépy, J. (2010) Delivering cargoes into cancer cells using DNA aptamers targeting internalized surface portals. *Biochimica et Biophysica Acta* 12, 6.

Orio, J., Bellard, E., Baaziz, H., Pichon, C., Mouritzen, P., Rols, M.-P., Teissié, J., Golzio, M., and Chabot, S. (2013) Sub-cellular temporal and spatial distribution of electrotransferred LNA/DNA oligomer. *Journal of RNAi and Gene Silencing* 9, 479-485.

Pendergrast, P.S., Marsh, H.N., Grate, D., Healy, J.M., and Stanton, M. (2005) Nucleic acid aptamers for target validation and therapeutic applications. *Journal of Biomolecular Techniques: JBT* 16, 224-234.

Radi, A.-E. (2011) Electrochemical aptamer-based biosensors: recent advances and perspectives. *International Journal of Electrochemistry* 2011

Roh, C., Kim, S.E., and Jo, S.-K. (2011) Label free inhibitor screening of hepatitis C virus (HCV) NS5B viral protein using RNA oligonucleotide. *Sensors* 11, 6685-6696.

Ryttsén, F., Farre, C., Brennan, C., Weber, S.G., Nolkrantz, K., Jardemark, K., Chiu, D.T., and Orwar, O. (2000) Characterization of single-cell electroporation by using patch-clamp and fluorescence microscopy. *Biophysical Journal* 79, 1993-2001.

Sampson, T. (2003) Aptamers and SELEX: the technology. *World Patent Information* 25, 123–129.

Scheller, F.W., Wollenberger, U., Warsinke, A., and Lisdat, F. (2001) Research and development in biosensors. *Current Opinion in Biotechnology* 12, 35-40.

Sefah, K., Shangguan, D., Xiong, X., O'Donoghue, M.B., and Tan, W. (2010) Development of DNA aptamers using Cell-SELEX. *Nature Protocols* 5, 1169-1185.

Song, K.M., Lee, S., and Ban, C. (2012) Aptamers and their biological applications. *Sensors* 12, 612-631.

Song, S., Wang, L., Li, J., Zhao, J., and Fan, C. (2008) Aptamer-based biosensors. *Trends in Analytical Chemistry* 27, 108–117.

Soundararajan, S., Chen, W., Spicer, E.K., Courtenay-Luck, N., and Fernandes, D.J. (2008) The nucleolin targeting aptamer AS1411 destabilizes Bcl-2 messenger RNA in human breast cancer cells. *Cancer Research* 68, 2358-2365.

Sperber, M. (2016) Impedance-based analysis of the cellular response to microparticles: Theory, assay development and model study. PhD Thesis, Universität Regensburg

Sperber, M., Hupf, C., Lemberger, M.-M., Goricnik, B., Hinterreiter, N., Lukic, S., Oberleitner, M., Stolwijk, J.A., and Wegener, J. (2016) Monitoring the impact of nanomaterials on animal cells by impedance analysis: a noninvasive, label-free, and multimodal approach. In Measuring Biological Impacts of Nanomaterials, J. Wegener, ed. (Springer International Publishing), pp. 45-108.

Stanlis, K.K., and McIntosh, J.R. (2003) Single-strand DNA aptamers as probes for protein localization in cells. *Journal of Histochemistry and Cytochemistry* 51, 797-808.

Stolwijk, J.A., Hartmann, C., Balani, P., Albermann, S., Keese, C.R., Giaever, I., and Wegener, J. (2011) Impedance analysis of adherent cells after in situ electroporation: Non-invasive monitoring during intracellular manipulations. *Biosensors and Bioelectronics* 26, 4720–4727.

Stolwijk, J.A., Michaelis, S., and Wegener, J. (2012) Cell growth and cell death studied by electric cell-substrate impedance sensing. In Electric cell-substrate impedance sensing and cancer metastasis, W.G. Jiang, ed. (Dordrecht: Springer Netherlands), pp. 85-117.

Szulcek, R., Bogaard, H.J., and van Nieuw Amerongen, G.P. (2014) Electric cell-substrate impedance sensing for the quantification of endothelial proliferation, barrier function, and motility. *Journal of Visualized Experiments:JoVE* 28, 51300.

Theis, M.G., Knorre, A., Kellersch, B., Moelleken, J., Wieland, F., Kolanus, W., and Famulok, M. (2004) Discriminatory aptamer reveals serum response element transcription regulated by cytohesin-2. *Proceedings of the National Academy of Sciences of the United States of America* 101, 11221-11226.

Tuerk, C., and Gold, L. (1990) Systematic evolution of ligands by exponential enrichment: RNA ligands to bacteriophage T4 DNA polymerase. *Science* 249, 505-510.

Velasco-Garcia, M.N., and Missailidis, S. (2009) New trends in aptamer-based electrochemical biosensors. *Gene Therapy and Molecular Biology* 13, 1-10.

Wasungu, L., and Hoekstra, D. (2006) Cationic lipids, lipoplexes and intracellular delivery of genes. *Journal of Control Release* 116, 255-264.

Wegener, J., Keese, C.R., and Giaever, I. (2002) Recovery of adherent cells after in situ electroporation monitored electrically. *Biotechniques* 33, 348 - 352.

White, R.R., Sullenger, B.A., and Rusconi, C.P. (2000) Developing aptamers into therapeutics. *Journal of Clinical Investigation* 106, 929-934.

Zamay, T.N., Kolovskaya, O.S., Glazyrin, Y.E., Zamay, G.S., Kuznetsova, S.A., Spivak, E.A., Wehbe, M., Savitskaya, A.G., Zubkova, O.A., Kadkina, A., et al. (2014) DNA-aptamer targeting vimentin for tumor therapy in vivo. *Nucleic Acid Therapeutics Journal* 24, 160-170.

Zhang, Y., Hong, H., and Cai, W. (2011) Tumor-targeted drug delivery with aptamers. *Current Medicinal Chemistry* 18, 4185-4194.

Zichel, R., Chearwae, W., Pandey, G.S., Golding, B., and Sauna, Z.E. (2012) Aptamers as a sensitive tool to detect subtle modifications in therapeutic proteins. *PLoS One* 7, e31948.

8 Delivery of Small Interfering RNA into Cells

8.1 Introduction

Double-stranded RNA molecules, able to induce gene silencing in a sequence-specific manner, are called short interfering RNA (siRNA), as they contain usually 21 or 22 nucleotides. RNA interference (RNAi) is a pathway present in eukaryotic cells (Elbashir et al., 2001a) and it was initially described by Andrew Fire and Craig C. Mello in 1998, when they discovered that introduction of double-stranded RNA (dsRNA) into *Caenorhabditis elegans* led to silencing of specific genes (Fire et al., 1998). The importance of siRNA machinery was recognized within the following years and the work of Fire and Mello on iRNA was awarded with Nobel Prize in Physiology and Medicine in 2006. When sequence-specific double-stranded siRNA is present in the mammalian cell, it is able to induce cleavage of the mRNA with a homologous nucleotide sequence (Elbashir et al., 2001b). Subsequent degradation of mRNA molecules leads to inability of the cell to produce gene product of interest and thus the inhibition of the corresponding protein.

Double-stranded RNA contains 21 - 23 nucleotides (RNA fragments) and mRNA cleavage takes place within the region of complementarity with dsRNA (Zamore et al., 2000). Once inside the cell, siRNA composed of two strands is cleaved by Dicer and two strands, sense and antisense, are divided. One of the strands (guide strand) incorporates into a multiprotein complex called RNA-induced silencing complex (RISC) or Slicer. Guide strand, along with the RISC identifies the mRNA of interest and cleaves it by an enzyme activity, thus inducing its degradation (Fire, 2007). After several years spent on investigation of siRNA mechanism, it has been revealed that the component endonuclease argonaute 2 – AGO2 of RISC complex separates sense strand (passenger strand) of siRNA from the antisense strand (guide strand), which remains associated within the RISC (Lam et al., 2015). Antisense strand within the RISC recognizes target mRNA, since it has a complementary sequence and AGO2 from RISC cleaves the mRNA (Pecot et al., 2011). The maturation of siRNA is a process catalysed by dsRNA-specific RNase-III-type endonucleases (Drosha and Dicer), which contain catalytic RNase III and dsRNA-binding domains (dsRBDs) (Meister and Tuschl, 2004). After years of intensive research, it has been concluded that the siRNA-induced gene knockdown, according to the above described mechanism, takes place both in cytoplasm and cell nucleus (Castel and Martienssen, 2013; Robb et al., 2005). The siRNA machinery can target virtually any gene and thus the expression of the corresponding proteins can be suppressed.

Besides siRNA, microRNA (miRNA) is recognized for its ability to silence genes. Whereas

siRNA acts highly specific, targeting only one mRNA, miRNA can have multiple targets (Lam et al., 2015). The miRNA mechanism can be based on two different approaches: miRNA inhibition and miRNA replacement. For miRNA inhibition, antisense single-stranded RNA (antagomir) inhibits the endogenous miRNA (van Rooij et al., 2012). In the replacement approach, miRNA mimics the function of the endogenous miRNA, which leads to a mRNA knockdown (Bader et al., 2010; Lam et al., 2015).

Besides the naturally synthesized dsRNA molecules, artificially synthesized inducers for the suppression of endogenous and heterologous genes can be produced to be applied for gene-specific therapeutics, or as a powerful tool for studying gene function in different types of mammalian cells (Elbashir et al., 2001a). A successful application of siRNA for gene silencing in mice was demonstrated in 2002 (McCaffrey et al., 2002) and since then, efforts have been made to integrate siRNA-induced gene knockdown within various applications, including target identification and validation in drug development, therapy and in the clinic (Drosopoulos and Linardopoulos, 2013).

Gene silencing effect usually takes 3–7 days in rapidly dividing cells, or can last for several weeks in non-dividing cells (Bartlett and Davis, 2006). This implies that for the therapeutic application, siRNA has to be administered repeatedly to achieve a persistent effect, as siRNA gets diluted intracellularly over time (Whitehead et al., 2009).

The dsRNAs are considered to be non-toxic and highly effective, since they are naturally employed by cells to regulate gene expression. Although dsRNA mechanism holds a great potential for a variety of application, there are several major problems which have to be solved in order to allow wide application of siRNA *in vivo*. The RNA molecules are very sensitive to serum nucleases and are susceptible to nucleases-mediated degradation. Unmodified or naked RNA can be rapidly hydrolyzed after its administration into a living system (they have short half-life) (Layzer et al., 2004). In addition, poor stability of RNA is a great obstacle for various therapeutic approaches, as well as the possible off-target (nonspecific) effects (Deng et al., 2014). Therefore, various chemical modifications of RNA have been developed recently, which can help reduction of immunogenicity, overcome instability of these molecules, increase their resistivity to nucleases and minimize off-target effects, whereas at the same time introduced modifications should not compromise RNA-induced gene silencing activity (Lam et al., 2015). Some of the possible modifications linked to the RNA molecules are: ribose 2′- OH group modification (the substitution of the ribose 2′-OH group with other chemical groups: 2′-O-methyl (2′-O-Me), 2′-fluoro (2′-F) and 2′-methoxyethyl (2′-O-MOE) (Molenaar et al., 2001), locked nucleic acids (containing a methylene bridge between the 2′-O and the 4′-C of the sugar - a stable “locked” ring

conformation), unlocked nucleic acids and backbone modifications (phosphorothioate-PS) (Veedu and Wengel, 2010; Vaish et al., 2011; Campbell et al., 1990; Lam et al., 2015). Extensive research has been conducted over past years in order to develop various therapeutic antisense nucleic acids and the three major groups of nucleic acid-based gene-silencing molecules can be distinguished: chemically modified antisense oligodeoxyribonucleic acids (ODNs), ribozymes and siRNAs (Dorsett and Tuschl, 2004; Scherer and Rossi, 2003). One should mention also peptide nucleic acids (PNAs), morpholino phosphorodiamidates, DNAzymes, etc.

Nevertheless, since the silencing effect by dsRNA has been discovered, a greatest barrier for its wide application in therapy and clinics is the delivery of such oligonucleotides to their site of action – cytoplasm and nucleus. For therapeutic application, synthetic RNA has to be delivered into cells of interest, in order to elicit RNA interference.

8.1.1 Methods of Introducing Double-Stranded RNA into Cells

Small interfering RNA (siRNA) and other antisense oligonucleotides causing RNA interference are novel candidates considered for application in therapy of various disorders (infections and cancer). However, internalization of such molecules within the cells is poor, due to their hydrophilicity, negative charge, size (~ 15 kDa) and susceptibility to degradation by nucleases (Dominska and Dykxhoorn, 2010). Delivery of siRNA remains a great obstacle for its widespread use, especially for the therapeutic applications. Therefore, it is necessary to develop non-toxic delivery systems, which can facilitate safe and effective transfer of siRNA across the cell membrane (Whitehead et al., 2009).

Once inside the cells, oligonulceotides have to be released into cytosol or reach the nucleus in order to successfully perform their action – gene knockdown and inhibition of protein expression. However, many delivery systems are based on an intracellular delivery of oligonucloetides by some kind of endocytosis, whereby it is essential to take into account that there are multiple routes of endocytosis (endocytotic pathway) present in the cell (Juliano et al., 2008). Complex trafficking pathways present in the cell, usually described as endocytosis include: (i) clathrin coated pathway, (ii) caveolar pathway, (iii) one or more noncaveolar, clathrin-independent pathways (CLIC), (iv) macropinocytosis and (v) phagocytosis. If oligonucloetide binds to the cell surface before it is being internalized, the process is called receptor-mediated endocytosis (Juliano et al., 2008).

As already mentioned, numerous delivery systems are based on endocytosis and endosomatic pathway. In the beginning, oligonucleotides are internalized within early endosomal vesicles. Thereafter, vesicles fuse with sorting endosomes and in the end,

content arrives to the late endosomes or even further to lysosomes. During their journey from vesicles to lysosomes, oligonucleotides are exposed to decreasing pH values within each of these cell organelles (compartments) and thus the possibility for oligonucleotides denaturation increases. Therefore, oligonucleotides should escape from endosomes into the cytosol, before they arrive to the lysosomes, the acidic cellular compartments with low pH, which often contain nucleases. Endosomal escape is essential for siRNA, in order to reach cytosol and nucleus (Meister, 2008), where it can find its targets (Dominska and Dykxhoorn, 2010). Although there are many effective viral carriers available for the nucleic acids (e.g. adenoviral vectors (Ad), adeno-associated virus vectors (AAV), retroviral vectors (RV), herpes simplex virus vectors (HSV), lentiviruses, etc.), there are certain concerns for their application, considering their safety (high immunogenicity and potential mutagenesis), low packaging capacity and high costs of production (Lam et al., 2015; Pereyra and Hereñu, 2013). Therefore, big efforts have been made to find alternatives to them in a form of various nonviral delivery systems.

As the most often applied nonviral RNA carriers are described: cationic lipids (liposomes, lipid-like materials) (Drummond et al., 1999), cationic polymers (polymer complexes) (Tiera et al., 2006) or various polymeric nanoparicles (Pridgen et al., 2007; Juliano et al., 2008), which by the electrostatic complexation bind the negatively charged oligonucleotides. Thereafter, positively charged lipid- and polymer-based systems (carrying nucleic acids) bind to the negatively charged cell membrane and can be taken up by the cell via adsorptive pinocytosis or endocytosis (Dominska and Dykxhoorn, 2010; Zabner et al., 1995). The encapsidation of siRNAs into nanoparticles (with lipid- or cationic polymer-based systems) increases their resistance to nucleases. Lipid-based transfection reagents are among the most popular nucleic acid delivery agents due to their high transfection efficiency *in vitro*, but there are some serious concerns regarding their safety for therapeutic use, such as: toxicity reported both *in vitro* and *in vivo* (Lv et al., 2006; Akhtar and Benter, 2007), unwanted inflammatory and immune response, as well as the possible off-target effects of siRNA (Whitehead et al., 2009; Hollins et al., 2007). PEGylation is a commonly employed strategy to reduce immunogenicity and toxicity of such cationic carriers (Lam et al., 2015). Furthermore, cationic polymers with linear or branched structure were shown to be efficient transfection agent, since they form stable polyplexes with siRNA and stimulate nonspecific endocytosis and endosomal escape (Boussif et al., 1995; Putnam, 2006). Preparation of polyplexes is simple and mostly applied polymer materials as oligonucleotides carriers are: PEI, cyclodextrin, highly branched dendrimers, etc. (Whitehead et al., 2009; Juliano et al., 2008). Lipoplexes are introduced recently as a combination of polymers and lipids in an

attempt to overcome the limitations of polymer-based and lipid-based delivery systems by combining the advantageous characteristics of both (Lam et al., 2015; Schaefer et al., 2010). Besides different nanocarriers, lipid- and polymer-based carriers, extensively investigated and usually described in the literature as non-invasive methods of delivery (Hoekstra et al., 2007; Kabanov, 2006, Akhtar and Benter, 2007), there are also so-called invasive delivery systems, such as electropermeabilization (electroporation) and microinjection (Dokka and Rojanasakul, 2000).

Microinjection is a highly effective process, whereby different type of molecules, including oligonucleotides (Chin et al., 1990; Leonetti et al., 1991; Fisher et al., 1993), can be introduced into a single cell with a micropipette. After their transfer into the cytosol, oligonucleotides can rapidly accumulate in the nucleus. Besides high transfection efficiency, this method allows delivery of different probes with the controlled (high) purity levels, directly into the cell cytoplasm (circumventing endocytotic pathway), but the great disadvantage is certainly a low throughput of this technique, as only a single cell at a time can be treated. Applicability of microinjection only on a limited number of cells makes it inappropriate for the applications *in vivo* (Dokka and Rojanasakul, 2000). In addition, special equipment is usually necessary to perform microinjection. There are several examples demonstrating that microinjection can be successfully applied for the delivery of siRNA into the single cells (Gruber et al., 2005; Ohrt et al., 2006; O'Meara et al., 2011).

Finally, application of electic field to transfer negatively charged oligonucleotides into the cell cytosol (electropermeabilization) was successfully demonstrated in the past, both with cells in suspension (Paganin-Gioanni et al., 2011; Chabot et al., 2013) and the confluent cell monolayer (Jain et al., 2012; Fujimoto et al., 2010).

Considering dsRNA molecules as very promising candidates for different applications in research and therapy, there is a great interest in finding a convenient method to overcome the greatest obstacle standing in their way to the wide application, which is delivery of dsRNAs into cells and tissues. In this work, *in situ* electroporation using ECIS technology was employed to facilitate successful, effective and non-toxic introduction of different types of siRNA molecules into various mammalian cell lines. Proof-of principle experiments are presented in the following chapters including delivery of membrane-impermeable siRNAs into cells by *in situ* electroporation (ISE) and impedance monitoring of the cellular behavior before and after siRNA entered the adherent cells. In the further text and figures abbreviation ELPO is often applied, having the same meaning as ISE – *in situ* electroporation. Delivery of siRNA by electroporation and with the common commercial cationic lipid-based transfection reagent is compared. For microscopic evaluation of transfection efficiency by electroporation,

chemical transfection and in some cases, fixation and permeabilization, confocal laser scanning microscopy (CLSM) and microscopy in an epi-mode were applied.

8.2 Delivery of Transfection Indicator siGLO Red into Cells

First siRNA type tested in this work was commercially available transfection indicator siGLO Red. This fluorescently-labeled siRNA with random non-targeting sequence is created by a manufacturer to accumulate in the cell nucleus, in case when transfection of the cells has been successful. This simple principle should ease the evaluation of transfection efficiency by different methods and at the same time, different incorrect (or unclear) interpretations can be thus avoided. The siGLO Red transfection indicator gives bright red (or red-orange) fluorescence signal within the cells (**Figure 8.1**), which was observed during microscopy.

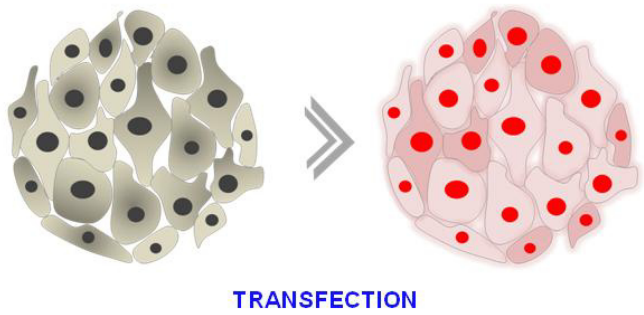

Figure 8.1 Schematic illustration showing adherent cells before (left) and after (right) their transfection in presence of fluorescently-labeled siRNA – siGLO Red. Successful delivery of siGLO Red into cells induces bright red fluorescence signal coming in the nuclei.

8.2.1 Delivery of siGLO Red into CHO-GFP Cells

8.2.1.1 Delivery of siGLO Red by *In Situ* Electroporation

Cell line CHO-GFP was applied as a first cell model to study an introduction of fluorescently-labeled siRNA into confluent cells using different transfection methods. Experimental procedure for *in situ* electroporation was conducted on 8W4Eμ electrode array and $EBSS^{++}$ was applied as an assay buffer.

Typical time course of the normalized impedance before, during and after *in situ* electroporation of CHO-GFP cells in presence of 1 or 2 μM siGLO Red is presented in **Figure 8.2**. Cells were pulsed using optimal combination of pulse parameters for this cell line: 40 kHz, 4 V and 500 ms either once, or three times successively, as indicated by the

arrows - a: 1st pulse, b: 2nd pulse and c: 3rd pulse application. Impedance measurement is presented at 16 kHz and data are normalized to the last time point before first electroporation pulse was applied. Impedance profiles vary after every pulse application, in most cases impedance slightly decreases and this is especially visible after first pulse application. Between the pulses, cells were allowed to return to the pre-pulse impedance values before the next pulse was applied and after the last electric pulse, cells were allowed to fully stabilize before impedance measurement was finished and microscopy followed.

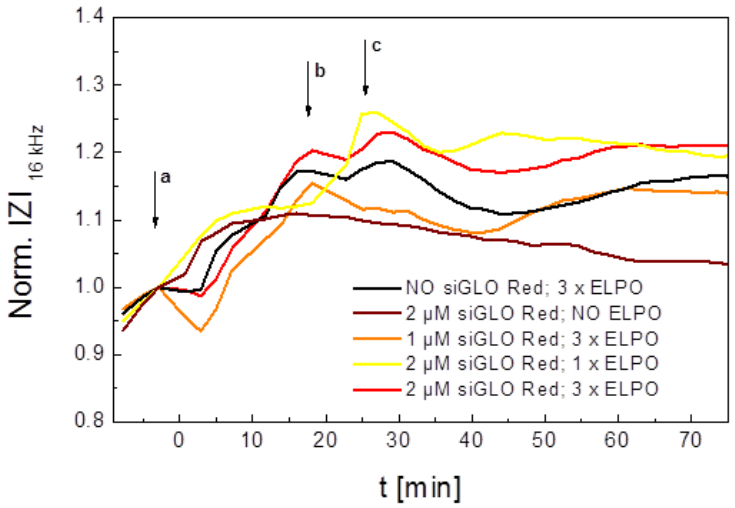

Figure 8.2 Typical time course of the normalized impedance at 16 kHz before, during and after *in situ* electroporation of CHO-GFP cells in presence of 1 and 2 µM siGLO Red. ISE was applied three times successively - **a**: 1st pulse, **b**: 2nd pulse and **c**: 3rd pulse application, using optimal combination of pulse parameters for this cell line: 40 kHz, 4 V and 500 ms. Impedance values are normalized to the last time point before first electroporation pulse was applied. After cellular recovery from the last pulse, impedance measurement (at 37 °C) was finished and microscopy followed to evaluate electroporation efficiency.

CHO-GFP cells were electroporated three times (red line), or only once (yellow line) in presence of 2 µM siGLO Red. They were also pulsed three times in presence of 1 µM siGLO Red (orange line) to check if and how loading efficiency correlates with the number of pulses. Corresponding controls where siGLO Red was present but no pulse was applied (brown line) and where cells were being electroporated in absence of siGLO Red (black line) were acquired as well during the experiment.

Exemplary phase-contrast and fluorescence micrographs are summarized in **Figure 8.3**. Fluorescence micrographs were taken in an epi-mode (presented in the second and third column) and subsequently using CLSM (presented in the fourth column) on the same microscope (details given in chapter 4.3.1). All micrographs were taken with 10-fold

magnification objective and confocal fluorescence micrographs (fourth column) were additionally zoomed 3 fold in order to better visualize cells on the electrodes.

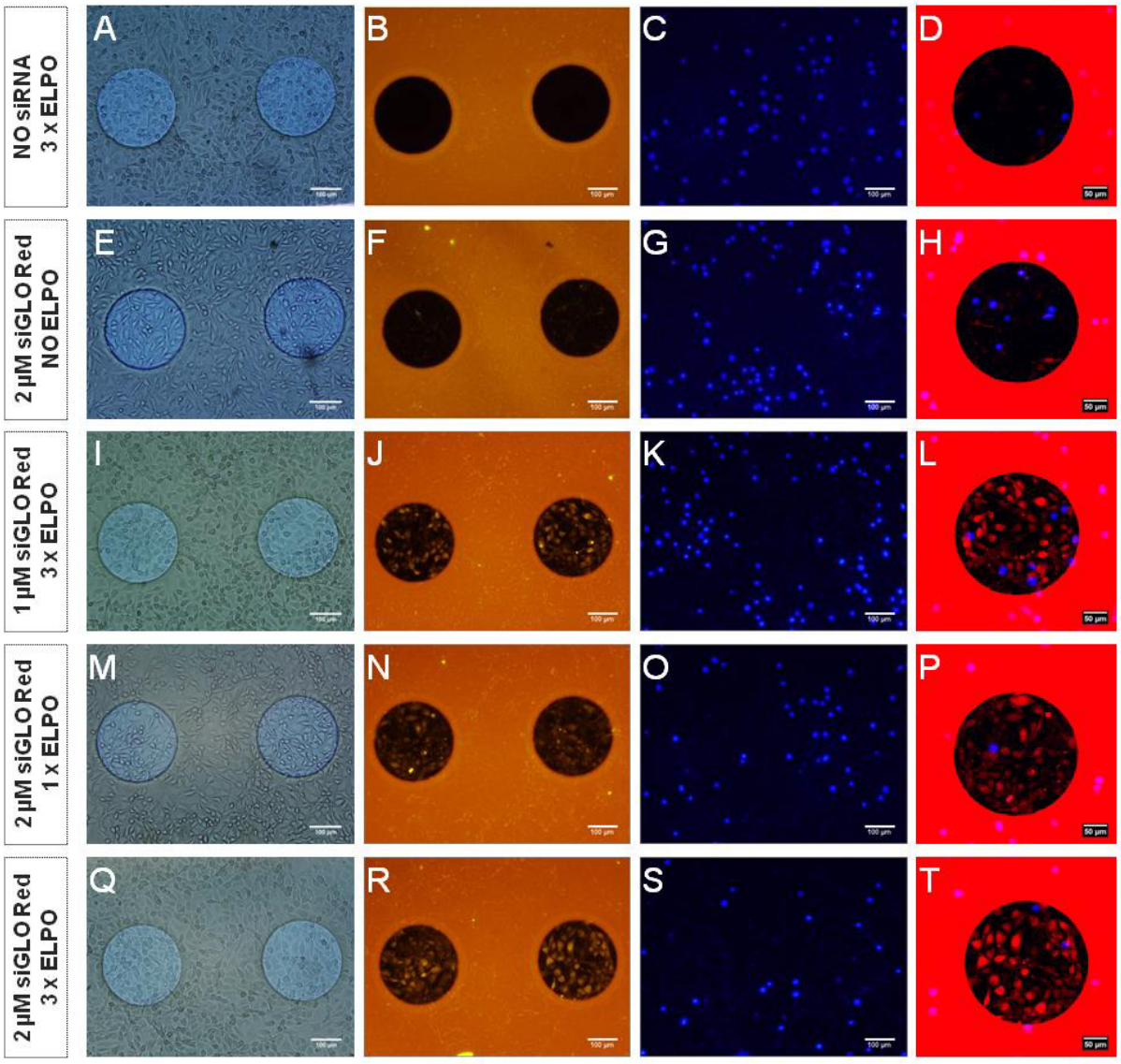

Figure 8.3 Exemplary phase-contrast (first column) and fluorescence micrographs (second to fourth column) taken after *in situ* electroporation was applied for delivery of 1 and 2 µM siGLO Red to CHO-GFP cells. Experiment was performed at 37 °C. Second column-epi-mode: siGLO Red signal; third column-epi-mode: DAPI staining; fourth column-CLSM: overlay of siGLO Red and DAPI at the single electrode. The scale bar in micrographs of first, second and third column corresponds to 100 µm and in micrographs of fourth column scale bar represents 50 µm. All micrographs were taken using 10-fold magnification objective.

Micrographs presented in the second column show fluorescence signal of the cells loaded with siGLO Red and the third column shows cells stained with DAPI. These micrographs

taken in epi-mode are not presented as overlay in order allow easier visualization of siGLO Red signal. Instead, subsequently taken confocal fluorescence micrographs (taken by CLSM, fourth column) show overlay in fluorescence signal between the red and blue channel (siGLO Red / DAPI). Micrographs in the second and fourth column show that layer of photopolymer surrounding the electrodes gives the background - red/orange fluorescence signal.

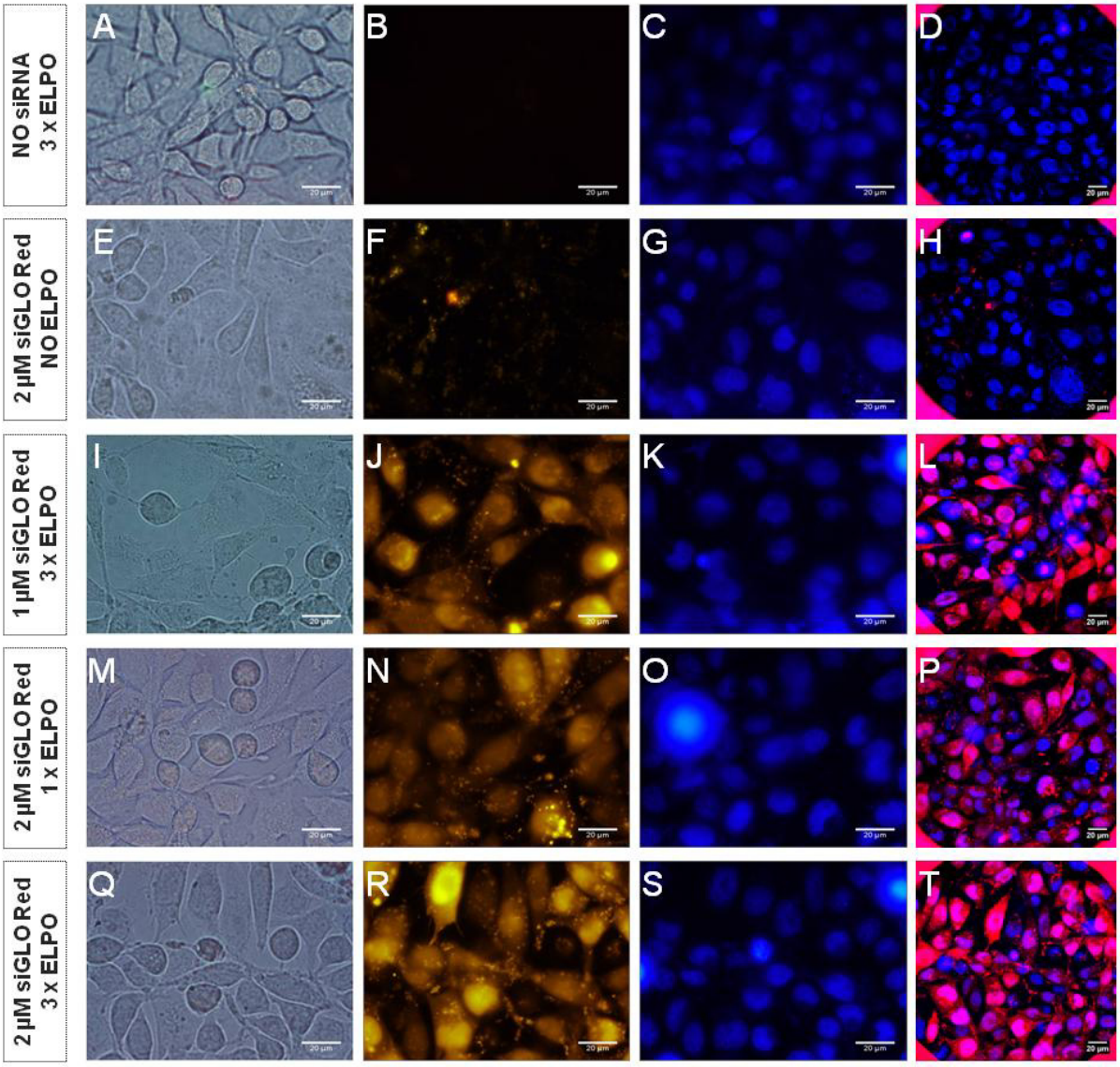

Figure 8.4 Exemplary phase-contrast (first column) and fluorescence micrographs (second to fourth column) taken after *in situ* electroporation was applied for delivery of 1 and 2 µM siGLO Red to CHO-GFP cells. Experiment was performed at 37 °C. Second column-epi-mode: siGLO Red signal; third column-epi-mode: DAPI staining; fourth column-CLSM: overlay of siGLO Red and DAPI at the single electrode. Scale bar in all micrographs corresponds to 20 µm. All micrographs were taken using 60-fold magnification objective.

Fluorescence micrographs presented in the second and fourth column show that non-electroporated CHO-GFP cells and those electroporated in absence of siGLO Red appear completely dark, since siGLO Red did not enter their cytosol (nuclei). The cells residing on the electrodes exposed to electroporation in presence of 1 or 2 µM siGLO Red exhibit red (or bright orange) fluorescence signal. Difference in fluorescence intensity between the cells pulsed once or three times and those exposed to 1 and 2 µM siGLO Red are better visualized in the micrographs taken with higher magnification objective (60-fold) and respective exemplary phase-contrast and fluorescence micrographs are summarized in **Figure 8.4**. CHO-GFP cells pulsed three times in presence of 1 µM siGLO Red (third row) exhibited slightly higher level of fluorescence intensity than the cells pulsed once in presence of 2 µM siGLO Red (fourth row), whereby siGLO Red was localized mostly within cell nuclei and only to small extent in the cytoplasm in both cases. In comparison to them, CHO-GFP cells pulsed three times with 2 µM siGLO Red exhibited significantly higher fluorescence signal and in addition, localization of siGLO Red within nuclei was found in a bigger fraction of cells. In fact, siGLO Red signal was found in the nucleus of almost every cell residing on one of the electrodes. Such observations are consistent with the level of siGLO Red signal observed in the respective micrographs presented in fourth column (taken by CLSM). These micrographs show overlay of siGLO Red and DAPI staining (of cell nuclei) and co-localization was observed in most of the cells presented in the micrograph **T** (**Figure 8.4**). Micrograph **F** of the same figure shows small level of unspecific siGLO Red uptake by the cells. Micrographs in **Figure 8.3** and **Figure 8.4** presenting DAPI staining show that DAPI did not enter nuclei of all cells and this is explained by the fact that cells were not fixed and permeabilized prior to DAPI addition, as they should be according to the standard protocol (described in chapter 4.3.4.2), but only incubated in presence of DAPI stain for a prolonged period of time in order to avoid potential leaking of siGLO Red from the fixed and permeabilized CHO-GFP cells.

In situ electroporation enabled delivery of siGLO Red into CHO-GFP cells and loading efficiency was enhanced with the higher siGLO Red concentration and by multiple pulse application. Thus, fluorescence signal of siGLO Red was found in the nuclei of majority of the cell population present on the electrodes.

8.2.1.2 Delivery of siGLO Red by Chemical Transfection

A widespread chemical lipid-based transfection (abbreviated CH TR) with commercial chemical transfection reagent Lipofectamine® was applied to make a comparison with siGLO Red delivery by *in situ* electroporation. CHO-GFP cells were chemically transfected in

presence of 33 and 50 nM siGLO Red according to the protocol described in chapter 4.4.2.3. Concentrations of siGLO Red were chosen based on recommendations for siRNA transfection given by the manufacturer of Lipofectamine (Thermo Fisher Scientific™). Transfection efficiency was evaluated app. 24 hours after transfection.

Exemplary phase-contrast and fluorescence micrographs were taken app. 24 hours after transfection of the cells and are summarized in **Figure 8.5**. Fluorescence micrographs were taken in an epi-mode (presented in the second and third column), and subsequently using CLSM (presented in the fourth column) on the same microscope (details given in chapter 4.3.1). Micrographs were taken with 10-fold magnification objective and confocal fluorescence micrographs (fourth column) were additionally zoomed 3 fold in order to better visualize appearance of the cells. In addition, micrographs were also taken with 60-fold magnification and respective exemplary micrographs are summarized in **Figure 8.6**.

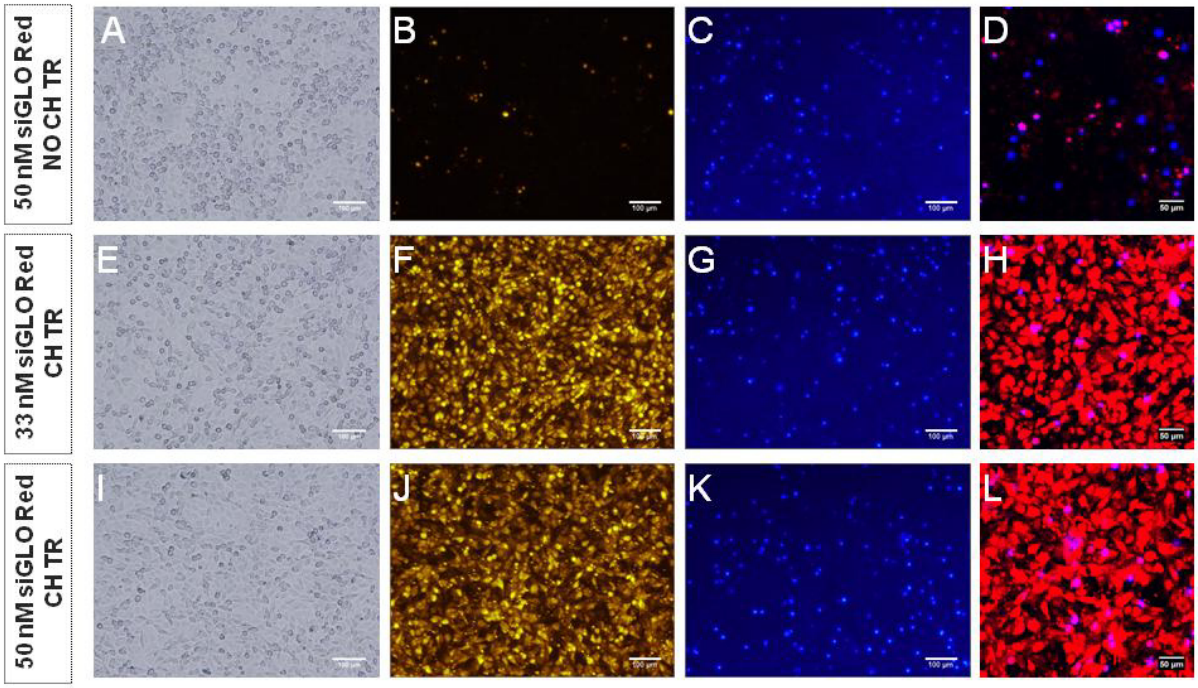

Figure 8.5 Exemplary phase-contrast (first column) and fluorescence micrographs (second to fourth column) taken app. 24 hours after chemical transfection of CHO-GFP cells in presence of 33 nM (second row) and 50 nM (third row) siGLO Red. Experiment was performed at 37 °C. Second column-epi-mode: siGLO Red signal; third column-epi-mode: DAPI staining; fourth column-CLSM: overlay of siGLO Red and DAPI staining. The scale bar in micrographs of first, second and third column corresponds to 100 µm and in micrographs of the fourth column, scale bar represents 50 µm. All micrographs were taken using 10-fold magnification objective.

Micrographs in both **Figure 8.5** and **Figure 8.6** show siGLO Red signal in the second column

(epi-mode), DAPI staining in the third (epi-mode) and the fourth column shows overlay in fluorescence signal between the red and blue channel (siGLO Red / DAPI) in micrographs taken by CLSM. Fluorescence images in the second and fourth columns of **Figure 8.5** reveal significant difference in appearance of CHO-GFP cells exposed to siGLO Red in the presence and absence of chemical transfection reagent. Whereas cells subjected to siGLO Red in absence of Lipofectamine showed only small amount of unspecific siGLO Red uptake, cells chemically transfected in presence of either 33 or 50 nM siGLO Red showed high level fluorescence intensity originating from siGLO Red.

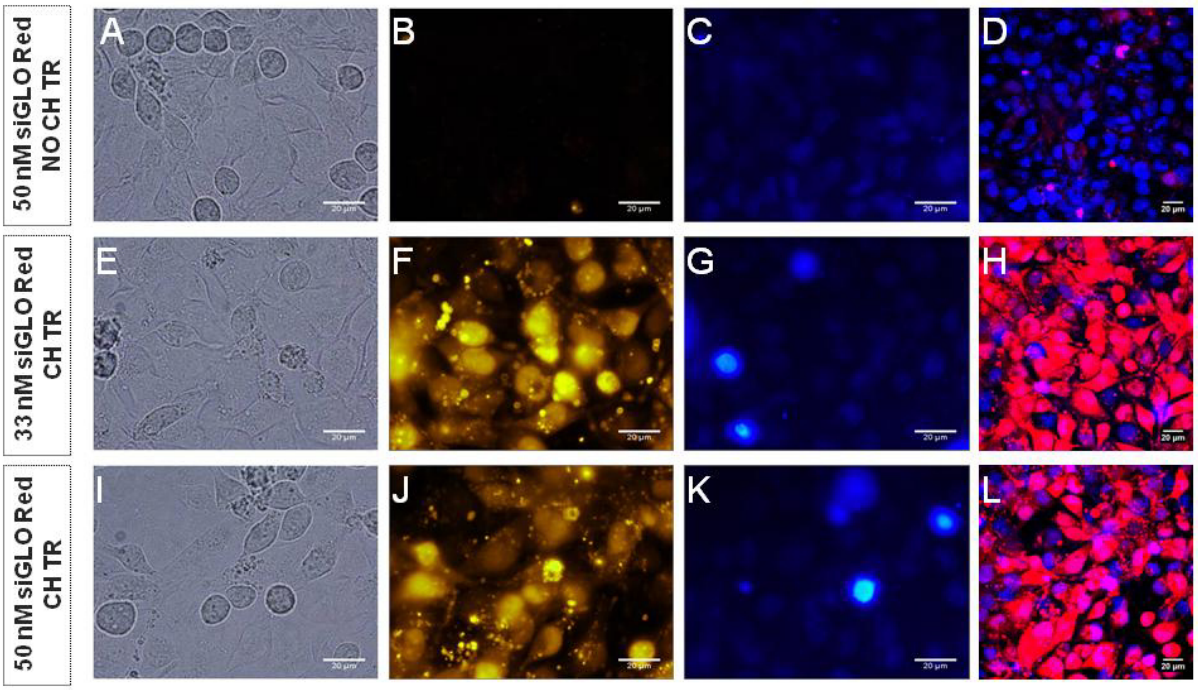

Figure 8.6 Exemplary phase-contrast (first column) and fluorescence micrographs (second to fourth column) taken app. 24 hours after chemical transfection of CHO-GFP cells in presence of 33 nM (second row) and 50 nM (third row) siGLO Red. Experiment was performed at 37 °C. Second column-epi-mode: siGLO Red signal; third column-epi-mode: DAPI staining; fourth column-CLSM: overlay of siGLO Red and DAPI staining. Scale bar in all micrographs corresponds to 20 µm. All micrographs were taken using 60-fold magnification objective.

Figure 8.6, presenting micrographs with higher magnification, reveals that fluorescence signal in transfected cells originates both from nuclei and cytoplasm, whereby most of the cells exhibited loading of nuclei with siGLO Red. However, presence of characteristic punctuated pattern is visible within the cell cytoplasm, indicating accumulation of siGLO Red within vesicles. Interestingly, it was observed that CHO-GFP cells transfected with 33 nM siGLO Red exhibited slightly higher extent of fluorescence signal within nuclei (more siGLO

Red and DAPI co-localization observed in the micrograph **Figure 8.6 H**) than the cells subjected to 50 nM siGLO Red (less co-localization between siGLO Red and DAPI in **Figure 8.6 L** than in the **Figure 8.6 H**). Therefore, it was concluded that sufficient level of transfection efficiency is achieved with 33 nM siGLO Red.

8.2.1.3 Delivery of siGLO Red into Fixed and Permeabilized Cells

The localization of 2 µM siGLO Red after its free diffusion through disrupted membrane of fixed and permeabilized CHO-GFP cells (abbreviated F + P) was investigated in order to verify if any correlation with previously obtained results after electroporation and chemical transfection can be made. The spatial distribution of 2 µM siGLO Red within CHO-GFP cells, after their exposure to fixation and permeabilization agents, paraformaldehyde and Triton-X-100, respectively, was documented using epi-mode and subsequently CLSM on the same microscope. Exemplary phase-contrast (first column) and fluorescence micrographs (second to fourth column) are summarized in **Figure 8.7**.

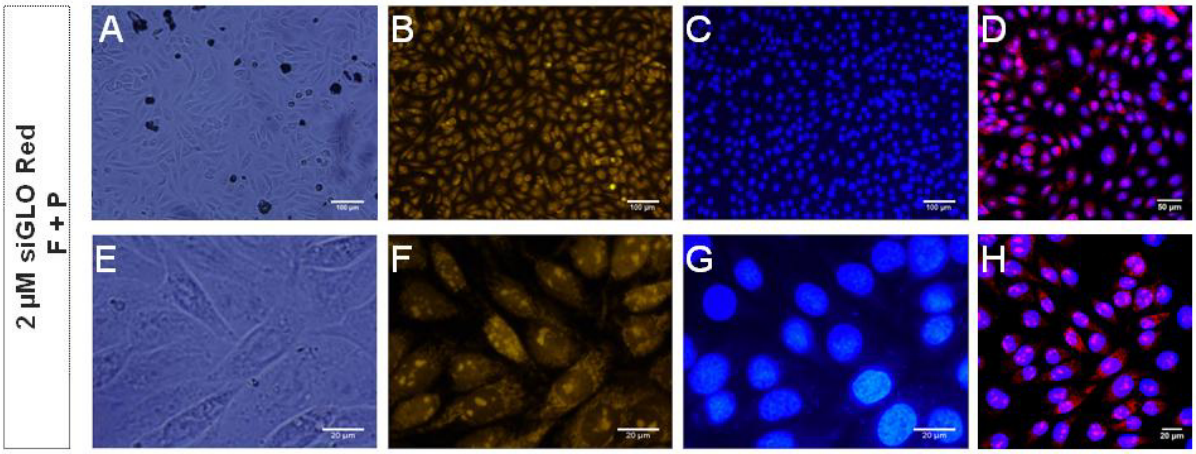

Figure 8.7 Exemplary phase-contrast (first column) and fluorescence micrographs (second to fourth column) taken app. 1 hour after 2 µM siGLO Red was added to fixed and permeabilized CHO-GFP cells. Experiment was performed at 37 °C. Second column-epi-mode: siGLO Red signal; third column-epi-mode: DAPI staining; fourth column-CLSM: overlay of siGLO Red and DAPI staining. The scale bar in micrographs **A**, **B** and **C** corresponds to 100 µm, in micrograph **D** to 50 µm and in micrographs **E**-**H** to 20 µm. Micrographs in the upper row were taken using 10-fold magnification and micrographs in the lower panel using 60-fold magnification objective.

Micrographs were taken using 10-fold (upper panel) and 60-fold (lower panel) magnification objective app. 1 hour after addition of 2 µM siGLO Red to fixed and pemeabilized cells. Fluorescence signal of siGLO Red is well visualized in micrographs of the second column

(taken in epi-mode) and it is shown that siGLO Red diffused into every cell, but stained only some specific cell structures. Within the nuclei, siGLO Red accumulated within the small bright spots, whilst within the cytoplasm it stained grained structure, which could be possibly lysosomes or mitochondria. Such observations were confirmed by confocal fluorescence micrographs (in fourth column), which show overlay in fluorescence signal between siGLO Red and DAPI. In addition, DAPI staining of cell nuclei is very well visible in this experiment, both in micrographs with lower and higher magnification objective, due to the fact that cells were previously fixed and permeabilized and not only incubated in presence of DAPI stain (details described in chapter 4.3.4.2). Thus, DAPI was allowed to freely diffuse into cytoplasm and it accumulated in the nuclei of every cell. It is surprising that level of siGLO Red accumulation within the cell nuclei was lower than the level observed after electroporation or chemical transfection.

8.2.2 Delivery of siGLO Red into NRK Cells

8.2.2.1 Delivery of siGLO Red by *In Situ* Electroporation

In addition to CHO-GFP, NRK cells were applied as a cell model for investigation of siRNA delivery using different transfection strategies. Fluorescent siRNA probe siGLO Red was applied to investigate and optimize possible delivery of siRNA into NRK cells. Experimental procedure for *in situ* electroporation (ISE or ELPO) was conducted on 8W4Eμ electrode array and $EBSS^{++}$ was applied as an assay buffer.

Typical time course of the normalized impedance before, during and after *in situ* electroporation of NRK cells in presence of 2, 4, or 6 μM siGLO Red is presented in **Figure 8.8**. NRK cells were pulsed, using optimal combination of pulse parameters for this cell line: 40 kHz, 4 V and 200 ms, three times successively as indicated by the arrows - a: 1^{st} pulse, b: 2^{nd} pulse and c: 3^{rd} pulse application. Impedance measurement is presented at 4 kHz and data are normalized to the last time point before first electroporation pulse was applied. After every pulse application, significant drop in impedance signal was observed and cells were allowed to return to the pre-pulse impedance values before the next pulse was applied. Time intervals between the pulses were app. 20 min and after the third and last electric pulse, cells were allowed to fully recover and stabilize before impedance measurement was finished. Microscopy followed to determine transfection efficiency.

During the experiment, corresponding controls were acquired where (4 μM) siGLO Red was present but no pulse was applied (brown line) and where cells were pulsed in absence of siGLO Red (black line). As expected, no significant difference in impedance signal was

observed during electroporation of NRK cells in presence of 2 µM siGLO Red (yellow line), 4 µM siGLO Red (orange line) and 6 µM siGLO Red (red line).

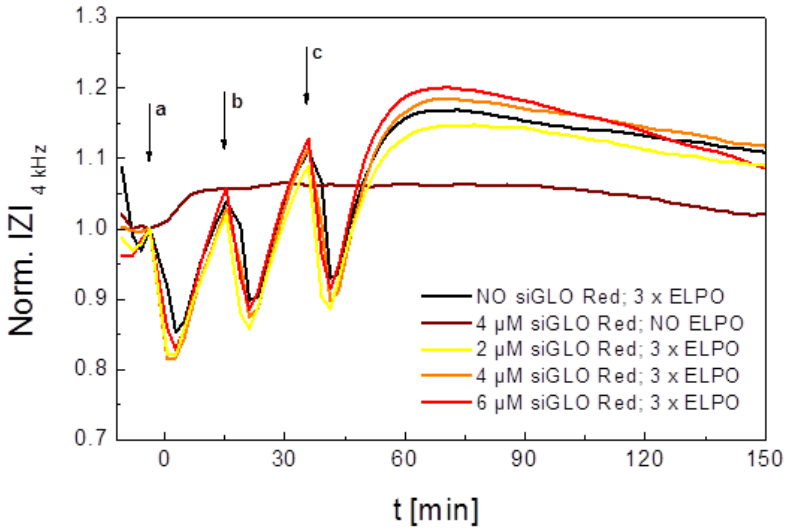

Figure 8.8 Typical time course of the normalized impedance at 4 kHz before, during and after *in situ* electroporation of NRK cells in presence of 2, 4 and 6 µM siGLO Red. ISE was applied three times successively - **a**: 1st pulse, **b**: 2nd pulse and **c**: 3rd pulse application, using optimal combination of pulse parameters for this cell line: 40 kHz, 4 V and 200 ms. Impedance values are normalized to the last time point before first electroporation pulse was applied. After cellular recovery from the third and last pulse, impedance measurement (at 37 °C) was finished and microscopy followed to evaluate electroporation efficiency.

Exemplary phase-contrast and fluorescence micrographs are summarized in **Figure 8.9** (micrographs taken with 10-fold magnification) and in **Figure 8.10** (micrographs taken with 60-fold magnification objective). Fluorescence micrographs were taken in epi-mode (presented in the second and third column of each figure) and subsequently using CLSM (presented in the fourth column of each figure) on the same microscope (details given in chapter 4.3.1). Confocal fluorescence micrographs (fourth column) were additionally zoomed 3 fold in order to better visualize cells on the electrodes.

Same as previously presented for CHO-GFP cells (chapter 8.2.1), micrographs in the second column show fluorescence signal of siGLO Red (taken in epi-mode), in the third fluorescence of DAPI staining (taken in epi-mode) and the fourth column shows overlay in fluorescence signal between siGLO Red and DAPI (taken by CLSM). Whereas phase-contrast micrographs do not show any difference between the cells in samples and controls, fluorescence micrographs reveal difference in appearance of the cells treated under different experimental conditions. Cells incubated with 4 µM siGLO Red without exposure to electric

pulse took up very small amounts of the probe unspecifically. NRK cells exposed to triple ISE (ELPO) in presence of different concentrations of siGLO Red, exhibited concentration-dependant intensity of fluorescence signal within the cells. High level of siGLO Red signal (red to bright orange) was observed within cell nuclei and cytoplasm. With higher siGLO Red concentration, both fluorescence intensity and fraction of loaded cells increased.

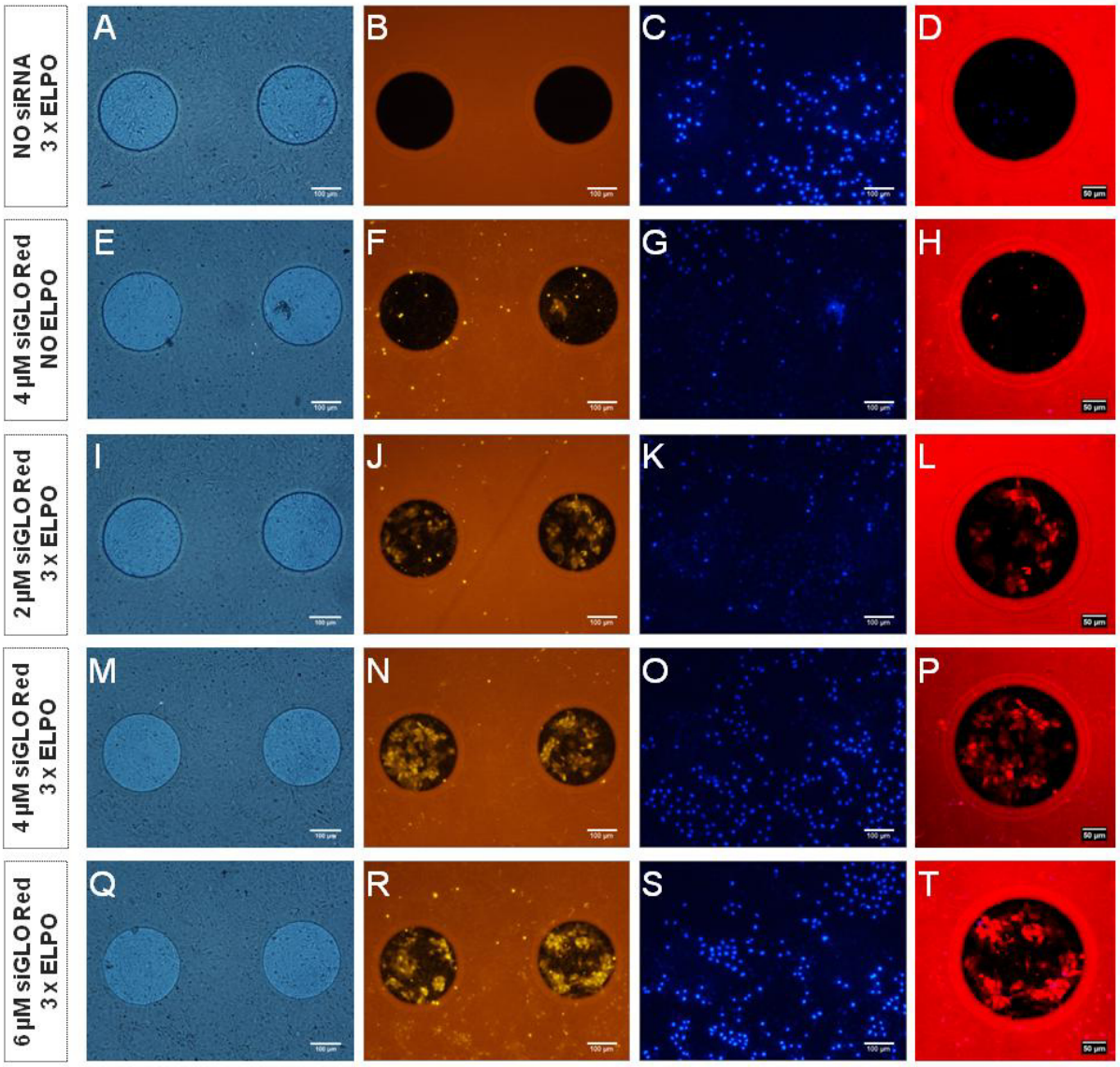

Figure 8.9 Exemplary phase-contrast (first column) and fluorescence micrographs (second to fourth column) taken after *in situ* electroporation was applied for delivery of 2, 4 and 6 µM siGLO Red to NRK cells. Experiment was performed at 37 °C. Second column-epi-mode: siGLO Red signal; third column-epi-mode: DAPI staining; fourth column-CLSM: overlay of siGLO Red and DAPI at the single electrode. The scale bar in micrographs of the first, second and third column corresponds to 100 µm and in micrographs of the fourth column scale bar represents 50 µm. All micrographs were taken using 10-fold magnification objective.

Such trend is visible in micrographs taken with lower magnification objective (**Figure 8.9**) and is even better visualized in micrographs taken with higher magnification (**Figure 8.10**), where concentration-dependent accumulation of siGLO Red within nuclei is obvious.

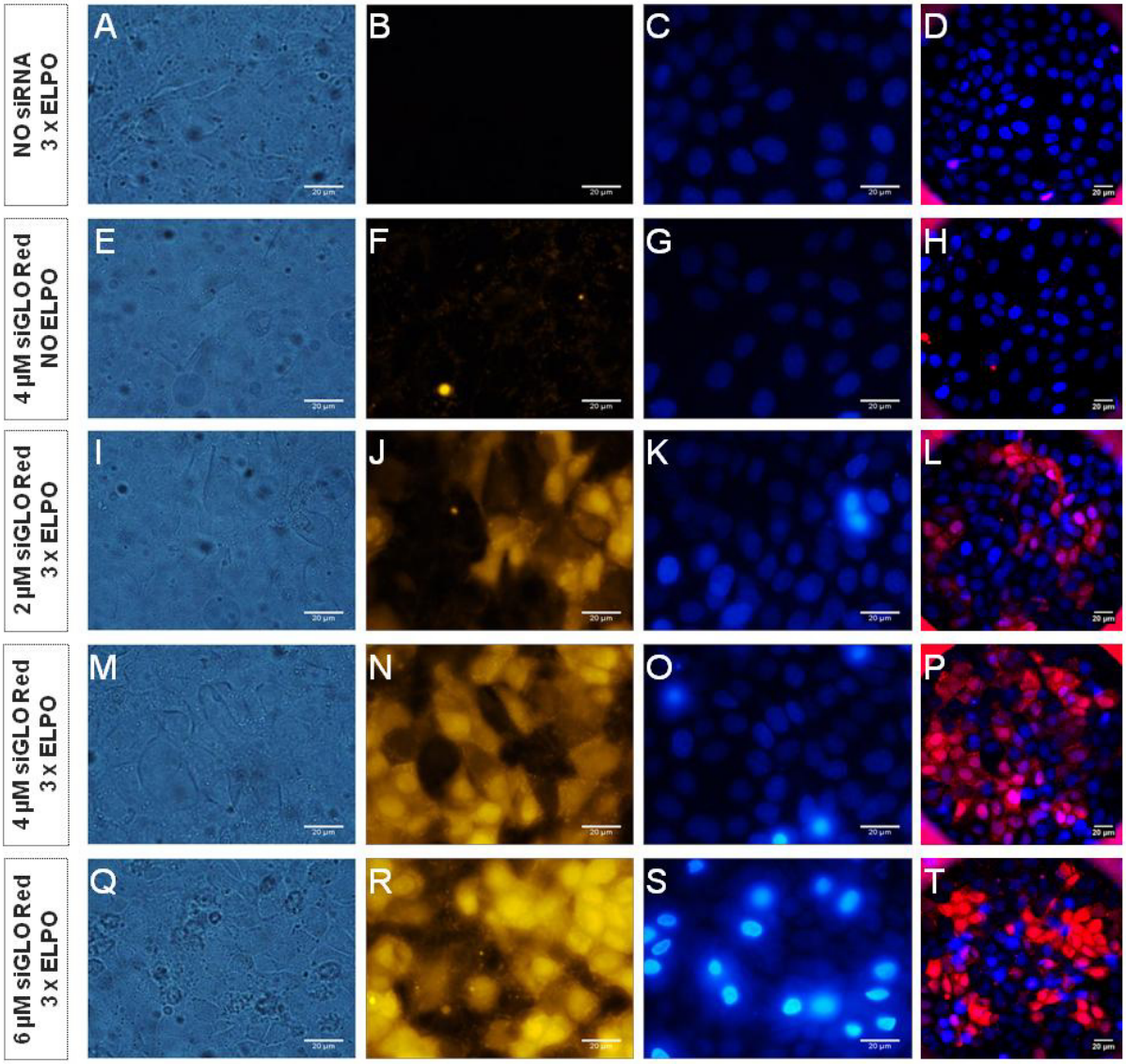

Figure 8.10 Exemplary phase-contrast (first column) and fluorescence micrographs (second to fourth column) taken after *in situ* electroporation was applied for delivery of 2, 4 and 6 µM siGLO Red to NRK cells. Experiment was performed at 37 °C. Second column-epi-mode: siGLO Red signal; third column-epi-mode: DAPI staining; fourth column-CLSM: overlay of siGLO Red and DAPI at the single electrode. Scale bar in all micrographs corresponds to 20 µm. All micrographs were taken using 60-fold magnification objective.

Micrographs taken by CLSM (fourth column of each figure) showed as well more fluorescence signal in NRK cells with higher siGLO Red concentration, however, co-

localization of siGLO Red and DAPI was lower than expected. This is most probably due to the fairly low fluorescence intensity of DAPI staining observed in this experiment. Obviously, only small amounts of DAPI stain managed to cross intact cell membrane, as staining of nuclei appeared very weak. NRK cells were not fixed and permeabilized (as recommended by the protocol for DAPI staining; chapter 4.3.4.2) before microscopy, to avoid potential leakage of previously loaded siGLO Red.

Experiment showed that *in situ* electroporation facilitated successful loading of NRK cells with siGLO Red and accumulation of siGLO Red in the cell nuclei increased with its increasing concentration. The best transfection efficiency was acquired when cells were pulsed three times in presence of 6 µM siGLO Red.

8.2.2.2 Delivery of siGLO Red by Chemical Transfection

Analogously to CHO-GFP cells, comparison of the siGLO Red delivery by *in situ* electroporation was made with common chemical lipid-based transfection reagent. Using Lipofectamine as a transfection mediator, NRK cells were initially subjected to lower concentrations of siGLO Red (33 and 50 nM), similarly as CHO-GFP cells, but transfection efficiency was surprisingly low. In addition, producer of Lipofectamine suggested, in one of the cell-specific protocols, that NRK cells might require higher amounts of siRNA to achieve good transfection efficiency. Therefore, concentration of siGLO Red was increased to 200 nM and NRK cells were chemically transfected according to the protocol described in chapter 4.4.2.3. Microscopic evaluation of transfection efficiency was conducted app. 24 hours after transfection.

Micrographs were taken using 10-fold and 60-fold magnification objective and the exemplary (phase-contrast and fluorescence) micrographs are summarized in **Figure 8.11** and **Figure 8.12**, respectively. Same as during previous experiments, fluorescence micrographs were taken in epi-mode (presented in the second and third column of each figure), and subsequently using CLSM (presented in the fourth column of each figure). Confocal fluorescence micrographs (fourth column) were additionally zoomed 3 times to better visualize the cells. Signal of siGLO Red is presented in the second column (epi-mode), DAPI staining in the third (epi-mode), whereas fourth column gives the overlay in fluorescence signal between the red and blue channel (siGLO Red / DAPI) in micrographs taken by CLSM. Fluorescence micrographs in the second and fourth columns of **Figure 8.11** and **Figure 8.12** show drastic difference in appearance of NRK cells, depending on Lipofectamine presence during incubation with siGLO Red. Whereas NRK cells incubated with siGLO Red in absence of transfection reagent showed minor unspecific uptake, NRK

cells subjected to chemical reagent and 200 nM siGLO Red showed rather high fluorescence signal 24 hours after transfection.

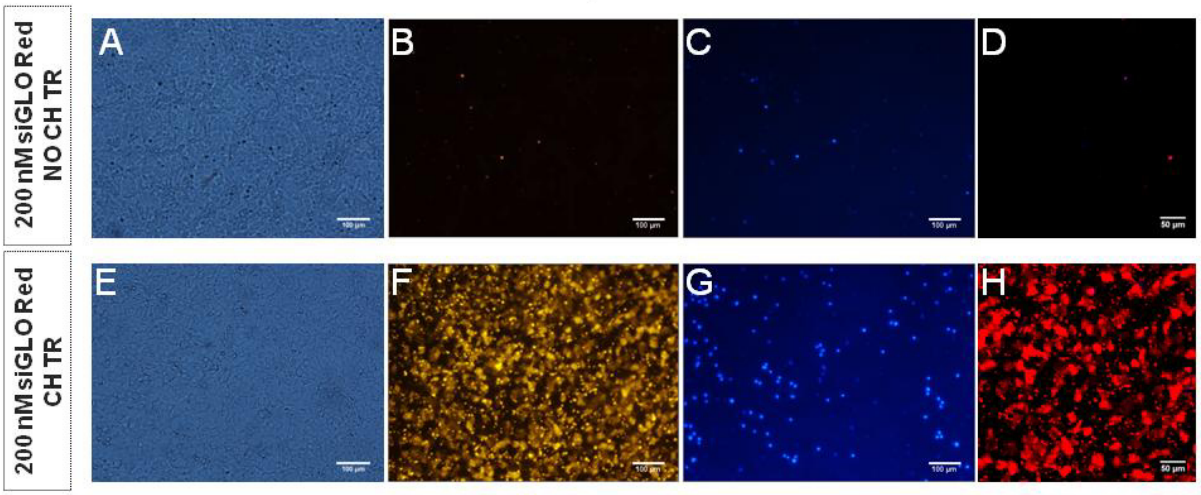

Figure 8.11 Exemplary phase-contrast (first column) and fluorescence micrographs (second to fourth column) taken app. 24 hours after chemical transfection of NRK cells in presence of 200 nM siGLO Red. Experiment was performed at 37 °C. Second column-epi-mode: siGLO Red signal; third column-epi-mode: DAPI staining; fourth column-CLSM: overlay of siGLO Red and DAPI staining. Scale bar in micrographs of first, second and third column corresponds to 100 µm and in micrographs of the fourth column, scale bar represents 50 µm. All micrographs were taken using 10-fold magnification objective.

Fluorescence micrographs taken with higher magnification (**Figure 8.12**) show localization of siGLO Red in nuclei and cytoplasm of some cells but predominantly, signal was observed in vesicles, since characteristic punctuated pattern was recognized. It is noticeable that transfection efficiency on NRK was lower compared to CHO-GFP cells, where more nuclear staining and higher fluorescence intensity was observed, even though applied concentrations of siGLO Red were much lower.

Punctuated pattern and fluorescence stains across the cell population were also observed in confocal fluorescence micrographs presented in the fourth column of each figure. Co-localization with DAPI was low for two reasons: limited localization of siGLO Red within the nuclei and very low DAPI signal achieved in the entire experiment. In this case, same as in the previous experiment, NRK cells were not fixed and permeabilized before DAPI staining (to avoid potential leakage of previously loaded material), but only incubated for app. 15 min in the presence of DAPI stain (protocol described in chapter 4.3.4.2). Obviously, very low amounts of DAPI material managed eventually to enter the cytosol of NRK cells and therefore, staining of the nuclei was very low. Even the micrographs taken with high magnification show very low signals originating from the DAPI stain (**Figure 8.12 C**, **D**, **G**, **H**).

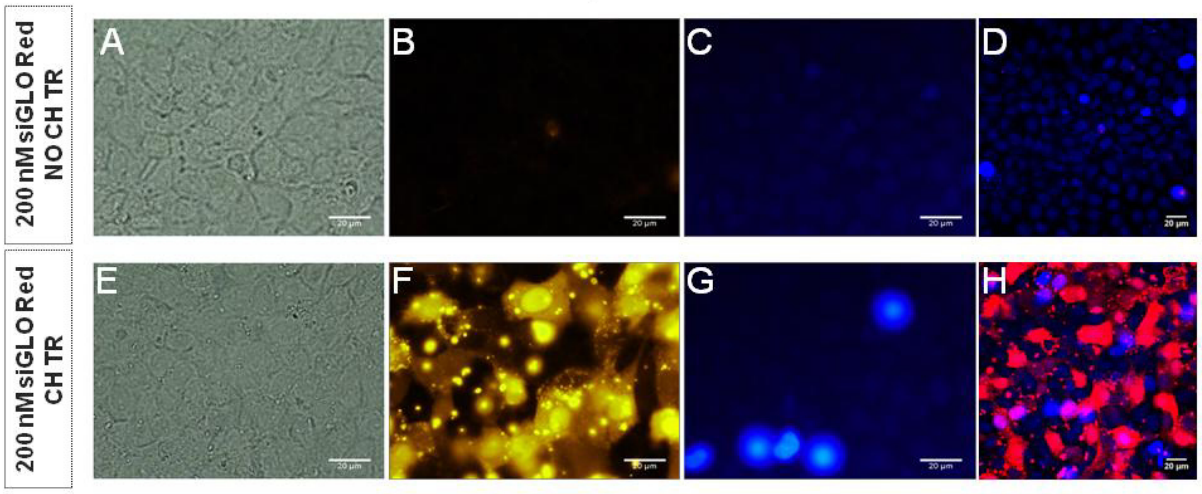

Figure 8.12 Exemplary phase-contrast (first column) and fluorescence micrographs (second to fourth column) taken app. 24 hours after chemical transfection of NRK cells in presence of 200 nM siGLO Red. Experiment was performed at 37 °C. Second column-epi-mode: siGLO Red signal; third column-epi-mode: DAPI staining; fourth column-CLSM: overlay of siGLO Red and DAPI staining. Scale bar in all micrographs corresponds to 20 µm. All micrographs were taken using 60-fold magnification objective.

Chemical transfection allowed entry of siGLO Red into cytosol of NRK cells, however, signal was mostly localized in vesicles, whereas part of the signal was observed in nuclei and cytoplasm. Transfection efficiency was overall lower than with CHO-GFP cells.

8.2.2.3 Delivery of siGLO Red into Fixed and Permeabilized Cells

Fixed and permeabilized NRK cells were applied for localization study including 4 µM siGLO Red, after its free diffusion through the disrupted cell membrane. This experiment was performed to acquire an additional control for previously conducted electroporation and chemical transfection of NRK cells. After addition of 4 µM siGLO Red to fixed and permeabilized NRK cells (according to the protocol described in chapter 4.5.1), they were incubated for app. 40 min at 37 °C and microscopy followed to evaluate localization of siGLO Red within the cells.

Exemplary phase-contrast (first column) and fluorescence micrographs (second to fourth column) are summarized in **Figure 8.13**. Micrographs were taken using 10-fold (upper panel) and 60-fold (lower panel) magnification app. 1 hour after addition of 4 µM siGLO Red to the cells. Fluorescence signal of siGLO Red is visible in the micrographs of second column (taken in epi-mode) and fourth column (taken by CLSM). Obviously, siGLO Red diffused into every NRK cell, however, only small level of fluorescence was found directly in nuclei.

Fluorescence was rather distributed between nucleus and plasma membrane within each cell. Similarly as with CHO-GFP; certain grained structure was recognized within cytoplasm, which could be possibly lysosomes or mitochondria. Confocal fluorescence micrographs presenting overlay of siGLO Red and DAPI staining (in fourth column) show very low level of co-localization and overall very different loading pattern between siGLO Red and DAPI. Staining of nuclei with DAPI was very well visible in this experiment, both in micrographs with lower and higher magnification, due to the fact that cells were previously fixed and permeabilized and not only incubated in presence of DAPI stain.

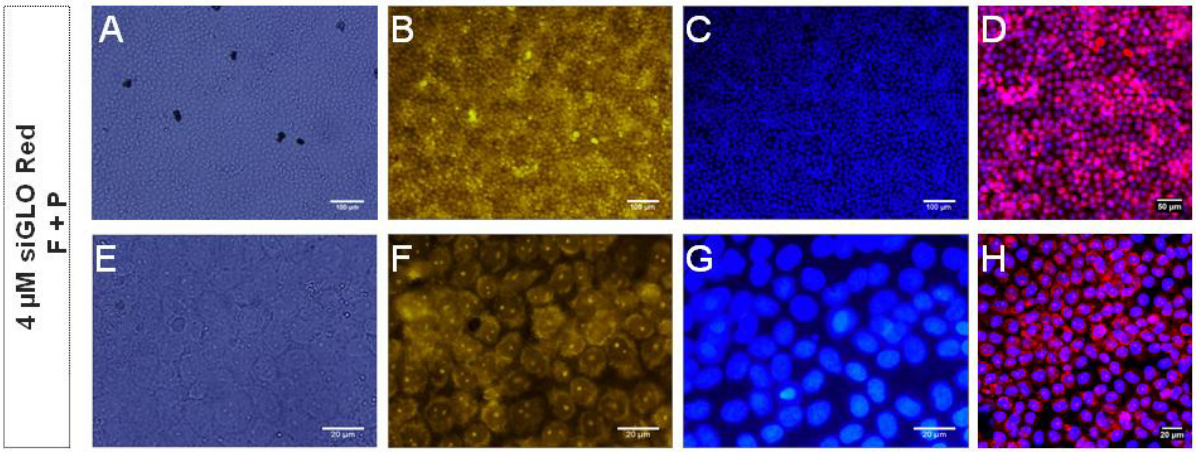

Figure 8.13 Exemplary phase-contrast (first column) and fluorescence micrographs (second to fourth column) taken app. 1 hour after 4 µM siGLO Red was added to fixed and permeabilized NRK cells. Experiment was performed at 37 °C. Second column-epi-mode: siGLO Red signal; third column-epi-mode: DAPI staining; fourth column-CLSM: overlay of siGLO Red and DAPI staining. The scale bar in micrographs **A**, **B** and **C** corresponds to 100 µm, in micrograph **D** to 50 µm and in micrographs **E**-**H** to 20 µm. Micrographs in the upper row were taken using 10-fold magnification and micrographs in the lower panel using 60-fold magnification objective.

8.2.3 Delivery of siGLO Red into NIH-3T3 Cells

Since NIH-3T3 cells were meant to serve as an additional cell model for delivery of siRNA into cells, the chemical transfection was investigated using fluorescently-labeled siRNA siGLO Red. NIH-3T3 cells were chemically transfected in presence of 25 and 50 nM siGLO Red according to the protocol described in chapter 4.4.2.3 and transfection efficiency was evaluated after app. 24 hours.

Exemplary phase-contrast (first column) and fluorescence micrographs (second and third column) are summarized in **Figure 8.14** (taken with 10-fold magnification) and in **Figure 8.15**

(taken with 60-fold magnification objective). Fluorescence micrographs were taken in epi-mode (second column of each figure), and using CLSM (third column of each figure). Fluorescence micrographs visualize siGLO Red signal and obviously, small amount of siGLO Red was taken up by the cells unspecifically (**Figure 8.14 B** and **Figure 8.15 B**). The fraction of transfected cells was relatively small and siGLO Red signal was found mainly in cytoplasm and vesicles (with the characteristic punctuated staining pattern). Almost no cells were found with the siGLO Red accumulated in their nuclei. Moreover, cells transfected with 50 nM siGLO Red exhibited slightly more fluorescence signal than the cells transfected with 25 nM, however, no difference in a loading pattern was observed.

Considering the fact that siGLO Red was rarely found in the nuclei of NIH-3T3 cells, chemical transfection of this cell line with siGLO Red is considered unsuccessful. *In situ* electoporation of NIH-3T3 cells was attempted, however, also without success, as during washing steps, cells were usually washed away from the substrate.

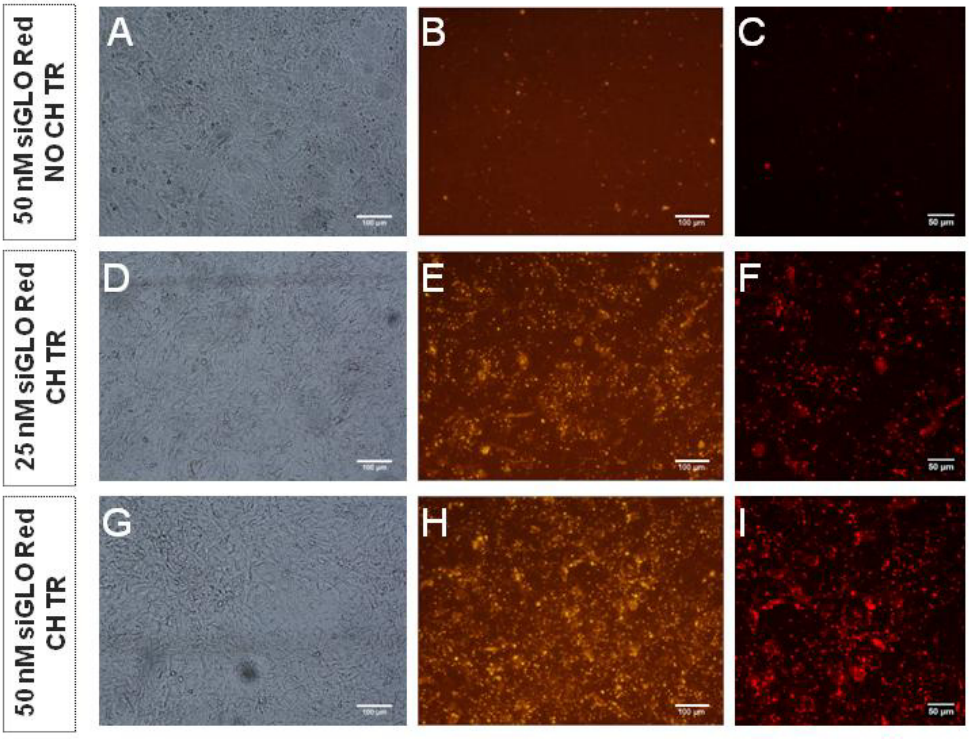

Figure 8.14 Exemplary phase-contrast (first column) and fluorescence micrographs (second to third column) taken app. 24 hours after chemical transfection of NIH-3T3 cells in presence of 25 nM (second row) and 50 nM (third row) siGLO Red. Experiment was performed at 37 °C. Second column shows fluorescence micrograph taken in epi-mode and third column shows fluorescence micrograph taken by CLSM. The scale bar in micrographs of the first and second column corresponds to 100 µm and in micrographs of the third column, scale bar represents 50 µm. All micrographs were taken using 10-fold magnification objective.

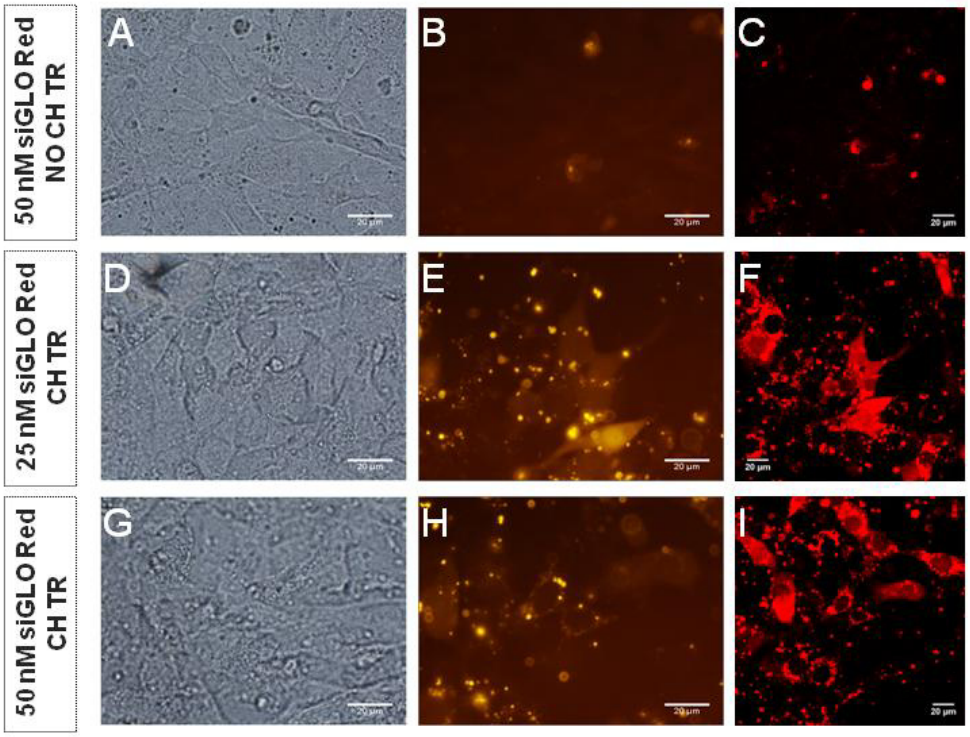

Figure 8.15 Exemplary phase-contrast (first column) and fluorescence micrographs (second to third column) taken app. 24 hours after chemical transfection of NIH-3T3 cells in presence of 25 nM (second row) and 50 nM (third row) siGLO Red. Experiment was performed at 37 °C. Second column shows fluorescence micrograph taken in epi-mode and third column shows fluorescence micrograph taken by CLSM. Scale bar in all micrographs corresponds to 20 µm. All micrographs were taken using 60-fold magnification objective.

8.3 Delivery of Small Interfering RNA Targeting EGFP into Cells

After delivery of siRNA into different mammalian cell lines was initially investigated using fluorescently-labeled non-targeting probe – siGLO Red and experimental conditions for cell lines CHO-GFP and NRK were optimized with this transfection indicator, specific siRNA type was applied. The sequence-specific siRNA targeting genes responsible for expression of enhanced green fluorescent protein (EGFP) was chosen as a functional siRNA probe (siEGFP) to be tested on CHO-K1 cells, genetically modified to stably express EGFP (CHO-GFP cells). This implies that successful transfection of CHO-GFP cells with siEGFP would cause knockdown (silencing) of genes responsible for EGFP expression, green fluorescence expressed by CHO-GFP cells would be inhibited and the affected cells would appear dark (illustrated in **Figure 8.16**). The level of expression of EGFP in CHO-GFP cells after transfection by *in situ* electroporation or by using conventional chemical transfection reagent was evaluated using confocal laser scanning microscopy (CLSM).

Besides siEGFP as a functional sequence-specific probe, siRNA with random unspecific sequence was applied as a negative control during all experiments, so-called scrambled siRNA (siSCR). Taking into account siSCR should help to exclude possible off-target (unspecific) effects during the experiments.

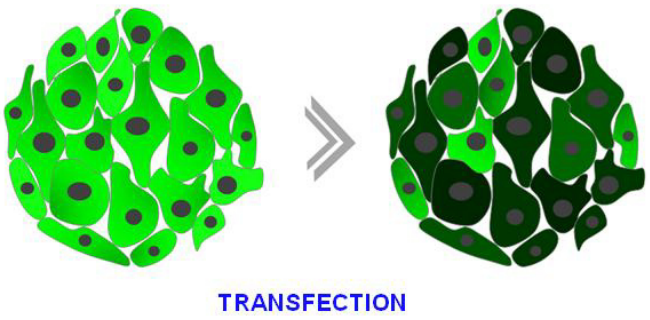

Figure 8.16 Schematic illustration showing adherent cells before (left) and after (right) their transfection in presence of siRNA targeting enhanced green fluorescent protein (EGFP) - siEGFP. Successful delivery of siEGFP into cells induces reduction or complete knockdown of bright green fluorescence signal expressed by CHO-GFP cells.

8.3.1 Delivery of siEGFP by *In Situ* Electroporation

The sequence-specific probe siEGFP was transfected into CHO-GFP cells by *in situ* electroporation using ECIS technology. Electroporation efficiency and effects of this siRNA type onto CHO-GFP cells were evaluated by CLSM either 48, or 72 hours after performing the electroporation, whereby experimental procedure for *in situ* electroporation (abbreviated ISE or ELPO) was performed according to the same protocol (more details described in chapter 4.2.2.5). $EBSS^{++}$ was applied as an assay buffer, working volume was 30 µL per well and experiments were conducted on 8W4Eµ electrode array. Since CHO-GFP was chosen as a cell model to study introduction and effects of siEGFP, *in situ* electroporation was applied using optimal combination of pulse parameters for this cell line: 40 kHz, 4 V and 500 ms. During impedimetric monitoring, electroporation was applied three times successively, as a strategy to improve transfection efficiency (multiple electroporation was studied in more details within chapter 5.1.3).

Knockdown Efficiency Evaluated after 48 Hours

Typical time course of the normalized impedance before, during and after *in situ* electroporation of CHO-GFP cells in presence of 2 µM siEGFP and 2 µM siSCR is presented in **Figure 8.17**. The experiment included control where cells were only incubated with 2 µM

siEGFP in absence of pulse application and the control where cells were pulsed in absence of siRNA. Impedance measurement is presented at 16 kHz and data are normalized to the last time point before first electroporation pulse was applied. CHO-GFP cells were electroporated three times successively, as indicated by the arrows - a: 1st pulse, b: 2nd pulse and c: 3rd pulse application. Impedance signal decreased and returned to the pre-pulse values within 20 – 30 min after every pulse application and after the last pulse, cells were allowed to fully recover before impedance measurement was finished. Thereafter, assay buffer was exchanged with the complete medium and cells were cultured for 48 hours before microscopy by CLSM was conducted to evaluate silencing effect of siEGFP on CHO-GFP.

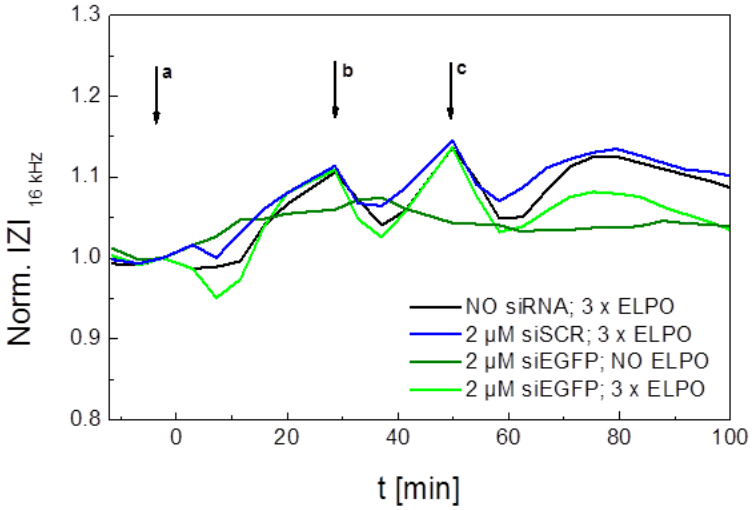

Figure 8.17 Typical time course of the normalized impedance at 16 kHz before, during and after *in situ* electroporation of CHO-GFP cells in presence of 2 µM siEGFP and 2 µM siSCR. ISE was applied three times successively - **a**: 1st pulse, **b**: 2nd pulse and **c**: 3rd pulse application, using optimal combination of pulse parameters for this cell line: 40 kHz, 4 V and 500 ms. Impedance values are normalized to the last time point before first electroporation pulse was applied. After cellular recovery from the last pulse, impedance measurement (at 37 °C) was finished, buffer was exchanged with the complete medium and microscopy by CLSM followed app. 48 hours later to evaluate knockdown efficiency.

App. 48 hours after electroporation, microscopy by CLSM was performed using 10-fold and 60-fold magnification objective. Exemplary phase-contrast and confocal fluorescence micrographs are summarized in **Figure 8.18**, and micrographs in the second column were additionally zoomed 1.5 fold to better visualize the appearance of the cells. During microscopy, imaging settings were kept constant (and detector of the same sensitivity was applied) in order to acquire fairly comparable fluorescence micrographs. This is evidenced by

the micrographs (taken with red channel) given in Appendix (**Figure 11.7 A**), which correspond to the micrographs shown in the second column (**Figure 8.18**). Red stars are added to the micrographs of first column to indicate which of the two presented electrodes is enlarged in the respective fluorescence micrograph in the third column. White circles in the micrographs of second column delineate area of electrodes, thus allowing one easier assessment of the fluorescence pattern.

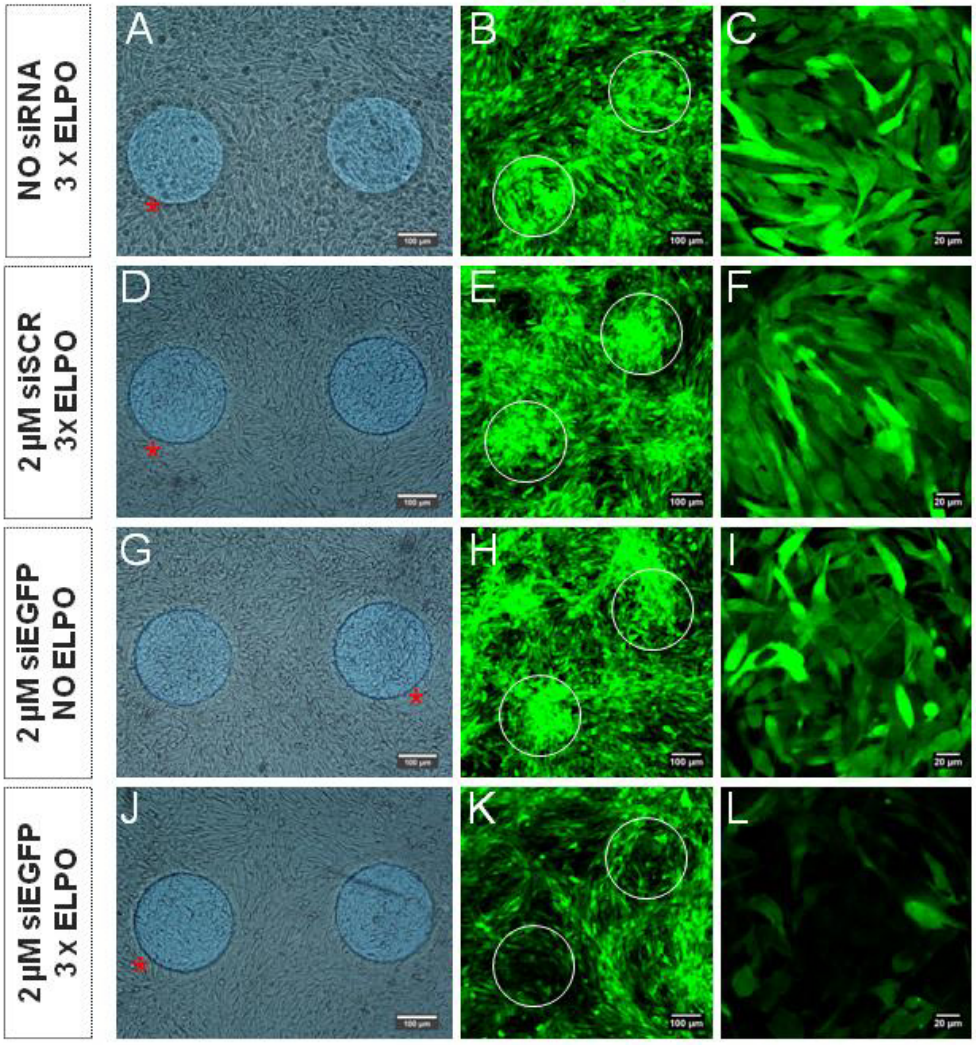

Figure 8.18 Exemplary phase-contrast (first column) and confocal fluorescence micrographs (second and third column) taken app. 48 hours after *in situ* electroporation was applied for delivery of 2 µM siEGFP and 2 µM siSCR to CHO-GFP cells. Experiment was performed at 37 °C. Red starts in the micrographs of first column indicate which of the two presented electrodes is enlarged in the respective micrograph in the third column. White circles in the micrographs of second column delineate area of electrodes. The scale bar in micrographs of the first and second column corresponds to 100 µm, whereas in micrographs of the third column scale bar represents 20 µm. Micrographs were taken using 10-fold (first and second column) and 60-fold (third column) magnification objective.

By observing phase-contrast micrographs, no difference between three controls and are encountered. However, fluorescence mcrographs show that CHO-GFP cells in controls (**A-I**) exhibit their regular levels of EGFP expression, as all cells appear bright. In the sample (**J-L**), CHO-GFP cells on the electrodes and around the electrodes appear darker than the cells residing on the photopolymer (background). Darker appearance of the cells electroporated in presence of 2 µM siEGFP is well visualized in the fluorescence micrograph **L**, where EGFP expression of majority of the cells on the electrode is completely silenced, whereas in some cells, EGFP expression is only reduced. Besides, fluorescence intensity of the cells on the electrodes appears overall higher due to a reflexion from the gold surface (of the electrode) and this has to be taken into account when assessment of fluorescence signal of the cells on the electrodes is evaluated.

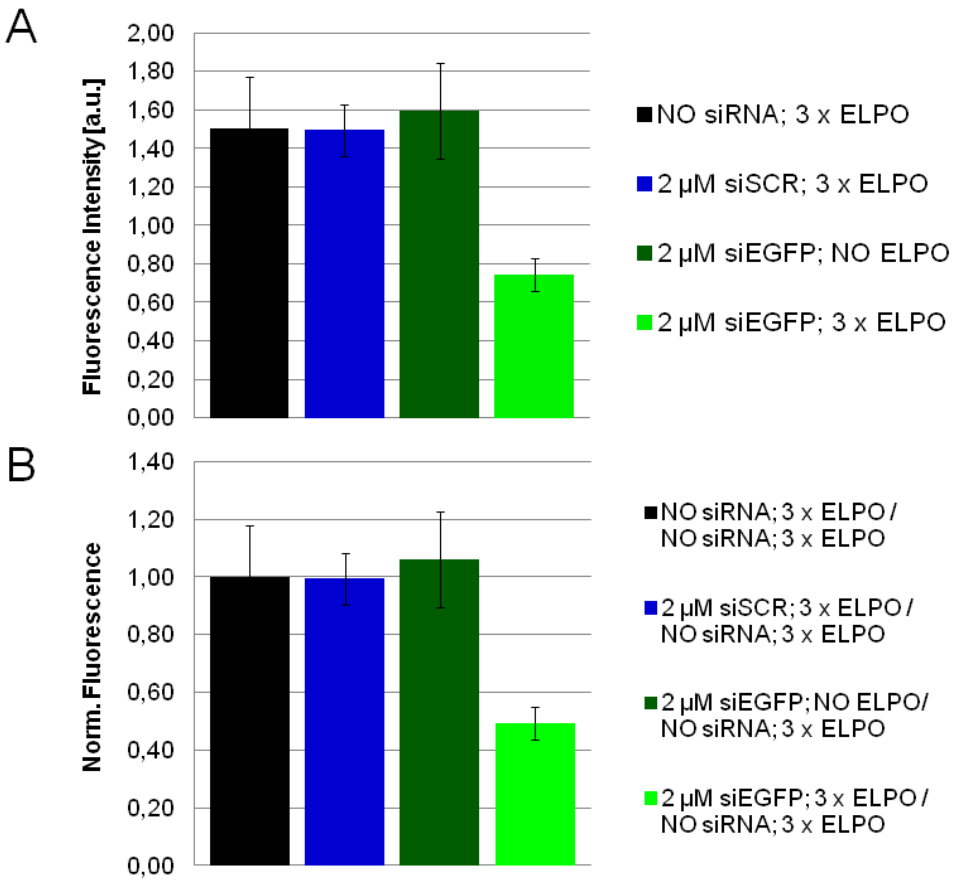

Figure 8.19 Bar plots presenting fluorescence intensity of EGFP on the micrographs taken 48 hours after *in situ* electroporation of CHO-GFP cells to facilitate delivery of siEGFP into the cell cytosol. **A** Bar plots show fluorescence intensity of EGFP in three controls and a sample. **B** Bar plots show the same data as given in **A**, but normalized to the control where cells were electroporated in absence of siRNA. 4 - 7 different micrographs taken for every experimental condition within 2 independent experiments were quantified using ImageJ; mean value ± standard deviation; n= 4 - 7.

Micrographs documented during microscopy app. 48 after *in situ* electroporation were quantified using ImageJ program and evaluated statistically, according to the scheme described in **Figure 4.15 A** within chapter 4.3.5. The fluorescence intensity value for a pair of electrodes was normalized to the average intensity of the background at the micrographs taken for every measured experimental condition. The experimental procedure for delivery of siEGFP into CHO-GFP cells by ISE was conducted within two independent experiments and altogether 4 - 7 different micrographs were analyzed for each experimental condition (n= 4 - 7). The results are evaluated in the form of bar plots presented in **Figure 8.19** (mean value ± standard deviation; n= 4 - 7). **Figure 8.19 A** shows bar plots representing fluorescence intensity of EGFP 48 hours after ISE and **Figure 8.19 B** shows bar plots representing the same data as given in **A**, but normalized to the control where cells were subjected to electroporation in absence of siRNA.

Image analysis (given in **A**) indicates that CHO-GFP cells electroporated in absence of siRNA (black bar) and in the presence of siSCR (blue bar) exhibited app. the same level of fluorescence intensity (1.51 ± 0.27 and 1.50 ± 0.13, respectively), whereas cells which were not electroporated but only incubated with 2 µM siEGFP (olive green bar) exhibited slightly higher fluorescence intensity (1.59 ± 0.25) than the other two controls. The fluorescence intensity of a sample (bright green bar) was 0.74 ± 0.09 and was significantly lower than any of three controls. Bar plots presented in **B** show the same data as in graph **A**, but fluorescence intensity values were normalized to the control where electroporation was applied only in buffer. Normalized data indicated again that cells electroporated in absence of siRNA (black bar) exhibited app. the same level of normalized fluorescence intensity as the cells electroporated in presence of siSCR (blue bar) (1.00 ± 0.18 and 0.99 ± 0.09, respectively). Cells which were not electroporated but only incubated with 2 µM siEGFP (olive green bar) exhibited slightly higher normalized fluorescence intensity than the other controls (1.06 ± 0.17). The normalized fluorescence intensity of the sample (bright green bar) was 0.49 ± 0.06, indicating that EGFP fluorescence was reduced 51 % app. 48 hours after siEGFP delivery into CHO-GFP cells by *in situ* electroporation.

Interestingly, quantification of fluorescence micrographs showed that cells exposed to siEGFP in absence of electric pulse exhibited higher fluorescence intensity than the cells pulsed with siSCR or without siRNA. Such results might suggest that reduction of fluorescence intensity in the sample is contributed by the reduction of fluorescence due to the cell damage induced by application of multiple invasive electric pulses.

Based on this data it was concluded that *in situ* electroporation facilitated successful transfection of CHO-GFP cells with siEGFP, and as a consequence, EGFP expression was

reduced for 50 % 48 hours after transfection.

Knockdown Efficiency Evaluated after 72 Hours

As already mentioned, transfection and knockdown efficiency were not only evaluated 48 hours, but also 72 hours after *in situ* electroporation of CHO-GFP cells in presence of 2 µM siEGFP and 2 µM siSCR. Experimental protocol and conditions were kept the same as during the experiments where effects of siEGFP were evaluated after 48 hours. Therefore, only the most important facts regarding the experiment will be mentioned to avoid unnecessary repeating and observed differences between two assays will be compared.

Typical time course of the normalized impedance at 16 kHz before, during and after *in situ* electroporation of CHO-GFP cells in presence of 2 µM siEGFP and siSCR is presented in **Figure 8.20**. CHO-GFP cells were pulsed three times successively using optimal combination of pulse parameters for this cell line. After cells recovered from the third pulse and stabilized, assay buffer was exchanged with complete medium and cells were cultured for 72 hours before microscopy by CLSM was performed to evaluate silencing effect of siEGFP on CHO-GFP cells.

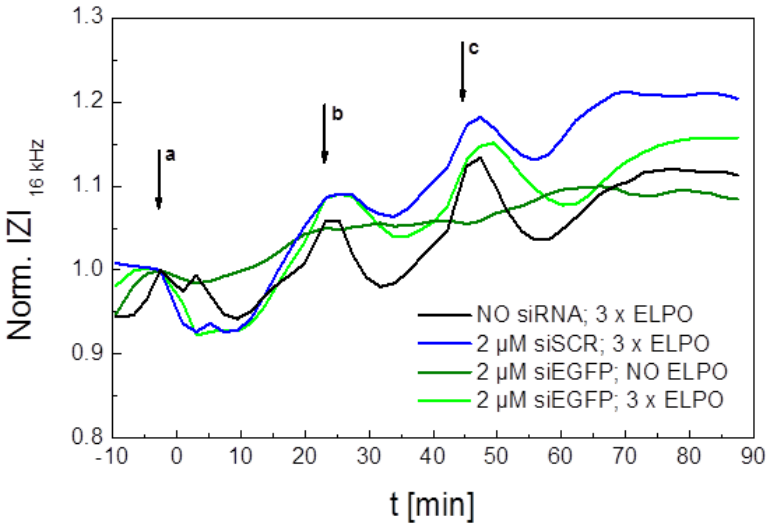

Figure 8.20 Typical time course of the normalized impedance at 16 kHz before, during and after *in situ* electroporation of CHO-GFP cells in presence of 2 µM siEGFP and 2 µM siSCR. ISE was applied three times successively - **a**: 1st pulse, **b**: 2nd pulse and **c**: 3rd pulse application, using optimal combination of pulse parameters for this cell line: 40 kHz, 4 V and 500 ms. Impedance values are normalized to the last time point before first electroporation pulse was applied. After cellular recovery from the third and last pulse, impedance measurement (at 37 °C) was finished, buffer was exchanged with the complete medium and microscopy by CLSM followed app. 72 hours later to evaluate knockdown efficiency.

Microscopy by CLSM was conducted app. 72 hours after electroporation. Exemplary phase-contrast and confocal fluorescence micrographs are summarized in **Figure 8.21**. Red stars indicate which of the two presented electrodes is enlarged in the respective micrograph in the third column. White circles delineate electrodes area. Imaging settings were kept constant during microscopy (including detector with the same sensitivity), and this is shown by the micrographs taken with red channel given in Appendix (**Figure 11.7 B**).

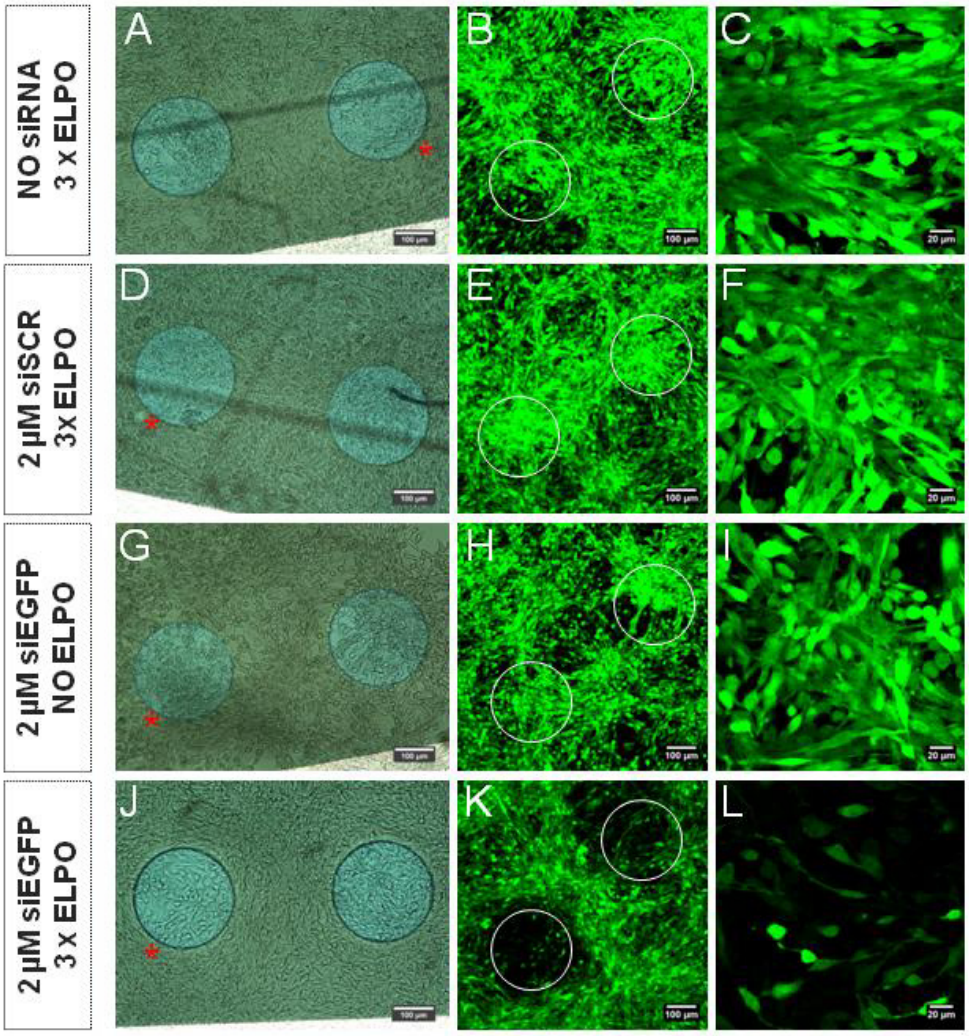

Figure 8.21 Exemplary phase-contrast (first column) and confocal fluorescence micrographs (second and third column) taken app. 72 hours after *in situ* electroporation was applied for delivery of 2 µM siEGFP and 2 µM siSCR to CHO-GFP cells. Experiment was performed at 37 °C. Red starts in the micrographs of first column indicate which of the two presented electrodes is enlarged in the respective micrograph in the third column. White circles in the micrographs of second column delineate area of electrodes. The scale bar in micrographs of the first and second column corresponds to 100 µm, whereas in micrographs of the third column, scale bar represents 20 µm. Micrographs were taken using 10-fold (first and second column) and 60-fold (third column) magnification objective.

Fluorescence micrographs show that cells in all three controls (**A-I**) exhibited their regular levels of EGFP expression, whereas cells previously subjected to electric pulses in presence of siEGFP (**J-L**) appeared darker than the cells of the background. The fluorescence micrograph **L** (in **Figure 8.21**) shows CHO-GFP cells in the central part of the electrode, previously pulsed in presence of 2 µM siEGFP, and they obviously appear significantly darker than the cells in the corresponding control images (**C**, **F** and **I**).

Fluorescence micrographs taken app. 72 hours after *in situ* electroporation were quantified using ImageJ program and evaluation was performed in a same manner as previously described for the micrographs taken 48 hours after ISE. Delivery of siEGFP into CHO-GFP cells by ISE was conducted within two independent experiments and altogether 4 - 8 different micrographs were analyzed for each experimental condition (n= 4 - 8). Resulting bar plots with mean value ± standard deviation; n= 4 - 8 are presented in **Figure 8.22.**

Figure 8.22 A shows bar plots representing fluorescence intensity of EGFP 72 hours after ISE and **Figure 8.22 B** shows bar plots representing the same data as given in **A**, but normalized to the control where cells were subjected to electroporation in absence of siRNA. The bar plots indicate very similar results to those obtained 48 hours after ISE. Cells electroporated in absence of siRNA (black bar) and in the presence of siSCR (blue bar) exhibited app. the same fluorescence intensity (1.44 ± 0.32 and 1.44 ± 0.25, respectively). Cells incubated with 2 µM siEGFP without pulsing exhibited again slightly higher fluorescence intensity values (1.54 ± 0.28) than the other two controls and cells pulsed with 2 µM siEGFP showed the lowest fluorescence intensity 0.64 ± 0.18.

Bar plots in **Figure 8.22 B** show the same data as in **A**, but fluorescence intensity values were normalized to the control where cells were electroporated only in buffer. Cells pulsed in absence of siRNA (black bar) exhibited the same level of normalized fluorescence intensity as the cells electroporated in presence of siSCR (blue bar) (1.00 ± 0.22 and 1.00 ± 0.18, respectively). Non-pulsed cells incubated with 2 µM siEGFP (olive green bar) exhibited normalized fluorescence intensity 1.07 ± 0.19). The normalized fluorescence intensity of the sample (bright green bar) was 0.45 ± 0.13.

Such results indicate that EGFP fluorescence was reduced 55 % app. 72 hours after siEGFP delivery into CHO-GFP cells by *in situ* electroporation.

Cells exposed to siEGFP in absence of electric pulse exhibited again slightly higher fluorescence intensity than the cells pulsed with siSCR or without siRNA, which supports strongly the hypothesis that overall reduction of fluorescence intensity observed for the pulsed cells is caused by the invasiveness of the ISE method and very small fraction of CHO-GFP cells is permanently damaged by the multiple pulse application.

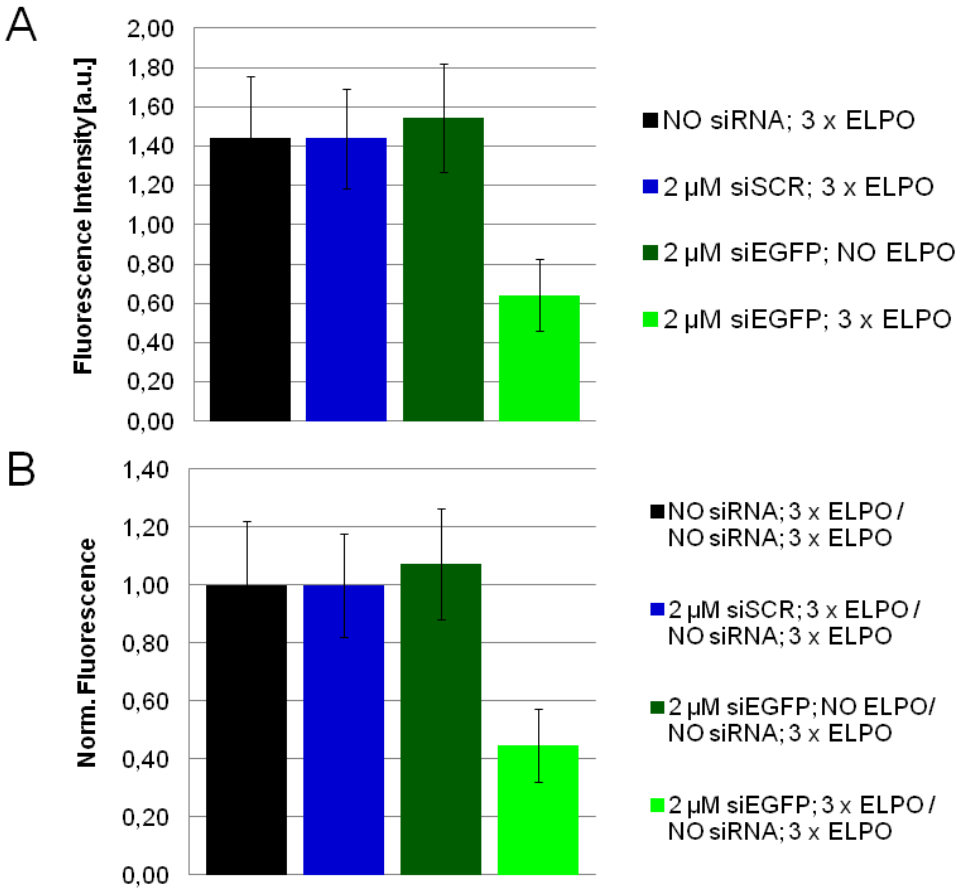

Figure 8.22 Bar plots presenting fluorescence intensity of EGFP on the micrographs taken 72 hours after *in situ* electroporation of CHO-GFP cells to facilitate delivery of siEGFP into the cell cytosol. **A** Bar plots show fluorescence intensity of EGFP in three controls and a sample. **B** Bar plots show the same data as given in **A**, but normalized to the control where cells were electroporated in absence of siRNA. 4 - 8 different micrographs taken for every experimental condition within 2 independent experiments were quantified using ImageJ; mean value ± standard deviation; n= 4 - 8.

8.3.2 Delivery of siEGFP by Chemical Transfection

Delivery of siEGFP into CHO-GFP cells by *in situ* electroporation was compared to the delivery of siEGFP by the widespread chemical lipid-based transfection (abbreviated CH TR). The CHO-GFP cells were chemically transfected in presence of either 33 nM siEGFP, or 33 nM siSCR using commercial chemical transfection reagent Lipofectamine, according to the protocol described in chapter 4.4.2.3. In addition, cells were exposed to chemical transfection mediator in absence of siRNA. App. 48 h after chemical transfection, transfection efficiency and silencing effect of siEGFP on CHO-GFP cells was evaluated by CLSM. Exemplary phase-contrast and fluorescence micrographs are summarized in **Figure 8.23**. Fluorescence micrographs in the third column were additionally zoomed 3 times to better

visualize the difference in fluorescence signal between the cells in the sample and in controls. Obviously, CHO-GFP cells in controls (first and second row) exhibited their regular level of EGFP expression, whereas entire population of cells exposed to siEGFP and Lipofectamine appeared much darker, due to reduction or complete knockdown of EGFP expression. It was concluded that chemical transfection with Lipofectamine induces very successful transfection of CHO-GFP cells with siEGFP, and as a consequence, EGFP was efficiently silenced.

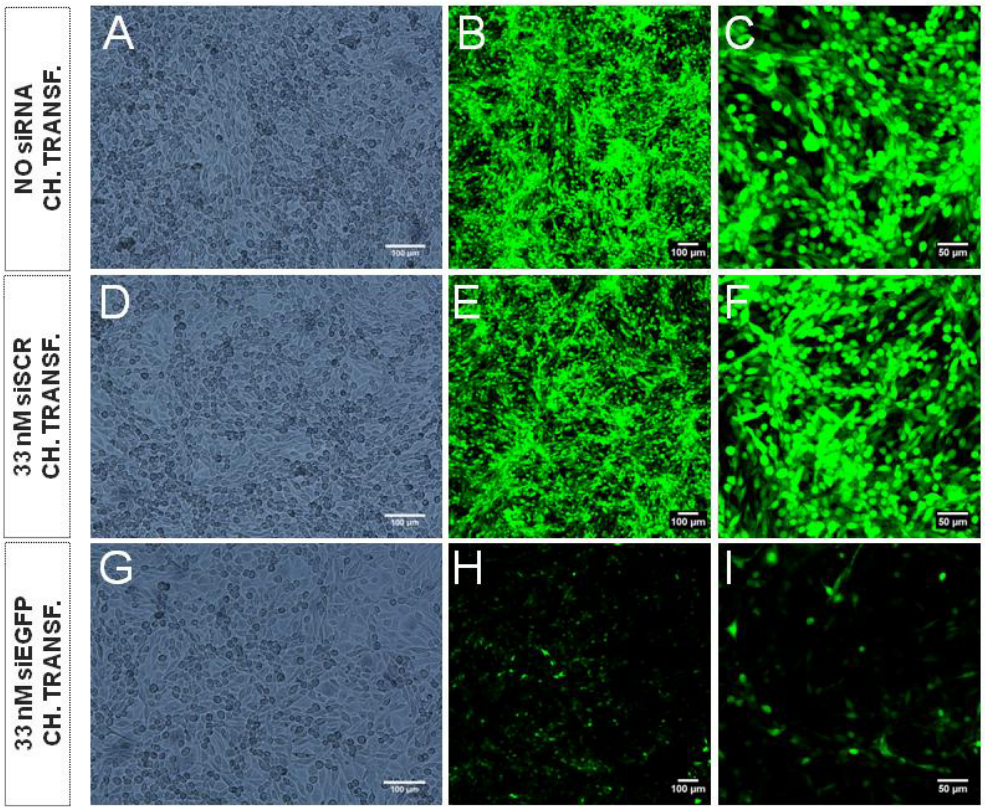

Figure 8.23 Exemplary phase-contrast (first column) and confocal fluorescence micrographs (second and third column) taken app. 48 hours after chemical transfection of CHO-GFP cells in presence of 33 nM siEGFP, or 33 nM siSCR. Experiment was performed at 37 °C. The scale bar in micrographs of the first and second column corresponds to 100 µm and scale bar in micrographs of the third column represents 50 µM. All micrographs were taken using 10-fold magnification objective.

8.4 Delivery of Cell Death siRNA into Cells

Besides specific siRNA targeting genes responsible for expression of EGFP, another sequence-specific siRNA type was applied for investigation of siRNA delivery into cells by *in situ* electroporation and chemical transfection, whereby cellular behavior before and after

delivery was monitored impedimetrically using ECIS technology. After delivery of siRNA into different mammalian cell lines was initially investigated using fluorescently-labeled non-targeting probe – siGLO Red and experimental conditions for every cell line were optimized, specific Cell Death siRNA type (siCD) was applied.

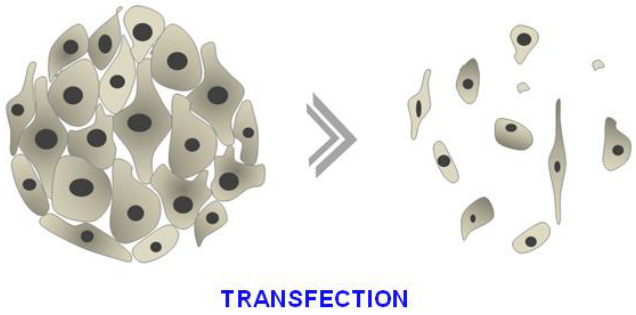

Figure 8.24 Schematic illustration showing adherent cells before (left) and after (right) their transfection in presence of siRNA targeting vital genes responsible for cell viability (Cell Death siRNA - siCD). Successful delivery of siCD into cells induces high level of cell death.

This commercially avaliable sequence-specific siRNA is created to target genes of mice and rats, essential for their survival. The exact gene targets are proprietary but successful transfection of the cells with siCD should induce knockdown (silencing) of genes responsible to sustain cell viability, so that affected cells undergo apoptosis and die (illustrated in **Figure 8.24**), as indicated by the name of this siRNA type. To study effects of siCD on the different cell lines, cellular behavior was monitored by ECIS technology after either *in situ* electroporation, or conventional chemical transfection of the cells in presence of siCD. In addition, micrographs were taken to visualize appearance of the cells under study before and after treatment with siCD.

Besides siCD as a functional sequence-specific probe, siRNA with random (unspecific) sequence, so-called scrambled siRNA (siSCR) was applied as a negative control during all experiments. Taking into account siSCR should help to exclude possible off-target (unspecific) effects of siRNA.

8.4.1 Delivery of Cell Death siRNA into CHO-GFP Cells

The first cell line applied as a cell model to study delivery of siCD into cells was CHO-GFP. After previous optimization of siRNA entry into this cell line using siGLO Red and studies of siEGFP delivery, it was concluded that CHO-GFP cells would be an appropriate cell model to study introduction of siCD into cells. Its potential cytotoxic effect on the cells was monitored

using ECIS platform and microscopy was used to visualize the appearance of the cells. The sequence-specific probe siCD was transfected into CHO-GFP cells by *in situ* electroporation and by chemical transfection. Thereafter, the effects of siCD onto cells were monitored by ECIS for 20 – 70 hours.

8.4.1.1 Delivery of siCD by *In Situ* Electroporation

Introduction of siCD into CHO-GFP by *in situ* electroporation was conducted (according to the experimental procedure described in chapter 4.2.2.5) on 8W4Eμ electrode array and $EBSS^{++}$ was applied as the assay buffer. Working volume was 30 μL per well. Typical time course of the normalized impedance at 16 kHz before, during and after *in situ* electroporation of CHO-GFP cells in presence of 2 μM CD is presented in **Figure 8.25 A**. After multiple electroporation of the cells (**A**), measurement was paused and assay buffer was exchanged with complete medium. Thereafter, impedance measurement was resumed and response of CHO-GFP cells was monitored for app. 45 hours. **Figure 8.25 B** shows time course of the normalized impedance magnitude (at 16 kHz) and **Figure 8.25 C** shows time course of the normalized capacitance (at 32 kHz) during the entire measurement. CHO-GFP cells were electroporated in presence of 2 μM siCD (purple line) and corresponding controls were included: (i) with cells electroporated in absence of siRNA (black line), (ii) with cells electroporated in presence of 2 μM siSCR (blue line) and (iii) with cells only incubated but not electroporated in presence of 2 μM siCD (light rose line).

In graph **A**, impedance monitoring of *in situ* electroporation is presented (zoomed in), whereby electric pulses were applied three time successively (using optimal combination of pulse parameters for CHO-GFP: 40 kHz, 4 V and 500 ms), as indicated by the arrows - a: 1^{st} pulse, b: 2^{nd} pulse and c: 3^{rd} pulse application. Impedance magnitudes were normalized to the last time point before first electroporation pulse was applied. Time course of the normalized impedance shows that impedance signal first decreased and then returned to the pre-pulse values within 20 - 30 min after every pulse application. Between the pulses, cells were allowed to recover and after the third and final pulse, cells were allowed to fully recover and stabilize before measurement was paused and $EBSS^{++}$ buffer was exchanged with complete culture medium in every well. The pause in the data acquisition for buffer exchange is marked with d in graph **A**.

In graph **B**, impedance values at 16 kHz were normalized to the last time point before buffer was exchanged with medium, which is marked with a ($t_{norm.}$=a). After data acquisition was resumed, (normalized) impedance values increased as a consequence of cellular reaction to medium addition and to the temporary temperature changes cells experienced during the

break (for buffer exchange). After initial increase, impedance signals stabilized within app. 4 hours. Whereas in the controls, relatively constant impedance values and no significant fluctuations were seen afterwards, (normalized) impedance signal of a sample (purple line) started to decrease app. 13 hours after multiple electroporation.

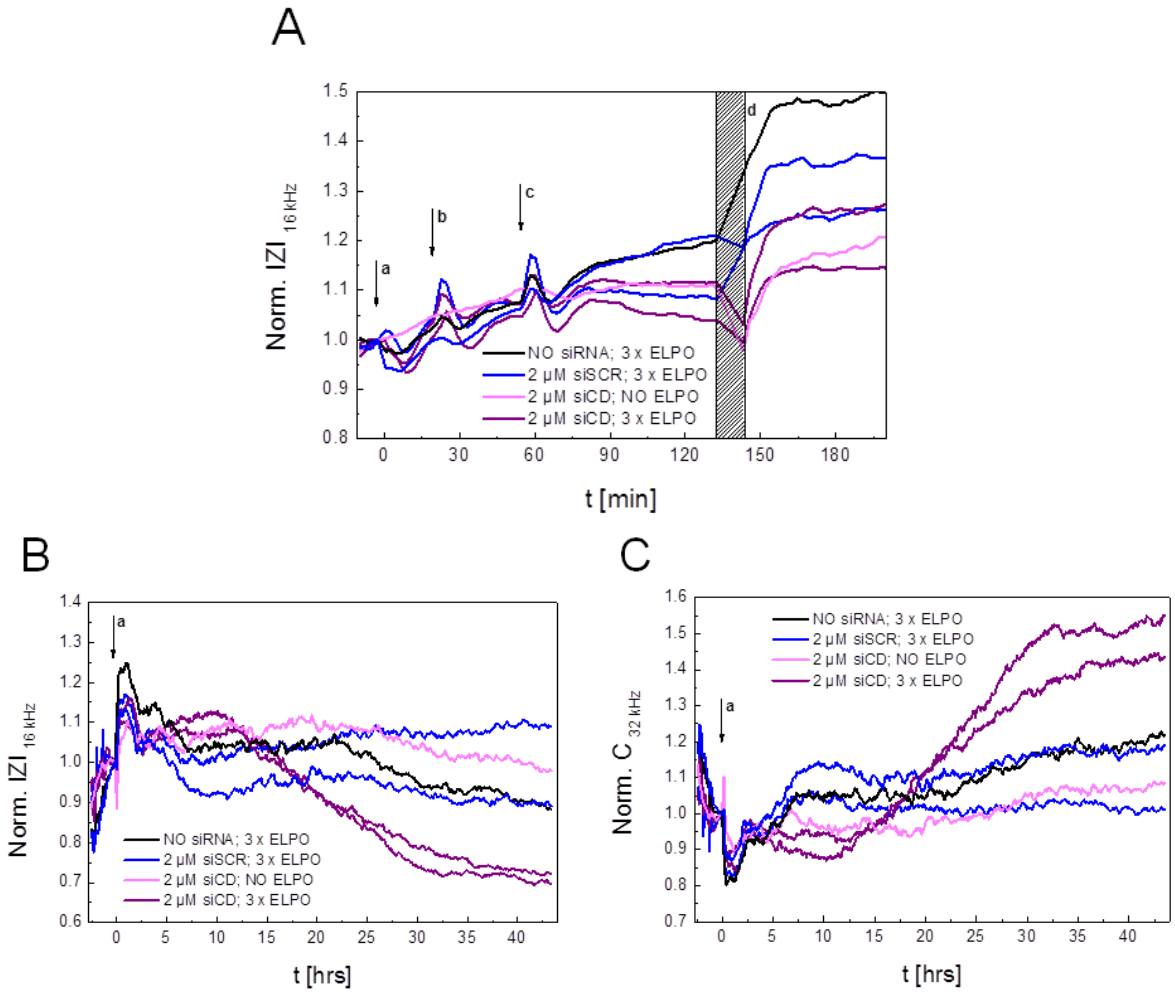

Figure 8.25 A Typical time course of the normalized impedance at 16 kHz before, during and after *in situ* electroporation of CHO-GFP cells in presence of 2 µM siCD and 2 µM siSCR. ISE was applied three times successively - **a**: 1st pulse, **b**: 2nd pulse and **c**: 3rd pulse application, using optimal combination of pulse parameters for this cell line: 40 kHz, 4 V and 500 ms. Impedance values are normalized to the last time point before first electroporation pulse was applied. After cellular recovery from the third pulse, impedance measurement was paused, assay buffer was exchanged with the complete medium (marked with **d**) and data acquisition was resumed. Impedance monitoring continued for app. 45 hours to evaluate cytotoxic effect of siCD. **B** Typical time course of the normalized impedance at 16 kHz for the entire measurement. **C** Typical time course of the normalized capacitance at 32 kHz for the entire experiment. Impedance (**B**) and capacitance (**C**) were normalized to the last time point before buffer exchange was executed (marked with arrow **a**).

Such downtrend was continued and by the end of the measurement (app. 45 h after electroporation), normalized impedance values for the sample (purple line) decreased to the values of app. 0.68 – 0.73, indicating rounding of the cells on the electrodes. For comparison, normalized impedance at 16 kHz dropped down to ~ 0.53 immediately after CHO-GFP cells were exposed to electric wounding in culture medium (more details described in chapter 8.4.1.3) and this value corresponds to the value when cells get killed on the electrode. Control with cells being electroporated in presence of 2 µM siSCR (blue line) exhibited slight decrease of impedance signal after media exchange and subsequent stabilization.

In graph **C**, capacitance values at 32 kHz were normalized to the last time point before buffer was exchanged with medium, which is marked with a ($t_{norm.}$=a). Values of (normalized) capacitance at high frequencies (here 32 kHz) indicate coverage of the cells on the electrodes (Keese et al., 2004) and correlation between cytotoxic effect of siCD on CHO-GFP cells and cell coverage was evaluated. Apart from some unspecific effect observed on the cells exposed to siSCR (capacitance increase 5 – 15 hours after media exchange), all controls showed fairly stable signals. The normalized capacitance of the sample (purple line) increased and reached values of 1.45 – 1.55 by the end of the measurement, indicating rounding of the cells on the electrodes. For comparison, normalized capacitance at 32 kHz increased to ~ 2.25 upon exposure of CHO-GFP cells to electric wounding in culture medium (details described in chapter 8.4.1.3).

After time-resolved monitoring of cellular response to siCD was finished, level of cell death induced by siCD was evaluated by CLSM. CHO-GFP cells were stained with 4 µM Ethidium-Homodimer-1 (EthD-1) according to the protocol described in chapter 4.3.4.1. EthD-1 is a fluorescent probe which diffuses into damaged and dead cells and stains their nuclei with bright red fluorescence signal.

Exemplary confocal fluorescence micrographs taken with 10-fold magnification are summarized in **Figure 8.26**. Fluorescence micrographs in the left column were zoomed additionally 1.5 times and in the right column 3 times to better visualize staining of CHO-GFP cells on the electrodes. Micrographs showing the controls (**E**-**F**) certainly indicate presence of some damaged and dead cells on and around the electrodes. This was subscribed to the regular living cycle of the cells, but also to the fact that cells spent at least two days in a confluent state before microscopy. Micrographs showing the sample - cells exposed to 2 µM siCD during electroporation (**G** and **H**) indicate presence of a large number of damaged and dead cells residing on the electrodes and around them. Such observations indicate that siCD induced cell death in CHO-GFP cells app. 45 hours after its delivery into cytosol by multiple

in situ electroporation. In order to get more precise information on the level of cytotoxicity induced by siCD, and thus indirectly on electroporation efficiency, fluorescence micrographs depicting single electrodes were quantified using ImageJ program and evaluated statistically, according to the scheme described in **Figure 4.15 A** within chapter 4.3.5. The fluorescence intensity value for every electrode was normalized to the average fluorescence intensity of the background, at the micrographs taken for every measured experimental condition.

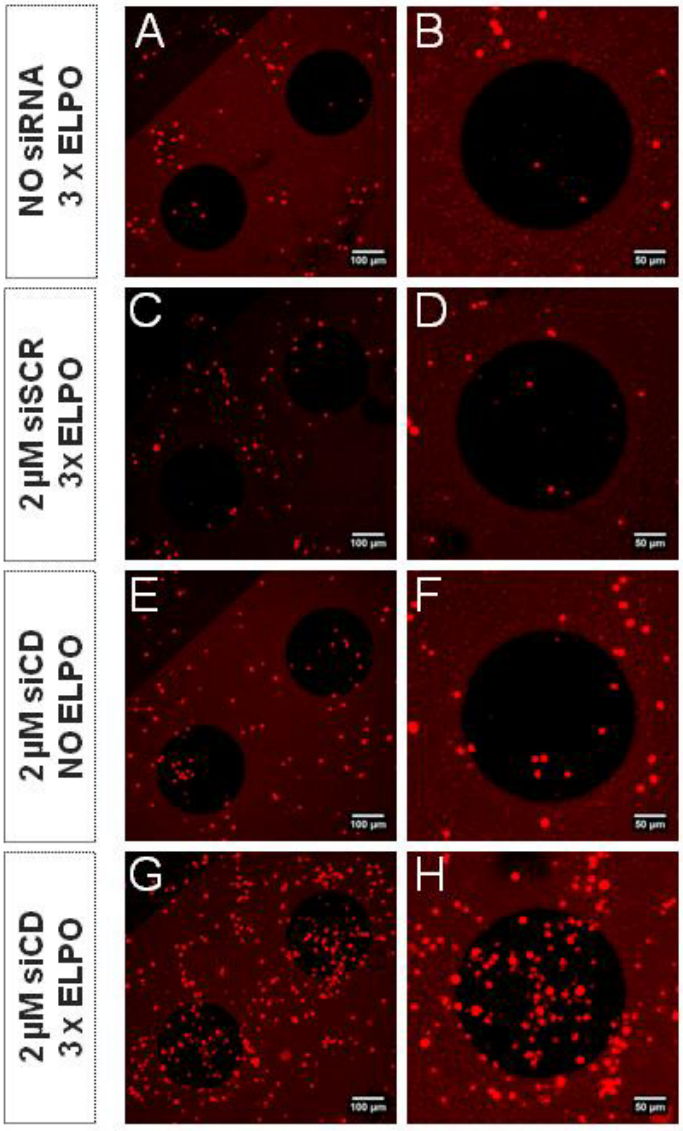

Figure 8.26 Exemplary confocal fluorescence micrographs taken after impedance monitoring of siCD effect on CHO-GFP cells (previously exposed to multiple *in situ* electroportion in presence of 2 µM siCD and 2µM siSCR). Damaged and dead CHO-GFP cells were stained with 4 µM Ethidium-Homodimer-1. The scale bar in micrographs of the left column corresponds to 100 µm and in micrographs of the right column to 50 µm. All micrographs were taken using 10-fold magnification objective.

Micrographs acquisition and their analysis after delivery of siCD into CHO-GFP cells by ISE was conducted only once and altogether 4 - 8 different micrographs were analyzed for each experimental condition (mean value ± standard deviation; n= 4 - 8). The results are evaluated in the form of bar plots presented in **Figure 8.27**.

The fluorescent intensities of EthD-1 in 3 controls: (i) cells electroporated in absence of siRNA (black bar; 0.05 ± 0.01), (ii) cells electroporated in presence of 2 µM siSCR (blue bar; 0.11 ± 0.04) and (iii) cells only incubated in presence of 2 µM siCD (light rose bar; 0.11 ± 0.03) were relatively low, compared to the intensity of cells electroporated in presence of 2 µM CD (purple bar; 0.38 ± 0.05). These results might indicate presence of some unspecific effect of siSCR on cells and possible endocytotic entry of siCD into non-electroporated cells. However, they might also show just the regular rate of cell death as in any cell population. In any case, fluorescence intensity of EthD-1 in the sample was significantly higher than in any of the three controls.

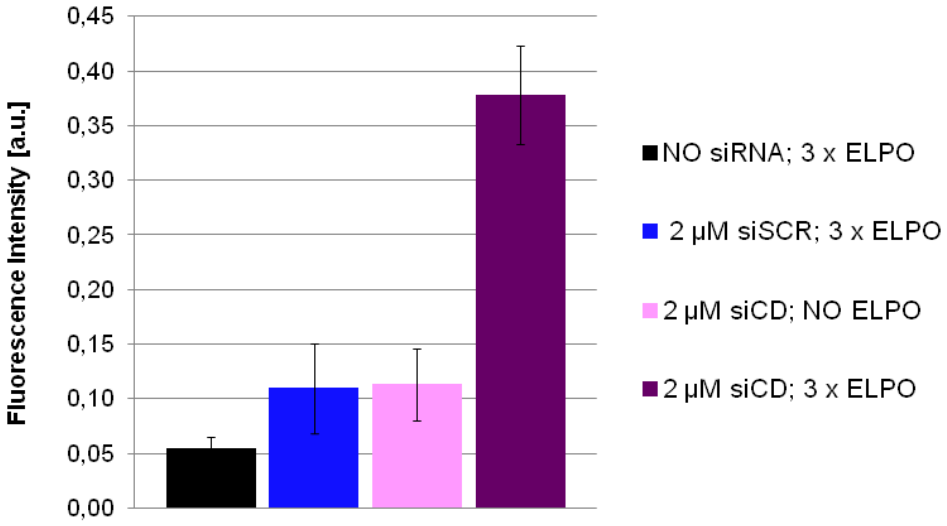

Figure 8.27 Bar plots presenting fluorescence intensity of EthD-1 staining on the micrographs taken app. 46 hours after *in situ* electroporation of CHO-GFP cells to facilitate delivery of siCD into the cell cytosol. Within one experiment, 4 - 8 different micrographs were taken for every experimental condition and were quantified using ImageJ; mean value ± standard deviation; n= 4 - 8.

In summary, successful delivery of siCD into CHO-GFP cells by multiple *in situ* electroporation was demonstrated, as only the cells exposed to ISE in presence of siCD exhibited high level of cell death. This is evidenced both by impedance (and capacitance) data recorded on ECIS and by microscopic evaluation conducted using CLSM.

8.4.1.2 Delivery of siCD by Chemical Transfection

Delivery of Cell Death siRNA (siCD) into CHO-GFP cells by *in situ* electroporation was compared with the widespread chemical lipid-based transfection (abbreviated CH TR) using commercial chemical transfection reagent Lipofectamine®. CHO-GFP cells were chemically transfected according to the protocol described in chapter 4.4.2.3 and immediately afterwards, monitoring of the cellular response (for app. 70 hours) was performed using ECIS. **Figure 8.28** shows typical time courses of (**A**) the normalized impedance at 16 kHz and (**B**) the normalized capacitance at 32 kHz, whereby every 10th time point is presented in order to reduce large data set (mean value ± standard deviation; n=2). App. 22 hours after chemical transfection, serum-free medium was exchanged by the complete culture medium (at the time point marked with a) and both impedance (**A**) and capacitance (**B**) dataset were normalized to the last time point before medium exchange ($t_{norm.}$=a).

Experimental procedure for chemical transfection of CHO-GFP cells included two samples, with cells being transfected in presence of either 33 nM, or 50 nM siCD (magenta and purple line, respectively) and two corresponding controls: with cells transfected in absence of siRNA (black line) and with cells being transfected in presence of 33 nM siSCR (blue line).

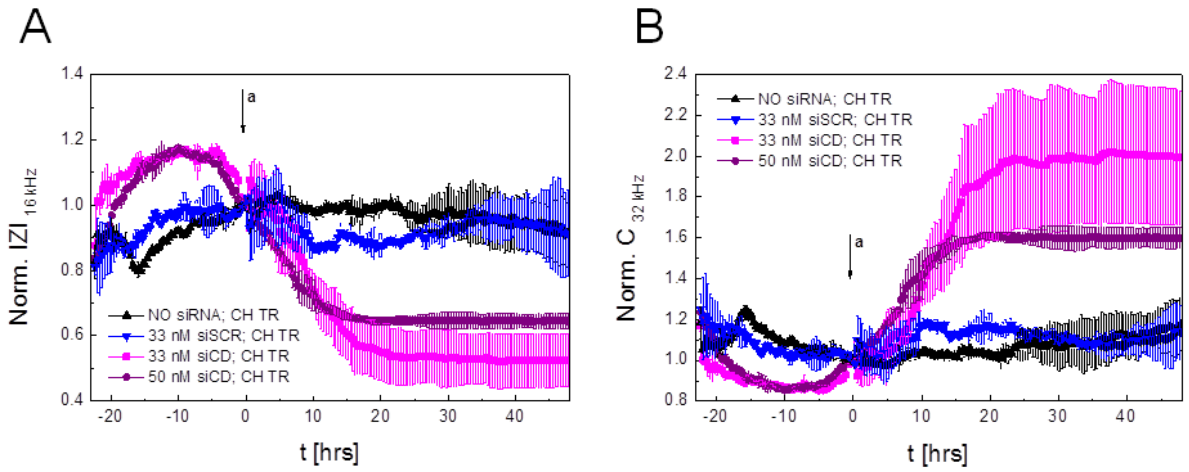

Figure 8.28 Typical time courses of (**A**) the normalized impedance at 16 kHz and (**B**) the normalized capacitance at 32 kHz during and after chemical transfection of CHO-GFP cells in presence of 33 and 50 nM siCD, including corresponding controls. Serum-free medium was exchanged by the complete culture medium (at the time point marked with arrow **a**) and monitoring of the cellular response was continued for app. 50 hours. Impedance (**A**) and capacitance (**B**) data are normalized to the last time point before medium exchange. Experiment was conducted at 37 °C. Every 10th time point during measurement is presented to reduce large data set; mean value ± standard deviation; n=2.

Graph **A** shows that impedance of both samples increased continuously for app. 10 – 15

hours after chemical transfection. Thereafter, impedance values started to decrease suddenly and were constantly sinking until they reached minimal values. Impedance signal of CHO-GFP cells treated with 50 nM siCD stabilized app. 42 hours after chemical transfection at the normalized impedance values of 0.6 ± 0.01, whereas impedance signal of the cells transfected with 33 nM siCD reached minimum app. 58 hours after transfection at the normalized impedance 0.52 ± 0.08. In contrast to samples, normalized impedance of both controls remained fairly constant during the entire measurement, without any major fluctuations.

Graph **B** shows that normalized capacitance of the cells exposed to siCD started to increase app. 17 hours after transfection and it reached maximal values app. 58 hours after transfection for the cells subjected to 33 nM siCD (2.02 ± 0.32). Normalized capacitance of cells exposed to 50 nM siCD reached maximal values 1.60 ± 0.02 app. 42 hours after chemical transfection. On the other hand, normalized capacitance of both controls exhibited relatively constant signal during the entire measurement.

Interestingly, such observations lead to conclusion that lower concentration of 33 nM siCD has higher impact on CHO-GFP viability than the higher concentration (50 nM). The raw data (not shown) indicated slightly slower signal decrease of impedance signal and lower minimal values when 33 nM siCD was applied. Even though cells exposed to higher siCD concentration (50 nM siCD) showed faster impedance decrease, their minimal impedance values were eventually higher than the values observed for 33 nM siCD. This indicates that stronger effect of lower siCD concentration observed in **Figure 8.28** is not an artifact, even though it is slightly enhanced by the normalization of the data.

These observations are in agreement with observations made after chemical transfection in presence of siGLO Red, where, same as here, slightly stronger effect was observed with lower siGLO Red concentration (33 nM, compared to 50 nM).

After ECIS measurement was finished, the appearance of CHO-GFP cells was evaluated under the microscope. The fraction of dead and damaged cells after their treatment with siCD in combination with Lipofectamine was easily accessed by phase-contrast imaging. Exemplary micrographs taken using 10-fold magnification objective are summarized in **Figure 8.29**. These phase-contrast micrographs revealed normal appearance and completely confluent monolayers of the cells in controls (**A**, **B**), whereas cell monolayers of both samples (**C**, **D**) were completely decomposed, with many rounded cells, detached from the substrate. The cell population was significantly reduced and remaining cells were isolated and scattered over the substrate surface.

This experiment was repeated in a very similar manner and without impedance monitoring to

document appearance of CHO-GFP subjected to siCD by fluorescence microscopy. The phase-contrast and confocal fluorescence micrographs were taken app. 48 h after chemical transfection of CHO-GFP cells in presence of 33 nM siCD and 33 nM siSCR. All micrographs were taken with 10-fold magnification objective and exemplary micrographs are summarized in **Figure 8.30**.

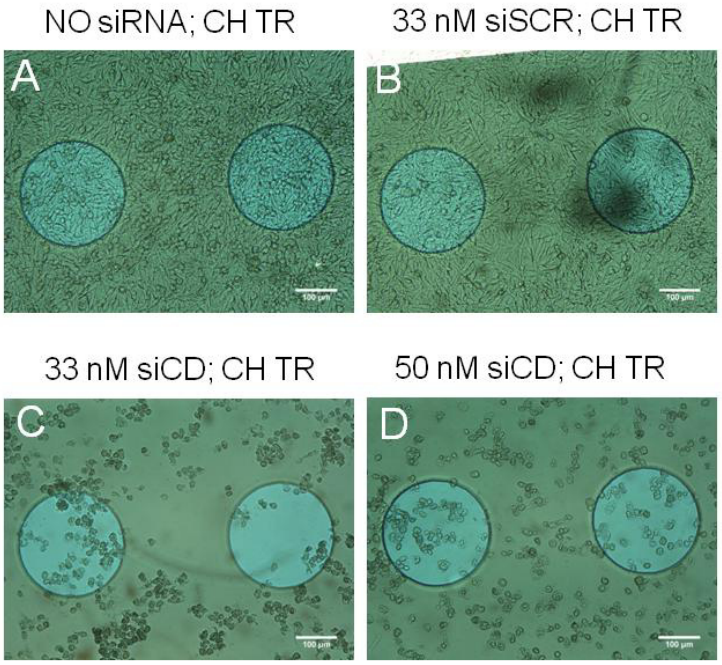

Figure 8.29 Exemplary phase-contrast micrographs taken app. 70 hours after chemical transfection of CHO-GFP cells in presence of 33 or 50 nM siCD and 33 nM siSCR. Experiment was performed at 37 °C and cellular behavior was followed by ECIS in real time. Scale bar in all micrographs corresponds to 100 µm. All micrographs were taken using 10-fold magnification objective.

Phase-contrast images in the first column show a clear difference in appearance of the cells in the sample and controls, similarly to **Figure 8.29**. Confocal fluorescence micrographs presented in the second and third column show difference in fluorescence signal between the sample: cells chemically transfected in presence of 33 nM siCD (**H**, **I**) and controls: cells chemically transfected in absence of siRNA (**B**, **C**) and cells chemically transfected in presence of 33 nM siSCR (**E**, **F**). The cells in controls maintained confluent monolayer, whereas monolayer of the cells exposed to siCD (third row) was completely decomposed. Remaining cells were isolated, scattered and contained apoptotic bodies.

In summary, acquired data indicate very successful introduction of siCD into CHO-GFP cells by chemical transfection. It was evidenced both by ECIS monitoring and microscopy that

CHO-GFP cells undergo cell death within hours after siCD enters the cytosol.

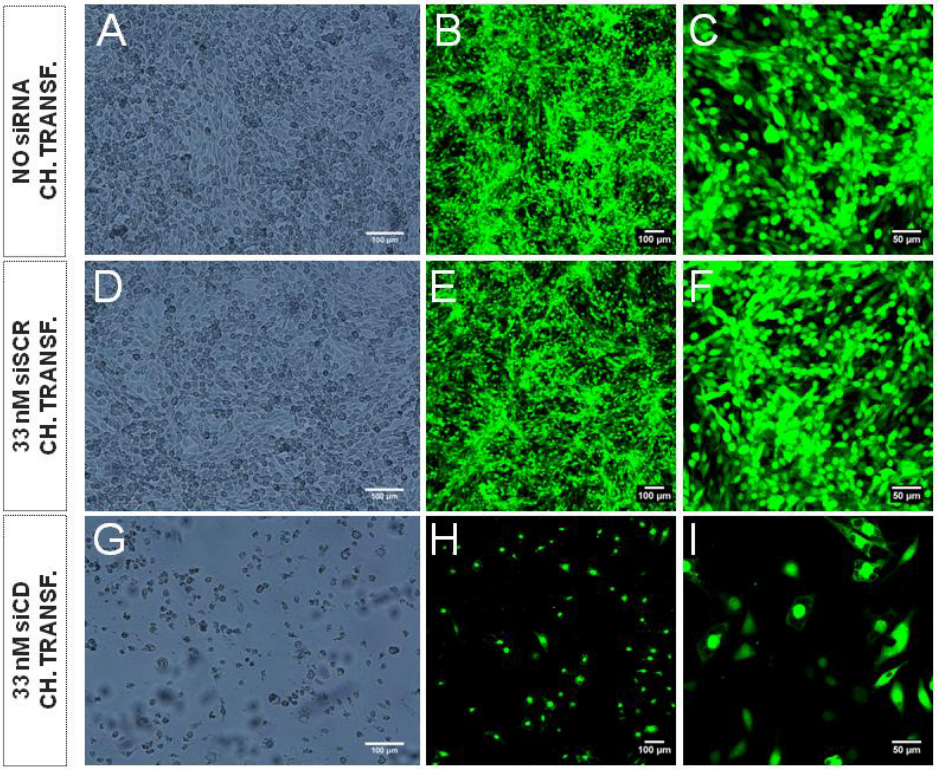

Figure 8.30 Exemplary phase-contrast (first column) and confocal fluorescence micrographs (second and third column) taken app. 48 hours after chemical transfection of CHO-GFP cells in presence of 33 nM siCD and 33 nM siSCR. Experiment was performed at 37 °C. Scale bar in micrographs of the first and second column corresponds to 100 µm and in the third column to 50 µm. All micrographs were taken using 10-fold magnification objective.

8.4.1.3 Cytotoxicity of Cell Death siRNA versus Wound/Healing

During previous experiments it was shown that siCD causes damage and death of CHO-GFP cells, several hours after its entry into cell cytoplasm. Such effect of siCD is, although much slower, quite comparable with an electric wounding of the cells. As described in chapter 3.2.4, invasive electric wounding causes irreversible permeabilization of cell membrane, cells detach from the substrate and get killed almost instantly. Even though this is much faster process than killing the cells by silencing their genes with siCD, aim of the following experiment was to make a comparison between the cellular recovery after exposure of the cells to siCD and after electric wounding.

CHO-GFP cells were subjected to electric wounding using standard pulse parameters: 40 kHz, 5 V and 30 s. Experiment was conducted on 8W4Eµ electrode array and cells were

bathed in complete culture medium during the entire experiment. Cellular behavior before, during and after electrical wounding was monitored by ECIS.

Figure 8.31 shows time courses of **A** the impedance at 16 kHz; **B** the capacitance at 32; **C** the normalized impedance at 16 kHz; **D** the normalized capacitance at 32 kHz before, during and after electric wounding. CHO-GFP cells were wounded at the time point marked with a, whereas cells in controls were not exposed to wounding (black line). In graphs **A** and **B** were integrated values for cell-free electrodes (grey lines) in the course of time. App. 2.5 hours after wounding, measurement was paused (marked with b) and phase-contrast micrographs were taken. Exemplary phase-contrast micrographs are given in **Figure 8.32**, along with the micrographs taken after the measurement was finished (marked with c).

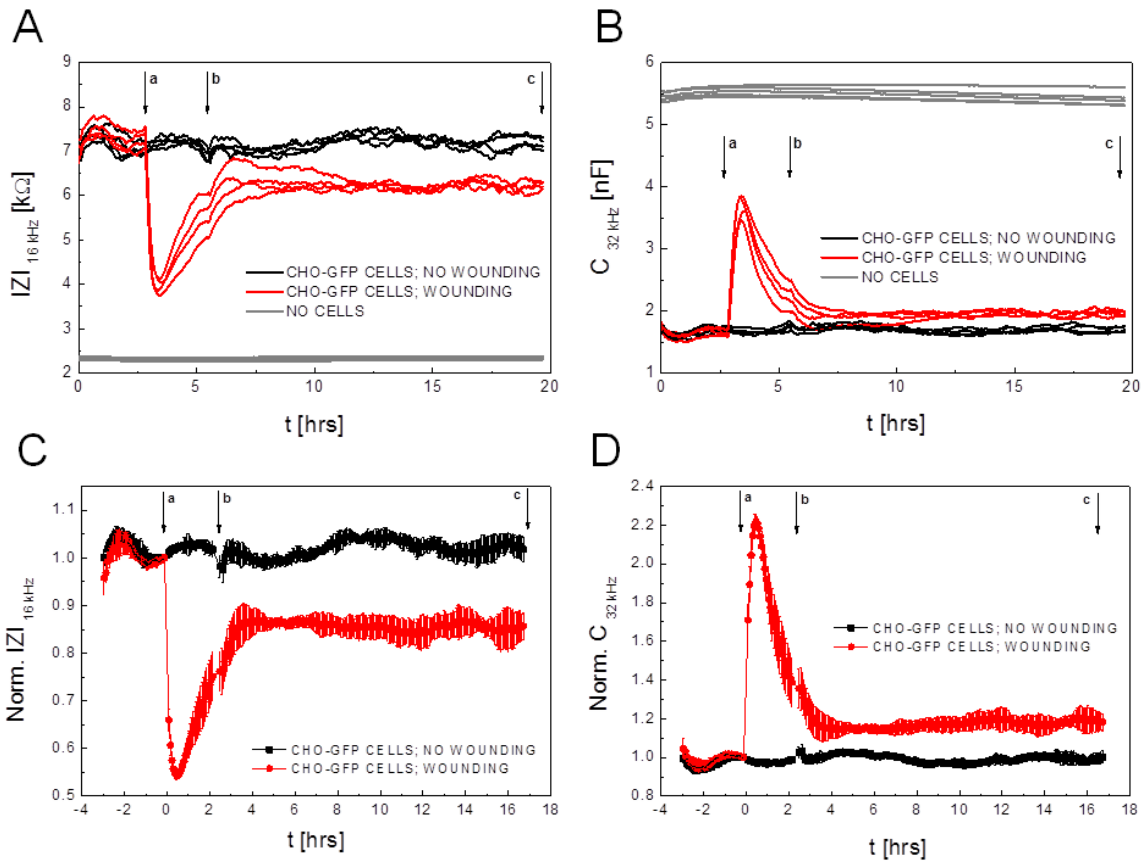

Figure 8.31 Typical time course of **A** the impedance at 16 kHz; **B** the capacitance at 32 kHz; **C** the normalized impedance at 16 kHz and **D** the normalized capacitance at 32 kHz before, during and after healing of an *in vitro* lesion introduced in CHO-GFP monolayers by invasive electric fields. Pulse parameters: 40 kHz, 5 V and 30 s. Impedance (**A**) and capacitance (**B**) are normalized to the last time point before wounding (marked with arrow **a**); mean value ± standard deviation; n=4. Experiment was conducted at 37 °C. Measurement was paused (**b**) to take micrographs and continued to follow recovery of the cells. After the measurement, phase-contrast micrographs were taken again (**c**) to evaluate appearance of the cells app. 17 hours after wounding.

Impedance (**A**) and capacitance (**B**) values of cell-free electrodes are included as a reference for impedance and capacitance values observed directly after wounding of CHO-GFP cells. The question arose if CHO-GFP cells instantly dye and detach from the cell surface upon application of strong electric fields (wounding), thus giving the respective impedance and capacitance values close to those of cell-free electrodes.

Graphs **C** and **D** depict the same measurement, only with normalized values of impedance (**A**) and capacitance (**B**), in order to evaluate and compare signal changes observed after wounding with those observed after transfection of CHO-GFP cells with siCD. Impedance (**C**) and capacitance (**D**) dataset was normalized to last time point before electric wounding was applied ($t_{norm.}$=a). Data represent mean value ± standard deviation; n=4.

Graph **A** shows that impedance signal immediately dropped after wounding and the minimum values were app.3.8 - 4.0 kΩ. Thereafter, impedance values started to increase and after app. 6 – 7 hours, they almost reached pre-pulse values. Surprisingly, impedance values, after wounding and subsequent recovery of the cells, did not reach and overlay with the impedance values of non-wounded cells in control. Instead, they remained constantly lower during the entire post-wounding time. In addition, impedance drop after electric wounding was not as large as expected and minimal impedance values did not correspond to the values of cell-free electrodes (app. 2.3 – 2.4 kΩ).

Capacitance (**B**) values jumped after pulsing and reached maximal plateau at app. 3.5 – 3.9 nF, however, capacitance values of the cell-free electrodes (5.4 – 5.5 nF) were not reached. Thereafter, capacitance started to decrease and eventually returned close to pre-pulse values. Signal remained at this level until the end of the measurement without major fluctuations.

Cell behavior observed in graphs **C** and **D** (depicting normalized impedance and normalized capacitance, respectively), corresponds to the cell behavior observed in **A** and **B**. With normalization, it becomes even more pronounced that impedance/ capacitance signals of wounded CHO-GFP cells do not return to the pre-pulse values. This might be a good indicator that CHO-GFP cells do not recover entirely after application of strong electric fields.

To evaluate appearance of CHO-GFP cells after wounding, micrographs were taken app. 2.5 hours after wounding and subsequently after ECIS monitoring was finished (app. 17 hours after wounding). Exemplary phase-contrast micrographs taken with 10-fold magnification are summarized in **Figure 8.32**.

As expected, cells in control, which were not exposed to wounding pulses, remained unchanged over the measurement time (**A**, **B**). However, CHO-GFP cells exposed to invasive wounding pulses partially detached from the electrodes surface and appeared

rounded and swollen (indicated by the arrows in **C**) app. 2.5 hours after wounding. Surprisingly, when the same cell population on the electrodes was observed app. 17 hours after wounding (**D**), the cells did not very much migrate or move from/to the electrodes, however, small group of dead cells was formed on the top of one electrode (indicated by the arrows in **D**). The cells partially recovered and reattached to the electrode surface. Parts of the electrodes where cells were missing shortly after wounding were still free of cells.

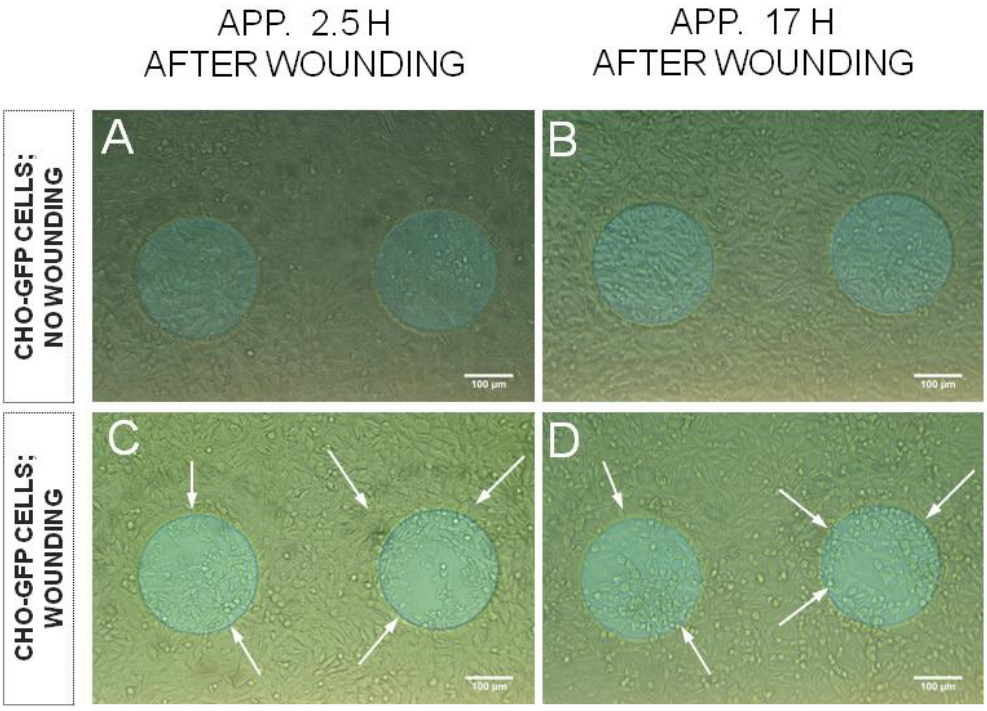

Figure 8.32 Exemplary phase-contrast micrographs taken 2.5 hours (**A**, **C**) and 17 hours (**B**, **D**) after healing of an *in vitro* lesion introduced in CHO-GFP monolayers by invasive electric fields. Scale bar in all micrographs corresponds to 100 µm. Micrographs were taken using 10-fold magnification objective.

This experiment showed that CHO-GFP population on the electrodes does not get killed entirely upon electric wounding, as cell-free values are not reached. However, it may be also concluded that their recovery is very slow and incomplete, as they do not recover entirely within 17 hours after the wounding.

8.4.2 Delivery of Cell Death siRNA into NRK Cells

Besides CHO-GFP, NRK cells were applied as a cell model to study introduction of siCD into monolayers and its possible effects on the vital genes. Since NRK cells were successfully transfected with siGLO Red, delivery of siCD into cells and its potential cytotoxic effects was monitored using ECIS technology, in combination with microscopy.

8.4.2.1 Delivery of siCD by *In Situ* Electroporation

Similarly as with CHO-GFP cells, the sequence-specific siCD was transfected into NRK cells by *in situ* electroporation and its effects were monitored by ECIS.

Experimental procedure was conducted on 8W4Eμ electrode array and $EBSS^{++}$ was applied as the buffer. Typical time course of the normalized impedance at 4 kHz before, during and after *in situ* electroporation of NRK cells in presence of siCD and siSCR is presented in **Figure 8.33 A**. *In situ* electroporation of NRK cells included 2 samples: cells being electroporated in presence of 2 μM siCD (magenta line) and 4 μM siCD (purple line), as well as the corresponding controls: (i) cells being electroporated in absence of siRNA (black line), (ii) cells electroporated in presence of 4 μM siSCR (blue line) and (iii) non-pulsed cells incubated with 2 μM siCD (light rose line).

After multiple electroporation of the cells (**A**), data acquisition was paused and assay buffer was exchanged with complete medium. Thereafter, impedance measurement was resumed and response of NRK cells was monitored for app. 36 hours.

Figure 8.33 B shows time course of the normalized impedance at 4 kHz and **Figure 8.33 C** shows time course of the normalized capacitance (at 32 kHz) during the entire measurement. Graph **A** shows impedance monitoring of multiple (3x) successive *in situ* electroporation (using optimal combination of pulse parameters for NRK: 40 kHz, 4 V and 200 ms), as indicated by the arrows - a: 1^{st} pulse, b: 2^{nd} pulse and c: 3^{rd} pulse application. Impedance values were normalized to the last time point before first electroporation pulse was applied. Time course of the normalized impedance shows typical impedance decrease after every pulse and recovery of the signal within 20 - 25 min after every pulse application. After last pulse and complete recovery of the cells, measurement was paused and $EBSS^{++}$ buffer was exchanged with complete culture medium in every well. The break in data acquisition for buffer exchange is marked with d.

In graph **B**, impedance values at 4 kHz were normalized to the last time point before buffer was exchanged with medium, which is marked with a ($t_{norm.}$=a). Unlike CHO-GFP, NRK cells showed only small signal change, as a reaction to the medium addition and temporary temperature changes. Overall trend of strong signal decrease started shortly after buffer exchange and it lasted for app. 3 – 4 hours when signal stabilized. Thereafter, all signals showed similar trend and eventually, impedance of cells exposed to 2 and 4 μM siCD started to decrease app. 16 hours after electroporation. App. 14 hours later, signals of samples returned back to the signal levels of controls. Even though impedance decrease in samples was rather small, it was distinct and it was correlated to the cytotoxic effect of siCD, which was shown by the micrographs taken app. 24 hours electroporation. Cells in controls did not

show significant changes and fluctuations in the signal, only exception was control including non-pulsed cells (incubated with siCD), however, this is subscribed to some unspecific factor.

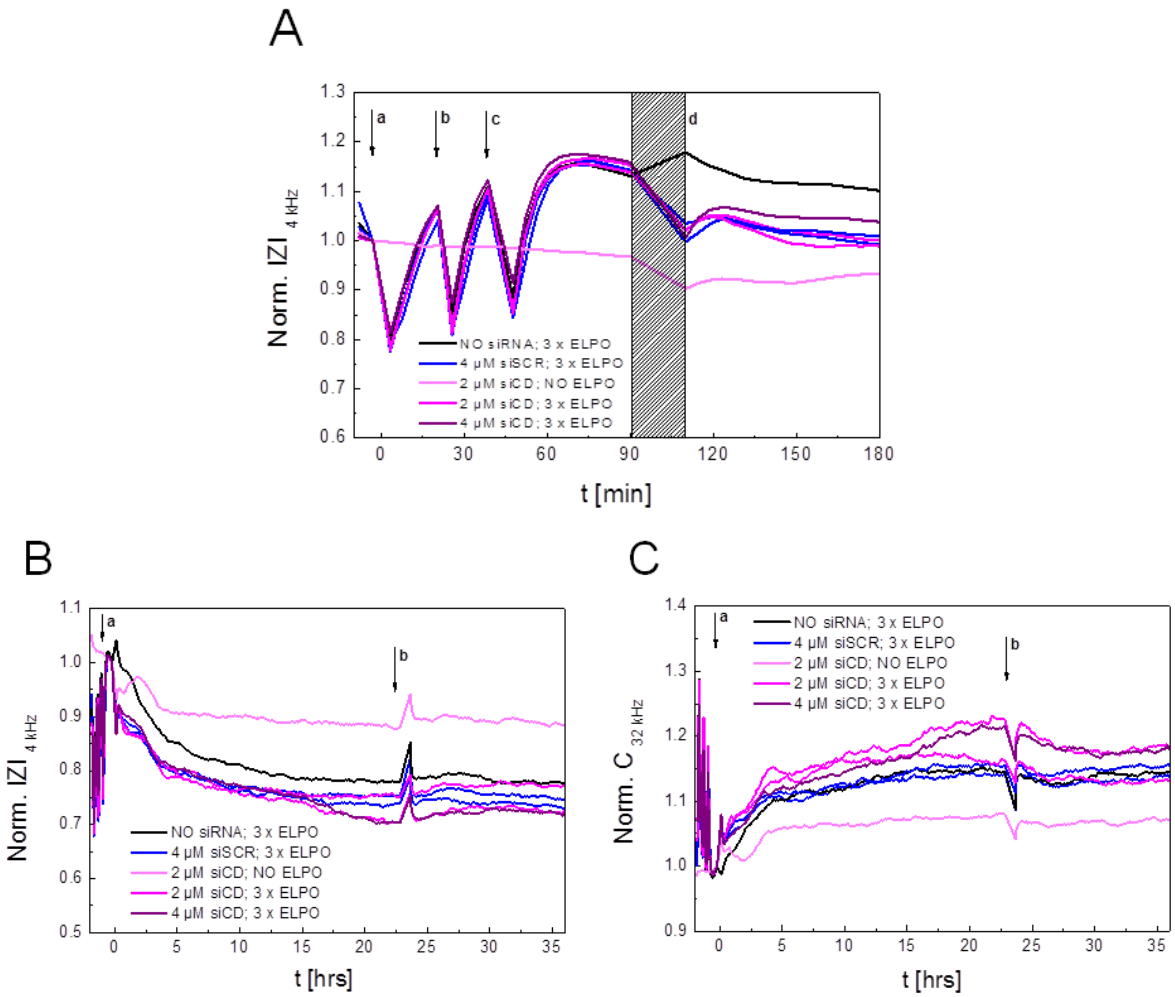

Figure 8.33 Typical time course of the normalized impedance at 4 kHz before, during and after *in situ* electroporation of NRK cells in presence of 2, or 4 µM siCD and 4 µM siSCR. ISE was applied three times - **a**: 1st pulse, **b**: 2nd pulse and **c**: 3rd pulse application, using pulse parameters: 40 kHz, 4 V and 200 ms. Impedance values are normalized to the last time point before first electroporation. After cellular recovery from the third pulse, measurement was paused and assay buffer was exchanged with the complete medium (marked with **d**). Data acquisition was resumed and impedance monitoring was continued for app. 36 hours to evaluate cytotoxic effect of siCD. Typical time course of **B** the normalized impedance at 4 kHz and **C** the normalized capacitance at 32 kHz for entire experiment. Impedance (**B**) and capacitance (**C**) were normalized to the last time point before buffer exchange was executed (marked with **a**). Measurement was paused to take micrographs at the time point **b**.

In graph **C**, capacitance values at 32 kHz were normalized to the last time point before buffer was exchanged with medium, which is marked with a ($t_{norm.}$=a). After buffer exchange,

normalized capacitance of the samples was constantly higher than the capacitance of controls. Difference in signals of samples and controls became more significant app. 16 hours after electoporation.

Micrographs taken in the course of experiment, by pausing the measurement app. 23 hours after media exchange (marked with b in graphs **B** and **C**) are summarized in **Figure 8.34**. The appearance of the cells and level of cell death induced by siCD were assessed by taking phase-contrast micrographs (using 10-fold magnification). As expected, there was no significant difference between the controls (**A**, **B** and **C**). However, micrographs showing samples (**D** and **E**) indicated that considerable population of damaged and dead cells was present on the top of the electrodes. These groups of cells and cell debris gathered on the top of the confluent, renewed cell monolayer on the electrodes appeared very similar to the cells several hours after their exposure to electrical wounding (chapter 8.4.2.3).

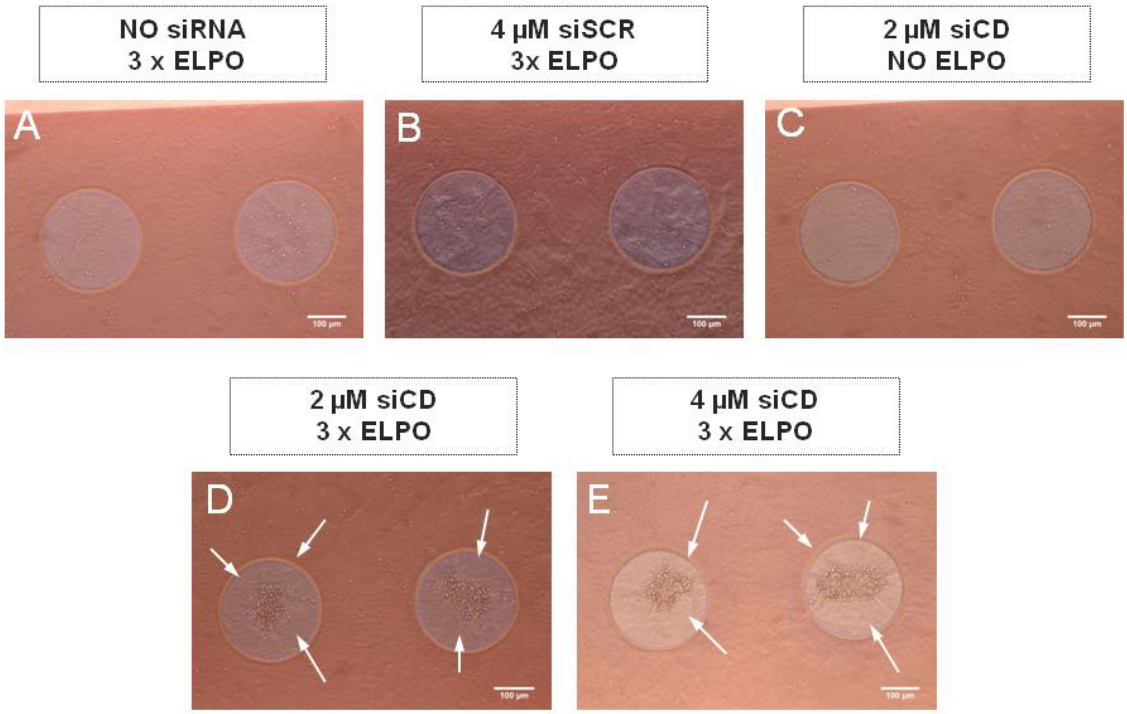

Figure 8.34 Exemplary phase-contrast micrographs taken app. 24 hours after *in situ* electroporation of NRK cells in presence of 2 and 4 µM siCD and 4 µM siSCR. Scale bar in all micrographs corresponds to 100 µm. All micrographs were taken using 10-fold magnification objective.

App. 37 hours after electroporation, measurement on ECIS was finished and micrographs were taken again. However, appearance of NRK cells on the electrodes was very similar to what has been observed on micrographs 23 hours after electroporation.

Surprisingly, effect of siCD on NRK cells after its introduction by ISE was muted. Even

though it is expected that NRK cells are efficiently loaded with siCD, cell dying was difficult to detect. Normalized capacitance (more than impedance) indicated changes in cell coverage which can be subscribed to apoptotic and dying cells. However, ECIS recordings, same as phase-contrast micrographs suggest that siCD does not induce dramatic changes in viability of NRK cells. In addition, recovery of the cells appears rapidly, damaged and dead cells are quickly moved aside (as evidenced by the micrographs), and monolayer composition remains intact as it is being renewed constantly.

8.4.2.2 Delivery of siCD by Chemical Transfection

Previously evaluated delivery of Cell Death siRNA (siCD) into NRK cells by *in situ* electroporation was compared with delivery of siCD by chemical lipid-based transfection. NRK cells were chemically transfected according to the protocol described in chapter 4.4.2.3 and immediately afterwards, impedance monitoring of the cellular behavior was started. Using ECIS platform, cell response was followed for app. 90 hours. **Figure 8.35** shows typical time courses of (**A**) the normalized impedance at 4 kHz and (**B**) the normalized capacitance at 32 kHz during and after transfection of NRK cells in presence of 200 nM of siCD and 200 nM siSCR. App. 20 hours after Lipofectamine treatment, serum-free medium was exchanged by the complete culture medium (at the time point marked with a) and both impedance (**A**) and capacitance (**B**) dataset were normalized to the last time point before this medium exchange ($t_{norm.}$=a). Graph **C** represents part of the dataset presented in **B**, only enlarged for the time interval between medium exchange (t=0) and 35 hours after that (t=35) to better visualize signal changes of treated cells in that period.

Graph **A** shows constant impedance decrease after Lipofectamine treatment, both in sample and in controls. For controls (chemical transfection with siSCR and without siRNA) such trend is visible only until medium exchange, whereas cells treated with siCD continued the downward path even after transient signal increase due to the addition of complete culture medium. Their signal stabilized app. 50 hours after medium exchange, whereas signal in controls started do decrease slowly again app 30 hours after medium exchange and such trend continued until the end of measurement. Based on such changes in normalized impedance, it is difficult to judge about cytotoxic effect of siCD on NRK cells after transfection. Even though impedance signals of cells exposed to siCD are reproducibly lower than those of controls, difference between them is not as large as it was with CHO-GFP cells. However, it is noticeable that the cells transfected with 200 nM siCD fluctuated much more frequently during the measurement, compared to the cells in controls.

These frequent fluctuations are even more obvious in graph **B**, during increase of normalized

capacitance after medium exchange. To better visualize intensive fluctuations of NRK cells exposed to siCD, graph **B** was additionally enlarged and graph **C** shows the same dataset with respect to the time period between medium exchange and 35 hours after that. Most intensive fluctuating of capacitance was observed within the time period of 15 - 30 hours after media exchange. Thereafter, signals surprisingly stabilized and no significant fluctuations were observed during the rest of the measurement. Such fluctuations, especially visible in the capacitance dataset, might be good indicator of NRK response to siCD effect and are probably result of intensive changes in the cell monolayer and its quick renewal, upon apoptosis and death which (at least part of the) NRK cells undergo after chemical transfection with siCD.

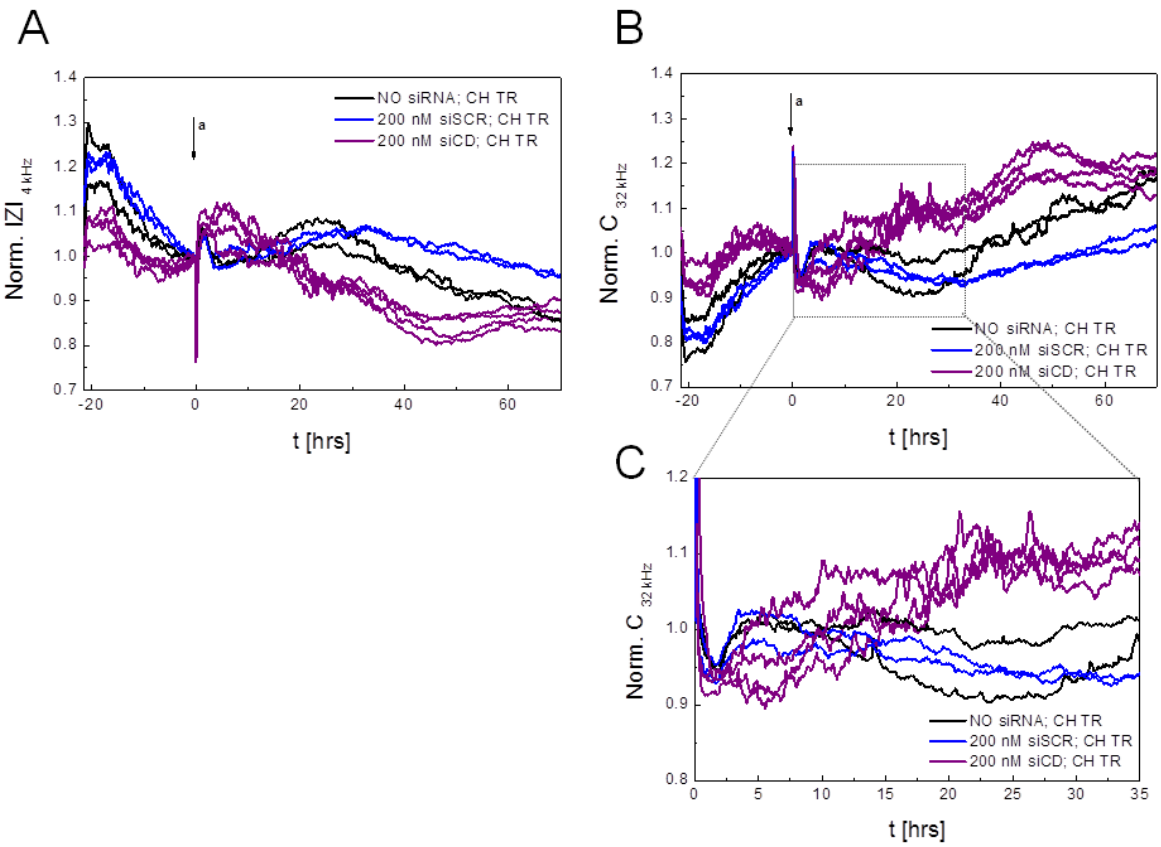

Figure 8.35 Typical time courses of (**A**) the normalized impedance at 4 kHz and (**B**) the normalized capacitance at 32 kHz during and after chemical transfection of NRK cells in presence of 200 nM siCD and 200 nM siCD. Experiment was conducted at 37 °C. Serum-free medium was exchanged by the complete culture medium (at the time point marked with arrow **a**) and monitoring of the cellular response was continued for app. 70 hours. Graph **C** represents enlarged segment of the graph **B**. Impedance (**A**) and capacitance (**B**, **C**) data are normalized to the last time point before medium exchange.

Obviously, app. 40 hours after medium exchange (and 50 hours after Lipofectamine treatment) monolayers of NRK cells are completely renewed and effect of siCD can no longer be observed. After ECIS measurement was finished, appearance of NRK cells was visualized under the microscope (data not shown). In the wells where NRK cells were treated with siCD, more dead and damaged cells was observed, than in the wells where cells were treated with siSCR, or just exposed to Lipofectamine. At the same time, confluent cell monolayers of NRK cells were preserved in all wells, which is in agreement with ECIS recordings and complete recovery of the cells treated with siCD, observed during impedance monitoring. In addition, these data are good indicator why very small signal changes were observed after delivery of siCD by ISE. Even when entire cell population in the well is exposed to siCD upon chemical tansfection, monolayers do not collapse and decompose but are rapidly renewed. Analogously, small cell populations residing on the electrodes, which are affected by siCD upon ISE, are being replaced even quicker by unaffected cells migrating to the electrodes and renewing constantly the cell monolayers.

8.4.2.3 Cytotoxicity of Cell Death siRNA versus Wound/Healing

Recovery of NRK cells after their exposure to siCD was compared to their recovery after electric wounding. As described in previous chapter, it is difficult to evaluate level of cytotoxicity induced by siCD, due to discrepancy between siCD effect and responses of NRK cells observed in ECIS recordings and by microscopy, indicating rapid renewal of the cell monolayer. Therefore, NRK cells were subjected to electric wounding and their recovery was monitored both by ECIS and microscopy. It was the aim to evaluate how fast monolayers of NRK cells recover after *in vitro* lesion is introduced by the invasive electric fields, and to compare it with the recovery of NRK cells after delivery of siCD by ISE and chemical transfection.

NRK cells were exposed to electric wounding in complete culture medium, using standard pulse parameters: 40 kHz, 5 V and 30 s. Experiment was conducted on 8W4Eμ electrode array. Cellular behavior before, during and after electric wounding was monitored by ECIS and phase-contrast micrographs were taken during and after the measurement.

Figure 8.36 shows time courses of **A** the impedance at 4 kHz; **B** the capacitance at 32; **C** the normalized impedance at 4 kHz; **D** the normalized capacitance at 32 kHz before, during and after electric wounding of NRK cells (red lines) at the time point marked with a, whereas cells in controls were not exposed to wounding (black lines). Impedance (**A**) and capacitance (**B**) values of cell-free electrodes are included as a reference for impedance and capacitance values observed upon wounding of NRK cells. Based on previous studies where wounding of

NRK cells was investigated (Stolwijk, 2012), it was expected that impedance and capacitance values will be close to those of cell-free electrodes directly after application of invasive electric fields.

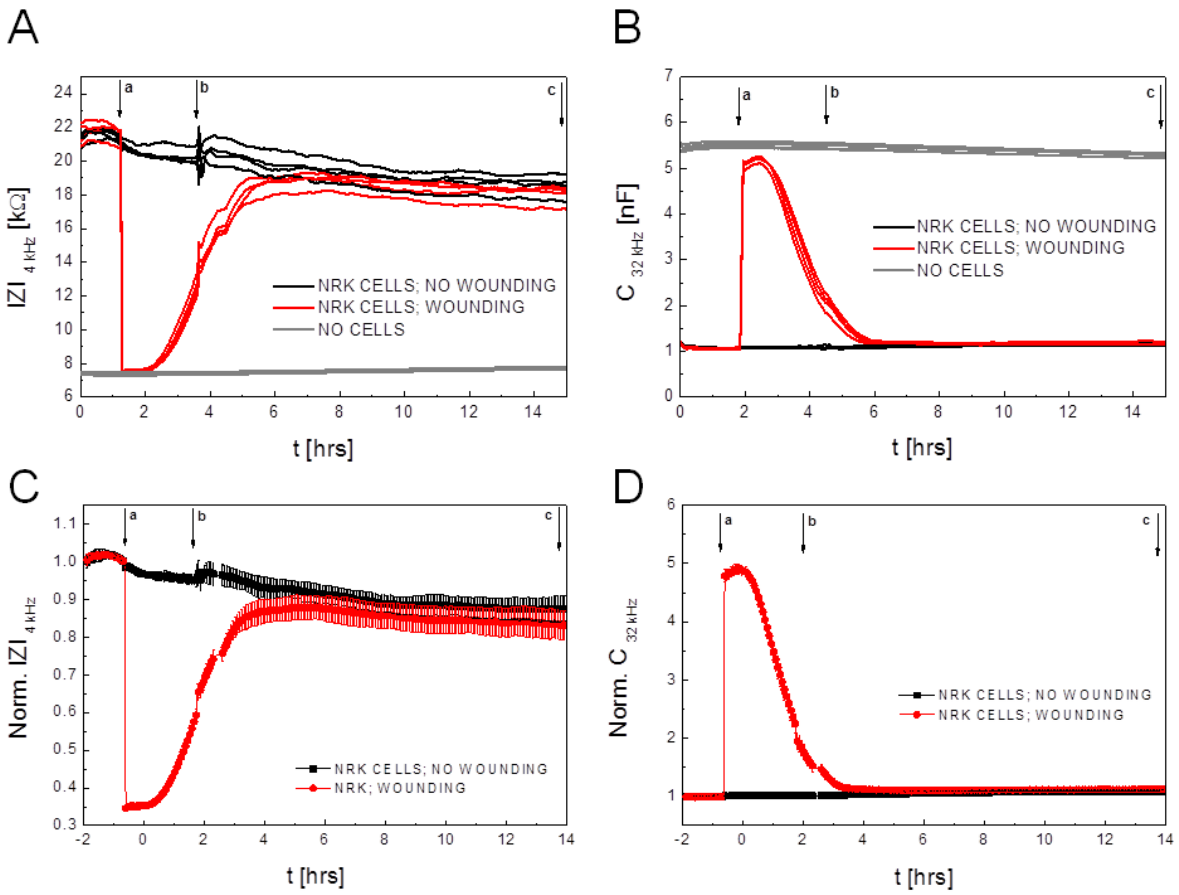

Figure 8.36 Typical time course of **A** the impedance at 4 kHz; **B** the capacitance at 32 kHz; **C** the normalized impedance at 4 kHz and **D** the normalized capacitance at 32 kHz before, during and after healing of an *in vitro* lesion introduced in NRK monolayers by invasive electric fields. Pulse parameters: 40 kHz, 5 V and 30 s. Impedance (**A**) and capacitance (**B**) are normalized to the last time point before wounding (marked with arrow **a**); mean value ± standard deviation; n=4. Experiment was conducted at 37 °C. Measurement was paused (**b**) to take micrographs and continued to follow recovery of the cells. After the measurement, phase-contrast micrographs were taken again (**c**) to evaluate appearance of the cells app. 14 hours after wounding.

Graphs **C** and **D** depict the same measurement, only with normalized values of impedance (**A**) and capacitance (**B**) to evaluate and compare signal changes observed after wounding with those observed after transfection of NRK cells with cell death inducing siCD. Impedance (**C**) and capacitance (**D**) dataset was normalized to last time point before electric wounding was applied ($t_{norm.}$=a). Data represent mean value ± standard deviation; n=4.

App. 2.5 hours after wounding data acquisition was paused (marked with b) and phase-contrast micrographs were taken. Exemplary phase-contrast micrographs are given in **Figure 8.37**, along with the micrographs taken after measurement was finished (arrow c).

Graph **A** shows immediate and sharp drop of impedance signal upon electric wounding and the minimum values were 7.5 - 8.0 kΩ, which was corresponding to the impedance values of cell-free electrodes (app. 7.5 kΩ). Thereafter, impedance started to increase and after app. 4 – 5 hours, it returned to the pre-pulse values. Capacitance (**B**) values immediately increased after pulsing and reached maximal values at 5.0 – 5.2 nF, thus approaching very closely to the capacitance values of cell-free electrodes (5.5 nF). Thereafter, capacitance started to decrease and eventually returned to the pre-pulse values after app. 4 - 5 hours. Signal remained at the same level until the end of the measurement.

Behavior of NRK cells upon electric wounding, presented in graphs **C** and **D** (depicting normalized impedance and normalized capacitance, respectively), corresponds to the cell behavior observed in **A** and **B**. Normalized data indicate significant signal changes upon application of strong electric fields, but also quite fast and importantly, complete recovery of cell monolayer afterwards. Obviously, such response of NRK cells after electric wounding is different from incomplete recovery of CHO-GFP cells, exposed to the same experimental and pulse parameter conditions.

To evaluate appearance of NRK cells after wounding, micrographs were taken app. 2.5 hours after wounding and subsequently, after ECIS monitoring was finished (app. 15 hours after wounding). Exemplary phase-contrast micrographs taken with 10-fold magnification are summarized in **Figure 8.37**. Cells in control, not being exposed to wounding, appeared the same in the course of the measurement (**A**, **B**). However, monolayers of NRK cells exposed to invasive wounding pulses were decomposed (within the electrode area) and cell debri were visualized (indicated by the arrows in **C**) app. 2.5 hours after wounding. When the same cell population on the electrodes was observed app. 15 hours after wounding (**D**), the cell monolayers were re-established, as the cells surrounding the electrodes re-populated electrode area free of cells. Thereby, dead and damaged cells gathered on the top of the renewed monolayer of cells (indicated by the arrows in **D**).

In summary, this experiment showed quite different behavior of NRK cells after wounding, compared to CHO-GFP. Impedance and capacitance of NRK reached cell-free values directly after wounding and this is very well in agreement with the previous reports that NRK cells get killed upon electric wounding (Stolwijk, 2012), mostly due to irreversible permeabilization of their membrane. However, recovery of NRK cells and their confluent monolayer is fast (taking place within app. 4 - 5 hours after pulsation) and complete. In

contrast, impedance and capacitance of CHO-GFP cells did not reach cell-free values of the electrodes and their incomplete recovery was evidence by ECIS and microscopy. By comparing response of NRK cells after the wounding and after their exposure to siCD, it is obvious that rapid and complete recovery of NRK cells mutes the cytotoxic effect of siCD.

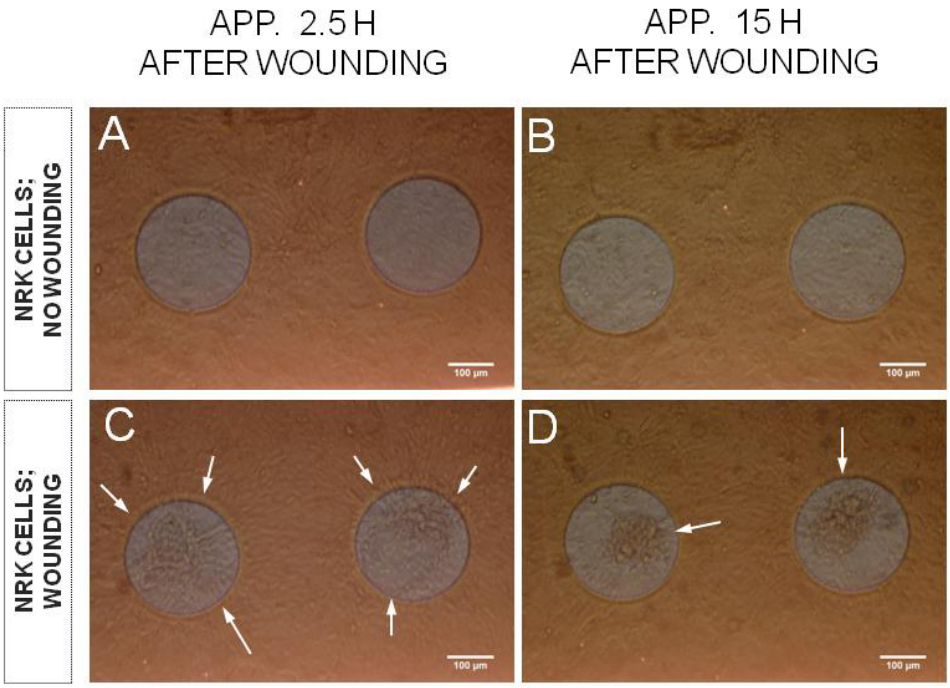

Figure 8.37 Exemplary phase-contrast micrographs taken 2.5 hours (**A**, **C**) and 15 hours (**B**, **D**) after healing of an *in vitro* lesion introduced in NRK monolayers by invasive electric fields. Scale bar in all micrographs corresponds to 100 µm. All micrographs were taken using 10-fold magnification objective.

8.4.3 Delivery of Cell Death siRNA into NIH-3T3 Cells

NIH-3T3 cells were investigated as an additional cell model to study introduction of siCD into cells. Experimental protocol for *in situ* electroporation did not give desired results, as the confluent NIH-3T3 cells detached rapidly from the substrate surface during pipetting and washing. Nevertheless, delivery of siCD into NIH-3T3 cells by chemical transfection was investigated according to the common experimental protocol described in chapter 4.4.2.3. Monitoring of the cellular response during and after chemical transfection was conducted using ECIS technology. **Figure 8.38** shows typical time courses of (**A**) the normalized impedance at 4 kHz and (**B**) the normalized capacitance at 32 kHz during and after transfection of NIH-3T3 cells in presence of 33 and 50 nM siCD and 33 nM siSCR. App. 20 hours after Lipofectamine treatment, serum-free medium was exchanged by the complete

culture medium (at the time point marked with a) and both impedance (**A**) and capacitance (**B**) dataset were normalized to the last time point before this medium exchange ($t_{norm.}$=a), whereby every 15th time point is presented in order to reduce large data set (mean value ± standard deviation, n=2).

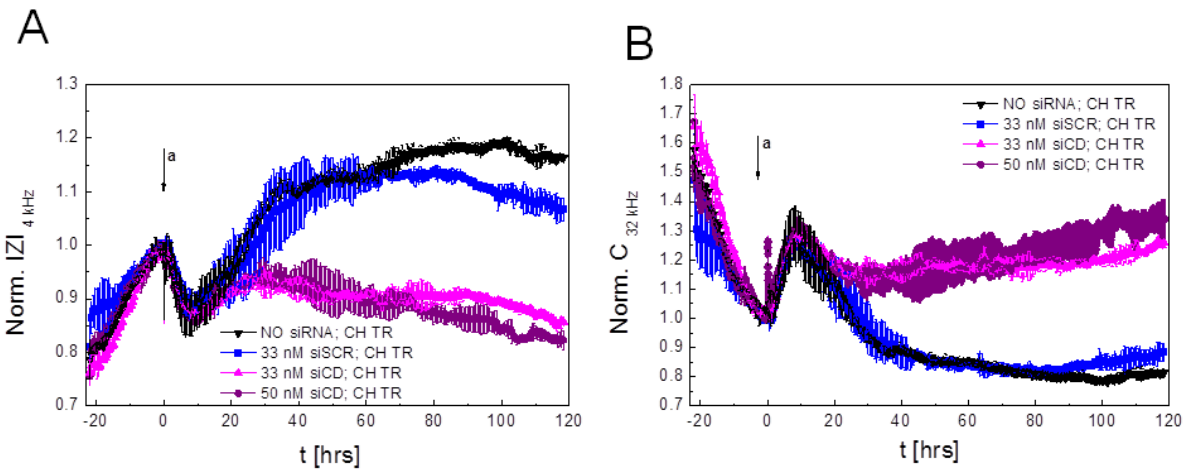

Figure 8.38 Typical time courses of (**A**) the normalized impedance at 4 kHz and (**B**) the normalized capacitance at 32 kHz during and after chemical transfection of NIH-3T3 cells in presence of 33 and 50 nM siCD, including corresponding controls. Serum-free medium was exchanged by the complete culture medium (at the time point marked with arrow **a**) and monitoring of the cellular response was continued for app. 120 hours. Impedance (**A**) and capacitance (**B**) data are normalized to the last time point before medium exchange. Experiment was conducted at 37 °C. Every 15th time point during measurement is presented to reduce large data set; mean value ± standard deviation; n=2.

Graph **A** shows impedance increase directly after chemical transfection, both for samples and controls and impedance values decreased for app. 10 hours after cell-free medium was exchanged by the complete culture medium. Thereafter, impedance signals of the cells corresponding to controls continued to increase and finally stabilized app. 30 hours later. Normalized impedance of the cells transfected with siCD stabilized quite rapidly after medium exchange, however, their values of normalized impedance were much lower than the values corresponding to the cells of controls.

Upward drifting of the signal exhibited by the cells in controls was unusual and surprising, as stable and flat impedance signals were observed in all wells before chemical transfection, when impedance of NIH-3T3 cells was shortly measured in complete medium (data not shown). Although NIH-3T3 cells did not show similar results to NRK and CHO-GFP, with respect to the trend of impedance signal, significant difference between the cells in samples and controls was observed. Thereby, NIH-3T3 cells exposed to 33 nM and 50 nM siCD

showed very similar response. However, it is unclear to which extent is this difference caused by siCD. Graph **B** depicting normalized capacitance showed as well obvious difference between the NIH-3T3 cells in samples and controls, with rather slow increase of normalized capacitance observed for cells exposed to siCD. After ECIS measurement was finished, appearance of NIH-3T3 cells was evaluated by the microscopy, however, cells in all wells (controls and samples) appeared very similar, with completely preserved and confluent cell monolayers. This leads to conclusion that siCD did not have significant cytotoxic effect on NIH-3T3 cells. Based on previous studies of siGLO Red delivery into NIH-3T3 cells, which was unsuccessful, it is assumed that chemical transfection of NIH-3T3 is inefficient. Lipofectamine might be inappropriate transfection reagent in the case of NIH-3T3, however, from the studies conducted in this work, NIH-3T3 appeared to be difficult-to-transfect.

8.5 Discussion

Within this chapter, efforts were described to deliver different types of siRNA molecules into three different mammalian cell lines by *in situ* electroporation (employing ECIS technology). Delivery of siRNA into adherent cells by invasive electric pulses was compared with the most common method for oligonucleotides delivery – chemical cationic lipid-based transfection. The response of cells during and after chemical transfection was monitored by ECIS. In addition, fate of siRNA after its free diffusion into cytosol of fixed and permeabilized cells was investigated. To assess changes in morphology of the cells after delivery of siRNA by different transfection methods, microscopy was performed. The main goal of these studies was to explore a possibility to apply *in situ* electroporation for delivery of dsRNA molecules into cells, while at the same time employing ECIS technology as a powerful analytical tool for non-invasive monitoring of the cellular behavior before and after introduction of siRNA molecules into the cytosol. Furthermore, ECIS was applied as an analytical tool to study cell response upon introduction of siRNA with another transfection method (lipid-based transfection).

Fluorescently-labeled siRNA probe (siGLO Red) was applied to investigate and optimize transfection protocols for every cell line. Thereafter, silencing effects of sequence-specific siRNA types were investigated: siEGFP targeting genes responsible for EGFP expression (silencing effects on cell morphology evaluated by microscopy) and siCD targeting genes essential for viability of mice and rats cells - Cell Death siRNA (silencing effects on morphology and viability of cells evaluated by ECIS and microscopy). Due to their hydrophilicity, size and negative charge, siRNAs cannot cross the cell membrane. Considering the fact that siRNAs often target molecules within the cell cytoplasm and

nucleus, crossing the membrane barrier is crucial for their widespread application in therapy, analytics or diagnostics. The cell membrane impermeability of siRNA is indeed the greatest obstacle nowadays, standing in the way to take advantage of a highly specific and effective nature of siRNA machinery (Dominska and Dykxhoorn, 2010). Since *in situ* electroporation combined with ECIS technology is a proven and well-established technique for delivery of various xenomolecules into mammalian cells (Wegener et al., 2002; Stolwijk et al., 2011; Albermann, 2004), proof-of-principle experiments were conducted within this work to demonstrate the capability of this experimental setup for efficient delivery of siRNA into cells and thus to provide appropriate solution for overcoming the membrane impermeability of siRNA. In addition, ECIS technique (Giaever and Keese, 1984, 1986) is employed as a versatile and powerful analytical tool for sensitive monitoring of the events before and after introduction of xenobiotics into cells.

8.5.1 Delivery of siGLO Red into Cells

The fluorescently-labeled siRNA probe siGLO Red is created by the manufacturer to accumulate exclusively within nuclei of the cells and thus qualitatively indicate successful transfection. Loading of cells with this commercially available transfection indicator was investigated on three different mammalian cell lines: CHO-GFP, NRK and NIH-3T3. Transfection of the cells was performed by *in situ* electroporation and chemical transfection, whilst fixation and permeabilization of the cells served as a control to check localization of siGLO Red after its free diffusion into the cytoplasm. Whereas CHO-GFP and NRK cells were successfully transfected with siGLO Red using all three methods, NIH-3T3 cells could be transfected only chemically and observed transfection efficiency was low.

Delivery of siGLO Red into CHO GFP Cells

CHO-GFP cells were subjected to multiple *in situ* electroporation to facilitate their efficient loading with the fluorescent probe sGLO Red. Optimal combination of pulse parameters (40 kHz, 4 V and 500 ms) and behavior of CHO-GFP cells upon their exposure to *in situ* electroporation were investigated during dye loading studies presented in chapter 5.1.2.2. Application of three successive electric pulses, as a strategy to enhance loading efficiency, resulted in successful loading of CHO-GFP cells with siGLO Red (**Figure 8.39 A**-**C** and **Figure 8.40 A**-**C**). With increasing concentration and increasing number of pulses (1 pulse vs. 3 pulses), loading efficiency was improved. Localization of siGLO Red signal predominantly within cell nuclei indicated efficient transfection. Chemical transfection of CHO-GFP cells facilitated entry of siGLO Red into cell interior as well, however, its

localization within nuclei was observed within a smaller fraction of cells and punctuated fluorescence signals were indicator of siGLO Red entrapment within the vesicles (**Figure 8.39 D**-**E** and **Figure 8.40 D**-**E**). This led to the conclusion that ISE facilitated more efficient delivery of siGLO Red into CHO-GFP cells than the common chemical lipid-based transfection.

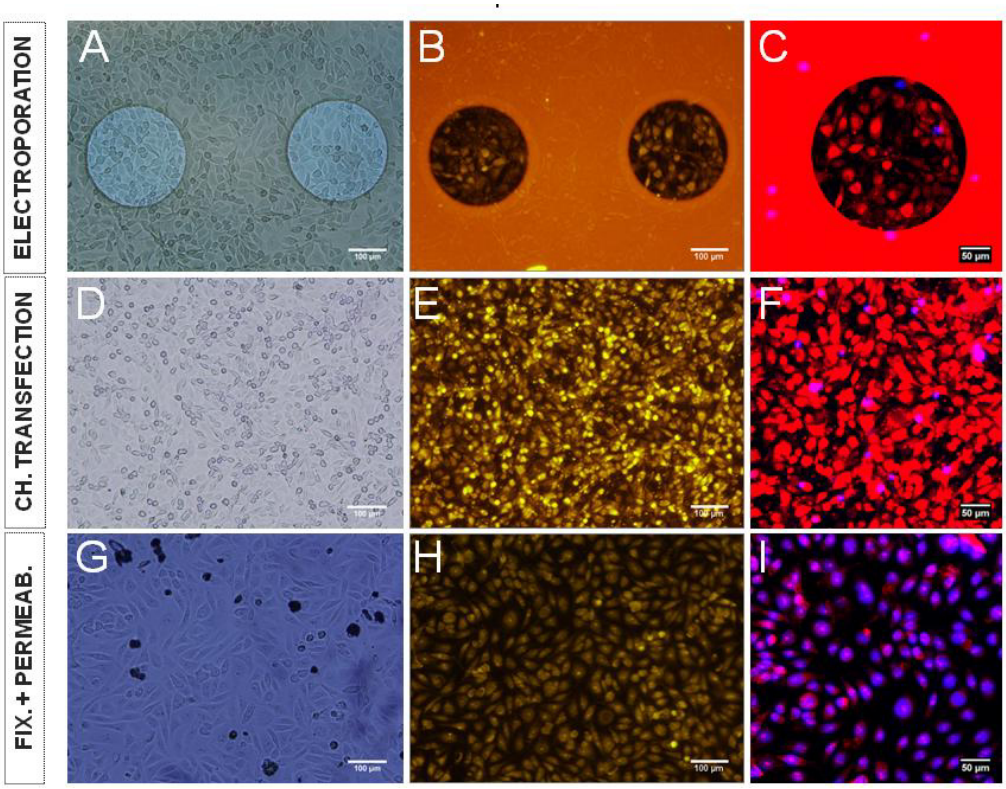

Figure 8.39 Summary of exemplary phase-contrast (first column) and fluorescence (second and third column) micrographs taken after *in situ* electroporation (**A-C**), chemical transfection (**D-F**) and fixation and permeabilization (**G-I**) of CHO-GFP cells in presence of the fluorescent probe siGLO Red. The scale bar in micrographs of the first and second column corresponds to 100 µm and in micrographs of the third column scale bar represents 50 µm. All micrographs were taken using 10-fold magnification objective.

Loading pattern of siGLO Red within chemically transfected CHO-GFP cells was compared to the study conducted by Breunig et al., 2008, who investigated application of various derivates of poly(ethylene imine) – PEI as the carriers for delivery of siRNA and compared delivery performance of PEI derivatives with the delivery by Lipofectamine. Transfection of CHO-K1 cells with 50 nM siGLO Green, using Lipofectamine as a transfection agent, resulted in homogeneous green fluorescence signal observed in nearly every cell. Most cell nuclei were loaded with siGLO Green, however, significant level of the fluorescence signal

was also found in small intracellular spots, interpreted as siRNA entrapped in endosomes or in the cytoplasm. Another study reported on application of Lipofectamine as a transfection agent for reverse transfection of cells on microarray arrays for high throughput screening (Erfle et al., 2007; Genovesio et al., 2011). This group found siGLO Red signal predominantly in cytoplasm of U2OS cells and to some smaller extent in the nuclei. Furthermore, Inoue et al., 2008 transfected H4IIEC3 cells using Lipofectamine to introduce fluorescently labeled siRNA probe. The group reported on nuclear localization of fluorescent siRNA and its homogenous distribution within the cytoplasm. In addition, large amount of fluorescent signal was found in the endosomal compartments. Microscopic examination of cells loaded with fluorescent siRNA was conducted 8 hours after transfection.

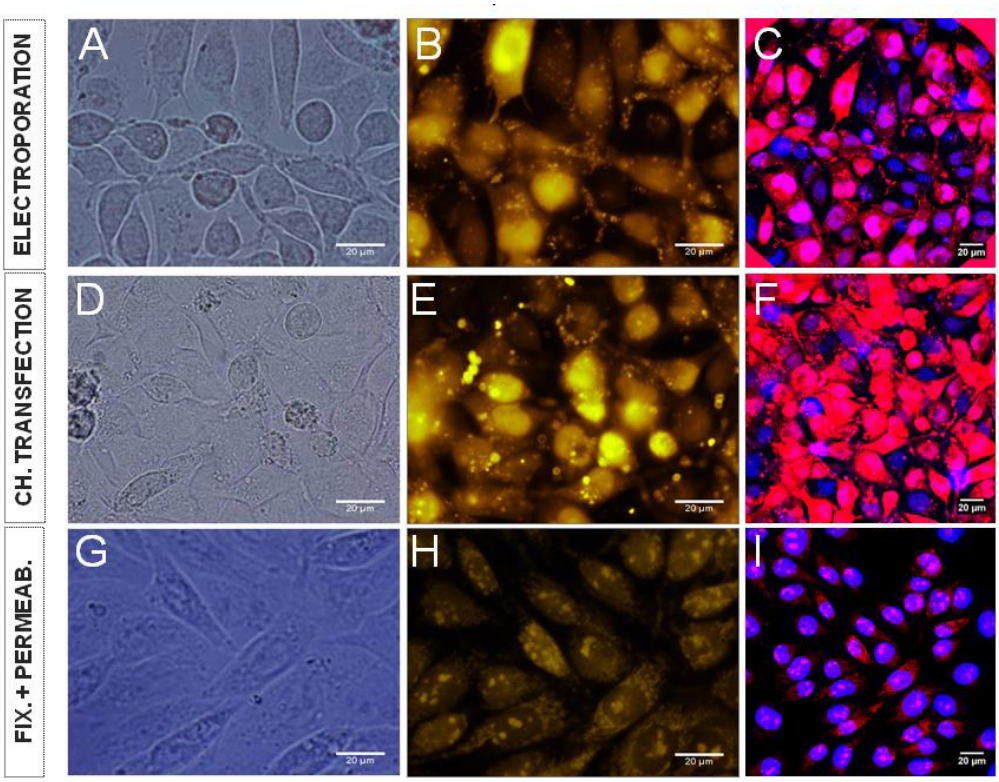

Figure 8.40 Summary of exemplary phase-contrast (first column) and fluorescence (second and third column) micrographs taken after *in situ* electroporation (**A-C**), chemical transfection (**D-F**) and fixation and permeabilization (**G-I**) of CHO-GFP cells in presence of the fluorescent probe siGLO Red. The scale bar in all micrographs corresponds to 20 µm. All micrographs were taken using 60-fold magnification objective.

Obviously, various groups of scientists reported similar localization pattern of fluorescently-labeled siRNA after its delivery into cells by chemical transfection reagent Lipofectamine. These are in agreement with the studies of siGLO Red delivery by Lipofectamine performed

on different cell lines in this work and confirm that, upon chemical transfection, significant amount of siRNA remains captured within acidic compartments of the cell. Within current work, CHO-GFP cells were subjected to siGLO Red at two concentrations: 33 and 50 nM and surprisingly, fluorescence micrographs indicted slightly better loading of cells with lower siGLO Red concentration. CHO-GFP cells exposed to 33 nM siGLO Red exhibited higher extent of fluorescence signal within cell nuclei and based on that, it was concluded that 33 nM siGLO Red is sufficient for efficient chemical transfection. This was in agreement with experiments performed later on with Cell Death siRNA (siCD). Impedance and capacitance monitoring of chemical transfection of CHO-GFP cells with 33 nM and 50 nM siCD revealed that siCD efficiently induced cell death at both concentrations, however, siCD at lower concentration induced slightly stronger cytotoxic effect.

Fixation and permeabilization of CHO-GFP cells allowed for free diffusion of siGLO Red across the disrupted cell membrane and surprisingly, only weak fluorescence signal was found in the cell nuclei (with very little co-localization with DAPI stain). Besides small spots stained within cell nuclei, siGLO Red mostly stained grained structures within the cytoplasm (**Figure 8.39 G-I** and **Figure 8.40 G-I**). It was expected that fluorescent siRNA will mostly accumulate within cell nuclei, similarly as the fluorescently-labeled aptamers did after their diffusion through the pores of irreversibly permeabilized cell membrane (details described in chapter 7.4.3). Absence of siRNA within nuclei of fixed and permabilized cells suggests that siRNA cannot simply diffuse into the nucleus from cytoplasm, but its transport into nuclei is protein-assisted. Proteins and receptors which normally regulate and perform nuclear import of siRNA are paralyzed in fixed and permeabilized cells, therefore, siRNA mostly remains captured within cytoplasm (probably in vesicles or mitochondria). Exact mechanism of siRNA import from cytoplasm into nuclei is still poorly understood, however, several studies propose possible mechanisms of siRNA action within nuclei and its potential transport vehicles (Schraivogel and Meister, 2014; Kohler and Hurt, 2007; Nakielny and Dreyfuss, 1999).

Delivery of siGLO Red into NRK Cells

For delivery of siGLO Red into NRK cells, strategy of multiple *in situ* electroporation was applied, similarly as with CHO-GFP cells. NRK cells were pulsed three times successively using optimal combination of pulse parameters previously established for this cell line (40 kHz, 4 V and 200 ms; Wegener et al., 2002; Stolwijk et al., 2011). Successful loading of NRK cells with siGLO Red was evidenced by fluorescence microscopy (**Figure 8.41 A**-**C** and **Figure 8.42 A**-**C**) and fluorescence signal was predominantly found in cell nuclei. Fluorescence intensity of siGLO Red in NRK increased with its increasing concentration and

cells exposed to the highest concentration (6 µM siGLO Red) exhibited very bright fluorescence signal within almost every cell residing on the electrode. These results demonstrate applicability of ISE for delivery of siRNA into cells and point out high level of transfection efficiency achieved with an established protocol. Highly efficient delivery of fluorescent siRNA by electroporation, described in the current work, correlates very well with previous studies describing this method as a great tool to achieve high level of cell loading with siRNA. One of such reports is study performed by Jordan et al., 2008, who investigated electoporation of HUVEC cells in presence of fluorescently-labeled siRNA, using pulse parameters: 350 V, 500 µF and 1000 Ω. The group determined transfection efficiency of 94 % by flow cytometry and applied the same protocol for introduction of sequence-specific siRNA into cells.

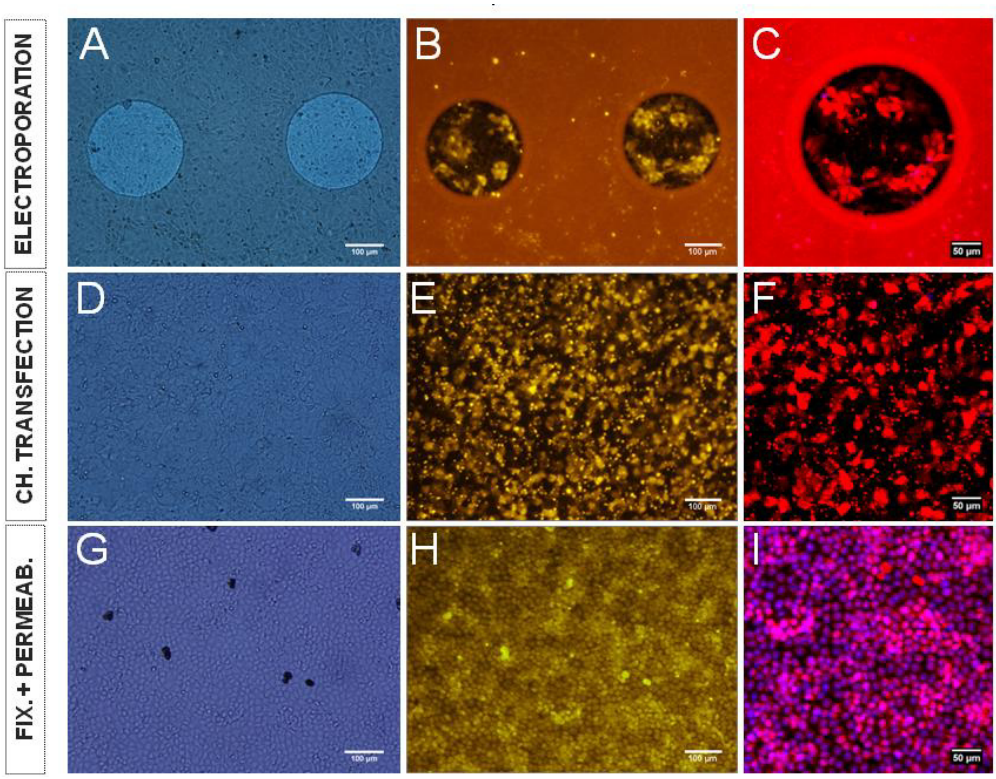

Figure 8.41 Summary of exemplary phase-contrast (first column) and fluorescence (second and third column) micrographs taken after *in situ* electroporation (**A-C**), chemical transfection (**D-F**) and fixation and permeabilization (**G-I**) of NRK cells in presence of the fluorescent probe siGLO Red. Scale bar in micrographs of the first and second column corresponds to 100 µm and in micrographs of the third column scale bar represents 50 µm. All micrographs were taken using 10-fold magnification objective.

Chemical transfection of NRK cells with siGLO Red resulted in localization of fluorescence signal in nuclei and cytoplasm of some cells, but fluorescent siRNA was mostly found in

vesicles, as indicated by the characteristic punctuated pattern (**Figure 8.41 D-E** and **Figure 8.42 D-E**). Interestingly, overall loading of NRK cells was less efficient than the loading of CHO-GFP cells, even though much higher concentration of siGLO Red was applied. Fixation and permeabilization of NRK cells allowed entry of siGLO Red into NRK cells, however, similarly as with CHO-GFP cells, the siRNA probe did not accumulate within nuclei. It stained structures within the cell cytoplasm and accumulated only in small spots within cell nuclei (**Figure 8.41 G-I** and **Figure 8.42 G**).

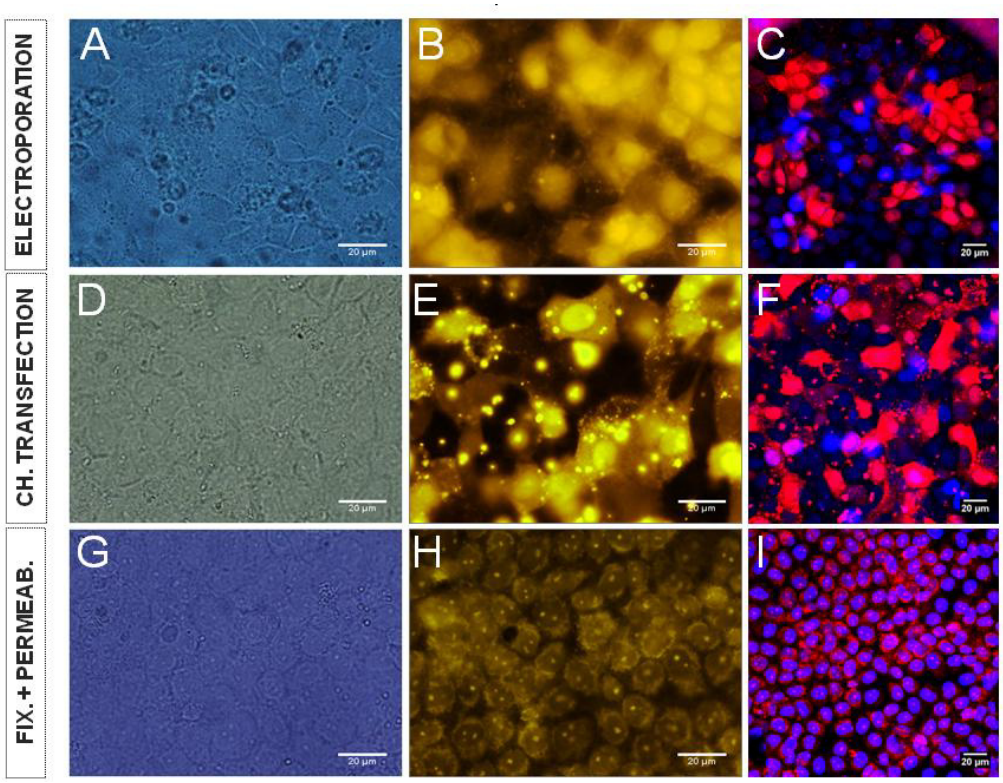

Figure 8.42 Summary of exemplary phase-contrast (first column) and fluorescence (second and third column) micrographs taken after *in situ* electroporation (**A-C**), chemical transfection (**D-F**) and fixation and permeabilization (**G-I**) of NRK cells in presence of the fluorescent probe siGLO Red. The scale bar in all micrographs corresponds to 20 µm. All micrographs were taken using 60-fold magnification objective.

Delivery of siGLO Red into NIH-3T3 Cells

Although *in situ* electroporation of NIH-3T3 cells in presence of 2 µM siGLO Red was performed, results are not discussed here. Loading of cells with siGLO Red was poor and instead, high level of unspecific siGLO Red uptake by the cells was observed. Although the fluorescent siRNA probe managed to enter nucleus of some cells, the results were not reproducible and overall transfection efficiency was much lower compared to CHO-GFP and

NRK cells. Optimization of electroporation parameters for this cell line was performed (details described in chapter 5.1.2.4), however, microscopic examination of NIH-3T3 cells was troublesome, mostly because confluent NIH-3T3 cells easily detach from the substrate surface. In addition, shear stress during pipetting and washing additionally challenges application of NIH-3T3 cells for electroporation studies. Adhesion of NIH-3T3 cells could be improved by coating of the culture substrate (ECIS electrode arrays) prior to every experiment, similarly as it was done prior to seeding of CHO-K1/ CHO-GFP or BAEC cells (protocol described in chapter 4.1.5). NIH-3T3 cells were successfully applied for electroporation studies in the past. Jain and Muthuswamy, 2007 developed 6x6 MEAs (microelectrode arrays) for electroporation of adherent cells with spatial and temporal control. They conducted dye loading studies on NIH-3T3 cells using propidium iodide and applied electric pulses with duration of 10 ms and voltages in a range 0.5 – 6 V. Cells exposed to pulses of 5 V got damaged or were killed by the pulse, as they vanished from the electrodes during post-electroporation washing of the MEAs surface.

Delivery of siGLO Red - General Remarks

Delivery studies conducted with siGLO Red as a probe demonstrated that both *in situ* electroporation and conventional chemical transfection allow for siRNA entry into the cytosol and thus help overcoming its poor cell uptake. However, for effective application of sequence-specific siRNA, it is essential to preserve its integrity and activity within the cell. Extensive research over the past years identified most of the siRNA targets within cytoplasm and nucleus of the cell (Meister and Tuschl, 2004; Ohrt et al., 2008; Castel and Martienssen, 2013). Therefore, localization of siRNA upon its entry to the cell has to be taken into account when efficiency of delivery method is being judged. Electroporation-mediated transfer of fluorescently-labeled siRNA into cell interior was studied on single-cell level by Paganin-Gioanni et al., 2011. They did direct microscopic visualization of the single adherent CHO cells before, during and after application of electric pulses (10 pulses of 5 ms, at 1 Hz and 300 V/cm). siRNA molecules entered the cells during pulse application and were homogeneously distributed in the cytoplasm. Several minutes after transfer, they still have not observed fluorescence signal located in the nucleus. Chabot et al., 2012 developed chemically-modified oligonucleotides LNA/DNA (locked nucleic acids combined with DNA; siLNA) and demonstrated successful delivery of LNA/DNA oligomer targeting anti-miR34a into cells by electroporation. The anti-miR34a siLNA decreased the level of the miR34a in the cells and induced its functional inhibition. Later on, the same group (Chabot et al., 2013) monitored transfer of (Cy5)-labeled LNA/DNA into CHO cells and observed its rapid entry in

the cytosol upon application of electric pulses (10 pulses of 5 ms, 0.3kV/cm, at 1 Hz). They monitored entry of Cy5-LNA/DNA (15 kDa) into single plated HeLa GFP-Rab7 cells before, during and several hours after application of electric pulses (Orio et al., 2013). With the pulse application, Cy5-LNA/DNA entered the cells and firstly diffused into cytoplasm. Few minutes after pulse application, Cy5-LNA/DNA entered nucleus and 2 hours after pulse application, fluorescence signal was still mainly present in the nucleus. Thereafter, fluorescence signal started to disappear from the nucleus and it was detected in cytoplasm. 4 - 9 hours after electroporation, fluorescence was localized in the cytoplasmic organelles and co-localization with MitoTracker® indicated fluorescence accumulation in mitochondria (due to nonspecific accumulation of Cy5). Interestingly, they did not find Cy5-LNA/DNA within lysosomes or endosomes, not even 24 hours after electroporation. These studies provide an interesting and important insight into dynamics and distribution of oligonucleotides, and suggest different loading pattern of siRNA and DNA. Their studies showed accumulation of DNA within nuclei and accumulation of fluorescently-labeled siRNA in the cytoplasm. It is important to emphasize they did not use transfection indicator which is created to localize in nucleus (as siGLO Red), as it was the case in this work. Observations of Chabot and collaborators can be correlated with the studies involving aptamers performed in this work (chapter 7), as in all investigated cell lines, fluorescently-labeled aptamers were found predominantly in cell nuclei.

Within current study, direct visualization of siRNA uptake by electroporated cells was not conducted, however, localization of siGLO Red within NRK cells was examined microscopically 24 hours after to multiple electroporation (data not shown). In contrast to predominantly nuclear localization of siGLO Red 1 – 2 hours after ISE, 24 hours after ISE, siGLO Red signal was mostly observed within cytoplasm, with only smaller fraction of cells containing fluorescence signal within their nuclei. Such observations can be correlated with studies of Chabot and collaborators, which describe shifting of oligonucleotides from nucleus to cytoplasm several hours after electroporation (Chabot et al., 2013; Orio et al., 2013).

Chemical transfecion of cells is often correlated with endocytotic pathways of oligonucleotides entry. Saleh et al., 2006 studied pathway for double-stranded RNA (dsRNA) uptake in Drosophila melanogaster S2 cells. After they incubated S2 cells with Cy3-labelled dsRNA, firstly they observed dsRNA binding to cell surface (after 5 min) in a form of punctate pattern, and in the course of 60 min, dsRNA entered the cells but remained in small punctate structures. In addition, they looked into temperature dependency of endogenous uptake of dsRNA and demonstrated that dsRNA-mediated silencing of firefly luciferase at 4 °C was inefficient, compared to the silencing at 25 ºC. Temperature-dependent uptake of

oligonucleotides was also reported by Shoji et al., 1991, Loke et al., 1989; Dokka and Rojanasakul, 2000, and suggest that transport of oligonucleotides across the cell membrane is active and energy-dependent process.

Hirsch and Helm, 2015 conducted studies of siRNA entry into adherent RBE4 cells chemically transfected with Oligofectamine® . They used FRET (fluorescence resonance energy transfer) method to monitor localization and integrity of siRNA inside the cells. siRNA duplexes were labeled with FRET pair Atto 488 / Atto 590. Close proximity of these dyes induces energy transfer and FRET signal is observed. They exploited FRET to determine fraction of siRNA molecules in which the dyes exhibit close spatial proximity, as measure of siRNA integrity. The group observed following classes of events in the course of 8 hours: (A) uptake of lipoplex structures containing siRNA, (B) release of siRNA and its rapid distribution in the cytosol, (C) depletion of siRNA fluorescence from the cytosol, (D) secondary (i.e. repeated) release in the same cell, (E) accumulation of partially degraded siRNA in the perinuclear structures, (F) occasionally observed transport of siRNA in the nuclei and (G) siRNA present in small endosomal structures, loss of integrity. The authors of this study described presence of fluorescent dots within all cells during the entire imaging. They suggested these are intact siRNA lipoplexes and differentiated them from perinuclear dots, as they exhibited higher integrity than the perinucelar dots and were more remote from the nucleus. Fluorescent dots can be very well correlated with punctuated pattern observed in the cells exposed to chemical transfection in this work. Hirsch and Helm observed co-localization of these small fluorescent dots with lysosomal marker which is in a good agreement with the co-localization studies of siGLO Red and LysoTracker conducted in this work. Fluorescence micrographs showed high level of co-localization of siGLO Red and LysoTracker afer chemical transfection of the cells, whereas, after *in situ* electroporation, siGLO Red and LysoTracker signal did not overlay. Hirsch and Helm indicated that first 60 min upon chemical transfection of cells are most dynamic, initial 4 hours are crucial for release of siRNA into cytosol and its subsequent distribution.

Finally, efforts made in this work to deliver fluorescent siRNA into adherent cells by *in situ* electroporation can be compared with the studies of Jain et al., 2009, who created microwell arrays for the high throughput electroporation studies which allow one to screen libraries of nucleic acids. HEK 293T cells were grown on transparent conductive Indium-Tin Oxide (ITO)-coated glass slides to allow cell imaging and thus evaluation of loading efficiency. They applied 1 square pulse of voltage 500 V/cm and pulse width of 1 ms to deliver Alexa Fluor 488-labeled siRNA into HEK 293T cells. Delivery of fluorescent siRNA by *in situ* electroporation resulted in transfection efficiency > 99 %. Thereby, high level of cell viability

was preserved. Similar transfection efficiency was also observed when mouse primary macrophages were exposed to electroporation in presence of fluorescently-labeled siRNA, indicating that electroporation can be applied for siRNA delivery into various cell types.
Within this work, efficient delivery of siGLO Red into CHO-GFP and NRK cells was demonstrated, allowing rapid import of siRNA to its sites of action (cytoplasm and nucleus). Established protocol, including multiple ISE of the cells was applied to deliver sequence-specific siRNA into cells, and respective changes in cell morphology were monitored by ECIS and/or by microscopy.

8.5.2 Delivery of Small Interfering RNA Targeting EGFP into Cells

Following the efficient delivery of fluorescently-labeled siGLO Red into CHO-GFP cells by *in situ* electroporation and chemical transfection, this cell line was applied as a cell model to study introduction of target-specific siRNA type. The siRNA addressing genes responsible for expression of EGFP was delivered into cells genetically modified to stably express EGFP (CHO-GFP). The cells exhibited EGFP expression homogenously, both in cytoplasm and nuclei (Seibel et al., 2007). CHO-GFP cells were exposed to multiple *in situ* electroporation and silencing effects of siEGFP were evaluated 48 and 72 hours after transfection by CLSM. Fluorescence micrographs revealed that cell population on the electrodes and a small fraction of cells around them appeared darker than the cells of the background (residing on the photopolymer). This indicated efficient loading of CHO-GFP cells with siEGFP, facilitated by ISE. However, silencing effect of siEGFP on EGFP expression was not strictly limited only to cell population residing on the electrodes, presence of dark(er) cells around the electrodes indicated that cells which were successfully loaded with siEGFP divided and migrated over period of time of 48 or 72 hours before microscopy. It is not difficult to imagine that cells, previously loaded with siEGFP divided and migrated from the electrode to the background and reverse, cells from the background (surrounding the electrodes during electroporation), moved partially to the electrode area. Such hypothesis may be confronted by the fact that CHO-GFP cells are not as “mobile” as NRK cells (this is going to be discussed in more details in the next subchapter), however, it is not difficult to envision that healthy, viable cells maintain their normal living functions, despite the fact that siRNA targeting EGFP entered their cytosol. The illustration of this phenomenon is given in **Figure 8.43**. This exemplary confocal fluorescence-micrograph shows CHO-GFP cells on the pair of electrodes app. 72 hours after their exposure to multiple ISE in presence of siEGFP. Small circles with solid line (marked with a) delineate area of gold film electrodes, where the population of dark cells is expected. Larger dashed circles (marked with b) indicate population of cells, where reduction

(inhibition) of EGFP was observed as well, however, unexpectedly. This fluorescence micrograph demonstrates as well that reduction or complete knockdown of EGFP is not homogeneously distributed within the cell population on the electrodes (and around them).

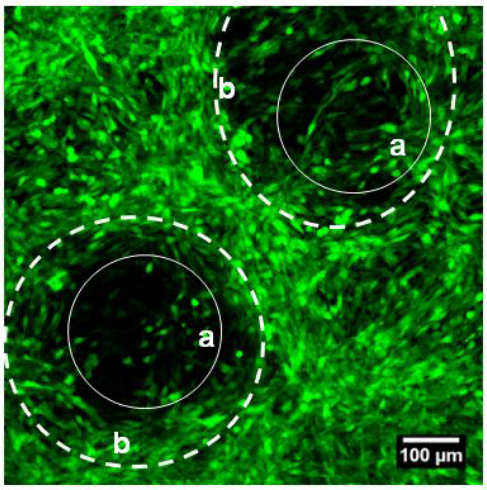

Figure 8.43 Exemplary confocal fluorescence micrograph taken app. 72 hours after *in situ* electroporation of CHO-GFP cells in presence of 2µM siEGFP. Scale bar represents 100 µm. Micrograph illustrates consequence of cell migration and division during time period of 72 hours (between siEGFP delivery into cells by electroporation and microscopy by CLSM).Circles **a** delineate area of electrodes and circles **b** indicate area of inhibited or reduced EGFP expression by siEGFP.

In order to quantify silencing effect of siEGFP on CHO-GFP cells, fluorescence micrographs were quantified using ImageJ program. As one can imagine, non-uniform distribution of dark siEGFP-treated cells on the electrodes and around them does not favor absolutely precise evaluation of silencing and thus transfection efficiency. Nevertheless, quantification was performed, firstly by comparing fluorescence intensity on the electrodes and around them (background). This way fluorescence on the electrodes was “corrected” with regards to an overall fluorescence of the cell population in one well. Clearly, background cells included also cells with reduced EGFP which were residing around the electrodes during microscopy. Nevertheless, when fluorescence intensities for every experimental condition were normalized to the control where cells were pulsed only in buffer, EGFP fluorescence was reduced by 50 % in cells observed 48 hours after ISE, whereas in the cells imaged 72 hours after ISE, EGFP was 55 % lower. It is important to mention that quantification of micrographs was also conducted by comparing the electrodes area only, regardless of the background (data not shown). As expected, such method of quantification resulted in even higher silencing efficiency; however, electrode-to-background comparison was chosen to be

presented as it still indicates highly efficient transfection achieved by ISE, after taking all controls into consideration.

These results are in agreement with previous studies conducted by Fujimoto and collaborators, who developed microarrays for high throughput *in situ* elecroporation-mediated transfection of cells with siRNA. They strategy included loading of siRNA targeting EGFP (GFP-siRNA) and poly(ethyleneimine) (PEI) on the electrode (layer-by-layer assembly) and subsequently grown d2EGFP-HEK cells were exposed to *in situ* electroporation. Single pulse (240 V/cm for 10 ms) was applied to facilitate loading of cells with GFP-siRNA and micrographs were taken 48 hours afterwards, to assess silencing and transfection efficiency (Fujimoto et al., 2008) Fluorescence of EGFP was reduced on the electrodes with GFP-siRNA and fluorescence reduction was dependent on the number of layers. Increasing number of layers resulted in more reduction of EGFP fluorescence signal. To improve storage of their microarrays they investigated addition of saccharides as additives to siRNA. Interestingly, they observed areas of dark cells - spots, corresponding to the area of their electrodes, after *in situ* electroporation. (Fujimoto et al., 2009). Furthermore, the group reported on concentration-dependent reduction of EGFP expression in d2EGFP-HEK cells 48 hours after their exposure to *in situ* electroporation. (Fujimoto et al., 2010). Similarly to the results in this work, they observed approximately the same level of EGFP expression in cells pulsed in presence of control siRNA (scrambled sequence) and cells pulsed in absence of siRNA. Interestingly, Fujimoto and collaborators investigated correlation between reduction of EGFP expression and time (24, 48 or 72 hours) after seeding of cells on siRNA-loaded microarrays. However, they found that siRNA loaded on electrodes maintained its silencing activity for 3 days under cell culture environment. After quantification of flow cytometry data, they determined silencing efficiency as a ratio of EGFP fluorescence on the electrode loaded with EGFP-siRNA and electrode loaded with control (non-binding) siRNA. Resulting silencing ratio was app. 70%.

Jain et al., 2012 studied electroporation-mediated delivery of siGFP into GFP-expressing primary mouse macrophages and measured knockdown of GFP, as a decrease in fluorescence intensity. *In situ* electroporation facilitated successful delivery of siGFP into cells and reduction of total GFP fluorescence was more than 60%, compared to the control, which is agreement with reduction of EGFP signal achieved in the current work. Moreover, various groups reported on reduction of fluorescent intensity after successful delivery of respective siRNA by electroporation (Fyrberg and Lotfi, 2010; Jordan et al., 2008). Paganin-Gioanni et al., 2011 evaluated efficiency of EGFP siRNA delivery into B16F10-EGFP melanoma cells by electotransfer *in vitro* (10 pulses, 5 ms duration, 500 V/cm at 1 Hz). They

observed significant decrease in EGFP expression within 2 days after the cells were subjected to electroporation. More precisely, reduction of 50 - 57% of EGFP expression was observed at days 2, 3, and 4 days after electroporation and such results correlate well with results obtained in the current work.

Silencing effect of siEGFP after electroporation was compared with conventional cationic lipid-based transfection using reagent Lipofectamine® RNAiMAX. Fluorescence micrographs taken 48 hours indicate excellent silencing efficiency achieved after chemical transfection, as almost entire cell population appeared dark. Knockdown effect of siEGFP in CHO-GFP cells was also evaluated app. 72 hours after chemical transfection (data not shown), however, results were again very similar to those obtained 48 hours after chemical transfection. Such observations are consistent with some of previously published reports on EGFP targeting by the respective siRNA, delivered into (sub)confluent cells by lipid-based transfection. Breunig and collaborators studied silencing efficiency when poly(ethylene imine) (PEI) was applied as a carrier for EGFP-targeting siRNA in CHO-GFP cells (Breunig et al., 2008). They reported that siRNA suppressed expression of EGFP in transfected cells and concentration-dependent effect was observed when commercial branched PEI (bPEI) and lPEI cross-linked via disulfide bonds (ssPEI) were applied. With bPEI silencing efficiency was app. 25 % and with ssPEI app 45 %. When anti-EGFP siRNA was delivered into CHO-GFP cells by chemical transfection using Lipofectamine, EGFP fluorescence was reduced to app. 10 %, which correlates well with results obtained with Lipofectamine in the current study, where very little EGFP expression was observed 48 hours after Lipofectamine treatment. Kwon et al., 2013 implemented chemical transfecion reagent for transfection of cells within high density spots microarrays. By application of reverse transfection of microRNAs and siRNA, cellular phenotype generated by microRNAs regulated NF-κB (RelA) expression, similarly to the siRNA. The group transfected HeLa cells with siRNA and miRNA targeting NF-κB (RelA) protein expression and visualized its reduction with anti-RelA/secondary antibody labeled with Alexa 488. They monitored reduction of green fluorescence as a measure of decrease in NF-κB protein expression. Interestingly, they concluded that cells should be transfected with minimal concentrations of siRNA and miRNA to avoid cytotoxic effects, however, their concentrations should be sufficiently high to induce silencing effect higher than 70 % on target protein. Even though no cytotoxic effect of siRNA was observed within current study, it has been observed with CHO-GFP cells that lower concentrations of siRNA induced better loading in cells (siGLO Red) and stronger silencing effect (siCD). Similarly as in this work, Kwon and collaborators followed silencing effect 48 and 72 hours after transfection, however, they observed that knockdown effect starts to disappear 96 hours after transfection and

recommended evaluation of silencing effects 48 hours after transfection. In contrast to the current study, this group could clearly visualize individual spots representing the area of transfection. No migration or movements of the cell monolayers during incubation time of 48 – 96 hours after transfection were reported. Since such effect was observed in CHO-GFP cells, the question arose how fast do these cells divide and (if) they share siRNA material. Bartlett and Davis, 2006 reported that species are diluted equally between the two daughter cells after each cell division. Moreover, they followed silencing effects in four different cell lines with various doubling time and concluded that the dilution effect due to cell division can alter the duration of gene silencing. Namely, cell lines with slower doubling times exhibit longer duration of silencing effects.

Nevertheless, assay involving siEGFP demonstrated its successful delivery by *in situ* electroporation and chemical transfection, as in both cases significant reduction of EGFP expression was determined within CHO-GFP cells.

8.5.3 Delivery of Cell Death siRNA into Cells

Besides siRNA targeting EGFP, which induces reduction of EGFP expression in the cells detectable only by the microscopy, another sequence-specific siRNA type was evaluated, so-called Cell Death siRNA (siCD). This highly potent siRNA causes knockdown of genes (present in mice and rats) indispensable for cell survival. Silencing of these genes induces cell death, which can be visualized by microscopy, but it can also be monitored / measured using ECIS technology. In this work, ECIS was applied as an analytical method to monitor cellular behavior before and after delivery of sequence-specific siCD into cells by *in situ* electroporation and by chemical transfection. It has been demonstrated that ECIS technology is able to detect alterations in cell morphology and viability, which occur as a direct consequence of siCD activity. Cell lines CHO-GFP, NRK and NIH-3T3 were applied as cell models to study introduction of this target-specific siRNA.

Delivery of Cell Death siRNA into CHO-GFP Cells

Cell Death siRNA was delivered into CHO-GFP cells by *in situ* electroporation applied three times successively and ECIS monitoring indicated that delivered siCD induced considerable levels of cell death in CHO-GFP cells. Time courses of the normalized impedance and capacitance showed distinct behavior of CHO-GFP cells after electroporation with siCD, compared to the respective controls. Subsequent microscopic examination of cells stained with EthD-1, confirmed silencing activity of siCD, as large number of dead and damaged cells was observed in wells where cells were exposed to siCD during ISE. Dead cells were

not only on the electrodes but also around them and this was in agreement with previous observations made after electroporation of cells with siEGFP, where similar pattern was observed 48 and 72 hours after ISE. Quantification of micrographs clearly indicated a correlation between the fluorescence signal (of dead cells) and cellular uptake of siCD.

Chemical transfection of CHO-GFP cells in presence of siCD resulted in a high level of cell death detected both by ECIS recordings and microscopy. Similarly to chemical transfection of CHO-GFP cells in presence of siGLO Red, lower concentration of siCD (33 nM) induced slightly stronger cytotoxic effects of siCD than the higher concentration (50 nM). Fluorescence micrographs taken app. 48 hours after chemical transfection showed completely decomposed monolayer of damaged and apoptotic cells.

Whereas strong silencing effect of siCD in CHO-GFP cells was exhibited both after ISE and chemical transfection, its effect on NRK cells appeared to be much lower than it was expected. Even though micrographs clearly showed dead and damaged cells gathered on the top of the electrodes after ISE with siCD, respective cytotoxic effect of siCD appeared minor in ECIS recordings. To investigate phenomena behind such discrepancy, cell death by siCD and by electric wounding was compared, not only in NRK cells but also in CHO-GFP. Upon wounding of CHO-GFP cells, impedance and capacitance values did not reach values of cell-free electrodes. In addition, impedance and capacitance signals did not return to pre-pulse values at least 17 hours after wounding. Respective ECIS recordings and micrographs taken in the course the measurement and after it indicated incomplete recovery of CHO-GFP cells after electric wounding.

Delivery of Cell Death siRNA into NRK Cells

Same as with CHO-GFP, *in situ* electroporation was applied three times successively to deliver Cell Death siRNA into NRK cells. After initial signal changes due to cellular reaction to transfection conditions and media exchange, impedance and capacitance signals stabilized and maintained at relatively constant values until the end of the measurement. Rather small differences between samples and controls were observed during time interval between 17 and 30 hours after electroporation. However, micrographs taken during that period showed a number of dead and damaged cells gathered on top of the confluent monolayer present the electrode. It was surprising that cytotoxic effect of siCD on NRK cells was not stronger and even more puzzling was a discrepancy between ECIS recordings and microscopic images. It was assumed that (i) dying of the cells on the electrodes and (ii) re-population of the electrodes by the healthy neighboring cells takes place at the same time, whereby second process (ii) was obviously quicker than the first one (i), thus masking cytotoxic activity of

siCD. Silencing effect of siCD was compared with electrical wounding of NRK cells, as it was assumed that rapid recovery and migration of NRK cells correlates in both cases with rapid renewal of the cell monolayer. Indeed, NRK cells on the electrodes after wounding and after ISE in presence of siCD appeared fairly similar. As expected, impedance and capacitance values reached values of cell-free electrodes immediately after introduction of lesion in the cell monolayers by highly invasive electric fields. During wound healing process, healthy cells surrounding the electrodes migrated to the electrode surface, filled an empty room and pushed damaged cells away from the substrate surface. Recovery of NRK cells after wounding was quick and complete.

Chemical transfection of NRK cells in presence of siCD induced relatively low extent of cell death. Microscopic examination of NRK cells affected by siCD showed significantly larger fraction of dead cells compared to controls. However, monolayers of these cells were still entirely confluent indicating again high rate of cell recovery.

Delivery of Cell Death siRNA into NIH-3T3 Cells

The third cell line tested on cytotoxic effect of Cell Death siRNA was NIH-3T3, however, cell response was only monitored during and after chemical transfection. ECIS recordings and subsequent microscopy did not reveal significant cytotoxic effect of siCD on NIH-3T3 and this is explained by low transfection efficiency observed after exposure of NIH-3T3 cells to siGLO Red in presence of Lipofectamine.

Delivery of siCD - General Remarks

Studies involving transfer of siCD across the cell membrane and monitoring of its cytotoxic effect, induced by siRNA-mediated silencing of genes essential for cell survival, were successfully conducted using CHO-GFP as a cell model. However, effect of siCD on NRK was difficult to detect using ECIS, even though aggregates of dead cells were observed in micrographs taken app. 24 hours after ISE, indicating presence of cytotoxic effect of siCD on NRK. Similar observations were previously reported by Stolwijk, 2012 who followed impedimetrically the effect of cytotoxic compounds delivered into NRK by ISE. Namely, after introduction of bleomycin (membrane-impermeable cytotoxic drug) into NRK by a single electroporation pulse (and subsequent cell recovery from pulse application), decrease in impedance signal (at 4 kHz) was observed, indicating cytotoxic effect of bleomycin on cells and transient minimum was recorded app. 13 hours after ELPO. Thereafter, impedance signal recovered fairly quickly and returned to the pre-pulse impedance values app. 25 hours after ISE. Such transient cell response to cytotoxic compound and fast recovery of the cells

is in agreement with the similar behavior of NRK detected in the current study. Another remarkable similarity between current work and studies of Stolwijk, is appearance of distinct fluctuations in impedance signal after exposure of the cells to the cytotoxic compound. Namely, Stolwijk observed that impedance signal at 32 kHz fluctuates intensively about 6.5 hours after ISE. In the current work, such fluctuations were observed after exposure of NRK cells to chemical transfection with siCD and fluctuations had transient character. Same as in the current work, Stolwijk did not observe similar fluctuations in the signal of control cell monolayers. Moreover, fluctuations were more visible at the higher frequencies (32 kHz) in both studies. Another significant similarity between current study with siCD and study with bleomycin performed by Stolwijk, was the appearance of NRK cells in micrographs taken after ISE. Stolwijk observed aggregates of dead cells on top of the confluent monolayer covering the electrode app 40 hours after ISE of NRK cells with 100 μM bleomycin. In contrast, no such structures were observed on the electrodes where cells were not treated with bleomycin in combination with ISE. Furthermore, Stolwijk compared behavior of NRK cells after their loading with bleomycin by ISE and after electric wounding. These studies revealed very similar appearance of the cells on electrodes after ISE with bleomycin and after electric wounding, with characteristic dead cell bodies aggregated on the top of the renewed monolayer covering the electrode, several hours after ISE and electrical wounding. In addition, Stolwijk analyzed effect of cytochalasin D on migration and wound healing capacity of NRK cells after ISE with bleomycin. Cytochalasin D inhibits cell motility and in this particular case, it was added to the assay buffer before electroporation. After subsequent electroporation of NRK cells with bleomycin in presence of cytochalasin, recovery of the cells and renewal of the cell monolayers was not observed during the measured time frame (24 hours). Characteristic fast recovery of NRK cells described in previous studies is thus consistent with behavior of this cell line observed in the current work and it clarifies very well processes behind moderate response of NRK cells to cytotoxic siCD observed in this work.

There are several reports which describe electroporation-mediated delivery of siRNA inducing cytotoxic effects in cells accomplished by electroporation. Fyrberg and Lotfi, 2010 described electroporation of hematopoetic (CEM) cells,which are difficult to transfect using classical chemical transfection. The group optimized electroporation protocol to achieve 70 – 80 % downregulation of enzyme (deoxycytidine – dCK) acivity and applied it for microarray analysis. The MTT assay was applied to assess citotoxicity in CEM cells after downregulation of dCK enzyme using siRNA. Interestingly, they found that applied electroporation protocol itself only moderately affected the number of cells, whereas proliferation of the cells was slowed down. Jain et al., 2012 applied their high throughout

microwell setup for efficient gene knockdown by surface-bound printed siRNAs. Before they tested electroporation of cells with siRNAs bound to the surface of microwell arrays, they did proof-of-principle assays by electroporating the cells with siRNAs suspended in buffer (in microwell arrays). They applied siRNA targeting ribosomal protein subunit 27a (siRPS27a) to induce cell death in HeLa and HEK 293 cells and observed high level of cell death (> 95 %) app. 48 hours after delivery of siRPS27a into these cell lines. They also subjected primary mouse macrophages to siRPS27a combined with electroporation and observed that more than 90 % cell died after 5 days.

Jordan et al., 2008 reported on successful silencing of glyceraldehyde phosphate dehydrogenase (GAPDH) expression in Jurkat cells already 4 h after electroporation (pulse parameters: 250 V, 300 µF, and 1000 Ω). The GAPDH expression was reduced by 88%, compared to the cells pulsed with non-specific sequence (scrambled control) and trend of further reduction of GAPDH expression continued for up to 48 h after electroporation. They optimized electroporation conditions using fluorescently-labeled siRNA in different cells, similarly as it was performed in the current work, and achieved 75% transfection efficiency for Neuro-2A, 93% for human primary fibroblasts, and 94% for HUVEC cells (analyzed by flow cytometry). The group emphasized quick optimization of the protocol for electroporation of cell suspensions and its applicability for transfection of cell types which are difficult-to-transfect using other methods.

Interestingly, above mentioned studies did not report on suppressing of siRNA-related cytotoxic effect by fast recovery of the cells. At the same time, only end-point evaluation of cytotoxic effect of siRNA on cells was conducted. Current work, similarly as previously described literature reports, demonstrate that electroporation-mediated delivery of siRNA molecules has highly efficient manner. The experimental protocol for delivery of siRNA into adherent cells by *in situ* electroporation, established and evaluated within the current work, combines advantages of this highly-efficient delivery method with time-resolved and non-invasive monitoring of the respective cell response by ECIS.

8.6 References

Akhtar, S., and Benter, I. (2007) Toxicogenomics of non-viral drug delivery systems for RNAi: potential impact on siRNA-mediated gene silencing activity and specificity. *Advanced Drug Delivery Reviews* 59, 164–182.

Albermann, S. (2004) In situ Elektroporation adhärenter Säugerzellen. PhD Thesis, Westfälische Wilhelms-Universität Münster.

Bader, A.G., Brown, D., and Winkler, M. (2010) The promise of microRNA replacement therapy. *Cancer Research* 70, 7027–7030.

Bartlett, D.W., and Davis, M.E. (2006) Insights into the kinetics of siRNA-mediated gene silencing from live-cell and live-animal bioluminescent imaging. *Nucleic Acids Research* 34, 322–333.

Boussif, O., Lezoualc'h, F., Zanta, M.A., Mergny, M.D., Scherman, D., Demeneix, B., and Behr, J.P. (1995) A versatile vector for gene and oligonucleotide transfer into cells in culture and in vivo: polyethylenimine. *Proceedings of the National Academy of Sciences of the United States of America* 92, 7297–7301.

Breunig, M., Hozsa, C., Lungwitz, U., Watanabe, K., Umeda, I., Kato, H., and Goepferich, A. (2008) Mechanistic investigation of poly(ethylene imine)-based siRNA delivery: Disulfide bonds boost intracellular release of the cargo. *Journal of Controlled Release* 130, 57–63.

Campbell, J.M., Bacon, T.A., and Wickstrom, E. (1990) Oligodeoxynucleoside phosphorothioate stability in subcellular extracts, culture media, sera and cerebrospinal fluid. *Journal of biochemical and biophysical methods* 20, 259–267.

Castel, S.E., and Martienssen, R.A. (2013) RNA interference in the nucleus: roles for small RNAs in transcription, epigenetics and beyond. *Nature Reviews Genetics* 14, 100-112.

Chabot, S., Orio, J., Castanier, R., Bellard, E., Nielsen, S.J., Golzio, M., and Teissie, J. (2012) LNA-based oligonucleotide electrotransfer for miRNA inhibition. *Molecular Therapy* 20, 1590-1598.

Chabot, S., Pelofy, S., Teissie, J., and Golzio, M. (2013) Delivery of RNAi-based oligonucleotides by electropermeabilization. *Pharmaceuticals* 6, 510-521.

Chin, D.J., Green, G.A., Zon, G., Szoka, F.C., Jr., and Straubinger, R.M. (1990) Rapid nuclear accumulation of injected oligodeoxyribonucleotides. *Nature: New Biology* 2, 1091-1100.

Deng, Y., Wang, C.C., Choy, K.W., Du, Q., Chen, J., Wang, Q., Li, L., Chung, T.K., and Tang, T. (2014) Therapeutic potentials of gene silencing by RNA interference: principles, challenges, and new strategies. *Gene* 538, 217–227.

Dokka, S., and Rojanasakul, Y. (2000) Novel non-endocytic delivery of antisense oligonucleotides. *Advanced Drug Delivery Reviews* 44, 35–49.

Dominska, M., and Dykxhoorn, D.M. (2010) Breaking down the barriers: siRNA delivery and endosome escape. *Journal of Cell Science* 123, 1183-1189.

Dorsett, Y., and Tuschl, T. (2004) siRNAs: Applications in functional genomics and potential as therapeutics. *Nature Reviews Drug Discovery* 3, 318-329.

Drosopoulos, K., and Linardopoulos, S. (2013) Integration of RNAi and small molecule screens to identify targets for drug development. *Methods in Molecular Biology* 986, 97–104.

Drummond, D.C., Meyer, O., Hong, K., Kirpotin, D.B., and Papahadjopoulos, D. (1999) Optimizing liposomes for delivery of chemotherapeutic agents to solid tumors. *Pharmacological Reviews* 51, 691–743.

Elbashir, S.M., Harborth, J., Lendeckel, W., Yalcin, A., Weber, K., and Tuschl, T. (2001a) Duplexes of 21-nucleotide RNAs mediate RNA interference in cultured mammalian cells. *Nature* 411, 494-498.

Elbashir, S.M., Lendeckel, W., and Tuschl, T. (2001b) RNA interference is mediated by 21- and 22-nucleotide RNAs. *Genes and Development* 15, 188-200.

Erfle, H., Neumann, B., Liebel, U., Rogers, P., Held, M., Walter, T., Ellenberg, J., and Pepperkok, R. (2007) Reverse transfection on cell arrays for high content screening microscopy. *Nature Protocols* 2, 392-399.

Fire, A.Z. (2007) Gene silencing by double-stranded RNA (Nobel Lecture). *Angewandte Chemie International Edition* 46, 6966 – 6984.

Fire, A.Z., Xu, S., Montgomery, M.K., Kostas, S.A., Driver, S.E., and Mello, C.C. (1998) Potent and specific genetic interference by double-strandedRNA in Caenorhabditis elegans. *Nature* 391, 806-811.

Fisher, T.L., Terhorst, T., Cao, X., and Wagner, R.W. (1993) Intracellular disposition and metabolism of fluorescently-labeled unmodified and modified oligonucleotides microinjected into mammalian cells. *Nucleic Acids Research* 21, 3857-3865.

Fujimoto, H., Kato, K., and Iwata, H. (2008) Electroporation microarray for parallel transfer of small interfering RNA into mammalian cells. *Analytical and Bioanalytical Chemistry* 392, 1309-1316.

Fujimoto, H., Kato, K., and Iwata, H. (2009) Prolonged durability of electroporation microarrays as a result of addition of saccharides to nucleic acids. *Analytical and Bioanalytical Chemistry* 393, 607-614.

Fujimoto, H., Kato, K., and Iwata, H. (2010) Layer-by-layer assembly of small interfering RNA and poly(ethyleneimine) for substrate-mediated electroporation with high efficiency. *Analytical and Bioanalytical Chemistry* 397, 571-578.

Fyrberg, A., and Lotfi, K. (2010) Optimization and evaluation of electroporation delivery of siRNA in the human leukemic CEM cell line. *Cytotechnology* 62, 497-507.

Genovesio, A., Giardini, M.A., Kwon, Y.-J., Dossin, F.d.M., Choi, S.Y., Kim, N.Y., Kim, H.C., Jung, S.Y., Schenkman, S., Almeida, I.C., et al. (2011) Visual genome-wide RNAi screening to identify human host factors required for Trypanosoma cruzi infection. *PLoS One* 6, e19733.

Giaever, I., and Keese, C.R. (1984) Monitoring fibroblast behavior in tissue culture with an applied electric field. *Proceedings of the National Academy of Sciences of the United States of America* 81, 3761-3764.

Giaever, I., and Keese, C.R. (1986) Use of electric fields to monitor the dynamical aspect of cell behavior in tissue culture. *IEEE Transactions on Biomedical Engineering* 33, 242-247.

Gruber, J., Manninga, H., Tuschl, T., Osborn, M., and Weber, K. (2005) Specific RNAi mediated gene knockdown in zebrafish cell lines. *RNA Biology* 2, 101-105.

Hirsch, M., and Helm, M. (2015) Live cell imaging of duplex siRNA intracellular trafficking. *Nucleic Acids Research* 43, 4650-4660.

Hoekstra, D., Rejman, J., Wasungu, L., Shi, F., and Zuhorn, I. (2007) Gene delivery by cationic lipids: in and out of an endosome. *Biochemical Society Transactions* 35, 68-71.

Hollins, A.J., Omidi, Y., Benter, I.F., and Akhtar, S. (2007) Toxicogenomics of drug delivery systems: exploiting delivery system-induced changes in target gene expression to enhance siRNA activity. *Journal of Drug Targeting* 15, 83–88.

Inoue, Y., Kurihara, R., Tsuchida, A., Hasegawa, M., Nagashima, T., Mori, T., Niidome, T., Katayama, Y., and Okitsu, O. (2008) Efficient delivery of siRNA using dendritic poly(l-lysine) for loss-of-function analysis. *Journal of Controlled Release* 126, 59-66.

Jain, T., McBride, R., Head, S., and Saez, E. (2009) Highly parallel introduction of nucleic acids into mammalian cells grown in microwell arrays. *Lab Chip* 9, 3557-3566.

Jain, T., and Muthuswamy, J. (2007) Microsystem for transfection of exogenous molecules with spatio-temporal control into adherent cells. *Biosensors and Bioelectronics* 22, 863–870.

Jain, T., Papas, A., Jadhav, A., McBride, R., and Saez, E. (2012) In situ electroporation of surface-bound siRNAs in microwell arrays. *Lab Chip* 12, 939-947.

Jordan, E.T., Collins, M., Terefe, J., Ugozzoli, L., and Rubio, T. (2008) Optimizing electroporation conditions in primary and other difficult-to-transfect cells. *Journal of Biomolecular Techniques: JBT* 19, 328-334.

Juliano, R., Alam, M.R., Dixit, V., and Kang, H. (2008) Mechanisms and strategies for effective delivery of antisense and siRNA oligonucleotides. *Nucleic Acids Research* 36, 4158-4171.

Kabanov, A.V. (2006) Polymer genomics: an insight into pharmacology and toxicology of nanomedicines. *Advanced Drug Delivery Reviews* 58, 1597–1621.

Keese, C.R., Wegener, J., Walker, S.R., and Giaever, I. (2004) Electrical wound-healing assay for cells in vitro. *Proceedings of the National Academy of Sciences of the United States of America* 101, 1554-1559.

Kohler, A., and Hurt, E. (2007) Exporting RNA from the nucleus to the cytoplasm. *Nature Reviews Molecular Cell Biology* 8, 761-773.

Kwon, Y.-J., Heo, J., Kim, H., Kim, J., Liuzzi, M., and Soloveva, V. (2013) Phenotypic microRNA microarrays. *Microarrays* 2, 63.

Lam, J.K.W., Chow, M.Y.T., Zhang, Y., and Leung, S.W.S. (2015) siRNA versus miRNA as therapeutics for gene silencing. *Molecular Therapy-Nucleic Acids* 4, e252.

Layzer, J.M., McCaffrey, A.P., Tanner, A.K., Huang, Z., Kay, M.A., and Sullenger, B.A. (2004) In vivo activity of nuclease-resistant siRNAs. *RNA Journal* 10, 766–771.

Leonetti, J.P., Mechti, N., Degols, G., Gagnor, C., and Lebleu, B. (1991) Intracellular distribution of microinjected antisense oligonucleotides. *Proceedings of the National Academy of Sciences of the United States of America* 88, 2702-2706.

Loke, S.L., Stein, C.A., Zhang, X.H., Mori, K., Nakanishi, M., Subasinghe, C., Cohen, J.S., and Neckers, L.M. (1989) Characterization of oligonucleotide transport into living cells. *Proceedings of the National Academy of Sciences of the United States of America* 86, 3474-3478.

Lv, H., Zhang, S., Wang, B., Cui, S., and Yan, J. (2006) Toxicity of cationic lipids and cationic polymers in gene delivery. *Journal of Controlled Release* 114, 100–109.

McCaffrey, A.P., Meuse, L., Pham, T.-T.T., Conklin, D.S., Hannon, G.J., and Kay, M.A. (2002) Gene expression: RNA interference in adult mice. *Nature* 418 38–39.

Meister, G. (2008) Molecular biology. RNA interference in the nucleus. *Science* 321, 496-497.

Meister, G., and Tuschl, T. (2004) Mechanisms of gene silencing by double-stranded RNA. *Nature* 431, 343-349.

Molenaar, C., Marras, S.A., Slats, J.C., Truffert, J.C., Lemaitre, M., Raap, A.K., Dirks, R.W., and Tanke, H.J. (2001) Linear 2' O-Methyl RNA probes for the visualization of RNA in living cells. *Nucleic Acids Research* 29, E89-89.

Nakielny, S., and Dreyfuss, G. (1999) Transport of proteins and RNAs in and out of the nucleus. *Cell* 99, 677-690.

O'Meara, C.M., Murray, J.D., Mamo, S., Gallagher, E., Roche, J., and Lonergan, P. (2011) Gene silencing in bovine zygotes: siRNA transfection versus microinjection. *Reproduction, Fertility and Development* 23, 534-543.

Ohrt, T., Merkle, D., Birkenfeld, K., Echeverri, C.J., and Schwille, P. (2006) In situ fluorescence analysis demonstrates active siRNA exclusion from the nucleus by Exportin 5. *Nucleic Acids Research* 34, 1369-1380.

Ohrt, T., Mutze, J., Staroske, W., Weinmann, L., Hock, J., Crell, K., Meister, G., and Schwille, P. (2008) Fluorescence correlation spectroscopy and fluorescence cross-correlation spectroscopy reveal the cytoplasmic origination of loaded nuclear RISC in vivo in human cells. *Nucleic Acids Research* 36, 6439-6449.

Orio, J., Bellard, E., Baaziz, H., Pichon, C., Mouritzen, P., Rols, M.-P., Teissié, J., Golzio, M., and Chabot, S. (2013) Sub-cellular temporal and spatial distribution of electrotransferred LNA/DNA oligomer. *Journal of RNAi and Gene Silencing* 9, 479-485.

Paganin-Gioanni, A., Bellard, E., Escoffre, J.M., Rols, M.P., Teissié, J., and Golzio, M. (2011) Direct visualization at the single-cell level of siRNA electrotransfer into cancer cells. *Proceedings of the National Academy of Sciences of the United States of America* 108, 10443–10447.

Pecot, C.V., Calin, G.A., Coleman, R.L., Lopez-Berestein, G., and Sood, A.K. (2011) RNA interference in the clinic: challenges and future directions. *Nature Reviews Cancer* 11, 59-67.

Pereyra, A., and Hereñu, C. (2013) Gene delivery systems. In Current Issues in Molecular Virology - Viral Genetics and Biotechnological Applications, P.V. Romanowski, ed. (InTech)

Pridgen, E.M., Langer, R., and Farokhzad, O.C. (2007) Biodegradable, polymeric nanoparticle delivery systems for cancer therapy. *Nanomedicine* 2, 669–680.

Putnam, D. (2006) Polymers for gene delivery across length scales. *Nature Materials* 5, 439–451.

Robb, G.B., Brown, K.M., Khurana, J., and Rana, T.M. (2005) Specific and potent RNAi in the nucleus of human cells. *Nature Structural and Molecular Biology* 12, 133-137.

Saleh, M.C., van Rij, R.P., Hekele, A., Gillis, A., Foley, E., O'Farrell, P.H., and Andino, R. (2006) The endocytic pathway mediates cell entry of dsRNA to induce RNAi silencing. *Nature Cell Biology* 8, 793-802.

Schaefer, J., Hoebel, S., Bakowsky, U., and Aigner, A. (2010) Liposome-polyethylenimine complexes for enhanced DNA and siRNA delivery. *Biomaterials* 31, 6892–6900.

Scherer, L.J., and Rossi, J.J. (2003) Approaches for the sequence-specific knockdown of mRNA. *Nature Biotechnology* 21, 1457–1465.

Schraivogel, D., and Meister, G. (2014) Import routes and nuclear functions of Argonaute and other small RNA-silencing proteins. *Trends in Biochemical Sciences* 39, 420-431.

Seibel, N.M., Eljouni, J., Nalaskowski, M.M., and Hampe, W. (2007) Nuclear localization of enhanced green fluorescein protein homomultimers. *Analytical Biochemistry* 368, 95–99.

Shoji, Y., Akhtar, S., Periasamy, A., Herman, B., and Juliano, R.L. (1991) Mechanism of cellular uptake of modified oligodeoxynucleotides containing methylphosphonate linkages. *Nucleic Acids Research* 19, 5543-5550.

Stolwijk, J.A. (2012) Electric manipulation and impedance analysis of adherent cells on gold-film electrodes. PhD thesis, Universität Regensburg

Stolwijk, J.A., Hartmann, C., Balani, P., Albermann, S., Keese, C.R., Giaever, I., and Wegener, J. (2011) Impedance analysis of adherent cells after in situ electroporation: Non-invasive monitoring during intracellular manipulations. *Biosensors and Bioelectronics* 26, 4720–4727.

Tiera, M.J., Winnik, F.O., and Fernandes, J.C. (2006) Synthetic and natural polycations for gene therapy: state of the art and new perspectives. *Current Gene Therapy* 6, 59–71.

Vaish, N., Chen, F., Seth, S., Fosnaugh, K., Liu, Y., Adami, R., Brown, T., Chen, Y., Harvie, P., Johns, R., et al. (2011) Improved specificity of gene silencing by siRNAs containing unlocked nucleobase analogs. *Nucleic Acids Research* 39, 1823–1832.

van Rooij, E., Purcell, A.L., and Levin, A.A. (2012) Developing microRNA therapeutics. *Circulation Research* 110, 496–507.

Veedu, R.N., and Wengel, J. (2010) Locked nucleic acids: promising nucleic acid analogs for therapeutic applications *Chemistry and Biodiversity* 7, 536–542.

Wegener, J., Keese, C.R., and Giaever, I. (2002) Recovery of adherent cells after in situ electroporation monitored electrically. *Biotechniques* 33, 348 - 352.

Whitehead, K.A., Langer, R., and Anderson, D.G. (2009) Knocking down barriers: advances in siRNA delivery. *Nature Reviews Drug Discovery* 8, 129-138.

Zabner, J., Fasbender, A.J., Moninger, T., Poellinger, K.A., and Welsh, M.J. (1995) Cellular and molecular barriers to gene transfer by a cationic lipid. *The Journal of Biological Chemistry* 270, 18997-19007.

Zamore, P.D., Tuschl, T., Sharp, P.A., and Bartel, D.P. (2000) RNAi: Double-stranded RNA directs the ATP-dependent cleavage of mRNA at 21 to 23 nucleotide intervals. *Cell* 101, 25–33.

9 Summary

Whole-cell biosensors are irreplaceable tool for studies of cellular mechanisms and behavior of the cell as a smallest living unit. Their development have progressed rapidly over past decades and nowadays we have powerful tools to study cell-based assays and to examine behavior of the cells exposed to different kinds of stimuli and challenges. Limited and selective permeability of the plasma membrane prevents the introduction of hydrophilic xenomolecules into the cytoplasm of mammalian cells. However, it is essential for many fields of cell biology, biomedicine or biotechnology to allow transport of such molecules (e.g. nucleic acids, antibodies, peptides or drugs) across the cell membrane. An ultimate goal of this thesis was to establish proof-of-principle assays for delivery of various bioactive molecules into adherent cells by *in situ* electroporation, and to monitor how these compounds influence cellular behavior, once they are internalized within the cell cytosol. Studies of *in situ* electroporation (ISE) were conducted using different types of mammalian cells (BAEC, CHO-K1/CHO-GFP, HaCaT, NRK and NIH-3T3) grown to confluence on small planar gold film electrodes. For every cell line individually, electric pulse parameters were optimized to achieve maximal loading efficiency, while keeping the invasiveness of the operation as low as possible. Impedance monitoring of *in situ* electroporation conducted with high time resolution showed biphasic changes of impedance signal after pulse application, indicating (i) fast recovery of the cell membrane integrity and (ii) relatively slow process of cell recovery after changes induced by membrane permeabilization. For the first time, release of intracellular material from the cells by ISE was studied using ECIS setup. Direct time-resolved imaging of NRK cells showed measurable efflux of fluorescence-labeled probes upon multiply applied electric pulses. *In situ* electroporation allowed transfer of second messenger (8-OH-)cAMP in the cell monolayers. Subsequent changes in impedance signal were in agreement with those observed after stimulation of the cells with membrane-permeable compounds CPT-cAMP and forskolin, as a consequence of triggering of the corresponding signaling cascades. Transport of nucleic acids into cytoplasm and nuclei of NRK and CHO-GFP cells was conducted in a highly-efficient manner. Besides fluorescent DNA aptamers, various types of siRNA molecules were successfully delivered into cells by *in situ* electroporation and their long-term sequence-specific silencing effect on cells was demonstrated and quantified by using microscopy and/ or impedance analysis. Transfection performance of ISE was compared with conventional and widespread delivery transfection method. In conclusion, this thesis demonstrated that *in situ* electroporation allows for highly efficient delivery of emerging types of molecules into monolayers of various types of cells.

10 Zusammenfassung

Zellbasierte Biosensoren sind ein unersetzbares Werkzeug um zelluläre Mechanismen und Funktionen der Zelle, als die kleinste lebende Einheit, zu erforschen. Zellbasierte Biosensoren haben sich in den letzten Jahrzehnten hin zu leistungsstarken Werkzeugen für Untersuchungen der zellulären Antwort auf verschiedene intra- und extrazelluläre Anregungen entwickelt. Dabei wird die Verfolgung von zellbasierten Assays ermöglicht. Die begrenzte und selektive Permeabilität von der Plasmamembran verhindert den Eintrag von den hydrophilen Molekülen in das Zytoplasma der Säugetierzellen. Für viele verschiedene Bereiche der Zellbiologie, Biomedizin, oder Biotechnologie ist es aber von großer Bedeutung, dass Moleküle wie z. B. Nukleinsäure, Antikörper, Peptide, oder Arzneimittel über die Zellmembran transportiert werden können. Ziel dieser Arbeit war es, die grundlegenden Assays für den Eintrag von bioaktiven Molekülen in adhärente Zellen mittels *in situ* Elektroporation zu etablieren. Dabei wurde verfolgt, wie Präsenz und Aktivität dieser Moleküle in dem Cytosol die Zellen beeinflusst. *In situ* Elektroporation (ISE) wurde an verschieden Zelllinien untersucht (BAEC, CHO-K1/CHO-GFP, HaCaT, NRK und NIH-3T3), welche auf kleinen planaren Goldfilmelektroden bis zur Konfluenz kultiviert wurden. Für jede Zelllinie wurden die Puls Parameter individuell für die Eintragsstudien optimiert, so dass die maximale Beladung mit möglichst wenig Invasivität erreicht wird. Impedanzmessungen mit hoher Zeitauflösung haben zweiphasige Signaländerungen nach dem elektrischen Puls gezeigt. Das bezeichnet (i) eine schnelle Erholung der Zellmembran und (ii) einen relativ langsamen Prozess der Zellerholung nach den Veränderungen, welche durch Zellmembranpermeabilisierung verursacht wird. Zum ersten Mal wurde die *in situ* Elektroporation in Kombination mit ECIS für die Freisetzung von dem intrazellulären Material aus den Zellen verwendet und untersucht. Direkte, zeitaufgelöste mikroskopische Bildgebung von NRK Zellen wurde verwendet, um das Ausströmen von Fluoreszenz-markierten Proben durch die sukzessive Zellmembranpermeabilisierung nachzuweisen. Außerdem ermöglicht *in situ* Elektroporation den Transfer von Second Messenger (8-OH-)cAMP in Zellmonoschichten. Die anschließenden Veränderungen des Impedanzsignals zeigten Übereinstimmung mit der Veränderung des Signals nach der Stimulation der Zellen in Gegenwart von membrangängigen cAMP-Stimulatoren CPT-cAMP und Forskolin. Der Transport von Nukleinsäuren in das Zytoplasma und den Nukleus der NRK und der CHO-GFP Zellen wurde erfolgreich als hoch effizient erwiesen. Neben den Fluoreszenz-markierten DNA Aptameren wurde der erfolgreiche Eintrag von den verschieden siRNA Typen durch *in situ* Elektroporation demonstriert. Dabei wurde ein langfristiger Sequenz-

spezifischer Silencing Effekt von siRNA auf die Zellen mittels mikroskopischer Aufnahmen oder über Impedanzmessungen quantifiziert. Die Effizienz von der Transfektion der *in situ* Elektroporation wurde mit konventionellen chemischen Transfektionsreagenzien verglichen. Diese Arbeit hat demonstriert, dass die *in situ* Elektroporation einen hoch effizienten Eintrag von verschiedenen bioaktiven Molekülen in die Zellmonoschichten ermöglicht.

11 Appendix

11.1 Abbreviations and Symbols

|Z|	impedance magnitude
×	-times
®	registered trade mark
2-APB	2-aminoethoxydiphenyl borate
8-OH-cAMP	8-hydroxyadenosine-3', 5'-cyclic monophosphate
8W1E	eight wells with one electrode in each
8W4E	eight wells with four electrodes in each
AC	alternating current
app.	Approximately
APT	aptamer
BAEC	bovine aortic endothelial cells
bp	base pairs
C	capacitance
Ca-AM	calcein-acetoxymethylester
cAMP	cyclic adenosine monophosphate
cGMP	cyclic guanosine monophosphate
CH TR	chemical transfection
CHO–GFP	Chinese hamster ovary cells expressing (enhanced) green fluorescent protein
CHO–K1	Chinese hamster ovary cells
CLSM	confocal laser scanning microscope
Cm	specific membrane capacitance (ECIS model)
CM	complete cell culture medium
CMN	calcimycin
CPE	constant phase element
CPT-cAMP	8-(4-chlorophenylthio) adenosine 3′,5′-cyclic monophosphate
CPT-cGMP	8-(4-chlorophenylthio) guanosine 3′,5′-cyclic monophosphate
d	distance
Da	Dalton
DAG	diacylglycerol
DAPI	4′,6-diamidino-2-phenylindole (dihydrochloride)
DC	direct current
DMEM	Dulbecco’s Modified Eagle’s Medium
DMSO	dimethylsulfoxide
DNA	desoxyribonucleic acid
DNase	deoxyribonuclease

DSMZ	Deutsche Sammlung von Mikroorganismen und Zellkulturen
E	electric field
e.g.	Lat.: *exempli gratia* - for example
$EBSS^{--}$	Earle's Balanced Salt Solution (without Mg^{2+} and Ca^{2+})
$EBSS^{+-}$	Earle's Balanced Salt Solution (with Mg^{2+}; without Ca^{2+})
$EBSS^{++}$	Earle's balanced salt solution (with Mg^{2+} and Ca^{2+})
ECIS	electric cell-substrate impedance sensing
EDTA	ethylenediaminetetraacetic acid
EGFP	enhanced green fluorescent protein
ELPO	electroporation
et al.	Lat.: *et alii* - and others
etc.	Lat.: *et setera* – and so on
EthD-1	ethidium homodimer
f	frequency
F + P	fixation and permeabilization
FBS	fetal bovine serum
FCS	fetal calf serum
FG	frequency generator
Fig.	figure
FITC	fluorescein isothiocyanate
FOR	forskolin
FRET	Förster resonance energy transfer
g	gravitational acceleration
G418	geneticin
HaCaT	human immortalized keratinocytes
HCl	hydrochloric acid
HTR	high time resolution
I	current
i	imaginary factor
i.e.	Lat.: *id est* - that is
IA	impedance analyzer
IDES	interdigitated electrodes
Im	imaginary fraction of a complex quantity
INT	I
IP3	inositol 1,4,5-triphosphate
IS	impedance spectroscopy
ISE	*in situ* electroporation
ITO	indium tin oxide
k	time constant

KCl	potassium chloride
kDa	kilo Dalton
KOH	potassium hydroxide
L-15	Leibovitz's L-15 medium
LDH	lactate dehydrogenase
LF®	Lipofectamine®
LNA	locked nucleic acid
$MgCl_2 \cdot 6H_2O$	magnesium chloride hexahydrate
mRNA	messenger ribonucleic acid
MV	mean value
Mw	molecular weight
n	number of
n.d.	not determined
NaCl	natrium chloride
NAD+	nicotinamide adenine dinucleotide (oxidizing agent)
NADH	nicotineamid adenine dinucleotide (reducing agent)
NaOH	natrium hydroxide
NIH-3T3	albino mouse embryonic cells
NLS	nuclear localization signal
Norm. |Z|	normalized impedance magnitude (|Z|)
NPC	nuclear pore complex
NRK	normal rat kidney cells, strain E52
Ø	diameter
OD	optical density
ON	oligonucleotide
p.a.	Lat.: *pro analysi* - for analysis
PBS^{--}	phosphate buffered saline (without Mg^{2+} and Ca^{2+})
PBS^{++}	phosphate buffered saline (with Mg^{2+} and Ca^{2+})
PC	personal computer
pDEAEMA	poly(diethylaminoethyl methylacrylate)
PDMS	polydimethylsiloxane
PEG	polyethyleneglycol
PEI	polyethyleneimine
PFA	paraformaldehyde
PI	propidium iodide
PKA	protein kinase A
PLL	poly(L-lysine)
PNA	peptide nucleic acid
QCM	quartz crystal microbalance

QD	quantum dot
r	radius
R	resistance (real fraction of the complex impedance)
r.u.	relative unit
Rb	specific barrier resistance (ECIS model)
Re	real fraction of a complex quantity
rms	root mean square
R	resistance
RNA	ribonucleic acid
RNase	ribonuclease
rpm	rounds per minute
RT	room temperature
SD	standard deviation
SFM	serum-free medium
siCD	Cell Death siRNA
siEGFP	siRNA targeting EGFP
siGLO Red	red transfection indicator
siRNA	small interfering RNA
siSCR	scrambled siRNA
SPR	surface plasmon resonance
T	temperature
t	time (point)
Tab.	table
TRITC	Tetramethylrhodamin isothiocyanate
tRNA	transfer ribonucleic acid
a.u.	arbitrary unit
U	voltage
UV	ultraviolet
Vit. C	vitamin c
vs.	versus
X	reactance (imaginary fraction of the complex impedance)
Z	impedance
α	parameter for cell-substrate junction (ECIS model)
Δ	difference
λ	wavelength
Φ	angle
φ	phase shift
ω	angular frequency
Ψ	membrane potential

11.2 Supplementary Figures

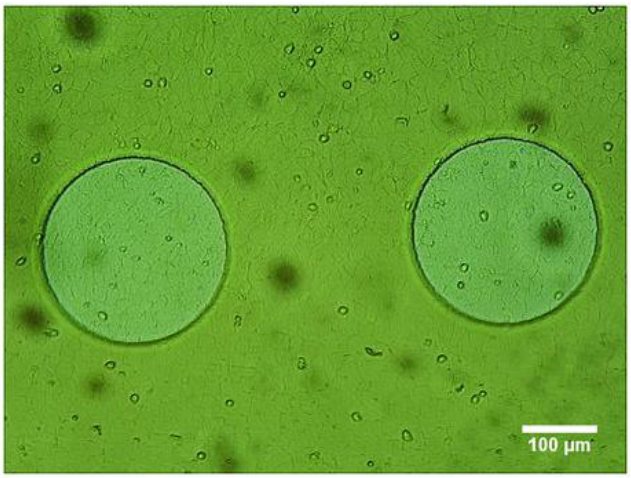

Figure 11.1 Exemplary phase-contrast micrograph taken after multiple *in situ* electroporation of NRK cells in presence of 2 mg/mL 250 kDa FITC-dextran monitored by time-resolved imaging (**Figure 5.18** and **Figure 5.19**, chapter 5.1.4). The scale bar corresponds to 100 µm. Micrograph is taken with 10-fold magnification objective.

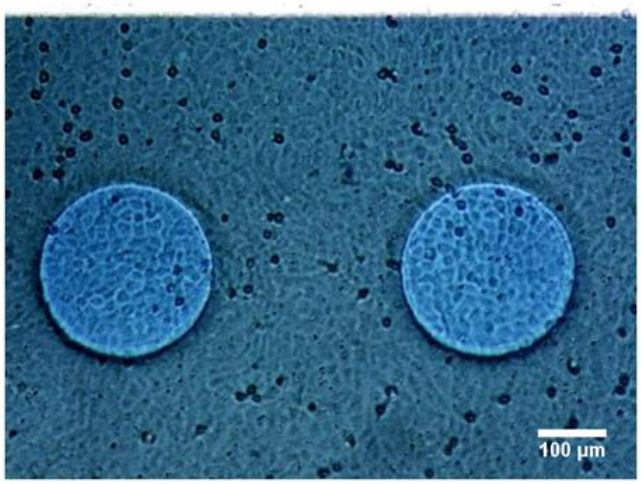

Figure 11.2 Exemplary phase-contrast micrograph taken after multiple *in situ* electroporation of NRK cells to facilitate release of calcein from the cytosol monitored by time-resolved imaging (**Figure 5.31**, chapter 5.3.1.3). The scale bar corresponds to 100 µm. Micrograph is taken with 10-fold magnification objective.

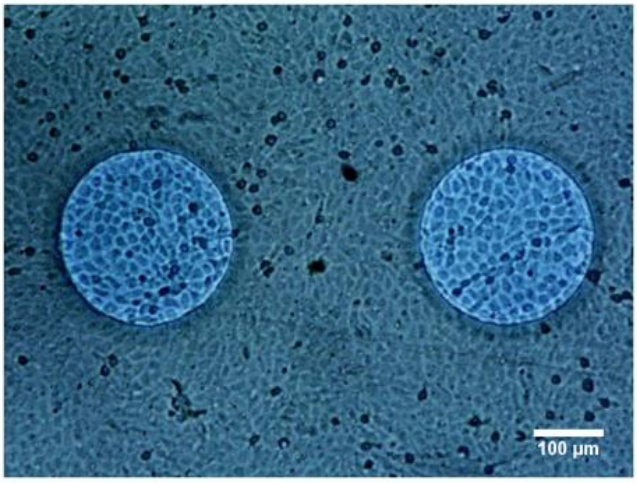

Figure 11.3 Exemplary phase-contrast micrograph taken after time-resolved imaging of NRK cells in absence of electric pulse application (**Figure 5.33**, chapter 5.3.1.3). The scale bar corresponds to 100 µm. Micrograph is taken with 10-fold magnification objective.

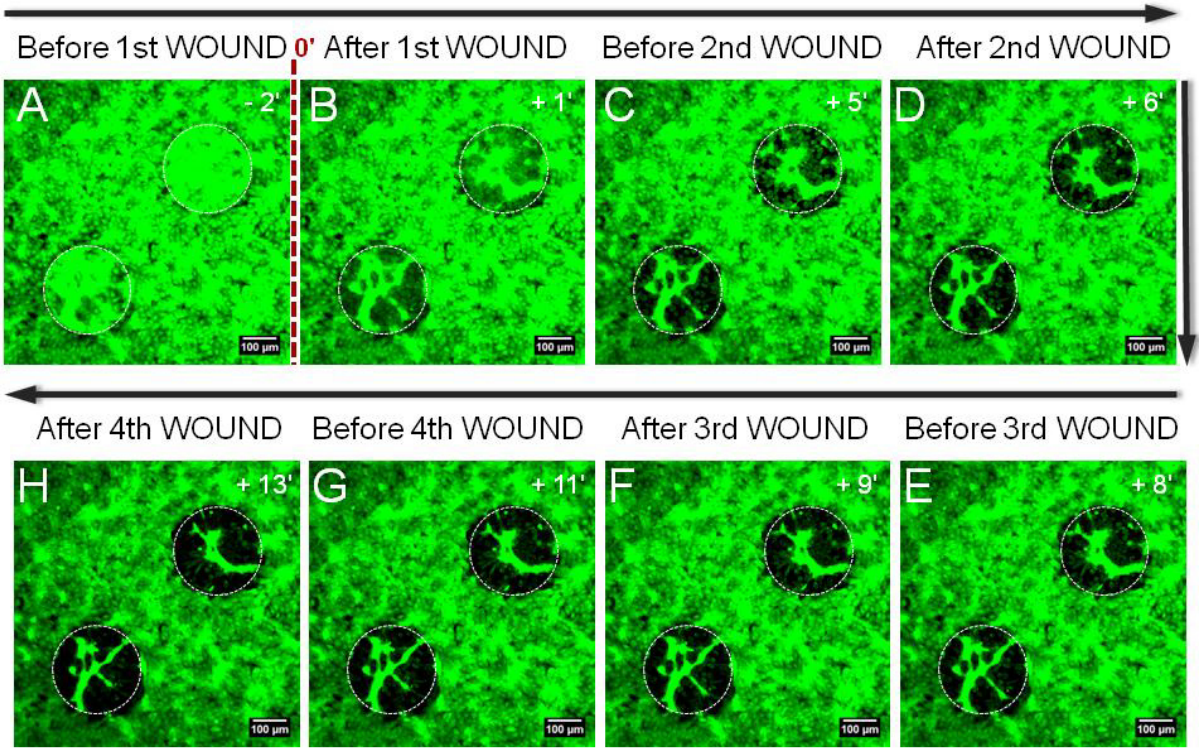

Figure 11.4 Microscopic images taken in real time by CLSM with 10-fold magnification objective before, during and after application of electric wounding (four times) to the confluent NRK cells. The scale bars represent 100 µm. White circles in the images delineate electrodes area. The damage of the cells on the electrodes increased with every electric pulse application.

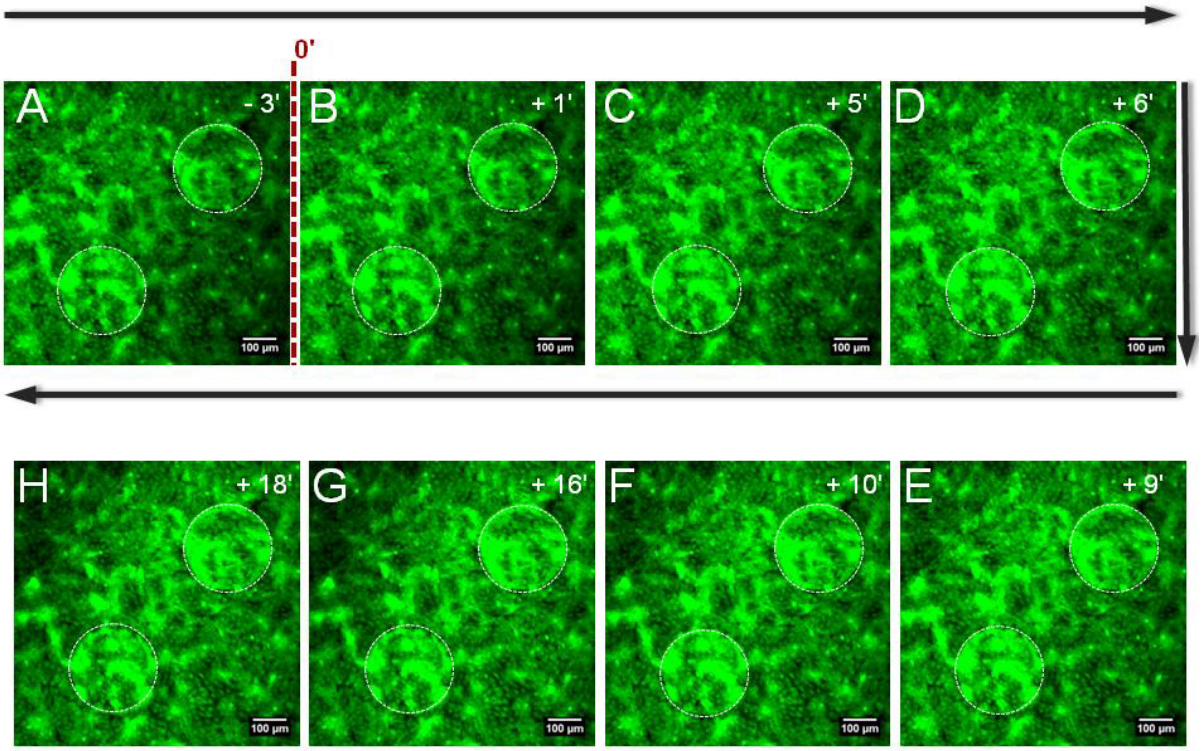

Figure 11.5 Series of microscopic images taken in real time by CLSM with 10-fold magnification objective in absence of electric pulse application. The scale bars represent 100 µm. White circles in the images delineate electrodes area. No cell damage was observed.

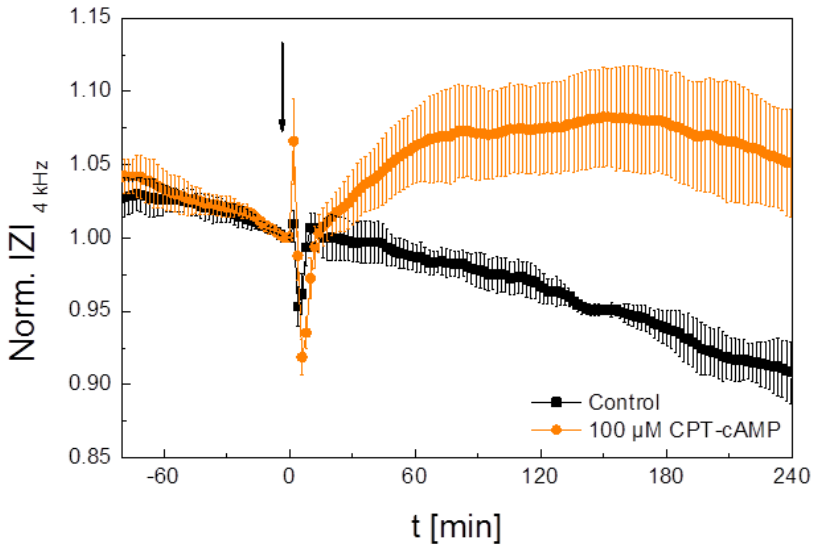

Figure 11.6 Time course of the normalized impedance magnitude at 4 kHz before, during and after stimulation of NRK cells (with passage number P28) with 100 µM CPT-cAMP. Data are normalized to the last time point before addition of CPT-cAMP (marked with an arrow). Error bars correspond to the values of standard deviation (mean value ± standard deviation; n=4).

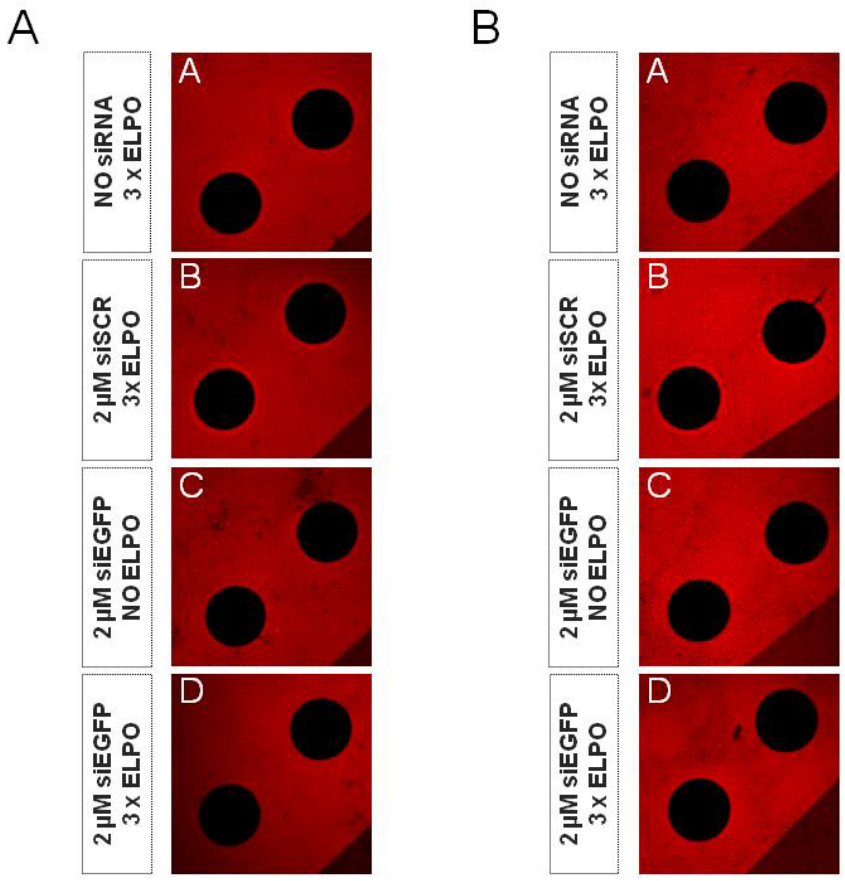

Figure 11.7 Confocal fluorescence micrographs taken (**A**) 48 hours and (**B**) 72 hours after *in situ* electroporation was applied for delivery of 2 µM siEGFP and 2 µM siSCR to CHO-GFP cells. Micrographs in the left column (**A**) correspond to the micrographs given in **Figure 8.18** and micrographs in the right column (**B**) correspond to the micrographs given in **Figure 8.21** (chapter 8.3.1).

11.3 Materials and Instrumentation

11.3.1 Materials for Cellbiological and Biophysical Work

2-APB	Sigma-Aldrich Chemie GmbH, Germany
8-OH-cAMP	BioLog Life Science Institute, Bremen, Germany
AllStars Negative Control siRNA (siSCR)	QIAGEN, Hilden, Germany
Buffered phosphate saline (PBS^{++})	Sigma-Aldrich Chemie GmbH, Germany
Buffered phosphate saline (PBS^{--})	Sigma-Aldrich Chemie GmbH, Germany
Calcein-AM	Sigma-Aldrich Chemie GmbH, Germany
Calcimycin	Sigma-Aldrich Chemie GmbH, Germany
Calcium chloride ($CaCl_2$)	Sigma-Aldrich Chemie GmbH, Germany

cAMP	BioLog Life Science Institute, Bremen, Germany
Cell Death siRNA (siCD)	QIAGEN, Hilden, Germany
cGMP	Sigma-Aldrich Chemie GmbH, Germany
CPT-cAMP	Sigma-Aldrich Chemie GmbH, Germany
CPT-cGMP	Sigma-Aldrich Chemie GmbH, Germany
Curing agent Sylgard® 184	Dow Corning, Michigan, MI, USA
DAPI	Sigma-Aldrich Chemie GmbH, Germany
Deionized ultrapure water (Milli-Q)	Millipore GmbH, Schwalbach, Germany
Dimethylsulfoxide (DMSO)	Carl Roth, Karlsruhe, Germany
DNA aptamer 1 (APT 1)	IBA, Goettingen, Germany
DNA aptamer 2 (APT 2)	IBA, Goettingen, Germany
Dulbecco's Modified Eagle's Medium (DMEM)	Sigma-Aldrich Chemie GmbH, Germany
Earle's Balanced Salt Solution ($EBSS^{++}$)	Sigma-Aldrich Chemie GmbH, Germany
Earle's Balanced Salt Solution ($EBSS^{--}$)	Gibco®, Life Technologies GmbH, Darmstadt, Germany
Elma clean 10	Elma Hans Schmidbauer GmbH, Singen, Germany
Ethanol	Merck KGaA, Darmstadt, Germany
Ethanol	Sigma-Aldrich Chemie GmbH, Germany
Ethidium-Homodimer	Molecular Probes®, Life Technologies GmbH, Darmstadt, Germany
EDTA	Carl Roth, Karlsruhe, Germany
EDTA BioUltra	Sigma-Aldrich Chemie GmbH, Germany
Fetal bovine serum (FBS Superior)	Biochrom AG, Berlin, Germany
Fetal calf serum (FCS Superior)	Biochrom AG, Berlin, Germany
FITC-dextran (10 kDa)	Sigma-Aldrich Chemie GmbH, Germany
FITC-dextran (250 kDa)	Sigma-Aldrich Chemie GmbH, Germany
FITC-dextran (4 kDa)	Sigma-Aldrich Chemie GmbH, Germany
Fluorescein	Fluka, Sigma-Aldrich Chemie GmbH, Germany
Forskolin	Fluka, Sigma-Aldrich Chemie GmbH, Germany
G418	InvivoGen, Toulouse, France
Gelatine	Sigma-Aldrich Chemie GmbH, Germany
Glutaraldehyde	Merck KGaA, Darmstadt, Germany
Ham's F-12	Sigma-Aldrich Chemie GmbH, Germany
HEPES, free acid	Carl Roth, Karlsruhe, Germany
Isoprenalin	Sigma-Aldrich Chemie GmbH, Germany
Leibovitz's L-15 Medium	Gibco®, Life Technologies GmbH, Darmstadt, Germany
L-Glutamine	Sigma-Aldrich Chemie GmbH, Germany
Lipofectamine® 3000 Reagent	Invitrogen™, Life Technologies GmbH, Darmstadt, Germany
Lipofectamine® RNAiMAX Reagent	Invitrogen™, Life Technologies GmbH, Darmstadt, Germany
LIVE/DEAD® cell viability assay	Molecular Probes®, Life Technologies GmbH, Darmstadt, Germany
Lucifer Yellow CH dipotassium salt	Sigma-Aldrich Chemie GmbH, Germany

LysoTracker® Blue DND-22	Molecular Probes®, Life Technologies GmbH, Darmstadt, Germany
Magnesium chloride hexahydrate ($MgCl_2$•$6H_2O$)	Sigma-Aldrich Chemie GmbH, Germany
Milli-Q water, DNase/RNase-free	Carl Roth, Karlsruhe, Germany
Natrium chloride (NaCl)	VWR International GmbH, Darmstadt, Germany
Natrium hydroxide (NaOH)	Merck KGaA, Darmstadt, Germany
Opti-MEM® I Reduced Serum Medium	Gibco®, Life Technologies GmbH, Darmstadt, Germany
Paraformaldehyde (PFA)	Sigma-Aldrich Chemie GmbH, Germany
PDMS base polymer Sylgard® 184	Dow Corning, Michigan, MI, USA
Penicillin	Sigma-Aldrich Chemie GmbH, Germany
Pierce™ LDH Cytotoxicity Assay Kit	Fisher Scientific GmbH, Schwerte, Germany
Potassium chloride (KCl)	Sigma-Aldrich Chemie GmbH, Germany
Potassium hydroxide pellets (KOH)	Merck KGaA, Darmstadt, Germany
Propidium Iodide	Sigma-Aldrich Chemie GmbH, Germany
siGLO™ Red Transfection Indicator	GE Healthcare Dharmacon, Inc., Lafayette, CO, USA
siRNA targeting EGFP (siEGFP)	Eurofins MWG Operon, Ebersberg, Germany
Streptomycin	Sigma-Aldrich Chemie GmbH, Germany
TRIS-HCl PUFFERAN®	Carl Roth, Karlsruhe, Germany
Triton-X-100	Sigma-Aldrich Chemie GmbH, Germany
Trypsin	Sigma-Aldrich Chemie GmbH, Germany

11.3.2 Instrumentation and Consumables

96-well PS-microplate (with flat bottom)	Greiner Bio-One GmbH, Frickenhausen, Germany
Aspiration station	HLC BioTech, Bovenden, Germany
Argon Plasma Cleaner PDC 32G-2	Harrick Plasma, Ithaca, NY, USA
Autoclave DX-45	Systec, Wettenberg, Germany
Buerker hemocytometer	Marienfeld-Superior, Lauda-Koenigshofen, Germany
Cell culture incubator Heraeus BB15	Thermo Scientific, Munich, Germany
Cell culture incubator CO2CELL (190 L)	MMM Medcenter Einrichtungen GmbH, Munich, Germany
Cell culture incubator CO2CELL (50 L)	MMM Medcenter Einrichtungen GmbH, Munich, Germany
Cell culture incubator Revco Ultima II	Thermo Scientific, Munich, Germany
Centrifuge Heraeus Multifuge 1S-R	Thermo Scientific, Munich, Germany
Centrifuge tube DNase/RNase-free CentriStar™ (50 mL)	Corning, Sigma-Aldrich Chemie, Germany
Centrifuge tubes (15 and 50 mL)	Sarstedt AG & Co., Nuembrecht, Germany
Centrifuge tubes Cellstar® (15 and 50 mL)	Greiner Bio-One GmbH, Frickenhausen, Germany
Confocal laser scanning microscope Nikon Eclipse 90i	Nikon instruments, Tokyo, Japan
Cryovial	Nunc®, Sigma-Aldrich Chemie GmbH, Germany
Disposable glass Pasteur pipettes (230 mm)	VWR International GmbH, Darmstadt, Germany
Disposable pipettes (1 and 2 mL)	TPP Techno Plastic Products AG, Trasadingen, Switzerland
Disposable pipettes Cellstar® (5, 10 and 25 mL)	Greiner Bio-One GmbH, Frickenhausen, Germany

Disposable scalpel	Feather safety razor Co., LTD. Osaka, Japan
ECIS 1600R	Applied BioPhysics, Troy, New York, USA
ECIS electrode arrays (8W1E, 8W4Eμ)	Applied BioPhysics, Troy, NY, USA
Filter tips DNase/RNase-free Biosphere® (10 and 100 µL)	Sarstedt AG & Co., Nuembrecht, Germany
Frequency generator type 33120A	Hewlett Packard-Agilent, Boeblingen, Germany
Gas Burner Bunsen Fireboy	Intergra Biosciences AG, Biebertal, Germany
Impedance analyzer SI 1260	Solartron Instruments, Farnborough, United Kingdom
Laminar flow hood HERAsafe®	Thermo Scientific, Munich, Germany
Latex gloves	Carl Roth, Karlsruhe, Germany
Microscope Nikon Diaphot	Nikon instruments, Tokyo, Japan
Mr. Frosty™ Freezing Container	Thermo Scientific™, Fisher Scientific GmbH, Schwerte, Germany
NanoDrop spectrophotometer	Fisher Scientific GmbH, Schwerte, Germany
Nitrile gloves	VWR International GmbH, Darmstadt, Germany
Petri dish	Greiner Bio-One GmbH, Frickenhausen, Germany
Petri dish tissue culture	Sarstedt AG & Co., Nuembrecht, Germany
pH – indicator paper (pH 6.4 – 8.0)	Merck KGaA, Darmstadt, Germany
Pipette controller accu-jet® pro	Brand GmbH & Co. KG, Wertheim, Germany
Pipette tips (10, 100 and 1000 µL)	Sarstedt AG & Co., Nuembrecht, Germany
Plastic tube DNase/RNase-free Biosphere® (0.5 mL)	Sarstedt AG & Co., Nuembrecht, Germany
Reaction tubes (0.5, 1.5 and 2.0 mL)	Greiner Bio-One GmbH, Frickenhausen, Germany
Reaction tubes (0.5, 1.5 and 2.0 mL)	Sarstedt AG & Co., Nuembrecht, Germany
Relay for electrode arrays	Applied BioPhysics, Troy, NY, USA
Silicone glue transparent for aquaria	Bauhaus AG, Mannheim, Germany
Sterile plastic culture flasks Cellstar®	Greiner Bio-One GmbH, Frickenhausen, Germany
Sterile plastic culture flasks	Sarstedt AG & Co., Nümbrecht, Germany
Tecan Reader Sunrise™	Tecan GmbH, Crailsheim, Germany
Ultrasonic water bath Sonorex Digitech	Bandelin Electronic GmbH & Co. KG, Berlin, Germany
Vortex mixer	Carl Roth, Karlsruhe, Germany
Water bath GFL	Julabo Labortechnik GmbH, Seelbach, Germany
Weighing instrument	Mettler-Toledo GmbH, Giessen, Germany

11.3.3 Software and Websites

ECIS™ software	Applied BioPhysics, Troy, NY, USA
ImageJ image processing program	ImageJ, USA
ECIS Viewer software	Written by Prof. Dr. Joachim Wegener, University of Regensburg
Lab View software	Labview
www.atcc.org	http://www.biophysics.com
http://dharmacon.gelifesciences.com	http://imagej.nih.gov/ij/

https://www.thermofisher.com/de/de/home/brands/product-brand/lipofectamine.html

Eidesstaatliche Erklärung

Hiermit erkläre ich an Eides statt, dass ich die vorliegende Arbeit selbstständig und nur unter Zuhilfenahme der angegebenen Mittel angefertigt habe.

Frankfurt am Main, den 24. Juli 2017

_____

Sonja Lukic

Acknowledgments

I thank my supervisor Prof. Dr. Joachim Wegener for giving me an opportunity to work on my doctoral thesis within his working group. The chance to do PhD project in his lab brought me a great experience and the time spent working on it was from many aspects life-changing for me. I would also like to thank him for all his support, advices and scientific discussions, as well as for the excellent working conditions in his group.

I would also like to thank PD Dr. Miriam Breunig and Prof. Dr. Antje J. Bäumner for taking over the roles of co-examiners and for their careful evaluation of this thesis. Moreover, I kindly thank to Apl. Prof. Dr. Rainer Müller for being a chairman of the examining board during the doctoral exam.

Furthermore, many thanks to Prof. Dr. Achim Göpferich, PD Dr. Miriam Breunig and Ms. Renate Liebl for kindly providing us CHO-K1/ CHO-GFP cells, different types of siRNA and transfection reagents at the beginning of the siRNA project. In addition, I thank Dr. Eva-Christina Wurster for her kind help with the protocol for annealing of the siRNA strands.

Many thanks as well to Dr. Stefanie Michaelis and Dr. Judith Stolwijk for their great support, especially at the beginning of this thesis, I also thank them for being nice labmates and a special thank to Steffi for always carefully reviewing my abstracts and posters. I am very thankful to Ms. Nicole Guber for her great help with all kinds of administrative work. Besides, I would like to thank all members of the working group for the fruitful discussions, team work and all the funny moments we shared in and outside of the lab.

I was very lucky to be a part of the Marie Curie Initial Training Network CHEBANA and thus had a chance to meet many great people from all over the world. Not only that we regularly exchanged research experience during our annual meetings, but we also became very good friends. Special thanks to Dr. Heike Mader and Prof. Dr. Frank-Michael Matysik for organization of CHEBANA events and their great involvement in the project. I had a great chance to spend three months in the lab of Prof. Dr. Manel del Valle from UAB Barcelona, as a visiting researcher and during that time, I learned a lot about aptamers and impedance spectroscopy. Many thanks to Prof. Dr. Manel del Valle, Dr. Cristina Ocaña and all members of the lab for their hospitality and for the great collaboration on the project.

Big thanks to all my friends for their understanding and support during these years, I appreciate it a lot. Also, many thanks to Stefan Balk for his love and support in good and bad times. Last but not least, I thank my parents and my brother for being there for me and supporting me for the whole time, despite the fact they are almost thousand kilometers away. Without you, I would not make it.

Curriculum Vitae

The CV is omitted in this electronic version due to privacy reasons.